



UNIVERSITY OF
LIVERPOOL

In vivo Measurement of Corneal Stiffness and Intraocular Pressure to Enable Personalised Disease Management and Treatment

*Thesis submitted in accordance with the requirements of
the University of Liverpool for the degree*

of

Doctor in Philosophy

by

Ashkan Eliasy

September 2020

(BLANK PAGE)

(BLANK PAGE)

Abstract

In ophthalmology, accurate measurement of intraocular pressure (IOP) and in vivo measurement of corneal material stiffness have been long-standing problems. Access to this information would transform the diagnosis and therapy of diseases and conditions such as glaucoma, refractive errors and keratoconus that are currently affecting over 50% of the world population. The aim of this study is to develop new methods for the accurate measurement of IOP and corneal material stiffness in vivo.

To achieve this goal, a mathematical method was developed to analyse tomography data of keratoconic corneas, to estimate the area, height and location of the keratoconic cone. This information was utilised in the development of representative numerical models of the ocular globe. A large parametric study was then conducted, and with the aid of custom-built programming tools, high-performance computing and optimisation techniques, new methods were developed. These methods enabled the use of information obtained from a non-contact tonometry device to estimate biomechanically corrected IOP and corneal material stiffness.

Methods developed in this study were validated on data collected from experimental tests as well as a large clinical database obtained from four continents. The results showed that the newly developed methods for measuring IOP are more accurate than those currently available in the market. IOP measurements were stable when compared in pre and post-surgical procedures such as refractive correction or corneal crosslinking. IOP values showed a weak/no correlation with geometrical or biomechanical parameters. Further methods for measuring corneal biomechanics in-vivo showed notable advancements compared to the existing method. Biomechanical values were weakly/not correlated with IOP and geometrical features while strongly correlated with age as an indication of changes in material stiffness. The experimental validation showed excellent agreement between the in-vivo measurements in comparison to ex-vivo findings.

The outcome of this research will have an impact on the better diagnosis of glaucoma by eliminating misdiagnosis due to IOP measurement inaccuracies. Further, it enables personalised disease management and treatment through in-vivo measurement of corneal biomechanics that leads to optimisation of surgical procedures, most notably corneal crosslinking and refractive surgeries.

(BLANK PAGE)

Declaration

Liverpool, on Friday, 25th of September 2020

I hereby certify that this thesis constitutes my own product, that where the language of others is set forth, quotation marks so indicate, and that appropriate credit is given where I have used the language, ideas, expressions or writings of another.

I declare that the thesis describes original work that has not previously been presented for the award of any other degree of any institution.

Ashkan Eliasy



(BLANK PAGE)

Acknowledgements

I would like to express my deep and sincere gratitude to my supervisor Professor Ahmed Elsheikh for his trust, continuous support, invaluable guidance and offering plenty of growth opportunities. Working under his leadership has been the most fulfilling moment of my life.

I wish to show my sincere appreciation to Dr Ahmed Abass for being always available to help at every stage of my research from coding to problem-solving and even brainstorming new ideas. I wish to extend my special thanks to Dr Bernardo Lopes and Dr Riccardo Vinciguerra for their support and for providing invaluable specialist clinical insights.

I am grateful to the following individuals who provided assistance throughout this project: Dr Sven Reisdorf, Dr Osama Maklad, Dr Kai Jung Chen, Dr Brendan Geraghty and Dr Junjie Wang.

I am incredibly grateful to my parents and both brothers for their love, caring, prayers and sacrifices that enabled me to reach this point.

I am sincerely thankful to the University of Liverpool for the PhD scholarship.

Ashkan Eliasy

(BLANK PAGE)

Nomenclature

Abbreviations

| | | | | | |
|-------------------|--|---|--|---|---|
| A | | EleFBFS8mm Best Fit Sphere within 8mm Diameter | O | | |
| A1 | First Aplanation | Et Tangent Modulus | OAG | Open-Angle Glaucoma | |
| A1L | A1 Length | F | | OCT Optical Coherence Tomography | |
| A1T | Applanation 1 Time | FFKC Forme Frust Keratoconus | OHT | Ocular Hypertension | |
| A1V | A1 Velocity | fIOP Fluid Structure Interaction | ONH | Optic Nerves Head | |
| ACG | Angle-closure Glaucoma | IOP | Op D | Optical Zone Diameter | |
| ACH | Anterior Cone apex Height | GAT Goldman Applanation Tonometry | ORA | Ocular Response Analyser | |
| AO | American Optical | G | | P | |
| API | Applanation Pressure 1 | GATAdj GAT Adjusted | PBS | | Phosphate Buffered Saline |
| AsphQFront | Anterior Surface Asphericity | H | | PCHM | Posterior Cone Apex Height Movement |
| B | | HC | Highest Concavity | PCT | Peripheral Corneal Thickness |
| BAD-D | Total Deviation of the Belin-Ambrosio Display | HCR | Radius at HC | PD | Peak Distance |
| BFS | Best Fit Sphere | HCT | Highest Concavity Time | PMMA | Polymethyl Methacrylate |
| BioEG | Biomechanical Engineering Group | I | | PRK | Transepithelial Photorefractive Keratectomy |
| bIOP | Biomechanically Corrected Intraocular Pressure | ICRS | Intrastromal Corneal Ring Segments | Q | |
| bPar | Base Parameters | IHA | Index of Height Asymmetry | QS | Quality Score |
| C | | IHD | Index of Height Decentration | R | |
| C | Cylinder | IOP | Intraocular Pressure | Rmin | Minimum Radius of Curvature |
| CBI | Corneal Biomechanical Index | IOPcc | Corneal Compensated IOP | S | |
| CCT | Central Corneal Thickness | IOPt | True Intraocular Pressure | S | Sphericity |
| CH | Corneal Hysteresis | ISV | Index of Surface Variance | SD | standard deviations |
| CKI | Centre keratoconus index | IVA | Index of Vertical Asymmetry | SE | Spherical Equivalent |
| CRF | Corneal Resistant Factor | K | | SMILE | Small Incision Lenticule Extraction |
| Cu D | Total Diameter of the Ablated Tissue | KC | Keratoconus | SP | Stiffness Parameter |
| CVS | Corvis ST | KCI | Keratoconus Index known as Klyce-Maeda | SPA1 | Stiffness Parameter at A1 |
| CVSIOP | Corvis uncorrected IOP | KI | Keratoconus index | SPHC | Stiffness Parameter at HC |
| CXL | corneal crosslinking | KMax | Maximum Front Surface Curvature | SSI | Stress-Strain Index |
| D | | KSI | Keratoconus Severity Index | T | |
| D | Diopter | KSS | Keratoconus Severity Score | Te | Term |
| DCR | Dynamic Corneal Response | L | | TKC | Topographic Keratoconus Classification |
| DCT | Dynamic Contour Tonometry | LASIK | Laser-Assisted in Situ Keratomileuses | U | |
| DeflAmpA1 | A1 Deflection Amp. | LVC | Laser Vision Correction | UV | Ultraviolet |
| DeflAmpMax | Deflection Amplitude Maximum | M | | UVA | Ultraviolet A |
| E | | M/F | Male Over Female Ratio | W | |
| E | Yong's Modulus | MD | Mean Deviation | WEM | Whole Eye Movement |
| | | mmHg | Millimetre of Mercury | | |
| | | N | | | |
| | | NCT | Non-Contact Tonometer | | |
| | | NTG | Normal-Tension Glaucoma | | |

Ophthalmology Terms

Ablation - surgical removal of tissue, typically using a cool beam laser

Ablation zone - the area of tissue that is removed during laser surgery

Anterior chamber - the fluid-filled space between the cornea and iris

Aqueous humor - the clear, watery fluid between the cornea and the front of the vitreous

Astigmatism - results from an irregularly-shaped or American football-shaped cornea which causes light to refract ineffectively

Ciliary body - the ring of muscle fibres that holds the lens of the eye. It also helps control intraocular pressure

Ciliary muscle - the smooth muscle portion of the ciliary body that is responsible for controlling the lens' shape as it narrows or thickens to focus on images at different distances

Cone - the irregular bulge on the surface of the cornea

Cornea - the dome-shaped window of the eye that provides most of the eye's optical power

Corneal transplantation - a surgical procedure to remove a diseased or scarred cornea and replace it with a healthy cornea from a deceased donor

Corneal cross-linking (CXL) - is a treatment for an eye problem called keratoconus

Diopter - a unit of measurement. It measures the degree to which light converges or diverges

Glaucoma - a group of diseases that result from increased intraocular pressure, which can result in damage to the optic nerve. A common cause of preventable vision loss

Hyperopia (farsightedness) - results when the eyeball is too short. Light rays hit the retina before they come into focus. Distant objects are clearer than near objects; however, even distant objects may appear blurry

Intracorneal ring - a tiny, transparent ring that can be inserted into the periphery of the cornea to change its shape and correct nearsightedness

Intraocular pressure (IOP) - is the fluid pressure inside the eye

Keratoconus - a hereditary, degenerative condition that causes the cornea to thin and protrude into a cone-like shape

LASIK - laser in situ keratomileusis. A surgical procedure during which the top layer of the cornea is pulled back and the middle layer is sculpted to eliminate refractive errors such as nearsightedness, farsightedness and astigmatism. The top layer of the cornea is then replaced to serve as a protective flap

Lens - the almond-shaped, elastic structure within the eye that focuses images onto the retina. It is curved on both its front and back surfaces; the lens narrows or thickens to focus on images at different distances

Myopia (nearsightedness) - a condition in which the visual images come to a focus in front of the retina of the eye because of defects in the refractive media of the eye or because of abnormal length of the eyeball, resulting especially in defective vision of distant objects

Optic nerve - the largest nerve of the eye, comprised of retinal nerve fibres (but no rods and cones), the optic nerve connects the retina to the primary visual cortex of the brain. Visual input from the

retina travels along the nerve fibres of the optic nerve to the brain. The brain interprets images sent by the optic nerve of each eye, reverses the images, and integrates them into the one three-dimensional image that you see

PRK - Photorefractive keratectomy (PRK) is a type of laser eye surgery. It's used to improve vision by correcting refractive errors in the eye

Retina - the innermost layer of blood vessels and nerves that serves as the “film” of the eye. The retina receives visual images and transmits signals to the optic nerve through its nerve endings, the rods and cones

Sclera - the tough outermost layer of the eye joining the cornea; the visible part is the white of the eye. The sclera has a transparent covering, the conjunctiva. The sclera helps maintain the eyeball's shape, which is about one inch (25mm) in diameter

Trabecular meshwork – a porous medium created by beam-like structures behind the iris that filters the aqueous humour and allows it to drain into the bloodstream

SMILE - Small incision lenticule extraction (SMILE) is a newer type of laser refractive surgery. This kind of surgery uses a laser to treat myopia (nearsightedness) and astigmatism (irregularly shaped cornea)

Uvea - the blood vessel-rich pigmented layers of the eye. It includes the iris, ciliary body and choroid. It contains the majority of the eye's blood vessels

Vitreotomy - surgical removal of the vitreous, blood, and/or membranes from the eye.

Vitreous or vitreous humour - the clear jelly that fills the eyeball behind the lens. It helps support the shape of the eye and transmits light to the retina

Visual field - field of vision, the entire area that can be seen when the eye is directed forward, including that which is seen with peripheral vision

These terminologies were obtained from the Dictionary of Eye Terminology, Second Edition, (1990), Barbara Cassin and Sheila A.B. Solomon, Melvin L. Rubin, M.D., Editor (Triad Publishing Company, Gainesville, Florida). EyeCenter ^{1,2}

List of Publications

JOURNAL PUBLICATIONS

1. Zhang, H., **Eliasy, A.**, Lopes, B., Abass, A., Vinciguerra, R., Vinciguerra, P., Ambrósio Jr, R., Roberts, C.J. and Elsheikh, A., 2021. Stress Strain Index Map: A New Way to Represent Corneal Material Stiffness. *Frontiers in Bioengineering and Biotechnology*, 9, p.155. <https://dx.doi.org/10.3389/fbioe.2021.640434>
2. Zhou, D., Abass, A., Lopes, B., **Eliasy, A.**, Hayes, S., Boote, C., Meek, K.M., Movchan, A., Movchan, N. and Elsheikh, A., 2021. Fibril density reduction in keratoconic corneas. *Journal of the Royal Society Interface*, 18(175), p.20200900. <https://dx.doi.org/10.1098/rsif.2020.0900>
3. Lopes, B.T., **Eliasy, A.**, Elhalwagy, M., Vinciguerra, R., Bao, F., Vinciguerra, P., Ambrósio, R., Elsheikh, A. and Abass, A., 2021, February. Determination of Optic Axes by Corneal Topography among Italian, Brazilian, and Chinese Populations. In *Photonics* (Vol. 8, No. 2, p. 61). Multidisciplinary Digital Publishing Institute. <https://dx.doi.org/10.3390/photonics8020061>
4. Shihab, A.H., **Eliasy, A.**, Lopes, B.T., Wu, R., White, L., Jones, S., Geraghty, B., Joda, A., Elsheikh, A. and Abass, A., 2021. Compressive behaviour of soft contact lenses and its effect on refractive power on the eye and handling off the eye. *Plos one*, 16(2), p.e0247194. <https://dx.doi.org/10.1371/journal.pone.0247194>
5. Aboulatta, A., Abass, A., Makarem, A., **Eliasy, A.**, Zhou, D., Chen, D., Liu, X. and Elsheikh, A., 2020. Experimental evaluation of the viscoelasticity of porcine vitreous. *Journal of the Royal Society Interface*, 18(175), p.20200849. <https://dx.doi.org/10.1098/rsif.2020.0849>
6. Doll, T., Moore, J., Shihab, A.H., Lopes, B.T., **Eliasy, A.**, Maklad, O., Wu, R., White, L., Jones, S., Elsheikh, A. and Abass, A., 2020. Which feature influences on-eye power change of soft toric contact lenses: Design or corneal shape?. *PloS one*, 15(11), p.e0242243. <https://dx.doi.org/10.1371/journal.pone.0242243>
7. Chang, S.H., Zhou, D., **Eliasy, A.**, Li, Y.C. and Elsheikh, A., 2020. Experimental evaluation of stiffening effect induced by UVA/Riboflavin corneal cross-linking using intact porcine eye globes. *Plos one*, 15(11), p.e0240724. <https://dx.doi.org/10.1371/journal.pone.0240724>

8. Curatolo, A., Birkenfeld, J.S., Martinez-Enriquez, E., Germann, J.A., Muralidharan, G., Palací, J., Pascual, D., **Eliasy, A.**, Abass, A., Solariski, J. and Karnowski, K., 2020. Multi-meridian corneal imaging of air-puff induced deformation for improved detection of biomechanical abnormalities. *Biomedical optics express*, 11(11), pp.6337-6355. <https://dx.doi.org/10.1364/BOE.402402>
9. **Eliasy, A.**, Abass, A., Lopes, B.T., Vinciguerra, R., Zhang, H., Vinciguerra, P., Ambrósio Jr, R., Roberts, C.J. and Elsheikh, A., 2020. Characterisation of cone size and centre in keratoconic corneas. *Journal of the Royal Society Interface*, 17(169), p.20200271. <https://doi.org/10.1098/rsif.2020.0271>
10. Maklad, O., **Eliasy, A.**, Chen, K.J., Wang, J., Abass, A., Lopes, B.T., Theofilis, V. and Elsheikh, A., 2020. Fluid-Structure Interaction Based Algorithms for IOP and Corneal Material Behavior. *Front. Bioeng. Biotechnol.* 8: 970. <https://dx.doi.org/10.3389/fbioe.2020.00970>
11. Abass, A., Roberts, C.J., Lopes, B., **Eliasy, A.**, Vinciguerra, R., Ambrósio, R., Vinciguerra, P. and Elsheikh, A., 2020. Can the Corvis ST Estimate Corneal Viscoelasticity?. *Journal of Refractive Surgery*, 36(5), pp.346-348. <https://doi.org/10.3928/1081597X-20200212-04>
12. **Eliasy, A.** and Przychodzen, J., 2020. The role of AI in capital structure to enhance corporate funding strategies. *Array*, 6, p.100017. <https://doi.org/10.1016/j.array.2020.100017>
13. Maklad, O., **Eliasy, A.**, Chen, K.J., Theofilis, V. and Elsheikh, A., 2020. Simulation of Air Puff Tonometry Test Using Arbitrary Lagrangian–Eulerian (ALE) Deforming Mesh for Corneal Material Characterisation. *International Journal of Environmental Research and Public Health*, 17(1), p.54. <https://dx.doi.org/10.3390/ijerph17010054>
14. Geraghty, B., Abass, A., **Eliasy, A.**, Jones, S.W., Rama, P., Kassem, W., Akhtar, R. and Elsheikh, A., 2020. Inflation experiments and inverse finite element modelling of posterior human sclera. *Journal of biomechanics*, 98, p.109438. <https://dx.doi.org/10.1016/j.jbiomech.2019.109438>
15. Moore, J., Lopes, B.T., **Eliasy, A.**, Geraghty, B., Wu, R., White, L., Elsheikh, A. and Abass, A., 2019. Simulation of the Effect of Material Properties on Soft Contact Lens On-Eye Power. *Bioengineering*, 6(4), p.94. <https://dx.doi.org/10.3390/bioengineering6040094>
16. Zhou, D., Abass, A., **Eliasy, A.**, Movchan, A., Movchan, N. and Elsheikh, A., 2019. Numerical Simulation of Corneal Fibril Reorientation in Response to External

- Loading. *International journal of environmental research and public health*, 16(18), p.3278.
<https://dx.doi.org/10.3390/ijerph16183278>
17. Abass, A., Lopes, B.T., **Eliasy, A.**, Salomao, M., Wu, R., White, L., Jones, S., Clamp, J., Ambrósio Jr, R. and Elsheikh, A., 2019. Artefact-free topography based scleral-asymmetry. *PloS one*, 14(7). <https://dx.doi.org/10.1371/journal.pone.0219789>
 18. Chen, K.J., **Eliasy, A.**, Vinciguerra, R., Abass, A., Lopes, B.T., Vinciguerra, P., Ambrósio Jr, R., Roberts, C.J. and Elsheikh, A., 2019. Development and validation of a new intraocular pressure estimate for patients with soft corneas. *Journal of Cataract & Refractive Surgery*, 45(9), pp.1316-1323. <https://dx.doi.org/10.1016/j.jcrs.2019.04.004>
 19. Lopes, B.T., **Eliasy, A.** and Ambrosio, R., 2019. Artificial Intelligence in Corneal Diagnosis: Where Are we?. *Current Ophthalmology Reports*, 7(3), pp.204-211. <https://dx.doi.org/10.1007/s40135-019-00218-9>
 20. Zhou, D., Abass, A., **Eliasy, A.**, Studer, H.P., Movchan, A., Movchan, N. and Elsheikh, A., 2019. Microstructure-based numerical simulation of the mechanical behaviour of ocular tissue. *Journal of the Royal Society Interface*, 16(154), p.20180685. <https://dx.doi.org/10.1098/rsif.2018.0685>
 21. **Eliasy, A.**, Chen, K.J., Vinciguerra, R., Lopes, B.T., Abass, A., Vinciguerra, P., Ambrósio Jr, R., Roberts, C.J. and Elsheikh, A., 2019. Determination of Corneal Biomechanical Behavior in-vivo for Healthy Eyes Using CorVis ST Tonometry: Stress-Strain Index. *Frontiers in bioengineering and biotechnology*, 7. <https://dx.doi.org/10.3389/fbioe.2019.00105>
 22. Kazaali, A., Lawman, S., Geraghty, B., **Eliasy, A.**, Zheng, Y., Shen, Y. and Akhtar, R., 2019. Line-Field Optical Coherence Tomography as a tool for In vitro characterisation of corneal biomechanics under physiological pressures. *Scientific reports*, 9(1), p.6321. <https://dx.doi.org/10.1038/s41598-019-42789-4>
 23. Zhou, D., **Eliasy, A.**, Abass, A., Markov, P., Whitford, C., Boote, C., Movchan, A., Movchan, N. and Elsheikh, A., 2019. Analysis of X-ray scattering microstructure data for implementation in numerical simulations of ocular biomechanical behaviour. *PloS one*, 14(4), p.e0214770. <https://dx.doi.org/10.1371/journal.pone.0214770>
 24. Abass, A., **Eliasy, A.**, Geraghty, B., Elabd, M., Hassan, A. and Elsheikh, A., 2019. Effect of freezing and thawing on the biomechanical characteristics of porcine ocular tissues. *Journal of biomechanics*, 87, pp.93-99. <https://dx.doi.org/10.1016/j.jbiomech.2019.02.024>
 25. Markov, P.P., **Eliasy, A.**, Pijanka, J.K., Htoon, H.M., Paterson, N.G., Sorensen, T., Elsheikh, A., Girard, M.J. and Boote, C., 2018. Bulk changes in posterior scleral

- collagen microstructure in human high myopia. *Molecular vision*, 24, p.818.
<https://www.ncbi.nlm.nih.gov/pubmed/30713421>
26. Abass, A., Lopes, B.T., **Eliasy, A.**, Wu, R., Jones, S., Clamp, J., Ambrósio Jr, R. and Elsheikh, A., 2018. Three-dimensional non-parametric method for limbus detection. *PloS one*, 13(11), p.e0207710.
<https://dx.doi.org/10.1371/journal.pone.0207710>
27. Vroon, J., de Jong, J.H., Aboulatta, A., **Eliasy, A.**, van der Helm, F.C.T., van Meurs, J.C., Wong, D. and Elsheikh, A., 2018. Numerical study of the effect of head and eye movement on progression of retinal detachment. *Biomechanics and modeling in mechanobiology*, 17(4), pp.975-983. <https://dx.doi.org/10.1007/s10237-018-1006-y>
28. **Eliasy, A.**, Chen, K.J., Vinciguerra, R., Maklad, O., Vinciguerra, P., Ambrósio Jr, R., Roberts, C.J. and Elsheikh, A., 2018. Ex-vivo experimental validation of biomechanically-corrected intraocular pressure measurements on human eyes using the CorVis ST. *Experimental eye research*, 175, pp.98-102.
<https://dx.doi.org/10.1016/j.exer.2018.06.013>
29. Chang, S.H., **Eliasy, A.**, Chen, K.J., Ji, Y.R., Young, T.H., Wang, T.J., Willoughby, C.E., Hamill, K.J. and Elsheikh, A., 2018. The relationship between mechanical properties, ultrastructural changes, and intrafibrillar bond formation in corneal UVA/Riboflavin cross-linking treatment for keratoconus. *Journal of Refractive Surgery*, 34(4), pp.264-272. <https://dx.doi.org/10.3928/1081597X-20180220-01>
30. Chen, K.J., Joda, A., Vinciguerra, R., **Eliasy, A.**, Sefat, S.M.M., Kook, D., Geraghty, B., Roberts, C.J. and Elsheikh, A., 2018. Clinical evaluation of a new correction algorithm for dynamic Scheimpflug analyser tonometry before and after laser in situ keratomileusis and small-incision lenticule extraction. *Journal of Cataract & Refractive Surgery*, 44(5), pp.581-588. <https://dx.doi.org/10.1016/j.jcrs.2018.01.023>
31. Boote, C., Palko, J.R., Sorensen, T., **Eliasy, A.**, Elsheikh, A., Komáromy, A.M., Pan, X. and Liu, J., 2016. Changes in posterior scleral collagen microstructure in canine eyes with an ADAMTS10 mutation. *Molecular vision*, 22, p.503.
<https://www.ncbi.nlm.nih.gov/pubmed/27212875>

CONFERENCES

-
1. **Eliasy, A.**, Lopes, B., Abass, A., Vinciguerra, R., Marcos, S. and Elsheikh, A., 2021. Evaluation of Stress-Strain Index (SSI) in Healthy and Keratoconic Corneas.

2. Abass, A., **Eliasy, A.**, Zhang, H., Lopes, B., Vinciguerra, R. and Elsheikh, A., 2021. Corneal Stress-Strain Index (SSI) Map.
3. Curatolo, A., Birkenfeld, J.S., Martinez-Enriquez, E., Germann, J., Palaci, J., Pascual, D., Muralidharan, G., **Eliasy, A.**, Abass, A., Solarski, J. and Karnowski, K., 2020. Detecting deformation asymmetries on multiple meridians in an ex vivo keratoconic eye model. *Investigative Ophthalmology & Visual Science*, 61(7), pp.4723-4723.
4. Birkenfeld, J.S., Curatolo, A., Nolan, A., McAuley, R., Abass, A., **Eliasy, A.**, Leahy, M., Elsheikh, A. and Marcos, S., 2020. Investigation of the corneal frequency response to modulated sound excitation. *Investigative Ophthalmology & Visual Science*, 61(7), pp.4717-4717.
5. Lopes, B., Wang, J., **Eliasy, A.**, Abass, A., Elsheikh, A., Early term results of the stress-strain index in patients with keratoconus submitted to corneal cross-linking, International CXL Experts Meeting 2019, Zurich, Switzerland, December 2019
6. Elsheikh, A., Zhou, D., **Eliasy, A.**, Lopes, B., Abass, A., Determination and mapping of corneal stiffness in keratoconic corneas, International CXL Experts Meeting 2019, Zurich, Switzerland, December 2019
7. Lopes, B., Wang, J., **Eliasy, A.**, Ambrosio, R., Elsheikh, A., *True Corneal Material Properties as a Risk Factor for Post-LASIK Ectasia*, ASCRS Annual Meeting, May 2019, San Diego, California
8. **Eliasy, A.**, Chen, K., Vinciguerra, R., Elsheikh, A., Novel Intraocular Pressure Measurement Algorithm for Patients with Keratoconus, *8th World Congress of Biomechanics*, Dublin, Ireland, July 2018
9. Elsheikh, A., Chen, K., **Eliasy, A.**, Vinciguerra, R., Obtaining biomechanical properties of corneal tissue in-vivo using a non-contact method, *8th World Congress of Biomechanics*, Dublin, Ireland, July 2018
10. Vinciguerra, R., **Eliasy, A.**, Chen, K., Roberts, C., Ambrosia, R., Vinciguerra, P., Elsheikh, A., Introducing new algorithms for in-vivo corneal material properties measurement for healthy and keratoconus populations using CorVis-ST tonometry, *best paper award contest ophthalmologists under 40, The International Congress of the Italian Society of Stem Cells and Ocular Surface*, Paestum, Italy, July 2018
11. **Eliasy, A.**, Chen, K., Elsheikh, A., Intraocular Pressure Measurement Pre- and Post Refractive Surgery Using GAT and CorVis ST bIOP Algorithm, *6th European Conference on Computational Mechanics (ECCM 6); 7th European Conference on Computational Fluid Dynamics (ECFD 7)*, Glasgow, UK, June 2018

12. Elsheikh, A., Zhou, D., **Eliasy, A.**, Boote, C., Numerical modelling of Ocular Biomechanical Behaviour Based on Fibril Density and Orientation Data for the Whole Eye Globe, *6th European Conference on Computational Mechanics (ECCM 6); 7th European Conference on Computational Fluid Dynamics (ECFD 7)*, Glasgow, UK, June 2018
13. Markov, P., Pijanka, J., **Eliasy, A.**, Elsheikh, A., Zhu, H., Blain, E., Boote, C., Building an integrated biomechanical model of the eye, Cardiff Institute of Tissue Engineering and Repair (CITER) Annual Scientific Meeting, Cardiff September 2017

BOOKS

1. **Eliasy, A.**, Zhou, D., Studer, H., Boote, C., Elsheikh, A., edited by: C.J. Roberts & W.J. Dupps Jr. & J.C. Downs (2018). Chapter 6: Material properties of the human cornea: anisotropy. In Book: *Biomechanics of the Eye*, 1st ed. Kugler Publications (presented at ARVO), ISBN: 978-90-6299-250-8

PATENTS

1. **Title:** System and method for obtaining ocular tissue biomechanical parameters, **Application Number:** PCT/IB2019/053554, **Date of receipt:** 30 April 2019/ *Madrid, Spain.*
2. **Title:** System and method of obtaining biomechanical parameters of ocular tissue through deformation of the ocular tissue, **Application Number:** EP20382067, **Date of receipt:** 02 February 2020/ *Madrid, Spain.*
3. **Title:** Method and system for screening ocular tissue abnormality through deformation of the ocular tissue, **Application Number:** EP20382178, **Date of receipt:** 11 March 2020/ *Madrid, Spain.*

Contents

| | |
|----------------------|------|
| ABSTRACT | I |
| DECLARATION | III |
| ACKNOWLEDGEMENTS | V |
| NOMENCLATURE | VII |
| LIST OF PUBLICATIONS | X |
| CONTENTS | XVI |
| LIST OF FIGURES | XXI |
| LIST OF TABLES | XXIX |

Chapter One

| | |
|-------------------------|----|
| 1. INTRODUCTION | 1 |
| 1.1 Preface | 1 |
| 1.2 Background | 4 |
| 1.2.1 Human Eye | 5 |
| 1.2.2 IOP | 7 |
| 1.2.3 Glaucoma | 8 |
| 1.2.4 Keratoconus | 9 |
| 1.2.5 Biomechanics | 10 |
| 1.3 Scope of the Study | 11 |
| 1.4 Aim and Objectives | 12 |
| 1.5 Thesis Structure | 12 |
| 1.6 Thesis Contribution | 13 |

Chapter Two

| | |
|----------------------|----|
| 2. LITERATURE REVIEW | 14 |
|----------------------|----|

| | | |
|------------|---|-----------|
| 2.1 | Introduction | 14 |
| 2.2 | Corneal Biomechanics | 14 |
| 2.2.1 | Elasticity | 15 |
| 2.2.2 | Ex-vivo Measurement of elasticity | 15 |
| 2.2.3 | In-plane Shear | 17 |
| 2.2.4 | Morphology and Ultrastructure | 17 |
| 2.2.5 | In-vivo Measurements of Biomechanics | 20 |
| 2.2.5.1 | Brillouin Microscopy | 20 |
| 2.2.5.2 | Elastography | 21 |
| 2.2.5.3 | Tonometry based systems | 22 |
| 2.3 | Sclera Biomechanics | 24 |
| 2.4 | Keratoconus | 25 |
| 2.4.1 | Epidemiology | 25 |
| 2.4.2 | Histopathology | 26 |
| 2.4.3 | Biomechanics | 26 |
| 2.4.4 | Aetiology | 27 |
| 2.4.5 | Morphology | 27 |
| 2.4.5.1 | Cone location and shape | 28 |
| 2.4.6 | Management of KC | 29 |
| 2.4.6.1 | Contact Lenses and spectacles | 29 |
| 2.4.6.2 | Collagen Crosslinking (CXL) | 30 |
| 2.4.6.3 | Corneal rings | 31 |
| 2.4.6.4 | Corneal transplantation | 31 |
| 2.5 | Intraocular Pressure (IOP) and Tonometry Devices | 32 |
| 2.5.1 | Commonly Used Tonometry Devices | 32 |
| 2.5.1.1 | Applanation Tonometry | 32 |
| 2.5.1.2 | Dynamic Contour Tonometry (DCT) | 34 |
| 2.5.1.3 | Non-Contact Tonometry | 35 |
| 2.5.1.3.1 | Ocular Response Analyser (ORA) | 35 |
| 2.5.1.3.2 | Corvis ST | 36 |
| 2.5.1.4 | Continuous Tonometry | 36 |
| 2.5.2 | Tonometry Methods Comparison | 37 |
| 2.6 | Concluding Remarks | 39 |

Chapter Three

| | | |
|------------|------------------------------------|-----------|
| 3. | METHODOLOGY | 41 |
| 3.1 | Introduction | 41 |
| 3.2 | KC Topography | 43 |
| 3.2.1 | Analysis of Curvature | 43 |
| 3.2.2 | Clinical Data | 44 |
| 3.2.3 | Corneal Maps and Indices | 45 |
| 3.3 | Numerical Model Development | 47 |
| 3.3.1 | Element Type | 47 |
| 3.3.2 | Boundary Conditions | 48 |
| 3.3.3 | Corvis ST Pressure | 48 |
| 3.3.4 | Mesh Convergence Study | 50 |
| 3.3.5 | Material Parameters | 51 |

| | | |
|------------|--|-----------|
| 3.4 | Validation of Numerical Models | 52 |
| 3.4.1 | Clinical Data | 52 |
| 3.4.2 | Comparison with Numerical Models | 54 |
| 3.4.2.1 | Generating Models | 55 |
| 3.4.2.2 | Reading Clinical Data | 55 |
| 3.4.2.3 | Whole Eye Movement | 55 |
| 3.4.2.4 | Reading the Numerical Model | 56 |
| 3.4.2.5 | Comparison between Clinical Data and Numerical Model | 57 |
| 3.5 | Parametric Study | 57 |
| 3.5.1 | Model Generation | 58 |
| 3.5.2 | KC Cone | 59 |
| 3.5.3 | Axial Power | 61 |
| 3.5.4 | Material Parameters | 62 |
| 3.5.5 | Application of IOP | 63 |
| 3.5.6 | Stress-Free Configuration | 64 |
| 3.5.7 | Corvis ST Air-puff | 65 |
| 3.5.8 | Model Analysis | 66 |
| 3.5.9 | Calculation of Dynamic Corneal Response (DCRs) parameters | 66 |
| | • Deflection Amplitude Maximum (<i>DeflAmpMax</i>): | 67 |
| | • Highest Concavity Time (<i>HCT</i>) | 67 |
| | • Peak Distance (<i>PD</i>) | 67 |
| | • Applanation 1 Time (<i>A1T</i>) | 67 |
| | • A1 Length (<i>A1L</i>) | 68 |
| | • A1 Deflection Amp. (<i>DeflAmpA1</i>) | 68 |
| | • A1 Velocity (<i>A1V</i>) | 68 |
| | • Applanation Pressure 1 (<i>AP1</i>) | 68 |
| | • Radius at HC (<i>HCR</i>) | 69 |
| | • Stiffness Parameter at A1 (<i>SPA1</i>) | 69 |
| | • Stiffness Parameter at HC (<i>SPHC</i>) | 69 |
| | • Corneal Asphericity (<i>P</i> and <i>R</i> Values): | 69 |
| 3.6 | Development of IOP and Material Stiffness Equations | 70 |
| 3.6.1 | Biomechanically Corrected IOP | 71 |
| 3.6.1.1 | biOP2 for Healthy (biOP2) | 71 |
| 3.6.1.2 | biOP2 for KC (biOP2-KC) | 72 |
| 3.6.2 | Stress-Strain Index | 72 |
| 3.6.2.1 | SSI2 for Healthy (SSI2-H) | 73 |
| 3.6.2.2 | SSI2 for KC (SSI2-KC) | 74 |
| 3.6.2.3 | SSI2 for Post LASIK and SMILE (SSI2-PLS) | 74 |
| 3.7 | Validation of Equations | 74 |
| 3.7.1 | Experimental Validation | 74 |
| 3.7.1.1 | Test Setup | 75 |
| 3.7.2 | Healthy Cases | 76 |
| 3.7.3 | Keratoconic Cases | 76 |
| 3.7.4 | Refractive Surgeries Cases | 77 |
| 3.7.5 | Glaucoma Cases | 78 |
| 3.7.6 | CXL Cases | 79 |
| 3.8 | Summary | 79 |

Chapter Four

| | | |
|-----------|----------------|-----------|
| 4. | RESULTS | 80 |
|-----------|----------------|-----------|

| | | |
|------------|---|------------|
| 4.1 | Introduction | 80 |
| 4.2 | KC Topography | 81 |
| 4.2.1 | Cone Characteristics | 82 |
| 4.2.2 | Cone Centre Location | 82 |
| 4.2.3 | Correlation between Cone Characteristics and Disease Severity | 83 |
| 4.2.4 | Posterior Cone Height in Relation to Anterior Cone | 85 |
| 4.2.5 | Correlation of Cone Height and Pathology Area with Radius of Optimum Sphere | 85 |
| 4.2.6 | Evaluation of Cone Properties with Pentacam Indices | 86 |
| 4.3 | Numerical Simulation | 89 |
| 4.3.1 | Element Type | 89 |
| 4.3.2 | Corvis ST Pressure | 89 |
| 4.3.3 | Mesh Density Study | 89 |
| 4.4 | Validation of Numerical Models | 91 |
| 4.5 | Equations | 91 |
| 4.5.1 | Biomechanically Corrected IOP (bIOP2) | 92 |
| 4.5.1.1 | bIOP2 Healthy Equation | 92 |
| 4.5.1.1.1 | Experimental Validation | 92 |
| 4.5.1.1.2 | Healthy Patients | 95 |
| 4.5.1.1.3 | Comparison between GAT, DCT, ORA and Corvis ST | 96 |
| 4.5.1.1.4 | Refractive Surgeries | 97 |
| 4.5.1.1.5 | CXL Data | 103 |
| 4.5.1.1.6 | Glaucoma Patients | 106 |
| 4.5.1.1.7 | Keratoconus Patients | 107 |
| 4.5.1.2 | bIOP2-KC Equation | 109 |
| 4.5.2 | Stress-Strain Index (SSI2) | 111 |
| 4.5.2.1 | SSI Healthy Equation | 111 |
| 4.5.2.1.1 | Experimental Validation | 112 |
| 4.5.2.1.2 | Healthy Patients | 113 |
| 4.5.2.1.3 | PRK Surgery | 114 |
| 4.5.2.2 | SSI2-KC Equation | 117 |
| 4.5.2.2.1 | Keratoconus Patients | 117 |
| 4.5.2.2.2 | Crosslinked Corneas | 119 |
| 4.5.2.3 | SSI-PLS for post LASIK and SMILE | 123 |
| 4.6 | Concluding Remarks | 129 |

Chapter Five

| | | |
|------------|---|------------|
| 5. | DISCUSSION | 130 |
| 5.1 | Overall Discussion | 130 |
| 5.1.1 | KC Topography Analysis | 131 |
| 5.1.2 | Biomechanically Corrected IOP 2 (bIOP2) | 134 |
| 5.1.3 | Stress-Strain Index 2 (SSI2) | 138 |
| 5.2 | Limitations of Study | 143 |
| 5.3 | Concluding Remarks | 145 |
| 5.4 | Recommendations for Future Studies | 146 |

REFERENCES ----- 147

Supplementary information

6. APPENDICES ----- 182

Section A - Biomechanically Corrected IOP (bIOP2) ----- 182

bIOP2 Healthy Equation ----- 182
Healthy Patients ----- 182
Refractive Surgeries ----- 189
CXL Data ----- 205
Glaucoma Patients ----- 211
Keratoconus Patients ----- 215
bIOP2-KC Equation ----- 223

Section B - Stress-Strain Index (SSI2) ----- 232

SSI Healthy Equation ----- 232
Healthy Patients ----- 232
PRK Surgery ----- 236
SSI2-KC Equation ----- 239
Keratoconus Patients ----- 239
Crosslinked Corneas ----- 249
SSI-PLS for post LASIK and SMILE ----- 254

List of Figures

| | |
|--|----|
| Figure 1-1 The eye structure conceived by Aristotle. At this time philosophers only recognised transparent cornea and sclera, and everything else was aligned with a hole which meant to be the pupil ⁵ | 1 |
| Figure 1-2 The anatomy of the eye as described by Galen. Many more components were identified at that time, including the crystalline lens, conjunctiva, choroid, retina, optic nerves, ciliary body, limbus and iris. ⁵ | 2 |
| Figure 1-3 Anatomy of the eye in the 17 th century ⁵ | 3 |
| Figure 1-4 Eye structure as it is currently known ¹⁹ | 4 |
| Figure 1-5 The eye cross-section with some important components ⁴⁹ | 6 |
| Figure 1-6 Corneal cross-section showing its main layers ⁵³ | 7 |
| Figure 1-7 Aqueous humour production and drainage ⁶⁴ | 8 |
| Figure 1-8 The eye anatomy comparison for healthy and glaucoma. ⁶⁶ | 8 |
| Figure 1-9 The comparison between health cornea (left) and keratoconic cornea (right) that led to thinning and deformation ⁸⁹ | 10 |
| Figure 1-10 The four features of viscoelasticity including (A) relaxation, (B) creep, (C) hysteresis and (D) time dependant strain | 11 |
| Figure 2-1 Stress-strain behaviour of the cornea in relation to age. ¹²³⁻¹²⁵ | 16 |
| Figure 2-2 Hierarchical structure of fibrils within tissue. (a) Collagen molecules are combined to form fibrils, fascicles and tendon fibres; the interaction between fibrils and molecules is shown in (b) and (c), respectively. C-L, cross-links between collagen molecules; PG, proteoglycan-rich matrix between fibrils. Adapted from ¹³⁸ | 18 |
| Figure 2-3 Lamellae structure within the cornea ¹⁴² | 19 |
| Figure 2-4 (a) The general arrangement of fibrils in the central cornea with preferred orientation in the vertical and horizontal directions ¹⁴⁵ ; (b) The 45-degree sectors of the central cornea where two-thirds of collagen fibrils have been observed to have a preferential orientation ¹⁴⁵ | 19 |
| Figure 2-5S The methodology used in Brillouin microscopy ¹⁴⁸ | 21 |
| Figure 2-6 The structure of Optical Coherence elastography ¹⁶⁵ | 22 |
| Figure 2-7 The deformations of the cornea under air puff application as it is monitored by Corvis-ST. Also, the Figure highlights the first and second applanation ¹⁸⁵ | 24 |
| Figure 2-8 The cone on the inferior side of the cornea of a patient with advance KC ²⁶⁴ | 28 |
| Figure 2-9 Collagen cross-linking application on the patient under UVA and the schematic view of structural changes between collagen fibrils ²⁹⁹ | 30 |
| Figure 2-10 The Intacs ICRS on the cornea and its position in the cross-sectional view. ³²⁶ | 31 |
| Figure 2-11 (a) The tonometer invented originally by Hjalmar Schiøtz that has various weights and could apply known pressure to the eye and measure deformations, (b) the Von Graefe tonometer able to measure IOP through eyelid in an era with no anaesthesia ³⁴⁰ | 33 |
| Figure 2-12 Goldmann tonometer and the position of the flattened cornea after the force is applied ³⁴⁹ | 34 |
| Figure 2-13 The DCT tonometer and the methodology of measuring pressure using this device ³⁵² | 35 |
| Figure 2-14 The methodology followed by ORA to estimate IOP and corneal biomechanics ³⁵⁹ | 36 |
| Figure 2-15 Sensimed Triggerfish contact lens (a) setup ³⁶⁶ and (b) device ³⁶⁷ | 37 |
| Figure 3-1 The overview of the methodology followed in this thesis. Each section is described in details in the following chapter | 42 |
| Figure 3-2 (A) The best-fit sphere of the posterior corneal surface and the distances from the centre of the sphere to multiple points on the posterior surface are calculated. The edge is detected using second derivatives of elevation and variations in the curvature of the cornea. (B) Is a graph indicating the Euclidean distance from corneal surface points to the best-fit sphere and the largest values suggest the cone height and apex location | 44 |
| Figure 3-3 A typical display of corneal topography that includes anterior surface curvature, the elevation of anterior and posterior surface and the thickness of the cornea. ⁴⁰⁸ | 46 |

| | |
|---|----|
| Figure 3-4 The difference between a 6-noded and a 15-noded element | 48 |
| Figure 3-5 Boundry condition of a typical model of the eye showing the equatorial and posterior points that were restricted on movement in different directions..... | 48 |
| Figure 3-6 (A) Reduction of pressure on the corneal surface away from apex and (B) variation of pressure on corneal apex and nozzle over time. | 49 |
| Figure 3-7 Optimum ocular model mesh showing cornea and surrounding sclera. The third ring is highlighted in red to clarify ring positions. | 50 |
| Figure 3-8 The model with different segmented rings where (a) has six segments and (b) has four segments | 51 |
| Figure 3-9 Corneal profile collected from Corvis ST in 140 measurements over a period of 32 ms from Temporal-Nasal axis. The figure only shows corneal deformation up to the point of corneal highest concavity at 16.8 ms..... | 54 |
| Figure 3-10 Corneal profile data with some information missing | 55 |
| Figure 3-11 Whole eye movement at a specific time point. The WEM was calculated on both sides of the cornea and a linear distribution was assumed when removing the eye movement from corneal displacement. D1 and D2 are the displacements calculated at each side..... | 56 |
| Figure 3-12 The Y-axis presents the elevations in mm, X-axis presents the distance in mm, and each colour is presenting a corneal profile at a different time point where (a) deformation obtained from clinical data that includes whole eye movement, (b) deformation obtained from clinical data after removal of eye movement, (c) deformation exported from numerical models and (d) adjusted deformation from numerical models to match clinical data | 57 |
| Figure 3-13 Process adopted to build the database required for the development of IOP and material stiffness estimation equations | 58 |
| Figure 3-14 The numerical model generated for this study with variation in thickness. Different colours are referring to different material segments. | 59 |
| Figure 3-15 Cross-section of a model showing a keratoconus cone appearing as a bulge on both the anterior and posterior surfaces | 61 |
| Figure 3-16 Axial power determined at a general point on a corneal surface. The power is calculated by identifying the radius of a circle that passes through the central axis while being perpendicular to the tangential line at this point. The derivate is calculated from the 3D coordinates of the surface collected from Pentacam or FE models. | 61 |
| Figure 3-17 The fluid cavity surface inside the ocular numerical model | 64 |
| Figure 3-18 Schematic figure describing the stress-free procedure. Source: Elsheikh et al. ⁴²⁶ | 65 |
| Figure 3-19 Corvis ST air pressure applied normal to the surface of each element (purple arrows).... | 65 |
| Figure 3-20 The blue region is the cornea, the red region is highlighting the cone area, and seven black lines are assuming different cone locations. In doing this, the cone was kept on the inferior side. | 66 |
| Figure 3-21 Schematic graphical description of Deflection Amplitude Maximum | 67 |
| Figure 3-22 Schematic graphical description of HC Time | 67 |
| Figure 3-23 Schematic graphical description of Peak Distance | 67 |
| Figure 3-24 Schematic graphical description of A1 Time | 68 |
| Figure 3-25 Schematic graphical description of A1 Length | 68 |
| Figure 3-26 Schematic graphical description of A1 Deflection Amp. | 68 |
| Figure 3-27 Schematic graphical description of A1 Velocity | 68 |
| Figure 3-28 Schematic graphical description of AP1 | 69 |
| Figure 3-29 Schematic graphical description of HC Radius | 69 |
| Figure 3-30 Optimisation method developed to generate equations | 71 |
| Figure 3-31 biomechanical behaviour of the cornea changes with age without any intersection as shown in figure "a" but instead consistently as shown in figure "b" that could translate to tangent modulus changes with stress as shown in figure "c". SSI equal by one represent the material stiffness of a healthy cornea at age 50 and as the age increases the stiffness increases and vice versa. | 73 |
| Figure 3-32 the diagram shows the structure of the test rig..... | 75 |
| Figure 4-1 Location of cone centre and transition zone estimated using the proposed method for the left eye of a 29-year-old patient with moderate keratoconus. The results are plotted on tangential curvature maps (A, B) and maps of elevation relative to the optimal sphere (C, D). | 81 |
| Figure 4-2 Frequency of cone centre location in (A) anterior surfaces of right eyes, (B) anterior surfaces of left eyes, (C) posterior surfaces of right eyes, and (D) posterior surfaces of left eyes | 83 |

| | |
|--|-----|
| Figure 4-3 Mean, standard deviation, minimum and maximum values of distance from cone centre to corneal apex (left column), cone height (middle column) and area of cone (right column) for eyes with mild KC (left = 90, right = 102), moderate KC (left = 148, right = 130) and advanced KC (left = 71, right = 77). Results are presented for anterior and posterior surfaces of right and left eyes..... | 84 |
| Figure 4-4 Correlation between anterior cone height and posterior cone height when considering all data (Note: the y axis is the extra change in the posterior cone height in comparison to the anterior cone height) | 85 |
| Figure 4-5 Correlation of cone height and pathology area with the radius of the sphere of optimal fit for both anterior and posterior surfaces | 86 |
| Figure 4-6 the mean and standard deviation of 280 cases and the pressure applied on the cornea.... | 89 |
| Figure 4-7 Mesh convergence study for cornea showing the deformation of apex under air puff pressure (left) and the computational time for corresponding rings (right) | 90 |
| Figure 4-8 Mesh convergence study for sclera showing the deformation of the apex under air puff (left) and the time of simulation for corresponding rings (right) | 90 |
| Figure 4-9 Comparison of numerical and clinical data for nine healthy corneas showing the deformation under air puff at the initial profile and highest concavity. The error presented above each plot is referring to the root mean squared of the deformation (mm) error across the full profile. | 91 |
| Figure 4-10 Correlation of IOP values from CVSIOP, bIOP and BIOP2 with CCT (left) and age (right) in Dataset 1..... | 95 |
| Figure 4-11 Correlation between DCT, GAT, ORA and three Corvis ST IOP measurements with age and CCT | 96 |
| Figure 4-12 Correlation of IOP values from CVSIOP, bIOP and BIOP2 with CCT (left) and age (right) in pre-surgery LASIK Dataset 1..... | 97 |
| Figure 4-13 Correlation of IOP values from CVSIOP, bIOP and BIOP2 with CCT (left) and age (right) in post-surgery LASIK Dataset 1 | 98 |
| Figure 4-14 The Bland Altman plots for (A) bIOP, (B) BIOP2 and (C) CVSIOP comparing the pre and post IOP values in LASIK Dataset 1..... | 99 |
| Figure 4-15 Correlation of IOP values from CVSIOP, bIOP and BIOP2 with CCT (left) and age (right) in pre-surgery SMILE Dataset 1..... | 100 |
| Figure 4-16 Correlation of IOP values from CVSIOP, bIOP and BIOP2 with CCT (left) and age (right) in post surgery SMILE Dataset 1 | 100 |
| Figure 4-17 The Bland Altman plots for (A) bIOP, (B) BIOP2 and (C) CVSIOP comparing the pre and post IOP values in SMILE Dataset 1..... | 101 |
| Figure 4-18 Correlation of IOP values from CVSIOP, bIOP and BIOP2 with CCT (left) and age (right) in Pre CXL Dataset 1..... | 103 |
| Figure 4-19 Correlation of IOP values from CVSIOP, bIOP and BIOP2 with CCT (left) and age (right) in early post CXL Dataset 1 | 104 |
| Figure 4-20 Correlation of IOP values from CVSIOP, bIOP and BIOP2 with CCT (left) and age (right) in late post CXL Dataset 1 | 105 |
| Figure 4-21 Correlation of IOP values from CVSIOP, bIOP and BIOP2 with CCT (left) and age (right) in HTG group of Dataset 1 | 106 |
| Figure 4-22 Correlation of IOP values from CVSIOP, bIOP and BIOP2 with CCT (left) and age (right) in OHT group of Dataset 1 | 107 |
| Figure 4-23 Correlation of IOP values from CVSIOP, bIOP and BIOP2 with CCT (left) and age (right) in KC Dataset 1..... | 108 |
| Figure 4-24 The changes in BIOP2 and bIOP in healthy, FFKC, Mild, Moderate and Severe keratoconic cases in Dataset 1 | 108 |
| Figure 4-25 Correlation of IOP values from BIOP2 and BIOP2-KC with CCT (left) and age (right) in KC Dataset 1..... | 110 |
| Figure 4-26 The changes in BIOP2 and BIOP2-KC in healthy, FFKC, Mild, Moderate and Severe keratoconic cases in Dataset 1..... | 110 |
| Figure 4-27 The comparison between SSI, SSI2-H and ex vivo SSI values obtained from human donor corneas against age in 7 different datasets (A-G) and all of them combined (H)..... | 112 |
| Figure 4-28 The correlation of SSI and SSI2-H with CCT (left), age (middle) and IOP (right) in Dataset 1 | 114 |

| | |
|--|-----|
| Figure 4-29 The Bland Altman plot for SSI2-H (top) and SSI (bottom) comparing the pre and post PRK surgery results in Dataset 1..... | 115 |
| Figure 4-30 The evaluation of correlation in changes in CCT with changes in SSI and SSI2-H in PRK group of Dataset 1 | 116 |
| Figure 4-31 The correlation of SSI and SSI2-H with CCT (left), age (middle) and IOP (right) in pre-surgery PRK group of Dataset 1 | 116 |
| Figure 4-32 The correlation of SSI and SSI2-H with CCT (left), age (middle) and IOP (right) in post-surgery PRK group of Dataset 1 | 117 |
| Figure 4-33 The correlation of SSI and SSI2-KC with CCT (left), age (middle) and IOP (right) in Dataset 1..... | 118 |
| Figure 4-34 The changes in SSI2-KC and SSI in healthy, FFKC, Mild, Moderate and Severe keratoconic cases in Dataset 1..... | 118 |
| Figure 4-35 The mean and standard deviation of pre-CXL and post-CXL data for SSI and SSI2-KC in the early group of CXL Dataset 1..... | 120 |
| Figure 4-36 The correlation of SSI and SSI2-KC with CCT (left), age (middle) and IOP (right) in the early pre-surgery group of CXL Dataset 1 | 121 |
| Figure 4-37 The correlation of SSI and SSI2-KC with CCT (left), age (middle) and IOP (right) in the early post-surgery group of CXL Dataset 1..... | 121 |
| Figure 4-38 The mean and standard deviation of pre-CXL and post-CXL data for SSI and SSI2-KC in the late group of CXL Dataset 1..... | 122 |
| Figure 4-39 The correlation of SSI and SSI2-KC with CCT (left), age (middle) and IOP (right) in the late pre-surgery group of CXL Dataset 1 | 122 |
| Figure 4-40 The correlation of SSI and SSI2-KC with CCT (left), age (middle) and IOP (right) in the late post-surgery group of CXL Dataset 1..... | 123 |
| Figure 4-41 Bland Altman plot for SSI2 (top) and SSI (bottom) comparing the pre and post SMILE surgery results in Dataset 1..... | 124 |
| Figure 4-42 The evaluation of correlation in changes in CCT with changes in SSI and SSI2 in SMILE group of Dataset 1 | 125 |
| Figure 4-43 The correlation of SSI and SSI2-H with CCT (left), age (middle) and IOP (right) in the pre-surgery SMILE group of Dataset 1..... | 125 |
| Figure 4-44 The correlation of SSI and SSI2-PLS with CCT (left), age (middle) and IOP (right) in the post-surgery SMILE group of Dataset 1..... | 126 |
| Figure 4-45 Bland Altman plot for SSI2 (top) and SSI (bottom) comparing the pre and post LASIK surgery results in Dataset 1..... | 127 |
| Figure 4-46 The evaluation of correlation in changes in CCT with changes in SSI and SSI2 in the LASIK group of Dataset 1 | 127 |
| Figure 4-47 The correlation of SSI and SSI2-H with CCT (left), age (middle) and IOP (right) in the pre-surgery LASIK group of Dataset 1..... | 128 |
| Figure 4-48 The correlation of SSI and SSI2-PLS with CCT (left), age (middle) and IOP (right) in the post-surgery LASIK group of Dataset 1..... | 128 |
| Figure 5-1 Components of overall stiffness | 139 |
| Figure 6-1 Correlation of IOP values from CVSIOP, bIOP and bIOP2 with CCT (left) and age (right) in Dataset 2..... | 182 |
| Figure 6-2 Correlation of IOP values from CVSIOP, bIOP and bIOP2 with CCT (left) and age (right) in Dataset 3..... | 183 |
| Figure 6-3 Correlation of IOP values from CVSIOP, bIOP and bIOP2 with CCT (left) and age (right) in Dataset 4..... | 184 |
| Figure 6-4 Correlation of IOP values from CVSIOP, bIOP and bIOP2 with CCT (left) and age (right) in Dataset 5..... | 185 |
| Figure 6-5 Correlation of IOP values from CVSIOP, bIOP and bIOP2 with CCT (left) and age (right) in Dataset 6..... | 186 |
| Figure 6-6 Correlation of IOP values from CVSIOP, bIOP and bIOP2 with CCT (left) and age (right) in Dataset 7..... | 187 |
| Figure 6-7 Correlation of IOP values from CVSIOP, bIOP and bIOP2 with CCT (left) and age (right) in Dataset 8..... | 188 |
| Figure 6-8 Correlation of IOP values from CVSIOP, bIOP and bIOP2 with CCT (left) and age (right) in pre surgery LASIK Dataset 2 | 189 |

| | |
|---|-----|
| Figure 6-9 Correlation of IOP values from CVSIOP, bIOP and bIOP2 with CCT (left) and age (right) in post surgery LASIK Dataset 2 | 189 |
| Figure 6-10 The Bland Altman plots for (A) bIOP, (B) bIOP2 and (C) CVSIOP comparing the pre and post IOP values in LASIK Dataset 2..... | 191 |
| Figure 6-11 Correlation of IOP values from CVSIOP, bIOP and bIOP2 with CCT (left) and age (right) in pre surgery LASIK Dataset 2 | 191 |
| Figure 6-12 Correlation of IOP values from CVSIOP, bIOP and bIOP2 with CCT (left) and age (right) in post surgery LASIK Dataset 2 | 192 |
| Figure 6-13 The Bland Altman plots for (A) bIOP, (B) bIOP2 and (C) CVSIOP comparing the pre and post IOP values in LASIK Dataset 2..... | 193 |
| Figure 6-14 Correlation of IOP values from CVSIOP, bIOP and bIOP2 with CCT (left) and age (right) in pre surgery LASIK Dataset 2 | 194 |
| Figure 6-15 Correlation of IOP values from CVSIOP, bIOP and bIOP2 with CCT (left) and age (right) in post surgery LASIK Dataset 2 | 194 |
| Figure 6-16 The Bland Altman plots for (A) bIOP, (B) bIOP2 and (C) CVSIOP comparing the pre and post IOP values in LASIK Dataset 2..... | 196 |
| Figure 6-17 The correlation of IOP values with CCT in PRK data for preoperative and 1,3 and 6 months postoperative | 199 |
| Figure 6-18 The correlation of IOP values with age in PRK data for preoperative and 1,3 and 6 months postoperative | 200 |
| Figure 6-19 The correlation of IOP values with CCT in LASIK data for preoperative and 1,3 and 6 months postoperative | 201 |
| Figure 6-20 The correlation of IOP values with age in LASIK data for preoperative and 1,3 and 6 months postoperative | 202 |
| Figure 6-21 The correlation of IOP values with CCT in SMILE data for preoperative and 1,3 and 6 months postoperative | 203 |
| Figure 6-22 The correlation of IOP values with age in SMILE data for preoperative and 1,3 and 6 months postoperative | 204 |
| Figure 6-23 Correlation of IOP values from CVSIOP, bIOP and bIOP2 with CCT (left) and age (right) in Pre CXL Dataset 2 | 205 |
| Figure 6-24 Correlation of IOP values from CVSIOP, bIOP and bIOP2 with CCT (left) and age (right) in Post CXL Dataset 2 | 206 |
| Figure 6-25 Correlation of IOP values from CVSIOP, bIOP and bIOP2 with CCT (left) and age (right) in Pre CXL Dataset 3 | 207 |
| Figure 6-26 Correlation of IOP values from CVSIOP, bIOP and bIOP2 with CCT (left) and age (right) in Post CXL Dataset 2 | 208 |
| Figure 6-27 Correlation of IOP values from CVSIOP, bIOP and bIOP2 with CCT (left) and age (right) in Pre CXL Dataset 4 | 209 |
| Figure 6-28 Correlation of IOP values from CVSIOP, bIOP and bIOP2 with CCT (left) and age (right) in Post CXL Dataset 4 | 210 |
| Figure 6-29 Correlation of IOP values from CVSIOP, bIOP and bIOP2 with CCT (left) and age (right) in healthy group of Dataset 2 | 211 |
| Figure 6-30 Correlation of IOP values from CVSIOP, bIOP and bIOP2 with CCT (left) and age (right) in NTG group of Dataset 2 | 212 |
| Figure 6-31 Correlation of IOP values from CVSIOP, bIOP and bIOP2 with CCT (left) and age (right) in HTG group of Dataset 2 | 213 |
| Figure 6-32 Correlation of IOP values from CVSIOP, bIOP and bIOP2 with CCT (left) and age (right) in OHT group of Dataset 2 | 214 |
| Figure 6-33 Correlation of IOP values from CVSIOP, bIOP and bIOP2 with CCT (left) and age (right) in KC Dataset 2..... | 215 |
| Figure 6-34 The changes in bIOP2 and bIOP in healthy, FFKC, Mild, Moderate and Severe keratoconic cases in Dataset 2 | 216 |
| Figure 6-35 Correlation of IOP values from CVSIOP, bIOP and bIOP2 with CCT (left) and age (right) in KC Dataset 3..... | 216 |
| Figure 6-36 The changes in bIOP2 and bIOP in healthy, FFKC, Mild, Moderate and Severe keratoconic cases in Dataset 3 | 217 |

| | |
|---|-----|
| Figure 6-37 Correlation of IOP values from CVSIOP, bIOP and bIOP2 with CCT (left) and age (right) in KC Dataset 4 | 218 |
| Figure 6-38 The changes in bIOP2 and bIOP in healthy, FFKC, Mild, Moderate and Severe keratoconic cases in Dataset 4..... | 218 |
| Figure 6-39 Correlation of IOP values from CVSIOP, bIOP and bIOP2 with CCT (left) and age (right) in KC Dataset 5 | 219 |
| Figure 6-40 The changes in bIOP2 and bIOP in healthy, FFKC, Mild, Moderate and Severe keratoconic cases in Dataset 5..... | 219 |
| Figure 6-41 Correlation of IOP values from CVSIOP, bIOP and bIOP2 with CCT (left) and age (right) in KC Dataset 6 | 220 |
| Figure 6-42 The changes in bIOP2 and bIOP in healthy, FFKC, Mild, Moderate and Severe keratoconic cases in Dataset 6..... | 220 |
| Figure 6-43 Correlation of IOP values from CVSIOP, bIOP and bIOP2 with CCT (left) and age (right) in KC Dataset 7 | 221 |
| Figure 6-44 The changes in bIOP2 and bIOP in healthy, FFKC, Mild, Moderate and Severe keratoconic cases in Dataset 7..... | 221 |
| Figure 6-45 Correlation of IOP values from CVSIOP, bIOP and bIOP2 with CCT (left) and age (right) in KC Dataset 8 | 222 |
| Figure 6-46 The changes in bIOP2 and bIOP in healthy, FFKC, Mild, Moderate and Severe keratoconic cases in Dataset 8..... | 222 |
| Figure 6-47 Correlation of IOP values from bIOP2 and bIOP2-KC with CCT (left) and age (right) in KC Dataset 2..... | 223 |
| Figure 6-48 The changes in bIOP2 and bIOP2-KC in healthy, FFKC, Mild, Moderate and Severe keratoconic cases in Dataset 2..... | 224 |
| Figure 6-49 Correlation of IOP values from bIOP2 and bIOP2-KC with CCT (left) and age (right) in KC Dataset 3..... | 224 |
| Figure 6-50 The changes in bIOP2 and bIOP2-KC in healthy, FFKC, Mild, Moderate and Severe keratoconic cases in Dataset 3..... | 225 |
| Figure 6-51 Correlation of IOP values from bIOP2 and bIOP2-KC with CCT (left) and age (right) in KC Dataset 4..... | 226 |
| Figure 6-52 The changes in bIOP2 and bIOP2-KC in healthy, FFKC, Mild, Moderate and Severe keratoconic cases in Dataset 4..... | 227 |
| Figure 6-53 Correlation of IOP values from bIOP2 and bIOP2-KC with CCT (left) and age (right) in KC Dataset 5..... | 227 |
| Figure 6-54 The changes in bIOP2 and bIOP2-KC in healthy, FFKC, Mild, Moderate and Severe keratoconic cases in Dataset 5..... | 228 |
| Figure 6-55 Correlation of IOP values from bIOP2 and bIOP2-KC with CCT (left) and age (right) in KC Dataset 6..... | 228 |
| Figure 6-56 The changes in bIOP2 and bIOP2-KC in healthy, FFKC, Mild, Moderate and Severe keratoconic cases in Dataset 6..... | 229 |
| Figure 6-57 Correlation of IOP values from bIOP2 and bIOP2-KC with CCT (left) and age (right) in KC Dataset 7..... | 230 |
| Figure 6-58 The changes in bIOP2 and bIOP2-KC in healthy, FFKC, Mild, Moderate and Severe keratoconic cases in Dataset 7..... | 230 |
| Figure 6-59 Correlation of IOP values from bIOP2 and bIOP2-KC with CCT (left) and age (right) in KC Dataset 8..... | 231 |
| Figure 6-60 The changes in bIOP2 and bIOP2-KC in healthy, FFKC, Mild, Moderate and Severe keratoconic cases in Dataset 8..... | 231 |
| Figure 6-61 The correlation of SSI and SSI2-H with CCT (left), age (middle) and IOP (right) in Dataset 2 | 232 |
| Figure 6-62 The correlation of SSI and SSI2-H with CCT (left), age (middle) and IOP (right) in Dataset 3 | 233 |
| Figure 6-63 The correlation of SSI and SSI2-H with CCT (left), age (middle) and IOP (right) in Dataset 4 | 233 |
| Figure 6-64 The correlation of SSI and SSI2-H with CCT (left), age (middle) and IOP (right) in Dataset 5 | 234 |

| | |
|--|-----|
| Figure 6-65 The correlation of SSI and SSI2-H with CCT (left), age (middle) and IOP (right) in Dataset 6 | 234 |
| Figure 6-66 The correlation of SSI and SSI2-H with CCT (left), age (middle) and IOP (right) in Dataset 7 | 235 |
| Figure 6-67 The correlation of SSI and SSI2-H with CCT (left), age (middle) and IOP (right) in Dataset 8 | 235 |
| Figure 6-68 Bland Altman plot for SSI2-H (top) and SSI (bottom) comparing the pre and post PRK surgery results in Dataset 2..... | 236 |
| Figure 6-69 The evaluation of correlation in changes in CCT with changes in SSI and SSI2-H in PRK group of Dataset 2 | 237 |
| Figure 6-70 The correlation of SSI and SSI2-H with CCT (left), age (middle) and IOP (right) in pre-surgery PRK group of Dataset 2 | 237 |
| Figure 6-71 The correlation of SSI and SSI2-H with CCT (left), age (middle) and IOP (right) in post-surgery PRK group of Dataset 2 | 238 |
| Figure 6-72 The correlation of SSI and SSI2-KC with CCT (left), age (middle) and IOP (right) in Dataset 2 | 239 |
| Figure 6-73 The changes in SSI2-KC and SSI in healthy, FFKC, Mild, Moderate and Severe keratoconic cases in Dataset 2 | 240 |
| Figure 6-74 The correlation of SSI and SSI2-KC with CCT (left), age (middle) and IOP (right) in Dataset 3 | 241 |
| Figure 6-75 The changes in SSI2-KC and SSI in healthy, FFKC, Mild, Moderate and Severe keratoconic cases in Dataset 3 | 241 |
| Figure 6-76 The correlation of SSI and SSI2-KC with CCT (left), age (middle) and IOP (right) in Dataset 4 | 242 |
| Figure 6-77 The changes in SSI2-KC and SSI in healthy, FFKC, Mild, Moderate and Severe keratoconic cases in Dataset 4 | 243 |
| Figure 6-78 The correlation of SSI and SSI2-KC with CCT (left), age (middle) and IOP (right) in Dataset 5 | 244 |
| Figure 6-79 The changes in SSI2-KC and SSI in healthy, FFKC, Mild, Moderate and Severe keratoconic cases in Dataset 5 | 244 |
| Figure 6-80 The correlation of SSI and SSI2-KC with CCT (left), age (middle) and IOP (right) in Dataset 6 | 245 |
| Figure 6-81 The changes in SSI2-KC and SSI in healthy, FFKC, Mild, Moderate and Severe keratoconic cases in Dataset 6 | 245 |
| Figure 6-82 The correlation of SSI and SSI2-KC with CCT (left), age (middle) and IOP (right) in Dataset 7 | 246 |
| Figure 6-83 The changes in SSI2-KC and SSI in healthy, FFKC, Mild, Moderate and Severe keratoconic cases in Dataset 7 | 247 |
| Figure 6-84 The correlation of SSI and SSI2-KC with CCT (left), age (middle) and IOP (right) in Dataset 8 | 248 |
| Figure 6-85 The changes in SSI2-KC and SSI in healthy, FFKC, Mild, Moderate and Severe keratoconic cases in Dataset 8 | 248 |
| Figure 6-86 The mean and standard deviation of pre-CXL and post-CXL data for SSI and SSI2-KC in the CXL Dataset 2 | 249 |
| Figure 6-87 The correlation of SSI and SSI2-KC with CCT (left), age (middle) and IOP (right) in the pre-surgery group of CXL Dataset 2..... | 250 |
| Figure 6-88 The correlation of SSI and SSI2-KC with CCT (left), age (middle) and IOP (right) in the post-surgery group of CXL Dataset 2..... | 250 |
| Figure 6-89 The mean and standard deviation of pre-CXL and post-CXL data for SSI and SSI2-KC in the CXL Dataset 3 | 251 |
| Figure 6-90 The correlation of SSI and SSI2-KC with CCT (left), age (middle) and IOP (right) in the pre-surgery group of CXL Dataset 3..... | 251 |
| Figure 6-91 The correlation of SSI and SSI2-KC with CCT (left), age (middle) and IOP (right) in post-surgery group of CXL Dataset 3..... | 252 |
| Figure 6-92 The mean and standard deviation of pre-CXL and post-CXL data for SSI and SSI2-KC in the CXL Dataset 4 | 252 |

| | |
|--|-----|
| Figure 6-93 The correlation of SSI and SSI2-KC with CCT (left), age (middle) and IOP (right) in the pre-surgery group of CXL Dataset 4..... | 253 |
| Figure 6-94 The correlation of SSI and SSI2-KC with CCT (left), age (middle) and IOP (right) in the post-surgery group of CXL Dataset 4..... | 253 |
| Figure 6-95 Bland Altman plot for (top) SSI2 and (bottom) SSI comparing the pre and post LASIK surgery results in Dataset 2..... | 254 |
| Figure 6-96 The evaluation of correlation in changes in CCT with changes in SSI and SSI2 in the LASIK group of Dataset 2..... | 255 |
| Figure 6-97 The correlation of SSI and SSI2-H with CCT (left), age (middle) and IOP (right) in the pre-surgery LASIK group of Dataset 2..... | 255 |
| Figure 6-98 The correlation of SSI and SSI2-PLSwith CCT (left), age (middle) and IOP (right) in the post-surgery LASIK group of Dataset 2..... | 256 |
| Figure 6-99 Bland Altman plot for SSI2 (top) and SSI (bottom) comparing the pre and post SMILE surgery results in Dataset 2..... | 257 |
| Figure 6-100 The evaluation of correlation in changes in CCT with changes in SSI and SSI2 in SMILE group of Dataset 2..... | 257 |
| Figure 6-101 The correlation of SSI and SSI2-H with CCT (left), age (middle) and IOP (right) in the pre-surgery SMILE group of Dataset 2..... | 258 |
| Figure 6-102 The correlation of SSI and SSI2-PLS with CCT (left), age (middle) and IOP (right) in the post-surgery SMILE group of Dataset 2..... | 258 |
| Figure 6-103 Bland Altman plot for SSI2 (top) and SSI (bottom) comparing the pre and post LASIK surgery results in Dataset 3..... | 259 |
| Figure 6-104 The evaluation of correlation in changes in CCT with changes in SSI and SSI2 in the LASIK group of Dataset 3..... | 260 |
| Figure 6-105 The correlation of SSI and SSI2-H with CCT (left), age (middle) and IOP (right) in the pre-surgery LASIK group of Dataset 3..... | 260 |
| Figure 6-106 The correlation of SSI and SSI2-PLS with CCT (left), age (middle) and IOP (right) in the post-surgery LASIK group of Dataset 3..... | 261 |
| Figure 6-107 Bland Altman plot for SSI2 (top) and SSI (bottom) comparing the pre and post SMILE surgery results in Dataset 3..... | 262 |
| Figure 6-108 The evaluation of correlation in changes in CCT with changes in SSI and SSI2 in SMILE group of Dataset 3..... | 262 |
| Figure 6-109 The correlation of SSI and SSI2-H with CCT (left), age (middle) and IOP (right) in the pre-surgery SMILE group of Dataset 3..... | 263 |
| Figure 6-110 The correlation of SSI and SSI2-PLS with CCT (left), age (middle) and IOP (right) in the post-surgery SMILE group of Dataset 3..... | 263 |

List of Tables

| | |
|---|-----|
| Table 2-1 Prevalence of KC based on the geographical positions | 26 |
| Table 3-1 demography for patents used to validate numerical models..... | 54 |
| Table 3-2 Constitutive parameters of Ogden material model in relation to age as found from experimental data..... | 63 |
| Table 4-1 Correlation between distance from corneal apex to cone centre, cone area and cone height with Pentacam parameters (p values that indicate significant correlation are highlighted in green).. | 88 |
| Table 4-2 Comparison between True IOP measured experimentally with CVSIOP, bIOP and bIOP2 | 93 |
| Table 4-3 The correlation between various IOP measurements and tonometry devices with CCT and age | 96 |
| Table 4-4 The differences between IOP values for CVSIOP, bIOP and bIOP2 for early and late post CXL in dataset 1 when compared to pre values. | 105 |
| Table 4-5 The correlation of Ex-vivo SSI, SSI2-H and SSI with age plus the mean and standard deviation of the differences between “ex-vivo and SSI” and “ex-vivo and SSI2-H ” in addition to Spearman’s rho correlation p-value | 113 |
| Table 4-6 Showing the mean, standard deviation (SD) and statistical comparison with the healthy group for SSI / SSI2-KC in the same format as shown here in Dataset 1..... | 119 |
| Table 6-1 Demographics and surgical parameters for LASIK, SMILE and PRK surgeries in Dataset 3. | 196 |
| Table 6-2 IOP values measured using three different methods for LASIK, SMILE and PRK in 1,3 and 6 months post operatively in Dataset 3 | 197 |
| Table 6-3 The differences between IOP measurements postoperatively in comparison to preoperative values for LASIK, SMILE and PRK surgeries in Dataset 3 | 198 |
| Table 6-4 the R and p values for evaluating correlations of IOP values with CCT for preoperative and 1,3 and 6 months postoperative in PRK data | 199 |
| Table 6-5 the R and p values for evaluating correlations of IOP values with age for preoperative and 1,3 and 6 months postoperative in PRK data | 200 |
| Table 6-6 the R and p values for evaluating correlations of IOP values with CCT for preoperative and 1,3 and 6 months postoperative in LASIK data | 201 |
| Table 6-7 the R and p values for evaluating correlations of IOP values with age for preoperative and 1,3 and 6 months postoperative in LASIK data | 202 |
| Table 6-8 the R and p values for evaluating correlations of IOP values with CCT for preoperative and 1,3 and 6 months postoperative in SMILE data | 203 |
| Table 6-9 the R and p values for evaluating correlations of IOP values with age for preoperative and 1,3 and 6 months postoperative in SMILE data | 204 |
| Table 6-10 Showing the mean, standard deviation (SD) and statistical comparison with the healthy group for SSI / SSI2-KC in the same format as shown here in Dataset 2..... | 240 |
| Table 6-11 Showing the mean, standard deviation (SD) and statistical comparison with the healthy group for SSI / SSI2-KC in the same format as shown here in Dataset 3..... | 241 |
| Table 6-12 Showing the mean, standard deviation (SD) and statistical comparison with the healthy group for SSI / SSI2-KC in the same format as shown here in Dataset 4..... | 243 |
| Table 6-13 Showing the mean, standard deviation (SD) and statistical comparison with the healthy group for SSI / SSI2-KC in the same format as shown here in Dataset 5..... | 244 |
| Table 6-14 Showing the mean, standard deviation (SD) and statistical comparison with the healthy group for SSI / SSI2-KC in the same format as shown here in Dataset 6..... | 246 |
| Table 6-15 Showing the mean, standard deviation (SD) and statistical comparison with the healthy group for SSI / SSI2-KC in the same format as shown here in Dataset 7..... | 247 |
| Table 6-16 Showing the mean, standard deviation (SD) and statistical comparison with the healthy group for SSI / SSI2-KC in the same format as shown here in Dataset 8..... | 248 |

Introduction

1.1 Preface

The eye has served as a topic of contradictory interpretations since ancient times. With the belief of philosophers and physicians in the eye as an active organ, Plato wrote in the 4th century B.C. that the emanated light rays from the eye capture the object and enable humans to see. With little knowledge of the eye anatomy, Aristotle rejected this theory, Figure 1-1. He believed it is unreasonable that seeing could occur by issuing something from the eye and advocated that the eye should be receiving rays.³ Beyond the philosophical discussions, Aristotle started to explore eye conditions. In his book, *De Generatione Animalium*, he discussed changes in eye colours which are believed to be related to glaucoma and more specifically acute angular-closure. This work was continued in the 1st century by Demosthenes Philalethes who described glaucoma in his book, *Ophthalmicus*, as the colouration of crystalline humour (lens) which he thought to be incurable. There seems to have been confusion between glaucoma and cataract in the literature during these early days. However, interestingly they were both believed to be due to thickening or hardening of intraocular humour.⁴

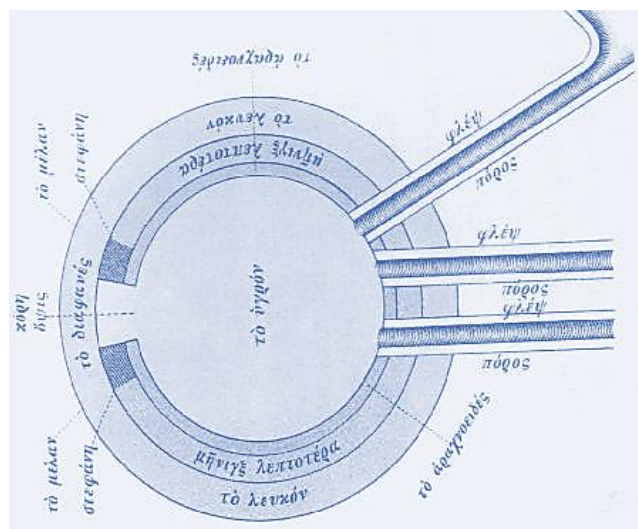


Figure 1-1 The eye structure conceived by Aristotle. At this time philosophers only recognised transparent cornea and sclera, and everything else was aligned with a hole which meant to be the pupil⁵

In the 1st century, interest in exploring light rays led to the book of *Optics* by the Greek philosopher Ptolemy who described convex lenses to aid with magnifying the image.⁶ Despite Aristotle’s view, 2nd century Galen hypothesised that light flows from the brain passing through an empty tube of optic nerves and leaves the eye. By taking advantage of the knowledge of Alexandria’s anatomists, Galen defined fundamental features of physiology and anatomy of the eye that served until the 7th century, Figure 1-2. Among those anatomists, Rufus of Ephesus described the eyelids, iris, cornea, retina, tear ducts, uvea and the two internal fluids, which he called the aqueous humour and vitreous. This knowledge enabled Galen to focus on the crystalline lens, which he described as the principal instrument of vision. Influenced by Galen, ophthalmology as a separate science started to appear from the 9th century and remained dominated by the emission theory and the significance of the crystalline lens. In the 10th century, the study of the dilation and contraction of the pupil and damage to the eye by intense light adhered to Aristotelian theory.³

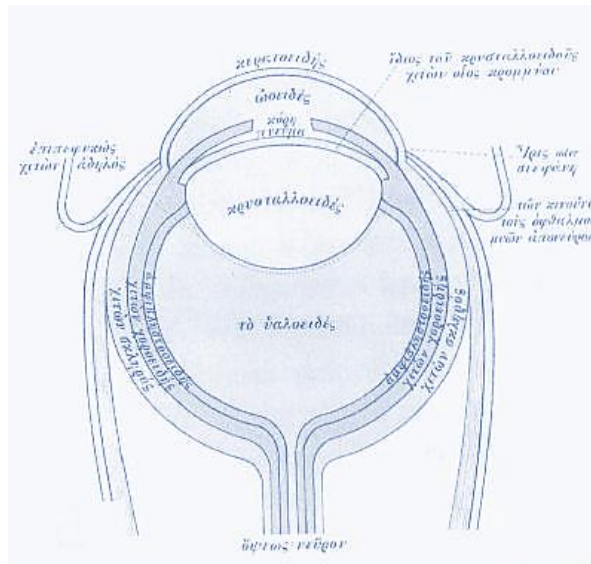


Figure 1-2 The anatomy of the eye as described by Galen. Many more components were identified at that time, including the crystalline lens, conjunctiva, choroid, retina, optic nerves, ciliary body, limbus and iris.

5

During this time, Ibn Sina described examination of glaucoma through ocular palpation and suggested cataract surgery was less suitable for those with hardening in the cornea.⁴ Ibn Sina and later 12th century Alhazen improved the description of the convex lenses, used for magnifying images from the 1st century, and explored in detail the light refraction and image formation.⁷ Ibn Sina’s and Alhazen’s work was followed by Nicolaus who described how the light passed through the cornea and crystalline lens and was transmitted by the optic nerve to the brain.³ Building on the resulting improvements in understanding of refraction, the use of reading stones became gradually more common in reading small texts.⁸ The first eyeglasses seem to have been produced in northern Italy during the 13th century.⁹ Important developments followed in the 16th century with Alessandro Achillini questioning the significance of the

crystalline lens, Vesalius denying the hollow structure of optic nerves and Felix Platter suggesting the optic nerve be the primary organ enabling vision and giving importance to the retina.³ During that time, Willebrord Snellius discovered the law of refraction.¹⁰

In the early 17th century, with more anatomical knowledge, Figure 1-3, Kepler theorised for the first time that the image is formed on the retina.³ In the 18th century, a German professor of anatomy and ophthalmologist surgeon, Burchard David Mauchart, documented for the first time keratoconus as a corneal disorder. This work was explored in more depth by British physician John Nottingham in the 19th century and keratoconus was distinguished from other corneal diseases.¹¹ In the latter part of that century, the first tonometer to measure the pressure inside the eye was developed by von Graefe. This was followed by Maklakoff who developed the earliest, relatively accurate applanation tonometer. During the 20th century, it became known that glaucoma was associated with elevated intraocular pressure, which became routinely monitored in clinical practice using the newly developed tonometers.¹² Later on, Joseph Dallos, William Feinbloom and Otto Wichterle developed contact lenses.¹³ This was followed by corneal reshaping techniques that were implemented manually by Jose Barraquer and later using laser following its invention in the 1950s¹⁴⁻¹⁶.

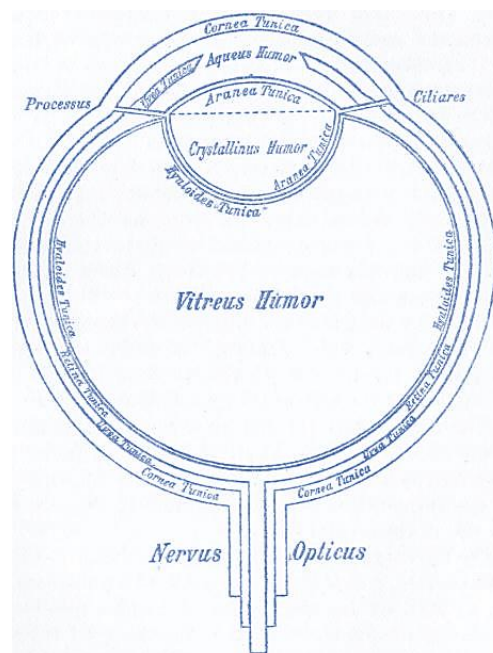


Figure 1-3 Anatomy of the eye in the 17th century⁵

Until the 20th century, and even with the detailed anatomical understanding depicted in Figure 1-4, the eye was known as an organ that transduces light into an image but never thought of as a biomechanical structure. It was considered a musculature thick shell that was pressurised to form its curved shape and provided with nutrition through fluid secretion and drainage along with a complex system of vascular as well as a variety of solute and fluid transport networks.¹⁷ The 9th edition of the veritable bible of ophthalmology, *Alde's Physiology of the Eye*, published in 1992, did not have any reference

to biomechanics, while the 11th edition, published in 2011, had only two relevant index entries.¹⁸

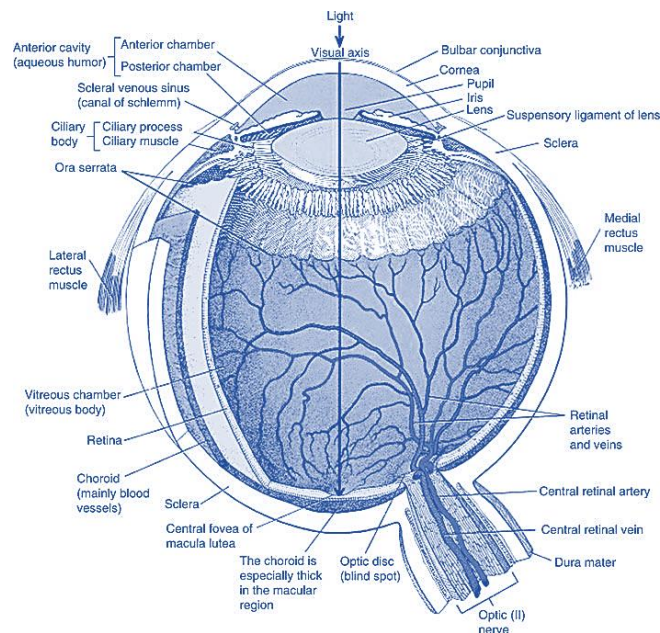


Figure 1-4 Eye structure as it is currently known¹⁹

From the late 20th century onwards, particular attention has been given to the field of ocular biomechanics, and the knowledge gained has transformed the diagnosis and therapies in ophthalmology.¹⁸ This research is part of efforts to improve understanding of ocular biomechanics and develop new technologies to improve clinical practice.

1.2 Background

Glaucoma management relies on lowering the eye's pressure (intraocular pressure or IOP) which is the only modifiable risk factor. The current inaccuracies in IOP measurement are reported to have contributed to 15% of patients with this condition are losing their eyesight while under treatment.^{20,21} This outcome is serious considering that glaucoma currently affects 66m people worldwide (11.2m of which suffer bilateral blindness as a result) and is expected to become more prevalent with an increasingly ageing population.²²

Most IOP measurement devices (tonometers) deform a central area of the cornea and assume that the resistance to deformation is related to the IOP.¹² While this operating principle makes device development simple, it leads to inaccuracies as the IOP measurements become affected by the natural variations in corneal thickness, curvature, astigmatism, tissue stiffness and corneal medical history.^{23,24} This had been a long-standing problem, and several attempts have been made, to varying degrees of success, to quantify the inaccuracies in various devices and produce reliable correction methods.

25-28

Goldmann applanation tonometer has served as the gold standard since 1954.²⁹ This tonometer makes contact with the cornea and requires the application of fluorescein and a local anaesthetic. This makes it time-consuming and uncomfortable to use. Also due to the contact, the device requires disinfection before it can be used on another patient. From 1972, with developments in non-contact tonometers such as non-contact tonometer (NCT), Keeler Pulsair, Ocular Response Analyser and Corvis ST, clinicians were able to monitor IOP as part of clinical routines. The advantages of non-contact tonometers are that they are quick, do not require disinfection and more importantly, are able to provide information on corneal movement under the puff of air.³⁰⁻³²

The ability to determine corneal biomechanical properties in-vivo – possibly using non-contact tonometers – is of great clinical importance as it can help optimise several treatments and management procedures that interact or interfere mechanically with the eye. Examples include measurement of intraocular pressure (IOP) for effective glaucoma management^{33,34}, refractive surgery planning^{35,36}, keratoconus risk profiling^{37,38}, optimisation and evaluation of different protocols of collagen crosslinking treatments³⁹, selection of intracorneal ring implants and even design of soft contact lenses where the mechanical interaction between the lens and the anterior eye is currently not considered.

There are two main challenges in estimating in vivo mechanical behaviour. First, the deformation of the cornea under an external load is dependant on the IOP and corneal stiffness. Both IOP and material stiffness are unknown factors and the inter-related link between them and deformation makes accurate measurements more challenging in-vivo.⁴⁰ Second, biological tissues and specifically the cornea and sclera behave in a nonlinear manner.^{17,41} This means the material stiffness (tangent modulus) changes with variation in strain or stress and therefore IOP affects the measured corneal stiffness value. This study aims to address these challenges through the development of methods to estimate IOP that is free of the effects of corneal stiffness, and in-vivo stress-strain estimates that are independent of the IOP and geometrical changes.

1.2.1 Human Eye

The main components of the eye relevant to this study are the cornea, limbus and sclera, Figure 1-5. The transparent cornea and the opaque sclera form the outer tunic of the ocular globe protect the eye's internal components.⁴² The border between the cornea and the sclera is the limbus, which contains the trabecular meshwork that allows outflow of the aqueous humour.⁴³

The cornea provides more than 60% of the eye's optical power through its unique microstructure, which results in tissue transparency, geometry and refractive index.⁴⁴ Anomalies in corneal shape, like those observed in keratoconus, can affect light

refraction and cause deterioration in visual acuity. The chamber between the cornea and iris (anterior chamber) and the space from the iris to the lens are filled with aqueous humour. This water-like fluid nourishes the lens and cornea while providing stability to the shape of the cornea.⁴⁵ The iris adjusts the amount of light that can enter the eye and reach the crystalline lens. The lens focuses the light that passes through the cornea onto the retina, and the retina detects light and transfers it to the brain through the optic nerve by creating electrical impulses.^{46,47} Ciliary muscle is responsible for changing the shape of the lens, and the ciliary epithelium produces aqueous humour. The part of the retina that provides visual clarity is called the macula and has a high density of light-sensitive cells. The sclera is filled with a colourless and transparent jelly-like substance, the vitreous humour, that helps the eye hold its shape and takes up around 80% of its internal volume.^{10,44,48}

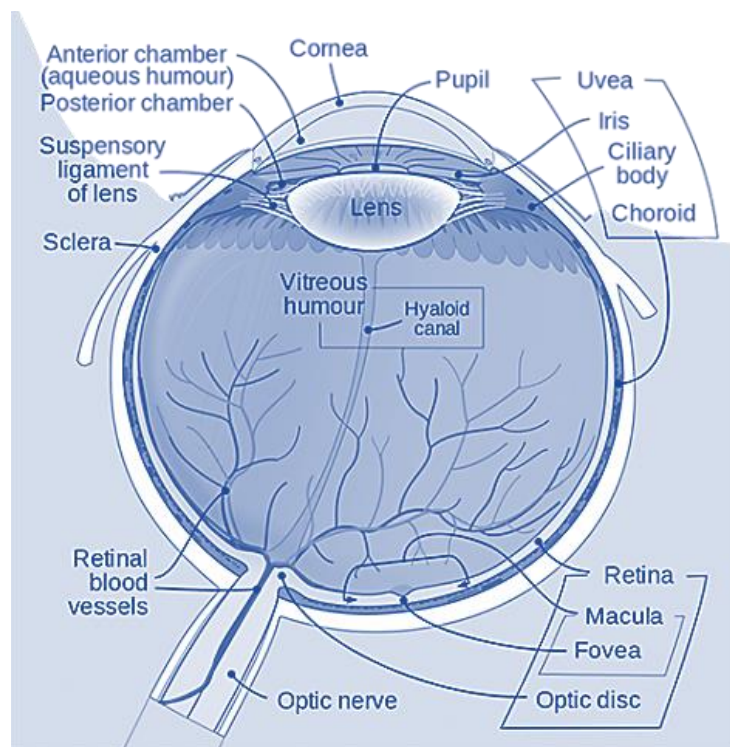


Figure 1-5 The eye cross-section with some important components⁴⁹

The non-regenerating governing layer (about 90% of corneal thickness) of the human cornea is the stroma which includes lamellae of organised collagen fibrils.⁵⁰ The anterior epithelium and posterior endothelium are cellular outer layers composed of keratinocytes. The epithelium with roughly 10% of corneal thickness, protects the eye from foreign bodies such as bacteria and water and absorbs cell nutrients and oxygen to transfer to the cornea.⁵¹ The thin endothelium's primary function is to pump fluid out of the stroma and prevent it from swelling while keeping it clear. If endothelium cells are lost, they cannot be regenerated.⁵² The function of non-regenerating acellular Bowman's layer with a thickness of 8-12 μm is not clear. The Descemet's membrane,

with roughly the same thickness as the Bowman's layer, is made of collagen, provides protection and can be regenerated after injury. Mechanical behaviour of the cornea is controlled by the stroma, and earlier studies showed that the epithelium's contribution to corneal biomechanics was negligible.^{53,54}

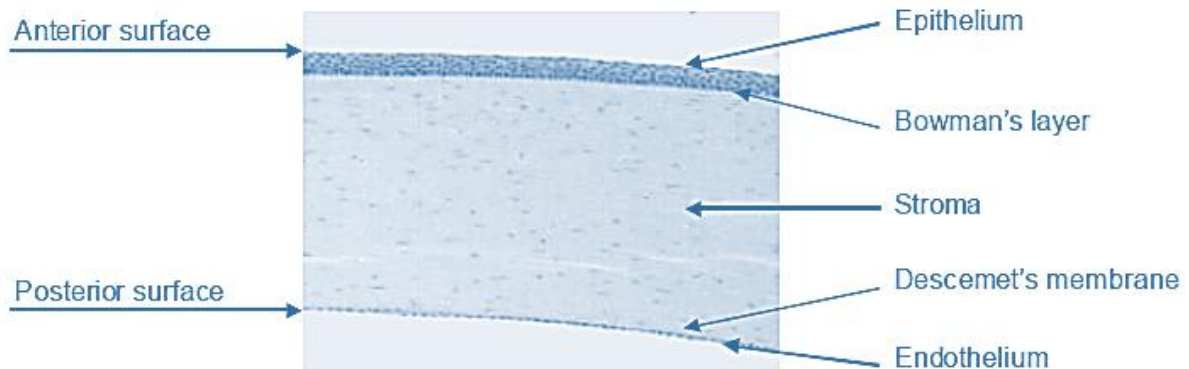


Figure 1-6 Corneal cross-section showing its main layers⁵³

1.2.2 IOP

The aqueous humour in the cornea is produced by the ciliary body and drained through the trabecular meshwork and uveoscleral outflow, Figure 1-7. The trabecular meshwork, made of a triangular porous tissue structure, is located in the angular base of the cornea. Through particular canals, it controls the outflow of aqueous humour and regulates IOP.⁵⁵⁻⁵⁷ Another drainage of aqueous humour is through an anatomical route called uveoscleral outflow.⁵⁸ IOP is adjusted by the balance between the production and drainage of aqueous humour that flows at an estimated rate of $2.75 \mu\text{l}/\text{min}$.⁵⁹ This pressure is uniformly distributed across the eye as a hydraulic unit.⁶⁰ The pressure in the eye can be measured by applying a known pressure on the cornea and measuring the resulting deformation. The higher the pressure, the smaller the deformation and vice versa. The healthy range of the IOP is between 10 and 21 mmHg, and it varies throughout the day.⁶¹ In the past, the IOP was examined by gentle pressure on the closed eyelids, and later using contact and non-contact tonometry devices. There are a number of inaccuracies associated with the majority of measurement methods as the corneal deformation is also influenced by the mechanical stiffness of the eye.⁶¹⁻⁶³

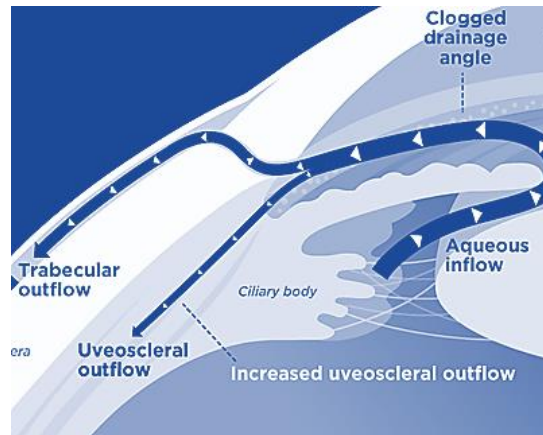


Figure 1-7 Aqueous humour production and drainage ⁶⁴

1.2.3 Glaucoma

Glaucoma, the second leading cause of blindness after cataract, is a gradual degeneration of the optic nerve that is irreversible and can lead to complete blindness. Most patients with glaucoma have elevated Intraocular Pressure (IOP) and around one-third maintain a normal pressure while developing optic nerve degeneration, Figure 1-8. Glaucoma is an umbrella term used to describe conditions that result in optic nerve degeneration. Currently, IOP is the only modifiable risk factor for most types of glaucoma. Due to inaccuracies associated with the measurement of IOP and the slow progression of glaucoma, in most cases, vision loss and damage to the optic nerve occur before being recognised by the clinicians or the patients.²¹ The main types of glaucoma include primary open-angle glaucoma (OAG), primary Angle-closure Glaucoma (ACG), secondary glaucoma and congenital glaucoma.⁶⁵

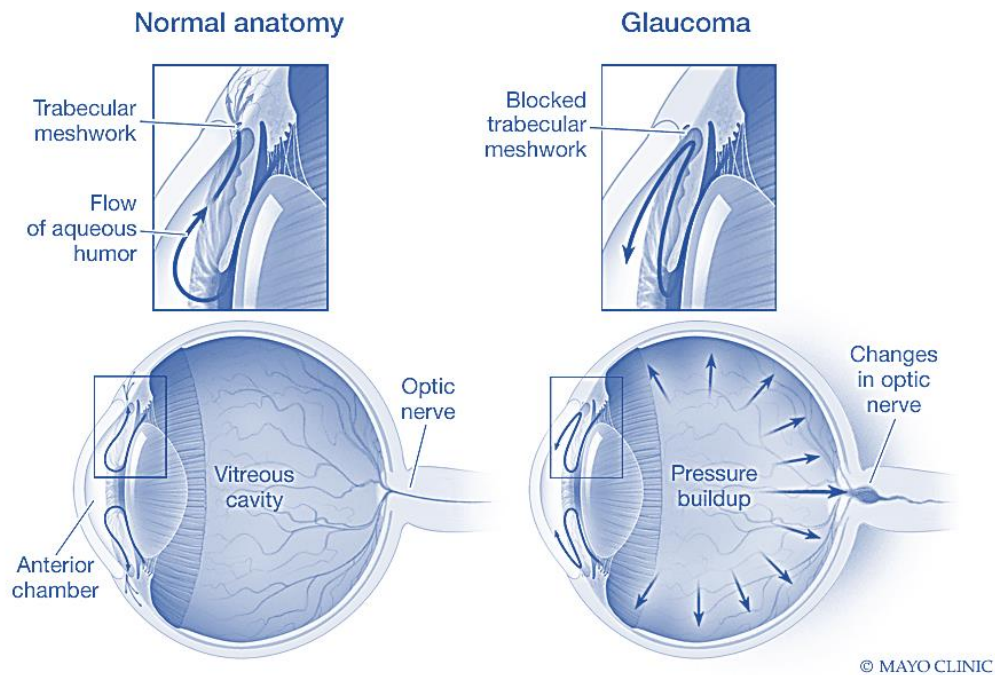


Figure 1-8 The eye anatomy comparison for healthy and glaucoma. ⁶⁶

The most common type of glaucoma in the west is OAG, in which the anterior chamber appears to be normal, but IOP is elevated. If there is any other identifiable factor for the change in IOP, it is then known as secondary glaucoma. If the IOP is in the normal range, but the vision is being affected, the condition is known as normal-tension glaucoma (NTG), which is a subset of OAG.⁶⁷ On the other hand, in ACG the problem is in the issue with the drainage of the aqueous humour. If there is any other trigger related to other conditions, then it is known as secondary glaucoma. ACG can be acute or chronic. In acute ACG, the blockage is due to the iris being moved forward and blocking the drainage channels, resulting in IOP increases. Some studies reported that secondary acute ACG resulted in greenish or bluish colour in a mid-dilated pupil.⁴ In the chronic type of ACG, the reason for elevated IOP remains the same and the only difference is that the condition develops very slowly. Finally, congenital glaucoma is a rare condition that develops in babies as a result of problems with the formation of the drainage systems before birth.⁶⁵ It is also important to learn about Ocular Hypertension (OHT) as it refers to a condition where the eye is healthy, but the IOP is higher than the normal range. Patients with OHT do not have glaucoma but should be monitored closely for the possible side effects of high IOP.⁶⁸

1.2.4 Keratoconus

Keratoconus (KC) is a condition that causes alterations in the curvature of the cornea and localised thinning, Figure 1-9⁶⁹⁻⁷². It commonly begins in early adolescence, progresses over the next two decades⁷³ and can significantly reduce visual acuity and vision-related quality of life^{74,75}. While the characteristic topographic patterns of keratoconus can be identified on corneal topographic and tomographic maps, it is still difficult to precisely locate the centre of the cone and the transition zone between the pathology area and the rest of the corneal tissue⁷⁶⁻⁸⁰. Classifying and managing keratoconus can be more efficient when the affected corneal region is located, especially in the case of customised corneal crosslinking⁸¹⁻⁸⁴. Hence techniques were developed to address this challenge⁸⁵⁻⁸⁷. However, some of the available techniques to detect the keratoconus cone are based on methods that analyse corneal tangential or axial curvature maps⁸⁵⁻⁸⁷. Tangential curvature at a point is defined as the curvature of the best fit sphere in the immediate local area surrounding this point. The standard management technique for keratoconus is corneal crosslinking (CXL), which is a surgical procedure that increases the stiffness of the cornea to prevent further distortion. In addition, there are several other methods used for improving the vision in KC eyes that includes the use of contact lenses, corneal implants or corneal transplants.⁸⁸

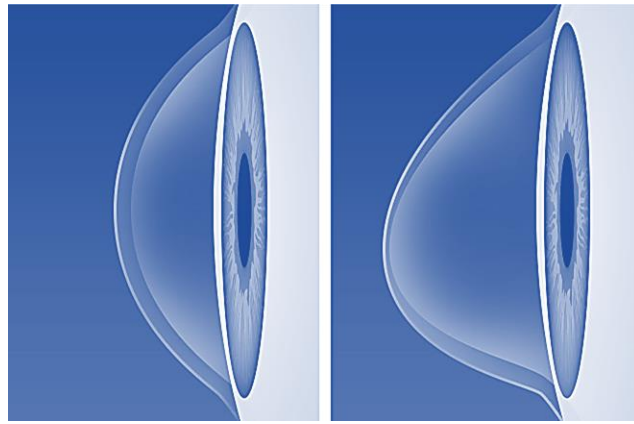


Figure 1-9 The comparison between health cornea (left) and keratoconic cornea (right) that led to thinning and deformation ⁸⁹

1.2.5 Biomechanics

Application of mechanics to biology for a better understanding of living systems' mechanics is defined as biomechanics. Thus the chemical and physical variations in tissue properties are being explored in biomechanics. The exponential progress in medicine that is mainly brought by advancements in the field of biomechanics made clinicians including ophthalmologists to become increasingly interested in the field.¹⁷ Understanding material behaviour such as elasticity is fundamental to the field of biomechanics. Elasticity refers to the ability of a material to recover its original shape after the applied force is removed. Stress and strain are the components used to define tissue behaviour.⁹⁰ The strain is the amount of stretch in comparison to its original dimensions and stress is the force pre-unit area.

When an external force is being applied, the structure deforms until the internal load cancel out the opposing force. Both forces and deformations can be decomposed into perpendicular and parallel tensor components, respectively defining normal and shear strain and stresses.⁹¹ If the energy density function defines the relationship between the stress-strain, it is termed hyperelastic.⁹² If the material behaviour is the same across the tissue, it is called isotropic. Otherwise, it is anisotropic, and there is no symmetry in mechanical properties. When the material is isotropic, elastic properties are the same regardless of the direction of the force and position of the tissue.^{93,94} If elastic material behaviour is linear, it is defined by Young's modulus and when nonlinear, it is described by tangent modulus. The word tangent is being used to indicate the stiffness is changing as the stress or strain values change.

When the cornea is subject to a fixed strain value, the stress will drop over time, and this behaviour is defined as relaxation, Figure 1-10-A. Similarly, when the tissue is subject to fixed stress value, it will stretch over time, and this is known as creep, Figure 1-10-B. The creep and relaxation in tissue were found to continue for a long time.^{95,96} These are viscoelasticity features and are mainly due to the hydration level of corneal tissue and collagen structures. One studies showed a strong correlation between

hydration and creep.⁹⁷ In that study, the corneal thickness was changed by controlling the hydration level, and the amount of strain under the applied load was found to be smaller in thinner corneas. Other viscoelastic features include hysteresis and time dependence deformation.⁹⁸⁻¹⁰⁰ If the loading and unloading of tissue do not follow the same path, it is described as hysteresis. Hysteresis is the amount of energy stored in the tissue that is equal to the area between the loading and unloading curves, Figure 1-10 (C). Time dependant strain means the faster the load is being applied, the stiffer the cornea becomes and the amount of deformation for a given stress value reduces, Figure 1-10 (D).

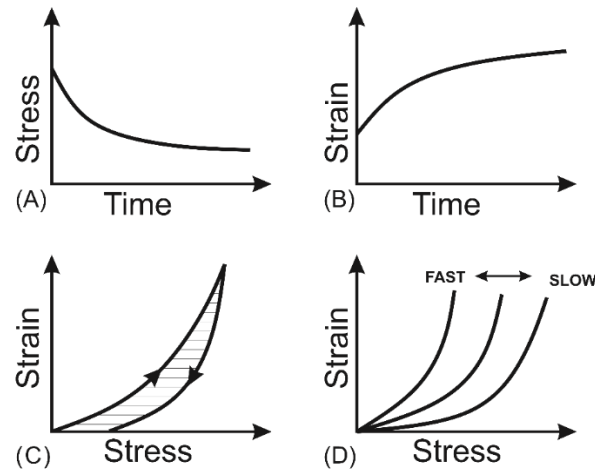


Figure 1-10 The four features of viscoelasticity including (A) relaxation, (B) creep, (C) hysteresis and (D) time dependant strain

1.3 Scope of the Study

Eye conditions such as glaucoma, refractive errors and keratoconus are currently affecting over 50% of the world population. Despite research and investment in this area over the past 30 years, the diagnosis and therapy of these conditions are made with inaccuracies, and largely relies on ophthalmologists' experience.

This study attempts to reduce inaccuracies and improve the process of diagnosis and treatment. It required knowledge in eye anatomy and vision, and involved mathematical and engineering analysis, programming, data management and high-performance computing. It relied on parametric studies conducted using representative numerical modelling of ocular behaviour of human eyes subjected to ocular pressure and a tonometry air puff. CorVis ST, developed by OCULUS Optikgeräte, Inc. (Wetzlar, Germany), was the chosen tonometer in this study as it provides more information on corneal behaviour compared to other devices such as Ocular Response Analyser (ORA). Corvis ST offers 140 images of corneal deformation during the 32 milliseconds of application of air puff.

The results of parametric studies were statistically analysed in order to develop methods to estimate biomechanically corrected IOP and Stress-Strain behaviour. These methods were subsequently validated with an experimental study on ex-vivo human eyes and a large clinical database. The new Stress-Strain Index (SSI) was developed in order to enable the customisation of surgical and therapeutic procedures, including early-stage diagnosis of corneal abnormalities, refractive surgeries and corneal crosslinking.

1.4 Aim and Objectives

The aim of this study is to develop new methods for the accurate measurement of IOP and corneal material stiffness in vivo. This aim is achieved through the fulfilment of the following objectives:

- Development of a mathematical method to analyse the tomography data of keratoconic corneas in order to estimate the area, height and location of the keratoconic cone
- Building representative numerical models of healthy and keratoconic corneas and simulation of Corvis ST air-puff application on the cornea
- Performing a parametric study with wide variations of important geometrical and biomechanical parameters exceeding the reported ranges
- Development of methods to predict IOP and corneal stiffness for the healthy and keratoconic eyes and those subjected to Laser-Assisted in Situ Keratomileuses (LASIK) and Small Incision Lenticule Extraction (SMILE) surgeries
- Validation of the IOP and corneal stiffness methods experimentally and using a large clinical database

1.5 Thesis Structure

The thesis includes five chapters providing a detailed description of the study's methodology and findings. It starts by providing an overview of how knowledge in ophthalmology has developed over the years, highlights the gaps and describes the contribution of this research. In Chapter 2, a literature review is provided to explore earlier studies and the lessons learnt in connection to the present research. The methodology that is followed to achieve the study aim and objectives is described in Chapter 3. The results obtained from numerical simulations are presented in Chapter 4. In addition, methods developed for IOP and corneal stiffness measurements were applied to clinical and experimental data and presented in this chapter. In the end, chapter 5 provides a thorough discussion of the main findings in comparison to earlier efforts. The conclusions and limitations of this study are also presented in the final chapter.

1.6 Thesis Contribution

The contributions of this thesis are:

- Development of a new method for estimating keratoconic cone properties including cone area, cone height and cone centre location
- Development of representative numerical models of keratoconic corneas that incorporated realistic cone shapes and distinctive material properties
- Thorough validation of the new IOP and corneal stiffness methods using thousands of clinical cases involving patients with various diseases and conditions collected from different clinical centres in four continents
- Evidence to show the new bIOP is able to compensate better for variations in corneal biomechanics in healthy and keratoconic eyes compared to previously developed equations
- Evidence to show that the new SSI parameter is independent of IOP and corneal biomechanics and can be applied to keratoconic eyes and those undergoing refractive or crosslinking surgeries

Chapter Two

Literature Review

2.1 Introduction

The following chapter presents a relevant review of literature on the biomechanics of the eye, keratoconus, intraocular pressure and tonometry devices. It starts with an overview of research carried out to characterise biomechanics of cornea and sclera. The chapter then proceeds to a review of keratoconus, and underlying research demonstrates how this disease influences corneal biomechanics and geometry, which makes it challenging to measure both Intraocular pressure (IOP) and mechanical behaviour in vivo. Finally, it presents a literature study conducted on IOP and tonometry devices and errors associated with each one. The key lessons learned from earlier studies are presented at the end of this chapter.

2.2 Corneal Biomechanics

The cornea is responsible for 2/3 of the refractive power of the eye. The shape of the eye and especially the cornea is dependent on the equilibrium between the intraocular pressure and biomechanics of the tissue.^{17,101-103} Corneal stiffness has an effect on most tonometry systems used to estimate IOP. The natural variation in corneal stiffness can lead to over or underestimation of IOP, which in results lead to deficiencies in glaucoma management. In diseases such as keratoconus, corneal stiffness reduces, which causes excessive deformation, and the cornea starts to change. The current management technique is based on corneal crosslinking (CXL), which is intended to restore the stiffness in the tissue. Stiffness is also affected by refractive surgery, which is intended to change the shape of the cornea to improve vision.¹⁰⁴ However, it leads to increased corneal deformation under IOP due to loss of stiffness caused by the surgeries which contribute to the deficiencies in the outcome of these surgeries.¹⁰⁵ For these reasons, it is important to understand corneal biomechanics and to be able to quantify corneal stiffness in particular in vivo, which was one of the main aims of this research.

2.2.1 Elasticity

Several types of hyperelastic constitutive models were presented in the literature, among which Neo-Hooke and Ogden were most commonly used for corneal modelling. The stress and strain relationship is defined using these models with constants that shape material properties.¹⁰⁶ It is reported that most biological tissues, including the cornea, are nonlinear and have different degrees of anisotropy.¹⁰⁷ The anisotropy is found to be mainly due to the constituent of collagen fibril microstructures in lamellae that are almost parallel to the corneal surface.¹⁰⁸ While anisotropic models are more accurate in representing tissue behaviour, they are computationally expensive.¹⁰⁸ Hence, the use of isotropic material models became essential for large size simulation-based studies. Research showed that the corneal mechanical response could be presented accurately using the Ogden material model.¹⁰⁹⁻¹¹²

2.2.2 Ex-vivo Measurement of elasticity

The experimental studies on the cornea are mainly dominated by uniaxial and inflation tests.¹¹³⁻¹¹⁷ Experiments using uniaxial test relied on excised strips of tissue being clamped on a device that applied axial forces to the tissues. Studies that performed these experiments started by applying some initial loading and unloading cycles to ensure the tissue behaviour is repeatable, and this process is known as preconditioning.¹¹⁸ Upon completion of the test, force and deformation data are converted to stress and strain curves that its slope enables the calculation of the tangent modulus. It is highlighted that uniaxial experiments are useful for quick studies or relative comparisons of biomechanics. It is noted that this method of testing is unable to provide accurate material behaviour for the cornea. This is first because the corneal tissue is naturally curved, and during the uniaxial test, it has to lose its natural shape and become flat. Second, by cutting a strip of tissue, fibres are unable to interact in a natural way, and only the remaining fibres are aligned towards the direction of the force and contribute to overall tissue deformation. As a result of these inaccuracies, the experimental studies obtained from the uniaxial test significantly vary from one another, mainly due to these limitations.^{119,120}

Attention gradually moved to test the tissue in its natural shape to overcome these problems. For this reason, inflation test rigs were developed that enable intact in vitro testing of cornea, sclera or whole eye.^{121,122} In these experiments, fluid pressure is applied to cause tissue deformation. This deformation is monitored using laser or digital cameras, and the pressure is measured and recorded. The analysis is more complex and computationally expensive; however, this method of characterising tissue biomechanics is used more and more. A study conducted on 57 human corneas between 30 to 99 years old using inflation provided reliable biomechanical properties. In this study, the cornea was loaded up to 60 mmHg while being clamped close to the limbus.¹²³ The tissue exhibited hyperelastic behaviour, and a nonlinear stiffening was reported with age. The relationship between stress and strain could be described accurately using exponential

Equation 2-1. This led to the development of a relationship between stress and strain in correspondence to age, Equation 2-2.

$$\sigma = A[e^{B\varepsilon}-1]$$

Equation 2-1

In Equation 2-1, constants A and B are obtained based on Equation 2-2 to enable obtaining the stresses (σ) in accordance with strain (ε) values.

$$A=35\times 10^{-9}age^2+1.4\times 10^{-6}age+1.03\times 10^{-3}, \quad B=0.0013\times age^2+0.013\times age+99$$

Equation 2-2

where age is provided in “year” and stress is obtained in “MPa”. By using Equation 2-2, the stress and strain relationship can be presented, as shown in Figure 2-1. The outcome of these equations showed a good match with experimental findings and has been used in numerical simulations.¹²³⁻¹²⁵ The effect of corneal hydration relationship with age is not clearly reported in the literature. One study reported that corneal thickness does not change with age and this indicates the hydration level stays more or less the same.¹²⁶ In contrast, another study found that corneal hydration is reduced with age.¹²⁷ Contradictory to both of these studies, Sharifipour, et al.¹²⁸ concluded that since Corneal Hysteresis (CH) and Corneal Resistance Factor (CRF) measured by Ocular Response Analyser are reduced with age, corneal hydration should increase with age to balance this relationship.

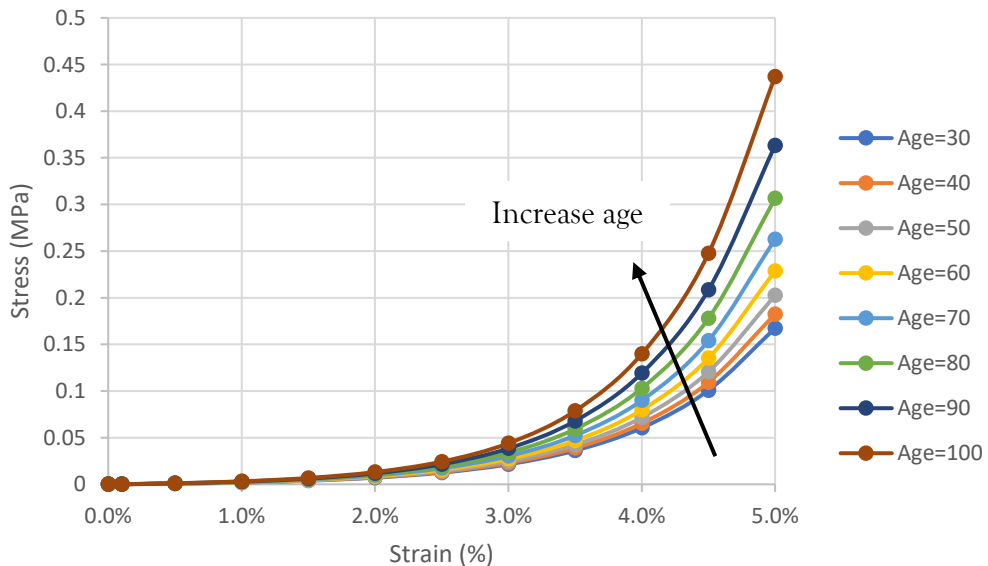


Figure 2-1 Stress-strain behaviour of the cornea in relation to age.¹²³⁻¹²⁵

2.2.3 In-plane Shear

It is found that deformation of the cornea due to shear force is methodologically challenging to measure. Although its value is estimated to be small ¹²⁹, its actual resistance is not known. Studies measured the shear modulus in the human eye to be between 2kPa to 20kPa ^{130,131} and another study showed this value is depth dependant and is higher in the anterior part ¹³². Since the value for shear modulus is relatively small, it is not considered in the majority of studies that used numerical simulations. There is a need to conduct more studies in this area to identify the shear modulus value accurately. This could have an impact on the improvement of accuracy in numerical simulations when the cornea is subjected to a bending force. ¹³³⁻¹³⁵

2.2.4 Morphology and Ultrastructure

The cornea and sclera have complex material behaviour including hyperelasticity (nonlinear stress-strain relationship), viscoelasticity (dependence on strain rate of deformation), regional variation of stiffness and dependence on age and medical history. In addition, the tissue is known to possess a high degree of anisotropy as its mechanical behaviour is dependent on the distribution of collagen fibres, the main load-carrying components of the tissue. With the collagen fibres showing significant regional variations in density and orientation, the biomechanical behaviour of the tissue changes accordingly, experiencing stiffness values that vary with location and direction, and making ocular biomechanics a highly complex topic.

Soft tissues generally consist of two main constituents: cells and extracellular matrix. According to Humphrey ¹³⁶, the extracellular matrix (ECM) – made of proteins, glycosaminoglycan and water – contributes to the eyes' material properties in a number of ways; one such contribution is the provision of tissue stiffness and, as such, the ECM may be regarded as the main source of mechanical properties which affect tissue behaviour. Proteins included within the ECM include the collagen fibrils (one of the most abundant proteins), elastin and proteoglycan (which together form the tissues' unique microstructure).

A total of 28 categories of collagen types have been identified ¹³⁷, among which collagen type one (fibrillar collagen) is the most common and abundant ¹³⁸. In addition, types II, III, V, VI and XI are all regarded as fibrillar collagens, differentiated by their individual self-assembly processes ¹³⁹. These collagens contribute to the formation of bands of fibrils in a staggered arrangement, organised into fibres, which provide mechanical support ¹³⁷ and whose production has been described thoroughly in the literature ^{139,140}, Figure 2-2. As such, the detailed synthesis of fibrillar collagen from cell to ECM will not be given herein, although the hierarchical structure of fibrils will be briefly outlined for its important role in biomechanics.

Collagen fibrils may be treated as the fundamental building blocks in collagen-rich tissues and, as such, may be used to understand the tissues' mechanical characteristics. The collagen molecules, which form the fibrils, can be observed via x-ray scattering, to allow the analysis of the tissues' regional microstructure. On the other hand, the ground substance matrix around the fibrils is used to describe all other components including, but not limited to, proteoglycans, water and elastin, Figure 2-2^{138,141}.

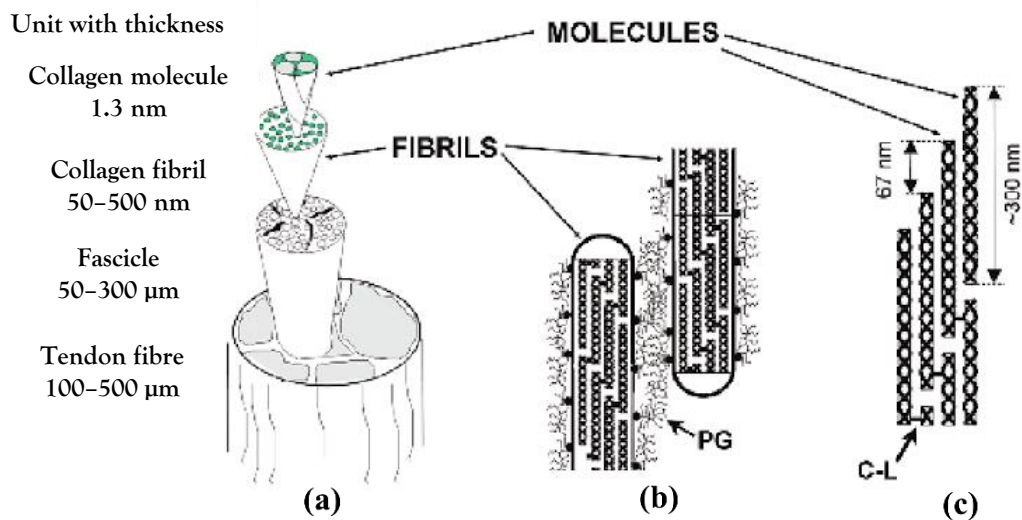


Figure 2-2 Hierarchical structure of fibrils within tissue. (a) Collagen molecules are combined to form fibrils, fascicles and tendon fibres; the interaction between fibrils and molecules is shown in (b) and (c), respectively. C-L, cross-links between collagen molecules; PG, proteoglycan-rich matrix between fibrils. Adapted from¹³⁸.

Individual collagen fibrils are cross-linked via proteoglycans and packed together, in a parallel form, in lamellae, which in turn are organised – layered in varying orientations – to form a composite material, providing the tissue with the general architecture shown in Figure 2-3. The parallel organisation of fibrils within individual lamellae leads to higher stiffness in the direction of the fibrils and reduced stiffness in other directions, resulting in the tissue's anisotropy.¹⁴²

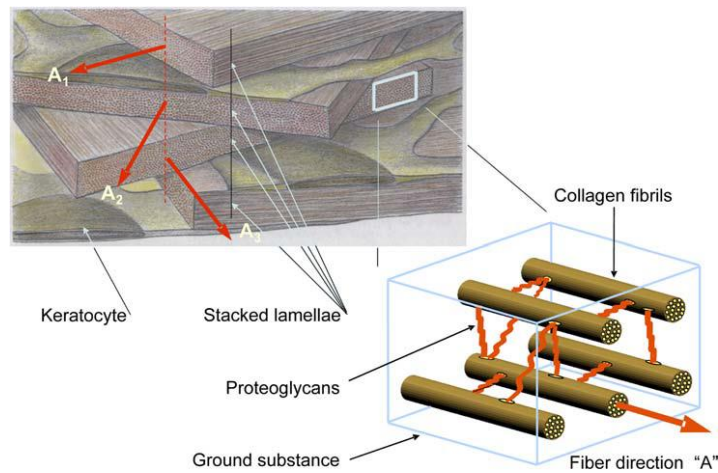


Figure 2-3 Lamellae structure within the cornea ¹⁴²

In the human eye, the number of lamellae within the stroma varies from approximately 300 at the centre of the cornea to 500 at the limbus ¹⁴². According to Meek, et al. ¹⁴³, two preferred meridional orientations of collagen fibrils have been found in the central human cornea by synchrotron X-ray diffraction – inferior-superior and temporal-nasal. This arrangement continues from the corneal apex to 1-2 mm from the limbus, where it becomes circumferential. Indeed, Aghamohammadzadeh, et al. ¹⁴⁴ demonstrated maintenance of the vertical and horizontal directions of fibrils to 1 mm from the limbus, which, in contrast, has a circular disposition of fibrils (Figure 2-4-a). Among all fibrils in the central cornea, one third are orientated within 45 degrees of the superior-inferior meridian and a similar quantity around the temporal-nasal direction (Figure 2-4-b); leaving one third in the diagonal directions in between ¹⁴⁵. This observation is concluded based on studies on healthy corneas and may not necessarily apply in other cases, for example, in keratoconic cases where the collagen fibrils do not seem to have clear preferred orientations ¹⁴⁶.

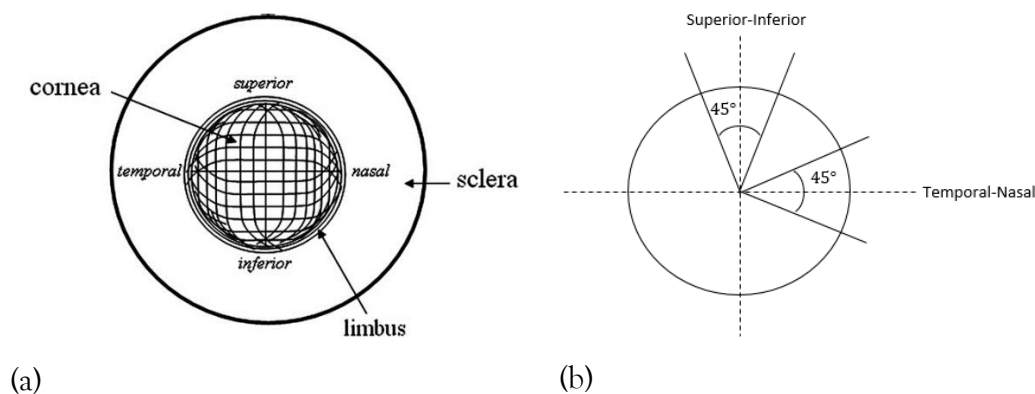


Figure 2-4 (a) The general arrangement of fibrils in the central cornea with preferred orientation in the vertical and horizontal directions ¹⁴⁵; (b) The 45-degree sectors of the central cornea where two-thirds of collagen fibrils have been observed to have a preferential orientation ¹⁴⁵

2.2.5 In-vivo Measurements of Biomechanics

In this section, three commonly used methods for measuring in vivo corneal biomechanics are reviewed. These include Brillouin Microscopy, Elastography and Tonometry based systems.

2.2.5.1 Brillouin Microscopy

Research showed that acoustic waves in the cornea are the result of thermal variations of molecules that produce volatility of pressure which propagates at around 1620 m/s, close to the speed of sound in the water. An effect known as Doppler frequency shift occurs as a result of the interaction between the reflection of the light with the modulation of the refractive index. Doppler effect is when the relative movement of the observer in regard to the wave source causes a change in the frequency of a wave. This shift in the cornea was found to be proportional to the speed of sound, which is equal to the square of longitudinal modulus. Brillouin microscopy is a low power laser, in addition to a high res confocal spectrometer to measure frequency. The longitudinal modulus obtained from this device is believed to be correlated to shear modulus and reported to map the localised properties. The rationale behind this is that the polarisation of scattered light from shear phonons assumed orthogonal to the longitudinal Brillouin scattering that enabled the separation of shear from longitudinal signals. When experimentally tested on Amorphous Polycarbonate (Lexan), Kim et al. showed an ability to measure the shear modulus.¹⁴⁷ However, in contrast, Wu et al. proved that Brillouin measurements are influenced by the level of hydration in the tissue as it influences acoustic waves and not tissue stiffness.^{148,149} The measurement value is useful for comparative studies, for instance, evaluation of changes in the same tissue before and after CXL or identifying localised changes in keratoconic eyes.¹⁵⁰⁻¹⁵³ Although this technology offers easy measurement and is a non-contact painless method, so far, it has not been able to gather enough information to measure tissue mechanical behaviour on its own. The method described here is called the spontaneous Brillouin scattering. It is believed that advancements in the second method, stimulated Brillouin, can address some of the shortfalls.¹⁵⁴

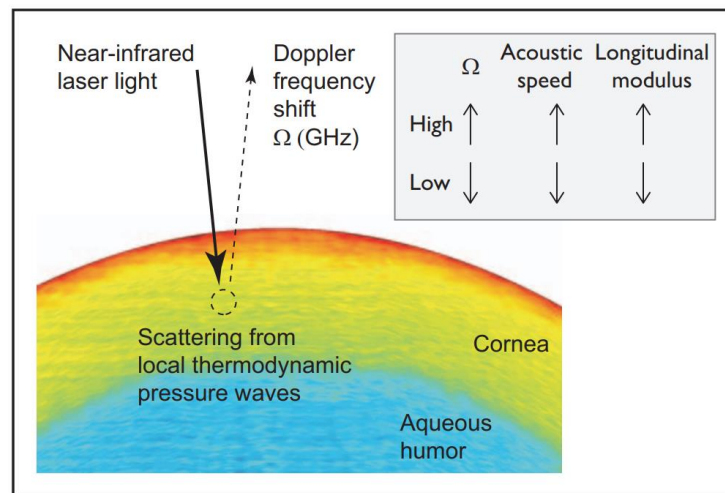


Figure 2-5S The methodology used in Brillouin microscopy ¹⁴⁸

2.2.5.2 Elastography

Elastography has been used commonly to diagnose diseases such as fibrosis or steatosis in the liver, breast, prostate and thyroid cancers. ¹⁵⁵⁻¹⁵⁷ It is based on a concept that creates some distortion in the tissue and then observes and analyses the response. The distortion is produced through three different methods of pushing or vibrating, acoustic radiation force impulse and ultimately, physiological distortions such as heartbeat or pulses. They are mostly based on ultrasound or magnetic resonance systems. By observing the response of the tissue, this method enables the detection of abnormal stiffness in the tissue. It was shown that if the tissue is deforming less or the wave travels more slowly than expected, the tissue can be identified as stiffer than normal. The ophthalmic application of this device requires ultrafast imaging to capture high-resolution images with a shear wave of around 15MHz. ¹⁵⁸⁻¹⁶⁰ The elastic modulus obtained from the healthy corneas in the literature ranges from 50 to 190 kPa using this method. ^{161,162} The drawback with this technique is reported to be the requirement of contact with the tissue, which causes patient discomfort. Studies noted that the new versions of OCT-based (Optical Coherence Tomography) imaging are likely to overcome this problem, Figure 2-6. However, the accuracy of estimating corneal biomechanics using these devices is not yet known. ¹⁶³⁻¹⁶⁵

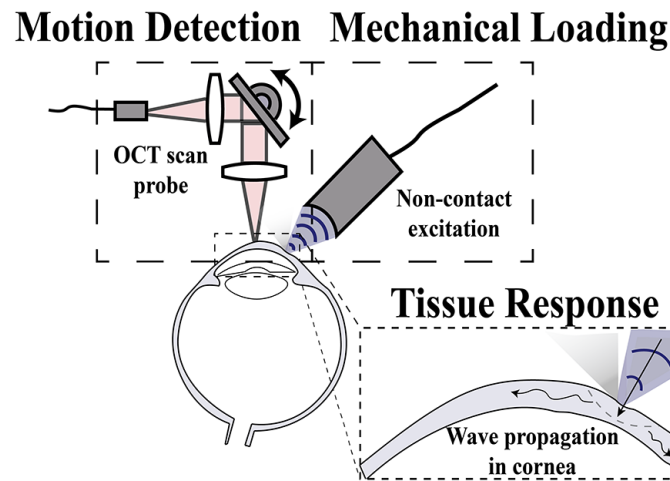


Figure 2-6 The structure of Optical Coherence elastography¹⁶⁵

2.2.5.3 Tonometry based systems

In recent years, there have been many advancements in how intraocular pressure is being measured. These devices have the advantage of being non-contact and apply puff of air to deform the cornea and monitor its deformation.¹⁶⁶ More information on this is provided in section 2.5. Ocular Response Analyser (ORA; Reichert Ophthalmic Instruments, Depew, NY) was the first to introduce biomechanical parameters to their device.¹⁶⁷ The problem with this device is that it only captures the cornea in two positions, at first and second applanations. Hence by knowing the pressure and time it takes to reach these two positions, two parameters of Corneal Hysteresis (CH) and Corneal Resistance Factor (CRF) have been estimated.^{168,169} Although the CH parameter in ORA is correlated with CCT, it appeared to provide useful insights into biomechanics. For instance, a study revealed a correlation between these parameters and the progression of open-angle glaucoma.^{170,171} Another study indicated that ORA could identify patients with keratoconus, although the accuracy was not great.¹⁷²

Further developments in non-contact tonometry led to the development of Corvis ST (Oculus Optikgeräte GmbH, Wetzlar, Germany) that combined air puff with the high-speed Scheimpflug camera system that monitors the deformation throughout the application of pressure, Figure 2-7. This new information enabled the development of new biomechanical parameters such as Stiffness Parameter (SP) and Corneal Biomechanical Index (CBI). In brief, CBI is a multivariate regression model that can separate healthy and KC corneas. SP is the differences between the IOP minus the pressure at applanation one divided by the maximum deflection minus applanation one deflection¹⁷³⁻¹⁷⁵ Both parameters are influenced by IOP and corneal geometrical parameters and unable to measure true material stiffness.^{176,177}

Studies on both ORA and Corvis ST showed some ability (to a varying degree of success) to differentiate between KC and healthy or hyperopia and myopia.¹⁷⁸⁻¹⁸⁰ A more recent

study developed a parameter called Stress-Strain Index (SSI) that is able to measure corneal biomechanics in vivo for healthy eyes with little influence from IOP and CCT.¹⁸¹ This parameter showed a good performance in healthy patients, but when tried on larger studies indicated a need for improvements to be less dependant on geometry (CCT) and IOP.^{182,183} Also, it demands notable improvement for diseased cornea and those after surgical procedures as the equation was developed with the intention to be applied only to healthy corneas. This thesis will tackle this issue of in vivo biomechanical measurements by developing a new biomechanical parameter that can be applied to all types of corneas with different diseases while remains independent or weakly correlated to IOP and geometrical parameters. This parameter should show a significant correlation with age as a measure of stiffness. There is one significant drawback with the use of noncontact air-puff tonometry to measure biomechanics which was reported in the literature. The drawback is the large deformation caused by air puff, and the small monitoring region of deformation, which hides the information requires for determining the localised variation of corneal biomechanics.¹⁸⁴

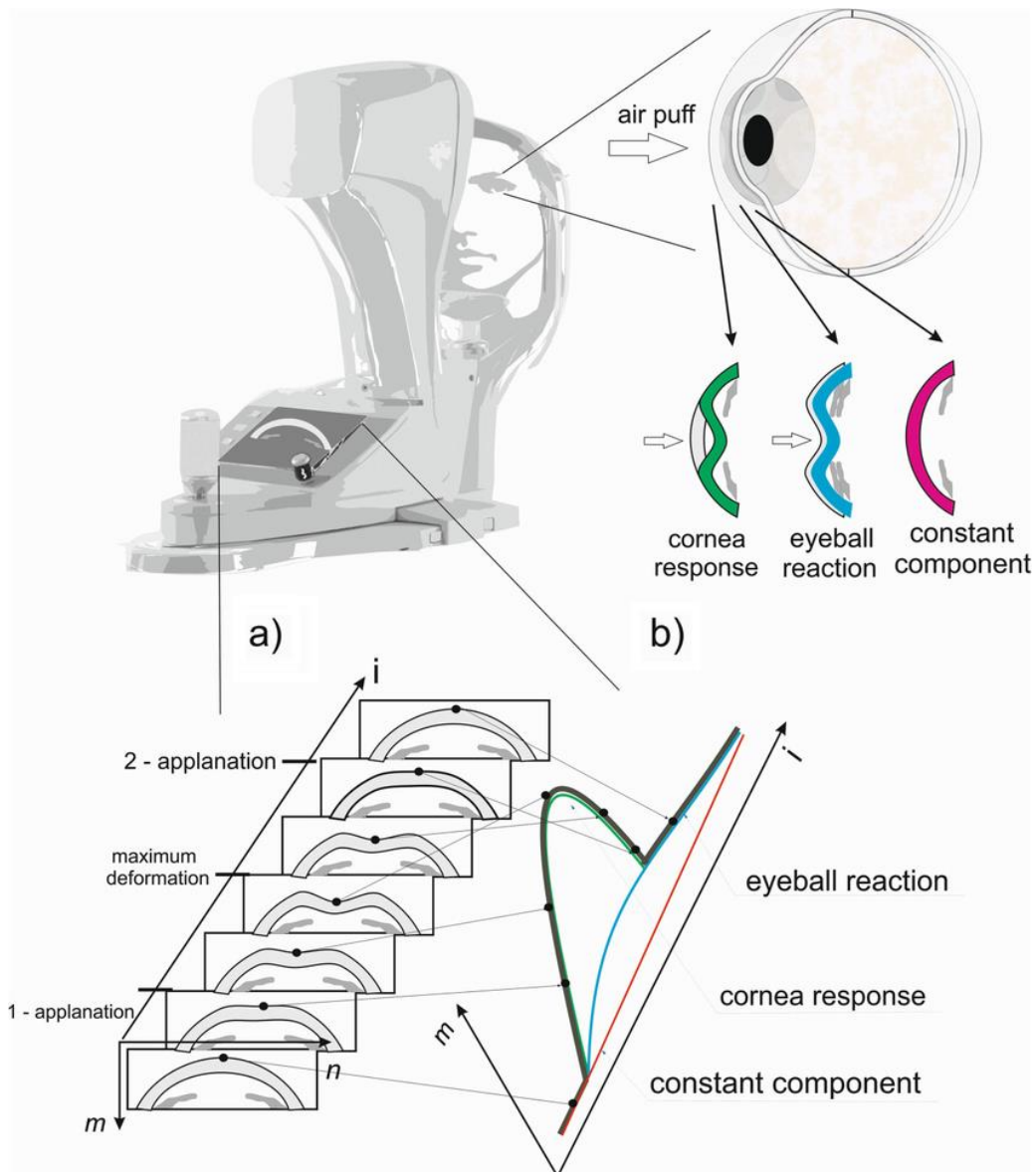


Figure 2-7 The deformations of the cornea under air puff application as it is monitored by Corvis-ST. Also, the Figure highlights the first and second appplanation ¹⁸⁵

2.3 Sclera Biomechanics

An eye that is able to see far away images sharply is referred to as emmetropia. Emmetropization is the process the eye adjusts its axial length to the focal length during childhood. ¹⁸⁶ Myopic eyes in comparison to the emmetropic ones are known to have elongated sclera. This prevents the eye to focus the light on the retina and causes blurry vision. Posterior sclera elongation is reported to be the cause of changes in axial length. ¹⁸⁷ Myopia as the most common refractive error roughly affects 23% of the world population and estimated to increase to over 50% by 2050. ¹⁸⁸ In addition to myopia, other diseases such as glaucoma, retinal detachment, and macular degeneration relate directly to sclera biomechanics. ¹⁸⁹⁻¹⁹² Hence knowledge of sclera biomechanics became necessary for tackling these unmet clinical needs.

The sclera was found to be the primary load-bearing avascular tissue between the cornea and the optic nerve that provides structural stability against intraocular and extraocular forces. IOP is an intraocular force, and extraocular forces include saccades, muscle forces and blinking. Structural stability should be maintained to allow the retina to receive the light rays in the correct locations to enable clear vision.¹⁸⁷ Studies showed that the thickness of the sclera varies from one location to another, but it is thinnest around the equatorial and thickest at the posterior pole.^{118,193} Majority of the sclera tissue is made of water (68%) followed by collagens (29%) proteoglycans, elastin and other proteins.¹⁹⁴ The distribution of collagen fibres in the sclera does not follow any pattern, and this randomness resulted in opaque material. Due to this randomness, simulation of microstructure based numerical models of sclera has become more complicated.^{195,196}

It was found that the nature of collagen fibres and their structure results in the tissue behaving in a nonlinear manner similar to the cornea. This means the increase in strain leads to an increase in stiffness. Understanding sclera biomechanics is essential to evaluate the eye globe responses to surgeries, tonometric pressure, IOP, extraocular muscles and fat, and better understand diseases and conditions such as retinal detachment and glaucoma. An ex vivo experimental study on 36 human scleras obtained the material behaviour, thickness variation and correlation of sclera with age.¹¹⁸ The current thesis is relying on the information obtained from this study to simulate sclera behaviour. Although the variation in localised stiffness of the sclera has no impact on the outcome of this thesis, still sclera is considered age dependant and split into three different regions. More on this is explained in chapter three, section 3.3.5.

2.4 Keratoconus

Keratoconus was first identified by Nottingham in 1854 and was distinguished from other ectatic diseases.¹⁹⁷ After more than 160 years of research, the pathogenesis of this disease remains uncertain. Today it is diagnosed by the steepening and thinning of the cornea through the study of corneal topography and remains the most common ectatic disorder. If not diagnosed and controlled, continuous progression of keratoconus can lead to visual impairment. In this section, a review of relevant literature is provided.

2.4.1 Epidemiology

There are many studies conducted on the epidemiology of keratoconus with significant variations. These variations may be subjected to geography, time and inhabitants factors. Keratoconus with an incidence rate below 1/2000 was classified as a rare disease.^{73,198} The prevalence varies from one country to another and is summarised in Table 2-1. A meta-analysis concluded that the rate of 138/100,000 is the global prevalence for keratoconus. The data suggest a higher prevalence in Asian backgrounds.¹⁹⁹

Table 2-1 Prevalence of KC based on the geographical positions

| Country | Prevalence (out of 100,000) |
|---|-----------------------------|
| Russia (Gorskova and Sevost'ianov ²⁰⁰) | 0.2 |
| UK (Pearson, et al. ²⁰¹) | 4.5 |
| Macedonia (Ljubic ²⁰²) | 6.8 |
| Japan (Tanabe, et al. ²⁰³) | 17.3 |
| Finland (Ihalainen ²⁰⁴) | 30 |
| UK Asians (Pearson, et al. ²⁰¹) | 32.3 |
| South Korea (Hwang, et al. ²⁰⁵) | 37.4 |
| US (Kennedy, et al. ¹⁹⁸) | 54.5 |
| Denmark (Nielsen, et al. ²⁰⁶) | 86 |
| Netherlands (Godefrooij, et al. ²⁰⁷) | 265 |
| France (Santiago, et al. ²⁰⁸) | 1190 |
| New Zealand (Papali'i-Curtin, et al. ²⁰⁹) | 520 and 2250 |
| Isreal (Millodot, et al. ²¹⁰) | 2340 |
| Iran (Hashemi, et al. ²¹¹) | 3300 |
| Lebanon (Waked, et al. ²¹²) | 3300 |
| Saudi Arabia (Netto, et al. ²¹³) | 4790 |

2.4.2 Histopathology

Studies showed that the pathology of KC could be identified from three categories of (1) stroma layer thinning, (2) changes in Bowman's membrane and (3) deposition of iron in the epithelium (basal layer). ⁷³ The thickness of epithelium is the centre of discussion as some reported thinning, others reported thickening and one study suggested a pattern can be identified in KC eyes' epithelium. ²¹⁴⁻²¹⁶ It is reported that the Bowman's membrane is distorted through penetration of collagens from stroma or the cellular elements from the epithelium. ²¹⁷⁻²¹⁹ In stroma collagenous lamellae and keratocytes are reduced, followed by widening and flattening of lamellae and degradation of the collagenous matrix by non-keratocyte cells. ^{219,220} This results in softening of the tissue as stroma occupies around 90% of corneal tissue. In advanced KC, damage to Descemet's membrane and stromal edema is reported. ²²¹ In advanced stages, vision is severely influenced due to irregular astigmatism, high myopia and corneal scarring, among whom 12% to 20% have to undergo corneal transplants. ^{72,222-225}

2.4.3 Biomechanics

The above-described microstructure changes in corneal tissues are expected to lead to changes in corneal biomechanics. Various studies using ORA showed that Corneal Hysteresis (CH) and Corneal Resistance Factor (CRF) reduced in KC. ^{38,226} Also using Brillouin Microscopy, it was demonstrated that there was a reduction in longitudinal tissue modulus. ¹⁵⁰ Further studies conducted on the Corvis ST showed that the Dynamic Corneal Response (DCR) parameters related to corneal biomechanics had lower values

in comparison to healthy eyes.²²⁷⁻²²⁹ These studies suggest softening of the cornea with KC progression. However, it remains unclear that when the biomechanical alteration starts to occur. This requires longitudinal studies of tissue stiffness across the corneal surface of patients who have not yet developed KC signs. No study has been found to cover this area.

2.4.4 Aetiology

Genetic factors have been studied and identified to be the reason for keratoconus in some cases.²³⁰ A recent study estimated that those who had KC in their ancestor have a prevalence of 15% to 67% higher than the general population.²³¹ There are studies conducted to identify the mode of inheritance, but it is still not clear.²³²⁻²³⁴ There are several environmental factors identified to be highly correlated with KC. Demography data of patients with KC indicated that the disease starts in adolescence and young adulthood (as early as 4) and develops during the second decade. The earlier the disease starts, the more rapid its progression is expected to be.²³⁵⁻²³⁸ KC development is reported in older patients. The predominance of gender in KC varies significantly as in the UK the M/F ratio reported being 3.34 for Caucasians and 1.63 for Asians, 1.33 in the US, 0.58 in Iran and 0.29 in India.^{201,211,225,239,240} Eye rubbing was also traditionally identified as a risk factor, and some studies reported that eye rubbing causes a faster progression of the disease.^{197,241} It remains unclear whether eye rubbing has any influence at all or it remains as a secondary or primary cause of KC. One study concluded that the contact lens movement in the cornea, especially alongside eye rubbing, can promote KC progression.²⁴² Other causes of the disease reported in the literature include inflammation and atopy, exposure to UV light, body weight, pregnancy and hormones.^{199,243-249}

2.4.5 Morphology

Characterisation of keratoconus is based on the morphology of the anterior corneal surface. Most keratoconic corneas have a cone that is higher and steeper than the natural corneal surface. The characterisation of cone became a tool to categorise corneas.^{245,250} For instance keratometry value higher than 46 diopters are considered as KC.²⁵¹ Literature concluded that 72% of cones are in the mid-periphery region and around 25% in the central region.²⁵²⁻²⁵⁴ The posterior surface movement starts at incipient phases of KC then leads to the thinning of the cone area.²⁵⁵ One study looked at the correlation between the corneal radius, shape factor, thinnest point and power of anterior and posterior surfaces. This study concluded an excellent correlation between two surfaces in the 61 eyes that were studied.²⁵⁶ another study compared the spherical power and astigmatism on the anterior-posterior surface of 31 patients and concluded that the posterior surface must be observed for better diagnosis.²⁵⁷ Clinicians find the interpretation of cone data to be difficult using available information reported by topography machines.^{258,259} There is only one parameter that was introduced with the

ability to detect the location and magnitude of the cone called CLMI (Cone Location and Magnitude Index). This algorithm works by searching a circular area with a defined radius on the surface of the cornea. At any location, the circle is comparing the curvature of the cornea with a mirrored location on the other side of the cornea. If the difference between curvature of these two locations are large, it is identified as abnormal area. This method is susceptible to other irregularities on the surface of the cornea such as astigmatism.^{260,261}

2.4.5.1 Cone location and shape

A study conducted on 827 KC patients using photokeratoscope reported steepening on mid-peripheral corneal at early stages of the diseases with a tendency to be located towards temporal and inferior sides, Figure 2-8. As the disease progressed in these patients, an egg-shaped ring was formed around the central part of the cornea and steepening progress to the periphery and inferonasal quadrant.²⁶² With technology advancements and the use of digitalised videokeratoscope another researcher conducted a similar study on 14 KC eyes. Through comparison of power maps, the asymmetry between paired eyes and steepness of central cornea was confirmed. The curvature of inferior and superior sides found to be significantly different, with an average of 8 diopters higher than healthy. A superimposed irregular bowtie shape was proposed as a diagnosis observation in KC eyes.⁷⁶ The topography of 62 KC eyes collected using photokeratoscope indicated that 72% of patients had peripheral cones that could reach limbus and were bound to two quadrants. The remaining had central cones, and paired eyes showed significant non-superimposable symmetry. Interestingly paired eyes showed variation in the power with a mean difference of 8.2 ± 6.0 D in apex power and 4.3 ± 2.7 D in cylindrical power. In this study majority of cones were located in inferonasal side in contradiction to the previous study.²⁵² Another study showed no influence of contact lens wear on topography which is contradictory to what is believed today.²⁶³



Figure 2-8 The cone on the inferior side of the cornea of a patient with advance KC²⁶⁴

Unilaterality incidence attracted attention and a study relied on 164 moderate to advanced KC cases and concluded low incidence rate and found even those who are initially unilateral, progress to bilateral with disease advancements. This limited performing refractive surgeries on the fellow healthy eyes.²⁶⁵ These eyes that show no sign of KC are diagnosed as Forme-Frust KC (FFKC).^{266,267} Later, age was found correlated with the shape of the cone in a study that recruited 251 patients with 482 KC eyes. This study concluded bowtie power maps for younger (<21 years), inferior cone for middle-aged (21-40 years) and inferotemporal cone for older (>40 years) groups. With a higher occurrence rate (7-20%) for cones on the temporal side, the study suggested attention to this area, especially in the younger group.²⁶⁸ The power maps became increasingly important, and keratoconus suspect corneas were identified by a bowtie posterior or localised anterior steepening shapes using Placido.^{269,270} With advancements in topographer a study using Orbscan IIz (Bausch & Lomb Surgical, Rochester, NY) and OPD-Scan (Corneal Navigator; Nidek Co., Ltd.) showed variation in thickness from the thinnest point to the periphery to be significant between FFKC or KC and healthy patients.²⁷¹ Future studies developed a number of parameters that could be used to help with the diagnosis of KC. Hence many recent studies looked at correlations of these parameters with the shape of the cornea or KC stage.²⁷²⁻²⁷⁷

2.4.6 Management of KC

The review of the literature showed that various grading systems were developed to identify the KC stage. The most common one is Amsler-Kurmeich which classified based on the amount of astigmatism and myopia, corneal scarring or thickness and central power.²⁷⁸ The use of KSS (Keratoconus Severity Score) which is based on root mean squared of the power of the cornea and Shabayek-Alio which is based on analysis of higher-order aberrations are also used often in the literature.^{279,280} Treatment monograms are also developed to work with various grading systems to standardise the procedure and improve management. However, a standard approach is not yet being followed or found to be reliable for this purpose, and the goal of an ophthalmologist is to enhance vision and stop vision loss. In this section, various management techniques are discussed.

2.4.6.1 Contact Lenses and spectacles

It is advised that at the early stages of the disease, spectacles can be provided to improve the vision. However, once cornea develops irregular astigmatism, spectacles would not be suitable and contacts being offered to patients.²⁸¹ Researchers found that at the early stages, Toric soft lenses could provide enough correction for astigmatism and myopia. As the disease progresses, more special lenses such as Rose K, piggy-back, hybrid or scleral lenses are needed to correct the vision. However, due to the irregular shape of the cornea, patients may experience discomfort in wearing them.^{282,283} It is reported that

contact lenses can improve the vision even after corneal grafting, crosslinking or ring implantation.^{281,284}

2.4.6.2 Collagen Crosslinking (CXL)

This invasive method of controlling KC progression relies on UVA interaction with topical riboflavin (vitamin B) for 30 minutes to form new bonds among collagen fibrils, Figure 2-9. One study reported an increase of nearly three times after CXL on strips of the porcine cornea.¹¹⁷ A number of studies suggested improvement of corneal ectasia and safety in the long term, which led to the recommendation to use it for younger patients who are at higher risk of progression.²⁸⁵⁻²⁹² The standard CXL method is Dresden Protocol and is suitable for corneas with a minimum thickness of 400 microns. In advanced KC cases, the thickness may fall below this limit, and other methods such as hypo-osmolar riboflavin solution are used to avoid endothelial cell loss.^{288,290,293} The procedure can be done with both epithelium on and off; however, the former is not recommended, and inconsistent results were reported.²⁹⁴⁻²⁹⁶ New protocols increase the irradiation intensity and reduce the time of CXL to reduce patient discomfort. These new methods are also found to be effective in controlling progression.^{297,298}

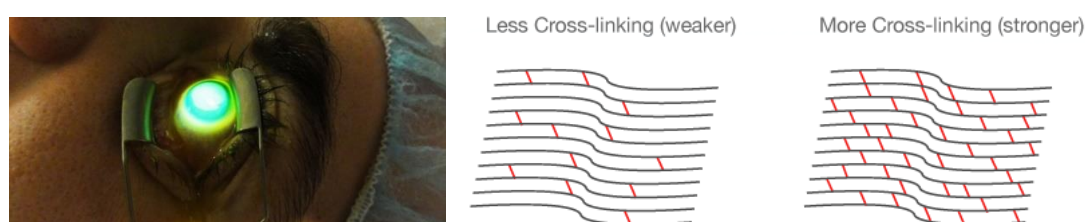


Figure 2-9 Collagen cross-linking application on the patient under UVA and the schematic view of structural changes between collagen fibrils²⁹⁹

The complications associated with CXL include infection, edema, haze and rarely melting despite the fact that the success rate is very high.³⁰⁰⁻³⁰⁵ To increase the efficiency of CXL, it is combined with other procedures including PRK, LASIK, Intacts, thermal keratoplasty and orthokeratology.^{290,291,306-308} The amount of stiffening in CXL is varying significantly from one study to another. Two studies on 23 and 17 enucleated porcine eyes tested under inflation reported a 58% increase in young's modulus.^{309,310} Another study also done with inflation on 4 human corneas reported an 80% increase in anterior cornea and a 90% increase in the posterior cornea after standard CXL.³¹¹ Using atomic force microscopy on 12 pairs of cadaver human eyes showed a 90% increase in Yong's modulus following Dresden protocol.³¹² Another study on 14 porcine eye globes using ultrasound showed an increase of 5% in stiffness after CXL.³¹³ Finally, a study on 72 porcine cornea strips showed a 30% increase when stress-strain curves were compared.³¹⁴

2.4.6.3 Corneal rings

Vision correction for both myopia and KC can also be achieved through the flattening of the cornea. For this reason, Intrastromal Corneal Ring Segments (ICRS) made of polymethyl methacrylate (PMMA) were developed to be implanted in the stroma, Figure 2-10. In addition to flattening, in KC cases, ICRS can also prevent further deformation of the cornea.³¹⁵⁻³¹⁷ Clinicians choose implants when contacts and spectacles do not work, and visual acuity is reduced severely, but patients have a clear cornea, CCT above 400 microns and age 21 or older. It is possible that the implant penetrates through the cornea in some cases, and if this happens, keratoplasty is the only option to restore vision.³¹⁸ Stable results achieved in 3 to 12 months postoperatively.³¹⁹ A study on 12 patients who developed ectasia after LASIK operation concluded the depth of 60% to 80% is suitable for implants to achieve desired flattening.³²⁰ The commonly used types of ICRS are Intacs (Addition technology Inc., IL, USA), Keraring (Mediphacos, MG, Brazil) and Ferrara Rings (Ferrara ophthalmics, MG, Brazil). The challenge in selecting suitable corneal rings remain untackled as it relies on clinicians experience and monograms do not always lead to a desirable outcome. ICRS can also be combined with other procedures such as PRK and CXL.³²¹⁻³²³ There are other types of implants that include MyoRing as intracorneal continuous rings and Phakic Intraocular lenses.^{324,325}

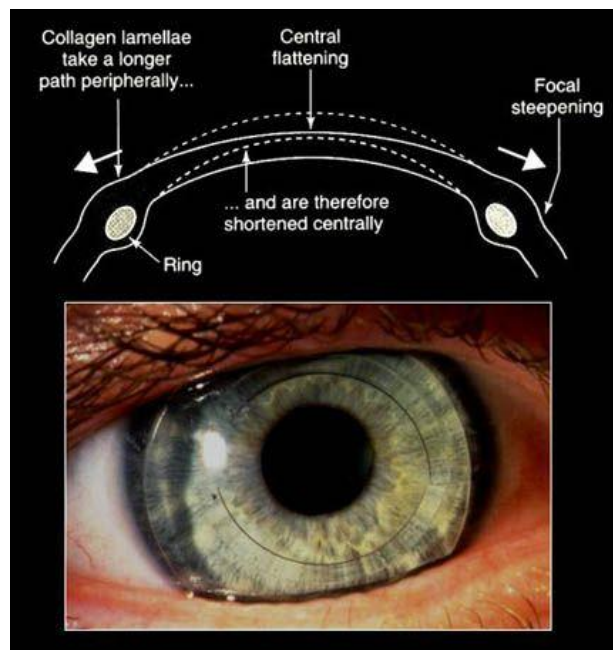


Figure 2-10 The Intacs ICRS on the cornea and its position in the cross-sectional view.³²⁶

2.4.6.4 Corneal transplantation

If necessary results cannot be achieved using other methods, the last option is to go with corneal transplants. It is reported that the surgery is being conducted on less than one-fifth of KC patients, and among them include age over 70 years old.^{327,328} Most patients achieve good vision with spectacles with penetrating keratoplasty after one year, although the rejection rate was reported at 5.8% to 41% in the first 24 months.^{224,329-332}

Deep anterior lamellar keratoplasty has shown a higher success rate and lower chance of rejection which is now the standard technique for keratoconus management. In this technique, a partial thickness of the cornea is being removed and transplanted, which enables endothelium and Descemet membrane to stay intact.^{333,334}

2.5 Intraocular Pressure (IOP) and Tonometry Devices

Intraocular pressure is the only modifiable factor for managing glaucoma, and its measurement is the principal test for diagnosing this disease. Glaucoma is the second cause of blindness and the most common eye disease. It is reported that 64.3 million people between the age of 40 to 80 had glaucoma in 2013, increasing to 76 million in 2020 and by 2050 this will reach 112 million people.²² African has a higher prevalence in primary open-angle glaucoma, and Asian are higher in angle-closure glaucoma.³³⁵ In 2002, WHO estimated 4.4 million people out of 37 million were blind due to glaucoma, which was 12.3% of the blind population.³³⁶ Hence this gave significant weight to accurate IOP monitoring as part of daily clinical examinations. The commonly used tonometry devices are explored first in this section. In the second part, a critical literature review is provided to enable comparisons between their measurement techniques.

2.5.1 Commonly Used Tonometry Devices

This part reviews literature theories and the development of some of the commercially available tonometry devices. All tonometry devices in today's market are functioning based on an old concept. These theories gradually improved with technological advancements over the past 200 years, and this fascinating area of literature is explored in this section.

2.5.1.1 Applanation Tonometry

A Berlin professor, Von Graefe, invented the first indentation tonometer in 1862 that could apply a known pressure to the eyelid and measure its deformation, Figure 2-11-A. There were a few further developments of this device in the next few decades, but still, hand examination remained as the standard practice. Hand examination was less painful for the patient and a more comfortable method of examination. In 1897, Professor Hjalmar Schiøtz developed a new impression tonometer that could relate the deformation of the eye to the amount of pressure more easily and was widely used for the next 50 years or so, Figure 2-11-B. Since the tonometer was making contact, disinfection using alcohol or heat was needed before testing a new patient to avoid infectious diseases.³³⁷⁻³³⁹

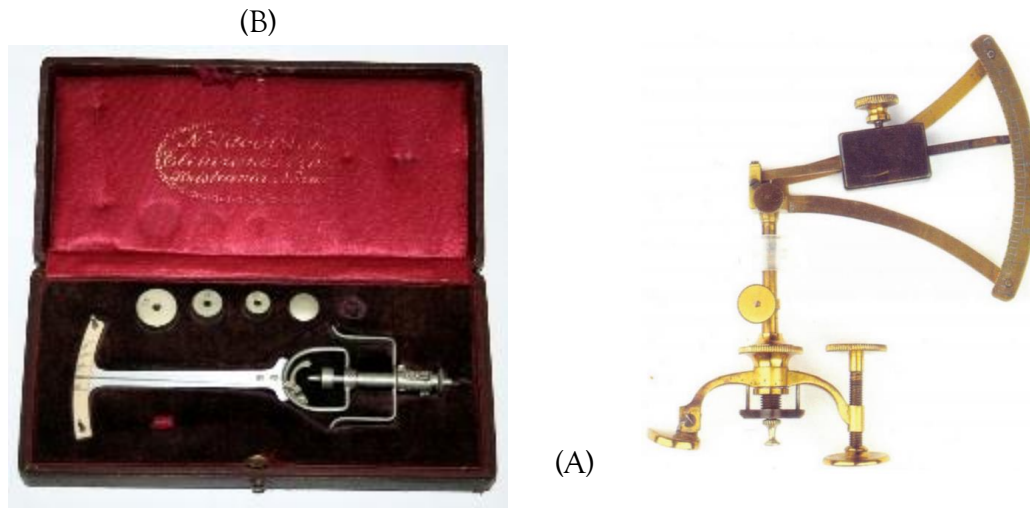


Figure 2-11 (a) The tonometer invented originally by Hjalmar Schiøtz that has various weights and could apply known pressure to the eye and measure deformations, (b) the Von Graefe tonometer able to measure IOP through eyelid in an era with no anaesthesia³⁴⁰

The gold standard applanation tonometer designed by Hans Goldmann in 1954, referred to as the Goldmann tonometer, became globally accepted and still commonly used in clinical practice, Figure 2-12.²⁹ This instrument overcomes some of the problems with other instruments such as avoiding the influence of ocular rigidity by applying it on the cornea and use of small plexiglass plate instead of metal that reduced pain and patient discomfort. This tonometer was working based on a concept that the pressure could gradually increase until flattened cornea could be achieved. Perkins Hand Held Applanation Tonometer introduced in the 80s is similar to the Goldmann tonometer (GAT) with the difference of being portable.³⁴¹ In 1988 the digital handheld and portable version of indentation tonometry was invented, called Tonopen. This device had the advantage of having a smaller tip that could be more suitable for abnormal corneas. The downside is that this reduces reliability and multiple measurements (4-6) are required to ensure an accurate reading.³⁴² All these tonometers function based on a simple concept.³⁴³ They follow the Imbert-Fick principle which says the pressure inside a dry sphere with a thin wall is equal by force required to flatten a surface divided by the area of the surface, Equation 2-3.³⁴⁴

$$P = \frac{F}{A}$$

Equation 2-3

where P is the pressure in N/mm^2 , F is the force in N , and A is the area in mm^2 . Considering this theory assumes dry, perfectly spherical and infinitely thin wall; its application to measure intraocular pressure will lead to inaccurate measurements. In this theory, a surface area of 3.06 mm^2 was calculated to cancel the rigidity of corneal thickness (assumed 520 microns in this case) and the attraction of tear meniscus.³⁴⁵ As a result, this is the area used in applanation tonometry to flatten the cornea. In clinical

practice, patients have a different corneal thickness, rigidity and curvature, and these factors influence accuracy. These inaccuracies in measuring IOP, contribute to high statistics of undiagnosed or misdiagnosed glaucoma patients to remain at 50% of all glaucoma patients.^{346,347} One major issue with the use of Goldmann is the application of local anaesthetic and fluorescein before starting the examination. Also, the measurements are influenced by human errors as the process is entirely manual.³⁴⁸

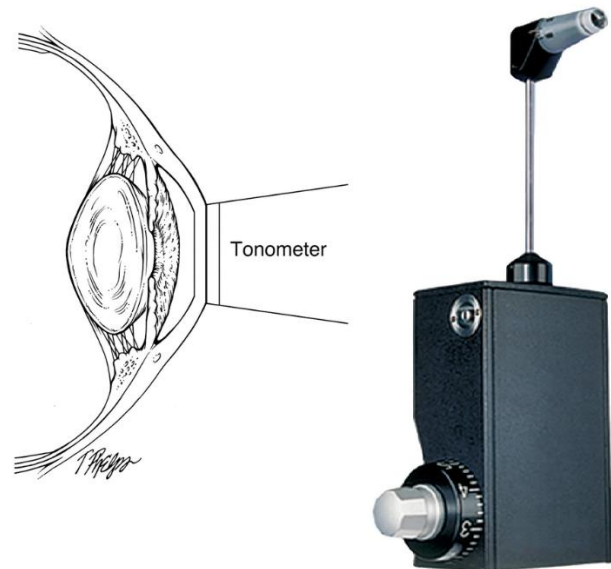


Figure 2-12 Goldmann tonometer and the position of the flattened cornea after the force is applied³⁴⁹

2.5.1.2 Dynamic Contour Tonometry (DCT)

DCT was developed to overcome problems associated with the deformation of the cornea. This tonometer was found to be less correlated with corneal biomechanics as the cornea does not need to deform. It provides a continuous measurement that lasts for 6 seconds. Different from applanation tonometry, this tonometer is based on the law of hydrostatic pressure by Blaise Pascal. It says in gasses and liquids, the pressure is constant and is applied to all boundaries perpendicularly.³⁴⁸ The tonometer is made of 7mm ring that matches the topography of an average cornea. The device applies a small pressure to force the cornea into its curvature of 10.5 mm, and a small piezoelectric sensor in the centre of the hollow tube measures the pressure accurately, Figure 2-13.³⁵⁰ This pressure is measured from the outside and assumed to be equal to internal pressure. This device is among the most accurate tonometry techniques available in the market. It requires the application of a local anaesthetic but is independent of human errors as the process is semi-automated. The significant drawback is the duration of each measurement, which takes over 2.5 minutes, and most patients require more than one readings.³⁵¹

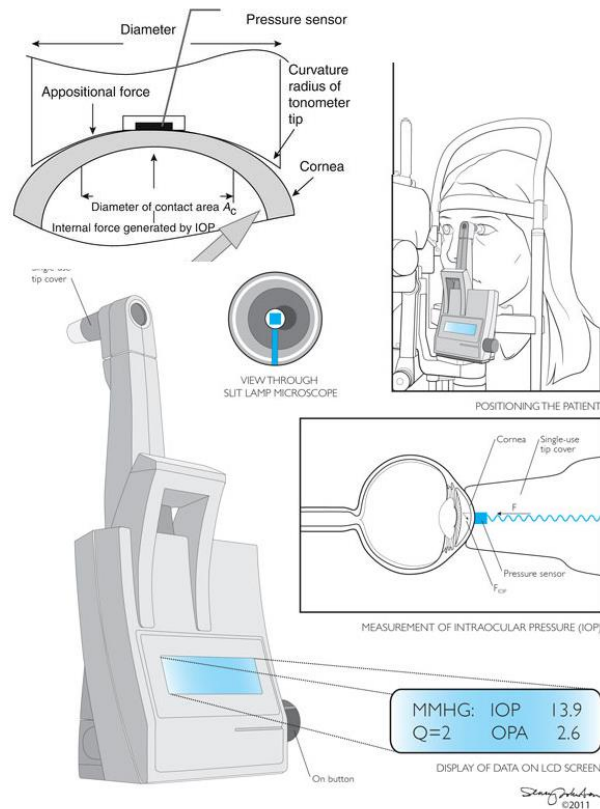


Figure 2-13 The DCT tonometer and the methodology of measuring pressure using this device ³⁵²

2.5.1.3 Non-Contact Tonometry

By introducing the non-contact tonometry, routing glaucoma screening became more feasible. One of the earliest non-contact tonometry systems is AO NCT (American Optical) introduced in 1972. This device applied a burst of air to the cornea to deform the cornea and measured the pressure at which the cornea reached first appplanation. The need for contact with the cornea was eliminated that led to a negligible retraction of the eyelid. The only discomfort is the noisy nature of the burst, which causes the patient to blink. Before measurement begins, the patient is asked to look at a fixation light to ensure proper alignment with the corneal surface. ³⁰ Keeler Pulsair, introduced in 1986, was among the most commonly used tonometers that eliminated the need for specialist staff to use it. ³⁵³ As part of the modern non-contact tonometries, Ocular Response Analyser (ORA) and CorVis ST have attracted attentions and discussed next.

2.5.1.3.1 Ocular Response Analyser (ORA)

ORA is not only able to measure IOP, but also provides insights into corneal biomechanics. Traditionally, in non-contact tonometry, an electro-optical sensor identifies the flattened time. In ORA, made in 2005, both inward and outward corneal movements are being monitored, Figure 2-14. This new information could provide insights into the viscoelasticity of the cornea. The differences in time between the first and second applications is called corneal hysteresis, and the comparison velocity

provides corneal resistant factor (CRF).³⁵⁴ Although IOP measurements in ORA are correlated with corneal biomechanics, they are not identical to GAT.³⁵⁵⁻³⁵⁷ The measurement takes a few milliseconds, and as a result, it is shown to be influenced by ocular pulses and cardiac cycles.³⁵⁸

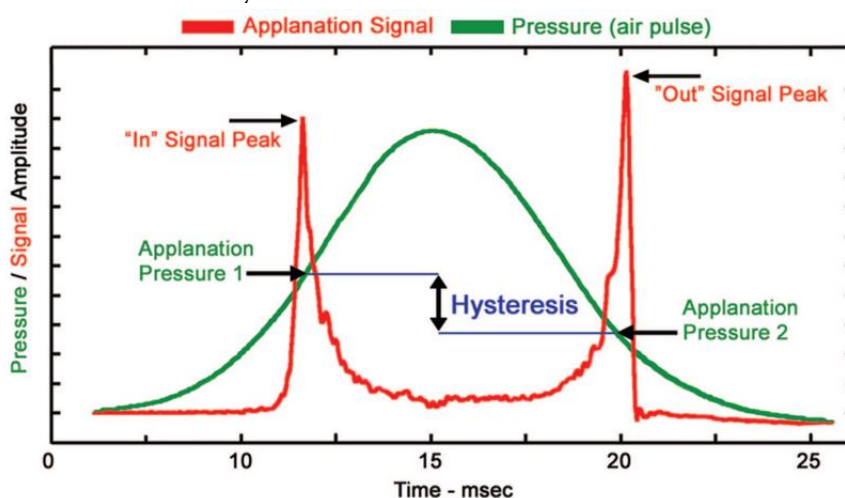


Figure 2-14 The methodology followed by ORA to estimate IOP and corneal biomechanics³⁵⁹

2.5.1.3.2 Corvis ST

The more detailed investigation into the dynamic corneal response (DCR) to the air puff became possible with Corvis ST. This device was made in 2010 and using a high-speed camera able to take 4330 frames per second, DCRs information could be accurately obtained. This camera is based on the Scheimpflug principle and can cover 8.5 mm of the horizontal corneal cross-section.³² This principle is commonly used in corneal topography mapping. Corvis ST can provide information from the posterior surface of the cornea, which enables measurement of the thickness. Extensive research has been conducted to produce parameters able to analyse corneal biomechanics and provide more accurate IOP measurements. Among these parameters, biomechanically corrected IOP (bIOP) and Stress-strain index (SSI) provide crucial information.^{104,181,360} Corneal Biomechanical Index (CBI) is able to separate between healthy and keratoconus.²²⁸ Stiffness Parameter (SP) is able to measure the overall stiffness of the cornea.³⁶¹

2.5.1.4 Continuous Tonometry

Research showed that IOP changes throughout the day. Hence continuous measurement of IOP is required to accurately diagnose patients who are likely to develop glaucoma. Sensimed Triggerfish claims to be able to monitor pressure for 24 hours and wirelessly communicates and transfers information, Figure 2-15. This device is placed on the cornea like a contact lens and monitors changes in the pressure. It records 144 readings during 24-hour use.^{362,363} Since this device measures the changes in the curvature of the cornea, IOP measurements are not very accurate.³⁶⁴ At the moment, this device is rarely used in clinical practice. A wireless intraocular pressure transducer

is another way of obtaining continuous measurement. However, this device requires a surgical procedure to be implanted and is only prescribed for patients with glaucoma who are in danger of having their optic nerve head damaged due to fluctuations of IOP.

365

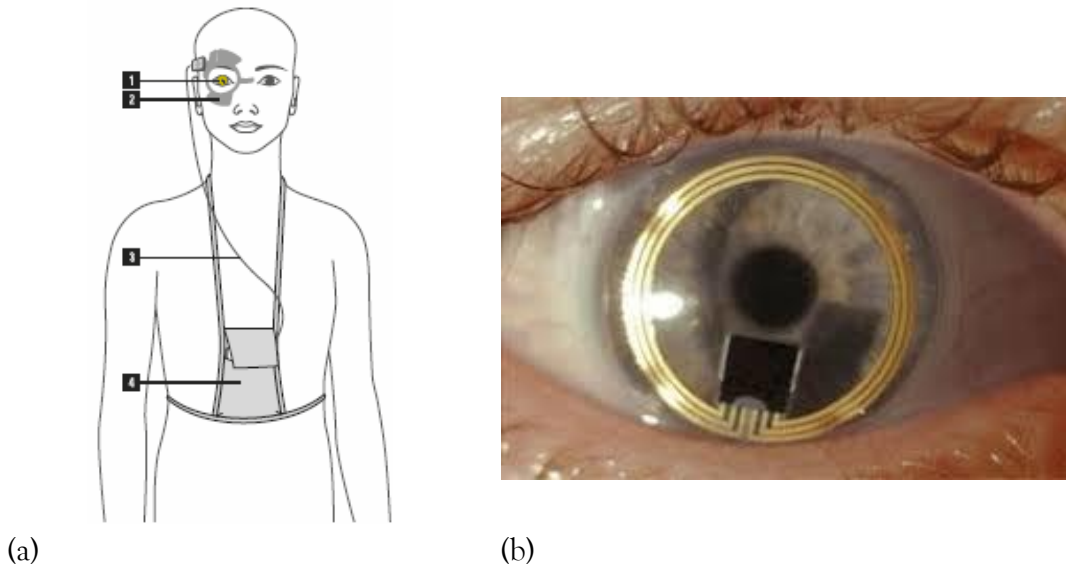


Figure 2-15 Sensimed Triggerfish contact lens (a) setup³⁶⁶ and (b) device³⁶⁷

2.5.2 Tonometry Methods Comparison

A study conducted on 59 patients out of which 36 cases had glaucoma compared Corvis ST (CVS) IOP with GAT. They found CVSIOP 18.9 ± 5.8 mmHg and GAT 20.3 ± 5.7 mmHg with no statistically significant differences between them.³² At this time, CVS was recently launched, and the tonometer performed similarly to contact applanation tonometry. DCT was found to be more repeatable than ORA and GAT, while the IOP values from the three devices were not interchangeable.^{355,368} NCT was found to be correlated with CCT more significantly than GAT. Since NCT is influenced by ocular pulse amplitude, multiple measures were needed.^{369,370} GAT is most accurately represent the IOP of corneas with CCT 520 microns.^{24,371} Knowing CCT varies significantly by diseases and ethnicity, many patients were misclassified as normal-tension glaucoma with GAT.^{372,373} For instance, Caucasian corneas CCT estimated between 580 to 600 microns, whereas African American was around 520 to 540.³⁷⁴ Patients with Ocular Hypertension were found to have CCT greater than 600 microns which could lead to a higher estimation of IOP using GAT.³⁷⁵ Every 10 microns increase in CCT was found to affect IOP measurements in healthy corneas using GAT between 0.18-0.24 mmHg.³⁷⁶

CCT is important in diagnosing primary open-angle glaucoma patients as it was found that with disease progression, corneal thickness reduces.³⁷⁷ On the other hand, patients

who undergo LASIK surgery found to have lower GAT IOP and the reduction in IOP was correlated to the amount of correction.³⁷⁸ GAT requires calibration and a study on 132 GAT tonometers found only 4% of them were calibrated to an acceptable tolerance of ± 0.5 mmHg.³⁷⁹ A study used GAT and DCT on 39 patients who undergo LASIK for myopia and concluded GAT reduced significantly postoperatively by 3.0 ± 1.9 mmHg while no significant changes were found in DCT (-0.2 mmHg ± 1.5 mmHg).³⁸⁰ Comparison of GAT, ORA and DCT showed that both DCT and GAT were able to provide repeatable findings with coefficients of 2.3 and 2.2 mmHg respectively. ORA corneal compensated IOP (IOPcc) measurements had higher repeatability coefficients of 4.3 mmHg and it is believed to be due to high correlation with ocular pulse amplitude. GAT underestimated IOP in comparison to DCT and ORA by around 2 mmHg. In this study DCT had the most repeatable results.³⁸¹ Another study conducted on 694 subjects using GAT, DCT and ORA found the mean IOP for GAT to be 14.1 ± 2.8 mmHg and for ORA IOPg and IOPcc to be 15.9 ± 3.2 mmHg and 16.6 ± 3.2 mmHg respectively and DCT to be 16.9 ± 2.7 mmHg. In this study, DCT again showed the smallest standard deviation among all three, followed by GAT. The values of IOP found not to be interchangeable.³⁸² The high value of IOPcc in normal-tension glaucoma patients suggested that the value of IOP may be underestimated using GAT, DCT and IOPg.³⁸³

In a comparison of four devices on 76 healthy subjects, GAT, ORA, DCT and CSV values were respectively found to be 15.62 ± 2.33 mmHg, 15.99 ± 3.58 mmHg, 17.44 ± 2.51 mmHg and 17.24 ± 3.44 mmHg. In this study, GAT and ORA plus CSV IOP and DCT were found to be not significantly different.³⁸⁴ CVS IOP was also found to be less affected with LASIK in comparison to GAT (3.4 mmHg), IOPcc (1.0 mmHg) and IOPg (3.8 mmHg).³⁸⁵ Another study on healthy patients found similar values between GAT (15.5 ± 2.8 mmHg) and CSV IOP (15.4 ± 2.8 mmHg). In 2015 a new biomechanically corrected equation (bIOP) was introduced for CSV. The bIOP reduced the correlation of measurements with CCT and Age (stiffness) when compared to non-corrected IOP values.³⁸⁶ With some further improvement, the equation was applied to 14 LASIK and 22 SMILE corneas and compared with GAT. This study found the IOP decrease with GAT in both surgeries by -3.2 ± 3.4 mmHg and -3.2 ± 2.1 mmHg respectively, while the same comparison for bIOP was 0.1 ± 2.1 mmHg and 0.8 ± 1.8 mmHg.³⁶⁰ Later bIOP was validated experimentally and was found to estimate values close to the true IOP (0.3 ± 1.6 mmHg, $P = 0.989$) and better than the non-corrected CSV IOP equation (7.5 ± 3.2 mmHg, $P < 0.001$).¹⁰⁴

Although the bIOP equation performed reasonably well in most cases, it was still underestimating IOP in keratoconic corneas. Hence a new equation was developed to be used on these eyes and termed IOP for soft corneas or bIOPs. This equation had the mean IOP in KC eyes similar to the healthy with no statistically significant differences.³⁸⁷ Comparison of bIOP to GAT in patients with OHT and OAG in 122 eyes found overall bIOP (15.2 ± 3.0 mmHg) was higher than GAT (14.1 ± 3.2 mmHg) and concluded

that it is less affected by corneal biomechanics.³⁸⁸ Another study in 94 healthy subjects compared bIOP with GAT and ORA. They found bIOP to be 16.11 ± 1.66 , which in comparison to both GAT (3.02 ± 2.60 mmHg) and IOPcc (1.09 ± 1.96 mmHg) had higher values.³⁸⁹ The comparison of four tonometry devices of GAT, DCT, ORA and CSV in healthy subjects found respective IOP values of 12.9 ± 2.4 mmHg, 16.1 ± 2.6 mmHg, 15.6 ± 3.3 mmHg and 13.5 ± 2.4 mmHg. This study concluded that bIOP is more close to GAT in comparison to ORA and DCT.³⁹⁰ bIOP was found to have good repeatability in healthy and KC eyes, although the mean value in KC eyes was lower than in the healthy group.³⁹¹

DCT was found to be less correlated with CCT than GAT, although the correlation was still significant.³⁹² Another study showed poor correlation with CCT in DCT ($r^2=0.01$, $P=0.017$) compared to GAT ($r^2=0.28$, $P<0.001$). Both devices showed a weak correlation with age and statistically not significant.³⁹³ ORA found to better compensate for changes in CCT than GAT as well.³⁹⁴ Another study found no association between CCT and IOPcc in the healthy group.³⁹⁵ ORA and GAT both showed significant correlations with corneal curvature.³⁹⁶ CCT was found to be correlated in GAT, ORA, NCT and DCT in a recent study. Although DCT seems to be more correlated with the corneal radius.³⁹⁷ The bIOP was showed to be less affected by CCT and Age.³⁶⁰

2.6 Concluding Remarks

This chapter aimed to review the literature relevant to this study. Discussions were kept for the final chapter of this thesis, and only what was found in the literature was presented. It provided a review of ocular biomechanics with more focus on the cornea. After presenting the findings on material behaviour including age dependency, scientific methods for measuring corneal biomechanics both in vivo and ex vivo were reviewed. It then progressed to keratoconus and covered a review in all the aspects of the disease, including morphological and biomechanical changes and management techniques including corneal crosslinking. It then reviewed studies related to the IOP and the field of tonometry and errors associated with IOP measurements. A critical comparison between commonly used tonometers was also provided.

As it was shown in this chapter, IOP measurements are influenced by corneal biomechanics and geometry. This is evident as patients with keratoconus and corneas after refractive surgeries consistently were measured with lower IOP. Non-contact tonometers with the ability to monitor the deformation of the cornea could also provide insights into corneal biomechanics. Hence this extra information was used to improve the accuracy of IOP measurements. Corvis ST introduced the new bIOP equation which at the moment is a measurement least associated with corneal biomechanics followed by DCT. This bIOP equation, however, still did not work well on patients with KC and a new equation was developed to measure IOP for these patients called bIOPs. However,

this method did not make it to the Corvis ST. This thesis develops a new bIOP equation and a universal method of measuring IOP that is not/weakly influenced by confounding factors.

On the other hand, biomechanical parameters obtained from Brillouin microscopy, ORA and Corvis ST were discussed in this chapter. ORA parameters that are CH and CRF showed to provide insights into biomechanical changes in the cornea; however, they are both correlated with IOP, biomechanics and geometrical factors. Brillouin microscopy works by the light reflections from corneal molecules and measures the corneal longitudinal modulus. Since no deformation is applied, until today, this device has been unable to estimate corneal mechanical behaviour and is more suitable for comparative studies or disease diagnosis. Corvis ST introduced several biomechanical parameters including CBI, SP and SSI as discussed in this chapter. SSI is the only parameter that is able to estimate mechanical behaviour in-vivo, and this was only developed for healthy corneas. This thesis offers a parameter that can provide stress-strain behaviour for all corneas with various diseases and geometries.

Chapter Three

Methodology

3.1 Introduction

The methodology used in this study to achieve the goal of developing new methods for estimating intraocular pressure (IOP) and corneal material stiffness in-vivo is described in this chapter, Figure 3-1. The chapter starts with a method used to obtain properties of the cone in keratoconus patients. This method relied on elevation data collected from commercially available topographers. Cone properties obtained with this method included the cone centre location, area and height. This is followed by an introduction to the numerical models used for simulating the corneal response to air-puff tonometry, and their validation. Next, a description is provided of the information exported from analyses of the numerical models and how dynamic corneal response (DCR) parameters were calculated.

A better understanding of corneal behaviour was needed to develop equations for estimating corneal mechanical response and IOP in vivo. For this reason, parameters such as corneal geometry, mechanical properties and abnormalities due to ectatic diseases were modified and simulated in numerical models. These models were subjected to IOP followed by Corvis ST air puff pressure. The deformations of these models were analysed and DCR parameters were exported that construct the database. This large database could explain the corneal response to air puff and used to develop the required equations (to estimate both IOP and material stiffness). To develop these equations, a custom software package was produced. This software, which is explained in section 3.6, read the data obtained from numerical models, generated new parameters by combining the DCRs and through multiple optimisation methods, equations were developed.

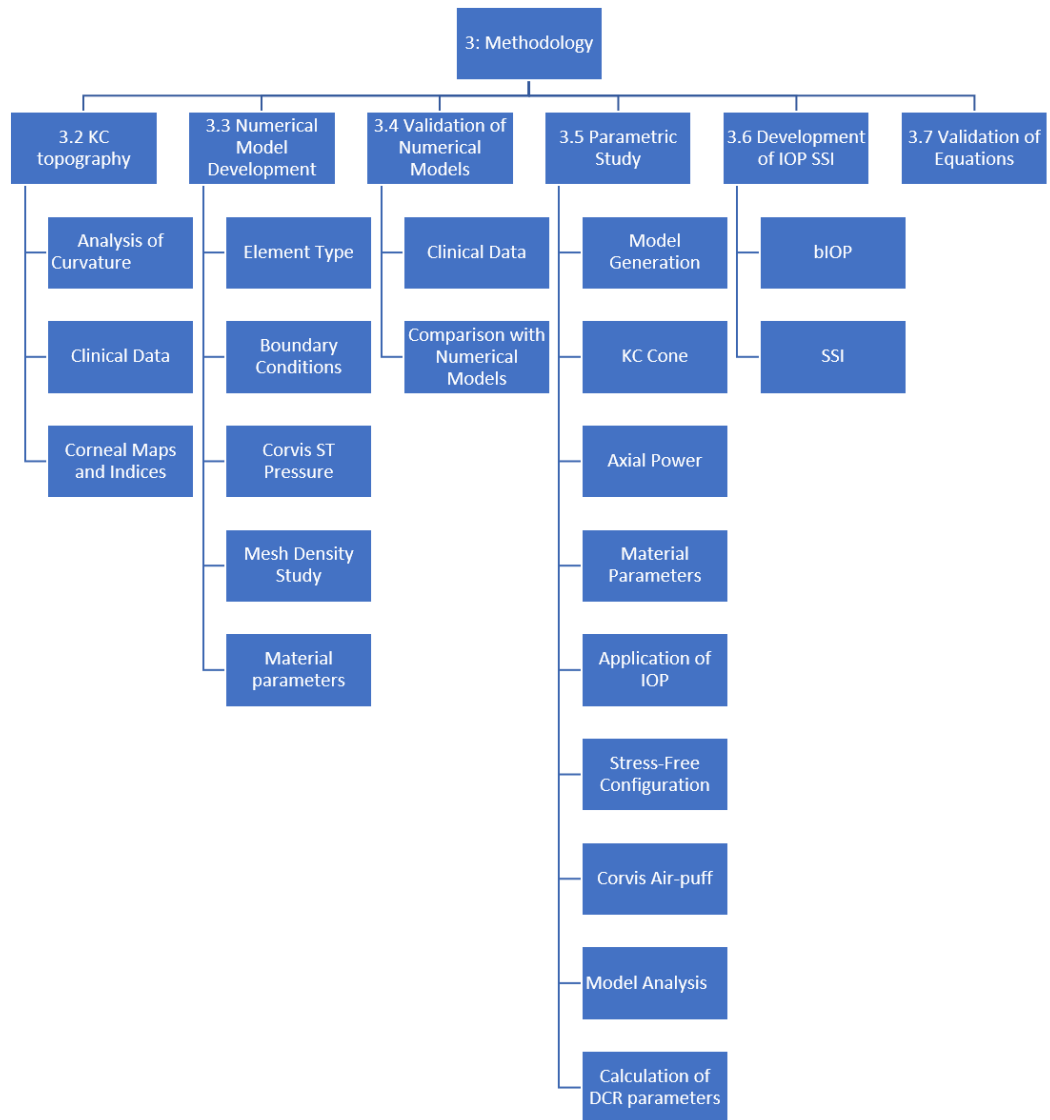


Figure 3-1 The overview of the methodology followed in this thesis. Each section is described in details in the following chapter.

At this stage, the objective was for the IOP equation to estimate actual IOP values set in the numerical models. Similarly, the material stiffness equation needed to estimate the true corneal material properties that were set in the numerical models. The optimisation continued until the differences between equations outcome, and true values were minimised. Then these equations were applied to healthy clinical data, and some final adjustments were made. These adjustments were necessary as numerical models can simulate ideal scenarios, whereas clinical data include a significant amount of noise. Through these adjustments, equations performed well in healthy clinical cases and then applied to other clinical data for validation. At the end of this chapter, an explanation of clinical data is provided. For IOP, a second equation was developed to improve the accuracy of predictions in keratoconic eyes when the topography of the cornea is known. For material stiffness, two other equations were developed to compensate for changes

in corneal biomechanics in keratoconic or corneal crosslinked eyes and the flap/cap thickness in LASIK and SMILE.

3.2 KC Topography

This section describes the method adapted to analyse the topography of keratoconic eyes in order to determine the cone height and location of cone centre and cone edge. This information was needed to enable the accurate representation of keratoconic cones in the construction of numerical models of KC eyes. This method is intended to be generic, so it can be applied to data collected from various topography machines and independent of any device-specific information. The method and its main findings were published in the *Journal of the Royal Society Interface*.³⁹⁸

3.2.1 Analysis of Curvature

A custom-built MATLAB (2018b, The MathWorks, Inc., Natick, Massachusetts, United States) code was developed to process clinical data. Initially, the raw elevation data for anterior and posterior maps were imported for all patients. Only records that had a quality score “OK” were processed. A sphere was then fitted to the central 4 mm radius of each cornea using a Matlab function, and the coordinates of the centre point and the radius of the sphere were identified. The distance from each data point on the corneal surface to the centre of the sphere was calculated. The distances were then subtracted from the radius of the sphere and the position and magnitude of the largest distance were assumed to point at the location and height of the cone centre, respectively. It was demonstrated in the literature that the radius of the cone is much smaller than the radius of the cornea.³⁹⁸ Hence in corneas with KC, the fitted sphere will not be dominated by the cone curvature. However, in rare cases the cone is so large that it dominates a large portion of the cornea, this method will be susceptible to errors.

To locate the boundary of the cone, a second derivative of the elevation data was calculated along radially extending lines from the cone centre with a fixed angle and while the relevant elevation data was determined using Matlab built-in function through triangle-based cubic interpolation³⁹⁹. As the first derivative of elevation would represent the gradient of the tangent to the surface, a second derivative represents the rate of change of this gradient. Since corneal curvature changes direction when the point of interest moves from the cone area to the surrounding healthy area, a sudden change in the sign of the rate of change in tangent gradient is indicative of an intersection with the boundary of the cone, Figure 3-2. Locating the cone boundary using this method then allowed calculating the cone area.

Once the cone boundary was identified, the cone area was removed from the topography in an iterative process. During this stage, the above procedure including a sphere fitting

and calculation of the cone properties including cone height, cone apex and cone boundary were repeated until the difference between two subsequent analyses became smaller than 1.0 micron. At this point, cone properties were recorded and used for further analysis. This procedure was repeated for both anterior and posterior surfaces for every patient.

The correlation of these cone parameters (location and height of cone apex and area of the cone) with disease severity and Pentacam keratoconus parameters were explored using the correlation coefficient 'R' and the corresponding significance value p using bespoke MATLAB code. The code was designed to analyse topography data and perform statistical analysis.

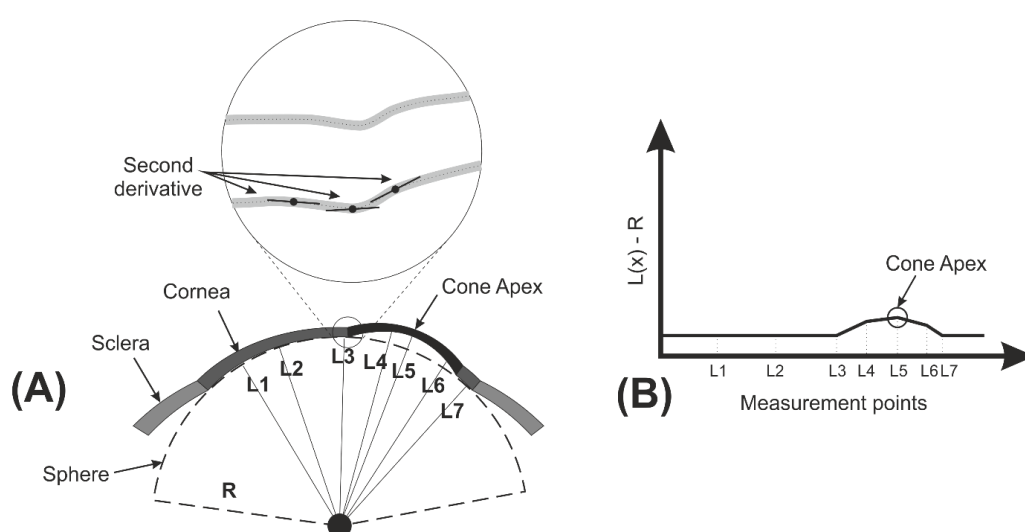


Figure 3-2 (A) The best-fit sphere of the posterior corneal surface and the distances from the centre of the sphere to multiple points on the posterior surface are calculated. The edge is detected using second derivatives of elevation and variations in the curvature of the cornea. (B) Is a graph indicating the Euclidean distance from corneal surface points to the best-fit sphere and the largest values suggest the cone height and apex location

3.2.2 Clinical Data

In this retrospective study, the tomography maps of right and left eyes of 309 clinically-diagnosed keratoconus patients enrolled in the Vincিয়েye Clinic, and Humanitas Clinical and Research Hospital (Milan, Italy) were reviewed. The institutional review board of the University of Liverpool ruled that approval was not obligatory for this record review study. However, the ethical standards set out in the 1964 Declaration of Helsinki and their revision in 2013 were observed, and all patients provided informed written consent before using their de-identified data in the study.

The inclusion criteria were the diagnosis of keratoconus made by an experienced cornea specialist (Paolo Vinciguerra) based on typical topographic patterns (e.g., inferior steepening, asymmetric bowtie, skewed axis) and/or characteristic slit-lamp findings (e.g., Vogt's striae, Fleischer's ring, apical thinning, or Rizutti's sign). Exclusion criteria

included eye diseases other than keratoconus, extensive corneal scarring, former ocular procedures such as collagen crosslinking or implantation of intracorneal rings, connective tissue disease, as well as pregnancy or early puberty. All participants underwent a complete ophthalmic examination, including a Pentacam HR (Oculus Optikgeräte GmbH; Wetzlar, Germany) exam. Raw elevation data with a reference plane set at the corneal apex (from U12 file) were extracted using customised Pentacam software (version 1.21r41) and stored in comma-separated values (CSV) format⁴⁰⁰. The data covered a square grid that was 14 mm wide and had a regular spacing of 0.01 mm.

Patients were divided according to disease severity into three groups; mild, moderate and advanced, based on the Topographic Keratoconus Classification (TKC) provided by the Pentacam topographer⁴⁰¹. Mild keratoconus was defined with TKC classification of “Abnormal”, “Possible”, “-“ and “1”, moderate keratoconus included TKC grades “1-2”, “2” and “2-3”, and advanced keratoconus included TKC grades “3”, “3-4” and “4”.

Other tomographic parameters exported for this study included total deviation of the Belin-Ambrosio display (BAD-D), corneal thickness at the thinnest point, corneal astigmatism, maximum front surface curvature (KMax), anterior surface asphericity (AsphQFront), the custom Oculus topometric indices: index of surface variance (ISV), index of vertical asymmetry (IVA), keratoconus index (KI), centre keratoconus index (CKI), index of height asymmetry (IHA), index of height decentration (IHD) and the relative front surface elevation at the thinnest point in relation to the best fit sphere (BFS) with 8mm diameter (EleFBFS8mmThinnest). These parameters and the important topography maps are explained next.

3.2.3 Corneal Maps and Indices

Keratoconus diagnosis and management rely on corneal maps and topography indices. Most studies in the literature were unable to process cone-specific properties such as height, area and location of the cone as this technology has not been available and information could not be obtained from any of the commercially available topographers. In clinical practice, clinicians look at the topography maps and identify the cone location and its existence, Figure 3-3. The three most commonly used maps are (1) curvature keratometric, (2) elevations and (3) thickness maps. It is needed to understand the usability of these maps to appreciate the underlying error in visual interpretations. Curvature keratometric maps provide information about the curvature of points on the surface of the cornea in a graphical manner set by the device manufacturer.⁴⁰² Similarly, elevation maps show the difference between the measured points on the surface of the cornea and the reference maps. Elevation maps are accurate for data processing and numerical analysis. The reference map is playing a pivotal role, and usually, the best fit sphere is used to highlight subtle changes.⁴⁰³ They usually cover the central 8mm diameter on the cornea, and some of the data may be missing due to shadows cast from eyelashes and eyelids.^{404,405} Finally, thickness maps are produced by processing elevation

data, and they may not be as accurate as elevation maps.^{406,407} To assist with the better diagnosis of keratoconus and disease stage, multiple indices were developed for different topographers among which some of them are being discussed in this section.

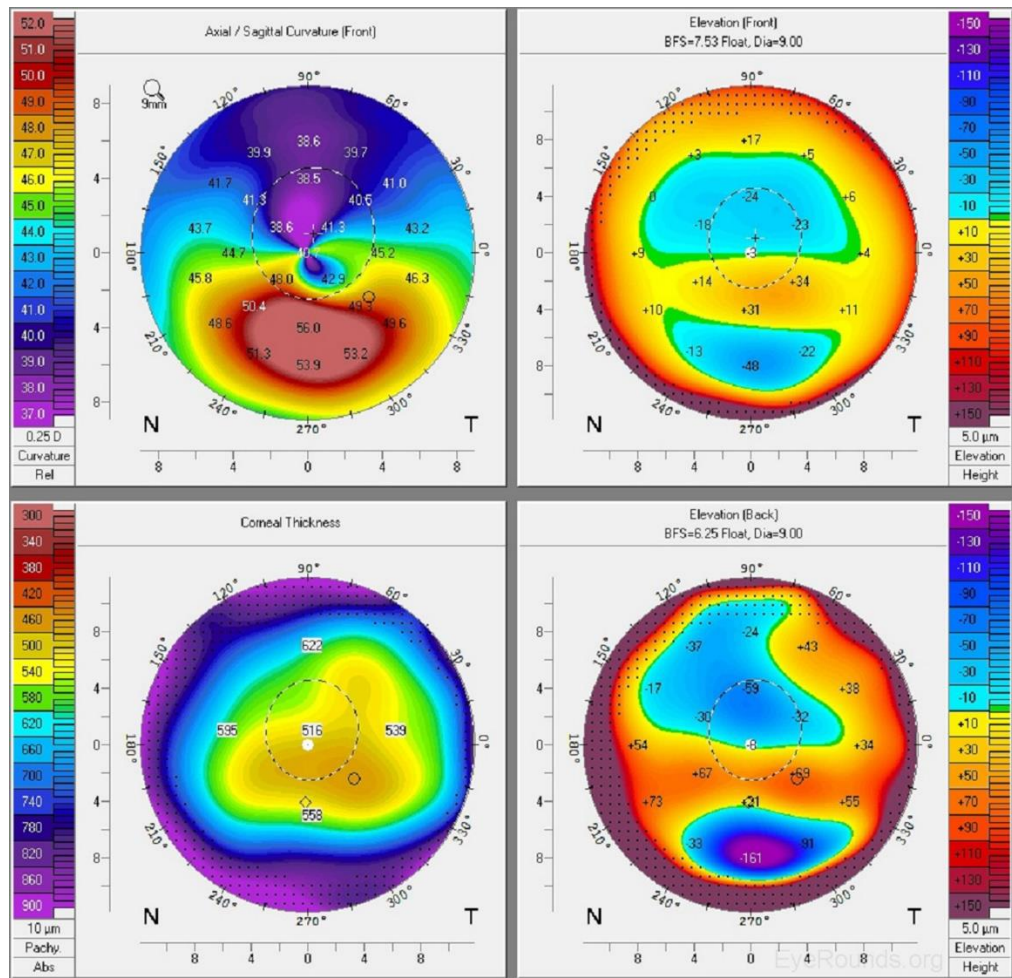


Figure 3-3 A typical display of corneal topography that includes anterior surface curvature, the elevation of anterior and posterior surface and the thickness of the cornea.⁴⁰⁸

Maximum front surface curvature (KMax): Using curvature data it finds the maximum value across the cornea and reports in dioptre⁴⁰⁹

Anterior surface asphericity (AsphQFront): The value is “0” if the anterior surface is a perfect sphere, negative if it is prolate and positive if it is oblate⁴⁰⁹

Index of surface variance (ISV): Evaluates irregularity of corneal surface⁴⁰⁹

Index of vertical asymmetry (IVA): Evaluates the symmetry of the curvature in comparison to horizontal axis⁴⁰⁹

Keratoconus index (KI): Calculates the mean radius between upper and lower segments and reports the ratio between them⁴⁰⁹

Centre keratoconus index (CKI): Calculates the mean radius between the periphery and central segments and reports the ratio between them⁴⁰⁹

Index of height asymmetry (IHA): Evaluates the symmetry of the elevation points in comparison to the horizontal axis⁴⁰⁹

index of height decentration (IHD): Within a 3mm ring, Fourier analysis is performed to obtain the amount of vertical decentralisation.⁴⁰⁹

EleFBFS8mmThinnest: Relative front surface elevation at the thinnest point in relation to the best fit sphere (BFS) within 8mm diameter⁴⁰⁹

Total deviation of the Belin-Ambrosio display (BAD-D): This index is developed using regression analysis on multiple parameters. Values (higher than 2.1) can detect ectatic disease and showed to be able to diagnose KC with high accuracy^{409,410}

Further information on other parameters can be found in published articles.⁴¹¹ It should be noted that these parameters are developed with the intention to provide more information about the corneal morphology and minimise the error associated with the qualitative judgment of maps by clinicians. None of these indexes can provide a universal solution for diagnosing the disease, and to a large extent, early diagnosis is subject to the experience of the clinician. In this thesis, a method is developed to address this shortfall.

3.3 Numerical Model Development

Numerical models were developed for a parametric study to understand the corneal response to Corvis ST tonometry. In all models, the rigid-body motion was prevented, section 3.3.2. The fluid cavity was introduced as an incompressible fluid with a density of 1,000 kg/m³ to behave similarly to vitreous and aqueous⁴¹².

This section starts by exploring the model structure, including the element type. This is followed by the development of a Matlab software code that simulated the application of Corvis ST air pressure on the cornea of these numerical models. A mesh density study was conducted to choose the optimum model formation to acquire reliable results as quickly as possible. The material parameters for the cornea were obtained through an inverse analysis process.

3.3.1 Element Type

Previous research in the Biomechanical Engineering Group (BioEG) at the University of Liverpool relied on the use of six-noded numerical models. It was found that these models are unstable for soft corneas.⁴¹³ A study was conducted to generate idealised numerical models for both 6-noded and 15-noded models using a custom-built mesh generator software which was developed by Wang⁴¹⁴, Figure 3-4. In this study, the same model geometries with the same material properties were generated. Both models were compared in terms of simulation time and rate of convergence. The outcome of this study was to recommend the use of 15-noded elements in future work, including this project. It should be noted that mass is not associated with the element and inertia is not at play in numerical models. In this study deformation of the cornea is only considered from the initial state to the highest concavity. Hence oscillation during this phase could be ignored as the data were extracted at two snapshots, when the cornea

becomes flat (applanation one) and when it reaches its maximum deformation (highest concavity).

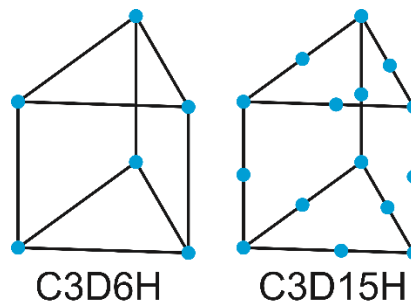


Figure 3-4 The difference between a 6-noded and a 15-noded element

3.3.2 Boundary Conditions

The rigid-body motion of the models was prevented by restricting the equatorial nodes in the anterior-posterior direction, allowing them to expand under IOP. Also, the posterior pole was fixed in both the superior-inferior and temporal-nasal directions, with the ability to move in the anterior-posterior direction. In addition, one point around the equatorial sclera was restricted on movement in superior-inferior direction to prevent the model from spinning around its central axis during the simulation, Figure 3-5.

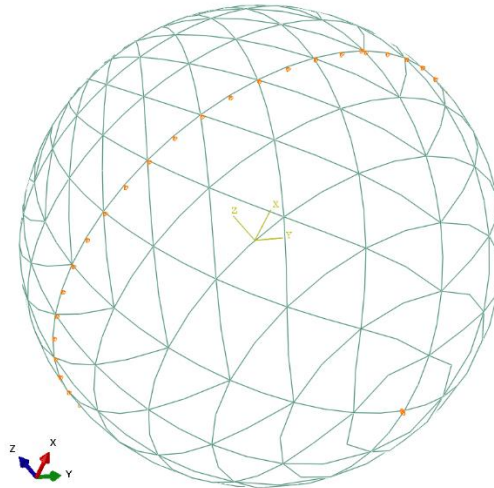


Figure 3-5 Boundary condition of a typical model of the eye showing the equatorial and posterior points that were restricted on movement in different directions

3.3.3 Corvis ST Pressure

Experimental studies revealed that the pressure released from the device nozzle was reduced by 50% when it reached the surface of the cornea, Figure 3-6¹⁸¹. In this thesis, pressure profiles of the left and right eyes of 140 healthy participants were evaluated over the 32-millisecond duration of air pressure. It was found that for all these 280 cases, the pressure profile followed a similar pattern with a standard deviation below 3.6% of

maximum applied pressure. Hence the mean profile obtained from this dataset was used as the pressure profile adopted in all numerical analyses. The spatial reduction of this pressure away from the corneal apex was obtained from an earlier study³⁸⁶. The distance from the corneal apex to the nozzle was assumed to be fixed to 11mm, similar to the Corvis ST and the results of the experimental study.

A PhD thesis developed numerical models in the context of a coupled models between computational fluid dynamics (CFD) and finite element analysis (FEA) using Arbitrary Lagrangian-Eulerian (ALE) deforming mesh.⁴¹⁵ It demonstrated that the effect of changing corneal shape during the application of the air puff is not significant on the distribution of air-puff pressure on the corneal surface compared to a model without fluid-structure interactions. In addition, performing CFD simulations would be too time-consuming and would not enable the conduct of a large parametric study that was needed for this thesis. Hence the pressure distribution that was obtained experimentally using sensors on a curved surface was used in this thesis, Figure 3-6.

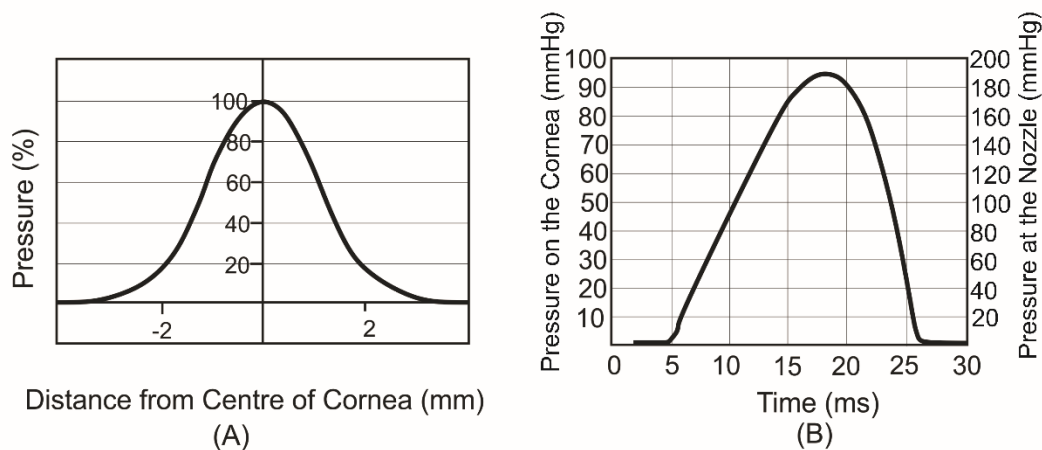


Figure 3-6 (A) Reduction of pressure on the corneal surface away from apex and (B) variation of pressure on corneal apex and nozzle over time.

The models produced by the mesh generator software included four files. These files included the input Abaqus commands, nodes, elements and material properties. A Matlab software code was developed to read the element files and locate the centre of each element on the anterior corneal surface. The distance from each centre point to the corneal apex was calculated and using linear interpolation, the value of pressure at this point was computed. The Matlab code then produced two files. The first defined how the pressure changed over time and during the simulation, while the second included the normalised value of pressure on each element. The number of elements that include a pressure value depends on the radial distance of the air pressure from the apex defined by the user in this code.

3.3.4 Mesh Convergence Study

The mesh density study was split into three parts to obtaining the optimum model, *Figure 3-7*. It started with a study on corneal rings, where models with 5, 10, 15, 25, 35 and 45 rings were generated. In this part, all models had 35 rings in the sclera and were subjected to inflation and air pressure. All parameters remained the same between these models apart from the number of corneal rings. Upon completion of the simulation, convergence time and deformation of cornea throughout the simulation were exported. The number for corneal rings was selected in a way to maintain model accuracy while using the smallest number of elements.

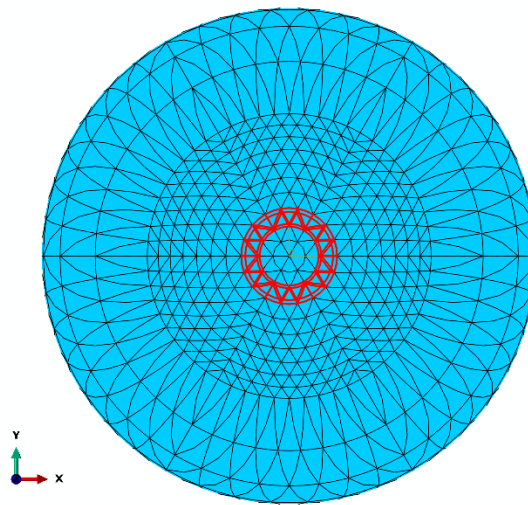


Figure 3-7 Optimum ocular model mesh showing cornea and surrounding sclera. The third ring is highlighted in red to clarify ring positions.

Once the optimum number of corneal element rings was determined, it was fixed in the second part of the study while varying the number of sclera rings. In this part, sclera rings were varied from 10 to 50 rings at steps of 10. In a similar manner to the previous step, deformations were compared, and the optimum number of rings was selected. After these two steps, a final stage of evaluating the number of segments on the cornea was needed. The numerical models of the eye could include four segments or six segments, as shown in *Figure 3-8*. The optimum mesh density values that were obtained for the cornea and sclera were used to generate both models. 6-segment models have more nodes and elements and result in longer computation times. Both models were subjected to inflation and air pressure. The deformations of the models were compared. Elements in Abaqus include integration points, which can adopt different biomechanical properties and have different stress values. As integration points are distributed through the thickness, a mesh density study through corneal thickness was not necessary. In addition, Keratoconus involves a slight change in geometry. Hence the mesh density should not be modified in KC eyes. Moreover, changing the mesh density

in cone area would create an artifact that could be responsible for differences between healthy and KC models that are not realistic.

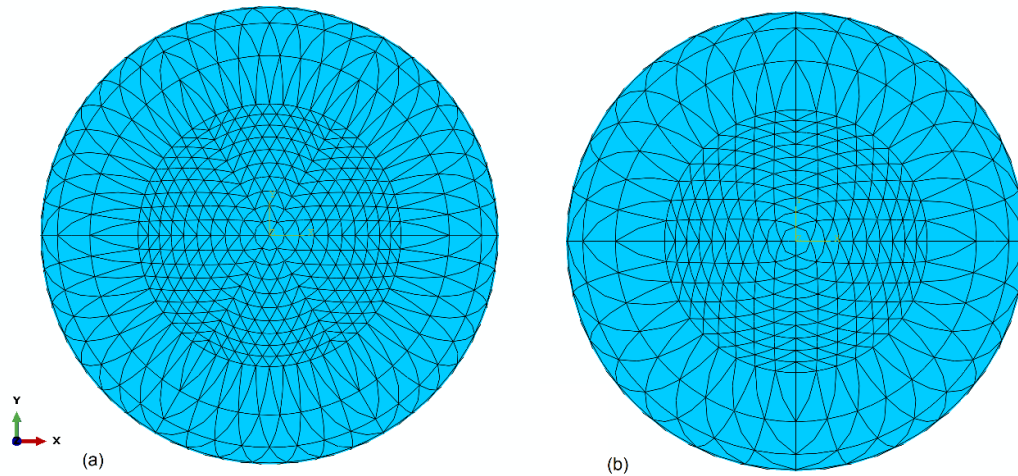


Figure 3-8 The model with different segmented rings where (a) has six segments and (b) has four segments

3.3.5 Material Parameters

An inverse analysis method was developed to obtain material properties of the models from previously published experimental data^{123,124}. The sclera was split into three different regions to match the tissue behaviour based on experimental findings¹¹⁸. The 15 noded models used in this study relied on Ogden constitutive material model. It was shown in the literature that the corneal material is viscoelastic and the Ogden material model can represent the soft tissue behaviour reasonably accurately^{181,354,416-420}. The hyperelastic Ogden strain energy equation is provided below and obtained from Abaqus Theory Guide documentation section 4.6.

$$U = \sum_{i=1}^N \frac{2\mu_i}{\alpha_i^2} (\lambda_1^{-\alpha_i} + \lambda_2^{-\alpha_i} + \lambda_3^{-\alpha_i} - 3) + \sum_{i=1}^N \frac{1}{D} (J_{el} - 1)^{2i}$$

Equation 3-1

where U is the strain energy, μ is the gradient of the line, α is the nonlinearity of the curve, N is the Ogden order, λ is the principal stretch in 3D, J_{el} is the volume of the particle and D is a constant. The stress-strain equation is derived from the equation above within the Abaqus. Ogden material model has proven to be able to present ocular material tissue and been used in a number of publications in this field.^{181,354,416-420} Hence no further investigation in this material model was needed in this study. It should be noted that Ogden does not incorporate viscoelastic material behaviour such as strain-rate dependency and hysteresis. In this study the rate of the applied pressure was constant and Ogden parameters were obtained to represent tissue behaviour at this rate. In addition, the behaviour of the cornea was considered only from the initial shape to the highest concavity. As a result of both of these, strain-rate dependency and hysteresis were not needed for numerical models.

A code was developed to use Matlab's built-in Particle Swarm Optimisation (PSO) function as an optimisation algorithm to obtain material parameters. There are two main reasons for using this metaheuristic approach. First, it has been used in this field and researchers are familiar with the algorithm and its performance which makes it more acceptable to be used in journal publications.⁴²¹ Second, PSO relies on particles with variable velocity property that enables quick convergence. The algorithm does not get stuck in local minimums and is a highly efficient search algorithm.⁴²² Since in this study optimisation is conducted alongside the FE models, the efficiency of the algorithm is crucial to reduce the overall time of the study.

In this study, the code located the target curve from previous experimental data. This data served as target curves for the inverse analysis procedure using the 15-noded model. Two material parameters for Ogden order one (N=1) were modified as described in Equation 3-1. It then used Equation 3-2 to calculate the error. If the error was below 10 microns, the analysis was terminated. Otherwise, it completed 200 iterations, and the lowest error was selected as the ideal material parameters that represent the same behaviour as experimental data. A python code was developed that could work with Abaqus ODB file for exporting deformations. Once the optimisation was completed for the defined target curves, and all parameters were obtained, the missing age groups could be identified using best-fit polynomials.

$$Error = \sqrt{\frac{\sum (Def_{Experimental} - Def_{Numerical})^2}{n}}$$

Equation 3-2

where $Def_{Experimental}$ and $Def_{Numerical}$ are representing the deformation obtained from experiments and vertical (Z-axis) deformation of corneal obtained from 15 noded models, and “n” is the number of target points.

3.4 Validation of Numerical Models

Now that the numerical models were prepared, they needed to be validated using clinical data. In this section, patient-specific numerical models were generated. These models were built with knowledge gained from the previous section in regards to the mesh density study and air pressure applied to the cornea. The deformation of corneal models was compared with the clinical data to evaluate the performance of numerical models.

3.4.1 Clinical Data

Clinical data obtained from 9 healthy participants enrolled at the Vincieye Clinic in Milan, Italy. Institutional review boards at the institution ruled that approval was not needed for this record review study. However, ethical approval for using the data in

research had been secured when the data was collected, anonymised, and used in earlier studies.^{228,423} Participants' informed and written consent was secured before collecting the data. Nevertheless, the ethical standards set out in the 1964 Declaration of Helsinki, and revised in 2000, were observed. All patients were evaluated with a complete ophthalmic examination, including the Corvis ST and Pentacam (OCULUS Optikgeräte GmbH; Wetzlar, Germany). All patients were free of any ophthalmic disease, with a Belin/Ambrósio Enhanced Ectasia total deviation index (BAD-D) derived from the Pentacam of smaller than 1.6 standard deviations (SD) from normative values in both eyes. Patients with previous ocular surgery or disease, myopia less than -10D, concurrent, or previous glaucoma or hypotonic therapies were excluded.

All Corvis ST exams were acquired by the same experienced technicians with good quality (QS) scores that enabled the calculation of all Corvis ST dynamic corneal response parameters (DCRs). Moreover, a frame-by-frame analysis of the exams was performed by an independent masked examiner to ensure the quality of each acquisition. Only one eye per patient was randomly included in the analysis to avoid the bias of the relationship between bilateral eyes that could influence the analysis result. Any Corvis ST readings with visible rotational misalignment in the corneal profile were excluded from the analysis. This data was previously published.¹⁸¹

This is important to note that there is a lot of noise in Crovis ST clinical data. Hence strict selection criteria had to be adapted to minimise these inconsistencies. Any measurement with quality standard not OK was rejected. Corvis ST does not necessarily shoot perpendicular to the corneal apex, and due to rotations caused by the visual axis, there can be a tilt in how the pressure is applied on the cornea. Hence in this part of the study, cases with rotation had to be excluded. In this study, it was assumed that the distance from the corneal apex to the nozzle was fixed to 11mm in numerical models. In clinics, the 11mm distance cannot be guaranteed. Hence any clinical cases with variation in distance to the nozzle as indicated by the Corvis ST DCRs parameters were excluded. Among the remaining cases, with consideration to cover various CCT, IOP and Age, nine cases were selected. The demography for these cases is as shown in Table 3-1. In the literature, other researchers have used 4 and 8 cases to validate their studies^{424,425}.

Table 3-1 demography for patents used to validate numerical models

| Case | Age (year) | Exam Eye: | QS | IOP [mmHg] | Pachy [μm] |
|------|------------|-----------|----|------------|-------------------------|
| 1 | 20 | Right | OK | 17 | 537 |
| 2 | 72 | Left | OK | 17 | 539 |
| 3 | 26 | Right | OK | 14.5 | 600 |
| 4 | 44 | Left | OK | 16.5 | 565 |
| 5 | 43 | Left | OK | 13 | 595 |
| 6 | 32 | Left | OK | 16.5 | 601 |
| 7 | 42 | Left | OK | 17.5 | 592 |
| 8 | 30 | Left | OK | 11.5 | 539 |
| 9 | 43 | Left | OK | 13 | 608 |

Using Corvis ST patient management software, the raw data were exported. These files included the deformation profile of the cornea throughout pressure application, Figure 3-9. This profile covered the central zone of the cornea with a 4mm radius. It included both anterior and posterior surfaces and contained 140 measurements taken during the 32 ms of air application. Only the loading part from the initial stage to the point of corneal highest concavity was considered.

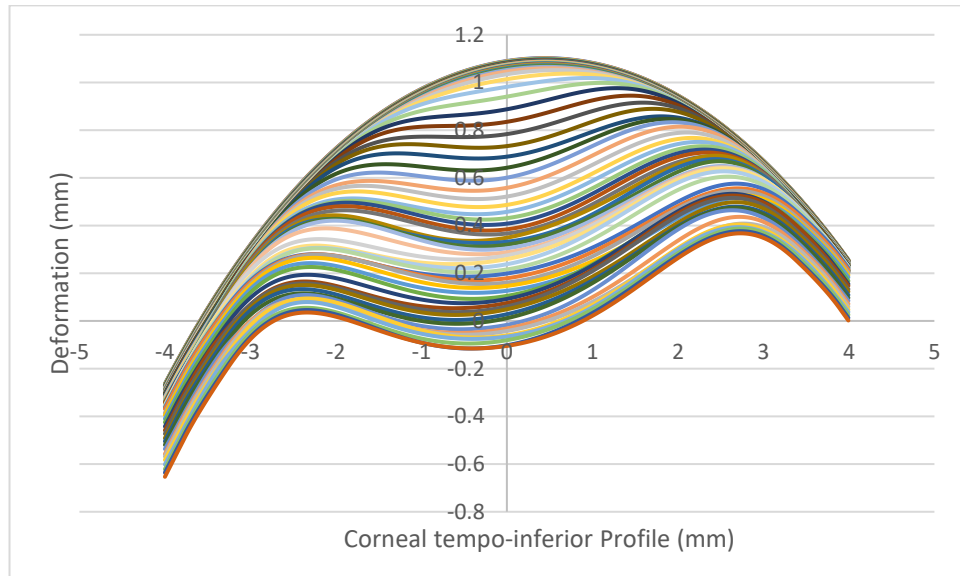


Figure 3-9 Corneal profile collected from Corvis ST in 140 measurements over a period of 32 ms from Temporal-Nasal axis. The figure only shows corneal deformation up to the point of corneal highest concavity at 16.8 ms.

3.4.2 Comparison with Numerical Models

A process had to be taken to enable comparison of the results obtained from clinical data with numerical models. To do this first patient-specific numerical models had to be generated. Next, the software had to be developed to read clinical data and remove

the whole eye movement. Finally, the deformation obtained from numerical models could be compared against those of clinical data for validation. These four steps are discussed below.

3.4.2.1 Generating Models

Patient-specific numerical models were generated using a bespoke mesh generator ⁴¹⁴. Before generating each model, IOP and the age of the patients were set to the values obtained from clinical data. After the numerical models were generated, they were inflated, and the stress-free form (explained in section 3.5.6) was obtained. Then Corvis ST pressure was added to these models using the code developed in section 3.3.3 ⁴²⁶. Upon completion of the simulation and using a python software code developed to extract the deformations, the data needed for the comparative study were collected in a text file. A new Matlab code was developed to analyse and compare this data.

3.4.2.2 Reading Clinical Data

The software started by reading a patient’s corneal deformation under Corvis ST loading obtained from clinical data. The patients who had missing points were excluded, Figure 3-10. A Matlab code was developed to process these files and identify the Corvis files that were suitable and had the required information to be used in this study.

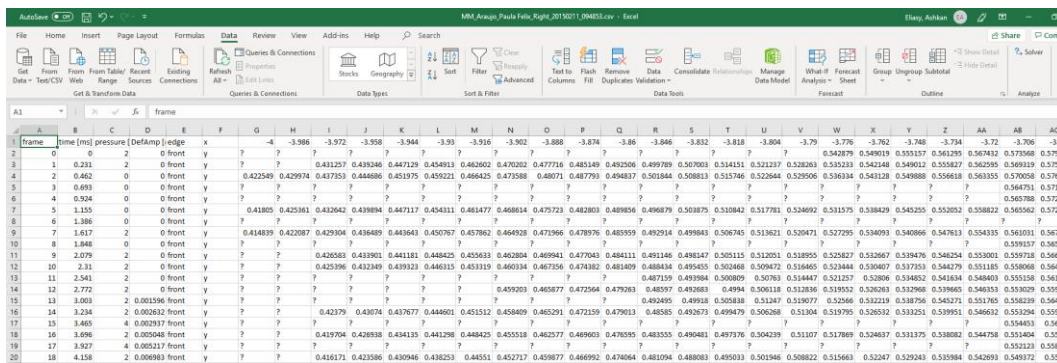


Figure 3-10 Corneal profile data with some information missing

3.4.2.3 Whole Eye Movement

In live patients, when the air-puff pushes against the cornea, the whole eye will move slightly backwards inside the orbit, this movement is called the Whole Eye Movement (WEM). Numerical models used in this study did not consider the muscles and orbital fat around the globe. Hence there was not any whole eye movement, and this deformation had to be excluded from the clinical data before it could be compared with the numerical predictions of displacement. To remove the WEM, a point within the 8mm Corvis ST profile was selected at a given profile. If this point is near the edge, it could be influenced by the edge effect and the fitting errors. Hence points that were 400 microns away from the edge of the 8mm region were found to be stable in all cases. At this location and to further reduce the noise, the elevation of all points within the

distance of 60 microns (from 400 to 460 microns) were averaged, and this value was recorded, *Figure 3-11*.

This process was repeated for the left and right sides of each corneal profile up to the point of highest concavity. The difference between the elevation value obtained from the first profile and subsequent profiles was considered as the WEM and was removed from the deformation of that profile. Knowing the WEM on the left and right sides, a linear change was assumed between them to remove this deformation from all points, as shown in *Figure 3-11*.

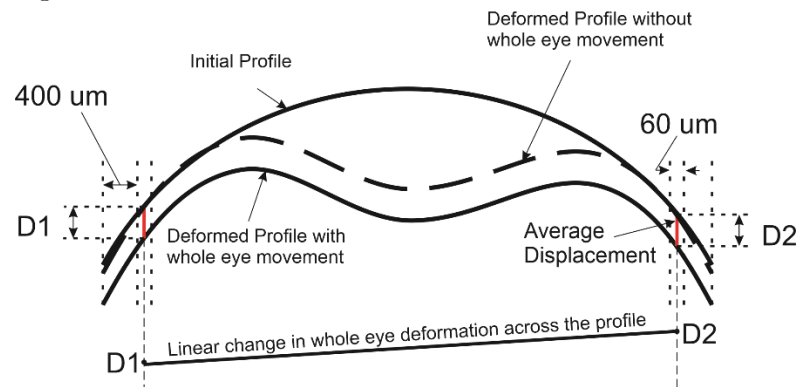


Figure 3-11 Whole eye movement at a specific time point. The WEM was calculated on both sides of the cornea and a linear distribution was assumed when removing the eye movement from corneal displacement. D1 and D2 are the displacements calculated at each side.

3.4.2.4 Reading the Numerical Model

As explained in section 3.4.2.1, the python file generated a text file with information on corneal deformation. This file included the position of the cornea at different time points during the 32ms air pressure simulation. Since a stress-free configuration (explained in section 3.5.6) was obtained, the inflated eye model had a matching profile with data obtained from the patient. Each profile was fitted to a polynomial order 12, similar to clinical data, to obtain an equation for that profile. A code was developed to prevent overfitting at this order, and order number 12 was obtained experimentally. Then using that equation, deformations at similar points as in clinical measurements were calculated. Also, a similar whole eye movement process was repeated to make sure all numerical model profiles were sitting on top of each other at the exact same point as in clinical data, *Figure 3-12*.

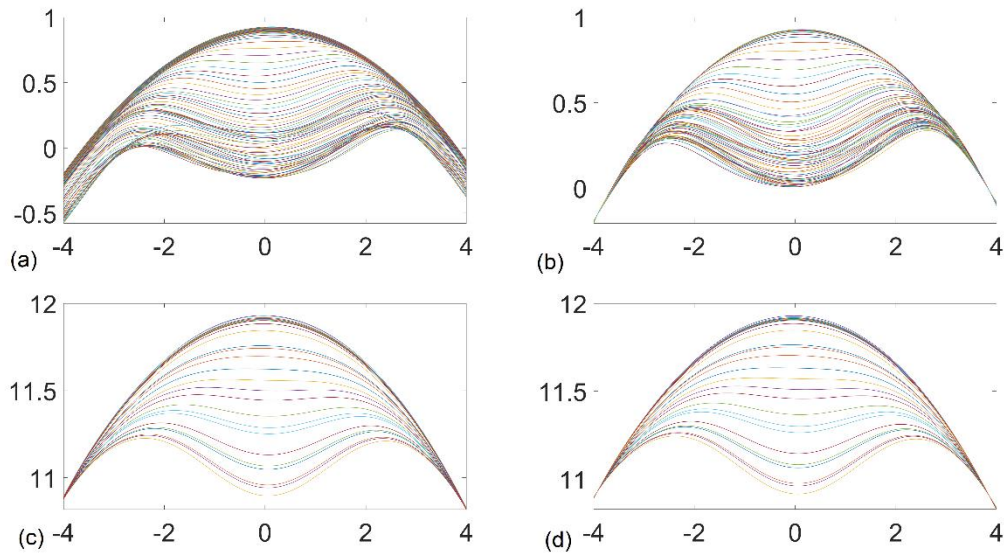


Figure 3-12 The Y-axis presents the elevations in mm, X-axis presents the distance in mm, and each colour is presenting a corneal profile at a different time point where (a) deformation obtained from clinical data that includes whole eye movement, (b) deformation obtained from clinical data after removal of eye movement, (c) deformation exported from numerical models and (d) adjusted deformation from numerical models to match clinical data

3.4.2.5 Comparison between Clinical Data and Numerical Model

The displacements of the cornea as measured clinically and predicted numerically were compared to validate the numerical models. In this method the known parameter is the deformation measured by the Corvis ST in clinics and the model behaviour was expected to match this behaviour. Deformation values were compared numerically and qualitatively (using plots) with the objective function as shown in, Equation 3-3. The output of this section is presented in the results section to serve as the validation of numerical models.^{386,415,427,428}

$$Error = \sqrt{\frac{\sum (Def_{clinical} - Def_{Numerical})^2}{n}}$$

Equation 3-3

where $Def_{clinical}$ and $Def_{Numerical}$ are representing the deformation obtained from Corvis ST and 15 noded model, and “n” is the number of data measurement points on clinical data.

3.5 Parametric Study

A large parametric study was conducted to build the database for the development of new equations to estimate IOP and material stiffness in vivo. The variable used in this study were selected in a way to control geometry and stiffness aspects of the eye model. Parameters number 1 to 4 changed the geometry and material stiffness of healthy eyes

while 5 to 7 introduced abnormalities to the cornea and number 8th varied the location of the abnormality in respect to Corvis ST profile. The parameters and the range defined for them are as below (in brackets the “x” refers to the total number of values considered for that variable):

- | | | |
|---|------------------------------|------|
| 1. CCT (um): | 395 to 645 at steps of 50 | (x6) |
| 2. Material Stiffness Ratio: | 0.25 to 2.0 at steps of 0.25 | (x8) |
| 3. Radius (mm): | 7.2, 7.8 and 8.4 | (x3) |
| 4. IOP (mmHg): | 10 to 35 at steps of 5 | (x6) |
| 5. Cone Radius (mm): | 0, 1 and 2 | (x3) |
| 6. Anterior Cone Height (um): | 0, 75 and 150 | (x3) |
| 7. Radial cone distance to corneal apex (mm): | 0, 1 and 2 | (x3) |
| 8. The angular position of the cone (degree): | 180 to 315 at steps of 22.5 | (x7) |

The suitable range for material, thickness variations, IOP and corneal radius were obtained from the literature^{118,181,429-433}. The values for cone properties (parameters 5-7) obtained from the study performed in section 3.2. The angular position was selected in a way that covers the most likely locations of the cone while keeping the number as low as possible. The total number of simulations for this database was 163,296, which is the largest parametric study performed in this field. Considering this, all steps for the parametric study had to be automated to be able to obtain these results on a reasonable time scale. Hence a great amount of time was spent on the development of the software to perform this study. The process taken to develop this software at this stage is shown in Figure 3-13, and each step is explained in more details later in this section.

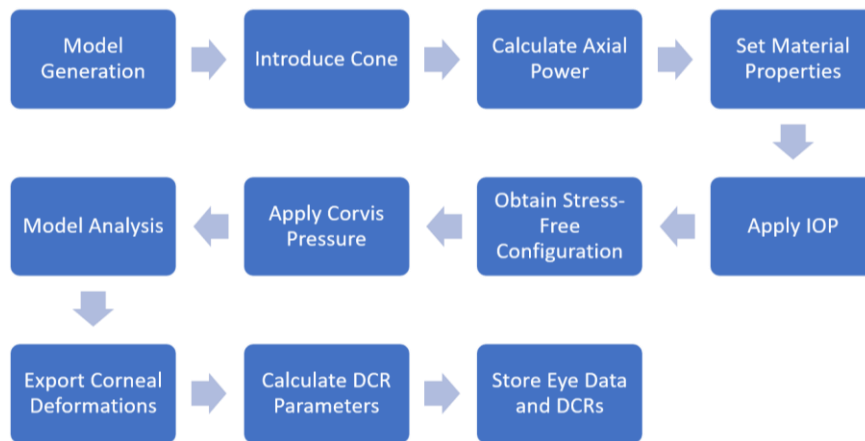


Figure 3-13 Process adopted to build the database required for the development of IOP and material stiffness estimation equations

3.5.1 Model Generation

Idealised eye models were generated using the bespoke mesh generator, Figure 3-14⁴¹⁴. At this stage, the number of corneal rings was set to 10, and the number of sclera rings was set to 10. Four segments models using 15-noded C3D15H elements were generated

based on the earlier mesh density study. Each model had a single layer with a total of 3606 nodes and 800 elements. The cornea was constructed from a single layer and the epithelium layer was not considered as a separate layer as its effect found to be negligible⁵⁴. However, its thickness was considered in total corneal thickness. There was no need to consider optic nerves head (ONH) as its effect was found insignificant on corneal deformation¹⁸¹.

Corneal radius and CCT was set based on selected parameters for this study. Corneal shape factor was set to 0.82, Peripheral Corneal Thickness (PCT) was 150 microns more than CCT, the limbal radius was 5.85 mm, and the scleral radius was 11.5 mm. Sclera thickness varied with PCT where equatorial set to 80% of PCT and posterior sclera set to 120% of PCT. All these values were obtained from the literature¹⁸¹. The sclera was divided into three segments to represent better the tissue behaviours based on the experimental studies conducted on various regions of sclera¹¹⁸. Apart from the sclera with three segments, the model had one segment for the whole cornea. This was modified later when the cone location was identified as described in section 3.5.2. The eye model's IOP was defined using a surface-based fluid cavity as described in 3.5.5. Stress-free was not performed at this stage.

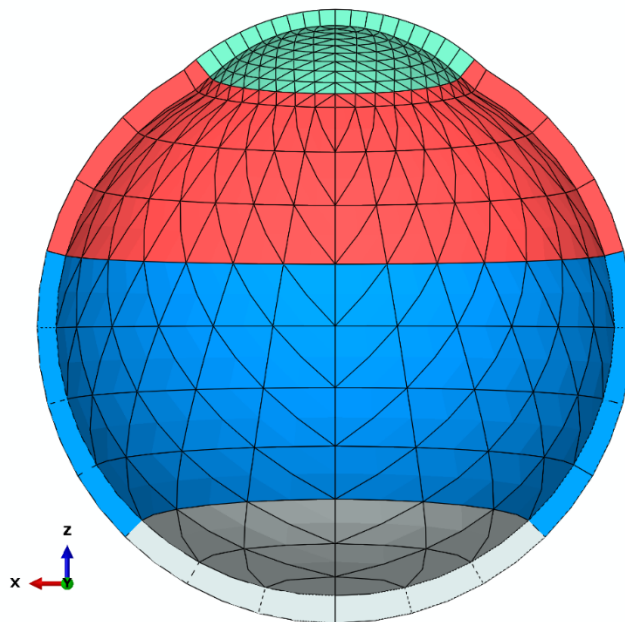


Figure 3-14 The numerical model generated for this study with variation in thickness. Different colours are referring to different material segments.

3.5.2 KC Cone

After desired idealised numerical models were generated, the corneal geometry had to be modified to introduce a cone. At this part, the knowledge of cone location on anterior and posterior surfaces, cone radius, cone height on anterior and posterior surfaces was required. The anterior cone height, cone radius and anterior cone location information defined by the parameters selected for this study and from section 3.2. Also

following the study in that section, more information was obtained about the remaining parameters, Equation 3-4, Equation 3-5 and Equation 3-6.

$$PCHM = 0.8138 \times ACH + 0.007$$

Equation 3-4

where $PCHM$ is the posterior cone apex height location changes in millimetres compared to the anterior cone height and ACH is the anterior cone apex height in millimetres.

$$X(Anterior) = 0.591 \times X(Posterior) - 0.296$$

Equation 3-5

$$Y(Anterior) = 0.7154 \times Y(Posterior) - 0.164$$

Equation 3-6

where $X(Anterior)$ and $X(Posterior)$ are the location of the cone in temporal-inferior meridian for anterior and posterior surfaces, $Y(Anterior)$ and $Y(Posterior)$ are the location of the cone in superior-inferior meridian for anterior and posterior surfaces. All units are in millimetres.

The software started by reading the node and element files. With the knowledge of the element type used in the model, nodes on the anterior surface, posterior surface and middle points were identified. Using the cone information provided by the user, the closest corneal point to the cone apex was identified. From the radius of the cone, all the corneal nodes within that range from cone apex were selected. At this stage, cartesian coordinates were converted to spherical coordinates to adjust the cone apex height to the desired value. Once the cone apex height is adjusted and with the information of the cone boundary, “griddata” function in Matlab was used that utilised triangle-based cubic interpolation to smoothly adjust all the corneal points within the cone area to be located between the cone apex and boundary.

This process was repeated for the posterior surface to adjust the coordinates of the points within the cone. Then using the coordinates of anterior and posterior surface, middle element points were recalculated, and the coordinates were updated. Then the node file was updated to reflect the cone coordinates in its geometry, Figure 3-15. Finally, the minimum corneal thickness was calculated to be used in future calculations. Then the input file was read in the Matlab code. Two node sets for anterior and posterior points of the cone and one element set that identified the cone area was introduced into the input file. A new reference for cone material was also defined to enable variation of cone material properties manually. The change in material stiffness is introduced as described in section 3.5.4. The mesh density did not need to be modified as described in section 3.3.4.

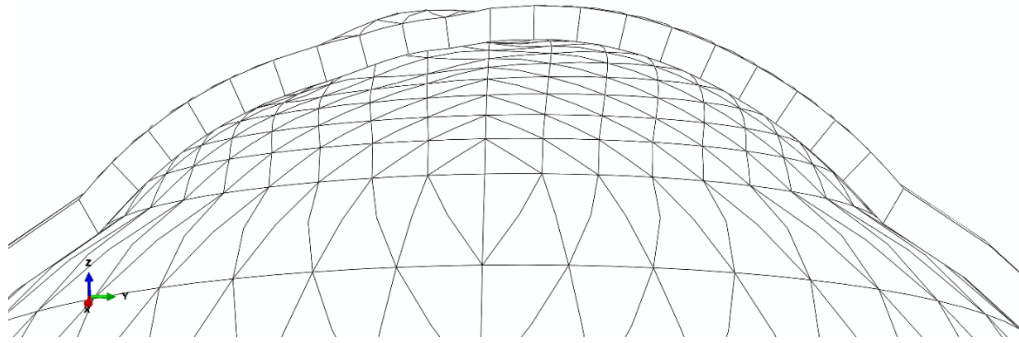


Figure 3-15 Cross-section of a model showing a keratoconus cone appearing as a bulge on both the anterior and posterior surfaces

3.5.3 Axial Power

It was necessary to calculate corneal axial power in the central 3mm diameter for identifying the material properties of the cone as described in the next section. Nodes from the anterior and posterior surface of the cornea were identified to calculate the axial power. The cornea was divided into 360 meridians where each meridian was analysed separately. Every point on every meridian was fitted to a circle in a way that the central point of the circle passed through the central line. This was done while maintaining a perpendicular tangential line to the radius of the circle, as shown in Figure 3-16. Once this point was identified, the radius from the centre of the circle to the point could be calculated.

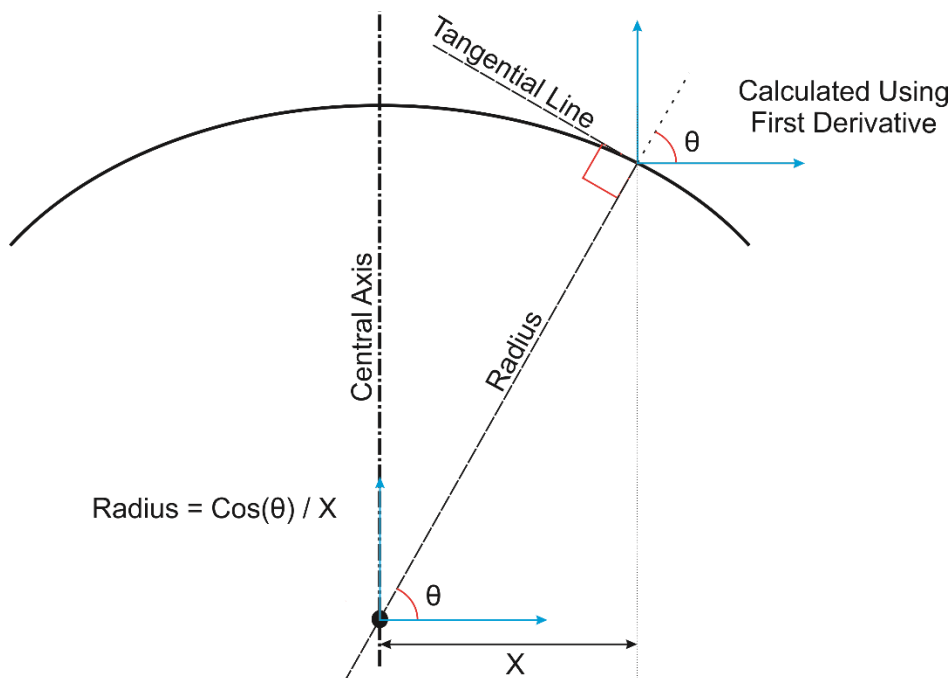


Figure 3-16 Axial power determined at a general point on a corneal surface. The power is calculated by identifying the radius of a circle that passes through the central axis while being perpendicular to the tangential line at this point. The derivate is calculated from the 3D coordinates of the surface collected from Pentacam or FE models.

Every point on the corneal surface had a different radius. This process was repeated for every point and across all meridians for both anterior and posterior surfaces. Once all radiuses were calculated, axial power at every point was estimated using Equation 3-7⁴³⁴. Then the average power of corneal central 3mm diameter was calculated as a single number to be used for the next step. This process was similar to what commercial topographer use to calculate power^{435,436}.

$$P = \frac{n_s - n_a}{R_A} + \frac{n_h - n_s}{R_P} - \frac{CCT}{n_s} \times \frac{n_s - n_a}{R_A} \times \frac{n_h - n_s}{R_P}$$

Equation 3-7

where P is the axial power in dioptre applied over the corneal surface, n_s is the refractive index of stroma (1.376), n_a is the refractive index of air (1.0), n_h is the refractive index of aqueous humour (1.336), R_A and R_P are the radius of anterior and posterior corneal surfaces respectively in microns and CCT is the central corneal thickness in microns^{437,438}.

The equation above is the correct method for calculating the refractive power of a thick lens, as described in the literature⁴³⁴. However, most topography devices use a thin lens equation, where the third part of the equation was excluded. Since in this study, it was required to compare these findings with a commercial topographer, a simplified version was used as in Equation 3-8.

$$P = \frac{n_s - n_a}{R_A} + \frac{n_h - n_s}{R_P}$$

Equation 3-8

3.5.4 Material Parameters

In this section, material properties were defined for cornea, sclera and cone. A recent study developed an equation that estimates the softening of the cone using some parameters, as described in Equation 3-9⁴³⁹.

$$C_r = -0.0406 \times C_A - 0.0073 \times P + 0.000165 \times t_{min} + 1.312$$

Equation 3-9

where C_r is the cone stiffness reduction factor, C_A is the cone area in mm, P is the power in central 3mm of the cornea in dioptre and t_{min} is the minimum corneal thickness. The material properties of the cornea were identified using age. Ogden material model and parameters used in the simulations were described in section 3.3.5. An equation was obtained from data that related the stiffness of the corneal tissue to age, Equation 3-10¹²³.

$$Beta = 0.5852 \times \exp^{0.0111 * Age}$$

Beta in the equation above provides the stress-strain behaviour of the cornea corresponding to a particular age. Using the equation above the stiffness variation between Age and material stiffness could be found and used as target curves. An optimisation technique was employed to obtain constitutive Ogden material parameters that provide the same behaviour as experimental data. A similar technique was used to obtain constitutive material parameters of the sclera in relation to age and using experimental data.¹²⁰ Hence the material properties of the whole eye could be now controlled using a single universal parameter, *age*,

Table 3-2. The software used this value to obtain all parameters and update the material file accordingly to be used for simulations.

Table 3-2 Constitutive parameters of Ogden material model in relation to age as found from experimental data.

| Age (year) | μ (MPa) | | | | λ | | | |
|---------------|-------------|--------------------|----------------------|---------------------|-----------|--------------------|----------------------|---------------------|
| | Cornea | Anterior Sclera | Equatorial Sclera | Posterior Sclera | Cornea | Anterior Sclera | Equatorial Sclera | Posterior Sclera |
| 0 | 0.104 | 1.678 | 0.922 | 0.443 | 119.80 | 31.543 | 41.521 | 53.016 |
| 25 | 0.115 | 1.913 | 1.081 | 0.554 | 119.80 | 35.303 | 43.876 | 53.016 |
| 50 | 0.132 | 2.224 | 1.291 | 0.743 | 119.80 | 40.265 | 46.983 | 53.016 |
| 75 | 0.157 | 2.633 | 1.568 | 1.096 | 119.80 | 46.815 | 51.084 | 53.016 |
| 100 | 0.197 | 3.174 | 1.934 | 1.830 | 119.80 | 55.458 | 56.497 | 53.016 |

3.5.5 Application of IOP

The IOP values of the parametric study were defined in the input file to apply this pressure in the form of a fluid cavity to the internal surface of the eye, Figure 3-17. At this stage, the input file was read, and the value of internal pressure in the first step of loading was modified to the desired value. This value was inserted in Mega Pascal (MPa) and was converted from millimetre mercury (mmHg) by being multiplied to “0.000133322” value.

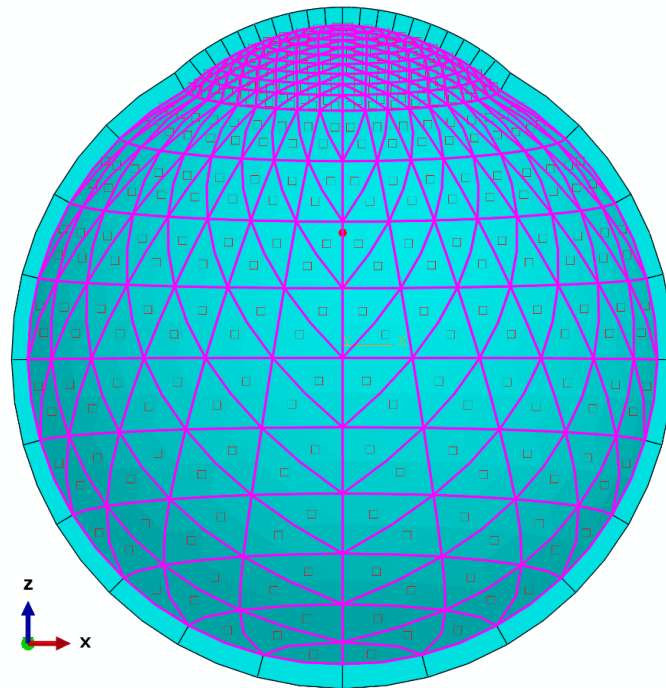


Figure 3-17 The fluid cavity surface inside the ocular numerical model

During the application of IOP, the pressure inside the eye is changing and this change in pressure results in expansion of the ocular shell. The fluid cavity allows for the pressure to change, however, there was no need to measure this change in pressure in this study. There are two effects involved here, one is the direct effect of the external pressure and the other is the effect of pressure waves inside the eye. The effect of these two is not separated in this study and the FE model considered both effects while calculating the behaviour.

Ocular rigidity is considered as the change in pressure that would be required to cause a unit change in volume, and this is commonly used as an overall measure of the stiffness of the ocular globe.⁴⁴⁰ The interest in this project is the stiffness of the ocular tissue and not the ocular globe. Hence the change in volume is considered in FE models however these data are not collected. In addition, the choroid is known to have a much lower tissue stiffness than the cornea and sclera and for this reason, it had been ignored in the numerical models. It is treated as part of the internal fluid of the eye due to this low stiffness.

3.5.6 Stress-Free Configuration

Until this step, the model included the desired geometry, IOP and material properties. However, the current geometry was before inflation, and the addition of IOP after running this model would change the geometry. For the parametric study, it was required for the model to have specific dimensions after being inflated. Hence it was required to find the geometry of the model at stress-free configuration⁴²⁶. In this

process, the model ran through multiple iterations, and the nodes' coordinates were modified at every iteration until the inflation model forms the desired geometry. In this study, this process was repeated five times to ensure the RMS between the desired geometry and inflated model was below 1 micron.

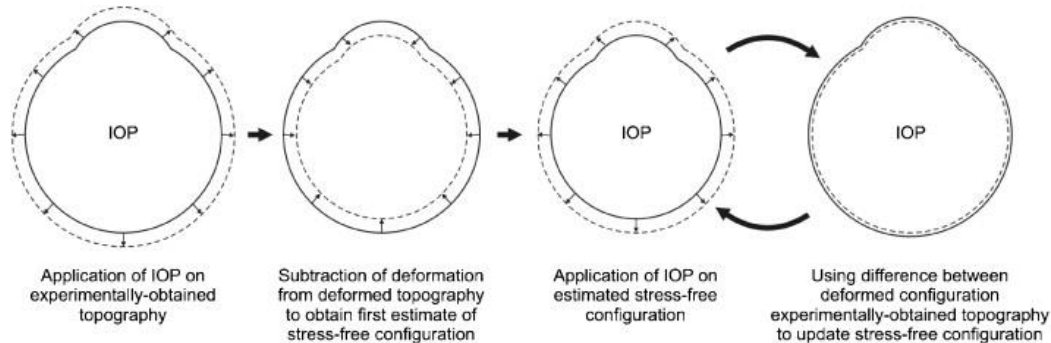


Figure 3-18 Schematic figure describing the stress-free procedure. Source: Elsheikh et al. ⁴²⁶

3.5.7 Corvis ST Air-puff

Once the stress-free configuration of the model was obtained, it was time to add a second loading step to the input file. At this stage, the input file reread by the software and Corvis ST pressure was added after the inflation step, Figure 3-19. This step simulated 32 ms of real air-puff application and required defining how the pressure changed over time and how much was the maximum pressure on every element during this process. This was done through the code developed for section 3.3.3 where a detailed explanation is provided on how the pressure was applied. It should be noted that the pressure was applied normal to the surface of each element. Outputs required for simulation was the coordinates and deformation of the model during the application of air pressure.

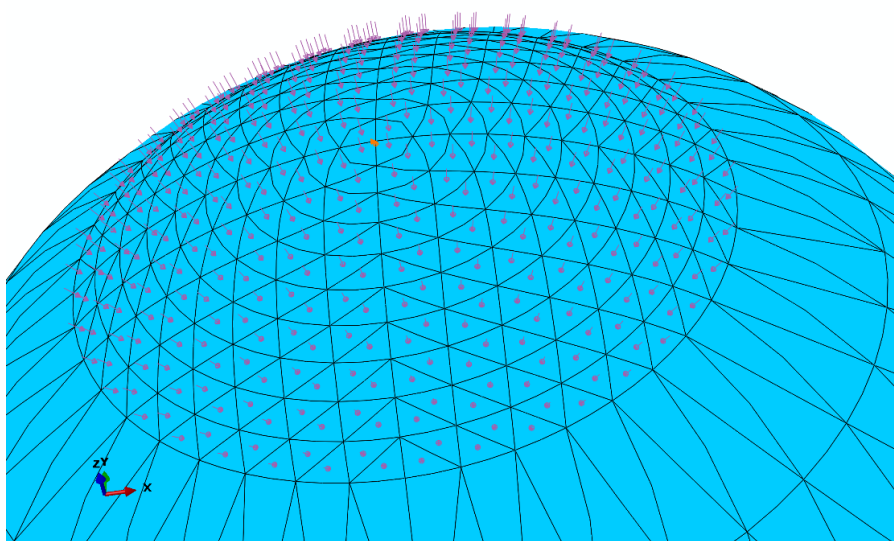


Figure 3-19 Corvis ST air pressure applied normal to the surface of each element (purple arrows)

3.5.8 Model Analysis

The models were ready at this stage for simulation. The previous seven steps were repeated in a loop, and a custom-built Matlab software code modified/generated and ran the models one by one. Upon completion of the simulation, it ran a python code to export corneal deformation for both anterior and posterior surfaces into a single text file. Then all the extra files generated during this process was removed to reduce the file size. The remaining files were those required to run the model again if necessary, plus the output text file. This process for every model took 4 minutes to complete. Considering there were 163,296 models, it would take 454 days and would not make the study feasible. Considering the nature of the models, seven different profiles of the cornea could be obtained from a single run, *Figure 3-20*. This meant instead of generating new models for every rotation of the cone and always exporting the horizontal line of the cornea; the cone remained the same, and different profiles were exported from a single model. This reduced the number of models to 23,328, reduced the total simulation time to 65 days until completion. This study was performed using a custom-built code and was performed on a Linux cluster at the University of Liverpool.

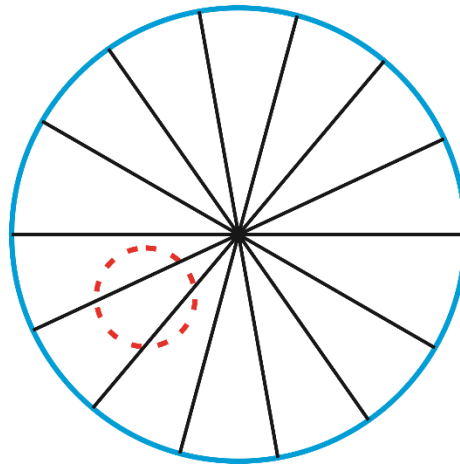


Figure 3-20 The blue region is the cornea, the red region is highlighting the cone area, and seven black lines are assuming different cone locations. In doing this, the cone was kept on the inferior side.

3.5.9 Calculation of Dynamic Corneal Response (DCRs) parameters

The text file generated from the python code explained in the previous step was read at this stage. It provided the cartesian coordinates of nodes on anterior and posterior surfaces of the corneal over time. Some information, including corneal radius, IOP, corneal material stiffness, cone height, cone radius and cone location, were provided from previous steps. At this stage, corneal CCT had to be recalculated. This is because CCT was influenced by the creation of the cone. Hence at this stage, the apex thickness was calculated. The Corvis ST profile was exported from the model similar to clinical data to perform DCR calculations. This profile was exported at different angles to

simulate the effect of cone movement around the eye and only on the inferior side, Figure 3-20. The Corvis ST parameters described below were calculated in this section are as below. Please note that the deformation parameters could not be calculated as there is no whole eye movement in these numerical models. Hence deflection in parameters below is referring to the corneal movement only.

- **Deflection Amplitude Maximum (*DeflAmpMax*):** This is the travelled distance from apex to the highest concavity. It was calculated by identifying the profile that has the highest deformation, Figure 3-21.

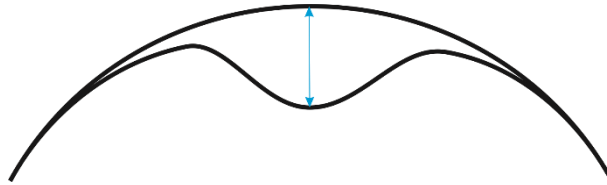


Figure 3-21 Schematic graphical description of Deflection Amplitude Maximum

- **Highest Concavity Time (*HCT*):** This is the time that cornea reached the highest concavity. It was obtained by estimating the time of the profile that deformed the most, Figure 3-22.

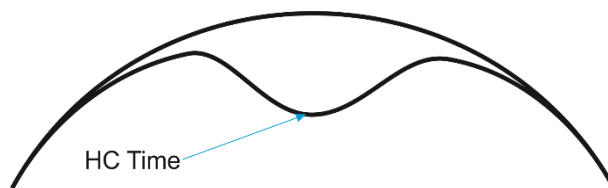


Figure 3-22 Schematic graphical description of HC Time

- **Peak Distance (*PD*):** This is the distance between two peaks at the highest concavity. This distance was calculated using the profile that deformed the most under Corvis ST pressure, Figure 3-23.

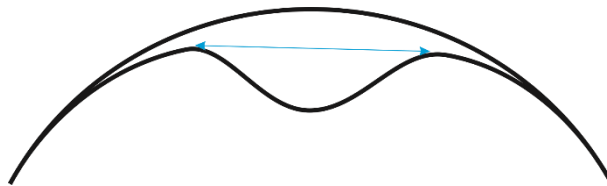


Figure 3-23 Schematic graphical description of Peak Distance

- **Applanation 1 Time (*AIT*):** This is the time at which the cornea becomes flat. This was calculated using the first derivate. This time was identified by selecting the profile before which cornea has three points with first derivate equal by zero, Figure 3-24.

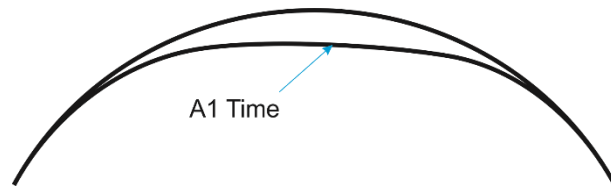


Figure 3-24 Schematic graphical description of A1 Time

- **A1 Length ($A1L$):** This is the length of all the points that have the first derivate between ± 10 microns. This value was obtained from the company, Figure 3-25.

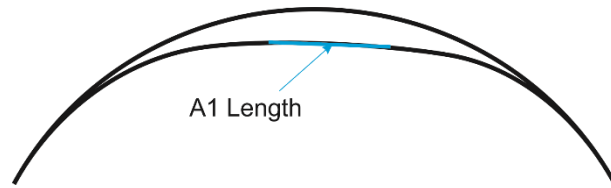


Figure 3-25 Schematic graphical description of A1 Length

- **A1 Deflection Amp. ($DeflAmpA1$):** This is the distance travelled by the cornea from natural position to A1 time, Figure 3-26.

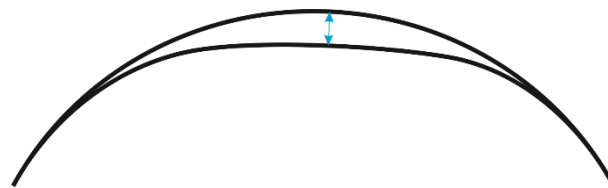


Figure 3-26 Schematic graphical description of A1 Deflection Amp.

- **A1 Velocity ($A1V$):** The velocity is calculated using the first derivate of corneal deformation over time. A1 Velocity is the sum of first derivate values until A1 time, Figure 3-27.

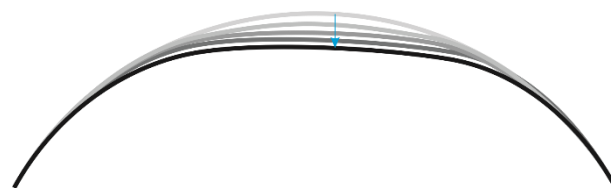


Figure 3-27 Schematic graphical description of A1 Velocity

- **Applanation Pressure 1 (API):** This is the pressure at the nozzle which was provided for the simulation using amplitude file, described in section 3.3.3 and shown in Figure 3-6. The precise value was obtained through interpolation, Figure 3-28.

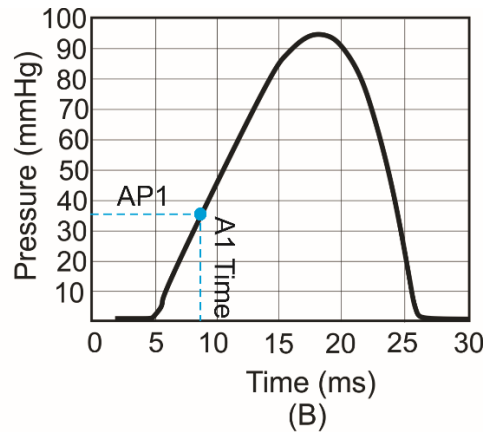


Figure 3-28 Schematic graphical description of AP1

- **Radius at HC (*HCR*):** This is the radius of the best fit circle at the highest concavity. It was calculated using a Matlab built-in function, Figure 3-29.

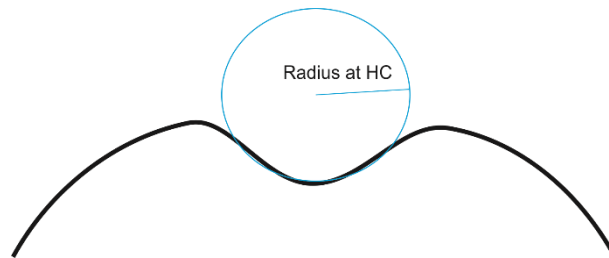


Figure 3-29 Schematic graphical description of HC Radius

- **Stiffness Parameter at A1 (*SPA1*):** This parameter which was initially introduced by Cynthia Roberts et al. ⁴⁴¹, is known to be correlated with overall corneal stiffness, Equation 3-11.

$$SPA1 = \frac{AP1 - IOP}{DeflAmpA1}$$

Equation 3-11

- **Stiffness Parameter at HC (*SPHC*):** This parameter is similar to SPA1, and the only difference is that it considers the deformation from A1 time to HC time, Equation 3-12.

$$SPHC = \frac{AP1 - IOP}{DeflAmpMax - DeflAmpA1}$$

Equation 3-12

- **Corneal Asphericity (*P* and *R* Values):** Using corneal asphericity Equation 3-13, coordinates of each profile at the relaxed position and after inflation was inserted into an optimisation algorithm to obtain shape factor (*P*) and apical radius (*R*) values.

The “fminsearch” Matlab function was used to minimise the error in differences between Y values predicted from Equation 3-13 and actual elevation data of corneal profile by optimising P and R .

$$Y^2 = 2 \times R \times X - P \times X^2$$

Equation 3-13

where: R = apical radius
 P = shape factor

when $P < 1$ prolate ellipse – flattens from centre to periphery
 $P = 1$ circle
 $P > 1$ oblate ellipse – steepens from centre to periphery

The analysis above was repeated for seven different corneal profiles at angles defined in section 3.5. This calculation took 1.5 minutes for each model, and as a result of analysing 23,328 models, this section took 25 days to complete. The analysis was performed on the University of Liverpool’s Linux cluster system.

3.6 Development of IOP and Material Stiffness Equations

For this study, two main equations needed to be developed to estimate biomechanically corrected Intraocular Pressure (bIOP2) and material stiffness or Stress-Strain Index (SSI2). Two healthy equations were developed that are applicable to the majority of eyes. In regards to bIOP2, to further improve the accuracy of estimation, a new equation was developed for a particular disease that distorts both geometry and corneal material stiffness, keratoconus. The parameters utilised in this equation incorporate topographical features that can be obtained from section 3.2.1. This new equation is denoted as bIOP2_{kc} to distinguish the difference from the healthy equation in this study. In terms of SSI2, two specialised equations were developed to improve the performance of estimating corneal mechanical behaviour in (1) patients who undergo LASIK and SMILE surgical procedures and (2) those who have keratoconus or done crosslinking. The method used to develop these equations are similar, and this is explained in the next section and also in Figure 3-30.

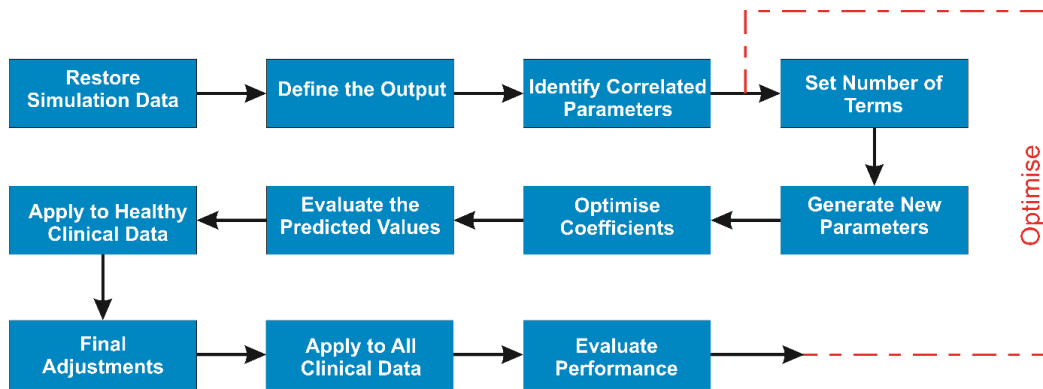


Figure 3-30 Optimisation method developed to generate equations

3.6.1 Biomechanically Corrected IOP

This section describes the method utilised to develop bIOP2 healthy and keratoconic equations. The data collected from the numerical simulation, as explained in section 3.5 was deployed into a Matlab script explicitly developed for finding optimum equations. Statistical analysis was performed to evaluate the correlation between various parameters and IOP. All parameters that showed any correlation with IOP were considered in the equation.

3.6.1.1 bIOP2 for Healthy (bIOP2)

The equation developed in this section was obtained through multiple optimisations procedures. The base parameters ($bPar$) selected for this equation as inputs are CCT , age , API , HCR , $DeflAmpA1$, $A1V$, $DefAmpMax$, HCT , PD , P and R while the output defined as IOP. In the optimisation algorithm developed for obtaining optimum equation, the base parameters were used in many different combinations to obtain a term (Te) that can predict the IOP with the highest accuracy. The formula for these terms is shown in Equation 3-14. The objective of this optimisation was to minimise the difference between predicted IOP and the actual IOP values set for numerical models. This code started from three terms for the equation. Each term could have one of the following forms.

1. $bPar_i$
2. $bPar_i^2$
3. $bPar_i^3$
4. $bPar_i \times bPar_j$
5. $bPar_i \times bPar_j \times bPar_k$

The code was able to change these parameters, add to the number of terms and in each case optimise the coefficients and calculate the error of the predicted IOP in comparison to the actual value, Equation 3-14. Once the optimisation was completed, and the

optimum terms were found, the equation was tested on clinical data obtained from healthy cases described in section 3.7.2.

$$\text{Output} = C_1 \times Te_i + C_2 \times Te_j + C_3 \times Te_k + \dots + C_4$$

Equation 3-14

Once the estimated IOP values were obtained from clinical data, output IOP correlation with CCT and Age was assessed, and final adjustments were made to improve the accuracy. The final equation was then applied to several different databases, including patients who underwent corneal crosslinking (CXL) or refractive surgeries and those who had glaucoma or keratoconus. It should be noted that corneal asphericity parameters were calculated for clinical data in the same manner as it was described in section 3.5.9. Since corneal profiles on clinical data were tilted, this equation was slightly modified to consider the rotation of the data as an extra parameter in optimisation.

3.6.1.2 bIOP2 for KC (bIOP2-KC)

The equation developed in section 3.6.1.1, provided good results when applied to keratoconic eyes. bIOP2 equation only used the information that could be obtained from Corvis ST. To further improve the accuracy of this equation, using the method developed in section 3.2.1, cone parameters that include cone height, cone area, cone distance to the apex and cone location were incorporated into the equation. A similar optimisation technique (section 3.6.1.1) was developed to optimise coefficients of these parameters and develop a new equation able to predict IOP in KC data with more accuracy. The accuracy in prediction was defined by the differences between the mean KC and healthy IOP values.

3.6.2 Stress-Strain Index

As described in chapter two, section 2.2, the corneal tissue behaviour is non-linear, which means it has a different stiffness at different stress or strain level. A previous study conducted by Biomechanical Engineering Group at the University of Liverpool found that there was a clear trend between stress-strain curves of different age groups^{123,442}. In simple form, as people aged, the corneal tissue became stiffer while the stress-strain curves did not intersect, Figure 3-31. The equation that described this relationship was discussed in section, 3.5.4. With this knowledge stiffness of the cornea at different age groups could be calculated in relation to stiffness at age 50. Hence with this one single parameter (SSI), the complete stress-strain curve could be obtained. Based on this, theoretically, if SSI could be obtained in clinics, then the mechanical behaviour of the patient could be measured in-vivo.

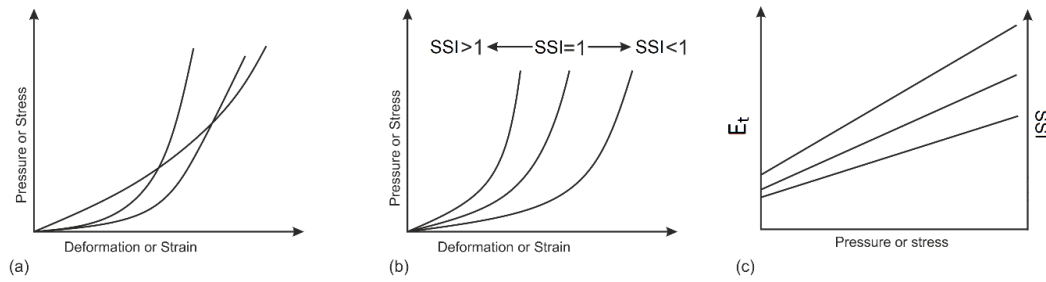


Figure 3-31 biomechanical behaviour of the cornea changes with age without any intersection as shown in figure “a” but instead consistently as shown in figure “b” that could translate to tangent modulus changes with stress as shown in figure “c”. SSI equal by one represent the material stiffness of a healthy cornea at age 50 and as the age increases the stiffness increases and vice versa.

This section describes the method utilised to develop SSI2 equations. An equation was developed that could predict the material properties of healthy corneas with no known abnormality or surgical procedures that could influence mechanical response. A second equation was developed that was able to incorporate changes in corneal biomechanics due to keratoconus. Finally, the third equation was able to compensate for changes in mechanical response after LASIK or SMILE refractive correction surgical procedures. If it is not known that the eye has undergone refractive correction or has keratoconus, the healthy equation could still be applied, but the accuracy would be lower. The methods utilised to develop these equations are described below.

3.6.2.1 SSI2 for Healthy (SSI2-H)

Following a similar optimisation procedure, as described in section 3.6.1, the healthy SSI2-H equation was developed. The base parameters (*bPar*) selected for this equation as inputs were CCT, IOP, Age, AP1, HCR, DeflAmpA1, A1V, DefAmpMax, HCT, PD, P and R Values, SPA1 and SPHC while the output defined as corneal material stiffness. The objective here was to minimise the differences between the predicted corneal material stiffness and the actual value that was set for the numerical models. The equation started with three terms, and each term could have the following forms.

1. $bPar_i$
2. $bPar_i^2$
3. $bPar_i^3$
4. $bPar_i \times bPar_j$
5. $bPar_i \times bPar_j \times bPar_k$
6. $bPar_i \div bPar_j$
7. $\frac{bPar_i + bPar_j + bPar_k}{bPar_w + bPar_r}$

Once the optimum equation was obtained (similar to Equation 3-14), it was applied to healthy clinical cases as described in section 3.6.1.1 and final adjustments in regards to the correlations with CCT, IOP and Age were made. The equation was able to predict the material stiffness with good accuracy for all patients, including those with KC and

post LASIK or SMILE surgeries. However, there was room for further improvement for these exceptional cases by introducing other parameters which demanded the development of two more equations.

3.6.2.2 SSI2 for KC (SSI2-KC)

When the healthy SSI2 equation was applied to clinical data described in section 3.7, the mean value of SSI2-H was reducing with disease progression as expected. However, there were considerable overlaps between KC and healthy groups. A new equation was developed to improve the accuracy for the moment that clinical diagnosis is available. To develop this equation, the expected corneal stiffness in these patients were used as a benchmark and the coefficient of the equation in section 3.6.2.1 were optimised to provide the desired results. This equation was then applied to clinical data and evaluated by comparing them to healthy cases. No further correction was applied from clinical data to this equation.

3.6.2.3 SSI2 for Post LASIK and SMILE (SSI2-PLS)

The healthy SSI2 equation was applied to three different types of refractive surgeries that are PRK, LASIK and SMILE. In the PRK group, the mean pre and post values were similar for SSI2, which is expected. However, in LASIK and SMILE, due to the nature of the procedure and the flap/cap that does not contribute much to overall mechanical behaviour, the post-op values were estimated lower than the pre. In this group, similar to SSI2 in KC patients, coefficients of the generic SSI2 equation were optimised to correct the error induced by surgery. When the equation was developed, it then applied to various clinical databases and evaluated. The reason for this difference is discussed in details in chapter five, section 5.1.3.

3.7 Validation of Equations

To validate equations developed in this study, they were applied to various clinical data. Some of the healthy and KC cases are previously described in sections 3.2.2 and 3.4.1. Other clinical data that used were as below. Please note that these data were provided by Oculus for this research and due to confidentiality agreements, the name of clinics are not revealed.

3.7.1 Experimental Validation

Five ex-vivo human ocular globes (age 69 ± 3 years) were obtained from the Fondazione Banca degli Occhi del Veneto Onlus, Venice, Italy, and tested within 3-5 days post mortem. Ethical approval to use the specimens in research was obtained by the eye bank in accordance with the Declaration of Helsinki. The central corneal thickness (CCT) was measured using a DGH 55 Pachmate pachymeter (DGH Technology, Exton, USA). After removing the extraocular tissues, a G14 needle was inserted through the posterior pole, glued around the insertion point to prevent leakage, and used to remove the

vitreous. The inside of the globe was washed with Phosphate Buffered Saline (PBS, P4417, Sigma-Aldrich, Darmstadt, Germany) a few times until a smooth movement of fluid was achieved through the needle and a syringe connected to it. The eye was then injected with a 10% Dextran solution (Sigma-Aldrich, Darmstadt, Germany) to prevent swelling during the experiment, before fitting it inside the test rig. Throughout these steps, the eye was kept moist using Everclear; a viscous tear film supplement (Melleson Pharma, Breda, Netherlands) to prevent drying. Information presented in this section was previously published.¹⁰⁴

3.7.1.1 Test Setup

A custom-built inflation rig was used in the study to control the IOP in ex-vivo eye globes, and measure it with the Corvis ST, Figure 3-32. The rig included a support mechanism for the eye to allow it to sit in its natural position with the cornea horizontally facing the Corvis ST while preventing both vertical and horizontal rigid-body motion. Inside the horizontal support, a skin-safe, soft silicone rubber padding (Ecoflex® Series, Smooth-On, Pennsylvania, USA.) was placed to simulate the effect of fatty tissue around the eye.

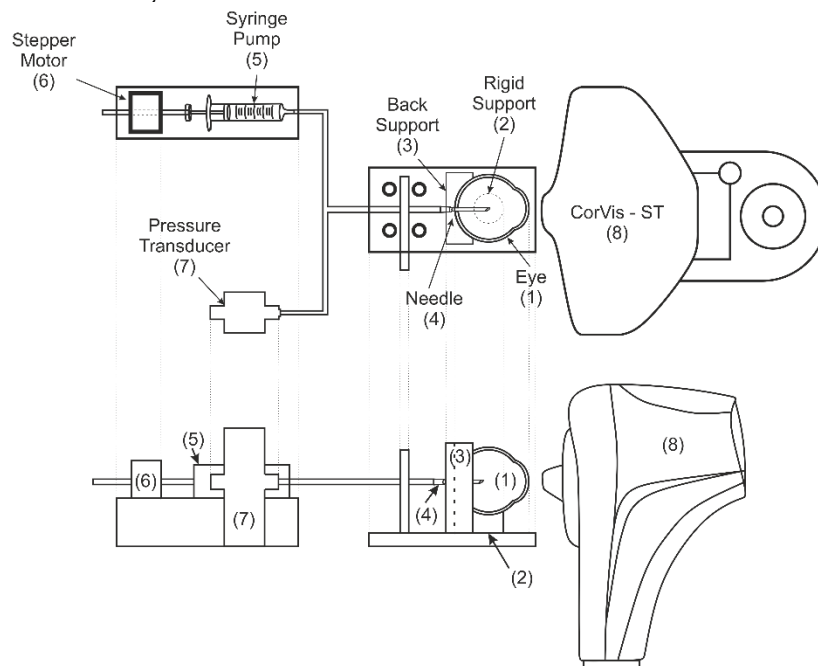


Figure 3-32 the diagram shows the structure of the test rig.

The needle that had been inserted through the posterior pole was connected to a 4mm diameter tube attached to a syringe pump, which was controlled using bespoke LabVIEW software. The pressure applied through the syringe pump on the inside of the globe was monitored using an FDW pressure transducer (RDP Electronics, Wolverhampton, UK) fixed at the same horizontal level as the centre of the eye to avoid pressure head differences. The readings of the pressure transducer were assumed to represent the true IOP (IOP_t) acting on the eye globe. IOP_t was controlled to vary

between values that covered the natural variation in IOP seen in ophthalmic practice; 10, 15, 20, 25 and 30 mmHg. These variations were introduced through the movement of a stepper motor connected to the syringe pump. After reaching each IOPt level, the eye was allowed to stabilise for 60 seconds before measuring IOP using the Corvis ST, which provided an uncorrected measurement (CVS-IOP) and a biomechanically-corrected measurement (bIOP and bIOP2). Corvis ST measurements, which included CCT, were taken at each IOPt level until at least three readings of acceptable quality were achieved. Acceptable quality was in reference to the Corvis ST built-in standards in assessing a reading, and as part of this assessment, the device could trace and record fully the deformation profiles of the cornea during the application cycle of the air puff. At least 120 seconds were allowed between successive Corvis measurements at the same IOPt that should enable the cornea to recover fully from the distortion caused by previous air puffs.

3.7.2 Healthy Cases

This section provides clinical information from data obtained from healthy participants. Institutional review boards at all institutions ruled that approval was not needed for record review studies. However, ethical approval for using the data in research had been secured at both institutions when the data was collected, anonymised, and used in earlier studies^{228,423}, before which participants' informed and written consent was secured before collecting the data. Nevertheless, the ethical standards set out in the 1964 Declaration of Helsinki, and revised in 2000, were observed. All patients were evaluated with a complete ophthalmic examination, including the Corvis ST and Pentacam (OCULUS Optikgeräte GmbH; Wetzlar, Germany). All patients were free of any ophthalmic disease, with a Belin/Ambrósio Enhanced Ectasia total deviation index (BAD-D) derived from the Pentacam of < 1.6 standard deviations (SD) from normative values in both eyes. Patients with previous ocular surgery or disease, myopia <-10D, concurrent, or previous glaucoma or hypotonic therapies were excluded.

All Corvis ST exams were acquired by the same experienced technicians with good quality scores (QS) that enabled the calculation of all Corvis dynamic corneal response parameters (DCRs). Moreover, a frame-by-frame analysis of the exams was performed by an independent masked examiner to ensure the quality of each acquisition. Only one eye per patient was randomly included in the analysis to avoid the bias of the relationship between bilateral eyes that could influence the analysis result. Any Corvis ST readings with visible rotational misalignment in the corneal profile were excluded from the analysis.

3.7.3 Keratoconic Cases

This multicenter retrospective study comprised persons enrolled at different hospitals to include variability from more than one continent. An institutional review board ruled

that approval was not obligatory for this study comprising a records review. However, the ethical standards set in the 1964 tenets of the Declaration of Helsinki and revised in 2000 were observed. All patients provided informed consent before their data were used in the study. All patients had a complete ophthalmic examination, including Corvis ST dynamic Scheimpflug analyzer and Pentacam rotating Scheimpflug camera (Oculus Optikgeräte GmbH) evaluations. Some of these data are previously published and used in this study.³⁸⁷

The inclusion criterion in the keratoconic groups was bilateral keratoconus without any former ocular surgeries, such as corneal crosslinking or intracorneal ring implantation. Moreover, to confirm the diagnosis, all examinations from each clinic were blindly reevaluated by a corneal expert at the other clinic. Only dynamic Scheimpflug analyzer examinations with good quality scores that enabled the calculation of all DCRs were included in the analysis. All measurements with the dynamic Scheimpflug analyzer were acquired by the same experienced technicians, and an additional manual frame-by-frame evaluation of the examinations, made by an independent masked examiner, was implemented to ensure the quality of acquisitions. Also, anterior and posterior topography maps were acquired using the rotating Scheimpflug camera and analyzed to determine the topography and thickness profiles of keratoconic eyes, which were then considered in the numerical parametric study. Only one eye per patient was randomly included in the analysis to avoid the possible effect of the relationship between bilateral eyes on the analysis results.

Further evaluation was performed by considering keratoconic eyes with different disease stages. For this purpose and based on the Topographic Keratoconus Classification (TKC) provided by the rotating Scheimpflug camera,⁴⁰¹ the keratoconus datasets were divided into three groups each as follows: mild, moderate, and advanced. According to this classification, mild keratoconus was defined as a TKC classification of abnormal, possible, -, and 1. Moderate keratoconus included TKC grade 1 to 2, 2, and 2 to 3, and advanced keratoconus included TKC grade 3, 3-pellucid marginal degeneration, 3 to 4, and 4.”

3.7.4 Refractive Surgeries Cases

Some of these clinical data are previously published by Joda et al. and reused in this study.⁴²⁵

Patients were treated for the correction of myopia or myopic astigmatism at different clinics. Inclusion criteria were myopia of fewer than 10 diopters (D) and/or astigmatism of less than 5D and a spherical equivalent (SE) higher than 1D but less than 10D. Patients with a central corneal thickness (CCT) less than 480 μ m, abnormal corneal topography, patients with glaucoma, glaucoma suspects, and patients receiving IOP-lowering medications were excluded from the study. The study was thoroughly discussed with each patient, and informed consent was obtained from all participants. The study

was approved by the local institutional review board and adhered to the tenets of the Declaration of Helsinki.

3.7.5 Glaucoma Cases

These data are previously published by Vinciguerra et al. and reused in this study.⁴⁴³

“Patients diagnosed using the criteria described below with Hypertension Glaucoma (HTG), Normal Tension Glaucoma (NTG), Ocular Hypertension (OHT) and healthy subjects were recruited over a period of 8 months in St Paul’s Eye Unit, Royal Liverpool University Hospital, UK. All patients provided informed consent for using their anonymised data in the study prior to the study commencement.

Inclusion criteria

POAG was defined as open-angle gonioscopy, glaucomatous optic disc and an abnormal visual field (VF) consistent with glaucoma confirmed by at least two reliable VF examinations. The definition of glaucomatous visual field defect was defined by two glaucoma hemifield tests graded “outside normal limits” and a cluster of three contiguous points at the 5% level on the pattern deviation plot, using the threshold test strategy with the 24-2 test pattern of the Zeiss-Humphrey field analyzer. Patients were divided into HTG and NTG based on an untreated GAT-IOP greater or lower than 21 mm Hg. OHT patients were defined as normal VF with an untreated GAT-IOP greater than 21 mm Hg, respectively. Healthy controls had an untreated GAT-IOP lower than 21 mm Hg, healthy discs and no ocular pathologies.

Exclusion criteria:

- Hypermetropia or myopia >5 diopters (D), and/or astigmatism >3 D, best-corrected visual acuity <20/40
- Ocular conditions that could mimic glaucomatous visual field loss, particularly congenital or acquired optic nerve diseases, or systemic conditions that could affect ocular blood flow, particularly diabetes mellitus and cerebrovascular diseases
- Previous ocular or intraocular surgery or previous trauma or corneal scarring

Ophthalmological examination

All participants underwent an initial complete ophthalmic examination. The OHT group also underwent automated perimetry using Humphrey Field Analyzer II (Carl Zeiss Meditec, Jena, Germany), with a full threshold 24–2 SITA standard programme. Global visual field parameters, including mean deviation (MD) and pattern SD (PSD), were recorded. IOP (mean of 3 measurements) and central corneal thickness (CCT) (mean of 25 measurements, one touch) were recorded using (GAT-IOP, Haag-Streit, Switzerland) and ultrasound pachymetry (DGH 55B Pachmate 2, DGH Technologies, Exton, Pennsylvania, USA), respectively, as well as corneal biomechanics and IOP measurement using the Corvis-ST. GAT-IOP was adjusted for pachymetry (GATAdj) using the manufacturer’s correction algorithm provided with the Pachmate 2, which is based on a reference corneal thickness of 545 μm from the work of Kohlhaas et al.⁴⁴⁴ Corvis measurements All measurements with the Corvis-ST (software V.6.08r22) were captured by the automatic release on alignment with the corneal apex and were all with ‘OK’ quality score. The DCRs used in the study were previously described.^{445,446} “

3.7.6 CXL Cases

Clinical data of patients were collected by different clinics. IRB approval in the form of written and informed consent was obtained to use the data in scientific research. The study followed the tenets of the Helsinki Declaration revised in 2013.

Patients with progressive keratoconus were identified from an increase in corneal curvature on instantaneous maps of at least 1.00D within the cone area whether accompanied by thinning of 20 μ m in the minimal corneal. These patients were referred to CXL and were included in this study. Exclusion criteria included other concomitant ocular diseases or the use of eye drops other than artificial tears, presence of central or paracentral corneal scars, corneal infection, systemic autoimmune diseases, pregnancy or breastfeeding. If both eyes of the same patients were submitted to the procedure, an eye was randomly chosen to conduct the analyses.

The data were obtained pre-CXL and at least four weeks after CXL using Corvis ST (OCULUS Optikgeräte GmbH; Wetzlar, Germany). The dynamic response parameters (DCR), including CCT and IOP values, were recorded and used to perform the statistical analysis required for this study. Data were collected using two different Corvis ST devices placed at two different centres. To increase the statistical power of the study, these data were combined to increase the reliability of the analysis. Also combining these data with reducing the biases associated with the data collection and variations between devices or technicians.

3.8 Summary

This section provided a detailed explanation of the methodology used to conduct this research and achieve the research goals. It started by introducing the newly developed method that was able to analyse tomography data obtained from commercially available devices to provide insights into cone properties in KC patients. It then dived into the development of numerical models and validation of models using clinical data. This was followed by running a complex parametric study to build the database needed for developing equations. After the simulation data were collected, they were analysed, DCR parameters were calculated and exported. Then through a new software program able to perform multiple optimisation processes, two main equations for BIOP2 and SSI2-H were developed. For specific conditions like keratoconus, CXL and those after LASIK and SMILE surgeries, further equations were developed to improve the accuracy of estimations. Finally, these equations were applied to a large clinical database with various eye conditions and experimental tests for validations.

Chapter Four

Results

4.1 Introduction

This chapter presents the main results produced by the methods and equations developed in this project. It starts by characterising cones of clinical cases, finding the cone centre locations, evaluating cone characteristics' (area, height and distance from the corneal apex) correlations with disease progression, analysing posterior cone's and establishing a relation between them and the anterior cones. Further analysis is provided for exploring cone height and area and the relation between cone characteristics and key topographical indices. The information obtained in this part fed into the development of numerical models and establishing a range of values used for parametric study. Section 4.3 is provided for numerical simulations that include results of the mesh density study that led to the optimum model structure. Once the model was developed, it was then validated by comparing patient-specific corneal FE models' deformations under air puff with nine healthy clinical cases, and the results are presented in section 4.4.

After the model validation and collection of parametric study data, new equations were developed to estimate IOP and material stiffness. The newly developed biomechanically corrected IOP is called bIOP2. Two bIOP2 equation were developed one for healthy, which relies purely on Corvis ST indices and another for keratoconic patients which in addition to Corvis ST, requires topographical analysis. This analysis of topography should be done using the method introduced in this thesis for the characterisation of the cone. Then bIOP2 equations are validated using experimental and clinical data. Experimental studies were conducted in a previous study.¹⁰⁴ The data of this study enabled a comparison between the new bIOP2 and true IOP values. Then bIOP2 applied to a large clinical data, including healthy and diseased and those after refractive surgery and corneal crosslinking. The bIOP2 values were compared with bIOP and Corvis ST uncorrected IOP (CVSIOP) and if available to Goldmann tonometry. This section is concluded by applying bIOP2-KC to eight datasets that included keratoconic patients, and the values were compared to bIOP2 to demonstrate improvements.

In this thesis, a new methodology was followed to develop equations for estimating the corneal material stiffness in vivo. This parameter is called Stress-Strain Index 2 (SSI2). There are three new equations developed for SSI2 that apply to different conditions. The discussion on this is provided in section 5.1.3. Initially, the results of SSI2-H is presented when applied to healthy eyes and those who undergo PRK surgery. Then the results for SSI2-KC are presented, and this equation was applied to keratoconic patients both before and after corneal crosslinking. Finally, the SSI-PLS developed specifically for post LASIK and SMILE corneas and evaluated in three different datasets. In all cases, the new SSI2 values were compared to previously developed SSI.¹⁰⁷ Finally, a brief conclusion is provided at the end of this chapter.

4.2 KC Topography

For the 309 keratoconic patients included in the study, the mean, standard deviation and range of age were 33 ± 11 years (9 - 72). The gender and ethnicity of patients were not recorded and therefore, not included in this analysis. Among the right eyes, those with mild, moderate and severe KC were 102, 130 and 77 respectively, while the corresponding numbers for left eyes were 90, 148 and 130. For each eye, the location and normal height of the cone centre and the transition zone between the cone-shape area and the remaining corneal tissue were estimated using the proposed method. Figure 4-1 presents a typical example where the cone centre and transition zone (presented by a black dot and a dashed line, respectively) are plotted on corneal tangential curvature maps and standard elevation maps for both the anterior and posterior surfaces.

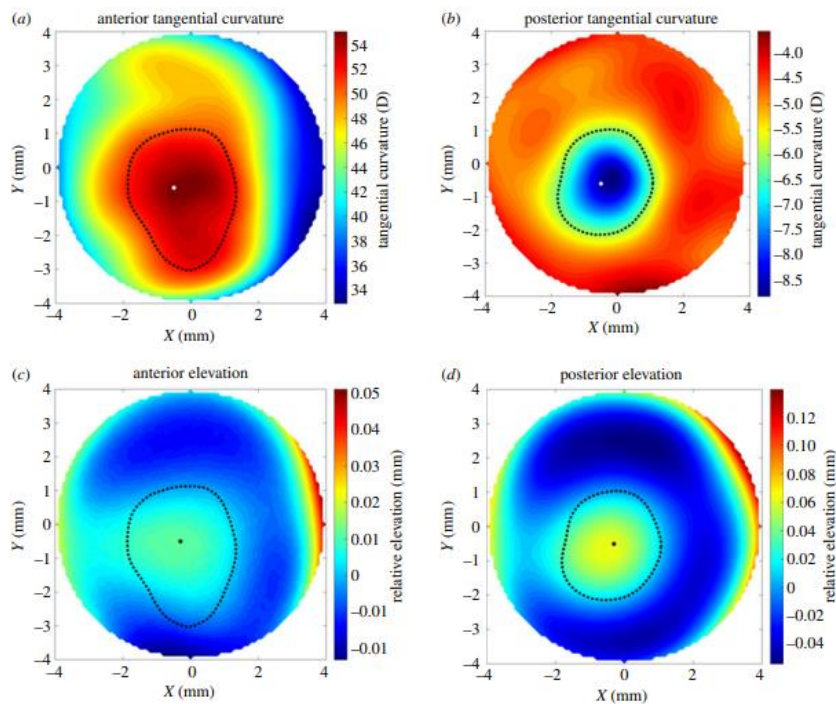


Figure 4-1 Location of cone centre and transition zone estimated using the proposed method for the left eye of a 29-year-old patient with moderate keratoconus. The results are plotted on tangential curvature maps (A, B) and maps of elevation relative to the optimal sphere (C, D).

4.2.1 Cone Characteristics

The results showed a mirror symmetry between right and left eye groups. Whereas in the right eyes, 76% and 82% of anterior and posterior cone centres were located in the temporal-inferior quadrant, respectively, the corresponding figures in the left eyes were 82% and 84%. The posterior cone centre was superiorly located relative to the anterior cone centre by 0.119 ± 0.216 mm in right eyes and 0.096 ± 0.227 mm in left eyes ($p=0.070$). The areas of the cone in the right and left eyes were also similar; with values of $7.36\pm 2.27\text{mm}^2$ (0.01 - 12.54) and $7.21\pm 2.22\text{mm}^2$ (1.13 - 12.54), respectively ($p=0.051$). The cone centre heights were also similar in right and left eyes at $36\pm 22\text{um}$ (2 - 107) and $37\pm 23\text{um}$ (3 - 129), $p=0.559$, in anterior surfaces and $74\pm 44\text{um}$ (8 - 244) and $75\pm 45\text{um}$ (5 - 243), $p=0.619$, in posterior surfaces. The results further demonstrate consistently that posterior cone height was larger than anterior cone height in 90% of cases and by $37\pm 24\text{um}$ (0 - 158) on average. On the other hand, the cone area presented was larger on the anterior surface ($7.77\pm 3.07\text{mm}^2$) than on the posterior surface ($7.26\pm 3.92\text{mm}^2$, $p<0.001$)

4.2.2 Cone Centre Location

Considering only the majority of the cones, which are located in the temporal-inferior quadrant, the anterior cone centre was located at 1.019 ± 0.403 mm (0.1 - 1.8) on the inferior side and 0.663 ± 0.434 (0.1 - 1.8) mm on the temporal side of the left eyes and located at 0.939 ± 0.388 (0.1 - 1.7) mm on the inferior side and 0.683 ± 0.424 (0.1 - 1.8) mm on the temporal side of right eyes. In posterior surfaces, the cone centre was located at 0.938 ± 0.344 (0.2 - 1.6) mm towards the inferior side and 0.610 ± 0.359 (0.1 - 1.4) mm towards the temporal side in left eyes and at 0.813 ± 0.345 (0.2 - 1.5) mm towards the inferior side and 0.734 ± 0.371 (0.1 - 1.5) mm towards the temporal side in right eyes, Figure 4-2.

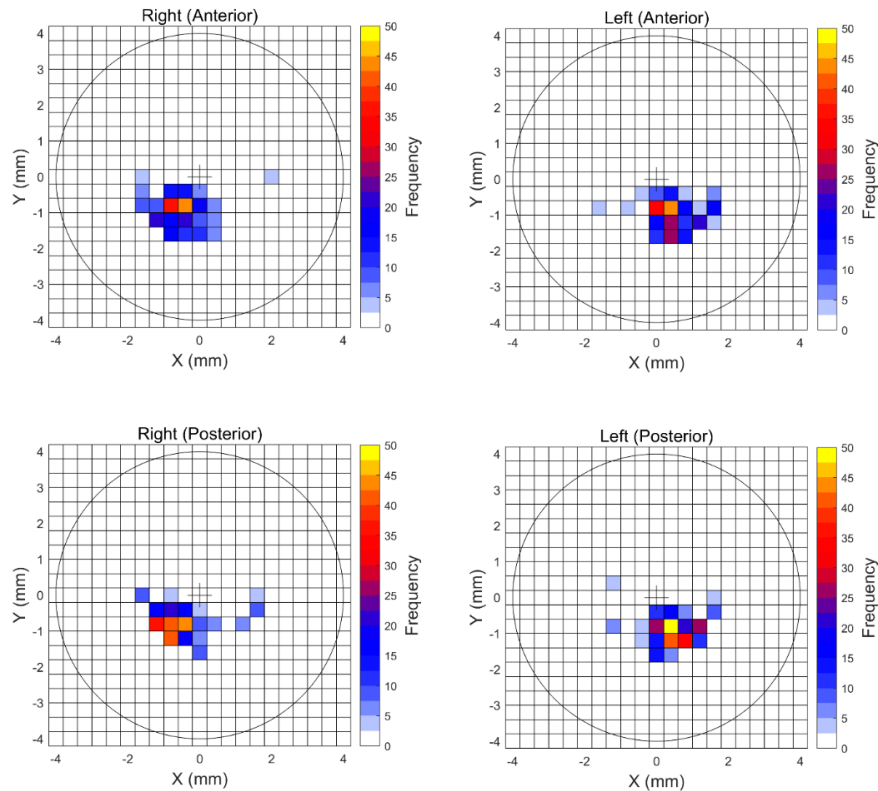


Figure 4-2 Frequency of cone centre location in (A) anterior surfaces of right eyes, (B) anterior surfaces of left eyes, (C) posterior surfaces of right eyes, and (D) posterior surfaces of left eyes

The results further show a strong correlation between the locations of cone centres on the anterior and posterior surfaces ($p < 0.001$). This correlation could be used to estimate the shifts between the two cone centres using the relationship used in chapter three, Equation 3-5 and Equation 3-6.

4.2.3 Correlation between Cone Characteristics and Disease Severity

The results showed evidence that with increased disease severity, the distance from corneal apex to cone centre reduced ($p < 0.001$, $R = -0.312$), while cone height increased ($p < 0.001$, $R = 0.716$). On the other hand, the cone area did not show statistically significant differences among the disease stages ($p = 0.002$, $R = -0.092$), Figure 4-3.

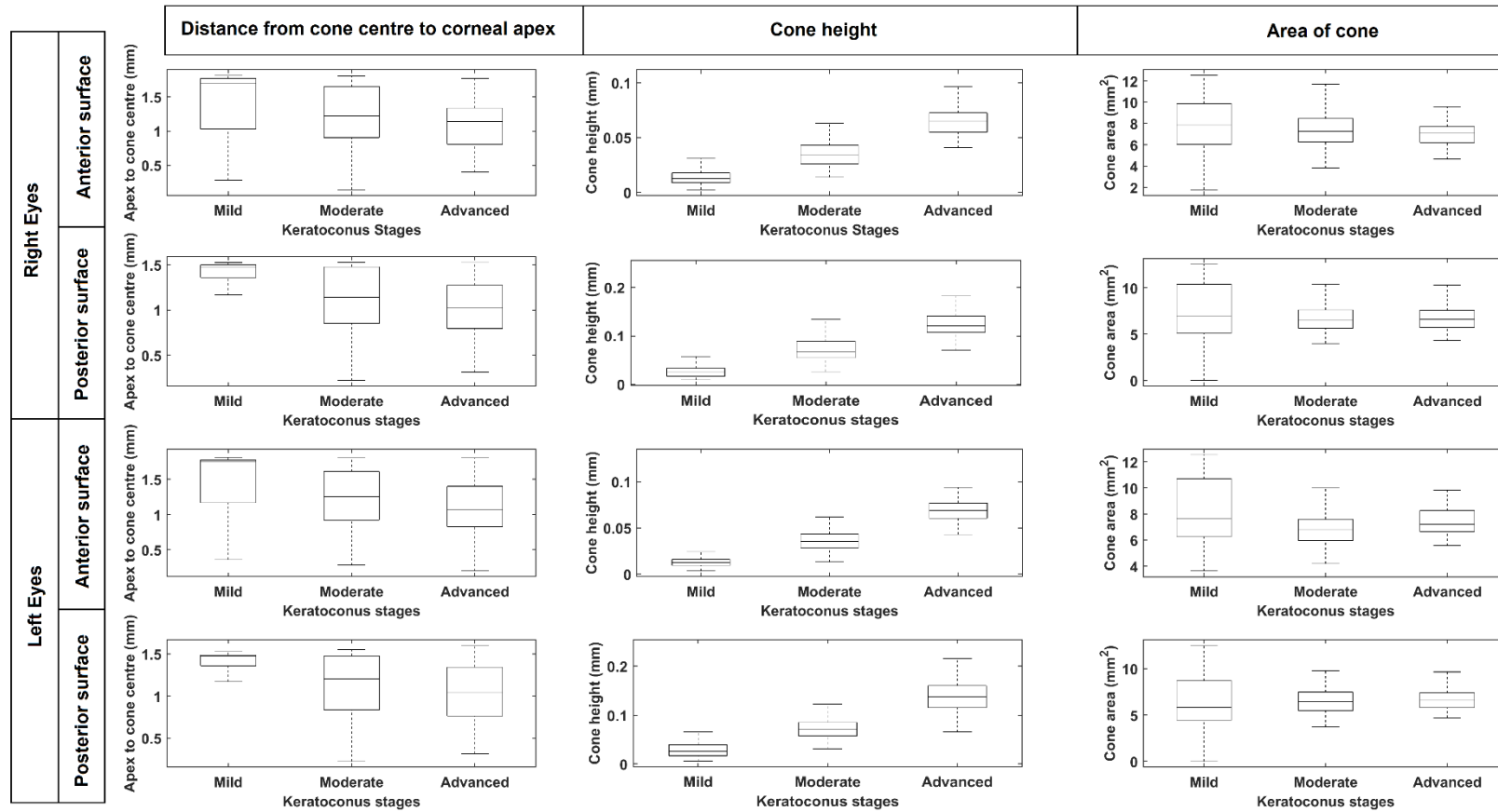


Figure 4-3 Mean, standard deviation, minimum and maximum values of distance from cone centre to corneal apex (left column), cone height (middle column) and area of cone (right column) for eyes with mild KC (left = 90, right = 102), moderate KC (left = 148, right = 130) and advanced KC (left = 71, right = 77). Results are presented for anterior and posterior surfaces of right and left eyes.

4.2.4 Posterior Cone Height in Relation to Anterior Cone

The results also show strong correlation between anterior cone height and posterior cone height ($p < 0.001$, $R = 0.784$ for right eyes and $p < 0.001$, $R = 0.774$ for left eyes). This strong correlation was evident when combining all the data or considering data separately for eyes with different KC severity extents, Figure 4-4. The relationship between the two cone heights follows the relationship used in chapter three, Equation 3-4

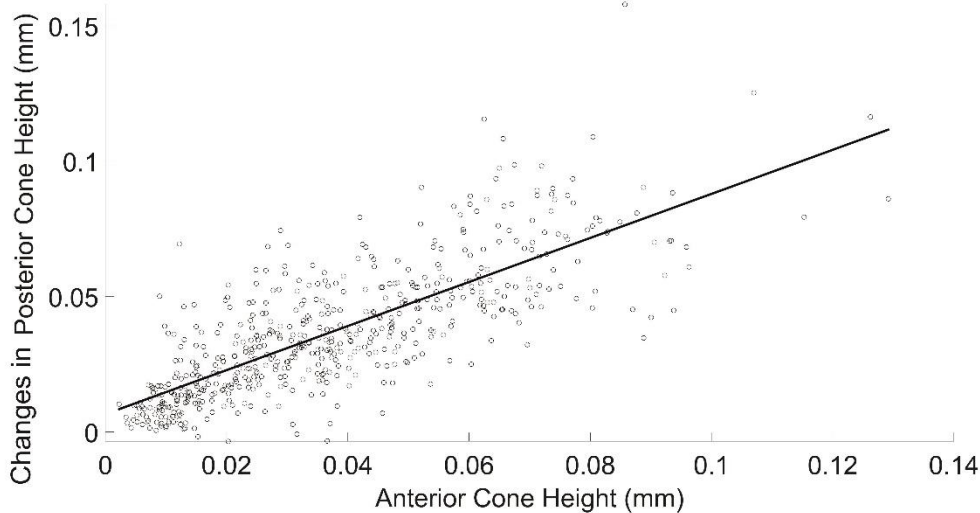


Figure 4-4 Correlation between anterior cone height and posterior cone height when considering all data (Note: the y axis is the extra change in the posterior cone height in comparison to the anterior cone height)

4.2.5 Correlation of Cone Height and Pathology Area with Radius of Optimum Sphere

The results show a significant correlation between the cone height and radius of the optimum sphere for anterior surfaces ($R = -0.584$, $p < 0.001$) and posterior surfaces ($R = -0.568$, $p < 0.001$) in all eyes. Meanwhile, there was no significant correlation between the area of pathology and the radius of the optimum sphere (obtained from sphere fitting to the cornea without the cone) for both anterior surfaces ($R = 0.012$, $p = 0.769$) and posterior surfaces ($R = 0.003$, $p = 0.945$), Figure 4-5.

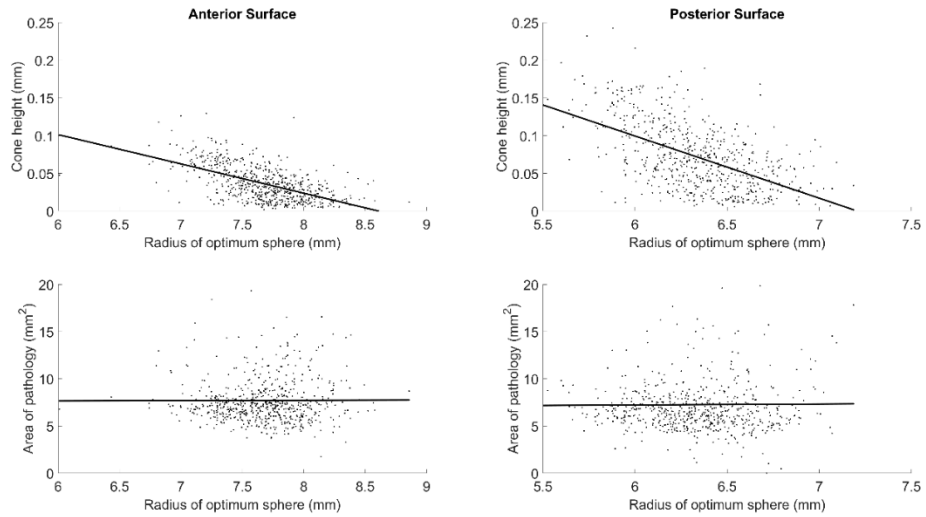


Figure 4-5 Correlation of cone height and pathology area with the radius of the sphere of optimal fit for both anterior and posterior surfaces

4.2.6 Evaluation of Cone Properties with Pentacam Indices

The correlations of cone height, cone area and distance from corneal apex to cone centre with age and key Pentacam parameters were explored in

Table 4-1, and showed similar results in the right and left eyes. As expected, cone height and location were not correlated with age in both right and left eyes and both corneal surfaces ($p > 0.11$). On the other hand, cone height was strongly correlated with almost all tomographic parameters, especially the BAD-D, KMax and EleFBFS8mm ($R > 0.9$). The distance to the corneal apex, as expected, showed a negative correlation with central metrics like central asphericity and CKI ($R < -0.6$).

Table 4-1 Correlation between distance from corneal apex to cone centre, cone area and cone height with Pentacam parameters (p values that indicate significant correlation are highlighted in green).

| Pentacam Parameters | | Right eyes | | | | Left eyes | | | |
|--|-----------|------------------|---------|-------------------|---------|------------------|---------|-------------------|---------|
| | | Anterior surface | | Posterior surface | | Anterior surface | | Posterior surface | |
| | | R Value | p Value | R Value | p Value | R Value | p Value | R Value | p Value |
| Distance from cone centre to corneal apex (mm) | BADD | -0.355 | 0 | -0.462 | 0 | -0.347 | 0 | -0.459 | 0 |
| | Pachy | 0.166 | 0.003 | 0.306 | 0 | 0.201 | 0 | 0.324 | 0 |
| | Age | 0.102 | 0.074 | -0.049 | 0.387 | 0.041 | 0.475 | 0.031 | 0.593 |
| | AstigD | -0.024 | 0.672 | -0.098 | 0.084 | 0.091 | 0.109 | -0.041 | 0.476 |
| | EleBFS8mm | -0.237 | 0 | -0.254 | 0 | -0.161 | 0.005 | -0.194 | 0.001 |
| | Kmax | -0.405 | 0 | -0.469 | 0 | -0.466 | 0 | -0.542 | 0 |
| | AsphQ | 0.645 | 0 | 0.634 | 0 | 0.727 | 0 | 0.732 | 0 |
| | ISV | -0.255 | 0 | -0.336 | 0 | -0.255 | 0 | -0.327 | 0 |
| | IVA | -0.091 | 0.11 | -0.158 | 0.005 | -0.084 | 0.142 | -0.138 | 0.015 |
| | KI | -0.227 | 0 | -0.279 | 0 | -0.244 | 0 | -0.297 | 0 |
| | CKI | -0.637 | 0 | -0.636 | 0 | -0.718 | 0 | -0.724 | 0 |
| | IHA | 0.001 | 0.987 | -0.023 | 0.685 | -0.164 | 0.004 | -0.202 | 0 |
| IHD | -0.146 | 0.01 | -0.222 | 0 | -0.16 | 0.005 | -0.199 | 0 | |
| Height of cone (mm) | BADD | 0.898 | 0 | 0.961 | 0 | 0.903 | 0 | 0.965 | 0 |
| | Pachy | -0.549 | 0 | -0.587 | 0 | -0.528 | 0 | -0.564 | 0 |
| | age | 0.071 | 0.214 | 0.094 | 0.118 | 0.033 | 0.56 | 0.088 | 0.141 |
| | AstigD | 0.594 | 0 | 0.553 | 0 | 0.555 | 0 | 0.486 | 0 |
| | EleBFS8mm | 0.926 | 0 | 0.886 | 0 | 0.922 | 0 | 0.887 | 0 |
| | Kmax | 0.895 | 0 | 0.882 | 0 | 0.862 | 0 | 0.833 | 0 |
| | AsphQ | -0.636 | 0 | -0.644 | 0 | -0.471 | 0 | -0.507 | 0 |
| | ISV | 0.96 | 0 | 0.911 | 0 | 0.97 | 0 | 0.913 | 0 |
| | IVA | 0.863 | 0 | 0.794 | 0 | 0.902 | 0 | 0.832 | 0 |
| | KI | 0.892 | 0 | 0.835 | 0 | 0.904 | 0 | 0.853 | 0 |
| | CKI | 0.721 | 0 | 0.72 | 0 | 0.629 | 0 | 0.644 | 0 |
| | IHA | 0.366 | 0 | 0.339 | 0 | 0.302 | 0 | 0.279 | 0 |
| IHD | 0.775 | 0 | 0.746 | 0 | 0.794 | 0 | 0.735 | 0 | |
| Area of cone (mm) | BADD | -0.174 | 0.002 | -0.158 | 0.008 | -0.123 | 0.031 | -0.025 | 0.671 |
| | Pachy | 0.104 | 0.069 | 0.077 | 0.196 | 0.054 | 0.347 | 0.015 | 0.802 |
| | age | 0.163 | 0.004 | 0.032 | 0.593 | 0.158 | 0.005 | 0.133 | 0.025 |
| | AstigD | -0.141 | 0.013 | -0.132 | 0.027 | -0.115 | 0.044 | -0.031 | 0.602 |
| | EleBFS8mm | -0.121 | 0.034 | -0.118 | 0.047 | -0.083 | 0.145 | 0.033 | 0.577 |

| | | | | | | | | |
|--------------|--------|-------|--------|-------|--------|-------|--------|-------|
| Kmax | -0.192 | 0.001 | -0.103 | 0.085 | -0.19 | 0.001 | 0.007 | 0.908 |
| AsphQ | 0.103 | 0.071 | -0.024 | 0.692 | 0.182 | 0.001 | -0.052 | 0.383 |
| ISV | -0.168 | 0.003 | -0.088 | 0.142 | -0.108 | 0.059 | 0.043 | 0.469 |
| IVA | -0.173 | 0.002 | -0.117 | 0.05 | -0.107 | 0.061 | 0.025 | 0.68 |
| KI | -0.121 | 0.034 | -0.054 | 0.366 | -0.089 | 0.118 | 0.039 | 0.513 |
| CKI | -0.12 | 0.036 | -0.005 | 0.935 | -0.136 | 0.017 | 0.069 | 0.249 |
| IHA | -0.103 | 0.072 | -0.139 | 0.02 | -0.127 | 0.026 | -0.085 | 0.152 |
| IHD | -0.248 | 0 | -0.183 | 0.002 | -0.176 | 0.002 | -0.053 | 0.37 |

4.3 Numerical Simulation

4.3.1 Element Type

In this study, two identical models with the only difference of element types were compared. Under air puff pressure, the 6-noded models with 5 and 15 corneal rings converged successfully. Models with 25, 35 and 45 corneal rings crashed during the simulation at different time points. Models with 15-noded elements converged in all cases. The details of these results are provided in section 4.3.3.

4.3.2 Corvis ST Pressure

The mean and standard deviation of Corvis ST pressure in 280 clinical cases were calculated. The pressure applied to the cornea was the mean pressure values at the nozzle that was reduced by 50%, as shown in Figure 4-6.

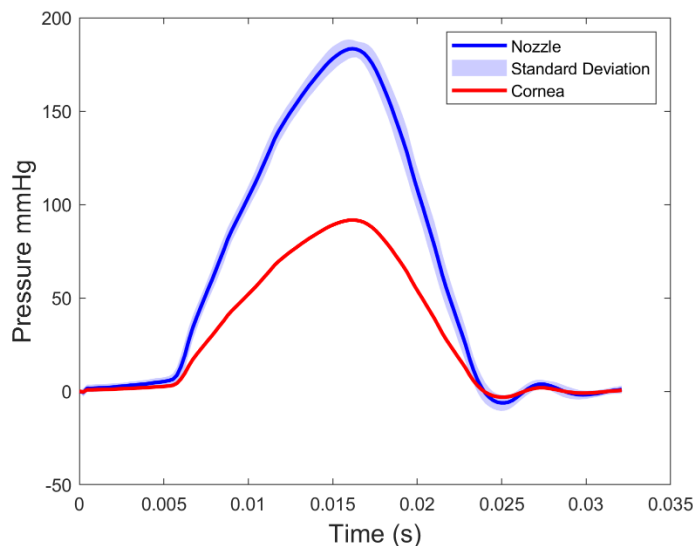


Figure 4-6 the mean and standard deviation of 280 cases and the pressure applied on the cornea

4.3.3 Mesh Density Study

Corneal rings were varied from 5 to 45 rings. Apex deformation under air puff with 10 to 45 rings produced similar results in 15-noded elements, Figure 4-7. The average corneal deformation under air puff for these cases were 798.2 ± 3 microns. The model

with ten rings was found to be closest to this value with a difference of only 2.3 microns, and this was the number of corneal rings selected for this study. This model could run in 16 minutes.

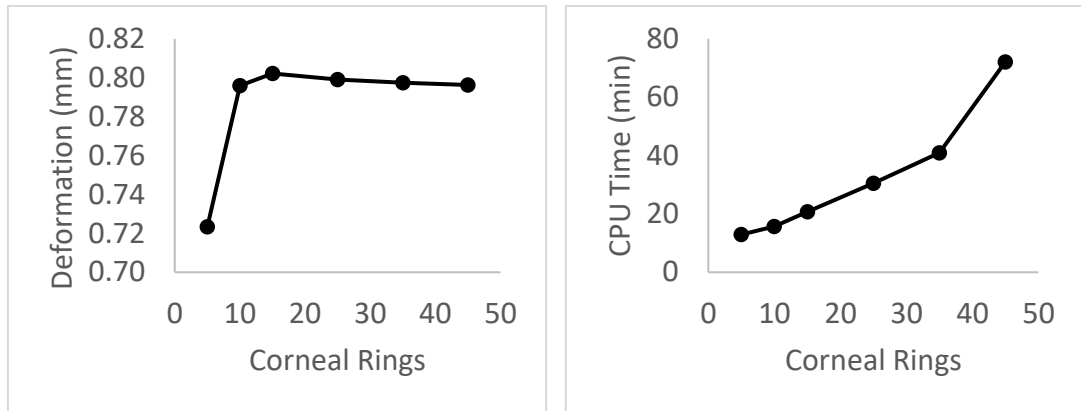


Figure 4-7 Mesh convergence study for cornea showing the deformation of apex under air puff pressure (left) and the computational time for corresponding rings (right)

The mesh convergence study for sclera followed a similar path to the cornea; the sclera rings were varied from 10 to 50, Figure 4-8. As can be seen from the deformations of the corneal apex, changes in sclera rings did not have a significant effect on the deformation of the cornea under air puff. The average value for this deformation was 795.7 ± 0.2 microns, and the closest model to this number had ten rings with a 0.2 microns difference. Hence the 10 rings model was selected for sclera in this study, and it reduced the simulation time to 3 minutes.

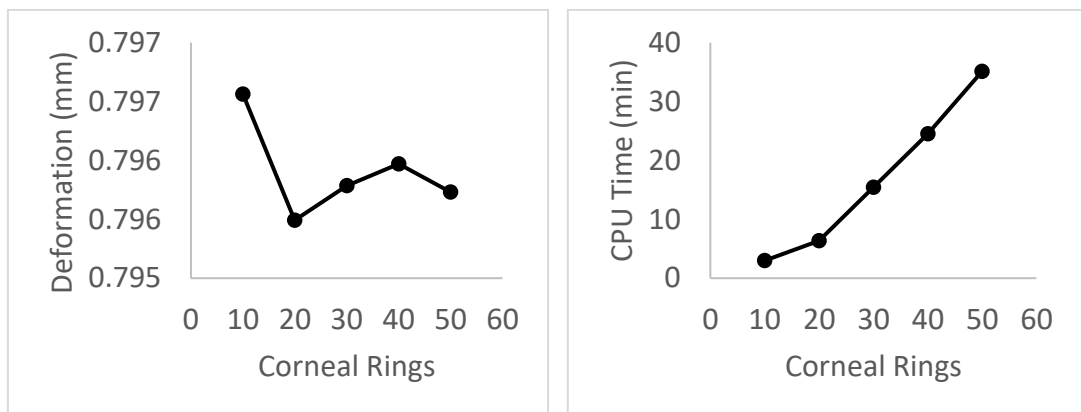


Figure 4-8 Mesh convergence study for sclera showing the deformation of the apex under air puff (left) and the time of simulation for corresponding rings (right)

When four and six segmented models were compared, no differences were found in corneal apex deformation throughout the simulation for both inflation and air pressure. The model with six segments took 2.7 minute, whereas four-segment models due to having fewer elements could run in 1.8 minutes. Hence the optimum mesh for the model was found with four-segment and used in the rest of the study.

4.4 Validation of Numerical Models

To validate the performance of numerical models and ensure they are representative of clinical data, nine healthy cases were tested. The demographics for these patients were provided in the methodology chapter section 3.4.1. The material stiffness of the cornea and sclera was adjusted based on the age of the patient and IOP was accordingly set as measured in the clinic. All models showed good agreement with clinical data, as shown in Figure 4-9. The RMS for these nine cases were found to be 31 ± 8 (20 - 45) microns across the 8 mm profile. Due to the stress-free process and the use of Pentacam topographies for each patient, the initial profile after inflation and before the start of air puff perfectly matched the clinical data.

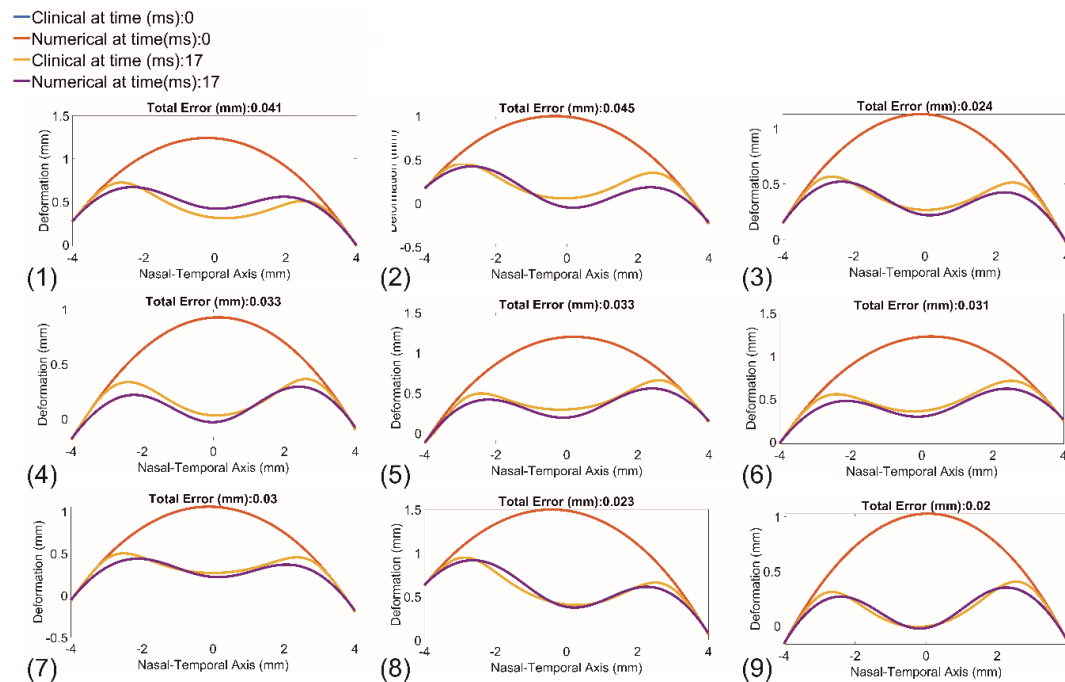


Figure 4-9 Comparison of numerical and clinical data for nine healthy corneas showing the deformation under air puff at the initial profile and highest concavity. The error presented above each plot is referring to the root mean squared of the deformation (mm) error across the full profile.

4.5 Equations

This section provides the results of applying methods developed in chapter three to clinical data. It starts with the bIOP2 equation in comparison to bIOP, CVSIOP and GAT. Then the comparison between bIOP2 and bIOP2-kc are provided. In terms of SSI2, all three equations were compared with SSI in healthy, KC, CXL and refractive surgery data. The aim of this section is to demonstrate that the bIOP2 has a weak correlation with CCT and *age* while SSI2 has a weak correlation with CCT and IOP with an increased correlation with *age*. This is the standard method of evaluation for IOP and material stiffness measurement methods in the literature.

4.5.1 Biomechanically Corrected IOP (bIOP2)

Two IOP equations were developed in this study, bIOP2 for healthy eyes which uses information collected from Corvis ST and bIOP2KC. The latter requires elevation data to be analysed, as described in section 4.2 and incorporates cone properties into the equations. The first section applies bIOP2 for healthy eyes on various clinical data. The second section explores bIOP2KC equation in comparison to bIOP2 in the KC database.

4.5.1.1 bIOP2 Healthy Equation

The bIOP2 equation for healthy eyes relies purely on parameters obtained from Corvis ST. This section applies this equation to various datasets, including KC eyes to evaluate its performance. The parameters presented in Equation 4-1 showed to be able to compensate for biomechanical and geometrical changes while estimating the IOP and hence they were selected for this equation.

$$bIOP2 = f(CCT, Age, AP1, PD, HCR, DeflAmpMax, A1V, DeflAmpA1, HCT)$$

Equation 4-1

where *CCT* is the central corneal thickness (microns), *AP1* is the pressure at applanation one (mmHg), *PD* is the Peak Distance (mm), *HCR* is the radius at highest concavity (mm), *DeflAmpMax* is the deflection amplitude maximum (mm), *A1V* is the velocity at applanation one (m/s), *DeflAmpA1* is the deflection amplitude at applanation one (mm) and *HCT* is the time at highest concavity (ms).

4.5.1.1.1 Experimental Validation

The experimental study was done in a previous study, and the data was available to evaluate the performance of bIOP2, ⁴⁴⁷. The purpose of this is to demonstrate how the IOP values measured from ex-vivo human eyes using Corvis ST compare to the true IOP that was set in strict laboratory conditions. In cases where *CCT* was above 600, the error in CVSIOP significantly increased, whereas in bIOP and bIOP2 there were no sudden changes in estimations. The average error in prediction of true IOP in percentage for CVSIOP found to be the highest 36 ± 37 (-3 - 155)% and consistently overestimating the true IOP. This was followed by bIOP where the error was -1 ± 1 (-3 - 19) % and bIOP2 with the error of 0 ± 4 (-6 - 15)%. Both bIOP and bIOP2 had underestimation and overestimation of IOP values with minimal standard deviations. Although bIOP2 overall performed better in predictions, the standard deviation of errors was smaller in bIOP results. No significant differences were found between both bIOP ($p=0.989$) and bIOP2 ($p=0.976$) with true IOP. CVSIOP was significantly different ($p < 0.001$) from the true IOP. The detailed comparisons of the findings are provided in Table 4-2.

Table 4-2 Comparison between True IOP measured experimentally with CVSIOP, bIOP and bIOP2

| # | Age (year) | CCT (microns) | True IOP (mmHg) | CVSIOP (mmHg) | Error (%) | bIOP (mmHg) | Error (%) | bIOP2 (mmHg) | Error (%) |
|---|------------|----------------------|-----------------|----------------------|-----------|----------------------|-----------|----------------------|-----------|
| 1 | 69 | 619±21.5 (598-639) | 10 | 25.5±0.9 (24.5-26.5) | 155% | 10.4±1.2 (8.7-11.5) | 4% | 11.5±0.6 (10.9-12.4) | 15% |
| | | 620.3±2.1 (618-622) | 15 | 30.5±0.5 (30-31) | 103% | 14.9±0.3 (14.6-15.2) | -1% | 15.5±0.6 (14.9-16) | 3% |
| | | 620.3±10.7 (611-632) | 20 | 36.2±0.3 (36-36.5) | 81% | 20±0.6 (19.4-20.4) | 0% | 19.8±0.5 (19.3-20.2) | -1% |
| | | 622.3±2.5 (620-625) | 25 | 41.3±0.6 (41-42) | 65% | 24.8±0.6 (24.4-25.5) | -1% | 24±0.6 (23.6-24.7) | -4% |
| | | 625.5±3.5 (623-628) | 30 | 47.3±0.4 (47-47.5) | 58% | 30.2±0.5 (29.8-30.5) | 0% | 28.6±0.4 (28.3-28.8) | -5% |
| 2 | 67 | 464.5±4.9 (461-468) | 10 | 14.8±0.4 (14.5-15) | 48% | 10.1±0.1 (10-10.1) | 1% | 9.5±0 (9.4-9.5) | -5% |
| | | 484.5±13.3 (472-503) | 15 | 19.3±1 (18-20.5) | 28% | 14.3±0.8 (13.3-15.2) | -5% | 15.6±0.3 (15.1-15.8) | 4% |
| | | 490±1.7 (489-492) | 20 | 23.5±0 (23.5-23.5) | 18% | 18.4±0.1 (18.3-18.5) | -8% | 21±0.3 (20.6-21.2) | 5% |
| | | 495.3±1.3 (494-497) | 25 | 28±0.4 (27.5-28.5) | 12% | 23±0.6 (22.1-23.5) | -8% | 24±0.3 (23.8-24.5) | -4% |
| | | 484.7±8.7 (475-492) | 30 | 31.8±1 (31-33) | 6% | 27.5±1 (26.5-28.4) | -8% | 30.2±1 (29.1-30.9) | 1% |
| 3 | 76 | 600±26.7 (560-615) | 10 | 13.3±1 (12.5-14.5) | 33% | 10±0.8 (8.9-10.8) | 0% | 10.3±0.3 (9.9-10.5) | 3% |

| | | | | | | | | | |
|---|---|----------------------|----|----------------------|-----|----------------------|------|----------------------|-----|
| | | 610.3±8 (602-618) | 15 | 17±0.5 (16.5-17.5) | 13% | 13.2±0.9 (12.4-14.1) | -12% | 15.3±0.4 (14.8-15.6) | 2% |
| | | 602.3±20 (582-622) | 20 | 21.8±0.8 (21-22.5) | 9% | 18±0.2 (17.9-18.2) | -10% | 19.7±0.4 (19.3-20.1) | -2% |
| | | 597±6.1 (590-601) | 25 | 27.2±0.3 (27-27.5) | 9% | 23±0.3 (22.7-23.3) | -8% | 24.7±0.1 (24.6-24.8) | -1% |
| | | 609±1 (608-610) | 30 | 31.2±1 (30-32) | 4% | 26.4±1 (25.2-27.1) | -12% | 29.8±0.8 (29-30.5) | -1% |
| 4 | 3 | 771±6 (765-777) | 10 | 16.5±0.5 (16-17) | 65% | 10.4±0.4 (10-10.8) | 4% | 9.4±0.2 (9.2-9.6) | -6% |
| | | 745±6.6 (738-751) | 15 | 21±0.5 (20.5-21.5) | 40% | 14.8±0.6 (14.3-15.4) | -1% | 15.5±0 (15.5-15.5) | 3% |
| | | 736±1 (735-737) | 20 | 28.5±0.5 (28-29) | 43% | 21.5±0.5 (21-22) | 8% | 20.5±0.4 (20.1-20.8) | 2% |
| | | 725±2.8 (723-727) | 25 | 33±0.7 (32.5-33.5) | 32% | 26.1±0.6 (25.6-26.5) | 4% | 24.8±0.3 (24.5-25) | -1% |
| | | 721.3±9.3 (711-729) | 30 | 37.8±0.6 (37.5-38.5) | 26% | 30.1±0.6 (29.7-30.8) | 0% | 30.1±1.4 (28.5-30.9) | 0% |
| 5 | 6 | 513.7±14.6 (500-529) | 10 | 12.7±0.8 (12-13.5) | 27% | 7±0.3 (6.8-7.4) | -30% | 10.4±0.2 (10.2-10.6) | 4% |
| | | 546.5±32.9 (499-570) | 15 | 16±0.4 (15.5-16.5) | 7% | 17.8±1.1 (16.9-19.3) | 19% | 14.9±0.7 (14.4-15.9) | -1% |
| | | 551.3±11.4 (540-565) | 20 | 19.5±0.4 (19-20) | -3% | 21.1±1.2 (20.3-22.9) | 5% | 20±0.7 (19-20.5) | 0% |
| | | 583±37.2 (560-649) | 25 | 26.7±0.9 (25.5-28) | 7% | 29.2±1.7 (27.2-31.9) | 17% | 24.9±0.4 (24.4-25.4) | 0% |
| | | 575.7±4.7 (572-581) | 30 | 31.7±0.8 (31-32.5) | 6% | 34.2±0.7 (33.8-35) | 14% | 29.7±0.4 (29.3-30.1) | -1% |

4.5.1.1.2 Healthy Patients

For brevity, only one of the datasets is presented in this section. A similar analysis was conducted on other datasets and results are available in Appendices, Section A.

Dataset 1

Dataset 1 includes 528 healthy patients with mean age of 39.9 ± 16.8 (7.0 -91.0) years and CCT of 537 ± 33 (444 -635) microns. The mean IOP values obtained from CVSIOP, bIOP and bIOP2 were 15.0 ± 2.7 (6.0 -29.0) mmHg, 14.4 ± 2.3 (9.1 -23.9) mmHg and 15.4 ± 1.3 (12.4 -22.6) mmHg, respectively. bIOP2 was least correlated with CCT ($p:0.285$, $R:-0.047$) and age ($p:0.050$, $R:0.085$). bIOP performed better in correlation with CCT ($p:0.139$, $R:-0.064$) than CVSIOP ($p:0.000$, $R:0.345$). CVSIOP showed weaker correlation ($p:0.011$, $R:0.111$) with age in comparison to bIOP ($p:0.004$, $R:-0.124$), Figure 4-10.

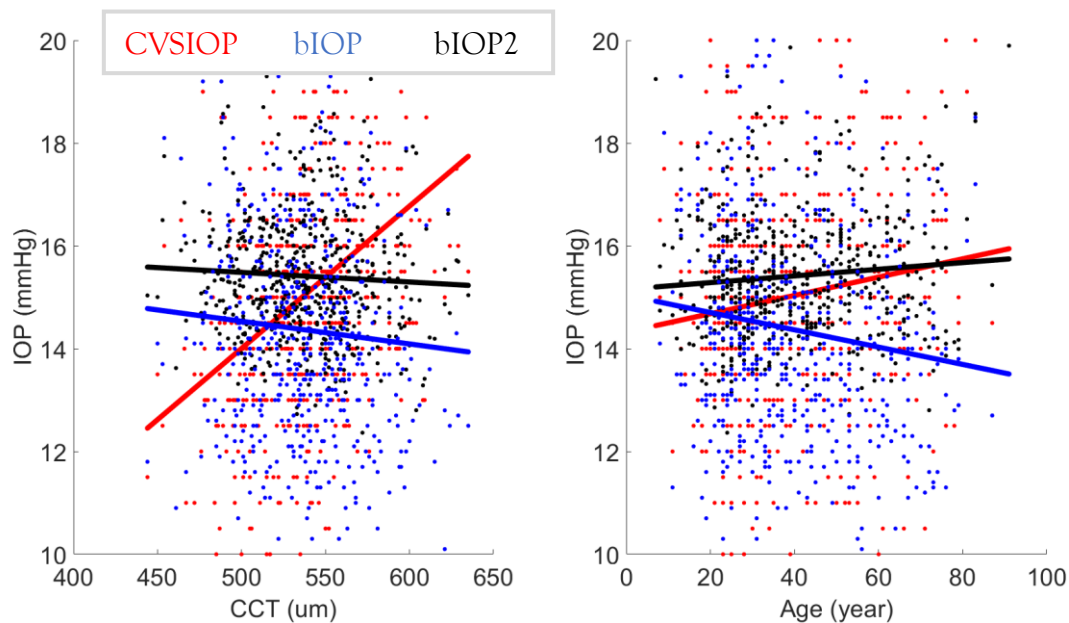


Figure 4-10 Correlation of IOP values from CVSIOP, bIOP and bIOP2 with CCT (left) and age (right) in Dataset 1

Summary of Results

bIOP2 was applied to 7 datasets with a total of 2117 healthy patients. Each dataset was obtained from a different clinic, located in various parts of the world. Specific details remain confidential based on the agreement in place with the device manufacturer and BioEG. The bIOP showed a weak correlation with CCT in the majority of these datasets. Although small improvements were achieved by bIOP2 in regards to CCT, it is not significant. Interestingly in six datasets, bIOP showed negative correlations with age whereas bIOP2 remained insignificant in all seven datasets. The overall comparison showed the correlation with CCT ($p:0.986$, $R:-0.000$) and age ($p:0.981$, $R:-0.001$) was weakest in bIOP2. bIOP showed weaker correlation with CCT ($p:0.972$, $R:-0.001$)

compared to CVSIOP ($p:0.000$, $R:0.367$). In terms of correlation with age, CVSIOP ($p:0.122$, $R:-0.034$) performed better than bIOP ($p:0.000$, $R:-0.196$).

4.5.1.1.3 Comparison between GAT, DCT, ORA and Corvis ST

This dataset consists of 422 healthy patients with a mean age of 27.114 ± 5.513 (17-42) years, CCT of 543 ± 28 (474-630) microns, DCT IOP of 17.2 ± 2.7 (10.3-28.1) mmHg, GAT IOP of 13 ± 2.2 (6.5-18.5) mmHg, ORA IOPg of 14.7 ± 2.7 (7.3-23.3) mmHg, ORA IOPcc of 15.4 ± 3.5 (8.5-26.5) mmHg, CVSIOP of 14 ± 1.9 (8.8-20.8) mmHg, bIOP of 13.7 ± 1.7 (9.4-19.1) mmHg and bIOP2 of 14.9 ± 1 (12.7-18.9) mmHg. The results of the correlation analysis are provided in Table 4-3. It is clear that all measurements are influenced by age apart from bIOP2 and all measurements are influenced with CCT apart from bIOP and bIOP2, Figure 4-11.

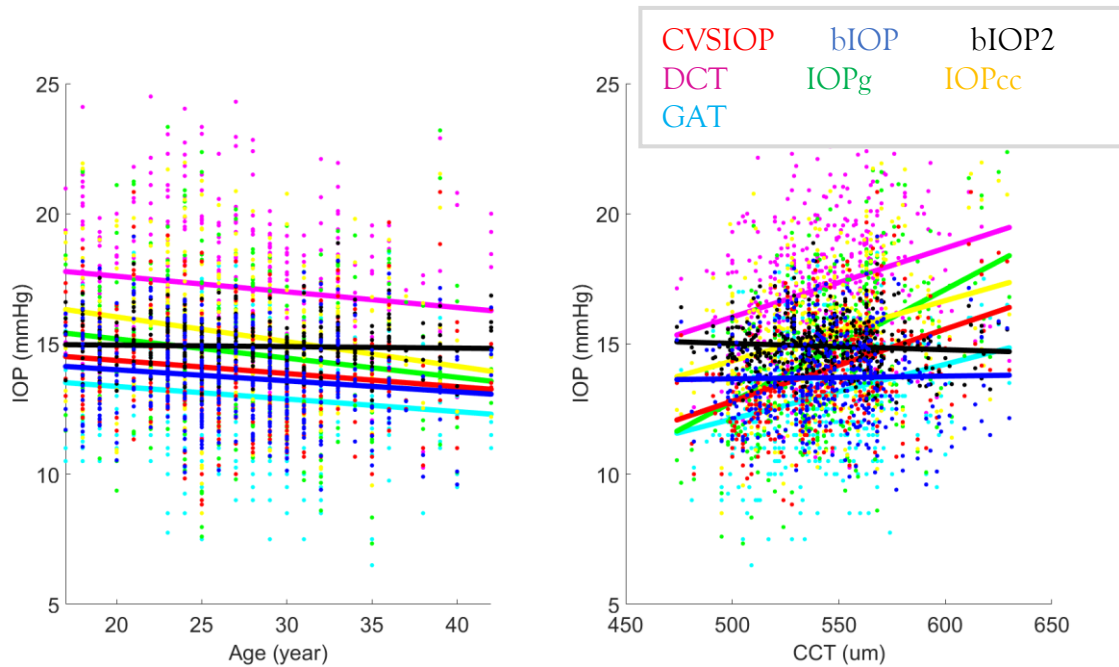


Figure 4-11 Correlation between DCT, GAT, ORA and three Corvis ST IOP measurements with age and CCT

Table 4-3 The correlation between various IOP measurements and tonometry devices with CCT and age

| | Age (year) | CCT (microns) |
|------------------|---------------------|---------------------|
| DCT IOP (mmHg) | R: -0.124, p: 0.012 | R: 0.274, p < 0.01 |
| GAT IOP (mmHg) | R: -0.120, p: 0.015 | R: 0.264, p < 0.01 |
| ORA IOPg (mmHg) | R: -0.151, p < 0.01 | R: 0.452, p < 0.01 |
| ORA IOPcc (mmHg) | R: -0.152, p < 0.01 | R: 0.189, p < 0.01 |
| CVSIOP (mmHg) | R: -0.143, p < 0.01 | R: 0.401, p < 0.01 |
| bIOP2 (mmHg) | R: -0.034, p: 0.497 | R: -0.071, p: 0.150 |
| bIOP (mmHg) | R: -0.138, p < 0.01 | R: 0.017, p: 0.726 |

Summary of Results

A comparison was conducted between different tonometers in 422 healthy eyes. In this study GAT, DCT, ORA and Corvis ST were used on patients. From ORA, two IOP values of IOPg and IOPcc were exported, and from Corvis ST three IOP values for CVSIOP, bIOP and bIOP2 were exported. In this study, all devices apart from Corvis ST showed significant correlations with age and CCT. Among Corvis ST values, CVSIOP was significantly correlated with both age and CCT. The correlation with CCT was not significant for both bIOP (R: 0.017, p: 0.726) and bIOP2 (R: -0.071, p: 0.150). In regards to age, bIOP2 (R: -0.034, p: 0.497) was the only parameter that showed no correlation. This study showed that with the use of bIOP2, Corvis ST becomes the only device able to estimate IOP values that are least influenced by corneal biomechanics and geometrical variations between patients.

4.5.1.1.4 Refractive Surgeries

For brevity, only one of the datasets is presented in this section. A similar analysis was conducted on other datasets and results are available in Appendices, Section A.

Dataset 1 - LASIK

Dataset 1 includes 52 patients who undergo LASIK surgery with mean age of 36.8 ± 6.7 (26.0 - 47.0) years, CCT of 543 ± 36 (473 - 611) microns, CVSIOP of 15.2 ± 3.2 (10.5 - 28.5) mmHg, bIOP of 14.8 ± 2.4 (11.6 - 25.2) mmHg and bIOP2 of 15.7 ± 1.5 (13.5 - 22.0) mmHg. The correlation with age was weak for CVSIOP (R:0.196, p:0.159), bIOP (R:0.088, p:0.532) and bIOP2 (R:0.235, p:0.090). CCT correlation was the weakest for bIOP2 (R:0.063, p:0.656) followed by bIOP (R:0.253, p:0.068) and CVSIOP (R:0.552, p:0.000), Figure 4-12.

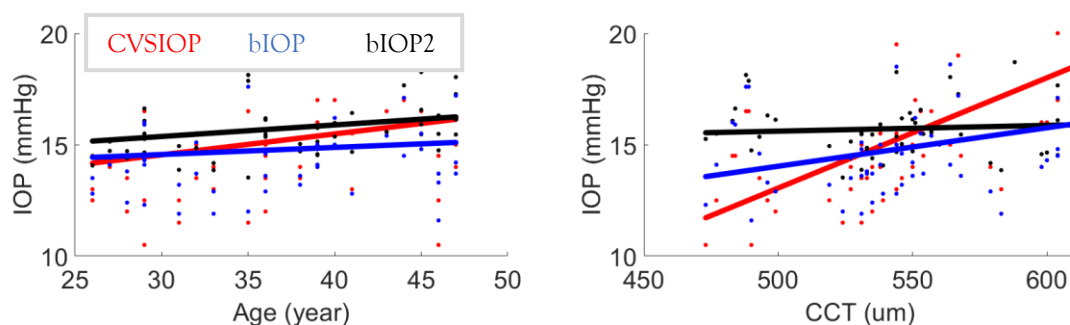


Figure 4-12 Correlation of IOP values from CVSIOP, bIOP and bIOP2 with CCT (left) and age (right) in pre-surgery LASIK Dataset 1

Demographics for post-operative data showed mean age of 37.1 ± 6.9 (27 - 48) years, CCT of 481 ± 33 (409 - 537) microns, CVSIOP of 11.6 ± 1.7 (7.5 - 14.5) mmHg, bIOP of 12.9 ± 1.5 (9.6 - 16.0) mmHg and bIOP2 of 15.3 ± 1.0 (13.0 - 17.2) mmHg. The

Wilcoxon signed-rank test showed no significant differences between pre and post-surgery measurements of bIOP2 ($p=0.088$), whereas both bIOP ($p=0.000$) and CVSIOP ($p=0.000$) were significantly different. The correlation remained weak with age for CVSIOP ($R:0.223$, $p:0.109$), bIOP ($R:0.043$, $p:0.760$) and bIOP2 ($R:-0.005$, $p:0.973$). The correlation with CCT was weakest for bIOP ($R:-0.090$, $p:0.520$) followed by bIOP2 ($R:-0.127$, $p:0.364$) and CVSIOP ($R:0.164$, $p:0.240$), Figure 4-13.

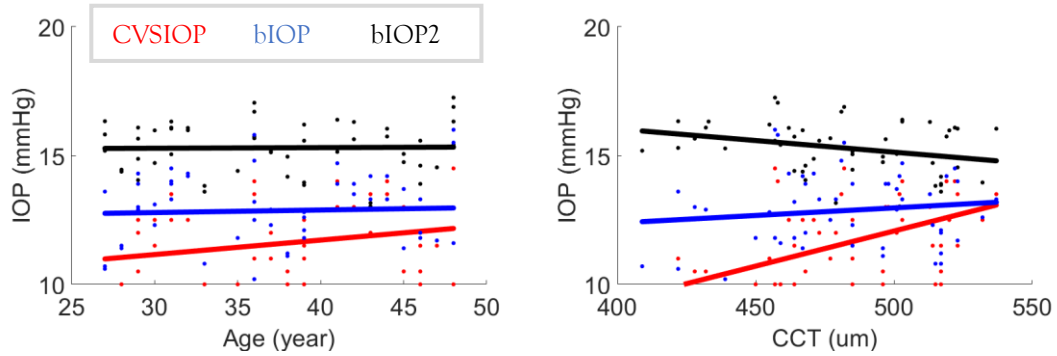
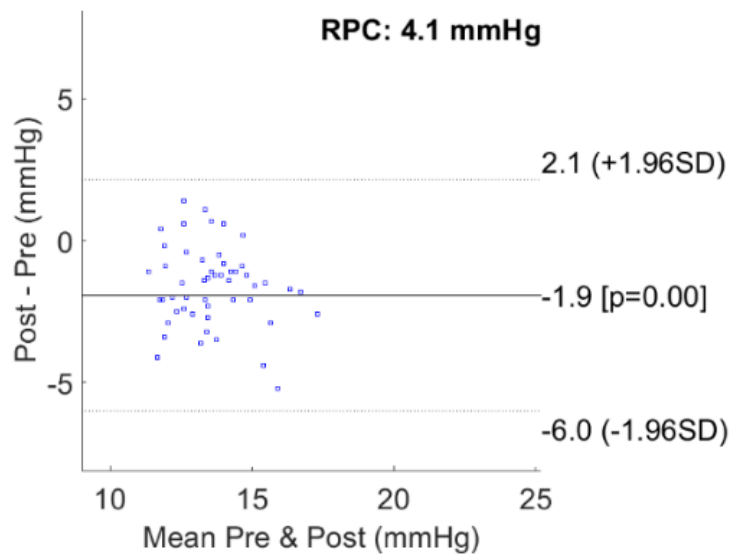
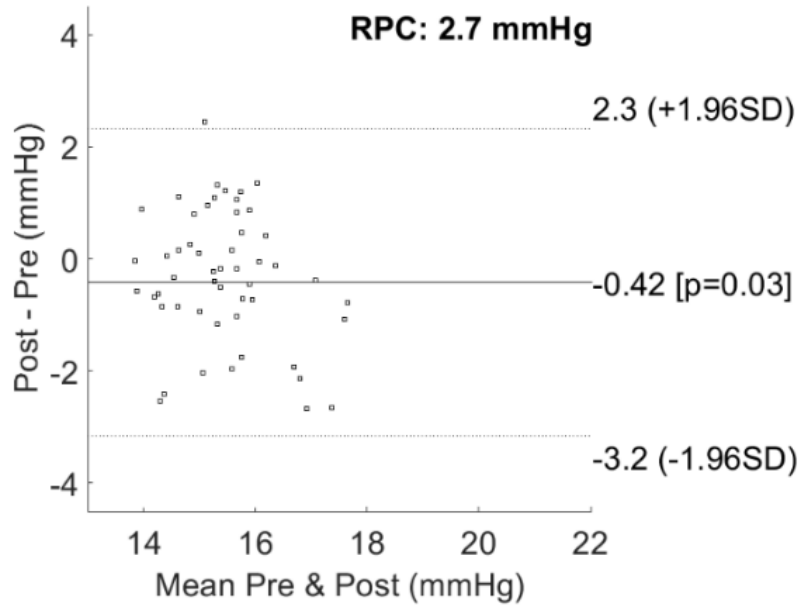


Figure 4-13 Correlation of IOP values from CVSIOP, bIOP and bIOP2 with CCT (left) and age (right) in post-surgery LASIK Dataset 1

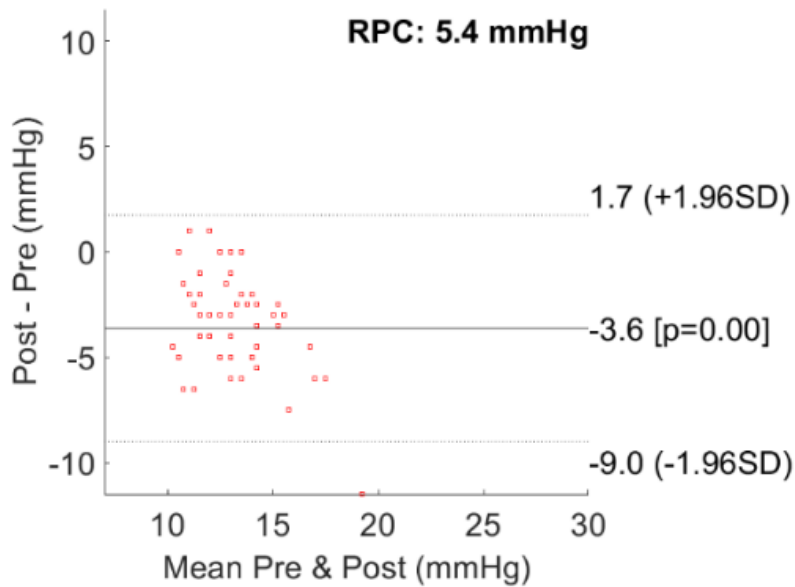
To better evaluate the differences between pre and post-refractive surgery data, Bland Altman plots were produced for each measurement method, Figure 4-14. Among all data, bIOP2 had the least differences in mean IOP values between pre and post with only 0.42 mmHg and the smallest standard deviation. This was followed by bIOP with differences of 1.9 mmHg and CVSIOP with differences of 3.6 mmHg.



(A)



(B)



(C)

Figure 4-14 The Bland Altman plots for (A) bIOP, (B) bIOP2 and (C) CVSIOP comparing the pre and post IOP values in LASIK Dataset 1

Dataset 1 - SMILE

Dataset 1 includes 82 patients who undergo SMILE surgery with mean age of 34.8 ± 7.7 (22.0 - 51.0) years, CCT of 541 ± 33 (480-642) microns, CVSIOP of 14.5 ± 2.4 (9.0 - 25.5) mmHg, bIOP of 14.3 ± 2.0 (9.6 - 21.1) mmHg and bIOP2 of

15.6 ± 1.3 (13.2 - 19.6) mmHg. The correlation with age was weak for CVSIOP (R:0.062, P:0.577), bIOP (R:0.062, P:0.581) and bIOP2 (R: 0.144, P:0.197). CCT correlation was the weakest for bIOP (R:-0.017, P:0.880) followed by bIOP2 (R:-0.132, P:0.238) and CVSIOP (R:0.354, P:0.001), Figure 4-15.

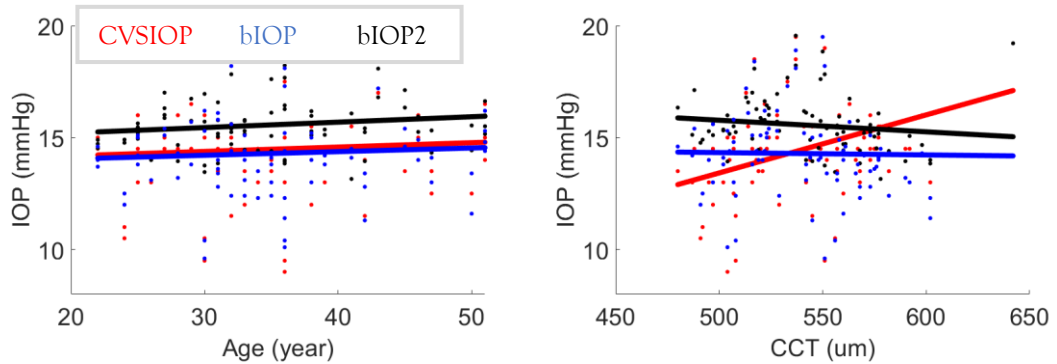


Figure 4-15 Correlation of IOP values from CVSIOP, bIOP and bIOP2 with CCT (left) and age (right) in pre-surgery SMILE Dataset 1

Demographics for post-operative data showed mean age of 35.2 ± 7.5 (22.0 -51.0) years, CCT of 444 ± 39 (351-545) microns, CVSIOP of 10.3 ± 2.2 (5.5 - 15.0) mmHg, bIOP of 12.3 ± 2.0 (8.1 -16.1) mmHg and bIOP2 15.7 ± 0.8 (12.5 -18.6) mmHg. The Wilcoxon signed-rank test showed no significant differences between pre and post-surgery measurements of bIOP2 (p:0.278), whereas both bIOP (p=0.000) and CVSIOP (p=0.000) were significantly different post-surgery. The correlation remained weak with age for CVSIOP (R:0.122, P:0.274), bIOP (R:0.021, P:0.854) and bIOP2 (R:0.090, P:0.421). The correlation with CCT was weakest for bIOP (R:0.111, P:0.320) followed by bIOP2 (R:-0.154, P:0.167) and CVSIOP (R:0.217, P:0.051), Figure 4-16.

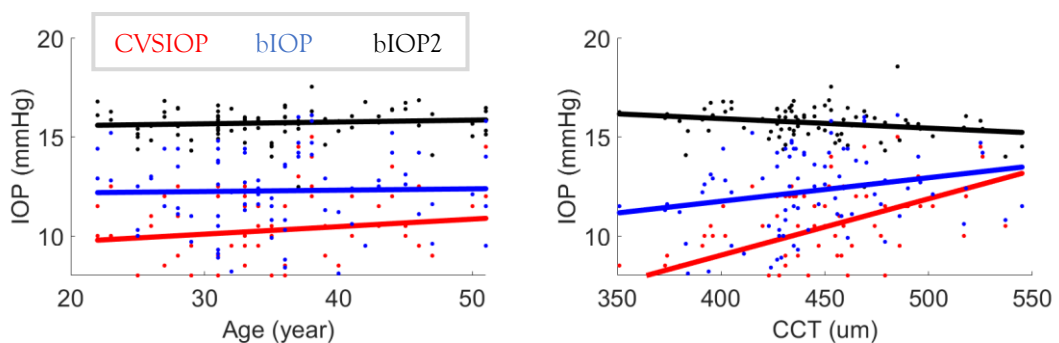
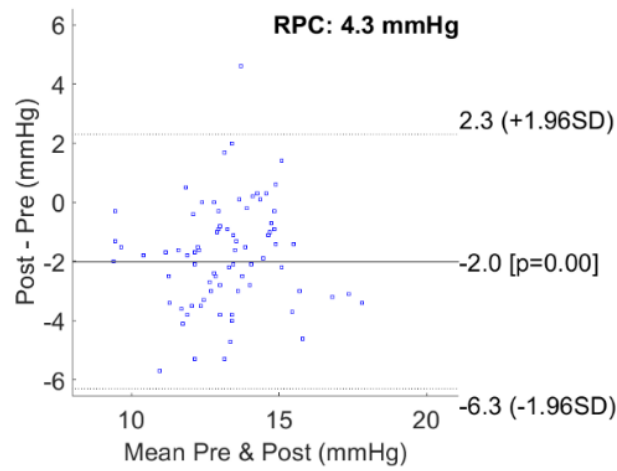
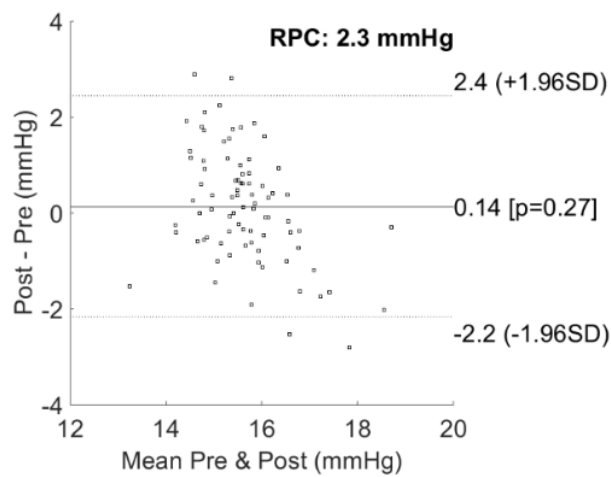


Figure 4-16 Correlation of IOP values from CVSIOP, bIOP and bIOP2 with CCT (left) and age (right) in post surgery SMILE Dataset 1

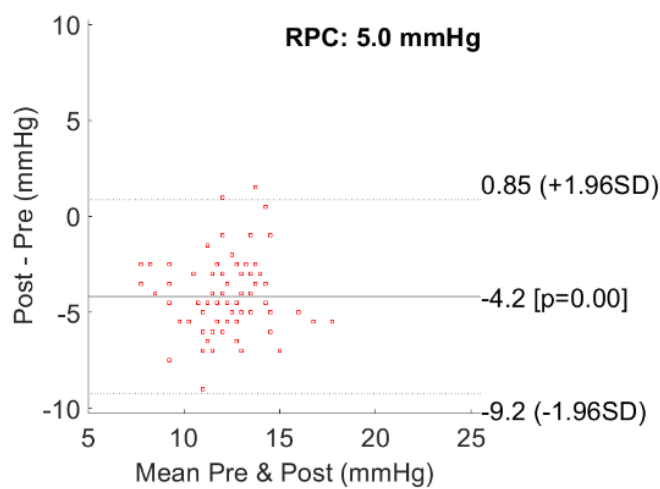
To better evaluate the differences between pre and post-refractive surgery, Bland Altman plots were produced for each IOP measurement method, Figure 4-17. Among all data, bIOP2 had the least differences in mean IOP values between pre and post with only 0.14 mmHg and the smallest standard deviation. This was followed by bIOP with differences of 2.0 mmHg and CVSIOP with differences of 4.2 mmHg.



(A)



(B)



(C)

Figure 4-17 The Bland Altman plots for (A) bIOP, (B) bIOP2 and (C) CVSIOP comparing the pre and post IOP values in SMILE Dataset 1

Summary of Results

IOP values were calculated in 4 different refractive surgery datasets. Each dataset was from a different clinic, different device and different country. The details of clinics must remain confidential, and they were only provided by Oculus for the development of new equations. In these datasets that included LASIK, SMILE and PRK surgeries, the IOP values pre and postoperatively were compared. Further, the correlations with CCT and age were evaluated for pre-op separate from the postoperative data. In these datasets, CCT significantly reduced after surgery which would enable assessment of the influence of change in geometrical components on the same patient while isolating biomechanical changes.

In Dataset one, there was no correlation between CCT and age in bIOP and bIOP2 measurements for pre and post LASIK and SMILE groups. Only bIOP2 values remained insignificant when compared to postoperative measurements for SMILE (p:0.278) and LASIK (p:0.088). Comparison in Bland Altman plots showed the mean differences (post minus pre) of 0.14 ± 2.3 mmHg for bIOP2, -2.0 ± 4.3 mmHg for bIOP and -4.2 ± 5.0 mmHg for CVSIOP. That indicates significant improvements in bIOP2. In Dataset two, weak or no correlations were observed with CCT and age for both bIOP and bIOP2. In PRK group bIOP (p:0.632) showed no significant changes between pre and post-surgery measurements. Looking closely at Bland Altman plots, the mean difference for bIOP of -0.12 ± 4.2 mmHg and for bIOP2 of 0.47 ± 2.1 mmHg and for CVSIOP of -2.9 ± 5.2 mmHg could be observed. This clearly highlights that although changes in bIOP2 were significant, the differences are less than 0.5 mmHg and in fact, bIOP2 improved on standard deviations and provided estimations with more stability. In LASIK (p:0.153) and SMILE (p:0.795) groups, bIOP2 was the only measurement method with no statistically significant differences with smallest means and standard deviations when pre and post data were compared.

Dataset 3 included all three surgeries in addition to longitudinal data at 1, 3 and 6 months postoperatively. This provided a unique opportunity to evaluate the performance of different IOP measurement methods over a more extended period of time. The CCT was reduced to around 100 microns on average for each patient. CVSIOP showed significant correlations with CCT in PRK and LASIK groups and no significant correlations in SMILE groups. bIOP showed no significant correlations with CCT in all three datasets and bIOP2 no significant correlation in preop data and some correlations with postoperative data in all groups. In PRK and LASIK, in all cases, bIOP2 was significantly correlated with CCT postoperatively while in SMILE group showed no significant correlations at six months data. Age was weakly correlated with all three measurement methods and in all cases. Looking closely at changes between the three methods CVSIOP reduced by 3.7 ± 2.0 ($-5.7 - 9.0$) mmHg after surgery while this value for bIOP was 1.4 ± 1.8 ($-8.3 - 6.3$) mmHg and for bIOP2 it increased by 0.5 ± 0.9 ($-5.4 - 3$) mmHg. This clearly showed that the bIOP2 values are less influenced

by geometrical changes and improved on both mean differences and significantly on standard deviations which are nearly half of the bIOP values. The statistical comparisons showed significant differences between pre and post IOP values for all measurements in all groups.

4.5.1.1.5 CXL Data

For brevity, only one of the datasets is presented in this section. A similar analysis was conducted on other datasets and results are available in Appendices, Section A.

Dataset 1

Dataset 1 includes 16 KC patients before and after CXL. Post CXL data divided into two groups, early (around One month after surgery) and late (3-6 months after surgery). The mean age was 31.1 ± 12.3 (18 - 62) years with CCT of 483 ± 47 (360 - 557) microns. Before surgery CVSIOP, bIOP and bIOP2 measurements were 12.3 ± 2.8 (5.5 - 16) mmHg, 13.7 ± 2.6 (7.4 - 18) mmHg and 16.0 ± 1.3 (14.3 - 19.0) mmHg respectively. There was no significant correlation with CCT for CVSIOP (R: 0.3536 ,p: 0.1791), bIOP (R: 0.0904,p: 0.7393), bIOP2 (R:-0.3031, p: 0.2537). Similarly no significant correlation was found with age for CVSIOP (R: -0.0215, p: 0.9370), bIOP (R: -0.0050 ,p: 0.9854) and bIOP2 (R: 0.3727 ,p: 0.1551), Figure 4-18.

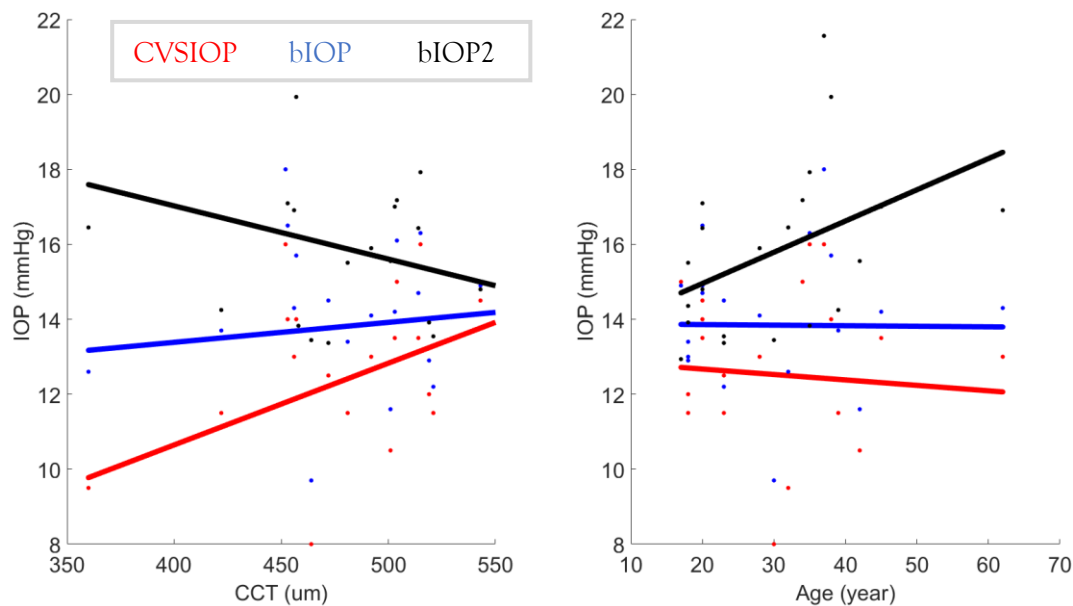


Figure 4-18 Correlation of IOP values from CVSIOP, bIOP and bIOP2 with CCT (left) and age (right) in Pre CXL Dataset 1

In early group, CCT was 461 ± 50 (328 - 518) microns, CVSIOP 14.2 ± 3.1 (8.0 - 20.5) mmHg, bIOP 15.8 ± 2.8 (10.6 - 21.7) mmHg and bIOP2 17.1 ± 1.4 (15.2 - 20.7) mmHg. The correlation with CCT was significant for CVSIOP (R: 0.6357, p: 0.0081) and on border line for bIOP (R: 0.4470 , p: 0.0826) and not significant for bIOP2 (R: 0.1331, p: 0.6232). The correlation with age was not significant for CVSIOP (R: -0.0046, p: 0.9864), bIOP (R: -0.1691, p: 0.5313) and bIOP2 (R 0.0105, p: 0.9691), Figure 4-19.

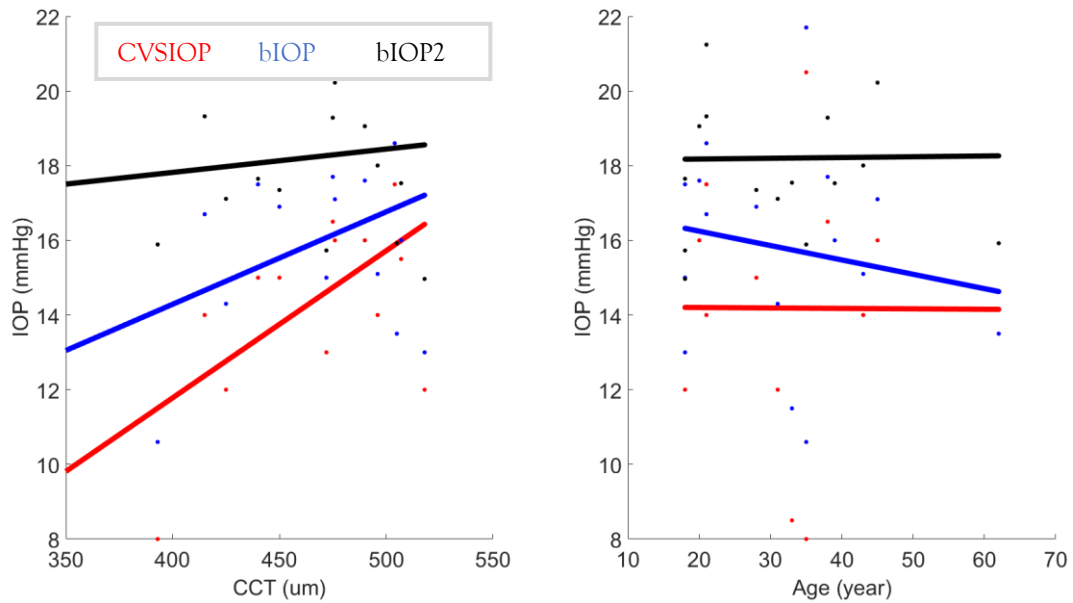


Figure 4-19 Correlation of IOP values from CVSIOP, bIOP and bIOP2 with CCT (left) and age (right) in early post CXL Dataset 1

In the late group, CCT was 468.7 ± 52.1 (351 - 559) microns, CVSIOP 13.19 ± 2.95 (9.00 - 20.50) mmHg, bIOP 14.71 ± 2.67 (10.20 - 21.10) mmHg and EIOP 16.01 ± 1.43 (12.65 - 19.44) mmHg. The correlation with CCT was not significant for CVSIOP (R: 0.4202, p: 0.0579), bIOP (R: 0.1618, p: 0.4834) and bIOP2 (R: -0.1868, p: 0.4176). The correlation with age was not significant for CVSIOP (R: -0.0646, p: 0.7807), bIOP (R: -0.0374, p: 0.8723) and bIOP2 (R: 0.1991, p: 0.3868), Figure 4-20. Comparison of pre and post values are shown in Table 4-4

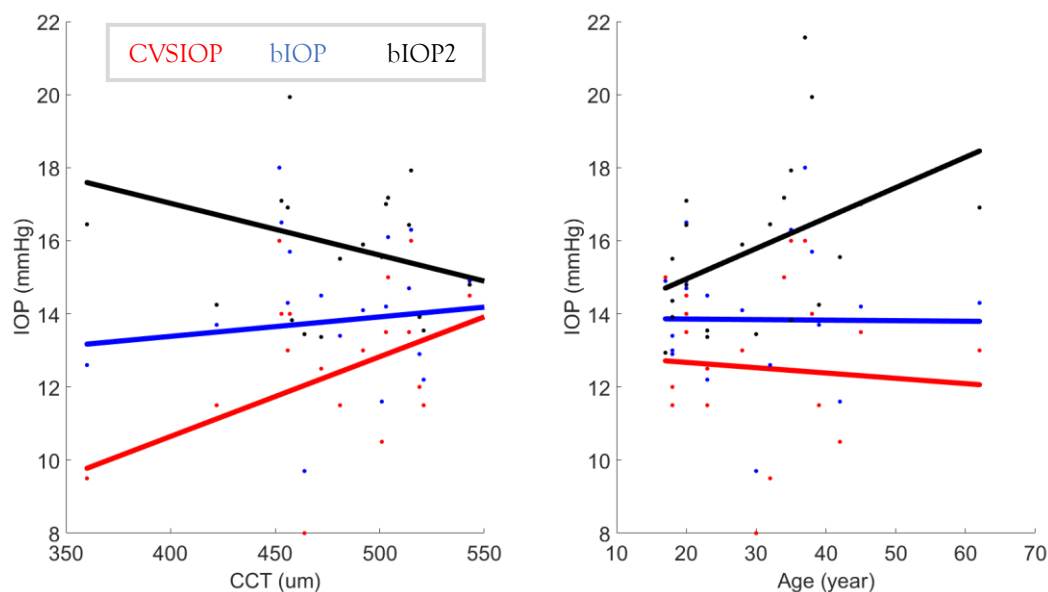


Figure 4-20 Correlation of IOP values from CVSIOP, bIOP and bIOP2 with CCT (left) and age (right) in late post CXL Dataset 1

Table 4.4 The differences between IOP values for CVSIOP, bIOP and bIOP2 for early and late post CXL in dataset 1 when compared to pre values.

| | CVSIOP (mmHg) | p Value | bIOP (mmHg) | p Value | bIOP2 (mmHg) | p Value |
|-------|-------------------------|------------|---------------------------|------------|----------------------------|------------|
| Early | -1.84±1.71 (-4.5 -1) | 0.012 | -2.09±2.07 (-5.4 -1.1) | 0.006 | -1.11±1.46 (-3.76 -1.4) | 0.03 |
| Late | -0.67±2.23 (-5 -3) | 0.21 | -0.87±2.22 (-4.8 -2.7) | 0.14 | -0.34±1.2 (-2.78 -1.57) | 0.259 |

Summary of Results

Evaluation of IOP values was also done on four different crosslinking datasets from different clinics and different countries. In all these data, both bIOP and bIOP2 showed no significant correlations with CCT and age. In dataset one for early data which was collected around one month post-op, all three methods showed significant differences with the pre IOP measurements while this was inverted for late (3 months or more) results. Similarly, dataset two showed no significant differences between pre and post IOP values for all methods. In dataset three, only bIOP2 was not significant, and in dataset four, all methods were significantly different. In all datasets, bIOP2 significantly improved on mean and standard deviations compared to bIOP when pre and post IOP values were compared. For instance, in dataset four, mean differences for bIOP2 was 1.2 ± 1.6 (-5 - 2.6) mmHg while bIOP was 2.5 ± 3 (-12.6 - 2.9) mmHg. In dataset three the mean bIOP2 was 0.59 ± 1.18 (-2.69 - 1.9) mmHg while bIOP was 1.56 ± 2.07 (-6.3 - 1.2) mmHg.

4.5.1.1.6 Glaucoma Patients

Dataset 1

Dataset 1 includes 111 patients with Hypertension Glaucoma (HTG) with mean age of 72.3 ± 9.7 (38.0 -91.0) years, CCT of 523 ± 31 (451 -597) microns, CVSIOP of 15.7 ± 4.0 (10.0 - 31.5) mmHg, bIOP of 14.6 ± 3.3 (9.8 -26.4) mmHg and bIOP2 of 15.5 ± 2.1 (11.4 - 22.6) mmHg. The correlation with CCT was significant with CVSIOP ($p:0.000$, $R:0.331$) and insignificant with bIOP ($p:0.243$, $R:0.112$) and bIOP2 ($p:0.199$, $R:0.123$). Age was not significantly correlated with CVSIOP ($p:0.702$, $R:-0.037$), bIOP ($p:0.543$, $R:-0.058$) and bIOP2 ($p:0.236$, $R:-0.114$), Figure 4-21.

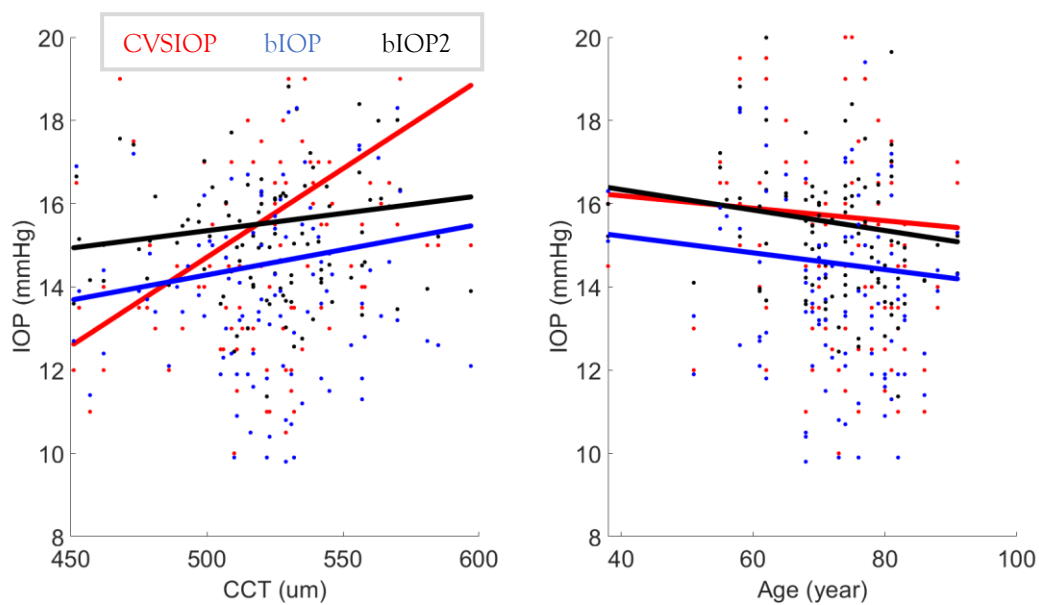


Figure 4-21 Correlation of IOP values from CVSIOP, bIOP and bIOP2 with CCT (left) and age (right) in HTG group of Dataset 1

Further, this dataset included 122 patients with Ocular Hypertension (OHT) with mean age of 65.1 ± 11.2 (34.0 -86.0) years, CCT of 552 ± 37 (476 -640) microns, CVSIOP of 19.0 ± 4.0 (11.5 -30.5) mmHg, bIOP of 16.9 ± 3.7 (9.0 -29.0) mmHg and bIOP2 of 17.4 ± 2.3 (12.5 -23.8) mmHg. The evaluation of bIOP ($p:0.007$, $R:-0.243$) showed significant correlation with CCT. CCT was not significantly correlated with EIOP ($p:0.080$, $R:-0.159$) and CVSIOP ($p:0.447$, $R:0.069$). Correlation with age was not significant with CVSIOP ($p:0.912$, $R:-0.010$), bIOP ($p:0.413$, $R:-0.075$) and bIOP2 ($p:0.157$, $R:-0.129$), Figure 4-22.

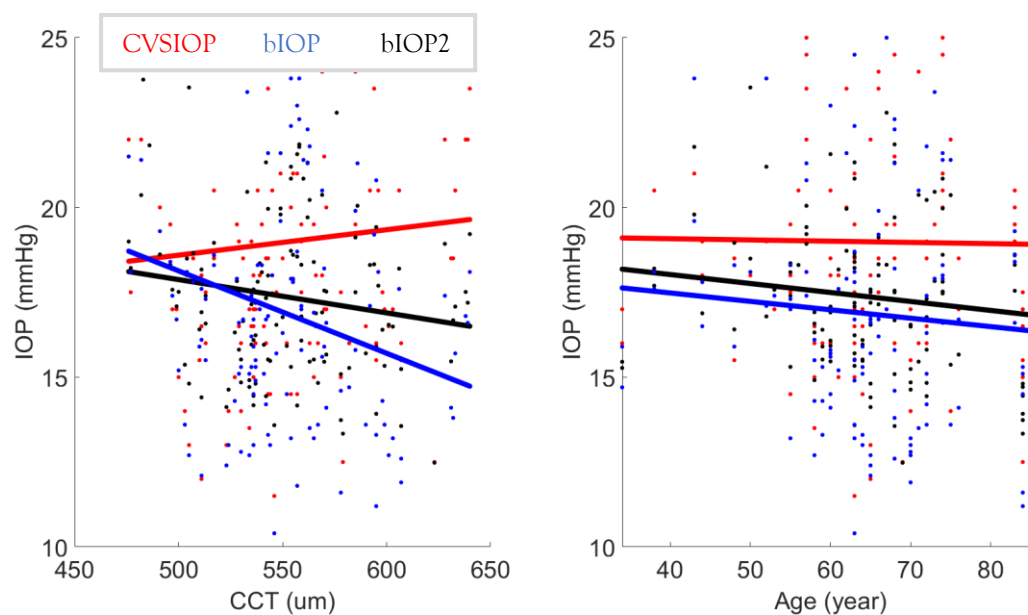


Figure 4-22 Correlation of IOP values from CVSIOP, bIOP and bIOP2 with CCT (left) and age (right) in OHT group of Dataset 1

Summary of Results

Two different datasets were used with patients who had Hypertension Glaucoma (HTG), Ocular Hypertension (OHT) and Normal-Tension Glaucoma (NTG). In dataset one, bIOP2 was not correlated with age and CCT while bIOP showed correlations with CCT in the HTG group. The mean values for CVSIOP of 15.7 ± 4.0 (10.0 - 31.5) mmHg, bIOP of 14.6 ± 3.3 (9.8 - 26.4) mmHg and bIOP2 of 15.5 ± 2.1 (11.4 - 22.6) mmHg showed that in HTG group bIOP had the lowest and CVSIOP had the highest values. Similarly in OHT mean CVSIOP of 19.0 ± 4.0 (11.5 - 30.5) mmHg, bIOP of 16.9 ± 3.7 (9.0 - 29.0) mmHg and bIOP2 of 17.4 ± 2.3 (12.5 - 23.8) mmHg showed similar trends. In the second dataset where GAT was also available, bIOP2 consistently did not have a significant correlation with both CCT and age in NTG, HTG and OHT groups. Whereas bIOP showed some correlation with CCT in the NTG group. In NTG group, the mean bIOP of 12.9 ± 2.3 (8.9 - 18.3) was the lowest IOP values and followed by CVSIOP of 13.4 ± 2.4 (8.5 - 17.5), GAT of 13.7 ± 1.0 (12.3 - 16.6), bIOP2 of 14.4 ± 1.0 (12.3 - 16.6) and AdjGAT of 16.3 ± 1.0 (12.3 - 16.6). In HTG, GAT and AdjGAT had the highest values and bIOP the lowest values while bIOP2 15.8 ± 1.9 (13.0 - 22.6) stayed in between. A similar trend was observed in the OHT group, where bIOP2 was 17.6 ± 2.4 (13.6 - 23.8). These results showed that bIOP2 values were higher than bIOP and lower than CVSIOP while GAT is sometimes higher and sometimes lower than bIOP2.

4.5.1.1.7 Keratoconus Patients

For brevity, only one of the datasets is presented in this section. A similar analysis was conducted on other datasets and results are available in Appendices, Section A.

Dataset 1

Consist of 255 KC patients with mean age of 34.8 ± 12.7 (13.0 -83.0) years, CCT of 481 ± 38 (353 -579) microns, bIOP of 13.9 ± 2.4 (6.1 -20.2) mmHg, CVSIOP of 12.6 ± 2.5 (4.5 -20.5) mmHg and bIOP2 of 15.5 ± 1.1 (13.0 -19.0) mmHg. Correlations with bIOP ($p:0.030$, $R:-0.145$), CVSIOP ($p:0.010$, $R:0.172$) and bIOP2 ($p:0.001$, $R:-0.228$) were significant with CCT. There was no significant correlations with age for bIOP ($p:0.501$, $R:-0.045$), CVSIOP ($p:0.155$, $R:0.095$), bIOP2 ($p:0.092$, $R:0.113$), Figure 4-23.

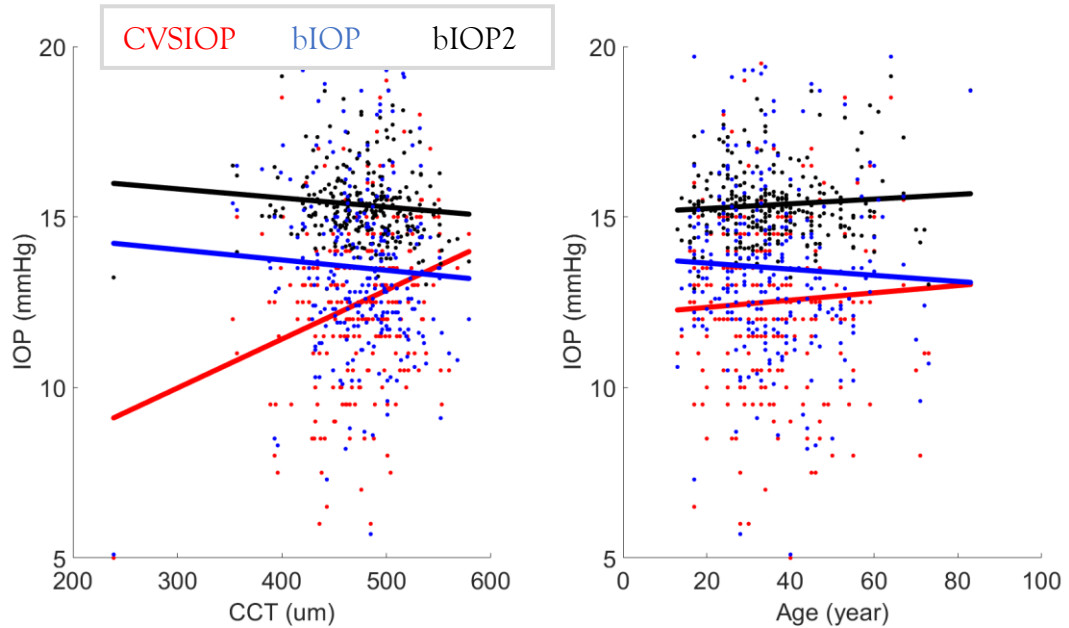


Figure 4-23 Correlation of IOP values from CVSIOP, bIOP and bIOP2 with CCT (left) and age (right) in KC Dataset 1

Comparison of healthy bIOP2 with different groups (based on disease severity) showed no significant differences with FFKC ($p: 0.8839$), Mild ($p: 0.9854$), Moderate ($p: 0.7467$) and Severe ($p: 0.6839$) KC IOP values. Whereas bIOP was significantly different ($p < 0.001$) in all cases. The mean differences are shown in Figure 4-24.

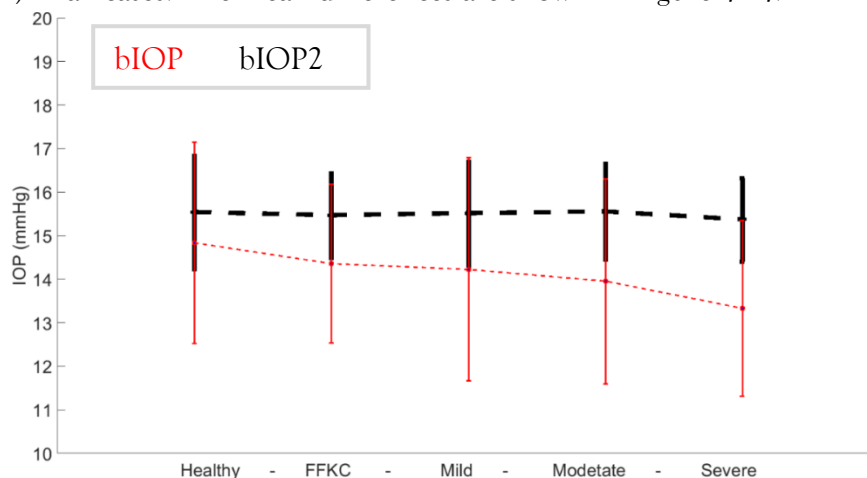


Figure 4-24 The changes in bIOP2 and bIOP in healthy, FFKC, Mild, Moderate and Severe keratoconic cases in Dataset 1

Summary of Results

The bIOP2 equation was applied to keratoconic eyes. In these seven datasets, overall, bIOP showed significant correlations with age and CCT while bIOP2 showed no correlation with Age and reduced correlation with CCT compared to bIOP. However, bIOP2 correlations with CCT remained significant in some cases. Next, a comparison between the IOP values of the healthy group and different stages of the disease, including FFKC, Mild, Moderate and Severe cases were conducted. These data showed that as the disease progressed, bIOP values were reduced in mean significantly. This is most likely due to the correlation with CCT as patients with more severe cases had thinner corneas. In contrast, bIOP2, consistently showed no change as the disease severity progressed. The change, in most cases, remained statistically not significant for bIOP2 while significant in all cases for bIOP.

4.5.1.2 bIOP2-KC Equation

This section shows the differences between bIOP2 healthy and bIOP2-KC. bIOP healthy only uses Corvis ST parameters, whereas bIOP-KC uses parameters obtained from Pentacam elevation data. The parameters used for developing bIOP2-KC are shown in Equation 4-2.

$$bIOP2 - kc = f(CCT, Age, AP1, PD, HCR, DeflAmpMax, A1V, DeflAmpA1, HCT, CH, CA, CDA, CL)$$

Equation 4-2

where CCT is the central corneal thickness (um), AP1 is the pressure at applanation one (mmHg), PD is the Peak Distance (mm), HCR is the radius at highest concavity (mm), DeflAmpMax is the deflection amplitude maximum (mm), A1V is the velocity at applanation one (m/s), DeflAmpA1 is the deflection amplitude at applanation one (mm), HCT is the time at highest concavity (ms), CH is the cone height (um), CA is the cone area (mm²), CDA is the cone distance to the corneal apex (mm), and CL is the cone location (degree).

The problems with bIOP in KC eyes were reviewed from the literature in section 2.5. The comparison between bIOP and bIOP2 is also presented in section 4.5.1.1.7. Since the performance of bIOP in KC eyes was not suitable and bIOP2 performed consistently better, the comparison in this section is only provided between bIOP2 and bIOP2-KC to demonstrate the improvements offered by considering new geometrical parameters. For brevity, only one of the datasets is presented in this section. A similar analysis was conducted on other datasets and results are available in Appendices, Section A.

Dataset 1

This dataset includes 222 KC eyes with a mean age of 34.9±12.7(13 -83) years, CCT of 480.7±38.1(353 -579) microns, bIOP2 of 15.5±1.1(13 -19) mmHg and bIOP2KC of 15.5±1.1(13.3 -18.9) mmHg. The correlation with CCT for bIOP2 (p:0.0007,

R: -0.2267) was significant while bIOP2KC (p:0.0889, R:-0.1144) remained insignificant. the correlations with age was no significant for bIOP2 (p:0.0926, R:0.1132 and significant for bIOP2-kc (p:0.0482, R:0.1328). There were no significant differences between the two IOP values (p:0.9732), Figure 4-25.

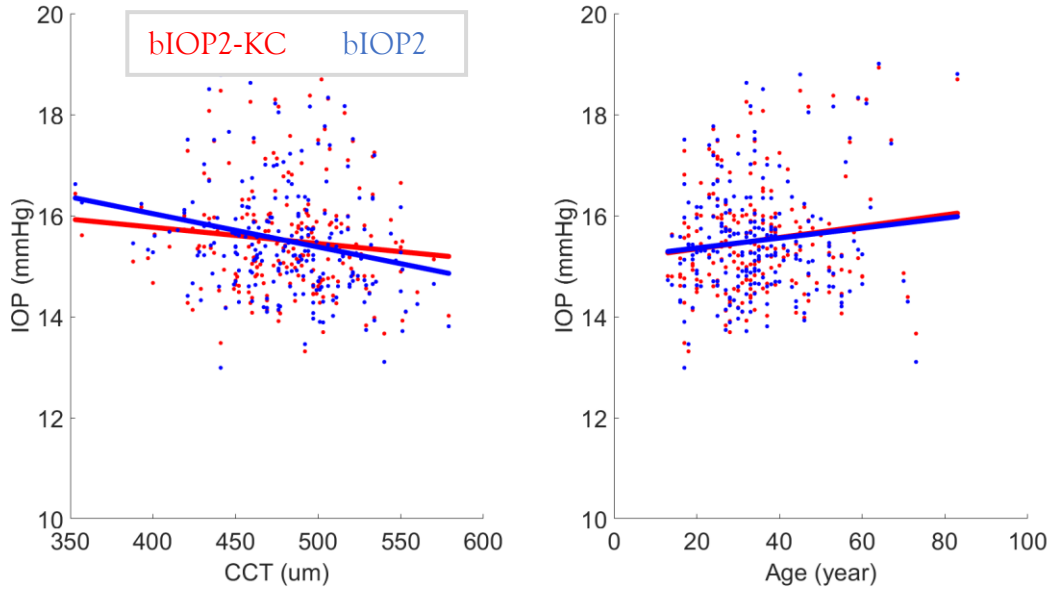


Figure 4-25 Correlation of IOP values from bIOP2 and bIOP2-KC with CCT (left) and age (right) in KC Dataset 1

The differences between IOP values in each group separated based on disease severity were compared to healthy and remained close to the previously calculated values in section 4.5.1.1.7. Hence the numbers are not presented again for this section as the conclusion remained the same, Figure 4-26.

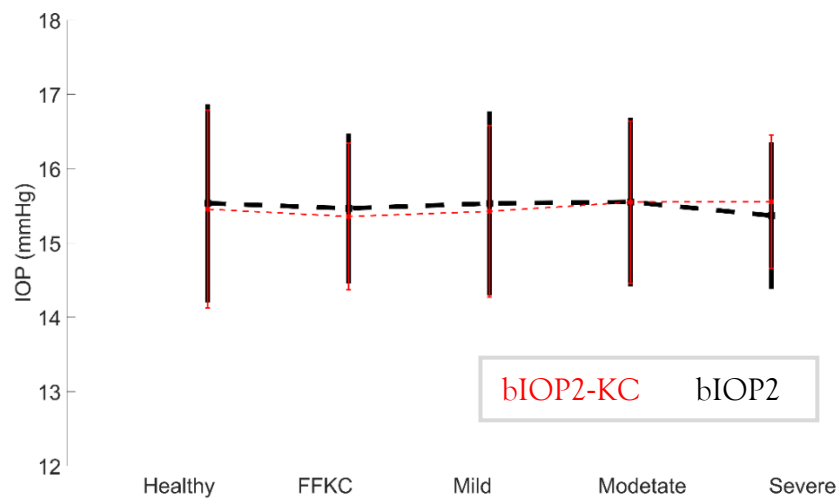


Figure 4-26 The changes in bIOP2 and bIOP2-KC in healthy, FFKC, Mild, Moderate and Severe keratoconic cases in Dataset 1

Summary of Results

The bIOP2 and bIOP2-KC were applied to seven KC datasets where elevation data were available. After processing the topographies and obtaining cone characteristics, a comparison was provided. Interestingly, when IOP values were compared between disease stages and healthy group, not a significant improvement was gained from bIOP2-KC. The difference between bIOP2 and bIOP2-KC was not statistically significant, and they were both not significantly different from the healthy group. Also, the correlation between bIOP2-KC and bIOP2 with age remained unchanged and not significant. However, bIOP2-KC performed better in terms of its correlation with CCT. All seven datasets showed reduced correlation with CCT and six of them not significantly correlated. Looking at all data combined, bIOP2 (p:0.000, R:-0.1204) showed significant correlations with CCT and bIOP2-KC (p:0.4228, R:-0.0207) remained uncorrelated in 1522 KC eyes.

4.5.2 Stress-Strain Index (SSI2)

In this study, three SSI2 equations were developed. All three SSI2 equations use Corvis ST parameters. The SSI2-H can be applied to the healthy cornea and post PRK surgery. The SSI2-KC equation is suitable for patients with distorted corneal geometry such as keratoconus and post CXL. Finally, SSI2-PLS is suitable for corneas post LASIK and SMILE surgeries. The reason why three different equation was required is discussed in the next chapter. All three equations were applied to clinical data accordingly and presented in this section.

4.5.2.1 SSI Healthy Equation

This section shows the differences between SSI2-H and the previously developed SSI. The SSI2 intends to improve on correlations with Age, CCT and IOP. The IOP formula use in this section is bIOP2 as it is believed to be less influenced by corneal biomechanics and provides a more accurate IOP value. The parameters used to develop SSI2-H are shown in Equation 4-3.

$$SSI2 - H = \int (CCT, bIOP2, Age, AP1, PD, HCR, DefAmpMax, A1V, DeflAmpA1, HCT)$$

Equation 4-3

where CCT is the central corneal thickness (um), bIOP2 is the newly developed biomechanically corrected IOP equation (mmHg), AP1 is the pressure at applanation one (mmHg), PD is the Peak Distance (mm), HCR is the radius at the highest concavity (mm), DeflAmpMax is the deflection amplitude maximum (mm), A1V is the velocity at applanation one (m/s), DeflAmpA1 is the deflection amplitude at applanation one (mm) and HCT is the time at highest concavity (ms).

4.5.2.1.1 Experimental Validation

An experimental test was conducted on ex-vivo human corneas using an inflation rig that concluded there is a relationship between age and corneal stiffness in healthy human corneas¹²³. This was explained in more details in Chapter three, section 3.5.4. In this section to validate the performance of the new equation, a comparison is provided between SSI and SSI2-H in healthy cornea against ex vivo expectations for that age in seven different datasets, Figure 4-27. The correlations between SSI, SSI2-H, and ex vivo SSI are compared and presented in Table 4-5. Both SSI and SSI2-H showed significant correlations with ex vivo results using Spearman's rho correlation as the data were not normally distributed. However, the new SSI showed a better correlation as it followed the trend almost parallel to the ex-vivo result. The details of these datasets are provided in section 4.5.1.1.2.

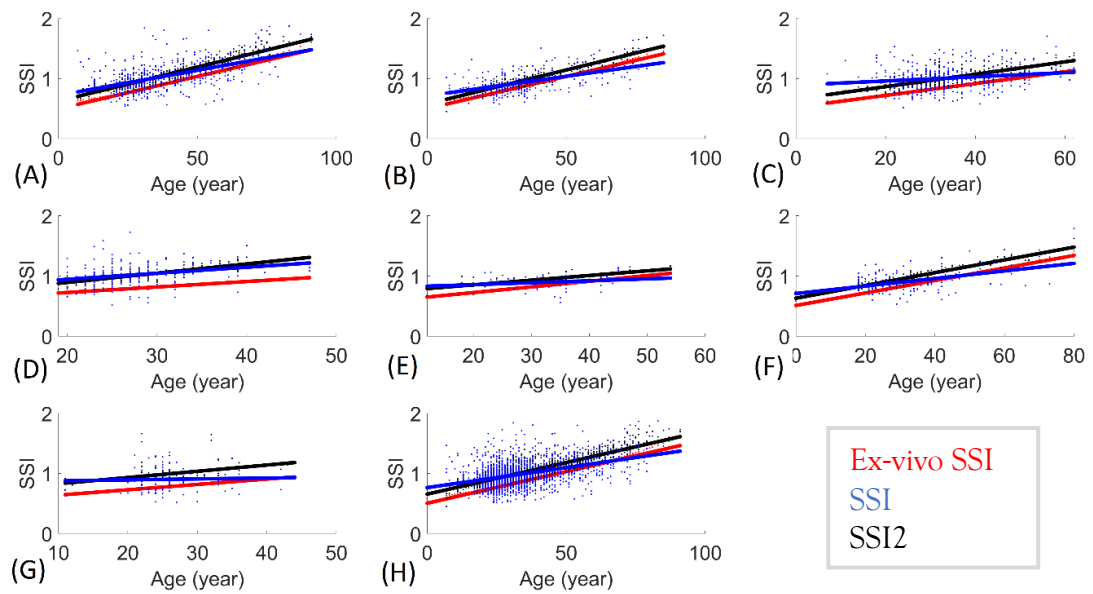


Figure 4-27 The comparison between SSI, SSI2-H and ex vivo SSI values obtained from human donor corneas against age in 7 different datasets (A-G) and all of them combined (H)

Table 4-5 The correlation of Ex-vivo SSI, SSI2-H and SSI with age plus the mean and standard deviation of the differences between “ex-vivo and SSI” and “ex-vivo and SSI2-H ” in addition to Spearman's rho correlation p-value

| Dataset | Ex-vivo SSI | SSI2-H | SSI | Ex vivo vs. SSI2-H Mean±SD | Ex vivo vs. SSI Mean±SD |
|---------|----------------------|---------------------|---------------------|-------------------------------|----------------------------|
| (A) | R:0.9943 (p<0.01) | R:0.905 (p<0.01) | R:0.540 (p<0.01) | 0.15±0.086 (p<0.01) | 0.127±0.218 (p<0.01) |
| (B) | R:0.9948 (p<0.01) | R:0.930 (p<0.01) | R:0.549 (p<0.01) | 0.1±0.071 (p<0.01) | 0.055±0.173 (p<0.01) |
| (C) | R:0.9974 (p<0.01) | R:0.709 (p<0.01) | R:0.174 (p<0.01) | 0.152±0.101 (p<0.01) | 0.148±0.201 (p<0.01) |
| (D) | R:0.999 (p<0.01) | R:0.730 (p<0.01) | R:0.266 (p<0.01) | 0.211±0.083 (p<0.01) | 0.226±0.191 (p<0.01) |
| (E) | R:0.9979 (p<0.01) | R:0.748 (p<0.01) | R:0.209 p:0.1578 | 0.106±0.06 (p<0.01) | 0.048±0.138 (p:0.159) |
| (F) | R:0.9943 (p<0.01) | R:0.911 (p<0.01) | R:0.465 (p<0.01) | 0.128±0.068 (p<0.01) | 0.056±0.173 (p<0.01) |
| (G) | R:0.9984 (p<0.01) | R:0.462 (p<0.01) | R:0.034 p:0.7633 | 0.213±0.112 (p<0.01) | 0.119±0.251 (p:0.484) |
| (H) | R:0.9945 (p<0.01) | R:0.841 (p<0.01) | R:0.418 (p<0.01) | 0.15±0.093 (p<0.01) | 0.124±0.207 (p<0.01) |

4.5.2.1.2 Healthy Patients

For brevity, only one of the datasets is presented in this section. A similar analysis was conducted on other datasets and results are available in Appendices, Section B.

Dataset 1

It included 414 patients with a mean age of 40.2±16.7(7-91) years, CCT of 541±32 (454 - 634) microns, bIOP of 15.5±1.3(12.4-22.8) mmHg, bIOP2 of 14.8±2.3(7.7-24.5) mmHg, SSI of 1.06±0.26(0.54-1.87) and SSI2-H of 1.08±0.21 (0.67- 1.74). Correlation with CCT for SSI was R:0.11 (p:0.026), and for SSI2-H, it became weaker with R:0.029 (p:0.552). Correlation with age for SSI was R:0.540 (p:0.000) and for SSI2-H was R:0.905 (p:0.000). Correlation with bIOP2 for SSI and SSI2-H was R:0.547 (p:0.000) and R:0.123 (p:0.012). Although the correlation of bIOP2 with SSI2-H is weaker, it is still significant and positively correlated, Figure 4-28.

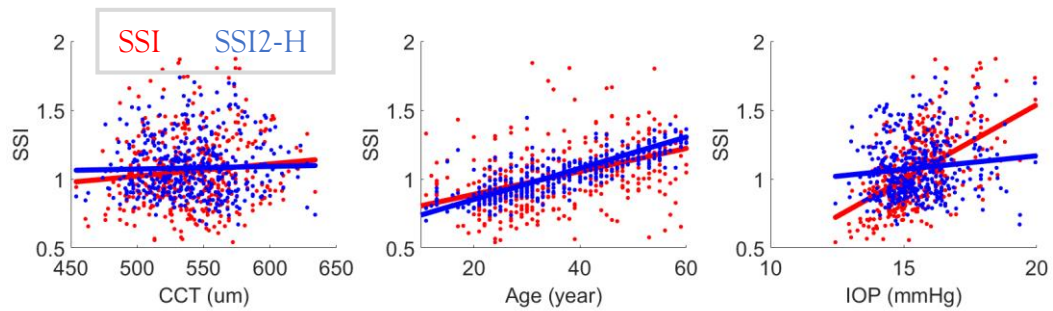


Figure 4-28 The correlation of SSI and SSI2-H with CCT (left), age (middle) and IOP (right) in Dataset 1

Summary of Results

Next, a correlation comparison was conducted in seven healthy datasets where SSI and SSI2 were evaluated against CCT, age and IOP. As described before, there should be no correlation between them and CCT or IOP, while the correlation with age should remain strong. In four datasets CCT was significantly correlated with SSI while only one dataset showed significant correlations with SSI2. Correlation with age was stronger in SSI2 consistently and in all datasets. Correlation with IOP was insignificant in five datasets for SSI2 while it remained significant with SSI in all cases. SSI2 consistently showed reduced correlation with IOP compared to SSI. Overall, analysis of 1410 patients showed correlation with CCT for SSI was significant with $R:0.111$ ($p:0.000$), while SSI2 was not correlated with $R:-0.003$ ($p:0.899$). Correlation with age for SSI was $R:0.419$ ($p:0.000$) and for SSI2 was $R:0.841$ ($p:0.000$). Correlation with bIOP2 for SSI and SSI2 was $R:0.471$ ($p:0.000$) and $R:0.000$ ($p:0.999$). This clearly showed that SSI2 is more representative of true material stiffness by being less correlated to IOP and CCT.

4.5.2.1.3 PRK Surgery

For brevity, only one of the datasets is presented in this section. A similar analysis was conducted on other datasets and results are available in Appendices, Section B.

Dataset 1

Dataset 1 consist of 38 patients who undergo PRK surgery with a mean CCT of 541 ± 33 (458 - 623) microns, age of 38.1 ± 10.7 (21 - 79) years, bIOP of 15.3 ± 2.2 (10.4 - 21.7) mmHg, bIOP2 of 15.9 ± 1.4 (13.2 - 19.9) mmHg, SSI of 0.94 ± 0.15 (0.59 - 1.27) and SSI2-H of 1.03 ± 0.16 (0.78 - 1.6). After LASIK these values changed to CCT of 414 ± 37 (343 - 502) microns, age of 39.8 ± 10.7 (23 - 80) years, bIOP of 15.2 ± 2.0 (11.2 - 19.6) mmHg, bIOP2 of 16.3 ± 0.9 (14.8 - 18.2) mmHg, SSI of 0.91 ± 0.23 (0.64-1.57), SSI2-H of 1.03 ± 0.16 (0.84 - 1.75). To evaluate the performance of SSI values, (Pre SSI - Post SSI)/ Pre SSI was calculated. This value for SSI was 0.006 ± 0.277 and for SSI2-H was 0.003 ± 0.071 . Bland Altman plots are provided to visualise these changes, Figure 4-29.

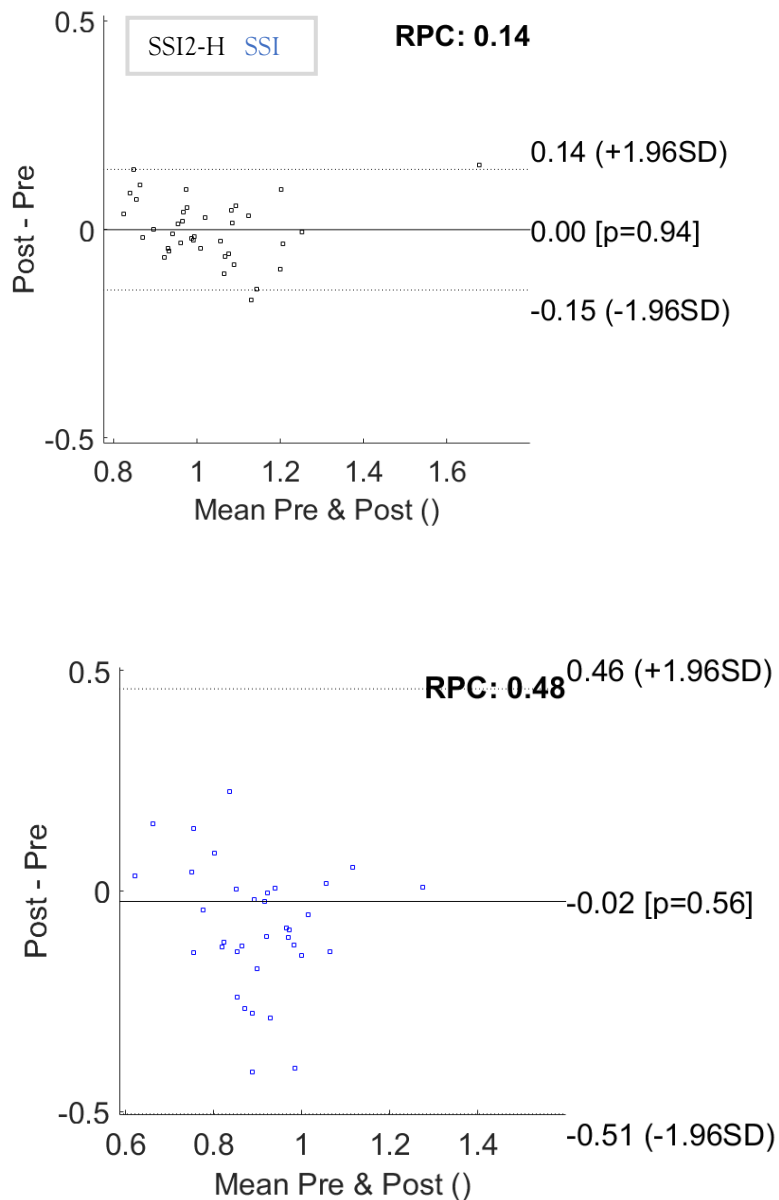


Figure 4-29 The Bland Altman plot for SSI2-H (top) and SSI (bottom) comparing the pre and post PRK surgery results in Dataset 1

Further, the correlations between changes in CCT and SSI/SSI2-H were evaluated. The correlation for SSI was $R:-0.203$ ($p:0.221$) and for SSI2-H was $R:0.319$ ($p:0.051$). both remained insignificant where SSI2-H had a positive correlation, and SSI was negatively correlated, Figure 4-30.

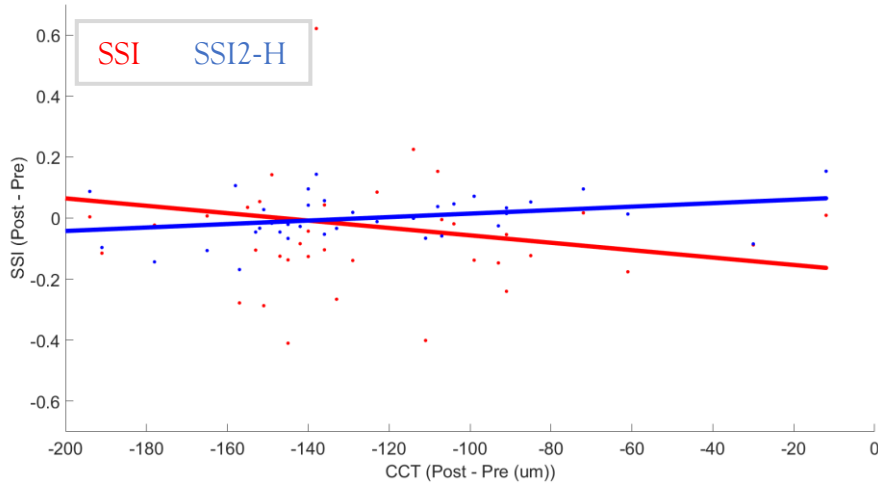


Figure 4-30 The evaluation of correlation in changes in CCT with changes in SSI and SSI2-H in PRK group of Dataset 1

Correlations with CCT before surgery for SSI was $R:-0.270$ ($p:0.101$) and for SSI2-H was weaker with $R:0.078$ ($p:0.643$). Age correlation with SSI was $R:0.575$ ($p:0.000$) and with SSI2-H was $R:0.840$ ($p:0.000$). Correlation of bIOP2 with SSI was high and significant with $R:0.559$ ($p:0.000$) while SSI2-H remained weak and insignificant with $R:0.021$ ($p:0.900$), Figure 4-31.

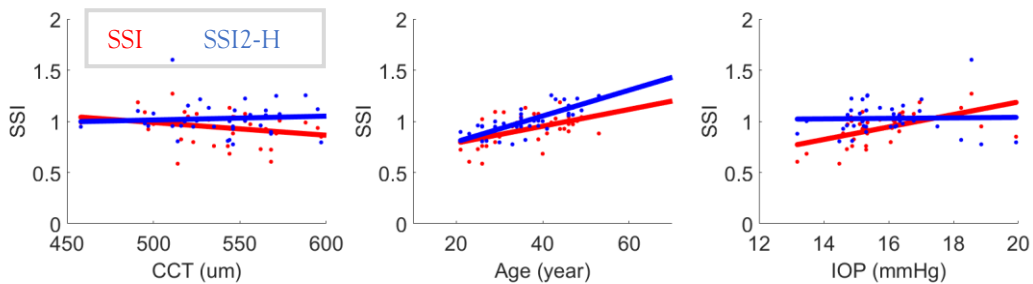


Figure 4-31 The correlation of SSI and SSI2-H with CCT (left), age (middle) and IOP (right) in pre-surgery PRK group of Dataset 1

Correlations with CCT after surgery for SSI was $R:0.133$ ($p:0.426$) and for SSI2-H was significant and stronger with $R:0.432$ ($p:0.007$). Age correlation with SSI was $R:0.143$ ($p:0.393$) and with SSI2-H was $R:0.898$ ($p:0.000$). Correlation of bIOP2 with SSI was strong and significant with $R:0.525$ ($p:0.000$) while SSI2-H remained insignificant and weak with $R:-0.081$ ($p:0.627$), Figure 4-32.

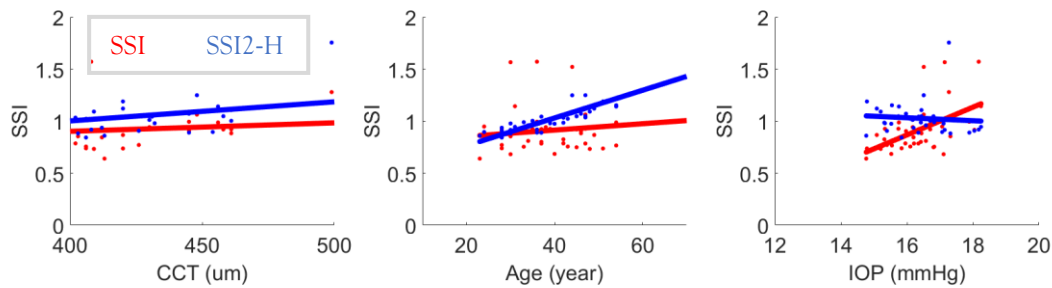


Figure 4-32 The correlation of SSI and SSI2-H with CCT (left), age (middle) and IOP (right) in post-surgery PRK group of Dataset 1

Summary of Results

The SSI2 was applied to patients who undergo PRK in two different datasets. In both cases for pre and post data, correlation with CCT and IOP was weaker in SSI2, and it had a stronger correlation with age. In SSI (0.02 ± 0.48 and 0.02 ± 0.37) and SSI2 (0.00 ± 0.14 and 0.02 ± 0.21), the mean differences between pre and post remained close to zero in both datasets. The differences in correlation with CCT between SSI ($p:0.221$) or SSI2 ($p:0.051$) remained insignificant in dataset one while it was only insignificant for SSI2 ($p:0.961$) in dataset two. This observation can now help explain the stability of SSI/SSI2 values following PRK. While the PRK ablation of stromal tissue and reduction in corneal thickness undoubtedly lead to a reduction in the cornea's geometric stiffness and hence overall stiffness, it should not lead to significant changes in the material stiffness measured by the SSI and SSI2. Perhaps the only material-related change that could be expected in this case is wound healing following surgery⁴⁴⁸. However, while there is still no agreement on the nature and magnitude of this effect (and whether it leads to increases or decreases in tissue stiffness), most evidence points at a small stiffness change affecting a thin zone immediately next to the incision surface^{449,453}.

4.5.2.2 SSI2-KC Equation

This section shows the differences between SSI2-KC and the previously developed SSI. The SSI2 intends to improve on correlations with Age, CCT and IOP. The IOP formula used in this section was bIOP2 as it is believed to be less influenced by corneal biomechanics and provides a more accurate IOP value. The parameters used to develop SSI2-KC equation are similar to healthy SSI2 and shown in Equation 4-3. Only the terms and coefficients were optimised to suit these data better.

4.5.2.2.1 Keratoconus Patients

For brevity, only one of the datasets is presented in this section. A similar analysis was conducted on other datasets and results are available in Appendices, Section B.

Dataset 1

It included 222 patients with a mean age of 34.9 ± 12.7 (13 - 83) years, CCT of 481 ± 38 (353 - 579) microns, bIOP of 13.9 ± 2.4 (6.1 - 20.2) mmHg, bIOP2 of

15.5 ± 1.1 (13 - 19) mmHg, SSI of 0.88 ± 0.26 (0.46 - 2) and SSI2-KC of 0.76 ± 0.18 (0.32 - 1.53). Correlation with CCT for SSI was R:0.212 (p:0.002), which is stronger than SSI2-KC with R:0.177 (p:0.008). Correlation with age for SSI was R:0.306 (p:0.000) and for SSI2-KC was R:0.778 (p:0.000). Correlation with bIOP2 for SSI with R:0.557 (p:0.000) was stronger than SSI2-KC with R:0.184 (p:0.006), Figure 4-33.

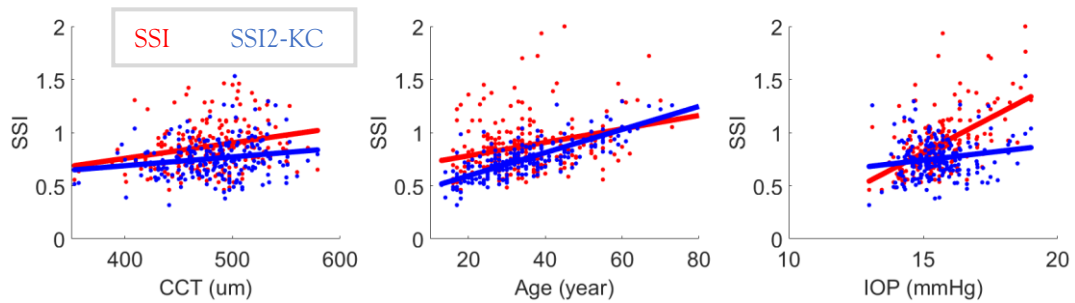


Figure 4-33 The correlation of SSI and SSI2-KC with CCT (left), age (middle) and IOP (right) in Dataset 1

When comparing the changes in SSI and SSI2-KC with disease progression, it is clear that both equations followed a clear trend. In severe cases, corneal biomechanics changed and became softer than less severe or healthy patients. SSI2-KC showed a more significant softening in Mild, Moderate and Severe cases, Figure 4-34. The detailed analysis for means, standard deviations and statistical comparison of SSI values to the healthy group is provided in Table 4-6.

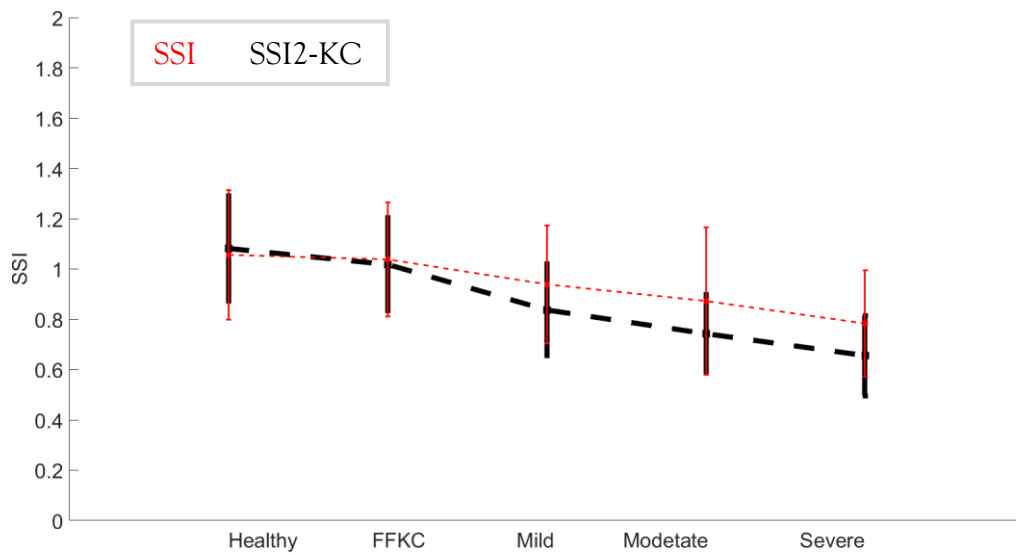


Figure 4-34 The changes in SSI2-KC and SSI in healthy, FFKC, Mild, Moderate and Severe keratoconic cases in Dataset 1

Table 4-6 Showing the mean, standard deviation (SD) and statistical comparison with the healthy group for SSI / SSI2-KC in the same format as shown here in Dataset 1

| | | | | | |
|----------------|-----------|-------------|-------------|-------------|-------------|
| Mean | 1.06/1.08 | 1.04/1.02 | 0.94/0.84 | 0.87/0.74 | 0.78/0.66 |
| SD | 0.26/0.21 | 0.23/0.18 | 0.23/0.18 | 0.29/0.16 | 0.21/0.16 |
| p value | 1/1 | 0.727/0.180 | 0.000/0.000 | 0.000/0.000 | 0.000/0.000 |

Summary of Results

SSI2-KC was compared with SSI in seven KC datasets. There was a clear strength in correlation with age in SSI2-KC in all cases compared to SSI. SSI2-KC showed weak correlations with CCT and IOP while SSI had positive and strong correlations with both. SSI2-KC showed a significant correlation with CCT in three datasets while SSI was correlated significantly in six datasets. The correlation with IOP was significant in only one dataset for SSI2-KC while it was significant with SSI in all cases. Overall, analysis of 1522 KC eyes showed correlation with CCT for SSI was strong with $R:0.257$ ($p:0.000$), and for SSI2 weaker with $R:0.131$ ($p:0.000$). Correlation with age for SSI was $R:0.164$ ($p:0.000$) and for SSI2 was $R:0.716$ ($p:0.000$). Correlation with bIOP2 for SSI was strong with $R:0.516$ ($p:0.000$) while SSI2 was weaker with $R:0.068$ ($p:0.008$) but still significant.

It is expected that as the keratoconus progresses, the material stiffness reduces.^{454,455} KC patients were split into four groups of FFKC, Mild, Moderate and Severe keratoconus. In all cases, SSI2-KC reduced with disease progression. On the other hand, SSI also reduced in most cases, but the reduction in values was smaller than SSI2-KC. The overall comparison showed SSI2-KC mean reduced from 1.03 in healthy eyes to 0.95, 0.74, 0.69 and 0.62 in FFKC, Mild, Moderate and Severe cases, respectively. On the other hand, in SSI this change was from 1.00 to 0.97, 0.87, 0.81 and 0.69. This showed there is a more consistent reduction in SSI2-KC with a larger gap between FFKC and Mild KC. Whereas, in SSI, there is a larger gap between Moderate and Severe KC cases. All changes were statistically significant when compared to healthy groups for both parameters.

4.5.2.2.2 Crosslinked Corneas

For brevity, only one of the datasets is presented in this section. A similar analysis was conducted on other datasets and results are available in Appendices, Section B.

Dataset 1 – Early Term Results

Dataset 1 consist of 16 patients who undergo CXL with a mean CCT of 482.8 ± 46.6 (360 - 557) microns, age of 31.1 ± 12.3 (18 - 62) years, bIOP of 13.7 ± 2.6 (7.4 - 18) mmHg, bIOP2 of 16 ± 1.3 (14.3 - 19) mmHg, SSI of 1 ± 0.3 (0.7 - 1.8) and SSI2-KC of 0.7 ± 0.1 (0.5 - 1). After crosslinking these value changed to a mean CCT of 461.1 ± 50.7 (328 - 518) microns, bIOP of 15.8 ± 2.8 (10.6 - 21.7) mmHg, bIOP2 of 17.1 ± 1.4 (15.2 - 20.7) mmHg, SSI of 1.2 ± 0.3 (0.6 - 1.7) and SSI2-KC of 0.7 ± 0.2 (0.4 - 1.1). In SSI, 25% of patients showed softening after crosslinking, whereas with SSI2-KC 37.5% showed softening, Figure 4-35.

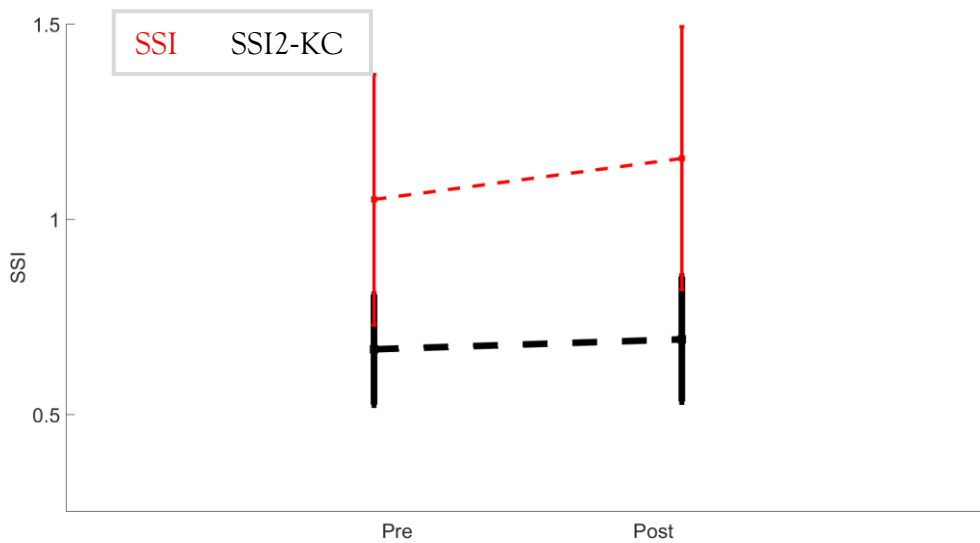


Figure 4-35 The mean and standard deviation of pre-CXL and post-CXL data for SSI and SSI2-KC in the early group of CXL Dataset 1

Correlations with CCT before crosslinking for SSI was strong and negative with R: - 0.526 (p:0.036) while SSI2-KC was weakly correlated and not significant R:0.046 (p:0.890). Age correlation with SSI was R:0.429 (p:0.097) and with SSI2-KC was R:0.731 (p:0.001). Correlation of bIOP2 with SSI and was strong and significant with R:0.625 (p:0.010) while SSI2-KC remained insignificant with R:0.288 (p:0.280), Figure 4-36.

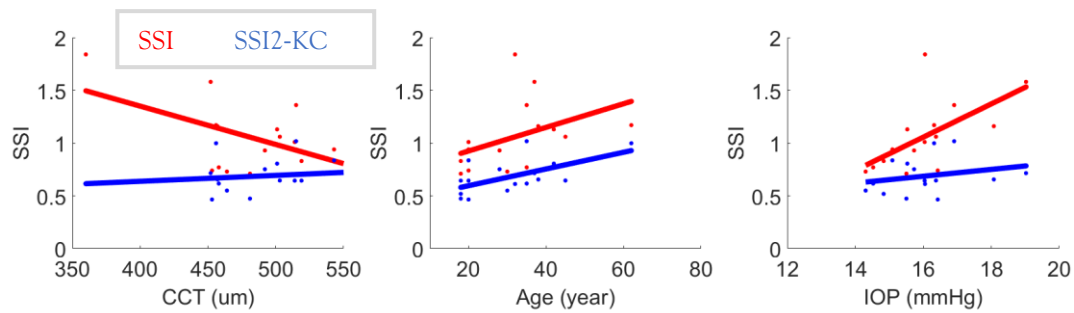


Figure 4-36 The correlation of SSI and SSI2-KC with CCT (left), age (middle) and IOP (right) in the early pre-surgery group of CXL Dataset 1

Correlations with CCT after crosslinking for SSI was strong with $R:0.444$ ($p:0.098$) and for SSI2-KC became weaker with $R:0.246$ ($p:0.359$). Age correlation with SSI was $R:0.359$ ($p:0.189$) and with SSI2-KC was $R:0.842$ ($p:0.000$). Correlation of bIOP2 with SSI was strong and significant with $R:0.516$ ($p:0.049$) while bIOP showed no significant correlations with $R:-0.095$ ($p:0.727$), Figure 4-37.

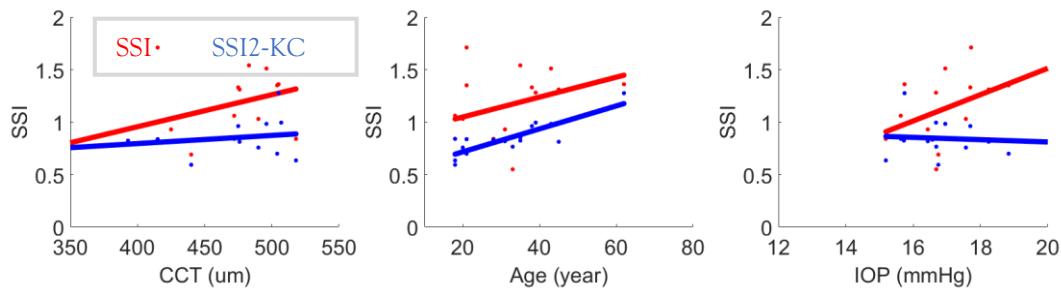


Figure 4-37 The correlation of SSI and SSI2-KC with CCT (left), age (middle) and IOP (right) in the early post-surgery group of CXL Dataset 1

Dataset 1 – Late-Term Results

Dataset 1 also consists of 21 patients who undergo CXL with a mean CCT of 486 ± 47 (360 - 563) microns, age of 30.2 ± 11.5 (17 - 62) years, bIOP of 13.8 ± 2.4 (7.4 - 18) mmHg, bIOP2 of 15.7 ± 1.3 (14-19) mmHg, SSI of 0.98 ± 0.32 (0.57 - 1.84) and SSI2-KC of 0.66 ± 0.14 (0.47-1). After crosslinking these value changed to a mean CCT of 469 ± 52 (351 - 559), bIOP of 14.7 ± 2.7 (10.2 - 21.1) mmHg, bIOP2 of 16 ± 1.4 (12.7 - 19.4) mmHg, SSI of 0.94 ± 0.28 (0.5 - 1.49) and SSI2-KC of 0.68 ± 0.19 (0.27 - 0.98). In SSI, 42.9% of patients showed softening after crosslinking, whereas with SSI2-KC 28.6% showed softening, Figure 4-38.

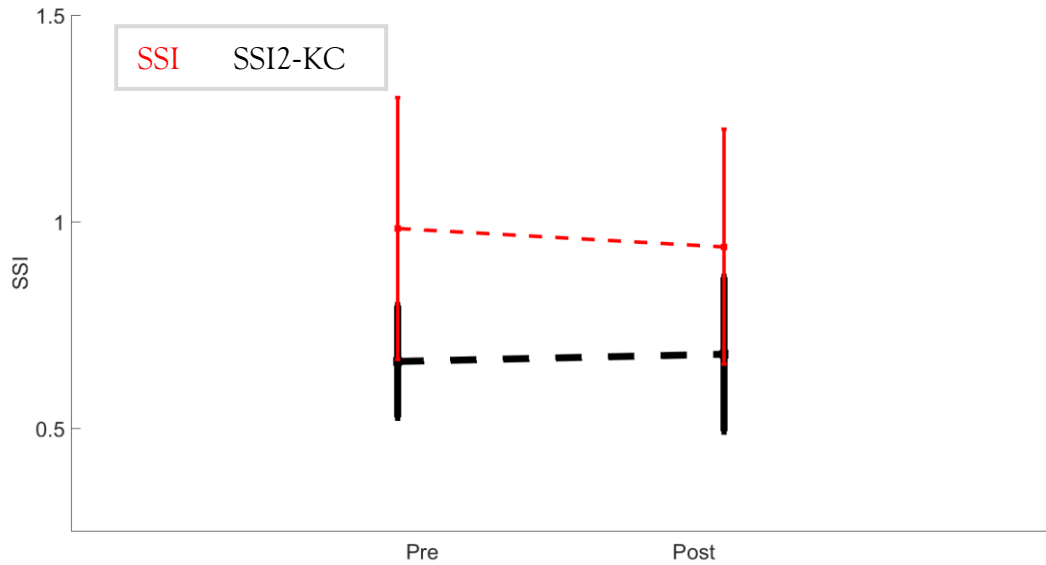


Figure 4-38 The mean and standard deviation of pre-CXL and post-CXL data for SSI and SSI2-KC in the late group of CXL Dataset 1

Correlations with CCT before crosslinking for SSI was negative and strong with $R: -0.405$ ($p:0.069$) while for SSI2-KC it remained insignificant and not correlated with $R:0.038$ ($p:0.870$). Age correlation with SSI was $R:0.440$ ($p:0.046$) and with SSI2-KC was $R:0.698$ ($p:0.004$). The correlation of bIOP2 with SSI was strong with $R:0.706$ ($p:0.000$) while SSI remained uncorrelated with $R:0.364$ ($p:0.105$), Figure 4-39.

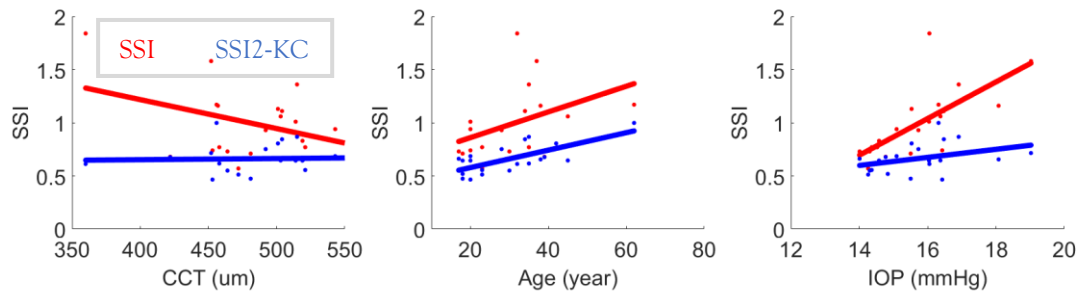


Figure 4-39 The correlation of SSI and SSI2-KC with CCT (left), age (middle) and IOP (right) in the late pre-surgery group of CXL Dataset 1

Correlations with CCT after crosslinking for SSI was $R:-0.145$ ($p:0.555$) and for SSI2-KC was $R:-0.119$ ($p:0.609$) where both remained insignificant and negatively correlated. Age correlation with SSI was $R:0.298$ ($p:0.215$) and with SSI2-KC was $R:0.444$ ($p:0.044$). Correlation of bIOP2 with SSI was strong and significant with $R:0.612$ ($p:0.005$) while SSI2-KC remained insignificant with $R:0.211$ ($p:0.360$), Figure 4-40.

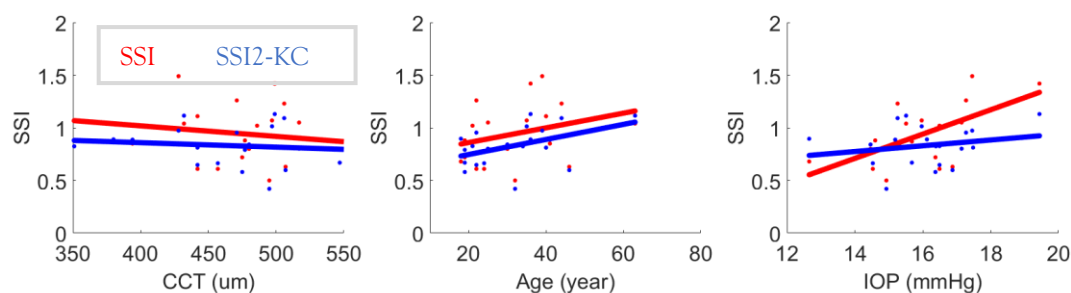


Figure 4.40 The correlation of SSI and SSI2-KC with CCT (left), age (middle) and IOP (right) in the late post-surgery group of CXL Dataset 1

Summary of Results

Application of SSI2-KC in five CXL datasets showed consistently weak correlations with CCT and IOP and strong positive correlations with age. In SSI the correlation with IOP was positive and strong in all cases, while the correlation with CCT and age were inconsistent (positive and negative). SSI values were then compared to pre and post surgeries. In three datasets, SSI showed a larger percentage of softening after CXL compared to SSI2-KC. Overall, the changes in SSI were larger than changes in SSI2-KC when pre and post data were compared. However, SSI2-KC values were consistently lower and in the severe KC region ($SSI2 \approx 0.65$) while SSI varied significantly and had the same values as for healthy corneas in 2 datasets. A possible explanation for the large variations in SSI could be its strong correlation with IOP. IOP after CXL is normally overestimated compared with the pre IOP measurements due to the influence of the changes in corneal biomechanics. However, since SSI2-KC is using bIOP2, which was shown to be less correlated with biomechanical changes, this error is reduced with SSI2. On average SSI2-KC showed a $6.5 \pm 4.3\%$ increase while SSI showed a $7.8 \pm 4.2\%$ increase after CXL. The mean SSI2-KC always increased after CXL, but in SSI it was reduced in one case. In the literature, changes in corneal stiffness varied from 5% ³¹³ to 90% ³¹². Hence the actual changes in corneal stiffness are not known, but it is believed that there will be an increase in stiffness or prevention of further softening and deformation in most patients.

4.5.2.3 SSI-PLS for post LASIK and SMILE

Similar to SSI2-KC, the equation developed for the SSI2-PLS incorporated the same parameters as the healthy equation. The main difference is that since the LASIK and SMILE surgeries leave a loose flap on the cornea, the thickness of the flap would result in different behaviour of the cornea as described in section 3.6.2.3. Hence in SSI2-PLS, this flap separation was considered while optimising coefficients and terms of the equation. Please note that in refractive surgery, patients have healthy eyes prior to the surgery. Hence SSI2-H was applied to pre-op data. And for post-op, the SSI2-PLS was applied to compensate for changes induced by the surgery. For brevity, only one of the datasets is presented in this section. A similar analysis was conducted on other datasets and results are available in Appendices, Section B.

Dataset 1

Dataset 1 consist of 82 patients who undergo SMILE Surgery with a mean CCT of 541 ± 33 (480 - 642) microns, age of 34.8 ± 7.7 (22 - 51) years, bIOP of 14.3 ± 2 (9.6 - 21.1) mmHg, bIOP2 of 15.6 ± 1.3 (13.2-19.6) mmHg, SSI of 1.18 ± 0.19 (0.62 - 1.57) and SSI2-H of 1.02 ± 0.2 (0.68-2.43). After SMILE these values changed to a mean CCT of 444 ± 39 (351 - 545) microns, age of 35.3 ± 7.5 (22 - 51) years, bIOP of 12.3 ± 2 (8.1 - 16.1) mmHg, bIOP2 of 15.7 ± 0.8 (12.5 - 18.6) mmHg, SSI of 1.06 ± 0.22 (0.69 - 1.81) and SSI2- PLSof 0.96 ± 0.11 (0.78 - 1.4). To evaluate the performance of SSI values, (Pre SSI - Post SSI) / Pre SSI was calculated. This value for SSI was 0.092 ± 0.163 and for SSI2 was 0.048 ± 0.114 . Bland Altman plots are provided to visualise these changes, Figure 4-41.

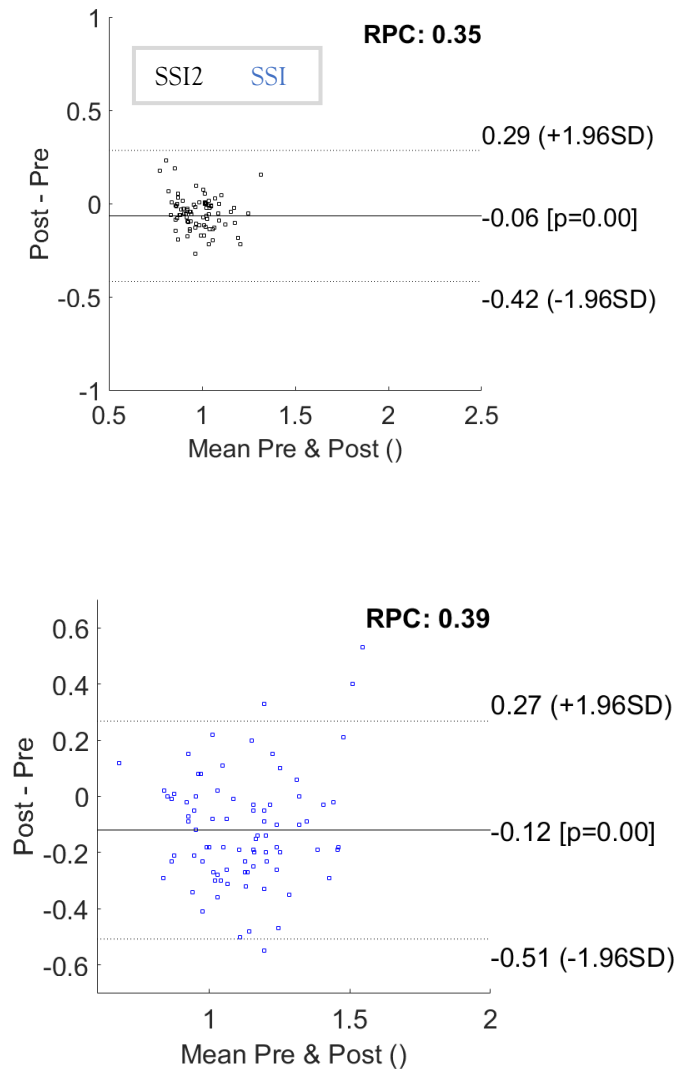


Figure 4-41 Bland Altman plot for SSI2 (top) and SSI (bottom) comparing the pre and post SMILE surgery results in Dataset 1

Further, the correlations between changes in CCT and SSI/SSI2 were evaluated. The correlation for SSI was $R:-0.187$ ($p:0.093$) and for SSI2 $R:-0.010$ ($p:0.372$). This showed changes in SSI2 had a weaker correlation with changes in CCT compared to SSI equation, Figure 4-42.

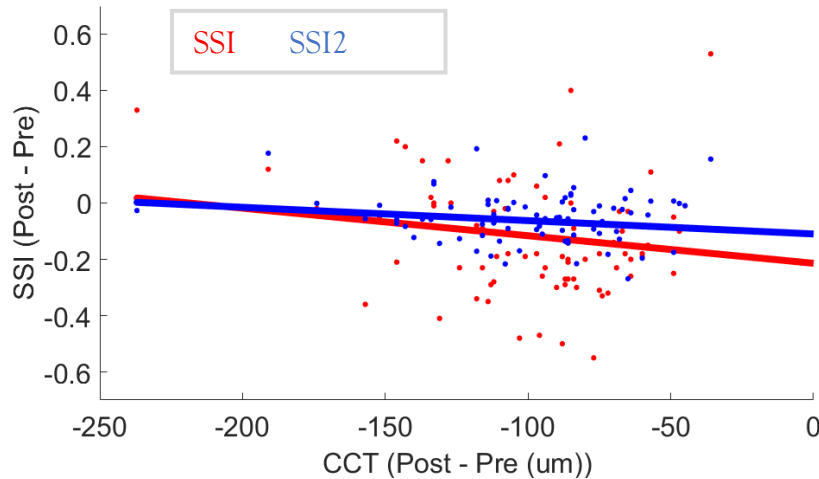


Figure 4-42 The evaluation of correlation in changes in CCT with changes in SSI and SSI2 in SMILE group of Dataset 1

Correlations with CCT before surgery for SSI was strong and significant with $R:-0.225$ ($p:0.042$) while SSI2-H was not correlated with $R:0.008$ ($p:0.946$). Age correlation with SSI was $R:0.403$ ($p:0.000$) and with SSI2-H was $R:0.528$ ($p:0.000$). Correlation of bIOP2 with SSI was significant and large with $R:0.564$ ($p:0.000$) while SSI2-H remained insignificant with $R:-0.133$ ($p:0.234$), Figure 4-43.

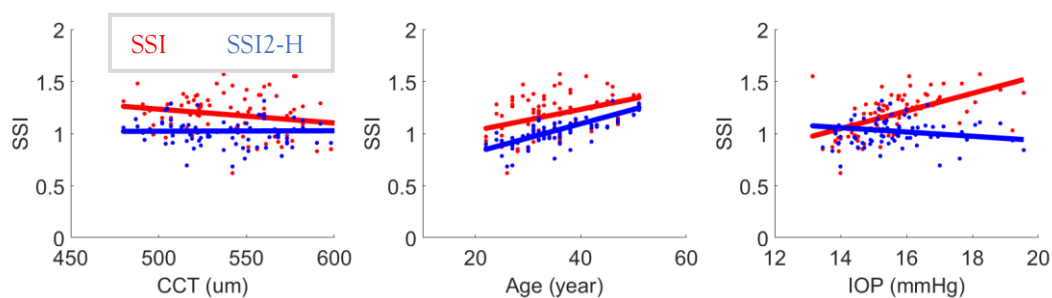


Figure 4-43 The correlation of SSI and SSI2-H with CCT (left), age (middle) and IOP (right) in the pre-surgery SMILE group of Dataset 1

Correlations with CCT after surgery for SSI remained strong with $R:0.269$ ($p:0.015$) and for SSI2-PLS became significant with $R:0.248$ ($p:0.025$). Age correlation with SSI was $R:0.388$ ($p:0.000$) and with SSI2-PLS was $R:0.799$ ($p:0.000$). Correlation of bIOP2 with SSI remained strong and significant with $R:0.515$ ($p:0.000$) while SSI2- PLS remained insignificant and not correlated with $R:0.017$ ($p:0.880$), Figure 4-44.

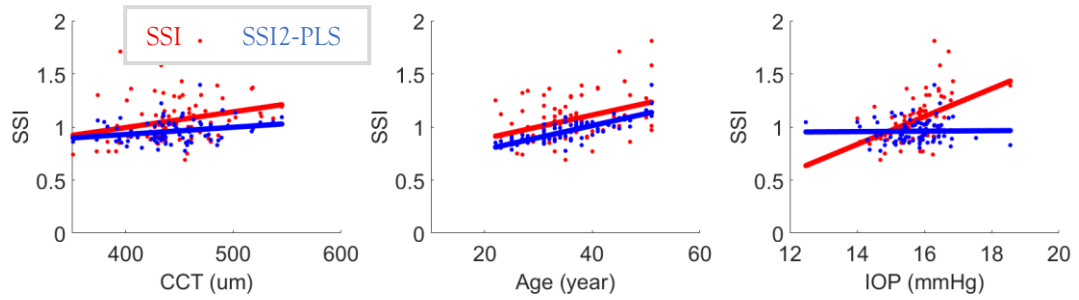
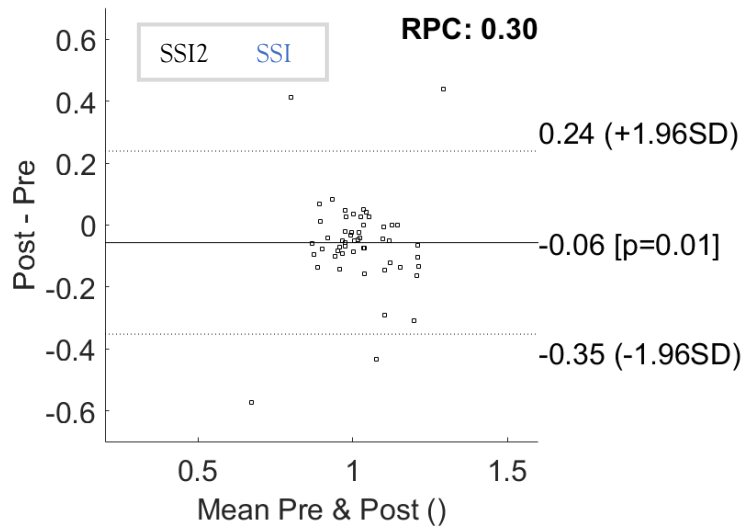


Figure 4-44 The correlation of SSI and SSI2-PLS with CCT (left), age (middle) and IOP (right) in the post-surgery SMILE group of Dataset 1

Dataset 1 includes 53 patients who undergo LASIK with a mean CCT of 543 ± 36 (473 - 611) microns, age of 36.8 ± 6.7 (26-47) years, bIOP of 14.8 ± 2.4 (11.6 - 25.2) mmHg, bIOP2 of 15.7 ± 1.5 (13.5-22) mmHg, SSI of 1.16 ± 0.21 (0.78-1.7) and SSI2-H of 1.05 ± 0.13 (0.59-1.35). After LASIK these values changed to a mean CCT of 481 ± 33 (409-537) microns, age of 37.1 ± 6.9 (27-48) years, bIOP of 12.9 ± 1.5 (9.6-16) mmHg, bIOP2 of 15.3 ± 1 (13-17.2) mmHg, SSI of 1.09 ± 0.26 (0.55-2.22) and SSI2-PLS of 0.99 ± 0.14 (0.39-1.51). To evaluate the performance of SSI values, $(\text{Pre SSI} - \text{Post SSI}) / \text{Pre SSI}$ was calculated. This value for SSI was 0.051 ± 0.242 and for SSI2 was 0.044 ± 0.163 . Bland Altman plots are provided to visualise these changes, Figure 4-45.



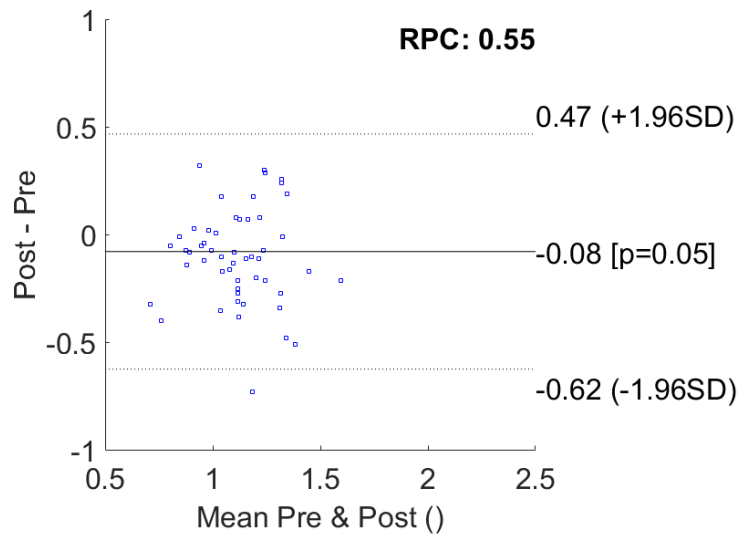


Figure 4-45 Bland Altman plot for SSI2 (top) and SSI (bottom) comparing the pre and post LASIK surgery results in Dataset 1

Further, the correlations between changes in CCT and SSI/SSI2 were evaluated. The correlation for SSI was $R:0.297$ ($p:0.031$) and for SSI2 $R:0.243$ ($p:0.080$). In this case, both had the same trend and closely related while SSI2 was insignificant, and SSI was significant, Figure 4-46.

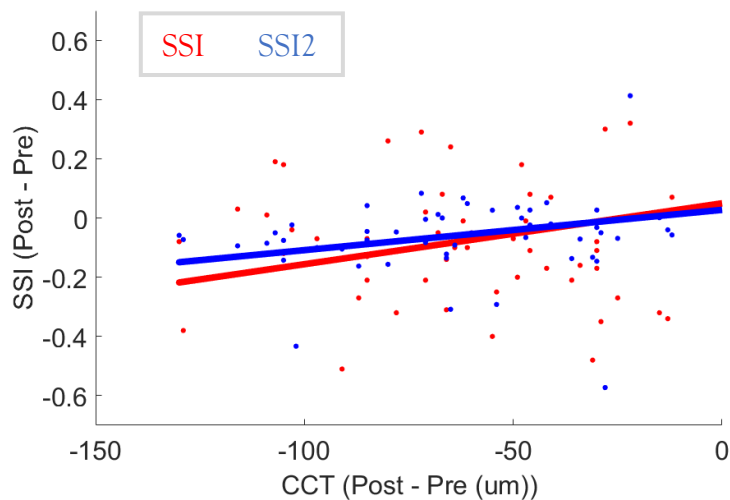


Figure 4-46 The evaluation of correlation in changes in CCT with changes in SSI and SSI2 in the LASIK group of Dataset 1

Correlations with CCT before surgery for SSI was negative with $R:-0.115$ ($p:0.414$) and for SSI2-H was stronger but insignificant with $R:0.249$ ($p:0.073$). Age correlation with SSI was $R:0.386$ ($p:0.004$) and with SSI2-H was $R:0.446$ ($p:0.001$). Correlation of bIOP2 with SSI was strong and significant with $R:0.366$ ($p:0.007$) while SSI2-H remained weakly correlated and insignificant with $R:0.098$ ($p:0.487$), Figure 4-47.

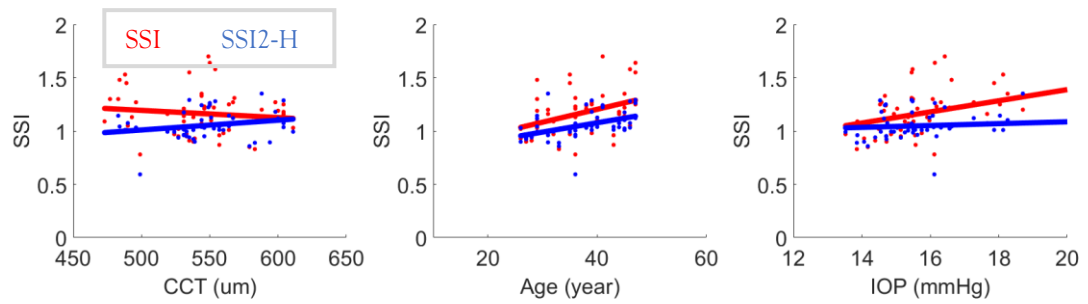


Figure 4-47 The correlation of SSI and SSI2-H with CCT (left), age (middle) and IOP (right) in the pre-surgery LASIK group of Dataset 1

Correlations with CCT surgery for SSI was $R:0.244$ ($p:0.078$) and for SSI2-PLS was $R:0.264$ ($p:0.056$) where both remained positive and insignificant. Age correlation with SSI was $R:0.168$ ($p:0.228$) and with SSI2-PLS was $R:0.541$ ($p:0.000$). Correlation of bIOP2 with SSI was significant and strong with $R:0.458$ ($p:0.000$) while SSI2-PLS was negatively and insignificantly correlated with $R:-0.192$ ($p:0.169$), Figure 4-48.

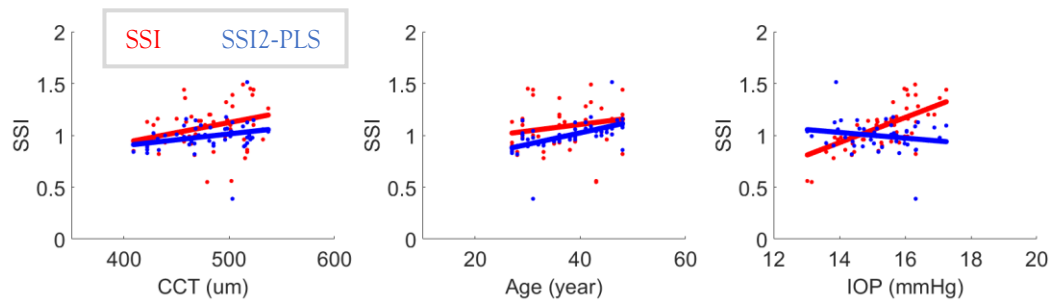


Figure 4-48 The correlation of SSI and SSI2-PLS with CCT (left), age (middle) and IOP (right) in the post-surgery LASIK group of Dataset 1

Summary of Results

In all four datasets, SSI2-PLS mean differences ranged from 0.01 to 0.06 reduction in values with standard deviations ranging from 0.13 to 0.35. On the other hand, SSI experienced a reduction of 0.08 to 0.15, with standard deviations ranging from 0.22 to 0.55. It is clear that SSI showed significant reductions in both means and standard deviations compared to SSI2-PLS. The correlation analysis showed that SSI was positively correlated with IOP and inconsistent correlations (positive and negative) with age and CCT. In general, the correlations with CCT and IOP was weakest in SSI2 for preoperatively and SSI2-PLS for postoperative data. Comparing the changes in CCT with changes in stiffness values, SSI2-PLS had a weaker correlation compared to SSI. With SSI2-PLS, it was possible to show that the material stiffness did not undergo significant changes following LASIK or SMILE.

4.6 Concluding Remarks

At the beginning of this chapter, a trend was found that could define the expected location of the cone and its geometry. The analysis for developing numerical models, including a mesh convergence study, was presented next. The numerical models were then validated using clinical cases. This chapter then presented the results of both bIOP2 and SSI2 equations on various clinical data in healthy, keratoconus, post crosslinking, refractive surgeries and glaucoma. In doing this, previously developed parameters were compared to demonstrate the improvements introduced by the new equations. These improvements were assessed in regards to correlations with CCT, age and IOP and through statistical analysis to compare pre and post-operative data. These results suggest noticeable improvements in estimating IOP and SSI compared to previously developed methods. These results are discussed in the next chapter.

Chapter Five

Discussion

5.1 Overall Discussion

This project started with the aim of enabling in vivo measurement of corneal biomechanics and further improve the diagnosis of glaucoma through a more accurate estimation of intraocular pressure (IOP). To achieve this, the study relied on representative numerical simulations to better understand corneal behaviour under tonometry air pressure. For numerical models to be representative, it was required to adopt realistic corneal geometry. This was particularly important in diseased eyes, such as those with keratoconus, where corneal geometry is distorted. The information that was available in the literature on this matter was not enough to construct these models. Hence a study was conducted to obtain this information. For this purpose, a method was developed that led to a software package that could receive elevation data from eye topographers and analyse them. This analysis was of particular importance in KC eyes so the cone properties could be characterised. These properties include the boundaries of the cone, the area of the cone, and its location and height.

Once the required information was obtained, the second piece of software was developed to utilise this information to build realistic numerical models, conduct a large parametric study and estimate corneal behaviour. This automated process alongside parallel and high-performance computing ability enabled conducting a large parametric study. Upon completion of these simulations, there was a need to analyse a large amount of data which would not be feasible by using manual techniques. Hence the third piece of software was designed to not only analyse the data collected from numerical models but also to calculate the dynamic corneal response parameters. Then the fourth and final piece of software was developed to read this information, and through having a detailed and multiplex objective function find the best parameters, build equations and estimate the required output with the smallest possible error.

This novel approach led to the development of new equations for biomechanically corrected IOP 2 (bIOP2) and Stress-Strain Index 2 (SSI2) which was a measure of corneal biomechanical stiffness in vivo. Upon development of these equations, their output was compared with previously developed parameters within Corvis ST and other

devices such as the DCT, ORA and GAT where their readings were available. This comparison was made with both previously conducted experimental data and a large clinical database. The clinical database included healthy, keratoconus and glaucoma patients in addition to post-surgery patients such as those who underwent refractive corrections and corneal crosslinking. These analyses served to validate the new methodologies and equations in addition to providing a holistic view of the performance of each. This section provides an overall discussion of all three main outcomes of (1) KC topography analysis, (2) biomechanically correlated IOP2 (bIOP2) and (3) Stress-Strain Index 2 (SSI2).

5.1.1 KC Topography Analysis

Keratoconus (KC) is a condition that causes an alteration in the curvature of the cornea and localised thinning^{69,72}. It commonly begins in early adolescence, progresses over the next two decades⁷³ and can significantly reduce visual acuity and vision-related quality of life^{74,75}. While the characteristic topographic patterns of keratoconus can be identified on corneal topographic and tomographic maps, it is still difficult to precisely locate the centre of the cone and the transition zone between the pathology area and the rest of the corneal tissue⁷⁶⁻⁸⁰. As classifying and managing keratoconus can be more efficient when the affected corneal region is located, especially in the case of customized corneal crosslinking⁸¹⁻⁸⁴, techniques were developed to address this challenge⁸⁵⁻⁸⁷. However, some of the available techniques to detect the keratoconus cone were based on methods that analysed corneal tangential or axial curvature maps, which were influenced by the variations in their algorithms⁸⁵⁻⁸⁷.

Tangential curvature maps typically have high noise-to-signal ratios and are based on the second derivative nature of the curvature calculation. This creates the need in elevation-based systems, such as Scheimpflug tomographers, for smoothing or low-pass filtering to derive tangential curvature from height data^{456,457}. Conversely, axial maps assume centre points of surface curvature to be always located on the central reference axis and this assumption reduces the sensitivity of the curvature maps in identifying surface changes due to cone development⁴⁵⁸. Mahmoud et al.⁸⁵ initially proposed a method using axial and tangential maps to locate the cone position and to quantify its magnitude. Later, axial and tangential curvature, and the relative elevation of both the anterior and the posterior surfaces, as well as the pachymetric maps were included in the method which exhibited improved accuracy in detecting the presence of keratoconus⁴⁵⁹. The Brillouin frequency shift at the point of maximum posterior elevation in relation to the best-fit sphere was also related to several curvature indices⁴⁶⁰. Its magnitude showed a high correlation with corneal stiffness reduction assessed by means of the Brillouin frequency shift⁴⁶⁰. Even though these methods have been demonstrated to be effective in detecting the presence of keratoconus cone and quantifying the relative stiffness reduction associated with the local pathology, they do not evaluate the size of

the pathologic area. Furthermore, as the cone centre is different in curvature, elevation, and pachymetry maps, there is a need for a method for detecting the location of the cone axis normal to the surface, in its natural three-dimensional position.

While estimating the area of pathology from the elevation data offers a direct method, a particular challenge is caused by the smooth transition between the natural curved shape of the corneal surface and the steeper curvature within the cone. Further, as the cone may be only a few microns above the curved shape of the cornea, it may be difficult to detect. This project attempted to overcome this difficulty by expressing corneal surface data normal to the surface and relative to the centre of the best-fit sphere to generate a 'spherical height map'. This map eliminates the effect of corneal surface curvature and hence increases the precision in locating cone centre and estimating the size of the affected area of the cornea.

A novel method to detect the cone centre and height normal to the surface, as well as the transition zone between the area of pathology and the surrounding healthy corneal tissue in keratoconic patients, was developed. The method relies on spherical coordinates relative to the centre of the cornea's optimal sphere fit and measured normal to the surface, in order to reduce the effect of the cornea's natural curvature in determining the cone's geometric features. When applying the method to 618 eyes of 309 KC patients, more than 80% of cases had infra-temporal cones, which is intermediate between the 95% figure reported by Auffarth, et al.⁴⁶¹ and 65% reported by Demirbas and Pflugfelder⁴⁶², but different from findings by Wilson, et al.⁴⁶³ where the majority of 48 eyes under study had the cone centre located in the inferior-nasal quadrant. The reason for this mismatch could be that Wilson, et al.⁴⁶³ used a relatively small sample that may have particular characteristics which cannot be generalised. These results also showed significant mirror-image symmetry (enantiomorphism) between right and left eyes in cone location, similar to what was reported by Rabinowitz and McDonnell⁷⁶ and Holland, et al.²⁶⁵. As no direct comparison was made between the fellow eyes of individual subjects in this study, the disease could be more advanced in one eye than the other.

The results further showed a trend of increased cone height ($R = 0.716$, $p < 0.001$) and reduced distance from corneal apex to cone centre ($R = -0.312$, $p < 0.001$) with disease severity – this trend was significant in both anterior and posterior surfaces of the right and left eyes. Cone height was also negatively correlated with the radius of the optimum fit sphere in both the anterior surfaces ($R = -0.584$, $p < 0.001$) and posterior surfaces ($R = -0.568$, $p < 0.001$).

In contrast, while having the radius of the optimal sphere as a co-variate, the cone area was not correlated with the disease stages in the anterior surface ($R = 0.002$, $p = 0.753$) and was weakly correlated in the posterior surface ($R = 0.093$, $p = 0.003$). This lack of

difference may be due to the simultaneous inclusion of different cone morphologies. Perry et al.,⁸¹ described two types of cone morphologies in advanced cases; the centrally restricted cone with nipple-shaped pattern and the peripheral cone with more oval shapes. As nipple cones typically have smaller areas and locate closer to corneal apex compared with oval cones in severe keratoconus, the use of both cone height and distance of cone centre to the apex as biomarkers for keratoconus severity may be less effective, leaving only cone height as a robust biomarker^{72,260,464,467}.

There is also strong evidence that the posterior cone increased in height faster in 90% of cases than the anterior cone, which was likely affected by epithelial remodelling. This finding supports the notion that the evaluation of both surfaces would be important for a reliable diagnosis²⁴⁵. The study also revealed a strong correlation between the shift of the posterior cone (relative to the anterior cone) and the height of the anterior cone. This is an important finding which can be used to provide a realistic representation of cone geometry in numerical simulations of the biomechanics of keratoconic eyes. It could also help the design and optimisation of corneal implants used to correct refractive errors in KC patients.

Another important earlier study by Mahmoud et al. identified the 2mm-diameter circular zone of the cornea with the steepest curvature and used it to locate the cone centre²⁶⁰. The method known as CLMI was initially developed for anterior surface axial and tangential curvature maps but later expanded to consider the posterior surface, surface elevation and corneal thickness maps. While this method was sensitive in separating keratoconic and normal corneas, and in locating and quantifying the alterations that occur in the central area of the disease, it was not designed to evaluate the cone shape or locate its transition zone.

The proposed method in this research is also different from the Belin/Ambrósio enhanced best-fit sphere method^{468,469}. In the Belin/Ambrosio method, the height of the cone is obtained by the difference in Z coordinate between the cornea and the BFS obtained after excluding a fixed area around the thinnest point. In the method presented in this study, the height is obtained by the radial differences between the cornea and the optimal sphere, calculated normal to the surface, obtained in an iterative process to exclude the pathologic area specific for each case.

This thesis provided a comparison between cone characteristics and key topographical indices obtained from the Pentacam. Cone area showed weak correlations with the majority of Pentacam indices related to KC diagnosis. Cone Height showed the strongest correlations with all parameters and specifically BADD, EleBFS8mm, Kmax, IVA and KI. The evaluation of distance from the cone centre to corneal apex showed moderate correlations with the majority of parameters where the correlation was highest in AsphQ and CKI. Comparison between anterior and posterior surfaces showed similar

correlations between them and Pentacam indices. In regards to cone height and distance from cone centre to corneal apex, all parameters apart from IHA showed similar correlations between left and right eyes. In regards to the area of the cone, no clear pattern could be detected between disease progression stages, Penatcam indices, anterior and posterior surfaces as well as left or right eyes.

With numerical simulations being used in ophthalmology, the findings of this study are valuable for future research. Numerical models require geometric information to be able to perform simulations and provide reliable results. To model eyes with keratoconus, the availability of the information provided in this research would enable modelling of corneal geometry, including the representation of the pathologic area which could then be simulated as softer than the surrounding area. The proposed method can also be used on data provided by different corneal topographers to identify the cone location, height and transition zone. This should enable researchers to develop computer programs based on this logic and analyse mass information in a customised manner using only the elevation data of the anterior and posterior cornea. In addition, in the era of artificial intelligence, access to large datasets is crucial for machine learning purposes. A problem with data collection is that information provided by different devices often cannot be used due to variations in data format^{466,470}. This method bridges this gap and enables consistent use of raw elevation data allowing multi-device data collection.

5.1.2 Biomechanically Corrected IOP 2 (bIOP2)

Measurement of intraocular pressure is an essential part of the treatment and screening of eye pathologies such as ocular hypertension, and glaucoma. IOP was identified as the only modifiable risk factor in glaucoma, which is one of the most common eye diseases and the second leading cause of blindness globally.⁴⁷¹ Every 1 mmHg increase in the IOP value was found to increase the risk of glaucoma by 11%.⁴⁷² Hence accurate measurement of IOP is extremely important to clinicians. Goldmann Applanation Tonometer (GAT) is the reference standard for measuring IOP.⁴⁷³ The details on how this device estimates IOP is discussed in Section 2.5.1.1. In brief, this device makes contact and applanates the cornea and assumes that the pressure applied to deform the cornea is equal to the internal pressure at first applanation. Although this assumption is true in an infinitely thin-walled sphere, in terms of the cornea it is susceptible to corneal thickness, curvature and biomechanics. As a result, measurements from GAT showed significant correlations with these confounding factors.^{474,475}

A number of attempts have been made to overcome these challenges and estimate more accurate IOP values. Among these attempts, newly developed devices such as Dynamic Contour Tonometer (DCT),³⁵⁰ Ocular Response Analyzer (ORA)⁴⁷⁶ and Corvis ST⁴⁷⁷ have been particularly successful to varying degrees. DCT is based on a completely different principle that is less influenced by corneal biomechanics, however, is

influenced by corneal geometrical parameters such as corneal radius.^{478,479} A detailed discussion is provided in section 2.5.1.2 on this topic. Both ORA and Corvis ST are non-contact tonometers that function based on the same concept as GAT. However, since they can capture more information about corneal deformation under external pressure, further adjustments could be introduced.^{25,480} Corvis ST has a high-speed Scheimpflug camera that enables monitoring the deformation of the anterior and posterior surfaces of the cornea at every location throughout the applanation process, section 2.5.1.3.2. ORA is using a laser-based system and can only identify the first and second applanation, section 2.5.1.3.1. In earlier studies, BIOP in Corvis ST was found to be the most accurate and least influenced by changes in corneal biomechanics and geometry.^{424,446} This was followed by DCT and then corneal-corrected IOP (IOPcc) in ORA.¹⁶⁶

The effectiveness of IOP measurements from different tonometers are obtained through clinical studies. In these studies, the correlation between the estimated IOP and various parameters and most importantly, central corneal thickness (CCT) and age (strongly correlated with stiffness) was examined.^{481,482} Some other researchers have compared the estimated IOP values with in-vivo manometry measurements with a limited number of patients due to practical reasons.^{483,484} Ex-vivo studies have been conducted that relied on measuring the pressure inside the eye using a transducer and comparing this true IOP value with what is estimated by a tonometry device. Although this is the most accurate method for measuring true IOP, difficulties in obtaining donor eye globes and the cost of experimental procedures have limited the ability to conduct large scale studies.⁴⁴⁷

The BIOP was developed using numerical modelling of healthy corneas through parametric studies and the equation included four parameters of CCT, age, API and Radius at Highest Concavity (RHC). The BIOP equation performed well, and studies had reported its better performance when compared to other IOP measurement methods. In particular, BIOP performed well in healthy eyes⁴⁸⁵ and when compared between pre and post-refractive surgeries³⁶⁰. In some publications, it was reported that BIOP was correlated with age³⁹⁰. Also, BIOP was not designed for keratoconic eyes, and a second equation was developed for soft corneas (bIOPs).³⁸⁷ In the development of bIOPs, a study on KC eyes was conducted and all corneas for healthy and KC patients were divided into five groups based on corneal curvature. Using this information, a rotationally symmetric FE parametric study was conducted which considered variations in CCT, corneal material stiffness, and corneal curvature.

In a study where bIOPs was compared to BIOP it showed improvement in estimating IOP values in the sense that the mean IOP of KC group was closer to the healthy eyes.³⁸⁷ However, there were three main flaws with this algorithm. First, it relied on an initially estimating corneal material stiffness which on its own is inter-related to IOP.

Inaccuracies in the estimation of material stiffness would lead to inaccurate IOP measurements. Second, it used rotationally symmetric numerical models to develop the parameter which is not representative of KC corneas. Third, numerical models did not consider the localised softening in the KC cornea. This simplification was found necessary to conduct that study using available resources, information and time span. The total number of models included in that study was 4500.⁴²⁸

A more recent study developed a new IOP algorithm (fIOP) for healthy eyes using more complex simulations.⁴⁸⁶ A novel multi-physics fluid-structure interaction model of the air-puff test was employed in a parametric numerical study simulating human eyes with a wide range of central corneal thickness (CCT), curvature (R), material stiffness and IOP. The models were internally loaded with IOP using a fluid cavity and externally with air-puff loading simulated using a turbulent computational fluid dynamics model. fIOP used the same parameters as bIOP, and the equation development strategy was the same.⁴¹⁵ It was concluded that fIOP performed as well as bIOP and no action was taken to implement the new algorithm into Corvis ST. Among the new fIOP, bIOP and bIOPs, only bIOP was implemented in Corvis ST and is in current use.

In this study, a new biomechanically-corrected IOP (bIOP2) was developed with the same goal as bIOP, which was to reduce the influence of biomechanics and geometrical components on IOP measurements. The FE models were also internally loaded using fluid cavity to introduce IOP. The fluid inside the cavity was described as incompressible so that the analysis would make sure the internal volume inside the ocular globe is maintained without change. Therefore, when the cornea is indented by the external load there will be a tendency to decrease the volume and increase the pressure. This pressure affects both cornea and sclera, adding to their surface tension and enlarging their size to accommodate the volume. This is compatible with the literature that the increase in IOP of biological eye globes would lead to the expansion of the sclera.⁴⁸⁷

In developing the new equation, several improvements were made, and some of them are presented here. (1) The numerical models were modified until full stability was achieved that enabled a 100% convergence rate. This was mainly achieved by modifying the element type, mesh density and constitutive material parameters from Ogden order three to order one. (2) The adjustments made in the model structure reduced the simulation time for every analysis to around 4 minutes. (3) The process of developing and analysing the numerical models, and exporting the data was entirely automated using a custom build software package allowing analysing several models in parallel and eliminating the time consumed by human interactions. (4) These points allowed expanding the size of the parametric study and looking at wider ranges of parameters. (5) In addition, more parameters were calculated and exported from the numerical simulations that enabled capturing more features from the corneal deformation under air puff.

(6) The strategy for developing the equation was improved where complex interconnected optimisation procedures were employed to automatically construct the most optimum equation. In contrast, in previous studies, the form of the equation was manually adjusted, and only the coefficients were optimised automatically.⁴²⁴ (7) A new innovative objective function was formed that enabled the development of the equation using numerical models while considering the noise and variations associated with clinical data. (8) In this project, a new methodology was developed to analyse and characterise KC cones for the first time. This led to the development of realistic asymmetric corneal models representing true conditions in clinical cases. Since this information has not been available until now, no FE model could be created with the precision as those in this thesis. (9) Asymmetric cone features and parameters were also varied in this study that included cone area, height and location in relation to Corvis ST monitoring line. (10) The stiffness in the cone area of FE models was reduced based on a recent study on KC microstructures of human corneas.⁴⁸⁸

(11) These new initiatives enabled a deeper understanding of corneal behaviour under air pressure that led to the development of an improved equation for bIOP2. The bIOP2 relied purely on parameters collected from Corvis ST to estimate IOP values for eyes with various conditions. Further, a second equation was developed to incorporate geometrical changes by collecting information from topography devices in addition to Corvis ST parameters. This equation was introduced as bIOP2-KC and is dedicated to keratoconic and distorted corneas. Cone characteristics utilised in this equation are based on the methodology developed in this study.

The improvements achieved in estimating IOP values were validated and verified through a large clinical study. This study expanded beyond exploring the effect only on healthy and keratoconic eyes as in previous studies. It evaluated the effect of surgical procedures, including refractive corrections and corneal crosslinking on the measurement of the IOP. It further evaluated the bIOP2 on glaucoma patients and in comparison with other tonometers including GAT, DCT and ORA. In addition to the clinical studies, experimental data were assessed where the true IOP was available and could be compared with the new IOP estimates. With this, a holistic view was provided on the performance of the new equations which is discussed next.

An ex vivo study previously conducted in the Biomechanical Engineering Group at the University of Liverpool controlled the IOP in five donor intact human eye globes under strict laboratory conditions.⁴⁴⁷ With access to the data of this study, the new bIOP2 was compared to bIOP and CVSIOP. Based on this, CVSIOP showed the largest differences compared to the true IOP with a mean of 6.1 ± 5.6 (-0.5-17.3) mmHg. This was followed by bIOP with a mean of -0.2 ± 2 (-3.6-4.2) mmHg and bIOP2 of 0.0 ± 0.6 (-1.4-1.5) mmHg. In that study, for each eye, multiple readings were taken, and the cases used in

this thesis may be different from those presented in a previous study.⁴⁴⁷ This led to minor changes in the means and standard deviations of values presented in the Results section. However, the message remained the same as bIOP was also recalculated for the cases used in this thesis. Based on these findings, bIOP2 improved on the prediction of true IOP in comparison to bIOP, slightly in mean values and significantly reduced the deviations that refer to the spread of estimations. Both bIOP2 ($p=0.976$) and bIOP ($p=0.989$) were not significantly different from the true IOP. Previous studies showed large errors with GAT when compared to actual IOP (1.7 ± 1.8 to 5.2 ± 1.6 mmHg).^{489,491} Inconsistent findings were reported when DCT errors were evaluated (0.58 ± 0.70 to 2.3 ± 2.4 mmHg).^{492,493}

The study on all clinical data, as explained in results section 4.5.1, clearly demonstrated that the bIOP2 is less influenced by corneal biomechanics compared to bIOP and other tonometry devices like DCT, ORA and GAT. This improvement in estimating IOP values for post-refractive surgeries post crosslinking, and in keratoconic eyes are significant. Also, the correlation with age in healthy datasets and with both CCT and age in KC datasets were reduced in bIOP2 measurements. However, bIOP2 showed some correlations with CCT in KC datasets and for this reason, a second equation was developed called bIOP2-KC. This equation can estimate improved IOP values if the topography information is available. In addition to all parameters used for bIOP2, in bIOP2-KC other parameters such as cone location, height and area were added.

5.1.3 Stress-Strain Index 2 (SSI2)

The last two decades experienced fast growth in interest in corneal biomechanics and its effect on the outcome of refractive surgery, measurement of intraocular pressure (IOP) and progression and management of keratoconus^{494,497}. This growth in interest has led to a few attempts to quantify corneal biomechanics in-vivo including, most notably, the Brillouin modulus, the Corneal Resistance Factor (CRF) and the Corneal Hysteresis (CH) provided by the Ocular Response Analyzer (ORA), and the Corvis ST deformation parameters including the Stiffness Parameter (SP) and the Integrated Inverse Radius (*IntInvR*)^{441,446,498,499}. A detailed discussion of these methods was provided in section 2.5. A more recent development is the Corvis Stress-Strain Index (SSI) which was designed to estimate the material stiffness of the cornea – rather than its overall stiffness – and seeks to determine the whole stress-strain behaviour rather than a particular value of the tangent modulus¹⁰⁷. This latter point is of particular importance since corneal tissue is known to have nonlinear pressure - deformation behaviour and stress-strain behaviour, and hence the tangent modulus (E_t) does not maintain a constant value but increases gradually with load, stress, deformation and strain⁵⁰⁰.

The cornea's overall stiffness is defined as its resistance to deformation under both internal loads (primarily the IOP) and external loads (such as eyelid pressure and tonometric loading). Stiffness has two major components; the geometric stiffness and the material stiffness, Figure 5-1. The geometric element is affected by corneal curvature and diameter but is dominated by corneal thickness, and this justifies the emphasis placed on the central corneal thickness (CCT) in correcting IOP measurements for the effects of corneal stiffness variations⁵⁰¹. All these parameters can be measured accurately, making the geometric stiffness of the cornea easy to quantify. In contrast, the corneal material stiffness presented significant challenges and until recently, it was not possible to estimate the full stress-strain behaviour in-vivo. The introduction of the SSI was intended to address this challenge and could, if successful, help, to detect the progression of keratoconus (where there is a deterioration in material stiffness) and assess the effectiveness of the collagen crosslinking treatment (by detecting increases in material stiffness)¹⁰⁷.

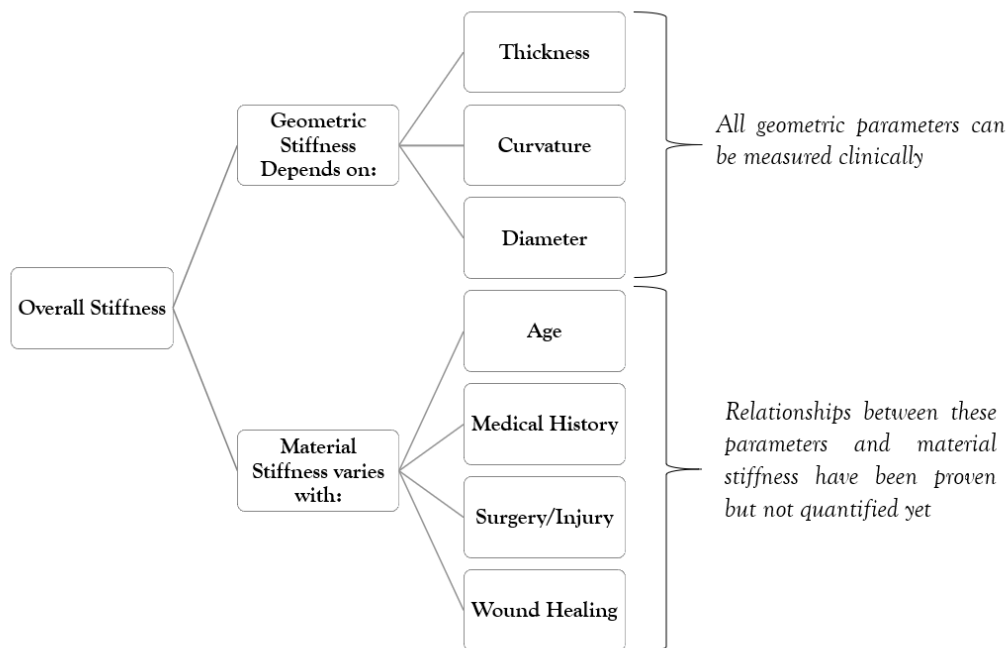


Figure 5-1 Components of overall stiffness

As explained in section 2.5.1.3, corneal deformation under air puff is influenced by both IOP and material stiffness. On the other hand, material behaviour is non-linear, which results in different corneal stiffness under different IOP values. The SSI was the first parameter that attempted to address this issue. The report on the SSI presented evidence of its independence of both corneal thickness and the IOP, and this point was illustrated using clinical data and experimental results of ex-vivo human corneas tested under artificial IOP¹⁰⁷. The development of SSI was based on numerical models and used three main parameters of CCT, bIOP and SP. In the parametric study done for

developing this algorithm, it was found that when material properties of the cornea changes, CCT, *bIOP* and *SP* can form a 3D surface presenting that particular material stiffness. Further, when the material stiffness was changed, these 3D surfaces did not intersect. Hence the idea was developed that using these three parameters and with the knowledge of the position of 3D surfaces from numerical models, the material stiffness of the cornea could be estimated.

Based on this logic, SSI became the first parameter that could provide insights into the actual material stiffness of the cornea. However, as it was shown in the previous section, *bIOP* was influenced by CCT and age (corneal biomechanics). Hence as this parameter was used in SSI, naturally there will be an adverse effect on the estimation of material properties of the cornea using this algorithm. Further, this equation could be susceptible to noise in clinical data as the 3D surfaces were developed purely based on numerical models. Hence upon application of the algorithm on more recent clinical data, there seemed to be a correlation with age and CCT to varying degrees. When it was tested on patients after refractive surgeries, changes in SSI was more than expected, and the value became lower than the pre SSI due to correlations with geometrical components.⁴²⁸

A second study attempted to develop a new equation to overcome these shortfalls by developing more complex models. This study relied on a multi-physics fluid-structure interaction model of the air-puff test and performed a parametric study on human eyes. The new equation (*fSSI*), employs similar parameters as SSI that were CCT, *SP* and *fIOP* as described in the previous section.⁴¹⁵ The performance of *fSSI* was found to be close to SSI, and hence the new equation was not implemented into Corvis ST. This thesis attempted to overcome these challenges by following a new methodology. The numerical simulations and the procedure for generating models, analysing them and collecting the data were completely revised as described in chapter 3.

Apart from that, this thesis did not try to build 3D surfaces and use a limited number of parameters to estimate material properties. Instead, the inter-connected blocks of optimisation algorithms that were developed for designing *bIOP2* were given the flexibility to obtain the optimum equation for SSI2. This brought a number of advantage to the new equation in addition to the 11 points mentioned earlier in section 5.1.2. These include (12) reduced dependency of SSI2 to only three parameters as in SSI, (13) compensating for noise in clinical data, (14) ability to use a more accurate IOP measurement that was developed in this thesis (*bIOP2*) and (15) utilising geometrically more representative numerical models. Hence to evaluate the performance of SSI2 equation, it was applied to clinical data of healthy and KC corneas and those who undergo surgeries such as refractive corrections and CXL. All values were compared with SSI to demonstrate the performance of the new equation and improvements brought by following the new methodology.

As another form of validation, correlations between SSI/SSI2 and age were compared with an earlier study involving inflation tests on ex-vivo human corneas^{123,502}. The study, which involved 57 corneas tested under inflation conditions with a posterior pressure simulating IOP, resulted in a stress-strain relationship of the form:

$$\sigma = A[e^{B\varepsilon} - 1]$$

Equation 5-1

where σ = stress, ε = strain, $A = 1.26 \times 10^{-3}$ and $B = 0.0013 \text{ age}^2 + 0.013 \text{ age} + 99$. Both parameters of A and B are dimensionless. As another form of validation, Equation 5-1 with respect to the strain leads to Equation 5-2:

$$E_t = \frac{d\sigma}{d\varepsilon} = AB e^{B\varepsilon} = B(\sigma + A)$$

Equation 5-2

where E_t is the tangent modulus. At the specific case with $\text{age} = 50$ years (at which $\text{SSI} = 1.0$), $B = 102.9$. Since the ratio between E_t at any age and E_t at $\text{age} = 50$ equals the ratio between SSI at this age and SSI at $\text{age} = 50$ years, which is 1.0, therefore SSI at any given age can be determined from Equation 5-3:

$$\frac{\text{SSI}_{\text{age } x}}{\text{SSI}_{50} = 1.0} = \frac{E_t(\text{age } x)}{E_t(\text{age } 50)}$$

Equation 5-3

This value of SSI, based on ex-vivo results given in terms of age, has been compared to the values of SSI obtained from the analysis of the in vivo results, obtained from the two clinical datasets. After the development of SSI2 for healthy corneas, there was a need to consider further variations in specific clinical conditions. First, a new equation was developed for patients with KC eyes. As shown in the first part of this chapter, the majority of KC cones are located on the inferior side of the cornea. Corvis ST only monitors the horizontal meridian located in the centre of the cornea. Hence it is unable to capture information from the cone area in the majority of KC eyes. If the clinician is aware that this eye is KC or not, then there is an opportunity to utilise this new information and improve the accuracy of corneal material estimation, and for this reason, SSI2-KC was developed.

In regards to refractive surgeries such as Femtosecond laser-assisted in situ keratomileusis (LASIK), Small incision lenticule extraction (SMILE) and Transepithelial Photorefractive keratectomy (PRK), there is a further complication. The three laser vision correction (LVC) procedures do affect corneal stiffness to different extents - while all three involve ablating tissue, only LASIK and SMILE also require tissue separation through the creation of a flap and a cap, respectively⁵⁰³. The flap and

the cap also have different characteristics with the flap having an almost complete separation from the residual stroma, and the cap maintaining a connection with the surrounding stroma except at the location of a short incision⁵⁰⁴. These differences in characteristics are expected to have different effects on corneal biomechanics in general, and corneal stiffness in particular⁵⁰⁵. As a result of this, another equation was developed to compensate for geometrical changes induced through these surgeries that specifically applies to patient post LASIK and SMILE, and it is called SS2-PLS.

The first validation started by comparing SSI and SSI2 of seven healthy clinical datasets with stiffness changes found experimentally using inflation tests of ex-vivo human corneas.¹²³ Both parameters showed a strong correlation with age and followed the same trend as ex vivo findings. The correlation between SSI and ex vivo results were weaker than the SSI2. SSI2 followed the ex vivo trend almost parallel to its linear regression line. The spread of the data in SSI2 was smaller than SSI. The mean values of SSI and SSI2 were slightly larger than ex vivo results. SSI2 maintained a significant correlation in all seven datasets while SSI showed insignificant correlations in two datasets with ex vivo findings. This validates SSI values and demonstrates improvements achieved by SSI2 in regards to correlations with age.

On the other hand, LASIK and SMILE are significantly different from PRK. Both surgeries involve tissue loss, similar to that of PRK, but they additionally require the separation of a top flap or cap⁵⁰⁶. While the cap is potentially more efficient than the flap in transmitting the surface tension caused by the IOP, they would behave similarly under the flexural action of the concentrated, external air puff⁵⁰⁷. In this case, the separation of the tissue into a thin anterior component (flap or cap) and a thicker posterior component (residual stroma), means that, under flexural actions (air-puff pressure), the contribution of the posterior component becomes dominant with that of the anterior flap or cap becoming negligible. Therefore, the effect of LASIK and SMILE is a reduction in geometric stiffness (due to both tissue ablation and separation), and this causes a large effect on the cornea's overall stiffness and more than PRK. Comparable observations were made in a series of publications in the literature^{505,508-510}.

Nevertheless, the material stiffness should remain stable after LASIK and SMILE, similar to what has been found after PRK. However, assessing this hypothesis met a challenge caused by the fact that the current SSI did not consider the tissue separation experienced in LASIK and SMILE¹⁰⁷. Therefore, considering the CCT measured postoperatively, which includes the thickness of the flap and cap, wrongly overestimates the geometric stiffness used in the calculations, and hence underestimates the material stiffness. For this reason, a new SSI algorithm was developed based on numerical modelling of the ocular globe that considered this difference in the two surgeries. The new parameter, which is called SSI2-PLS, was applied to three different datasets of patients who undergo LASIK and SMILE with the expectation that the pre and post

values remain the same, and they were compared to SSI. It should be noted that SSI was not designed to be applied to these datasets, and as a result, a larger reduction in values postoperatively is expected.

Based on the analysis presented in section 4.5.2, it is clear that SSI2 was able to significantly improve the estimation of corneal biomechanics more independent from geometrical changes and IOP values. This is a crucial step forward in enabling personalised medicine in the field of ophthalmology and the only available method for measuring in vivo corneal biomechanics at the moment. It is expected that the value of SSI2 will be used in software and devices used in ophthalmology to optimise procedures such as refractive corrections or crosslinking.

5.2 Limitations of Study

In this research, an attempt was made to minimise the influence of limitations associated with reaching the desired outcome of this study as much as possible. Although the goal of the study was well met, some limitations are mentioned below.

- The analysis of corneal elevation data based on the methodology proposed in this thesis is influenced by the accuracy of topographers. For instance, in Pentacam, the error is estimated to be around 100 microns, and this would influence the accuracy of cone characteristics parameters obtained from the methodology developed in this study.
- The reliance of the SSI2 and bIOP2 equations on a single meridian from horizontal corneal thickness profile obtained with the Corvis ST may introduce slightly higher variability than what could be achieved with other imaging techniques, such as the rotating scheinpflug tomographers.
- Another limitation is that the differences between the three surgeries in ablation profiles and the width of ablated tissue could have further effects on the cornea's geometric stiffness. However, these effects are unknown and expected to be small and had been ignored in this study to avoid introducing further complexity in the analysis.
- Measurements taken from different Corvis ST devices may be subjected to small inherent variations which could influence the precision of equations developed in this study.
- Readings taken from distorted eyes using Corvis ST may require manual triggering of air puff that could influence the behaviour of the cornea. This is because, in the simulations done in this study, the distance from the cornea to the nozzle was assumed 11 mm. Manual handling of the device would potentially change this distance and results in higher or lower pressure on the cornea. This is a potential source of error in keratoconic and crosslinked cornea.

- The data used for pre-surgery in CXL datasets must be collected on the day of the surgery. If the readings were taken a couple of months before the surgery date, corneal stiffness would potentially be higher in KC eyes and would result in errors when compared to postoperative data. The data presented in this study could not be confirmed to adhere to this protocol.
- The effect of wound healing in refractive surgery data is unknown, and its effect could not be considered in the development of equations. If this information could be provided, the accuracy of equations could be improved.
- The eye model did not include extracellular muscles and orbital fat. Hence the effect of whole eye movement was removed from Corvis ST readings to match the numerical models. A better understanding of the whole eye movement could improve the accuracy of equations.
- Lack of proper understanding of corneal hysteresis limited the use of data collected from the return of cornea from the highest concavity point back to the neutral position. This is because numerical simulations could not adapt to hysteresis behaviour, and this factor could not be considered in equation development.
- It is not known that if CXL would increase the flexural behaviour of the cornea. All studies conducted in this field, tested the cornea under tension and showed an increase in stiffness. One study that used ultrasound techniques should only 5% increase in stiffness. Hence although the new SSI2 equations show stiffening after CXL in the majority of cases, it is not known if the increased value of stiffening is representative of true changes in corneal biomechanics.
- Due to variations between geometrical and visual axes, Corvis ST does not always shoot perpendicular to the apex as it was simulated in this study. These variations could have affected the accuracy and spread of readings.
- An ideal method for validating SSI2 would be to test fresh donor human eyes ex-vivo and compare the Corvis ST estimate of the material stiffness with results obtained from inflation. However, obtaining human eyes is extremely difficult and costly and was not feasible for this study.
- Since Corvis ST captures the behaviour of the horizontal meridian of the central cornea, the estimation of material stiffness obtained from SSI or SSI2 is presenting overall corneal material stiffness separate from geometrical components. In diseases corneas, there is a localised variation in material stiffness, and this could not be measured in this study.
- With the ability to collect more information from the eye, it may be possible to develop one single equation for SSI2 and bIOP2. However, at this time, this would not be possible and led to the development of multiple equations that deal with specific clinical conditions.

5.3 Concluding Remarks

The aim of this study was to develop new methods to measure corneal biomechanics in vivo and estimate IOP independent of corneal biomechanics and geometric variations. Were this outcome to be achieved, personalised medicine would be possible in ophthalmology. Possible applications for SSI2 include optimising the strength of CXL, adjusting ablation thickness in refractive surgery based on corneal biomechanics, customising contact lenses by considering the mechanical interaction with the cornea, and improving glaucoma management. The new methods and equations were indeed achieved in this study, and validation using both experimental and clinical data was performed. In conclusion:

- This study proposed a new method to explore the changes in anterior and posterior corneal surfaces in patients with keratoconus and to define the cone-shaped area. The method is intended to help improve understanding of corneal shape as keratoconus progresses and customise treatment regimens such as collagen crosslinking and intracorneal ring implantation. Also, this information would now enable the development of numerical models representative of KC conditions in research.
- A large parametric study was conducted that adapted realistic KC corneal geometry with reduced localised material stiffness enabled a better understanding of corneal behaviour under air puff and led to the development of new equations for estimating IOP and corneal material stiffness in vivo.
- Three new equations were developed and validated for estimating corneal material stiffness in health eyes (SSI2), KC and CXL eyes (SSI2-KC), and those post LASIK and SMILE (SSI2-PLS).
- bIOP2 and SSI2 were validated with experimental data and evaluated on a large set of clinical data while being compared with previously developed equations and compared with key parameters.
- The bIOP2 equation has significantly reduced the correlation with CCT and age in comparison to bIOP. It was also less affected by biomechanical changes in keratoconus patients and crosslinked eyes and in eyes that underwent refractive surgeries.
- The bIOP2-KC performed better in reducing the correlation with CCT in KC eyes compared to bIOP2 and bIOP. However, the estimation of IOP using bIOP2-KC did not change significantly compared to bIOP2 equation.
- New SSI2 equations were superior to SSI in being less correlated with CCT and IOP while having a stronger correlation with age in line with earlier ex vivo experimental results.
- SSI2-KC was able to capture the changes in KC eyes with disease progression better than the previous equations. Also, when SSI and SSI2-KC were compared in pre and post CXL data, SSI2-KC performed better by showing a fewer number of corneas softening after surgery.

- SSI-PLS showed better stability when pre and post LASIK and SMILE surgery data were compared. This analysis proved that the new methodology adapted for developing SSI2 was more suitable for estimating corneal biomechanics and is less affected by noise in clinical data.

5.4 Recommendations for Future Studies

Some recommendations are provided for future research to improve the performance of the equations developed in this study and further expand to new areas. These recommendations are as below:

- Improving the Corvis ST fixation target to a more advanced adjustable method that ensures the air puff is shooting perpendicular to the corneal apex and aligned by geometrical axis instead of the visual axis.
- Ex vivo studies on fresh donor human eyes could enable better evaluation of the performance of SSI2. To do this, Corvis ST should be used to estimate biomechanics and then compared with inflation tests results as a measure of true material stiffness.
- A better understanding of corneal hysteresis could enable the improvement of numerical simulations and information obtained from the highest concavity of the cornea back to the neutral position could be utilised in the equations.
- If the true distance from the Corvis ST nozzle to the cornea could be measured, this new information could be used in numerical simulations to adjust the pressure on the cornea and improve the accuracy of equations.
- Ex vivo studies should be conducted on healthy and CXL corneas under flexural force to accurately measure the amount of stiffening with crosslinking under air puff loading.
- A better understanding of the wound healing effect could lead to more accurate simulations of the cornea after refractive surgeries and improve the accuracy of equations.
- Reducing the errors induced by human interactions, including manual triggering of the air puff, could lead to improved repeatability of results. The influence of this on measurements is not known, and a clinical study could be conducted to evaluate this.
- Capturing deformation of the cornea in more meridians could lead to a better understanding of corneal response at localised locations. Studies should be conducted to measure the suitable locations.
- The application of a large pressure such as air puff eliminates the ability to estimate localised changes in corneal biomechanics. Hence combining air puff with other techniques such as Brillouin microscopy or videography could enable measurement of corneal stiffness with the ability to adjust for localised variations on the corneal surface.

References

- 1 EyeCenter. *Ophthalmology Terms*,
<http://www.eyecenter.emory.edu/ophthalmology_terms.htm> (2020).
- 2 Care, U. o. I. H. *Glossary of Eye Terms*,
<<https://medicine.uiowa.edu/eye/patient-care/glossary-eye-terms>>
(2020).
- 3 Siraisi, N. G. *Medieval and early Renaissance medicine: an introduction to knowledge and practice*. (University of Chicago Press, 2009).
- 4 Leffler, C. T., Schwartz, S. G., Hadi, T. M., Salman, A. & Vasuki, V. The early history of glaucoma: the glaucous eye (800 BC to 1050 AD). *Clinical ophthalmology (Auckland, NZ)* **9**, 207 (2015).
- 5 Mrcophth. *Anatomy*,
<<http://www.mrcophth.com/Historyofophthalmology/anatomy.htm>> (
- 6 Smith, A. M. *Ptolemy's theory of visual perception: an English translation of the Optics*. Vol. 82 (American Philosophical Society, 1996).
- 7 Lindberg, D. C. & Lindberg, D. C. *Theories of Vision from al-Kindi to Kepler*. (University of Chicago Press, 1981).
- 8 Grant, E. *A source book in medieval science*. Vol. 13 (Harvard University Press, 1974).
- 9 Kriss, T. C. & Kriss, V. M. History of the operating microscope: from magnifying glass to microneurosurgery. *Neurosurgery* **42**, 899-907 (1998).
- 10 Colston, H. & Gibbs, R. A brief history of irony. *Irony in language and thought: A cognitive science reader*, 3-21 (2007).
- 11 Abdelaziz, L. & Barbara, R. History of the Development of the Treatment of Keratoconus. *International Journal of Keratoconus and Ectatic Corneal Diseases* **2**, 31-33 (2013).
- 12 Stamper, R. L. A history of intraocular pressure and its measurement. *Optometry and Vision Science* **88**, E16-E28 (2011).
- 13 Newton, M. J. *Contact lens practice: by Robert B. Mandell, OD, Ph. D., Springfield, Charles C Thomas, 1988, 1025 pp., illus. Price: \$69.75. Survey of Ophthalmology* **34**, 408 (1990).
- 14 Lengyel, B. A. *Lasers: generation of light by stimulated emission*. (1962).
- 15 Srinivasan, R. & Braren, B. Ultraviolet laser ablation of organic polymers. *Chemical Reviews* **89**, 1303-1316 (1989).
- 16 Peyman, G. A. (Google Patents, 1989).
- 17 Ethier, C. R., Johnson, M. & Ruberti, J. Ocular biomechanics and biotransport. *Annu. Rev. Biomed. Eng.* **6**, 249-273 (2004).

- 18 Roberts, C. J., Dupps, W. J. & Downs, J. C. *Biomechanics of the Eye*. (Kugler Publications, 2018).
- 19 Irsch, K. & Guyton, D. L. in *Encyclopedia of Biometrics* (eds Stan Z. Li & Anil Jain) 11-16 (Springer US, 2009).
- 20 Leske, M. C., Connell, A., Wu, S.-Y., Hyman, L. G. & Schachar, A. P. Risk factors for open-angle glaucoma: the Barbados Eye Study. *Archives of ophthalmology* **113**, 918-924 (1995).
- 21 McMonnies, C. W. Glaucoma history and risk factors. *Journal of optometry* **10**, 71-78 (2017).
- 22 Vajaranant, T. S., Wu, S., Torres, M. & Varma, R. The changing face of primary open-angle glaucoma in the United States: demographic and geographic changes from 2011 to 2050. *American journal of ophthalmology* **154**, 303-314. e303 (2012).
- 23 Brubaker, R. F. Tonometry and corneal thickness. *Archives of ophthalmology* **117**, 104-105 (1999).
- 24 Kohlhaas, M. *et al.* Effect of central corneal thickness, corneal curvature, and axial length on applanation tonometry. *Archives of ophthalmology* **124**, 471-476 (2006).
- 25 Park, S. J., Ang, G. S., Nicholas, S. & Wells, A. P. The effect of thin, thick, and normal corneas on Goldmann intraocular pressure measurements and correction formulae in individual eyes. *Ophthalmology* **119**, 443-449 (2012).
- 26 LOPEZ DE LA FUENTE, C., SANCHEZ-CANO, A., PINILLA, I., FUENTES BROTO, L. & SEGURA CLAVO, F. Relationship between IOP and biomechanical corneal values obtained by ORA. *Acta Ophthalmologica* **90** (2012).
- 27 Tonnu, P. *et al.* The influence of central corneal thickness and age on intraocular pressure measured by pneumotonometry, non-contact tonometry, the Tono-Pen XL, and Goldmann applanation tonometry. *British Journal of Ophthalmology* **89**, 851-854 (2005).
- 28 Asaoka, R. *et al.* The relationship between Corvis ST tonometry measured corneal parameters and intraocular pressure, corneal thickness and corneal curvature. *PloS one* **10** (2015).
- 29 Okafor, K. C. & Brandt, J. D. Measuring intraocular pressure. *Current opinion in ophthalmology* **26**, 103-109 (2015).
- 30 Myers, K. J. & Scott, C. A. The non-contact ("air puff") tonometer: variability and corneal staining. *American journal of optometry and physiological optics* **52**, 36-46 (1975).
- 31 Shah, S., Laiquzzaman, M., Yeung, I., Pan, X. & Roberts, C. The use of the Ocular Response Analyser to determine corneal hysteresis in eyes before and after excimer laser refractive surgery. *Contact lens and anterior eye* **32**, 123-128 (2009).

- 32 Hong, J. *et al.* A new tonometer—the Corvis ST tonometer: clinical comparison with noncontact and Goldmann applanation tonometers. *Investigative ophthalmology & visual science* **54**, 659-665 (2013).
- 33 Elsheikh, A. *et al.* Clinical Evaluation of Correction Algorithm for Corvis ST Tonometry. *Investigative Ophthalmology & Visual Science* **56**, 101-101 (2015).
- 34 Kaushik, S., Pandav, S. S., Banger, A., Aggarwal, K. & Gupta, A. Relationship between corneal biomechanical properties, central corneal thickness, and intraocular pressure across the spectrum of glaucoma. *American journal of ophthalmology* **153**, 840-849. e842 (2012).
- 35 Roberts, C. Biomechanics of the cornea and wavefront-guided laser refractive surgery. *Journal of Refractive Surgery* **18**, S589-S592 (2002).
- 36 Pepose, J. S., Feigenbaum, S. K., Qazi, M. A., Sanderson, J. P. & Roberts, C. J. Changes in corneal biomechanics and intraocular pressure following LASIK using static, dynamic, and noncontact tonometry. *American journal of ophthalmology* **143**, 39-47. e31 (2007).
- 37 Ambrosio, R., Jr. *et al.* Corneal Biomechanics in Ectatic Diseases: Refractive Surgery Implications. *Open Ophthalmol J* **11**, 176-193, doi:10.2174/1874364101711010176 (2017).
- 38 Ortiz, D., Piñero, D., Shabayek, M. H., Arnalich-Montiel, F. & Alió, J. L. Corneal biomechanical properties in normal, post-laser in situ keratomileusis, and keratoconic eyes. *Journal of Cataract & Refractive Surgery* **33**, 1371-1375 (2007).
- 39 Goldich, Y. *et al.* Clinical and corneal biomechanical changes after collagen cross-linking with riboflavin and UV irradiation in patients with progressive keratoconus: results after 2 years of follow-up. *Cornea* **31**, 609-614 (2012).
- 40 Liu, J. & Roberts, C. J. Influence of corneal biomechanical properties on intraocular pressure measurement: quantitative analysis. *Journal of Cataract & Refractive Surgery* **31**, 146-155 (2005).
- 41 Elsheikh, A. *et al.* Assessment of corneal biomechanical properties and their variation with age. *Current eye research* **32**, 11-19 (2007).
- 42 Maurice, D. M. in *Vegetative Physiology and Biochemistry* 289-368 (Elsevier, 1962).
- 43 Van Buskirk, E. M. The anatomy of the limbus. *Eye* **3**, 101-108 (1989).
- 44 Fatt, I. & Weissman, B. A. *Physiology of the eye: an introduction to the vegetative functions.* (Butterworth-Heinemann, 2013).
- 45 Goel, M., Picciani, R. G., Lee, R. K. & Bhattacharya, S. K. Aqueous humor dynamics: a review. *The open ophthalmology journal* **4**, 52 (2010).
- 46 Lowell, J. *et al.* Optic nerve head segmentation. *IEEE Transactions on medical Imaging* **23**, 256-264 (2004).

- 47 Bloemendal, H. *et al.* Ageing and vision: structure, stability and function of lens crystallins. *Progress in biophysics and molecular biology* **86**, 407-485 (2004).
- 48 Guyer, D. R. *et al.* Retina-vitreous-macula. *Retina* **19**, 265 (1999).
- 49 Wikipedia. Eye, <<https://en.wikipedia.org/wiki/Eye>> (
- 50 Meek, K. M. & Boote, C. The organization of collagen in the corneal stroma. *Experimental eye research* **78**, 503-512 (2004).
- 51 Vrana, N. E., Elsheikh, A., Builles, N., Damour, O. & Hasirci, V. Effect of human corneal keratocytes and retinal pigment epithelial cells on the mechanical properties of micropatterned collagen films. *Biomaterials* **28**, 4303-4310 (2007).
- 52 Tuft, S. & Coster, D. The corneal endothelium. *Eye* **4**, 389-424 (1990).
- 53 Elsheikh, A. *Understanding corneal biomechanics through experimental assessment and numerical simulation.* (Nova Science Publishers, 2010).
- 54 Elsheikh, A., Alhasso, D. & Rama, P. Assessment of the epithelium's contribution to corneal biomechanics. *Experimental eye research* **86**, 445-451 (2008).
- 55 Hogan, M. J. & Alvarado, J. A. Weddell JE: Histology of the Human Eye: An Atlas and Textbook. Philadelphia. London. Toronto: Saunders (1971).
- 56 Acott, T. S. & Kelley, M. J. Extracellular matrix in the trabecular meshwork. *Experimental eye research* **86**, 543-561 (2008).
- 57 Acott, T. S. *et al.* Intraocular pressure homeostasis: maintaining balance in a high-pressure environment. *Journal of Ocular pharmacology and therapeutics* **30**, 94-101 (2014).
- 58 Alm, A. & Nilsson, S. F. Uveoscleral outflow—a review. *Experimental eye research* **88**, 760-768 (2009).
- 59 Brubaker, R. F., Ritch, R., Shields, M. & Krupin, T. Measurement of aqueous flow by fluorophotometry. *The glaucomas* **1**, 337-344 (1989).
- 60 Abu-Hassan, D. W., Acott, T. S. & Kelley, M. J. The trabecular meshwork: a basic review of form and function. *Journal of ocular biology* **2** (2014).
- 61 Stamper, R. L., Lieberman, M. F. & Drake, M. V. *Becker-Shaffer's Diagnosis and Therapy of the Glaucomas E-Book.* (Elsevier Health Sciences, 2009).
- 62 Cook, J. A. *et al.* Systematic review of the agreement of tonometers with Goldmann applanation tonometry. *Ophthalmology* **119**, 1552-1557 (2012).
- 63 Whitacre, M. M. & Stein, R. Sources of error with use of Goldmann-type tonometers. *Survey of ophthalmology* **38**, 1-30 (1993).
- 64 Toris, C. & Kiel, J. Aqueous Outflow and Glaucoma Drug Mechanisms of Action, <<https://www.aaio.org/basic-skills/animation-of-aqueous-flow>> (2017).

- 65 Thompson, A. M. Moorfields Manual of Ophthalmology. *Clinical & Experimental Ophthalmology* 36, 690-690 (2008).
- 66 MFMER. *Glaucoma*, <<https://middlesexhealth.org/learning-center/diseases-and-conditions/glaucoma>> (2018).
- 67 Kwon, Y. H., Fingert, J. H., Kuehn, M. H. & Alward, W. L. Primary open-angle glaucoma. *New England Journal of Medicine* 360, 1113-1124 (2009).
- 68 Argus, W. A. Ocular hypertension and central corneal thickness. *Ophthalmology* 102, 1810-1812 (1995).
- 69 Appelbaum, A. Keratoconus. *Archives of Ophthalmology* 15, 900-921 (1936).
- 70 Bron, A. J. Keratoconus. *Cornea* 7, 163-169 (1988).
- 71 Krachmer, J. H., Feder, R. S. & Belin, M. W. Keratoconus and related non-inflammatory corneal thinning disorders. *Survey of Ophthalmology* 28, 293-322 (1984).
- 72 Krachmer, J. H., Feder, R. S. & Belin, M. W. Keratoconus and related noninflammatory corneal thinning disorders. *Survey of ophthalmology* 28, 293-322 (1984).
- 73 Rabinowitz, Y. S. Keratoconus. *Survey of ophthalmology* 42, 297-319 (1998).
- 74 Efron, N. & Hollingsworth, J. G. New perspectives on keratoconus as revealed by corneal confocal microscopy. *Clin Exp Optom* 91, 34-55, doi:10.1111/j.1444-0938.2007.00195.x (2008).
- 75 Nejabat, M., Khalili, M. R. & Dehghani, C. Cone location and correction of keratoconus with rigid gas-permeable contact lenses. *Contact Lens and Anterior Eye* 35, 17-21, doi:<https://doi.org/10.1016/j.clae.2011.08.007> (2012).
- 76 Rabinowitz, Y. S. & McDonnell, P. J. Computer-assisted corneal topography in keratoconus. *Journal of Refractive Surgery* 5, 400-408 (1989).
- 77 Klyce, S. D. Information fidelity in corneal topography. *Br J Ophthalmol* 79, 791-792 (1995).
- 78 Lebow, K. A. & Grohe, R. M. Differentiating contact lens induced warpage from true keratoconus using corneal topography. *The CLAO journal : official publication of the Contact Lens Association of Ophthalmologists, Inc* 25, 114-122 (1999).
- 79 Maguire, L. J. & Bourne, W. M. Corneal topography of early keratoconus. *Am J Ophthalmol* 108, 107-112 (1989).
- 80 Maeda, N., Klyce, S. D. & Smolek, M. K. Neural network classification of corneal topography. Preliminary demonstration. *Investigative ophthalmology & visual science* 36, 1327-1335 (1995).
- 81 Perry, H. D., Buxton, J. N. & Fine, B. S. Round and oval cones in keratoconus. *Ophthalmology* 87, 905-909 (1980).
- 82 Seiler, T. G. *et al.* Customized Corneal Cross-linking: One-Year Results. *Am J Ophthalmol* 166, 14-21, doi:10.1016/j.ajo.2016.02.029 (2016).

- 83 Scarcelli, G., Besner, S., Pineda, R. & Yun, S. H. Biomechanical characterization of keratoconus corneas ex vivo with Brillouin microscopy. *Investigative ophthalmology & visual science* **55**, 4490-4495, doi:10.1167/iovs.14-14450 (2014).
- 84 Dauwe, C. *et al.* Biomechanical and morphological corneal response to placement of intrastromal corneal ring segments for keratoconus. *J Cataract Refract Surg* **35**, 1761-1767, doi:10.1016/j.jcrs.2009.05.033 (2009).
- 85 Mahmoud, A. M. *et al.* CLMI: the cone location and magnitude index. *Cornea* **27**, 480-487, doi:10.1097/ICO.0b013e31816485d3 (2008).
- 86 Vega-Estrada, A. & Alio, J. L. The use of intracorneal ring segments in keratoconus. *Eye Vis (Lond)* **3**, 8, doi:10.1186/s40662-016-0040-z (2016).
- 87 Shetty, R. *et al.* A Novel Zernike Application to Differentiate Between Three-dimensional Corneal Thickness of Normal Corneas and Corneas With Keratoconus. *American Journal of Ophthalmology* **160**, 453-462.e452, doi:<http://dx.doi.org/10.1016/j.ajo.2015.06.001> (2015).
- 88 Parker, J. S., van Dijk, K. & Melles, G. R. Treatment options for advanced keratoconus: a review. *Survey of ophthalmology* **60**, 459-480 (2015).
- 89 Wachler, B. S. B. *Keratoconus: Causes, symptoms and 10 treatment options*, <<https://www.allaboutvision.com/conditions/keratoconus.htm>> (2019).
- 90 Edmund, C. Corneal elasticity and ocular rigidity in normal and keratoconic eyes. *Acta ophthalmologica* **66**, 134-140 (1988).
- 91 Bisplinghoff, R. L., Mar, J. W. & Pian, T. H. *Statics of deformable solids*. (Courier Corporation, 2014).
- 92 Ruberti, J. W., Sinha Roy, A. & Roberts, C. J. Corneal biomechanics and biomaterials. *Annual review of biomedical engineering* **13**, 269-295 (2011).
- 93 Olivier, N., Aptel, F., Plamann, K., Schanne-Klein, M.-C. & Beaurepaire, E. Harmonic microscopy of isotropic and anisotropic microstructure of the human cornea. *Optics express* **18**, 5028-5040 (2010).
- 94 Elliott, D. M. & Setton, L. A. Anisotropic and inhomogeneous tensile behavior of the human annulus fibrosus: experimental measurement and material model predictions. *J. Biomech. Eng.* **123**, 256-263 (2001).
- 95 Fung, Y.-c. *Biomechanics: mechanical properties of living tissues*. (Springer Science & Business Media, 2013).
- 96 Elsheikh, A. & Anderson, K. Comparative study of corneal strip extensometry and inflation tests. *Journal of the Royal Society Interface* **2**, 177-185 (2005).
- 97 Olsen, T. & Sperling, S. The swelling pressure of the human corneal stroma as determined by a new method. *Experimental eye research* **44**, 481-490 (1987).

- 98 Elsheikh, A., Wang, D., Rama, P., Campanelli, M. & Garway-Heath, D. Experimental assessment of human corneal hysteresis. *Current eye research* **33**, 205-213 (2008).
- 99 Boyce, B., Jones, R., Nguyen, T. & Grazier, J. Stress-controlled viscoelastic tensile response of bovine cornea. *Journal of biomechanics* **40**, 2367-2376 (2007).
- 100 Lombardo, M. *et al.* Biomechanics of the anterior human corneal tissue investigated with atomic force microscopy. *Investigative ophthalmology & visual science* **53**, 1050-1057 (2012).
- 101 Boote, C. *et al.* Scleral structure and biomechanics. *Progress in retinal and eye research*, 100773 (2019).
- 102 Levy, A. M., Fazio, M. A. & Grytz, R. Experimental myopia increases and scleral crosslinking using genipin inhibits cyclic softening in the tree shrew sclera. *Ophthalmic and Physiological Optics* **38**, 246-256 (2018).
- 103 Downs, J. C. & Girkin, C. A. Lamina cribrosa in glaucoma. *Current opinion in ophthalmology* **28**, 113 (2017).
- 104 Eliasy, A. *et al.* Ex-vivo experimental validation of biomechanically-corrected intraocular pressure measurements on human eyes using the CorVis ST. *Experimental eye research* **175**, 98-102 (2018).
- 105 Ambrósio Jr, R. *et al.* Suppl-1, M2: Corneal Biomechanics in Ectatic Diseases: Refractive Surgery Implications. *The open ophthalmology journal* **11**, 176 (2017).
- 106 Kim, B. *et al.* A comparison among Neo-Hookean model, Mooney-Rivlin model, and Ogden model for chloroprene rubber. *International Journal of Precision Engineering and Manufacturing* **13**, 759-764 (2012).
- 107 Eliasy, A. *et al.* Determination of Corneal Biomechanical Behavior in-vivo for Healthy Eyes Using CorVis ST Tonometry: Stress-Strain Index. *Front Bioeng Biotechnol* **7**, 105, doi:10.3389/fbioe.2019.00105 (2019).
- 108 Studer, H., Larrea, X., Riedwyl, H. & Büchler, P. Biomechanical model of human cornea based on stromal microstructure. *Journal of biomechanics* **43**, 836-842 (2010).
- 109 Alastrué, V., Calvo, B., Pena, E. & Doblaré, M. Biomechanical modeling of refractive corneal surgery. (2006).
- 110 Yu, J.-g. *et al.* Influence of glucocorticosteroids on the biomechanical properties of in-vivo rabbit cornea. *Journal of the mechanical behavior of biomedical materials* **29**, 350-359 (2014).
- 111 Elsheikh, A. & Wang, D. Numerical modelling of corneal biomechanical behaviour. *Computer methods in biomechanics and biomedical engineering* **10**, 85-95 (2007).
- 112 Anderson, K., El-Sheikh, A. & Newson, T. Application of structural analysis to the mechanical behaviour of the cornea. *Journal of the Royal Society Interface* **1**, 3-15 (2004).

- 113 Woo, S.-Y., Kobayashi, A., Schlegel, W. & Lawrence, C. Nonlinear material properties of intact cornea and sclera. *Experimental eye research* **14**, 29-39 (1972).
- 114 Andreassen, T. T., Simonsen, A. H. & Oxlund, H. Biomechanical properties of keratoconus and normal corneas. *Experimental eye research* **31**, 435-441 (1980).
- 115 Nash, I. S., Greene, P. R. & Foster, C. S. Comparison of mechanical properties of keratoconus and normal corneas. *Experimental eye research* **35**, 413-424 (1982).
- 116 Hoeltzel, D. A., Altman, P., Buzard, K. & Choe, K.-i. Strip extensimetry for comparison of the mechanical response of bovine, rabbit, and human corneas. (1992).
- 117 Wollensak, G., Spoerl, E. & Seiler, T. Stress-strain measurements of human and porcine corneas after riboflavin-ultraviolet-A-induced cross-linking. *Journal of Cataract & Refractive Surgery* **29**, 1780-1785 (2003).
- 118 Elsheikh, A. *et al.* Regional variation in the biomechanical properties of the human sclera. *Experimental eye research* **90**, 624-633 (2010).
- 119 Chang, S. H. *et al.* The relationship between mechanical properties, ultrastructural changes, and intrafibrillar bond formation in corneal UVA/Riboflavin cross-linking treatment for keratoconus. *Journal of Refractive Surgery* **34**, 264-272 (2018).
- 120 Geraghty, B., Jones, S. W., Rama, P., Akhtar, R. & Elsheikh, A. Age-related variations in the biomechanical properties of human sclera. *Journal of the mechanical behavior of biomedical materials* **16**, 181-191 (2012).
- 121 Boyce, B. L., Grazier, J. M., Jones, R. E. & Nguyen, T. D. Full-field deformation of bovine cornea under constrained inflation conditions. *Biomaterials* **29**, 3896-3904, doi:10.1016/j.biomaterials.2008.06.011 (2008).
- 122 Coudrillier, B. *et al.* The inflation response of normal and glaucomatous posterior human sclera. *Investigative Ophthalmology & Visual Science* (2011).
- 123 Elsheikh, A., Geraghty, B., Rama, P., Campanelli, M. & Meek, K. M. Characterization of age-related variation in corneal biomechanical properties. *J R Soc Interface* **7**, 1475-1485, doi:10.1098/rsif.2010.0108 (2010).
- 124 Elsheikh, A. *et al.* Assessment of corneal biomechanical properties and their variation with age. *Curr Eye Res* **32**, 11-19, doi:10.1080/02713680601077145 (2007).
- 125 Elsheikh, A., Alhasso, D. & Rama, P. Biomechanical properties of human and porcine corneas. *Experimental eye research* **86**, 783-790 (2008).
- 126 Siu, A. & Herse, P. The effect of age on human corneal thickness: statistical implications of power analysis. *Acta ophthalmologica* **71**, 51-56 (1993).

- 127 Polse, K. *et al.* Age differences in corneal hydration control. *Investigative ophthalmology & visual science* **30**, 392-399 (1989).
- 128 Sharifipour, F., Panahi-Bazaz, M., Bidar, R., Idani, A. & Cheraghian, B. Age-related variations in corneal biomechanical properties. *Journal of current ophthalmology* **28**, 117-122 (2016).
- 129 Maurice, D. M. in *The cornea: Transactions of the World Congress on the Cornea III*. 187-193 (Raven Press, New York).
- 130 Hatami-Marbini, H. Viscoelastic shear properties of the corneal stroma. *Journal of biomechanics* **47**, 723-728 (2014).
- 131 Whitford, C., Studer, H., Boote, C., Meek, K. M. & Elsheikh, A. Biomechanical model of the human cornea: considering shear stiffness and regional variation of collagen anisotropy and density. *Journal of the mechanical behavior of biomedical materials* **42**, 76-87 (2015).
- 132 Petsche, S. J., Chernyak, D., Martiz, J., Levenston, M. E. & Pinsky, P. M. Depth-dependent transverse shear properties of the human corneal stroma. *Investigative ophthalmology & visual science* **53**, 873-880 (2012).
- 133 Seiler, T. G., Shao, P., Frueh, B. E., Yun, S.-H. & Seiler, T. The influence of hydration on different mechanical moduli of the cornea. *Graefe's archive for clinical and experimental ophthalmology* **256**, 1653-1660 (2018).
- 134 Ramirez-Garcia, M. A., Sloan, S. R., Nidenberg, B., Khalifa, Y. M. & Buckley, M. R. Depth-Dependent Out-of-Plane Young's Modulus of the Human Cornea. *Current eye research* **43**, 595-604 (2018).
- 135 Kling, S. & Hafezi, F. Corneal biomechanics—a review. *Ophthalmic and Physiological Optics* **37**, 240-252 (2017).
- 136 Humphrey, J. D. in *Proceedings of the Royal Society of London A: Mathematical, Physical and Engineering Sciences*. 3-46 (The Royal Society).
- 137 Sherman, V. R., Yang, W. & Meyers, M. A. The materials science of collagen. *Journal of the mechanical behavior of biomedical materials* **52**, 22-50 (2015).
- 138 Fratzl, P. Collagen Structure and Mechanics. (2008).
- 139 Kadler, K. E., Holmes, D. F., Trotter, J. A. & Chapman, J. A. Collagen fibril formation. *Biochemical Journal* **316**, 1-11 (1996).
- 140 Michelacci, Y. M. Collagens and proteoglycans of corneal extracellular matrix. *Brazilian Journal of Medical and Biological Research* (2003).
- 141 Weiss, J. A., Maker, B. N. & Govindjee, S. Finite element implementation of incompressible, transversely isotropic hyperelasticity. *Computer Methods in Applied Mechanics and Engineering* **135**, 107-128, doi:Doi 10.1016/0045-7825(96)01035-3 (1996).
- 142 Pinsky, P. M., van der Heide, D. & Chernyak, D. Computational modeling of mechanical anisotropy in the cornea and sclera. *Journal of Cataract & Refractive Surgery* **31**, 136-145 (2005).
- 143 Meek, K. M., Blamires, T., Elliott, G. F., Gyi, T. J. & Nave, C. The Organization of Collagen Fibrils in the Human Corneal Stroma - a

- Synchrotron X-Ray-Diffraction Study. *Current Eye Research* **6**, 841-846 (1987).
- 144 Aghamohammadzadeh, H., Newton, R. H. & Meek, K. M. X-ray scattering used to map the preferred collagen orientation in the human cornea and limbus. *Structure* **12**, 249-256 (2004).
- 145 Boote, C., Dennis, S., Huang, Y., Quantock, A. J. & Meek, K. M. Lamellar orientation in human cornea in relation to mechanical properties. *J Struct Biol* **149**, 1-6, doi:10.1016/j.jsb.2004.08.009 (2005).
- 146 Daxer, A. & Fratzl, P. Collagen fibril orientation in the human corneal stroma and its implication in keratoconus. *Invest Ophthalmol Vis Sci* **38**, 121-129 (1997).
- 147 Kim, M. *et al.* Shear Brillouin light scattering microscope. *Optics express* **24**, 319-328 (2016).
- 148 Yun, S. H. & Chernyak, D. Brillouin microscopy: assessing ocular tissue biomechanics. *Current opinion in ophthalmology* **29**, 299 (2018).
- 149 Wu, P.-J. *et al.* Water content, not stiffness, dominates Brillouin spectroscopy measurements in hydrated materials. *Nature methods* **15**, 561-562 (2018).
- 150 Scarcelli, G., Besner, S., Pineda, R., Kalout, P. & Yun, S. H. In vivo biomechanical mapping of normal and keratoconus corneas. *JAMA ophthalmology* **133**, 480-482 (2015).
- 151 Naderan, M., Rajabi, M. T. & Zarrinbakhsh, P. Intereye asymmetry in bilateral keratoconus, keratoconus suspect and normal eyes and its relationship with disease severity. *British Journal of Ophthalmology* **101**, 1475-1482 (2017).
- 152 Denoyer, A., Ricaud, X., Van Went, C., Labbé, A. & Baudouin, C. Influence of corneal biomechanical properties on surgically induced astigmatism in cataract surgery. *Journal of Cataract & Refractive Surgery* **39**, 1204-1210 (2013).
- 153 Randleman, J. B., Su, J. P. & Scarcelli, G. Biomechanical Changes After LASIK Flap Creation Combined With Rapid Cross-Linking Measured With Brillouin Microscopy. *J Refract Surg* **33**, 408-414, doi:10.3928/1081597X-20170421-01 (2017).
- 154 Krug, B., Koukourakis, N. & Czarske, J. W. Impulsive stimulated Brillouin microscopy for non-contact, fast mechanical investigations of hydrogels. *Opt Express* **27**, 26910-26923, doi:10.1364/OE.27.026910 (2019).
- 155 Cochlin, D. L., Ganatra, R. & Griffiths, D. Elastography in the detection of prostatic cancer. *Clinical radiology* **57**, 1014-1020 (2002).
- 156 McKnight, A. L. *et al.* MR elastography of breast cancer: preliminary results. *American journal of roentgenology* **178**, 1411-1417 (2002).
- 157 Masuzaki, R. *et al.* Assessing liver tumor stiffness by transient elastography. *Hepatology international* **1**, 394-397 (2007).

- 158 Wang, H., Prendiville, P. L., McDonnell, P. J. & Chang, W. V. An ultrasonic technique for the measurement of the elastic moduli of human cornea. *Journal of biomechanics* **29**, 1633-1636 (1996).
- 159 He, X. & Liu, J. A quantitative ultrasonic spectroscopy method for noninvasive determination of corneal biomechanical properties. *Investigative ophthalmology & visual science* **50**, 5148-5154 (2009).
- 160 Liu, J., He, X., Pan, X. & Roberts, C. J. Ultrasonic model and system for measurement of corneal biomechanical properties and validation on phantoms. *Journal of biomechanics* **40**, 1177-1182 (2007).
- 161 Tanter, M., Touboul, D., Gennisson, J. L., Bercoff, J. & Fink, M. High-resolution quantitative imaging of cornea elasticity using supersonic shear imaging. *IEEE Trans Med Imaging* **28**, 1881-1893, doi:10.1109/TMI.2009.2021471 (2009).
- 162 Touboul, D. *et al.* Supersonic shear wave elastography for the in vivo evaluation of transepithelial corneal collagen cross-linking. *Invest Ophthalmol Vis Sci* **55**, 1976-1984, doi:10.1167/iops.13-13445 (2014).
- 163 Wang, S. & Larin, K. V. Noncontact depth-resolved micro-scale optical coherence elastography of the cornea. *Biomedical optics express* **5**, 3807-3821 (2014).
- 164 Singh, M. *et al.* Applanation optical coherence elastography: noncontact measurement of intraocular pressure, corneal biomechanical properties, and corneal geometry with a single instrument. *Journal of biomedical optics* **22**, 020502 (2017).
- 165 Kirby, M. A. *et al.* Optical coherence elastography in ophthalmology. *Journal of biomedical optics* **22**, 121720 (2017).
- 166 Luce, D. A. Determining in vivo biomechanical properties of the cornea with an ocular response analyzer. *Journal of Cataract & Refractive Surgery* **31**, 156-162 (2005).
- 167 Terai, N., Raiskup, F., Haustein, M., Pillunat, L. E. & Spoerl, E. Identification of biomechanical properties of the cornea: the ocular response analyzer. *Current eye research* **37**, 553-562 (2012).
- 168 Touboul, D. *et al.* Correlations between corneal hysteresis, intraocular pressure, and corneal central pachymetry. *Journal of Cataract & Refractive Surgery* **34**, 616-622 (2008).
- 169 Avetisov, S. E., Novikov, I. A., Bubnova, I. A., Antonov, A. A. & Siplivyi, V. I. Determination of corneal elasticity coefficient using the ORA database. *Journal of refractive surgery* **26**, 520-524 (2010).
- 170 Congdon, N. G., Broman, A. T., Bandeen-Roche, K., Grover, D. & Quigley, H. A. Central corneal thickness and corneal hysteresis associated with glaucoma damage. *American journal of ophthalmology* **141**, 868-875 (2006).
- 171 Wells, A. P. *et al.* Corneal hysteresis but not corneal thickness correlates with optic nerve surface compliance in glaucoma patients. *Investigative ophthalmology & visual science* **49**, 3262-3268 (2008).

- 172 Luz, A. *et al.* ORA waveform-derived biomechanical parameters to distinguish normal from keratoconic eyes. *Arquivos brasileiros de oftalmologia* **76**, 111-117 (2013).
- 173 Roberts, C. Two novel stiffness parameters for the Corvis ST. *OCULUS Special Supplement* (2016).
- 174 Chan, T. C., Wang, Y. M., Yu, M. & Jhanji, V. Comparison of corneal tomography and a new combined tomographic biomechanical index in subclinical keratoconus. *Journal of Refractive Surgery* **34**, 616-621 (2018).
- 175 Vinciguerra, R. *et al.* Should the Corvis biomechanical index (CBI) include corneal thickness parameters? *Journal of Refractive Surgery* **34**, 213-216 (2018).
- 176 Hafezi, F. Contributing Factors to Corneal Deformation in Air Puff Measurements. *Investigative ophthalmology & visual science* **54**, 5086-5086 (2013).
- 177 Ambrósio Jr, R. *et al.* Dynamic ultra high speed Scheimpflug imaging for assessing corneal biomechanical properties. *Revista Brasileira de Oftalmologia* **72**, 99-102 (2013).
- 178 Ali, N. Q., Patel, D. V. & McGhee, C. N. Biomechanical responses of healthy and keratoconic corneas measured using a noncontact scheimpflug-based tonometer. *Investigative ophthalmology & visual science* **55**, 3651-3659 (2014).
- 179 Mohammadpour, M. *et al.* Ocular response analyzer parameters in healthy, keratoconus suspect and manifest keratoconus eyes. *Oman journal of ophthalmology* **8**, 102 (2015).
- 180 Qazi, M. A., Roberts, C. J., Mahmoud, A. M. & Pepose, J. S. Topographic and biomechanical differences between hyperopic and myopic laser in situ keratomileusis. *Journal of Cataract & Refractive Surgery* **31**, 48-60 (2005).
- 181 Eliasy, A. *et al.* Determination of corneal biomechanical behavior in-vivo for healthy eyes using CorVis ST tonometry: Stress-Strain Index. *Frontiers in bioengineering and biotechnology* **7** (2019).
- 182 Han, F. *et al.* Effect of Biomechanical Properties on Myopia: a Study of New Corneal Biomechanical Parameters. (2020).
- 183 Liu, G. *et al.* Age Distribution and Associated Factors of Cornea Biochemical Parameter Stress-Strain Index in Chinese Healthy Population. (2020).
- 184 Dorronsoro, C., Pascual, D., Pérez-Merino, P., Kling, S. & Marcos, S. Dynamic OCT measurement of corneal deformation by an air puff in normal and cross-linked corneas. *Biomedical optics express* **3**, 473-487 (2012).
- 185 Koprowski, R. Automatic method of analysis and measurement of additional parameters of corneal deformation in the Corvis tonometer. *Biomedical engineering online* **13**, 150 (2014).

- 186 MJ, G.-F. The relationships between ocular optical components and implications in the process of emmetropization. *Arch Soc Esp Oftalmol* **83**, 307-316 (2008).
- 187 Rada, J. A. S., Shelton, S. & Norton, T. T. The sclera and myopia. *Experimental eye research* **82**, 185-200 (2006).
- 188 Holden, B. A. *et al.* Global prevalence of myopia and high myopia and temporal trends from 2000 through 2050. *Ophthalmology* **123**, 1036-1042 (2016).
- 189 Wang, F., Lee, H. P. & Lu, C. Biomechanical effect of segmental scleral buckling surgery. *Current eye research* **32**, 133-142 (2007).
- 190 Coudrillier, B. *et al.* Biomechanics of the human posterior sclera: age-and glaucoma-related changes measured using inflation testing. *Investigative ophthalmology & visual science* **53**, 1714-1728 (2012).
- 191 Nguyen, C. *et al.* Studies of scleral biomechanical behavior related to susceptibility for retinal ganglion cell loss in experimental mouse glaucoma. *Investigative ophthalmology & visual science* **54**, 1767-1780 (2013).
- 192 Trier, K. The sclera. *Advances in Organ Biology* **10**, 353-373 (2005).
- 193 Olsen, T. W., Aaberg, S. Y., Geroski, D. H. & Edelhauser, H. F. Human sclera: thickness and surface area. *American journal of ophthalmology* **125**, 237-241 (1998).
- 194 Meek, K. in *Collagen* 359-396 (Springer, 2008).
- 195 Zhou, D. *et al.* Analysis of X-ray scattering microstructure data for implementation in numerical simulations of ocular biomechanical behaviour. *PloS one* **14** (2019).
- 196 Zhou, D. *et al.* Microstructure-based numerical simulation of the mechanical behaviour of ocular tissue. *Journal of the Royal Society Interface* **16**, 20180685 (2019).
- 197 Nottingham, J. Practical observations on conical cornea: and on the short sight, and other defects of vision connected with it. (1854).
- 198 Kennedy, R. H., Bourne, W. M. & Dyer, J. A. A 48-year clinical and epidemiologic study of keratoconus. *American journal of ophthalmology* **101**, 267-273 (1986).
- 199 Ferrari, G. & Rama, P. The keratoconus enigma: A pathogenesis review. *The Ocular Surface* (2020).
- 200 Gorskova, E. & Sevost'ianov, E. Epidemiology of keratoconus in the Urals. *Vestnik Oftalmologii* **114**, 38-40 (1998).
- 201 Pearson, A., Soneji, B., Sarvananthan, N. & Sandford-Smith, J. Does ethnic origin influence the incidence or severity of keratoconus? *Eye* **14**, 625-628 (2000).
- 202 Ljubic, A. Keratoconus and its prevalence in Macedonia. *Macedonian Journal of Medical Sciences* **2**, 58-62 (2009).

- 203 Tanabe, U., Fujiki, K., Ogawa, A., Ueda, S. & Kanai, A. Prevalence of keratoconus patients in Japan. *Nippon Ganka Gakkai Zasshi* **89**, 407 (1985).
- 204 Ihalainen, A. Clinical and epidemiological features of keratoconus genetic and external factors in the pathogenesis of the disease. *Acta Ophthalmologica. Supplement* **178**, 1-64 (1986).
- 205 Hwang, S., Lim, D. H. & Chung, T.-Y. Prevalence and incidence of keratoconus in South Korea: a nationwide population-based study. *American journal of ophthalmology* **192**, 56-64 (2018).
- 206 Nielsen, K., Hjortdal, J., Aagaard Nohr, E. & Ehlers, N. Incidence and prevalence of keratoconus in Denmark. *Acta ophthalmologica Scandinavica* **85**, 890-892 (2007).
- 207 Godefrooij, D. A., De Wit, G. A., Uiterwaal, C. S., Imhof, S. M. & Wisse, R. P. Age-specific incidence and prevalence of keratoconus: a nationwide registration study. *American journal of ophthalmology* **175**, 169-172 (2017).
- 208 Santiago, P. *et al.* in *Investigative Ophthalmology & Visual Science*. S307-S307 (LIPPINCOTT-RAVEN PUBL 227 EAST WASHINGTON SQUARE, PHILADELPHIA, PA 19106).
- 209 Papali'i-Curtin, A. T. *et al.* Keratoconus prevalence among high school students in New Zealand. *Cornea* **38**, 1382-1389 (2019).
- 210 Millodot, M., Shneor, E., Albou, S., Atlani, E. & Gordon-Shaag, A. Prevalence and associated factors of keratoconus in Jerusalem: a cross-sectional study. *Ophthalmic epidemiology* **18**, 91-97 (2011).
- 211 Hashemi, H. *et al.* Prevalence of keratoconus in a population-based study in Shahroud. *Cornea* **32**, 1441-1445 (2013).
- 212 Waked, N., Fayad, A., Fadlallah, A. & El, H. R. Keratoconus screening in a Lebanese students' population. *Journal francais d'ophtalmologie* **35**, 23-29 (2012).
- 213 Netto, E. A. T. *et al.* Prevalence of keratoconus in paediatric patients in Riyadh, Saudi Arabia. *British Journal of Ophthalmology* **102**, 1436-1441 (2018).
- 214 Hollingsworth, J. G., Efron, N. & Tullo, A. B. In vivo corneal confocal microscopy in keratoconus. *Ophthalmic and Physiological Optics* **25**, 254-260 (2005).
- 215 Uçakhan, Ö. Ö., Kanpolat, A., Ylmaz, N. & Özkan, M. In vivo confocal microscopy findings in keratoconus. *Eye & contact lens* **32**, 183-191 (2006).
- 216 Zhou, W. & Stojanovic, A. Comparison of corneal epithelial and stromal thickness distributions between eyes with keratoconus and healthy eyes with corneal astigmatism ≥ 2.0 D. *PLoS One* **9** (2014).
- 217 Scroggs, M. W. & Proia, A. D. Histopathological variation in keratoconus. *Cornea* **11**, 553-559 (1992).

- 218 Sawaguchi, S. *et al.* Three-dimensional scanning electron microscopic study of keratoconus corneas. *Archives of Ophthalmology* **116**, 62-68 (1998).
- 219 Sherwin, T., Brookes, N., Loh, I.-P., Poole, C. & Clover, G. Cellular incursion into Bowman's membrane in the peripheral cone of the keratoconic cornea. *Experimental Eye Research* **74**, 473-482 (2002).
- 220 Mocan, M. C., Yilmaz, P. T., Irkeç, M. & Orhan, M. In vivo confocal microscopy for the evaluation of corneal microstructure in keratoconus. *Current eye research* **33**, 933-939 (2008).
- 221 Gaskin, J. C. F., Patel, D. V. & McGhee, C. N. Acute corneal hydrops in keratoconus—new perspectives. *American journal of ophthalmology* **157**, 921-928. e921 (2014).
- 222 Arnal, E., Peris-Martinez, C., Menezo, J. L., Johnsen-Soriano, S. & Romero, F. J. Oxidative stress in keratoconus? *Investigative ophthalmology & visual science* **52**, 8592-8597 (2011).
- 223 Lass, J. H. *et al.* Clinical management of keratoconus: a multicenter analysis. *Ophthalmology* **97**, 433-445 (1990).
- 224 Pramanik, S., Musch, D. C., Sutphin, J. E. & Farjo, A. A. Extended long-term outcomes of penetrating keratoplasty for keratoconus. *Ophthalmology* **113**, 1633-1638 (2006).
- 225 Wagner, H., Barr, J., Zadnik, K. & Group, C. L. E. o. K. S. Collaborative Longitudinal Evaluation of Keratoconus (CLEK) Study: methods and findings to date. *Contact Lens and Anterior Eye* **30**, 223-232 (2007).
- 226 Gkika, M., Labiris, G., Giarmoukakis, A., Koutsogianni, A. & Kozobolis, V. Evaluation of corneal hysteresis and corneal resistance factor after corneal cross-linking for keratoconus. *Graefe's Archive for Clinical and Experimental Ophthalmology* **250**, 565-573 (2012).
- 227 Elham, R. *et al.* Keratoconus diagnosis using Corvis ST measured biomechanical parameters. *Journal of current ophthalmology* **29**, 175-181 (2017).
- 228 Vinciguerra, R. *et al.* Detection of keratoconus with a new biomechanical index. *Journal of refractive surgery* **32**, 803-810 (2016).
- 229 Wang, Y. M., Chan, T. C., Yu, M. & Jhanji, V. Comparison of corneal dynamic and tomographic analysis in normal, forme fruste keratoconic, and keratoconic eyes. *Journal of Refractive Surgery* **33**, 632-638 (2017).
- 230 Gordon-Shaag, A. *et al.* Is consanguinity a risk factor for keratoconus? *Optometry and Vision Science* **90**, 448-454 (2013).
- 231 Wang, Y., Rabinowitz, Y., Rotter, J. & Yang, H. Genetic epidemiological study of keratoconus: evidence for major gene determination. *American journal of medical genetics* **93**, 403-409 (2000).
- 232 Tynismaa, H. *et al.* A locus for autosomal dominant keratoconus: linkage to 16q22. 3-q23. 1 in Finnish families. *Investigative ophthalmology & visual science* **43**, 3160-3164 (2002).

- 233 Nielsen, K., Hjortdal, J., Pihlmann, M. & Corydon, T. J. Update on the keratoconus genetics. *Acta Ophthalmologica* **91**, 106-113 (2013).
- 234 Khaled, M. L. & Liu, Y. in *Genetics and Genomics of Eye Disease* 219-235 (Elsevier, 2020).
- 235 Olivares, J. J., Guerrero, J. J., Bermudez, F. R. & Serrano, D. L. Keratoconus: age of onset and natural history. *Optometry and vision science: official publication of the American Academy of Optometry* **74**, 147-151 (1997).
- 236 Sabti, S., Tappeiner, C. & Frueh, B. E. Corneal cross-linking in a 4-year-old child with keratoconus and down syndrome. *Cornea* **34**, 1157-1160 (2015).
- 237 Kankariya, V. P., Kymionis, G. D., Diakonis, V. F. & Yoo, S. H. Management of pediatric keratoconus—evolving role of corneal collagen cross-linking: an update. *Indian journal of ophthalmology* **61**, 435 (2013).
- 238 Gordon, M. O. *et al.* Baseline factors predictive of incident penetrating keratoplasty in keratoconus. *American journal of ophthalmology* **142**, 923-930. e921 (2006).
- 239 Jonas, J. B., Nangia, V., Matin, A., Kulkarni, M. & Bhojwani, K. Prevalence and associations of keratoconus in rural maharashtra in central India: the central India eye and medical study. *American journal of ophthalmology* **148**, 760-765 (2009).
- 240 Woodward, M. A., Blachley, T. S. & Stein, J. D. The association between sociodemographic factors, common systemic diseases, and keratoconus: an analysis of a nationwide health care claims database. *Ophthalmology* **123**, 457-465. e452 (2016).
- 241 Harrison, R. *et al.* Association between keratoconus and atopy. *British Journal of Ophthalmology* **73**, 816-822 (1989).
- 242 Macsai, M. S., Varley, G. A. & Krachmer, J. H. Development of keratoconus after contact lens wear: patient characteristics. *Archives of Ophthalmology* **108**, 534-538 (1990).
- 243 Bawazeer, A. M., Hodge, W. G. & Lorimer, B. Atopy and keratoconus: a multivariate analysis. *British Journal of Ophthalmology* **84**, 834-836 (2000).
- 244 Alhawari, H. H. *et al.* Autoimmune Thyroid Disease and Keratoconus: Is There an Association? *International journal of endocrinology* **2018** (2018).
- 245 Gomes, J. A. *et al.* Global consensus on keratoconus and ectatic diseases. *Cornea* **34**, 359-369 (2015).
- 246 Fink, B. A. *et al.* The influence of gender and hormone status on the severity and progression of keratoconus. *Cornea* **29**, 65-72 (2010).
- 247 Stock, R. A., Thumé, T. & Bonamigo, E. L. Acute corneal hydrops during pregnancy with spontaneous resolution after corneal cross-linking for keratoconus: a case report. *Journal of medical case reports* **11**, 53 (2017).
- 248 Gatziofias, Z., Panos, G. D., Gkaragkani, E., Georgoulas, S. & Angunawela, R. Recurrence of keratoconus after deep anterior lamellar

- keratoplasty following pregnancy. *International journal of ophthalmology* **10**, 1011 (2017).
- 249 Hoogewoud, F., Gatzoufas, Z. & Hafezi, F. Transitory topographical variations in keratoconus during pregnancy. *Journal of Refractive Surgery* **29**, 144-146 (2013).
- 250 McGhee, C. N., Kim, B. Z. & Wilson, P. J. Contemporary treatment paradigms in keratoconus. *Cornea* **34**, S16-S23 (2015).
- 251 Zadnik, K. *et al.* Baseline findings in the Collaborative Longitudinal Evaluation of Keratoconus (CLEK) Study. *Investigative ophthalmology & visual science* **39**, 2537-2546 (1998).
- 252 Wilson, S. E., Lin, D. & Klyce, S. D. Corneal topography of keratoconus. *Cornea* **10**, 2-8 (1991).
- 253 Prisant, O., Legeais, J.-M. & Renard, G. Superior keratoconus. *Cornea* **16**, 693-694 (1997).
- 254 Weed, K., McGhee, C. & MacEwen, C. Atypical unilateral superior keratoconus in young males. *Contact Lens and Anterior Eye* **28**, 177-179 (2005).
- 255 Schlegel, Z., Hoang-Xuan, T. & Gatinel, D. Comparison of and correlation between anterior and posterior corneal elevation maps in normal eyes and keratoconus-suspect eyes. *Journal of Cataract & Refractive Surgery* **34**, 789-795 (2008).
- 256 Montalbán, R., Alio, J. L., Javaloy, J. & Piñero, D. P. Correlation of anterior and posterior corneal shape in keratoconus. *Cornea* **32**, 916-921 (2013).
- 257 Tomidokoro, A. *et al.* Changes in anterior and posterior corneal curvatures in keratoconus. *Ophthalmology* **107**, 1328-1332 (2000).
- 258 Smolek, M. K., Klyce, S. D. & Hovis, J. K. The Universal Standard Scale: proposed improvements to the American National Standards Institute (ANSI) scale for corneal topography. *Ophthalmology* **109**, 361-369 (2002).
- 259 Buey Salas, M. & Peris, M. Biomecánica y arquitectura corneal. *Spain: ELSEVIER* (2014).
- 260 Mahmoud, A. M. *et al.* CLMI the cone location and magnitude index. *Cornea* **27**, 480 (2008).
- 261 Lewis, J. R., Frueh, B. E., Tappeiner, C., Mahmoud, A. M. & Roberts, C. J. Keratoconus Screening Based On Broader Applications Of CLMI Algorithm. *Investigative Ophthalmology & Visual Science* **52**, 5167-5167 (2011).
- 262 Amsler, M. Le keratocone fruste au javal. *Ophthalmologica* **96**, 77-83 (1938).
- 263 Wilson, S. E., Lin, D. T., Klyce, S. D., Reidy, J. J. & Insler, M. S. Topographic changes in contact lens-induced corneal warpage. *Ophthalmology* **97**, 734-744 (1990).
- 264 Assil, K. *What is Keratoconus?*, <<https://assileye.com/conditions/keratoconus>> (2020).

- 265 Holland, D. R. *et al.* Unilateral keratoconus: incidence and quantitative topographic analysis. *Ophthalmology* **104**, 1409-1413 (1997).
- 266 Armitage, J. A., Bruce, A. S., Phillips, A. J. & Lindsay, R. G. Morphological variants in keratoconus: anatomical observation or aetiologically significant? *Aust N Z J Ophthalmol* **26 Suppl 1**, S68-70 (1998).
- 267 Amsler, M. The "forme fruste" of keratoconus. *Wien Klin Wochenschr* **73**, 842-843 (1961).
- 268 Ertan, A., Kamburoglu, G. & Colin, J. Location of steepest corneal area of cone in keratoconus stratified by age using Pentacam. *Journal of Refractive Surgery* **25**, 1012-1016 (2009).
- 269 Schlegel, Z., Hoang-Xuan, T. & Gatinel, D. Comparison of and correlation between anterior and posterior corneal elevation maps in normal eyes and keratoconus-suspect eyes. *J Cataract Refract Surg* **34**, 789-795, doi:10.1016/j.jcrs.2007.12.036 (2008).
- 270 Klyce, S. D. Chasing the suspect: keratoconus. *Br J Ophthalmol* **93**, 845-847, doi:10.1136/bjo.2008.147371 (2009).
- 271 Saad, A. & Gatinel, D. Topographic and tomographic properties of forme fruste keratoconus corneas. *Investigative ophthalmology & visual science* **51**, 5546-5555 (2010).
- 272 Du, X.-L., Chen, M. & Xie, L.-X. Correlation of basic indicators with stages of keratoconus assessed by Pentacam tomography. *International journal of ophthalmology* **8**, 1136 (2015).
- 273 Roshdy, M. M. S., Wahba, S. S., Elkitkat, R. S., Hakim, A. M. & Fikry, R. R. Effect of age on pentacam keratoconus indices. *Journal of ophthalmology* **2018** (2018).
- 274 Ramos-López, D. *et al.* Screening subclinical keratoconus with placido-based corneal indices. *Optometry and Vision Science* **90**, 335-343 (2013).
- 275 Zemova, E. *et al.* Interaction between topographic/tomographic parameters and dry eye disease in keratoconus patients. *Current eye research* **39**, 1-8 (2014).
- 276 Wahba, S. S., Roshdy, M. M., Elkitkat, R. S. & Naguib, K. M. Rotating Scheimpflug imaging indices in different grades of keratoconus. *Journal of ophthalmology* **2016** (2016).
- 277 Safarzadeh, M. & Nasiri, N. Anterior segment characteristics in normal and keratoconus eyes evaluated with a combined Scheimpflug/Placido corneal imaging device. *Journal of current ophthalmology* **28**, 106-111 (2016).
- 278 Ishii, R. *et al.* Correlation of corneal elevation with severity of keratoconus by means of anterior and posterior topographic analysis. *Cornea* **31**, 253-258 (2012).

- 279 McMahon, T. T. *et al.* A new method for grading the severity of keratoconus: the Keratoconus Severity Score (KSS). *Cornea* **25**, 794-800 (2006).
- 280 Alió, J. L. & Shabayek, M. H. Corneal higher order aberrations: a method to grade keratoconus. *Journal of Refractive Surgery* **22**, 539-545 (2006).
- 281 Smiddy, W. E., Hamburg, T. R., Kracher, G. P. & Stark, W. J. Keratoconus: contact lens or keratoplasty? *Ophthalmology* **95**, 487-492 (1988).
- 282 Rathi, V. M., Mandathara, P. S. & Dumpati, S. Contact lens in keratoconus. *Indian journal of ophthalmology* **61**, 410 (2013).
- 283 Fernandez-Velazquez, F. J. Kerasoft IC compared to Rose-K in the management of corneal ectasias. *Contact Lens and Anterior Eye* **35**, 175-179 (2012).
- 284 Buxton, J. N., Keates, R. H. & Hoefle, F. B. in *Contact lenses: The CLAO guide to basic science and clinical practice* (ed O H Jr. Dabeszies) Ch. 55, 55 (Grune and Stratton, 1984).
- 285 Raiskup-Wolf, F., Hoyer, A., Spoerl, E. & Pillunat, L. E. Collagen crosslinking with riboflavin and ultraviolet-A light in keratoconus: long-term results. *Journal of Cataract & Refractive Surgery* **34**, 796-801 (2008).
- 286 Ashwin, P. T. & McDonnell, P. J. Collagen cross-linkage: a comprehensive review and directions for future research. *British journal of ophthalmology* **94**, 965-970 (2010).
- 287 Caporossi, A., Baiocchi, S., Mazzotta, C., Traversi, C. & Caporossi, T. Parasurgical therapy for keratoconus by riboflavin-ultraviolet type A rays induced cross-linking of corneal collagen: preliminary refractive results in an Italian study. *Journal of Cataract & Refractive Surgery* **32**, 837-845 (2006).
- 288 Grewal, D. S. *et al.* Corneal collagen crosslinking using riboflavin and ultraviolet-A light for keratoconus: one-year analysis using Scheimpflug imaging. *Journal of Cataract & Refractive Surgery* **35**, 425-432 (2009).
- 289 Wittig-Silva, C. *et al.* A randomized, controlled trial of corneal collagen cross-linking in progressive keratoconus: three-year results. *Ophthalmology* **121**, 812-821 (2014).
- 290 Kontadakis, G. A. *et al.* Long-term comparison of simultaneous topography-guided photorefractive keratectomy followed by corneal cross-linking versus corneal cross-linking alone. *Ophthalmology* **123**, 974-983 (2016).
- 291 Kymionis, G. D. *et al.* Long-term results of combined transepithelial phototherapeutic keratectomy and corneal collagen crosslinking for keratoconus: Cretan protocol. *Journal of Cataract & Refractive Surgery* **40**, 1439-1445 (2014).

- 292 Richoz, O., Mavrakanas, N., Pajic, B. & Hafezi, F. Corneal collagen cross-linking for ectasia after LASIK and photorefractive keratectomy: long-term results. *Ophthalmology* **120**, 1354-1359 (2013).
- 293 Kanellopoulos, A. J. Comparison of sequential vs same-day simultaneous collagen cross-linking and topography-guided PRK for treatment of keratoconus. *Journal of Refractive Surgery* **25**, S812-S818 (2009).
- 294 Hafezi, F., Mrochen, M., Iseli, H. P. & Seiler, T. Collagen crosslinking with ultraviolet-A and hypoosmolar riboflavin solution in thin corneas. *Journal of Cataract & Refractive Surgery* **35**, 621-624 (2009).
- 295 Kymionis, G. D. et al. An overview of corneal collagen cross-linking (CXL). *Advances in therapy* **30**, 858-869 (2013).
- 296 Mazzotta, C., Balestrazzi, A., Baiocchi, S., Traversi, C. & Caporossi, A. Stromal haze after combined riboflavin-UVA corneal collagen cross-linking in keratoconus: in vivo confocal microscopic evaluation. *Clinical & experimental ophthalmology* **35**, 580-582 (2007).
- 297 Çınar, Y. et al. Accelerated corneal collagen cross-linking for progressive keratoconus. *Cutaneous and ocular toxicology* **33**, 168-171 (2014).
- 298 Hashemi, H. et al. Short-term comparison of accelerated and standard methods of corneal collagen crosslinking. *Journal of Cataract & Refractive Surgery* **41**, 533-540 (2015).
- 299 keratomania. *Corneal Collagen Cross-linking*, <<https://www.keratomania.com/corneal-collagen-crosslinking.html>> (2014).
- 300 Mangioris, G. F. et al. Corneal infiltrates after corneal collagen cross-linking. *Journal of refractive surgery* **26**, 609-611 (2010).
- 301 Holopainen, J. M. & Krootila, K. Transient corneal thinning in eyes undergoing corneal cross-linking. *American journal of ophthalmology* **152**, 533-536 (2011).
- 302 Kodavoor, S. K., Sarwate, N. J. & Ramamurthy, D. Microbial keratitis following accelerated corneal collagen cross-linking. *Oman journal of ophthalmology* **8**, 111 (2015).
- 303 Ivarsen, A. & Hjortdal, J. Collagen cross-linking for advanced progressive keratoconus. *Cornea* **32**, 903-906 (2013).
- 304 Labiris, G., Kaloghianni, E., Koukoula, S., Zissimopoulos, A. & Kozobolis, V. P. Corneal melting after collagen cross-linking for keratoconus: a case report. *Journal of medical case reports* **5**, 152 (2011).
- 305 Sloot, F., Soeters, N., van der Valk, R. & Tahzib, N. G. Effective corneal collagen crosslinking in advanced cases of progressive keratoconus. *Journal of Cataract & Refractive Surgery* **39**, 1141-1145 (2013).
- 306 Stojanovic, A., Zhou, W. & Utheim, T. P. Corneal collagen cross-linking with and without epithelial removal: a contralateral study with 0.5% hypotonic riboflavin solution. *BioMed research international* **2014** (2014).
- 307 Kılıç, A., Kamburoglu, G. & Akıncı, A. Riboflavin injection into the corneal channel for combined collagen crosslinking and intrastromal

- corneal ring segment implantation. *Journal of Cataract & Refractive Surgery* **38**, 878-883 (2012).
- 308 Spadea, L. & Mencucci, R. Transepithelial corneal collagen cross-linking in ultrathin keratoconic corneas. *Clinical Ophthalmology (Auckland, NZ)* **6**, 1785 (2012).
- 309 Kling, S., Remon, L., Pérez-Escudero, A., Merayo-Llodes, J. & Marcos, S. Corneal biomechanical changes after collagen cross-linking from porcine eye inflation experiments. *Investigative ophthalmology & visual science* **51**, 3961-3968 (2010).
- 310 Lanchares, E., Del Buey, M. A., Cristóbal, J. A., Lavilla, L. & Calvo, B. Biomechanical property analysis after corneal collagen cross-linking in relation to ultraviolet A irradiation time. *Graefes archive for clinical and experimental ophthalmology* **249**, 1223-1227 (2011).
- 311 Lombardo, M., Serrao, S., Rosati, M., Ducoli, P. & Lombardo, G. Biomechanical changes in the human cornea after transepithelial corneal crosslinking using iontophoresis. *Journal of Cataract & Refractive Surgery* **40**, 1706-1715 (2014).
- 312 Dias, J., Diakonis, V. F., Kankariya, V. P., Yoo, S. H. & Ziebarth, N. M. Anterior and posterior corneal stroma elasticity after corneal collagen crosslinking treatment. *Experimental eye research* **116**, 58-62 (2013).
- 313 He, X., Spoerl, E., Tang, J. & Liu, J. Measurement of corneal changes after collagen crosslinking using a noninvasive ultrasound system. *J Cataract Refract Surg* **36**, 1207-1212, doi:10.1016/j.jcrs.2009.12.047 (2010).
- 314 Schumacher, S., Oeftiger, L. & Mrochen, M. Equivalence of biomechanical changes induced by rapid and standard corneal cross-linking, using riboflavin and ultraviolet radiation. *Investigative ophthalmology & visual science* **52**, 9048-9052 (2011).
- 315 Schanzlin, D. J., Asbell, P. A., Burris, T. E. & Durrie, D. S. The Intrastromal Corneal Ring Segments: Phase II Results for the Correction of Myopia. *Ophthalmology* **104**, 1067-1078 (1997).
- 316 McQuaid, R., Cummings, A. B. & Mrochen, M. The theory and art of corneal cross-linking. *Indian journal of ophthalmology* **61**, 416 (2013).
- 317 Burris, T. E., Ayer, C. T., Evensen, D. A. & Davenport, J. M. Effects of intrastromal corneal ring size and thickness on corneal flattening in human eyes. *Journal of Refractive Surgery* **7**, 46-50 (1991).
- 318 Chou, B. & Wachler, B. S. B. Intacs for a keratocone: a promising new option? *Review of Optometry* **137**, 97-97 (2000).
- 319 Torquetti, L. *et al.* Intrastromal corneal ring segments implantation in patients with keratoconus: 10-year follow-up. *Journal of Refractive Surgery* **30**, 22-26 (2014).
- 320 Hashemi, H. *et al.* Efficacy of intacs intrastromal corneal ring segment relative to depth of insertion evaluated with anterior segment optical

- coherence tomography. *Middle East African journal of ophthalmology* **20**, 234 (2013).
- 321 Mohammadpour, M., Heidari, Z. & Hashemi, H. Updates on managements for keratoconus. *Journal of current ophthalmology* **30**, 110-124 (2018).
- 322 Shetty, R., D'Souza, S., Ramachandran, S., Kurian, M. & Nuijts, R. M. Decision making nomogram for intrastromal corneal ring segments in keratoconus. *Indian journal of ophthalmology* **62**, 23 (2014).
- 323 Legare, M. E. *et al.* Intacs with or without same-day corneal collagen cross-linking to treat corneal ectasia. *Canadian Journal of Ophthalmology* **48**, 173-178 (2013).
- 324 Mohammadpour, M., Hahemi, H. & Jabbarvand, M. Technique of simultaneous femtosecond laser assisted Myring implantation and accelerated intrastromal collagen cross-linking for management of progressive keratoconus: A novel technique. *Contact Lens and Anterior Eye* **39**, 9-14 (2016).
- 325 Leccisotti, A. & Fields, S. V. Angle-supported phakic intraocular lenses in eyes with keratoconus and myopia. *Journal of Cataract & Refractive Surgery* **29**, 1530-1536 (2003).
- 326 Abish, D. H. Corneal Ring, <<https://www.slideshare.net/astrodoha/corneal-rings>> (2015).
- 327 Castroviejo, R. Keratoplasty for the treatment of keratoconus. *Transactions of the American Ophthalmological Society* **46**, 127 (1948).
- 328 Jhanji, V., Sharma, N. & Vajpayee, R. B. Management of keratoconus: current scenario. *British Journal of Ophthalmology* **95**, 1044-1050 (2011).
- 329 Javadi, M. A. *et al.* Outcomes of penetrating keratoplasty in keratoconus. *Cornea* **24**, 941-946 (2005).
- 330 Severinsky, B., Behrman, S., Frucht-Pery, J. & Solomon, A. Scleral contact lenses for visual rehabilitation after penetrating keratoplasty: long term outcomes. *Contact Lens and Anterior Eye* **37**, 196-202 (2014).
- 331 Brahma, A., Ennis, F., Harper, R., Ridgway, A. & Tullo, A. Visual function after penetrating keratoplasty for keratoconus: a prospective longitudinal evaluation. *British journal of ophthalmology* **84**, 60-66 (2000).
- 332 Niziol, L. M., Musch, D. C., Gillespie, B. W., Marcotte, L. M. & Sugar, A. Long-term outcomes in patients who received a corneal graft for keratoconus between 1980 and 1986. *American journal of ophthalmology* **155**, 213-219. e213 (2013).
- 333 Tan, D., Anshu, A., Parthasarathy, A. & Htoon, H. Visual acuity outcomes after deep anterior lamellar keratoplasty: a case-control study. *British journal of ophthalmology* **94**, 1295-1299 (2010).
- 334 Feizi, S., Javadi, M. A. & Fekri, Y. Use of deep anterior lamellar keratoplasty (DALK) for keratoconus: indications, techniques and outcomes. *Expert Review of Ophthalmology* **11**, 347-359 (2016).

- 335 Tham, Y.-C. *et al.* Global prevalence of glaucoma and projections of glaucoma burden through 2040: a systematic review and meta-analysis. *Ophthalmology* 121, 2081-2090 (2014).
- 336 Bourne, R. (BMJ Publishing Group Ltd, 2006).
- 337 Moses, R. A. Theory of the Schiottz tonometer and its empirical calibration. *Transactions of the American Ophthalmological Society* 69, 494 (1971).
- 338 McLean, W. The development of a tonometer. *American Journal of Ophthalmology* 2, 417-419 (1919).
- 339 DO DNB, M. C. M. & MS, A. C. 180 years of evolution in tonometry. *Kerala Journal of Ophthalmology*, 173 (2009).
- 340 Wolffe, M. & Burrows, M. C. Tonometers, <<https://www.college-optometrists.org/the-college/museum/online-exhibitions/virtual-ophthalmic-instrument-gallery/tonometers.html#:~:text=In%201862%20Von%20Graefe%2C%20a,eye%20by%20a%20known%20weight.>> (2002).
- 341 Perkins, E. Hand-held applanation tonometer. *The British journal of ophthalmology* 49, 591 (1965).
- 342 Iester, M., Mermoud, A., Achache, F. & Roy, S. New Tonopen XL: comparison with the Goldmann tonometer. *Eye* 15, 52-58 (2001).
- 343 Kozin, M. P., Kudashov, N. V., Sakharov, J. I. & Fedorov, S. N. (Google Patents, 1988).
- 344 Stuckey, G. Tonometry and the Imbert-Fick Law. *Australian Journal of Ophthalmology* 2, 68-70 (1974).
- 345 Moses, R. A. The Goldmann applanation tonometer. *American journal of ophthalmology* 46, 865-869 (1958).
- 346 Nayak, B. K., Maskati, Q. B. & Parikh, R. The unique problem of glaucoma: under-diagnosis and over-treatment. *Indian journal of ophthalmology* 59, S1 (2011).
- 347 Elsheikh, A., Alhasso, D., Gunvant, P. & Garway-Heath, D. Multiparameter correction equation for Goldmann applanation tonometry. *Optometry and Vision Science* 88, E102-E112 (2011).
- 348 Schneider, E., Kanngiesser, H. E. & Kniestedt, C. in *Glaucoma* 47-63 (Springer, 2006).
- 349 Medicine, J. H. *Glaucoma: What Every Patient Should Know*, <<https://www.hopkinsmedicine.org/wilmer/services/glaucoma/book/ch06s01.html>> (
- 350 Kanngiesser, H. E., Kniestedt, C. & Robert, Y. C. Dynamic contour tonometry: presentation of a new tonometer. *Journal of glaucoma* 14, 344-350 (2005).
- 351 Anderson, M. F., Agius-Fernandez, A. & Kaye, S. B. Comparison of the utility of Pascal dynamic contour tonometry with Goldmann applanation tonometry in routine clinical practice. *Journal of glaucoma* 22, 422-426 (2013).

- 352 Sampaolesi, R., Sampaolesi, J. R. & Zárate, J. in *The Glaucomas* 153-159 (Springer, 2014).
- 353 Sponsel, W. E. *et al.* Evaluation of the Keeler Pulsair non-contact tonometer. *Acta ophthalmologica* **67**, 567-572 (1989).
- 354 Kotecha, A. What biomechanical properties of the cornea are relevant for the clinician? *Survey of ophthalmology* **52**, S109-S114 (2007).
- 355 Sullivan-Mee, M. *et al.* Factors influencing intermethod agreement between goldmann applanation, pascal dynamic contour, and ocular response analyzer tonometry. *Journal of glaucoma* **22**, 487-495 (2013).
- 356 Kotecha, A., White, E., Schlottmann, P. G. & Garway-Heath, D. F. Intraocular pressure measurement precision with the Goldmann applanation, dynamic contour, and ocular response analyzer tonometers. *Ophthalmology* **117**, 730-737 (2010).
- 357 Sullivan-Mee, M., Gerhardt, G., Halverson, K. D. & Qualls, C. Repeatability and reproducibility for intraocular pressure measurement by dynamic contour, ocular response analyzer, and goldmann applanation tonometry. *Journal of glaucoma* **18**, 666-673 (2009).
- 358 Xu, G., Lam, D. S. & Leung, C. K.-s. Influence of ocular pulse amplitude on ocular response analyzer measurements. *Journal of glaucoma* **20**, 344-349 (2011).
- 359 Oncel, B., Dinc, U. A., Gorgun, E. & Ilgaz Yalvaç, B. Diurnal variation of corneal biomechanics and intraocular pressure in normal subjects. *European journal of ophthalmology* **19**, 798-803 (2009).
- 360 Chen, K.-J. *et al.* Clinical evaluation of a new correction algorithm for dynamic Scheimpflug analyzer tonometry before and after laser in situ keratomileusis and small-incision lenticule extraction. *Journal of Cataract & Refractive Surgery* **44**, 581-588 (2018).
- 361 Lee, H., Roberts, C. J., Ambrósio Jr, R., Elsheikh, A. & Kang, D. S. Y. Changes in biomechanically corrected intraocular pressure and dynamic corneal response parameters before and after transepithelial photorefractive keratectomy and femtosecond laser-assisted laser in situ keratomileusis. *Journal of Cataract & Refractive Surgery* **43**, 1495-1503 (2017).
- 362 Leonardi, M., Pitchon, E. M., Bertsch, A., Renaud, P. & Mermoud, A. Wireless contact lens sensor for intraocular pressure monitoring: assessment on enucleated pig eyes. *Acta ophthalmologica* **87**, 433-437 (2009).
- 363 Mansouri, K. & Shaarawy, T. Continuous intraocular pressure monitoring with a wireless ocular telemetry sensor: initial clinical experience in patients with open angle glaucoma. *British Journal of Ophthalmology* **95**, 627-629 (2011).
- 364 Holló, G., Kóthy, P. & Vargha, P. Evaluation of continuous 24-hour intraocular pressure monitoring for assessment of prostaglandin-induced pressure reduction in glaucoma. *Journal of glaucoma* **23**, e6-e12 (2014).

- 365 Melki, S., Todani, A. & Cherfan, G. An implantable intraocular pressure transducer: initial safety outcomes. *JAMA ophthalmology* **132**, 1221-1225 (2014).
- 366 Mansouri, K. & Weinreb, R. N. Continuous 24-hour intraocular pressure monitoring for glaucoma-time for a paradigm change. *Swiss medical weekly* **142** (2012).
- 367 Medgadget. *SENSIMED Triggerfish Electronic Contact Lens Provides Continuous Monitoring of Intraocular Pressure*, <https://www.medgadget.com/2009/08/sensimed_triggerfish_electronic_contact_lens_provides_continuous_monitoring_of_intraocular_pressure.html> (2009).
- 368 Wang, A. S. *et al.* Repeatability and reproducibility of Goldmann applanation, dynamic contour and ocular response analyzer tonometry. *Journal of glaucoma* **22**, 127 (2013).
- 369 Ito, K., Tawara, A., Kubota, T. & Harada, Y. IOP measured by dynamic contour tonometry correlates with IOP measured by Goldmann applanation tonometry and non-contact tonometry in Japanese individuals. *Journal of glaucoma* **21**, 35-40 (2012).
- 370 Yaoeda, K. *et al.* Measurement of intraocular pressure using the NT-4000: a new non-contact tonometer equipped with pulse synchronous measurement function. *Journal of glaucoma* **14**, 201-205 (2005).
- 371 Feltgen, N., Leifert, D. & Funk, J. Correlation between central corneal thickness, applanation tonometry, and direct intracameral IOP readings. *British journal of ophthalmology* **85**, 85-87 (2001).
- 372 Copt, R.-P., Thomas, R. & Mermoud, A. Corneal thickness in ocular hypertension, primary open-angle glaucoma, and normal tension glaucoma. *Archives of ophthalmology* **117**, 14-16 (1999).
- 373 Doughty, M. J. & Zaman, M. L. Human corneal thickness and its impact on intraocular pressure measures: a review and meta-analysis approach. *Survey of ophthalmology* **44**, 367-408 (2000).
- 374 La Rosa, F. A., Gross, R. L. & Orengo-Nania, S. Central corneal thickness of Caucasians and African Americans in glaucomatous and nonglaucomatous populations. *Archives of ophthalmology* **119**, 23-27 (2001).
- 375 Brandt, J. D., Beiser, J. A., Kass, M. A., Gordon, M. O. & Group, O. H. T. S. Central corneal thickness in the ocular hypertension treatment study (OHTS). *Ophthalmology* **108**, 1779-1788 (2001).
- 376 Foster, P. J. *et al.* Central corneal thickness and intraocular pressure in a Mongolian population. *Ophthalmology* **105**, 969-973 (1998).
- 377 Gordon, M. O. *et al.* The Ocular Hypertension Treatment Study: baseline factors that predict the onset of primary open-angle glaucoma. *Archives of ophthalmology* **120**, 714-720 (2002).

- 378 Chang, D. H. & Stulting, R. D. Change in intraocular pressure measurements after LASIK: the effect of the refractive correction and the lamellar flap. *Ophthalmology* **112**, 1009-1016 (2005).
- 379 Choudhari, N. S., Jadhav, V., George, R. & Vijaya, L. Variability in the calibration error of the goldmann applanation tonometer. *Journal of glaucoma* **20**, 492-496 (2011).
- 380 Buckley, D. H., Swikert, M. & Johnson, R. L. Friction, Wear, and Evaporation Rates of Various Materials in Vacuum to 10⁻⁷ mm Hg. *ASLE TRANSACTIONS* **5**, 8-23 (1962).
- 381 Lam, A., Chen, D., Chiu, R. & Chui, W.-S. Comparison of IOP measurements between ORA and GAT in normal Chinese. *Optometry and Vision Science* **84**, 909-914 (2007).
- 382 Carbonaro, F., Andrew, T., Mackey, D., Spector, T. & Hammond, C. Comparison of three methods of intraocular pressure measurement and their relation to central corneal thickness. *Eye* **24**, 1165-1170 (2010).
- 383 Morita, T. *et al.* Intraocular pressure measured by dynamic contour tonometer and ocular response analyzer in normal tension glaucoma. *Graefes archive for clinical and experimental ophthalmology* **248**, 73 (2010).
- 384 Lanza, M. *et al.* Comparison between Corvis and other tonometers in healthy eyes. *Contact Lens and Anterior Eye* **38**, 94-98 (2015).
- 385 Hong, J. *et al.* Corvis ST tonometer for measuring postoperative IOP in LASIK patients. *Optometry and Vision Science* **92**, 589-595 (2015).
- 386 Joda, A. A., Shervin, M. M. S., Kook, D. & Elsheikh, A. Development and validation of a correction equation for Corvis tonometry. *Computer methods in biomechanics and biomedical engineering* **19**, 943-953 (2016).
- 387 Chen, K.-J. *et al.* Development and validation of a new intraocular pressure estimate for patients with soft corneas. *Journal of Cataract & Refractive Surgery* **45**, 1316-1323 (2019).
- 388 Ye, Y. *et al.* Comparison of Biomechanically Corrected Intraocular Pressure Obtained by Corvis ST and Goldmann Applanation Tonometry in Patients With Open-angle Glaucoma and Ocular Hypertension. *Journal of glaucoma* **28**, 922-928 (2019).
- 389 Sedaghat, M.-R. *et al.* Biomechanically-Corrected Intraocular Pressure Compared To Pressure Measured With Commonly Used Tonometers In Normal Subjects. *Clinical Optometry* **11**, 127-133 (2019).
- 390 Ramm, L. *et al.* Intraocular Pressure Measurement Using Ocular Response Analyzer, Dynamic Contour Tonometer, and Scheimpflug Analyzer Corvis ST. *Journal of ophthalmology* **2019** (2019).
- 391 Yang, K., Xu, L., Fan, Q., Zhao, D. & Ren, S. Repeatability and comparison of new Corvis ST parameters in normal and keratoconus eyes. *Scientific reports* **9**, 1-10 (2019).

- 392 Martinez-de-la-Casa, J. M. *et al.* Effect of corneal thickness on dynamic contour, rebound, and Goldmann tonometry. *Ophthalmology* **113**, 2156-2162 (2006).
- 393 Jordão, M., de Carvalho Lupinacci, A. P., Ferreira, E., Enomoto, I. & Costa, V. Influence of age, central corneal thickness, and quality score on dynamic contour tonometry. *Eye* **23**, 1364-1369 (2009).
- 394 Jorge, J. M. M., Gonzalez-Meijome, J. M., Queiros, A., Fernandes, P. & Parafita, M. A. Correlations between corneal biomechanical properties measured with the ocular response analyzer and ICare rebound tonometry. *Journal of glaucoma* **17**, 442-448 (2008).
- 395 Wasielica-Poslednik, J., Berisha, F., Aliyeva, S., Pfeiffer, N. & Hoffmann, E. M. Reproducibility of ocular response analyzer measurements and their correlation with central corneal thickness. *Graefe's Archive for Clinical and Experimental Ophthalmology* **248**, 1617-1622 (2010).
- 396 Goldich, Y., Barkana, Y., Avni, I. & Zadok, D. Goldmann applanation tonometry versus ocular response analyzer for intraocular pressure measurements in keratoconic eyes. *Cornea* **29**, 1011-1015 (2010).
- 397 Kouchaki, B., Hashemi, H. & Yekta, A. Comparison of current tonometry techniques in measurement of intraocular pressure. *Journal of current ophthalmology* **29**, 92-97 (2017).
- 398 Eliasy, A. *et al.* Characterization of cone size and centre in keratoconic corneas. *Journal of the Royal Society Interface* **17**, 20200271 (2020).
- 399 Renka, R. J., Renka, R. L. & Cline, A. K. A TRIANGLE-BASED C¹ INTERPOLATION METHOD. *The Rocky Mountain Journal of Mathematics* **14**, 223-237 (1984).
- 400 Belin, M. W. & Khachikian, S. S. An introduction to understanding elevation-based topography: how elevation data are displayed - a review. *Clin Experiment Ophthalmol* **37**, 14-29, doi:10.1111/j.1442-9071.2008.01821.x (2009).
- 401 Goebels, S. *et al.* Staging of keratoconus indices regarding tomography, topography, and biomechanical measurements. *Am J Ophthalmol* **159**, 733-738, doi:10.1016/j.ajo.2015.01.014 (2015).
- 402 Ambrósio Jr, R. *et al.* Evaluation of corneal shape and biomechanics before LASIK. *International ophthalmology clinics* **51**, 11-38 (2011).
- 403 Belin, M. W. & Ambrósio Jr, R. Scheimpflug imaging for keratoconus and ectatic disease. *Indian journal of ophthalmology* **61**, 401 (2013).
- 404 Chan, J. S., Mandell, R. B., Burger, D. S. & Fusaro, R. E. Accuracy of videokeratography for instantaneous radius in keratoconus. *Optometry and vision science: official publication of the American Academy of Optometry* **72**, 793-799 (1995).
- 405 Szczołka, L. B. & Thomas, J. Comparison of axial and instantaneous videokeratographic data in keratoconus and utility in contact lens curvature prediction. *The CLAO journal: official publication of the Contact Lens Association of Ophthalmologists, Inc* **24**, 22-28 (1998).

- 406 Emre, S., Doganay, S. & Yologlu, S. Evaluation of anterior segment parameters in keratoconic eyes measured with the Pentacam system. *Journal of Cataract & Refractive Surgery* **33**, 1708-1712 (2007).
- 407 Alió, J. L. *et al.* Keratoconus-integrated characterization considering anterior corneal aberrations, internal astigmatism, and corneal biomechanics. *Journal of Cataract & Refractive Surgery* **37**, 552-568 (2011).
- 408 Greenwald, M. F., Scruggs, B. A., Vislisel, J. M. & Greiner, M. A. *Corneal Imaging: An Introduction*, <<https://webeye.ophth.uiowa.edu/eyeforum/tutorials/Corneal-Imaging/Index.htm>> (2016).
- 409 Lopes, B. T., Ramos, I. C., Dawson, D. G., Belin, M. W. & Ambrosio Jr, R. Detection of ectatic corneal diseases based on pentacam. *Zeitschrift für Medizinische Physik* **26**, 136-142 (2016).
- 410 Muftuoglu, O., Ayar, O., Hurmeric, V., Orucoglu, F. & Kılıc, I. Comparison of multimetric D index with keratometric, pachymetric, and posterior elevation parameters in diagnosing subclinical keratoconus in fellow eyes of asymmetric keratoconus patients. *Journal of Cataract & Refractive Surgery* **41**, 557-565 (2015).
- 411 Cavas-Martínez, F., De la Cruz Sánchez, E., Martínez, J. N., Cañavate, F. F. & Fernández-Pacheco, D. Corneal topography in keratoconus: state of the art. *Eye and vision* **3**, 5 (2016).
- 412 Villamarin, A. *et al.* 3D simulation of the aqueous flow in the human eye. *Medical engineering & physics* **34**, 1462-1470 (2012).
- 413 Chen, K.-J. *Accurate Estimation of Intraocular Pressure and Corneal Material Behaviour Using a Non-Contact Method*, University of Liverpool, (2018).
- 414 Wang, J. *Numerical simulation of corneal refractive surgery based on improved reconstruction of corneal surface*, (2015).
- 415 Maklad, O. *Influence of Fluid-Structure Interaction on Human Eye Biomechanics Under Air Puff Non-Contact Tonometry*, University of Liverpool, (2019).
- 416 Ogden, R. W. *Non-linear elastic deformations*. (Courier Corporation, 1997).
- 417 Markert, B., Ehlers, W. & Karajan, N. in *PAMM: Proceedings in Applied Mathematics and Mechanics*. 245-246 (Wiley Online Library).
- 418 guo Yu, J. *et al.* Assessment of corneal biomechanical behavior under posterior and anterior pressure. *Journal of Refractive Surgery* **29**, 64-71 (2013).
- 419 Groves, R. B., Coulman, S., Birchall, J. C. & Evans, S. L. Quantifying the mechanical properties of human skin to optimise future microneedle device design. *Computer methods in biomechanics and biomedical engineering* **15**, 73-82 (2012).
- 420 Moran, R., Smith, J. H. & García, J. J. Fitted hyperelastic parameters for human brain tissue from reported tension, compression, and shear tests. *Journal of biomechanics* **47**, 3762-3766 (2014).

- 421 Magalhães, R., Elsheikh, A., Büchler, P., Whitford, C. & Wang, J. < b> Application of particle swarm optimization in inverse finite element modeling to determine the cornea's mechanical behavior. *Acta Scientiarum. Technology* **39**, 325-331 (2017).
- 422 Venter, G. & Sobieszczanski-Sobieski, J. Particle swarm optimization. *AIAA journal* **41**, 1583-1589 (2003).
- 423 Ambrósio, R. *et al.* Integration of Scheimpflug-based corneal tomography and biomechanical assessments for enhancing ectasia detection. *Journal of Refractive Surgery* **33**, 434-443 (2017).
- 424 Joda, A. A., Shervin, M. M., Kook, D. & Elsheikh, A. Development and validation of a correction equation for Corvis tonometry. *Comput Methods Biomech Biomed Engin* **19**, 943-953 (2016).
- 425 Chen, K.-J. *et al.* Clinical evaluation of a new correction algorithm for dynamic Scheimpflug analyzer tonometry before and after laser in situ keratomileusis and small-incision lenticule extraction. *Journal of Cataract & Refractive Surgery* (2018).
- 426 Elsheikh, A. *et al.* Stress free configuration of the human eye. *Med Eng Phys* **35**, 211-216, doi:10.1016/j.medengphy.2012.09.006 (2013).
- 427 Maklad, O., Theofilis, V. & Elsheikh, A. in *10th International Conference on Computational Fluid Dynamics, ICCFD 2018-Proceedings*.
- 428 Chen, K.-J. *Accurate Estimation of Intraocular Pressure and Corneal Material Behaviour Using a Non-Contact Method*, University of Liverpool, (2018).
- 429 Dubbelman, M., Weeber, H. A., van der Heijde, R. G. & Volker-Dieben, H. J. Radius and asphericity of the posterior corneal surface determined by corrected Scheimpflug photography. *Acta Ophthalmol Scand* **80**, 379-383 (2002).
- 430 Belin, M. W. & Khachikian, S. S. New devices and clinical implications for measuring corneal thickness. *Clinical & experimental ophthalmology* **34**, 729-731 (2006).
- 431 Gilani, F. *et al.* Comprehensive anterior segment normal values generated by rotating Scheimpflug tomography. *Journal of Cataract & Refractive Surgery* **39**, 1707-1712 (2013).
- 432 Avitabile, T., Marano, F., Uva, M. G. & Reibaldi, A. Evaluation of central and peripheral corneal thickness with ultrasound biomicroscopy in normal and keratoconic eyes. *Cornea* **16**, 639-644 (1997).
- 433 Ambrósio Jr, R., Alonso, R. S., Luz, A. & Velarde, L. G. C. Corneal-thickness spatial profile and corneal-volume distribution: tomographic indices to detect keratoconus. *Journal of Cataract & Refractive Surgery* **32**, 1851-1859 (2006).
- 434 Abass, A., Clamp, J., Bao, F., Ambrósio Jr, R. & Elsheikh, A. Non-orthogonal corneal astigmatism among normal and keratoconic Brazilian and Chinese populations. *Current eye research* **43**, 717-724 (2018).

- 435 Klein, S. A. Axial curvature and the skew ray error in corneal topography. *Optometry and vision science: official publication of the American Academy of Optometry* **74**, 931-944 (1997).
- 436 Salmon, T. O. & Horner, D. G. Comparison of elevation, curvature, and power descriptors for corneal topographic mapping. *Optometry and vision science: official publication of the American Academy of Optometry* **72**, 800-808 (1995).
- 437 Smith, G., George, S. & Atchison, D. A. *THE EYE AND VISUAL OPTICAL INSTRUMENTS. Edition en anglais.* (Cambridge University Press, 1997).
- 438 Vojniković, B. & Tamajo, E. Gullstrand's Optical Schematic System of the Eye-Modified by Vojniković & Tamajo. *Collegium antropologicum* **37**, 41-45 (2013).
- 439 Elsheikh, A., Zhou, D., Eliasy, A., Teixeira Lopes, B. & Abass, A. Determination and mapping of corneal stiffness in keratoconic corneas. (2019).
- 440 Detorakis, E. T. & Pallikaris, I. G. Ocular rigidity: biomechanical role, in vivo measurements and clinical significance. *Clinical & experimental ophthalmology* **41**, 73-81 (2013).
- 441 Roberts, C. J. *et al.* Introduction of Two Novel Stiffness Parameters and Interpretation of Air Puff-Induced Biomechanical Deformation Parameters With a Dynamic Scheimpflug Analyzer. *J Refract Surg* **33**, 266-273, doi:10.3928/1081597X-20161221-03 (2017).
- 442 Elsheikh, A., Geraghty, D., Alhasso, D. & Rama, P. Regional biomechanical behaviour of the human sclera and its variation with age. *Investigative Ophthalmology and Visual Science* **50**, E-Abstract 3948 (2009).
- 443 Vinciguerra, R. *et al.* Corneal biomechanics and biomechanically corrected intraocular pressure in primary open-angle glaucoma, ocular hypertension and controls. *British Journal of Ophthalmology* **104**, 121-126 (2020).
- 444 Kohlhaas, M. *et al.* Effect of central corneal thickness, corneal curvature, and axial length on applanation tonometry. *Arch Ophthalmol* **124**, 471-476, doi:10.1001/archophth.124.4.471 (2006).
- 445 Vinciguerra, R. *et al.* Detection of Keratoconus With a New Biomechanical Index. *J Refract Surg* **32**, 803-810, doi:10.3928/1081597X-20160629-01 (2016).
- 446 Vinciguerra, R. *et al.* Influence of Pachymetry and Intraocular Pressure on Dynamic Corneal Response Parameters in Healthy Patients. *J Refract Surg* **32**, 550-561, doi:10.3928/1081597X-20160524-01 (2016).
- 447 Eliasy, A. *et al.* Ex-vivo experimental validation of biomechanically-corrected intraocular pressure measurements on human eyes using the CorVis ST. *Experimental eye research* **175**, 98-102 (2018).
- 448 Kivanany, P. B., Grose, K. C., Tippani, M., Su, S. & Petroll, W. M. Assessment of Corneal Stromal Remodeling and Regeneration after

- Photorefractive Keratectomy. *Sci Rep* 8, 12580, doi:10.1038/s41598-018-30372-2 (2018).
- 449 McCarey, B. E., Napalkov, J. A., Phippen, P. A., Koester, J. M. & al
Reaves, T. Corneal wound healing strength with topical
antiinflammatory drugs. *Cornea* 14, 290-294, doi:10.1097/00003226-
199505000-00010 (1995).
- 450 Raghunathan, V. K. *et al.* Tissue and cellular biomechanics during
corneal wound injury and repair. *Acta Biomater* 58, 291-301,
doi:10.1016/j.actbio.2017.05.051 (2017).
- 451 Wilson, S. E. Analysis of the keratocyte apoptosis, keratocyte
proliferation, and myofibroblast transformation responses after
photorefractive keratectomy and laser in situ keratomileusis. *Trans Am
Ophthalmol Soc* 100, 411-433 (2002).
- 452 Netto, M. V. *et al.* Effect of prophylactic and therapeutic mitomycin C
on corneal apoptosis, cellular proliferation, haze, and long-term
keratocyte density in rabbits. *J Refract Surg* 22, 562-574 (2006).
- 453 Spadea, L. & Giovannetti, F. Main Complications of Photorefractive
Keratectomy and their Management. *Clin Ophthalmol* 13, 2305-2315,
doi:10.2147/OPHTH.S233125 (2019).
- 454 Roberts, C. J. Biomechanics in keratoconus. *Textbook on Keratoconus: New
Insights*, 29-32 (2011).
- 455 Bao, F., Geraghty, B., Wang, Q. & Elsheikh, A. Consideration of
corneal biomechanics in the diagnosis and management of keratoconus:
is it important? *Eye and vision* 3, 18 (2016).
- 456 Abass, A., Clamp, J., Bao, F., Ambrosio, R., Jr. & Elsheikh, A. Non-
Orthogonal Corneal Astigmatism among Normal and Keratoconic
Brazilian and Chinese populations. *Curr Eye Res*, 1-8,
doi:10.1080/02713683.2018.1433858 (2018).
- 457 Khurana, A. K. *Theory And Practice Of Optics And Refraction*. 3 edn,
(Elsevier India Pvt. Limited, 2008).
- 458 Lopes, B. T., Ramos, I. C., Dawson, D. G., Belin, M. W. & Ambrosio,
R., Jr. Detection of ectatic corneal diseases based on pentacam. *Z Med
Phys* 26, 136-142, doi:10.1016/j.zemedi.2015.11.001 (2016).
- 459 Mahmoud, A. M. *et al.* Expanding the cone location and magnitude
index to include corneal thickness and posterior surface information for
the detection of keratoconus. *Am J Ophthalmol* 156, 1102-1111,
doi:10.1016/j.ajo.2013.07.018 (2013).
- 460 Seiler, T. G., Shao, P., Eltony, A., Seiler, T. & Yun, S. H. Brillouin
Spectroscopy of Normal and Keratoconus Corneas. *Am J Ophthalmol*
202, 118-125, doi:10.1016/j.ajo.2019.02.010 (2019).
- 461 Auffarth, G. U., Wang, L. & Volcker, H. E. Keratoconus evaluation
using the Orbscan Topography System. *Journal of Cataract and Refractive
Surgery* 26, 222-228, doi:Doi 10.1016/S0886-3350(99)00355-7 (2000).

- 462 Demirbas, N. H. & Pflugfelder, S. C. Topographic pattern and apex location of keratoconus on elevation topography maps. *Cornea* **17**, 476-484 (1998).
- 463 Wilson, S. E., Lin, D. T. & Klyce, S. D. Corneal topography of keratoconus. *Cornea* **10**, 2-8 (1991).
- 464 Twa, M. D. *et al.* Characteristics of corneal ectasia after LASIK for myopia. *Cornea* **23**, 447-457 (2004).
- 465 Maguire, L. J. & Bourne, W. M. Corneal topography of early keratoconus. *American journal of ophthalmology* **108**, 107-112 (1989).
- 466 Maeda, N., Klyce, S. D. & Smolek, M. K. Neural network classification of corneal topography. Preliminary demonstration. *Investigative ophthalmology & visual science* **36**, 1327-1335 (1995).
- 467 Wilson, S. E. & Klyce, S. D. Screening for corneal topographic abnormalities before refractive surgery. *Ophthalmology* **101**, 147-152 (1994).
- 468 Belin, M. W. & Khachikian, S. S. Keratoconus/ectasia detection with the oculus pentacam: Belin/Ambrósio enhanced ectasia display. *Highlights Ophthalmol* **35**, 5-12 (2007).
- 469 Luz, A. *et al.* Enhanced combined tomography and biomechanics data for distinguishing forme fruste keratoconus. *Journal of Refractive Surgery* **32**, 479-494 (2016).
- 470 Smolek, M. K. & Klyce, S. D. Screening of prior refractive surgery by a wavelet-based neural network. *Journal of Cataract & Refractive Surgery* **27**, 1926-1931 (2001).
- 471 Stamper, R. L. A history of intraocular pressure and its measurement. *Optom. Vis. Sci.* **88**, E16-28, doi:10.1097/OPX.0b013e318205a4e7 (2011).
- 472 Bengtsson, B., Leske, M. C., Hyman, L., Heijl, A. & Group, E. M. G. T. Fluctuation of intraocular pressure and glaucoma progression in the early manifest glaucoma trial. *Ophthalmology* **114**, 205-209 (2007).
- 473 Goldmann, H. Un nouveau tonometre d'applanation. *Bull Soc Ophthalmol Fr* **67**, 474-478 (1955).
- 474 Ehlers, N., Hansen, F. K. & Aasved, H. Biometric correlations of corneal thickness. *Acta Ophthalmol (Copenh)* **53**, 652-659 (1975).
- 475 Herndon, L. W. *et al.* Central corneal thickness in normal, glaucomatous, and ocular hypertensive eyes. *Archives of Ophthalmology* **115**, 1137-1141 (1997).
- 476 Montard, R. *et al.* Ocular response analyzer: feasibility study and correlation with normal eyes. *Journal francais d'ophtalmologie* **30**, 978-984 (2007).
- 477 Hong, J. *et al.* A New Tonometer—The Corvis ST Tonometer: Clinical Comparison with Noncontact and Goldmann Applanation Tonometers IOP Measurement with Corvis ST, NCT, and GAT. *Investigative ophthalmology & visual science* **54**, 659-665 (2013).

- 478 Saenz-Frances, F. *et al.* Effect of corneal morphometry on dynamic contour and goldmann applanation tonometry. *Journal of glaucoma* **22**, 380-383 (2013).
- 479 Özcür, F., Yıldırım, N., Tambova, E. & Şahin, A. Evaluation of Goldmann applanation tonometry, rebound tonometry and dynamic contour tonometry in keratoconus. *Journal of optometry* **10**, 117-122 (2017).
- 480 Boszczyk, A., Kasprzak, H. & Siedlecki, D. Non-contact tonometry using Corvis ST: analysis of corneal vibrations and their relation with intraocular pressure. *JOSA A* **36**, B28-B34 (2019).
- 481 Doyle, A. & Lachkar, Y. Comparison of dynamic contour tonometry with Goldman applanation tonometry over a wide range of central corneal thickness. *Journal of glaucoma* **14**, 288-292 (2005).
- 482 Kniestedt, C. *et al.* Clinical comparison of contour and applanation tonometry and their relationship to pachymetry. *Archives of Ophthalmology* **123**, 1532-1537 (2005).
- 483 Eisenberg, D. L., Sherman, B. G., McKeown, C. A. & Schuman, J. S. Tonometry in adults and children: A manometric evaluation of pneumatonometry, applanation, and TonoPen in vitro and in vivo¹¹The authors have no commercial interest in any of the products mentioned. *Ophthalmology* **105**, 1173-1181 (1998).
- 484 Whitacre, M. M., Stein, R. A. & Hassanein, K. The effect of corneal thickness on applanation tonometry. *American journal of ophthalmology* **115**, 592-596 (1993).
- 485 Lee, S.-h., Moon, J.-i. & Jung, Y. H. Comparison of Intraocular Pressures Measured by the Corvis ST and Other Tonometers in Normal Eyes. *Journal of the Korean Ophthalmological Society* **60**, 1250-1256 (2019).
- 486 Maklad, O. *et al.* Fluid-Structure Interaction Based Algorithms for IOP and Corneal Material Behavior. *Front. Bioeng. Biotechnol.* **8**: 970. doi: 10.3389/fbioe (2020).
- 487 Sigal, I. A. *et al.* IOP-induced lamina cribrosa deformation and scleral canal expansion: independent or related? *Investigative ophthalmology & visual science* **52**, 9023-9032 (2011).
- 488 Zhou, D. *et al.* Fibril Density Reduction in Keratoconic Corneas. *Journal of The Royal Society Interface* **In-press** (2020).
- 489 Kniestedt, C., Nee, M. & Stamper, R. L. Dynamic contour tonometry: a comparative study on human cadaver eyes. *Arch Ophthalmol* **122**, 1287-1293, doi:10.1001/archophth.122.9.1287 (2004).
- 490 McCafferty, S., Levine, J., Schwiegerling, J. & Enikov, E. T. Goldmann applanation tonometry error relative to true intracameral intraocular pressure in vitro and in vivo. *BMC ophthalmology* **17**, 215 (2017).
- 491 Riva, I. *et al.* Dynamic contour tonometry and goldman applanation tonometry: correlation with intracameral assessment of intraocular pressure. *Eur J Ophthalmol* **22**, 55-62, doi:10.5301/ejo.5000067 (2012).

- 492 Kniestedt, C., Nee, M. & Stamper, R. L. Accuracy of dynamic contour tonometry compared with applanation tonometry in human cadaver eyes of different hydration states. *Graefes Arch Clin Exp Ophthalmol* **243**, 359-366, doi:10.1007/s00417-004-1024-6 (2005).
- 493 Riva, I. *et al.* Dynamic contour tonometry and Goldmann applanation tonometry: correlation with intracameral assessment of intraocular pressure. *European journal of ophthalmology* **22**, 55-62 (2012).
- 494 Ambrosio, R., Jr. Post-LASIK Ectasia: Twenty Years of a Conundrum. *Semin Ophthalmol* **34**, 66-68, doi:10.1080/08820538.2019.1569075 (2019).
- 495 Vinciguerra, R. *et al.* Corneal biomechanics and biomechanically corrected intraocular pressure in primary open-angle glaucoma, ocular hypertension and controls. *Br J Ophthalmol* **104**, 121-126, doi:10.1136/bjophthalmol-2018-313493 (2020).
- 496 Tomita, M. Combined laser in-situ keratomileusis and accelerated corneal cross-linking: an update. *Curr Opin Ophthalmol* **27**, 304-310, doi:10.1097/ICU.0000000000000281 (2016).
- 497 Dupps, W. J., Jr. & Roberts, C. J. Corneal biomechanics: a decade later. *J Cataract Refract Surg* **40**, 857, doi:10.1016/j.jcrs.2014.04.012 (2014).
- 498 Scarcelli, G., Pineda, R. & Yun, S. H. Brillouin optical microscopy for corneal biomechanics. *Invest Ophthalmol Vis Sci* **53**, 185-190, doi:10.1167/iovs.11-8281 (2012).
- 499 Luce, D. A. Determining in vivo biomechanical properties of the cornea with an ocular response analyzer. *J Cataract Refract Surg* **31**, 156-162, doi:10.1016/j.jcrs.2004.10.044 (2005).
- 500 Roberts, C. J. & Dupps, W. J., Jr. Biomechanics of corneal ectasia and biomechanical treatments. *J Cataract Refract Surg* **40**, 991-998, doi:10.1016/j.jcrs.2014.04.013 (2014).
- 501 Shih, C. Y., Graff Zivin, J. S., Trokel, S. L. & Tsai, J. C. Clinical significance of central corneal thickness in the management of glaucoma. *Arch Ophthalmol* **122**, 1270-1275, doi:10.1001/archophth.122.9.1270 (2004).
- 502 Girard, M. J., Suh, J.-K. F., Bottlang, M., Burgoyne, C. F. & Downs, J. C. Scleral biomechanics in the aging monkey eye. *Investigative ophthalmology & visual science* **50**, 5226-5237 (2009).
- 503 Guo, H., Hosseini-Moghaddam, S. M. & Hodge, W. Corneal biomechanical properties after SMILE versus FLEX, LASIK, LASEK, or PRK: a systematic review and meta-analysis. *BMC Ophthalmol* **19**, 167, doi:10.1186/s12886-019-1165-3 (2019).
- 504 Sekundo, W., Kunert, K. S. & Blum, M. Small incision corneal refractive surgery using the small incision lenticule extraction (SMILE) procedure for the correction of myopia and myopic astigmatism: results of a 6 month prospective study. *Br J Ophthalmol* **95**, 335-339, doi:10.1136/bjo.2009.174284 (2011).

- 505 Khamar, P. *et al.* Biomechanics of LASIK Flap and SMILE Cap: A Prospective, Clinical Study. *J Refract Surg* **35**, 324-332, doi:10.3928/1081597X-20190319-01 (2019).
- 506 Zhang, Y., Shen, Q., Jia, Y., Zhou, D. & Zhou, J. Clinical Outcomes of SMILE and FS-LASIK Used to Treat Myopia: A Meta-analysis. *J Refract Surg* **32**, 256-265, doi:10.3928/1081597X-20151111-06 (2016).
- 507 Wang, K. J., Wang, W. W., Tsai, C. L. & Wang, I. J. Intraocular pressure changes in eyes with small incision lenticules and laser in situ keratomileusis. *Clin Exp Optom* **102**, 399-405, doi:10.1111/cxo.12861 (2019).
- 508 Cao, K. *et al.* Changes in corneal biomechanics during small-incision lenticule extraction (SMILE) and femtosecond-assisted laser in situ keratomileusis (FS-LASIK). *Lasers Med Sci*, doi:10.1007/s10103-019-02854-w (2019).
- 509 Sefat, S. M. *et al.* Evaluation of Changes in Human Corneas After Femtosecond Laser-Assisted LASIK and Small-Incision Lenticule Extraction (SMILE) Using Non-Contact Tonometry and Ultra-High-Speed Camera (Corvis ST). *Curr Eye Res* **41**, 917-922, doi:10.3109/02713683.2015.1082185 (2016).
- 510 Osman, I. M., Helaly, H. A., Abdalla, M. & Shousha, M. A. Corneal biomechanical changes in eyes with small incision lenticule extraction and laser assisted in situ keratomileusis. *BMC Ophthalmol* **16**, 123, doi:10.1186/s12886-016-0304-3 (2016).

Appendices

Section A - Biomechanically Corrected IOP (bIOP2)

bIOP2 Healthy Equation

Healthy Patients

Dataset 2

Dataset 2 includes 329 healthy patients with mean age of 36.9 ± 16.4 (7.0 -85.0) years and CCT of 545 ± 34 (459 -681) microns. The IOP values obtained from CVSIOP, bIOP and bIOP2 were 15.5 ± 2.2 (10.5 -24.5) mmHg, 14.3 ± 2.0 (7.8 -21.7) mmHg and 15.5 ± 1.2 (12.8 -21.0) mmHg respectively. bIOP2 was least correlated with CCT (p:0.985, R:-0.001) and age (p:0.637, R:-0.026). bIOP performed better in correlation with CCT (p:0.531, R:-0.035) than CVSIOP (p:0.000, R:0.391). CVSIOP showed weaker correlation (p:0.896, R:-0.007) with age in comparison to bIOP (p:0.000, R:-0.265), Figure 6-1.

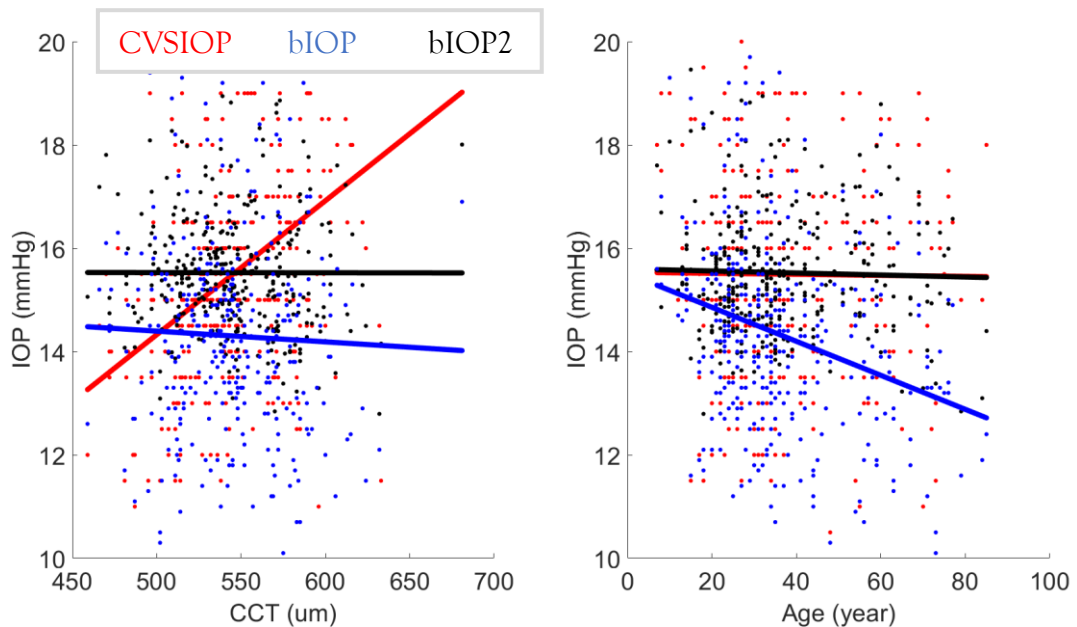


Figure 6-1 Correlation of IOP values from CVSIOP, bIOP and bIOP2 with CCT (left) and age (right) in Dataset 2

Dataset 3

Dataset 3 consist of 412 healthy patients with mean age of 34.4 ± 9.9 (7.0 -62.0) years and CCT of 545 ± 33 (441 -663) microns. The IOP values obtained from CVSIOP, bIOP and bIOP2 were 15.0 ± 2.7 (6.0 -28.5) mmHg, 15.0 ± 2.3 (9.4 -26.5) mmHg and 15.4 ± 1.3 (12.6 -21.7) mmHg respectively. In terms of correlation with CCT, bIOP ($p:0.853$, $R:0.009$) and bIOP2 ($p:0.757$, $R:-0.015$) showed weak correlations and CVSIOP ($p:0.000$, $R:0.348$) was significantly correlated. Correlation with age was weakest in bIOP2 ($p:0.715$, $R:0.018$), followed by CVSIOP ($p:0.620$, $R:0.024$) and bIOP ($p:0.600$, $R:-0.026$). None of the devices showed significant correlations with age, Figure 6-2.

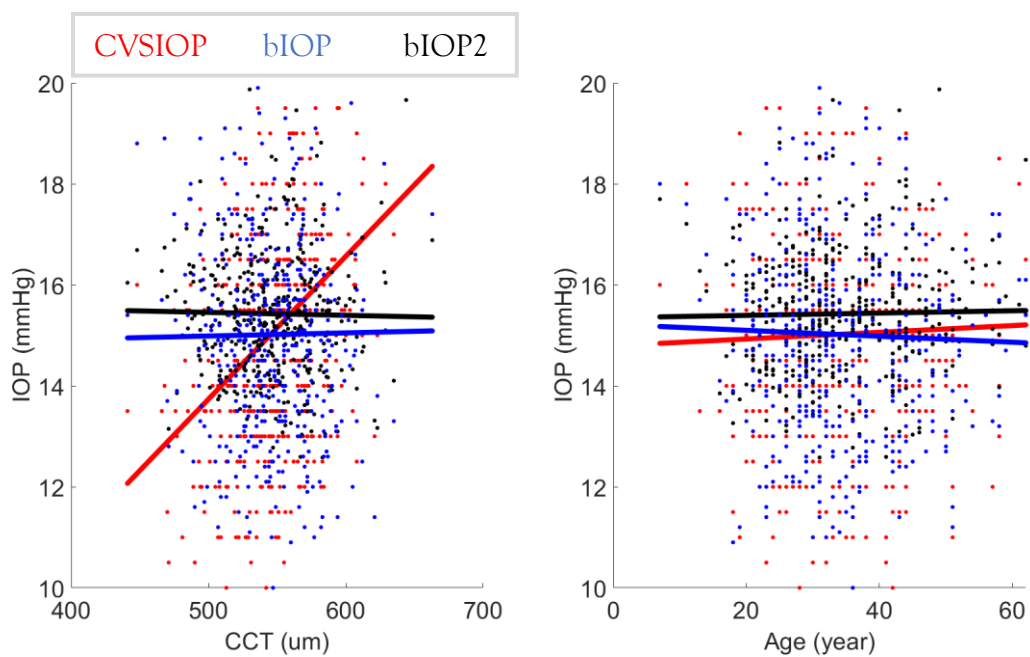


Figure 6-2 Correlation of IOP values from CVSIOP, bIOP and bIOP2 with CCT (left) and age (right) in Dataset 3

Dataset 4

Dataset 4 consist of 212 healthy patients with mean age of 27.1 ± 5.7 (15.0 -47.0) years and CCT of 550 ± 30 (418 -634) microns. The IOP values obtained from CVSIOP, bIOP and bIOP2 were 16.7 ± 2.3 (11.5 -24.0) mmHg, 16.0 ± 2.4 (11.7 -22.7) mmHg and 15.7 ± 1.4 (11.9 -19.4) mmHg respectively. The correlation with CCT was weakest for bIOP($p:0.719$, $R:0.025$) followed by bIOP2 ($p:0.063$, $R:-0.128$) and CVSIOP ($p:0.000$, $R:0.346$). Correlation with age was not significant in CVSIOP ($p:0.675$, $R:0.029$), bIOP ($p:0.800$, $R:0.017$) and bIOP2 ($p:0.574$, $R:0.039$), Figure 6-3.

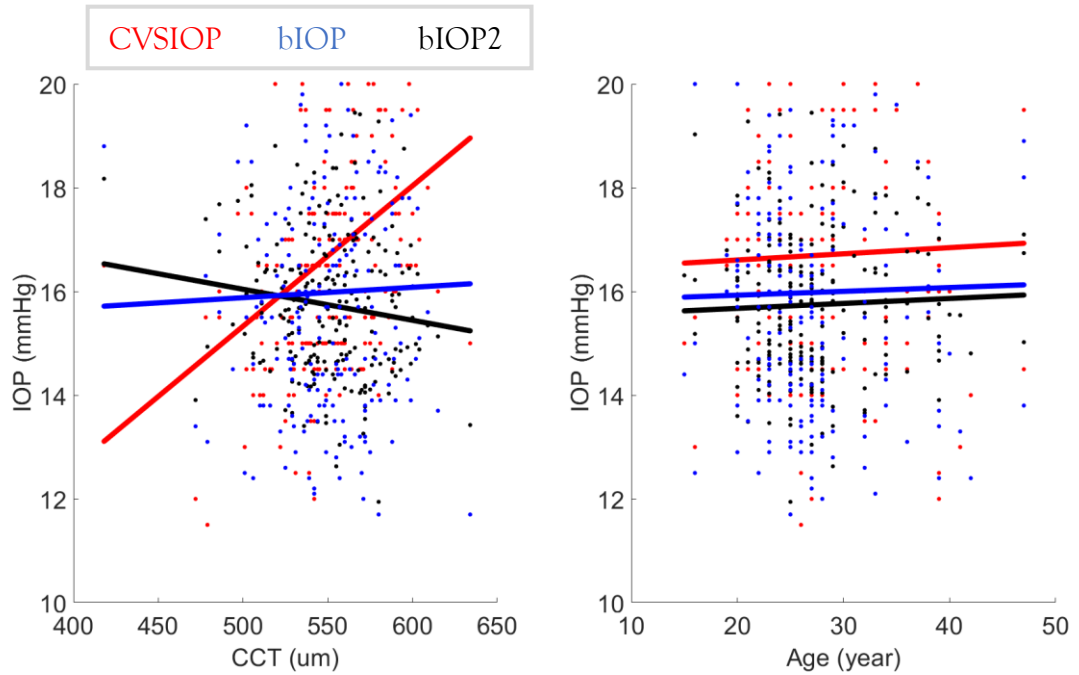


Figure 6-3 Correlation of IOP values from CVSIOP, bIOP and bIOP2 with CCT (left) and age (right) in Dataset 4

Dataset 5

Dataset 5 consist of 55 healthy patients with mean age of 34.6 ± 9.4 (12.0 -66.0) years and CCT of 552 ± 35 (459 -614) microns. The IOP values obtained from CVSIOP, bIOP and bIOP2 were 16.1 ± 2.3 (12.5 -20.5) mmHg, 14.9 ± 2.2 (10.5 -19.8) mmHg and 15.9 ± 1.3 (12.8 -18.5) mmHg respectively. The correlation with CCT (p:0.524, R:0.088) and age (p:0.294, R:-0.144) was weakest in bIOP2. bIOP showed weaker correlation (p:0.382, R:0.120) with CCT compared to CVSIOP (p:0.002, R:0.410). In terms of correlation with age, CVSIOP (p:0.028, R:-0.296) performed better than bIOP (p:0.013, R:-0.333), Figure 6-4.

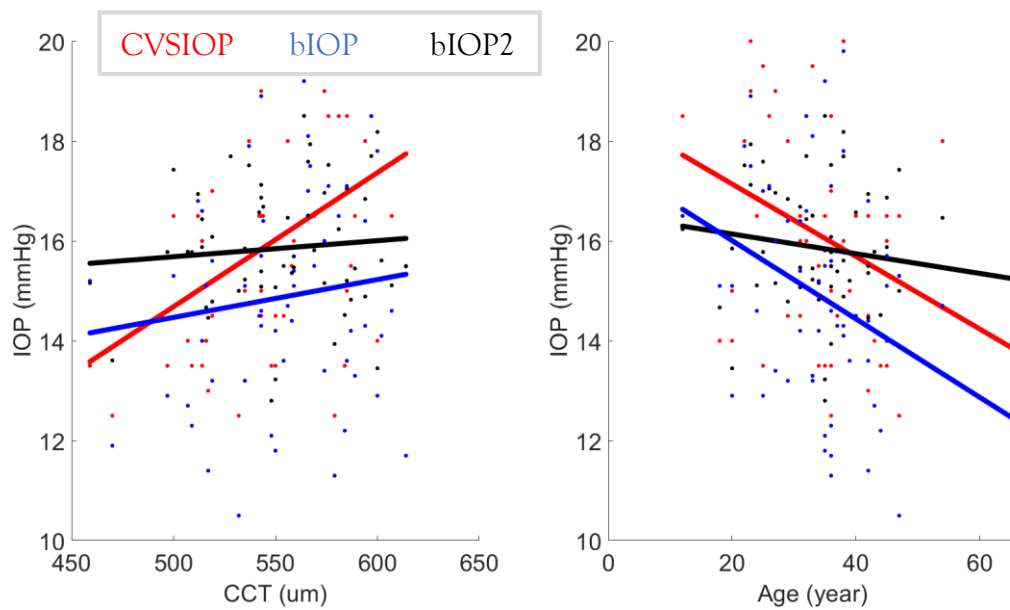


Figure 6-4 Correlation of IOP values from CVSIOP, bIOP and bIOP2 with CCT (left) and age (right) in Dataset 5

Dataset 6

Dataset 6 consist of 244 healthy patients with mean age of 32.9 ± 13.0 (7.0 -80.0) years and CCT of 549 ± 34 (435 -645) microns. The IOP values obtained from CVSIOP, bIOP and bIOP2 are 16.0 ± 2.1 (9.5 -24.0) mmHg, 14.5 ± 1.8 (9.8 -22.9) mmHg and 15.7 ± 1.1 (13.3 -19.5) mmHg respectively. The correlation with CCT (p:0.707, R:-0.024) and age (p:0.844, R:-0.013) was weakest in bIOP2. bIOP showed weaker correlation (p:0.241, R:-0.075) with CCT compared to CVSIOP (p:0.000, R:0.395). in terms of correlation with age, CVSIOP (p:0.328, R:-0.063) performed better than bIOP (p:0.001, R:-0.205), Figure 6-5.

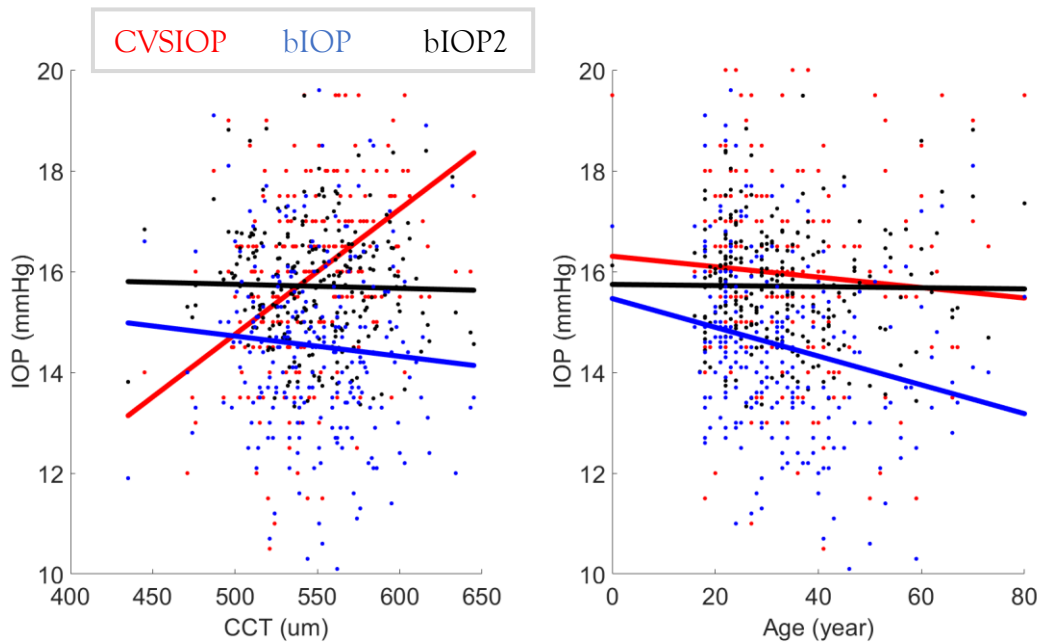


Figure 6-5 Correlation of IOP values from CVSIOP, bIOP and bIOP2 with CCT (left) and age (right) in Dataset 6

Dataset 7

Dataset 6 consist of 337 healthy patients with mean age of 25.7 ± 7.9 (10.0 -81.0) years and CCT of 526 ± 36 (424 -629) microns. The IOP values obtained from CVSIOP, bIOP and bIOP2 were 15.8 ± 2.5 (9.5 -27.5) mmHg, 15.3 ± 2.2 (9.9 -23.6) mmHg and 15.5 ± 1.3 (12.2 -20.9) mmHg respectively. The correlation with CCT ($p:0.117$, $R:0.086$) and age ($p:0.295$, $R:-0.057$) was weakest in bIOP2. bIOP showed weaker correlation ($p:0.029$, $R:0.119$) with CCT compared to CVSIOP ($p:0.000$, $R:0.447$). In terms of correlation with age, CVSIOP ($p:0.257$, $R:-0.062$) performed better than bIOP ($p:0.001$, $R:-0.173$), Figure 6-6.

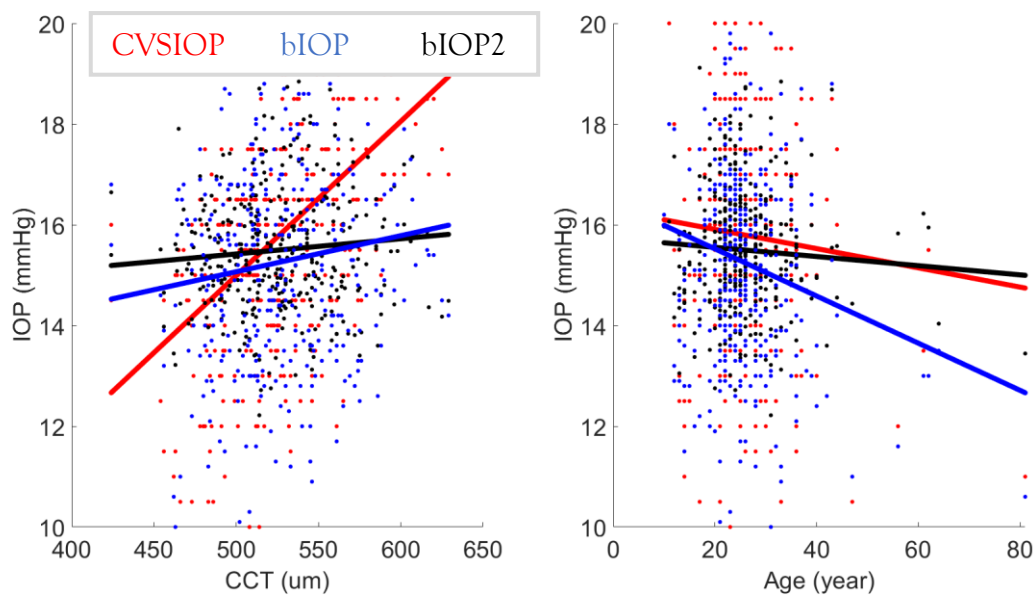


Figure 6-6 Correlation of IOP values from CVSIOP, bIOP and bIOP2 with CCT (left) and age (right) in Dataset 7

Dataset 8

Combining all data resulted in 2117 healthy patients with mean age of 33.9 ± 13.9 (7.0 - 91.0) years and CCT of 541 ± 34 (418 -681) microns. The IOP values obtained from CVSIOP, bIOP and bIOP2 were 15.5 ± 2.5 (6.0 -29.0) mmHg, 14.8 ± 2.2 (7.8 - 26.5) mmHg and 15.5 ± 1.3 (11.9 -22.6) mmHg respectively. The correlation with CCT (p:0.986, R:-0.000) and age (p:0.981, R:-0.001) was weakest in bIOP2. bIOP showed weaker correlation (p:0.972, R:-0.001) with CCT compared to CVSIOP (p:0.000, R:0.367). in terms of correlation with age, CVSIOP (p:0.122, R:-0.034) performed better than bIOP (p:0.000, R:-0.196), Figure 6-7.

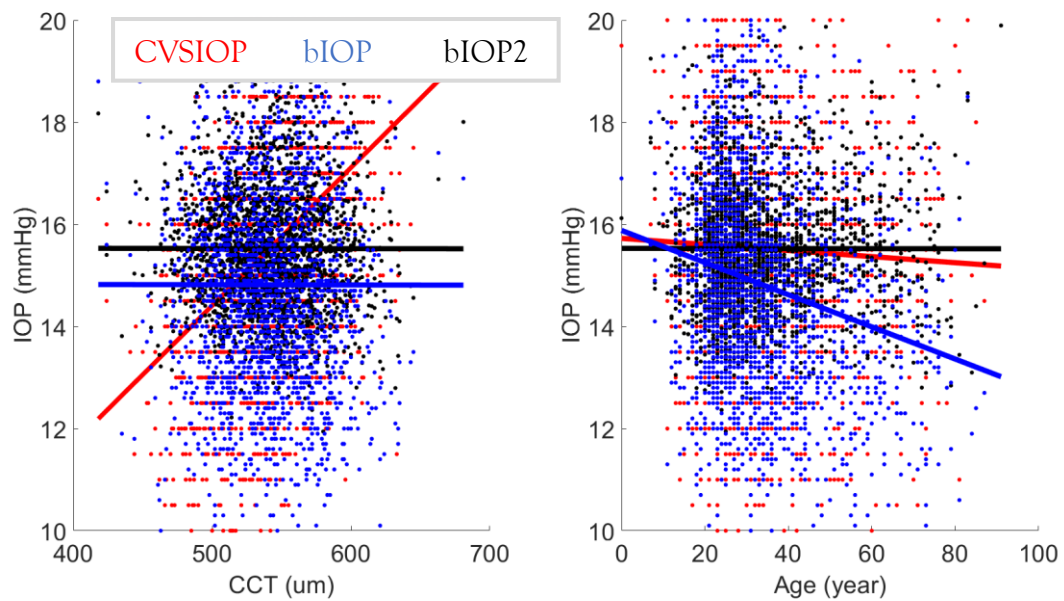


Figure 6-7 Correlation of IOP values from CVSIOP, bIOP and bIOP2 with CCT (left) and age (right) in Dataset 8

Refractive Surgeries

Dataset 2

Dataset 2 includes 38 patients who undergo PRK surgery with mean age of 38.1 ± 10.7 (21.0 - 79.0) years, CCT of 541 ± 33 (458 - 623) microns, CVSIOP of 15.8 ± 2.8 (10.5 - 24.5) mmHg, bIOP of 15.3 ± 2.2 (10.4-21.7) mmHg and bIOP2 of 15.9 ± 1.4 (13.1-19.9). The correlation with age was weak for CVSIOP (R:0.119, P:0.477), bIOP (R:0.018, P:0.915) and bIOP2 (R:0.185, P:0.267). Correlation with CCT was the weakest for bIOP2 (R:-0.041, P:0.807) followed by bIOP (R:0.167, P:0.316) and CVSIOP (R:0.492, P:0.002), Figure 6-8.

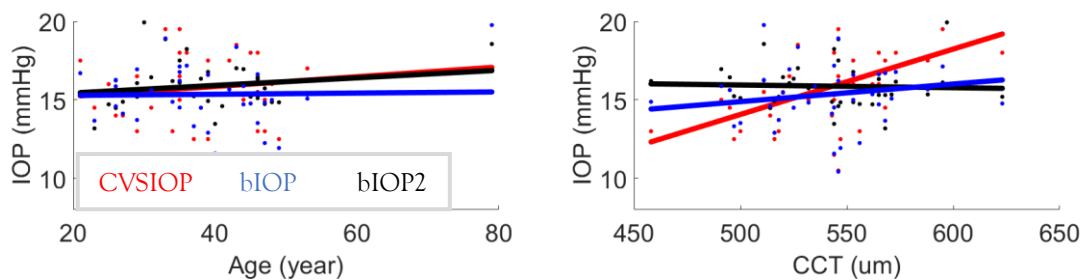


Figure 6-8 Correlation of IOP values from CVSIOP, bIOP and bIOP2 with CCT (left) and age (right) in pre surgery LASIK Dataset 2

Demographics for post operative data showed mean age of 39.8 ± 10.7 (23.0 - 80.0) years, CCT of 414 ± 37 (343-502) microns, CVSIOP of 12.9 ± 2.3 (8.5-20.5) mmHg, bIOP of 15.2 ± 2.0 (11.2-19.6) mmHg and bIOP2 of 16.3 ± 0.9 (14.8 - 18.2) mmHg. The Wilcoxon signed-rank test showed no significant differences between pre and post surgery measurements of bIOP ($p=0.632$), whereas both bIOP2 ($p=0.003$) and CVSIOP ($p=0.000$) were significantly different. The correlation remained weak with age for CVSIOP (R:0.300, P:0.067), bIOP (R:0.063, P:0.708) and bIOP2 (R:-0.189, P:0.255). The correlation with CCT was weakest for bIOP (R:-0.010, P:0.952) followed by bIOP2 (R:-0.167, P:0.318) and CVSIOP (R:0.019, P:0.908), Figure 6-9.

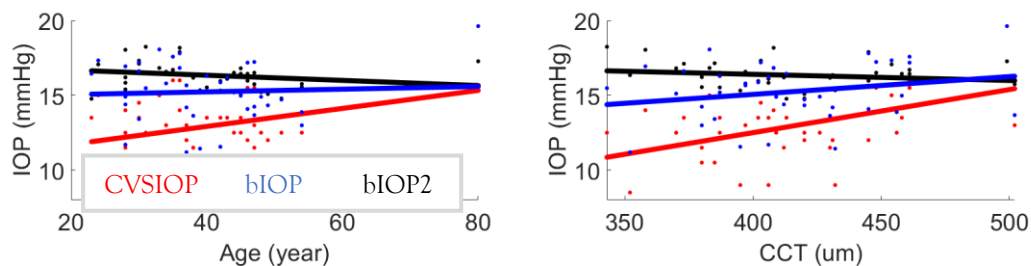
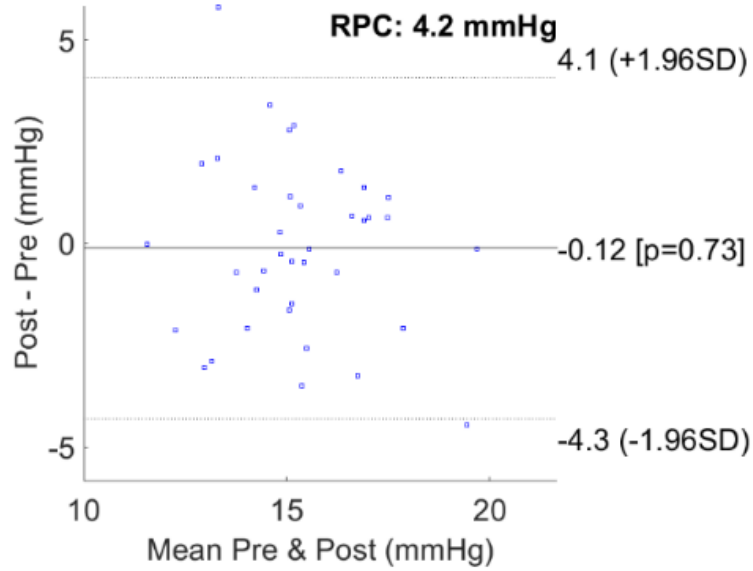


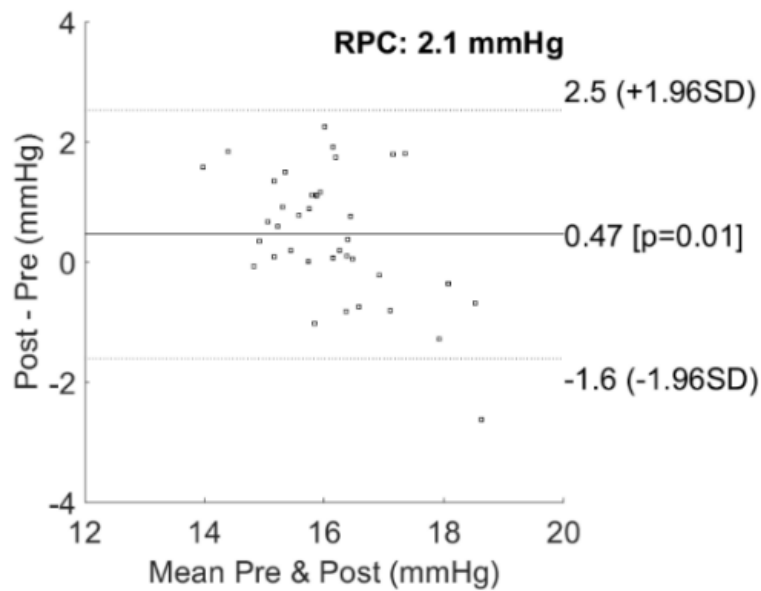
Figure 6-9 Correlation of IOP values from CVSIOP, bIOP and bIOP2 with CCT (left) and age (right) in post surgery LASIK Dataset 2

To better evaluate the differences between pre and post-refractive surgery, Bland Altman plots were produced for each IOP measurement method, Figure 6-10. Among all data, bIOP had the least differences in mean IOP values between pre and post with only 0.12 mmHg. This was followed by bIOP2 with differences of 0.47 mmHg and the

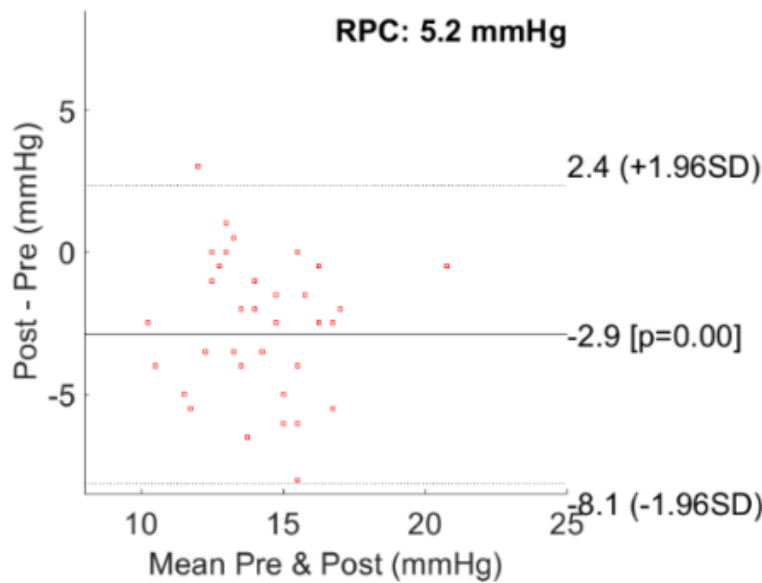
smallest standard deviation among all three. CVSIOP had the mean differences of 2.9 mmHg and the largest standard deviation.



(A)



(B)



(C)

Figure 6-10 The Bland Altman plots for (A) bIOP, (B) bIOP2 and (C) CVSIOP comparing the pre and post IOP values in LASIK Dataset 2

Dataset 2 also includes 47 patients who undergo LASIK surgery with mean age of 35.6 ± 7.4 (21.0-47.0) years, CCT of 549 ± 34 (476 - 632) microns, CVSIOP of 15.4 ± 2.8 (11.0 -25.0) mmHg, bIOP of 14.9 ± 2.2 (11.2 - 22.5) mmHg and bIOP2 of 15.7 ± 1.4 (13.8-18.8) mmHg. The correlation with age was weak for CVSIOP (R:-0.002, P:0.988), bIOP (R:-0.146, P:0.327) and bIOP2 (R:0.000, P:0.998). CCT correlation was the weakest for bIOP2 (R:0.117, P:0.434) followed by bIOP (R:0.124, P:0.408) and CVSIOP (R:0.485, P:0.001), Figure 6-11.

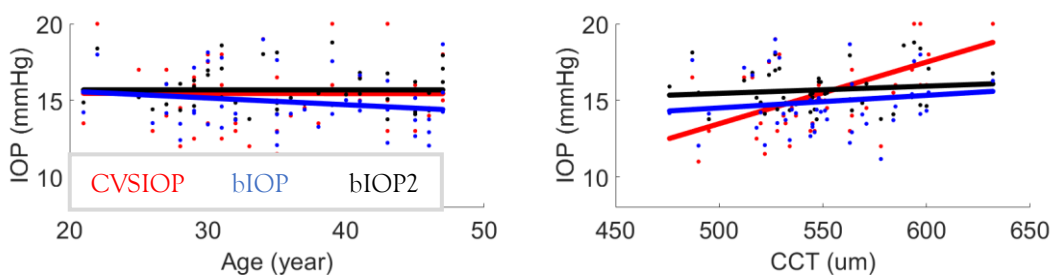


Figure 6-11 Correlation of IOP values from CVSIOP, bIOP and bIOP2 with CCT (left) and age (right) in pre surgery LASIK Dataset 2

Demographics for post operative data showed mean age of 36.1 ± 7.4 (21.0-48.0) years, CCT of 475 ± 51 (348-583) microns, CVSIOP of 12.0 ± 2.0 (6.5-17.0) mmHg, bIOP of 13.4 ± 1.8 (8.8 -17.3) mmHg and bIOP2 of 15.4 ± 0.9 (13.8-17.2). The Wilcoxon signed-rank test showed no significant differences between pre and post surgery measurements of bIOP2 (p:0.153), whereas both bIOP (p=0.000) and CVSIOP (p=0.000) were significantly different. The correlation remained weakest with age for bIOP2 (R:-0.103,

P:0.4901), followed by CVSIOP (R:-0.185, P:0.2135) and bIOP (R:-0.295, P:0.0441). The correlation with CCT was weakest for bIOP (R:0.031, P:0.836) followed by bIOP2 (R:0.117, P:0.434) and CVSIOP (R:0.319, P:0.029), Figure 6-12.

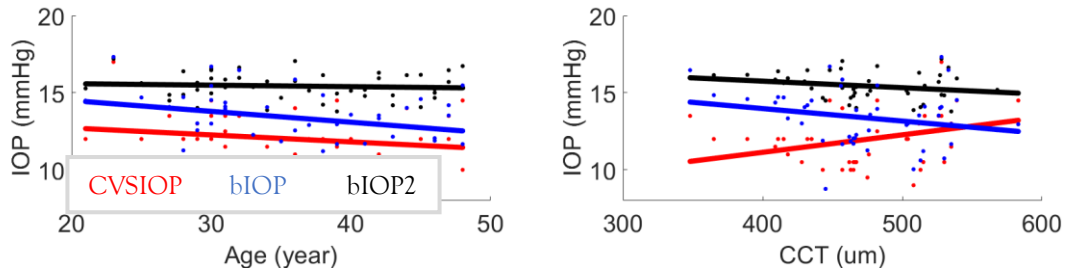
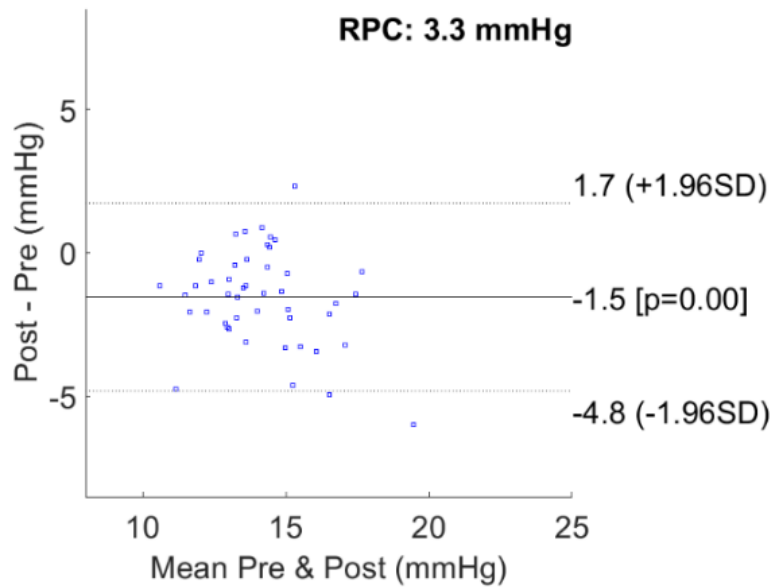
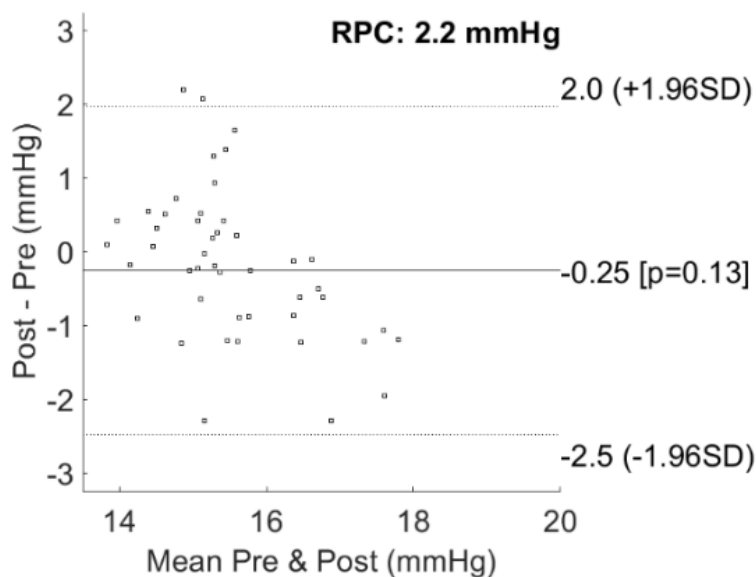


Figure 6-12 Correlation of IOP values from CVSIOP, bIOP and bIOP2 with CCT (left) and age (right) in post surgery LASIK Dataset 2

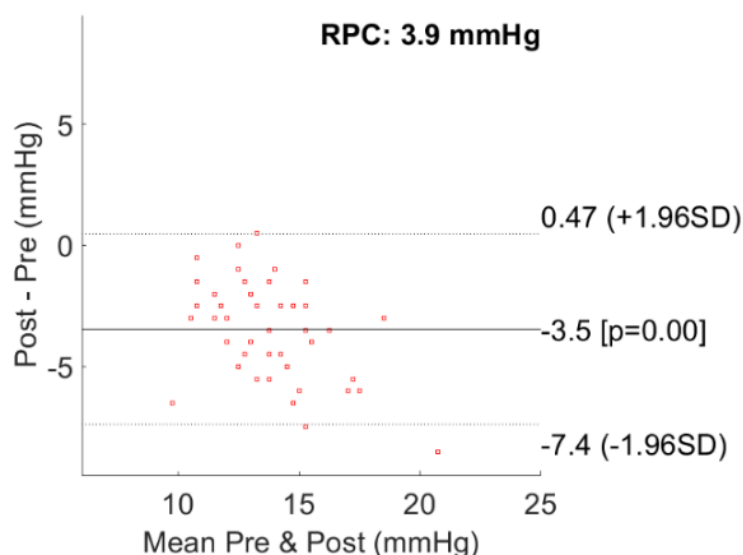
To better evaluate the differences between pre and post-refractive surgery data, Bland Altman plots were produced for each IOP measurement method, Figure 6-13. Among all data, bIOP2 had the least differences in mean IOP values between pre and post with only 0.25 mmHg and the smallest standard deviation. This was followed by bIOP2 with the differences of 1.5 mmHg and CVSIOP with 3.5 mmHg, which had the largest standard deviation too.



(A)



(B)



(C)

Figure 6-13 The Bland Altman plots for (A) bIOP, (B) bIOP2 and (C) CVSIOP comparing the pre and post IOP values in LASIK Dataset 2

Dataset 2 also includes 17 patients who undergo SMILE surgery with mean age of 24.1 ± 4.5 (18.0-31.0) years, CCT of 548 ± 22 (515-595) microns, CVSIOP of 17.2 ± 1.8 (14.5-20.5) mmHg, 16.8 ± 1.3 (14.5-19.0) mmHg and bIOP2 of 16.6 ± 0.8 (15.2 - 18.1) mmHg. The correlation with age was weak for CVSIOP (R:-0.134, P:0.608), bIOP (R:-0.145, P:0.579) and bIOP2 (R:-0.058, P:0.824). CCT correlation was weak for bIOP2 (R:0.229, P:0.376) and bIOP (R:0.219, P:0.399) but significant for CVSIOP (R:0.562, P:0.019), Figure 6-14.

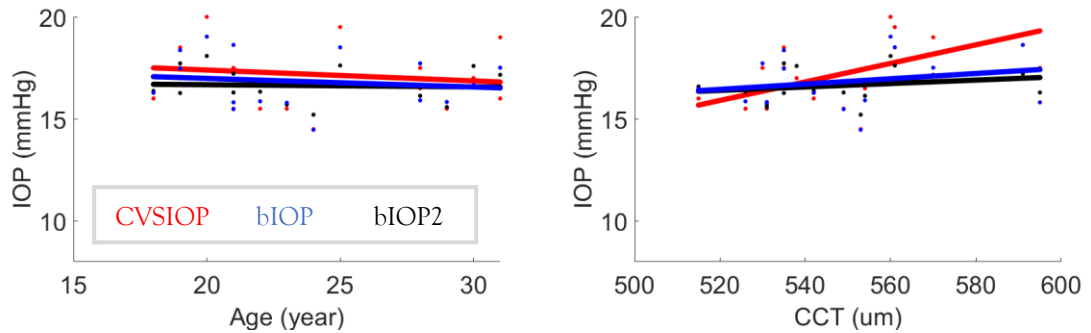


Figure 6-14 Correlation of IOP values from CVSIOP, bIOP and bIOP2 with CCT (left) and age (right) in pre surgery LASIK Dataset 2

Demographics for post operative data showed mean age of 24.8 ± 4.3 (19.0 -32.0) years, CCT of 450 ± 26 (409 -499) microns, CVSIOP of 14.1 ± 1.5 (12.0-16.5) mmHg, bIOP of 16.2 ± 1.5 (14.3-19.1) mmHg and bIOP2 of 16.6 ± 1.0 (15.1-19.3). The Wilcoxon signed-rank test showed no significant differences between pre and post surgery measurements of bIOP2 ($p=0.795$), whereas both bIOP ($p=0.000$) and CVSIOP ($p=0.000$) were significantly different post-surgery. The correlation with age for bIOP2 ($R:-0.335$, $P:0.189$), bIOP ($R:-0.334$, $P:0.191$) and CVSIOP ($R:-0.244$, $P:0.346$) remained weak. The correlation with CCT was weakest for bIOP ($R:-0.007$, $P:0.979$) followed by bIOP2 ($R:0.062$, $P:0.813$) and CVSIOP ($R:0.203$, $P:0.434$), Figure 6-15.

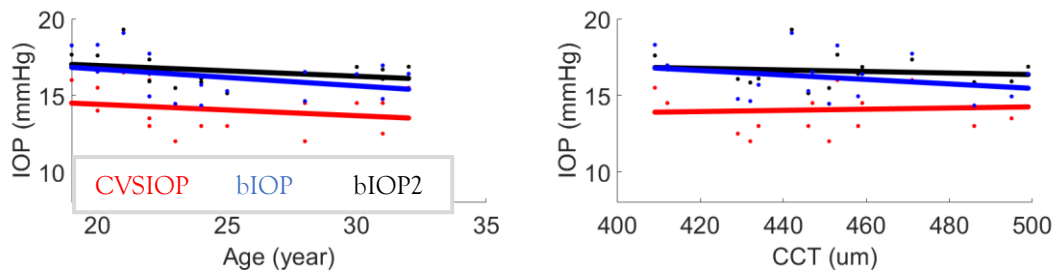
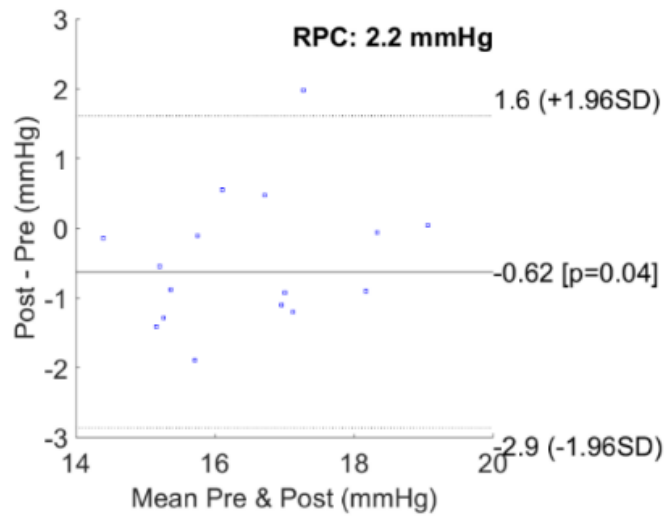
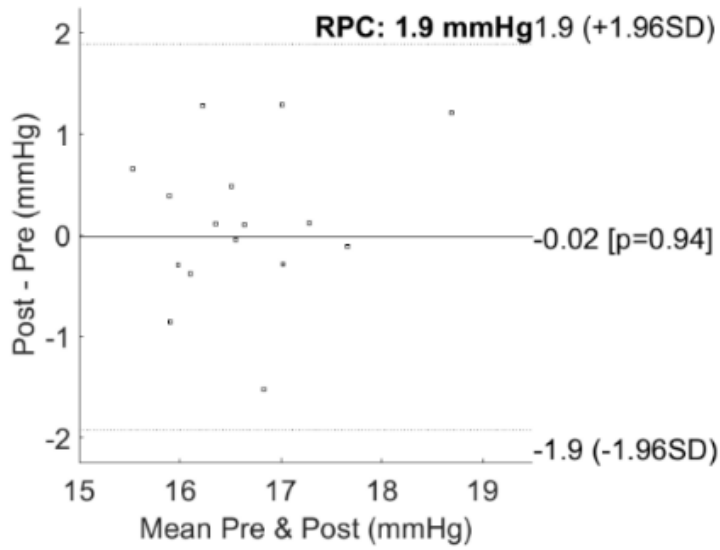


Figure 6-15 Correlation of IOP values from CVSIOP, bIOP and bIOP2 with CCT (left) and age (right) in post surgery LASIK Dataset 2

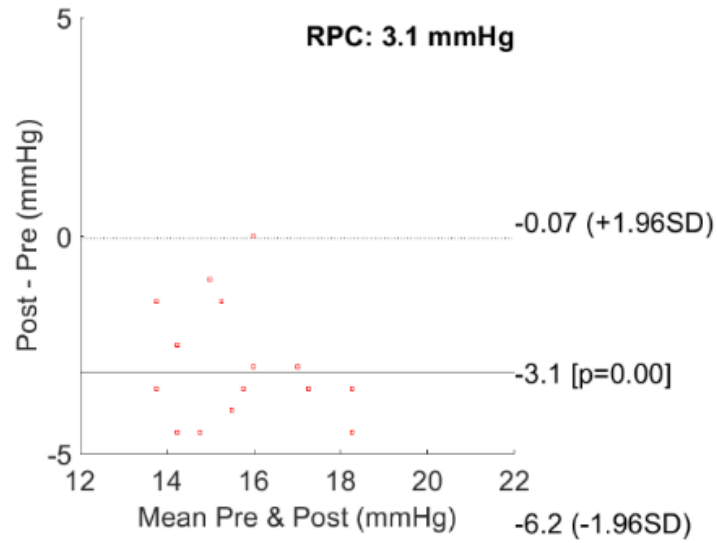
To better evaluate the differences between pre and post-refractive surgery data, Bland Altman plots were produced for each IOP measurement method, Figure 6-13. Among all data, bIOP2 had the least differences in mean IOP values between pre and post with only 0.02 mmHg and the smallest standard deviation. This was followed by bIOP2 with the value of 0.62 mmHg and CVSIOP with 3.1 mmHg, which had the largest standard deviation too.



(A)



(B)



(C)

Figure 6-16 The Bland Altman plots for (A) bIOP, (B) bIOP2 and (C) CVSIOPI comparing the pre and post IOP values in LASIK Dataset 2

Dataset 3

Dataset 3 includes longitudinal refractive surgery data including SMILE (60 eyes), LASIK (80 eyes) and PRK (62 eyes) surgeries recorded at 1, 3 and 6 months postoperatively. Detailed demographics, including operational parameters, are provided in Table 6-1. The IOP values measured using three different methods and reported in CVSIOPI, bIOP and bIOP2, Table 6-2.

Table 6-1 Demographics and surgical parameters for LASIK, SMILE and PRK surgeries in Dataset 3

| | PRK | LASIK | SMILE |
|-------------------|---------------------------|---------------------------|---------------------------|
| Age (year) | 25.7+4.9 (17 - 36) | 25.9+4.8 (17 - 37) | 26.3+6 (17 - 41) |
| Optical Zone (mm) | 6.6+0.4 (5.6 - 7.4) | 6.6+0.4 (5.9 - 7.3) | 6.6+0.2 (6 - 6.9) |
| SE (diopter) | -5.2+1.9 (-9.7 - -1.5) | -5.2+1.6 (-9.5 - -1.8) | -5.3+1.6 (-8.8 - -2.4) |
| S (diopter) | -4.8+1.9 (-9.2 - -1) | -4.9+1.5 (-9 - -1.5) | -4.9+1.6 (-8.3 - -2.1) |
| C (diopter) | -0.7+0.6 (-2.5 - 0) | -0.6+0.6 (-2.5 - 0) | -0.7+0.5 (-3 - 0) |
| Axis (degree) | 84.4+74.4 (0 - 180) | 51.5+68.9 (0 - 180) | 104.7+73.7 (0 - 180) |
| Op D (mm) | 6.6+0.4 (5.6 - 7.4) | 6.6+0.4 (5.9 - 7.3) | 6.6+0.2 (6 - 6.9) |

| | | | |
|-------------------------------------|-------------------------|---------------------------|--------------------------|
| Cu D (mm) | 8.1+0.4 (6.9 - 8.8) | 7.7+0.4 (6.9 - 8.3) | 7.3+0.4 (7 - 7.6) |
| Depth (microns) | 139+22.2 (85 - 187) | 88.4+21.1 (35 - 122) | 104.5+20.1 (63 - 145) |
| Residual Thickness (microns) | 402+36.3 (323 - 481) | 352.2+28.7 (302 - 429) | 321+22 (284 - 376) |

Table 6-2 IOP values measured using three different methods for LASIK, SMILE and PRK in 1,3 and 6 months post operatively in Dataset 3

| PRK | Pre | 1M Post | 3M Post | 6M Post |
|----------------------|-----------------------------|-------------------------------|-------------------------------|-----------------------------|
| CCT (microns) | 556+26.5 (509 - 603.7) | 446.4+40.5 (351 - 543) | 445.4+41.6 (347 - 539.7) | 443.8+38.8 (350.6 - 518) |
| CVSIOP (mmHg) | 14.3+1.9 (10.8 - 19.8) | 11.2+2.6 (6.5 - 21.2) | 10.9+2.2 (6.5 - 16.8) | 10.9+2 (7.5 - 15.8) |
| bIOP (mmHg) | 14+1.6 (10.1 - 17.5) | 13.3+2.4 (9.2 - 23.6) | 13.1+2 (9.2 - 18.5) | 13+1.8 (8.8 - 17.5) |
| bIOP2 (mmHg) | 15.1+1 (12.9 - 17.1) | 16.2+1.1 (14.5 - 21.7) | 15.9+0.8 (12.7 - 18) | 15.7+0.6 (14.4 - 17.2) |
| LASIK | | | | |
| CCT (microns) | 554.4+21.9 (511.2 - 603) | 450.6+33.6 (376.3 - 540.7) | 454.3+34.6 (377.4 - 538.8) | 453.8+33.3 (380.3 - 539) |
| CVSIOP (mmHg) | 13.9+1.9 (10.5 - 18.2) | 10+1.9 (6 - 14) | 10.1+1.8 (6.5 - 14.1) | 10.1+1.7 (6.7 - 14.9) |
| bIOP (mmHg) | 13.7+1.7 (10.1 - 18.4) | 12.1+1.7 (8.3 - 15.8) | 12.2+1.6 (9.4 - 15.9) | 12.1+1.6 (9.2 - 16) |
| bIOP2 (mmHg) | 15+1 (13.4 - 17.9) | 15.5+0.6 (14.2 - 17.1) | 15.4+0.7 (13.7 - 17.1) | 15.4+0.6 (14 - 16.8) |
| SMILE | | | | |
| CCT (microns) | 557+23.7 (506 - 634.7) | 458.2+23.7 (415 - 517.3) | 460.2+21.5 (420.5 - 518) | 459.4+21 (418 - 510) |
| CVSIOP (mmHg) | 14.1+1.9 (9.5 - 17.7) | 10.4+1.8 (7.1 - 17.5) | 10.3+1.8 (6.8 - 17.8) | 10.3+1.6 (7.8 - 14) |
| bIOP (mmHg) | 13.8+1.7 (9.4 - 16.9) | 12.5+1.8 (8.2 - 19.8) | 12.4+1.8 (8.3 - 20.3) | 12.4+1.6 (9.7 - 15.7) |
| bIOP2 (mmHg) | 15.1+1 (12.7 - 18.1) | 15.7+0.8 (13.9 - 18.7) | 15.5+0.7 (13.6 - 19.3) | 15.4+0.6 (13.8 - 16.8) |

Statistical analysis showed significant differences between all three IOP values and CCT when compared with preoperative measurements, Table 6-3. However, looking closely

at the differences between these values, CVSIOP had the largest differences and standard deviation with the mean of $3.7+2.0(-5.7 - 9.0)$ mmHg for all three surgeries. This was followed by bIOP with differences of $1.4+1.8(-8.3 - 6.3)$ mmHg and bIOP2 of $-0.5+0.9 (-5.4 - 3)$ mmHg. These results show that bIOP2 estimated postoperative IOP values more accurately than the other three while having the smallest standard deviation. It should be noted that on average the CVSIOP and bIOP underestimated IOP values, whereas bIOP2 slightly overestimated IOP by 0.5 mmHg in this dataset. This difference in IOP value is minimal and clinically has no impact on diagnosis.

Table 6-3 The differences between IOP measurements postoperatively in comparison to preoperative values for LASIK, SMILE and PRK surgeries in Dataset 3

| PRK | 1M Post (Diff) | 3M Post (Diff) | 6M Post (Diff) |
|---------------|------------------------------|------------------------------|------------------------------|
| CCT (microns) | 109.7+30.6 (21 - 175) | 110.6+32.2 (24.3 - 179) | 112.3+29.9 (44 - 175.4) |
| CVSIOP (mmHg) | 3.1+2.7 (-5.7 - 9) | 3.3+2 (-1 - 8) | 3.4+1.8 (-1.8 - 7.7) |
| bIOP (mmHg) | 0.6+2.5 (-8.3 - 6.3) | 0.9+1.8 (-2.8 - 5.5) | 1+1.7 (-3.1 - 5) |
| bIOP2 (mmHg) | -1+1.2 (-5.4 - 2.1) | -0.8+0.9 (-2.8 - 1.1) | -0.6+0.9 (-2.8 - 2.2) |
| LASIK | | | |
| CCT (microns) | 103.8+26.3 (51.1 - 163.7) | 100.1+27.3 (49.7 - 162.6) | 100.6+26.5 (52.8 - 166.9) |
| CVSIOP (mmHg) | 3.9+2 (-0.2 - 8.7) | 3.8+2.1 (-1 - 9) | 3.8+1.9 (-1.9 - 8) |
| bIOP (mmHg) | 1.6+1.8 (-2.2 - 5.9) | 1.6+1.9 (-2.4 - 6.1) | 1.6+1.7 (-3.3 - 5.4) |
| bIOP2 (mmHg) | -0.5+0.9 (-2.2 - 2.2) | -0.4+1 (-2 - 2.2) | -0.3+0.9 (-2.3 - 2) |
| SMILE | | | |
| CCT (microns) | 98.7+21.3 (62.3 - 151.7) | 96.7+20.3 (58 - 158) | 97.6+19.3 (54.3 - 152.7) |
| CVSIOP (mmHg) | 3.7+1.7 (-1 - 8) | 3.8+1.7 (-1.3 - 7.5) | 3.8+1.6 (0.8 - 7.8) |
| bIOP (mmHg) | 1.3+1.5 (-3 - 5) | 1.4+1.5 (-3.5 - 5) | 1.4+1.5 (-1.3 - 5.2) |
| bIOP2 (mmHg) | -0.6+0.9 (-2.3 - 2.4) | -0.4+0.9 (-2.7 - 3) | -0.3+0.9 (-2 - 2.9) |

In PRK data CVSIOP found to be correlated with CCT at all time points. bIOP and bIOP2 were both uncorrelated with CCT in preoperative data. However, in

postoperative data bIOP was found to be least correlated with CCT followed by bIOP2 and CVSIOP, Figure 6-17. The statistical comparison is provided in Table 6-4.

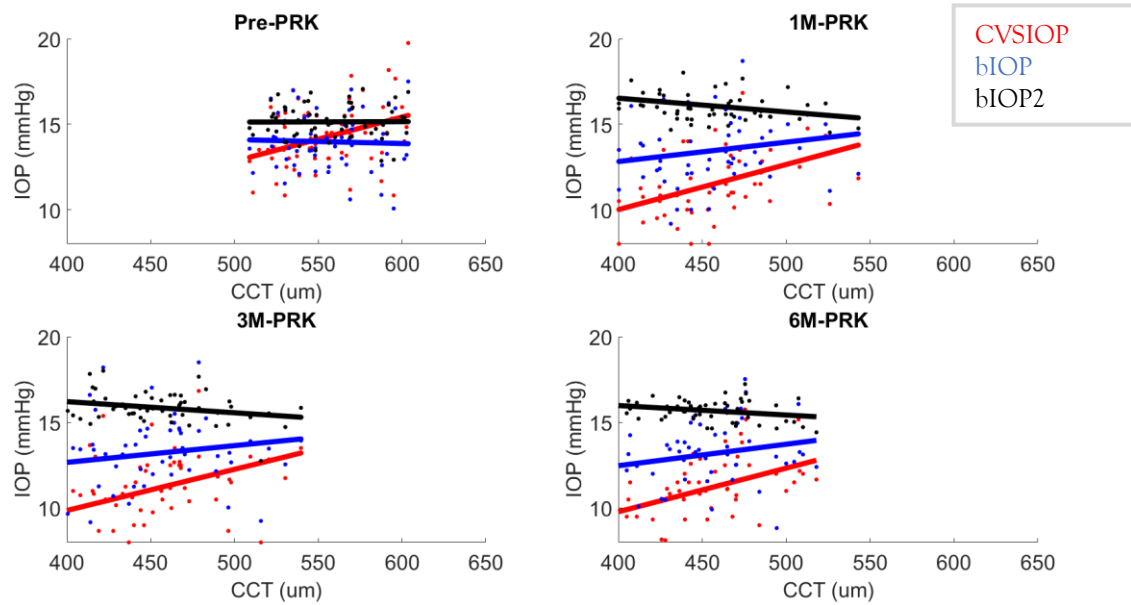


Figure 6-17 The correlation of IOP values with CCT in PRK data for preoperative and 1,3 and 6 months postoperative

Table 6-4 the R and p values for evaluating correlations of IOP values with CCT for preoperative and 1,3 and 6 months postoperative in PRK data

| | Pre | | 1M Post | | 3M Post | | 6M Post | |
|---------------|---------|---------|---------|---------|---------|---------|---------|---------|
| | R Value | p Value | R Value | p Value | R Value | p Value | R Value | p Value |
| CVSIOP (mmHg) | 0.363 | 0.004 | 0.419 | 0.001 | 0.464 | 0.000 | 0.506 | 0.000 |
| bIOP (mmHg) | -0.038 | 0.767 | 0.188 | 0.143 | 0.205 | 0.109 | 0.277 | 0.029 |
| bIOP2 (mmHg) | 0.007 | 0.956 | -0.300 | 0.018 | -0.327 | 0.009 | -0.339 | 0.007 |

In terms of PRK data, there was no significant correlation with age in all groups and all measurement methods, Figure 6-18. The difference between the three methods are small and detailed analysis is provided in Table 6-5.

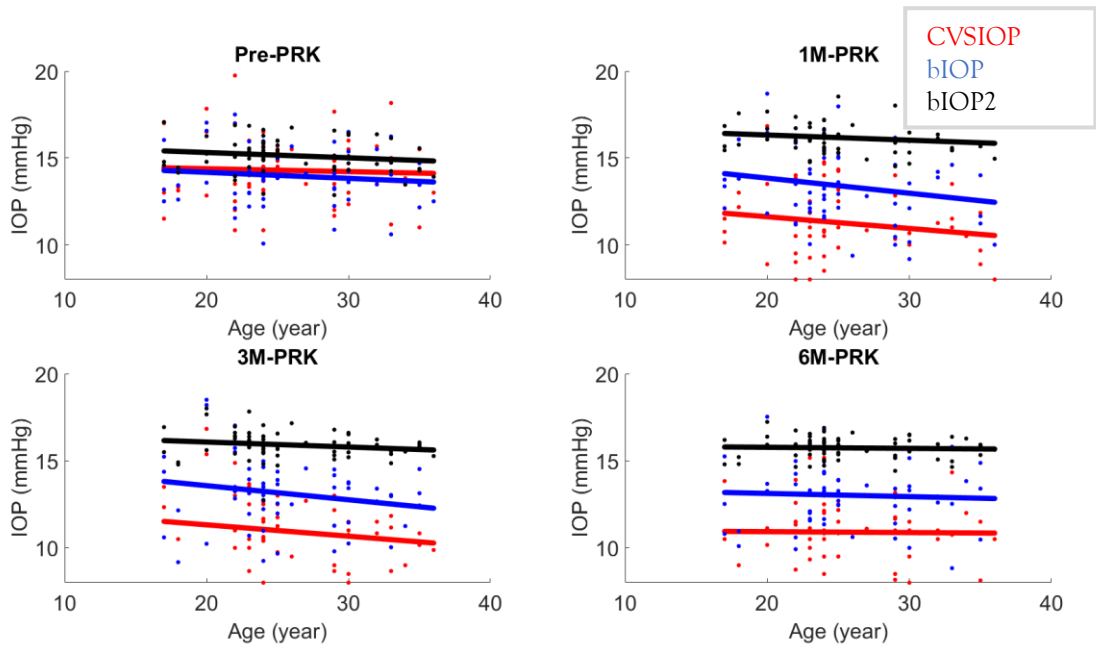


Figure 6-18 The correlation of IOP values with age in PRK data for preoperative and 1,3 and 6 months postoperative

Table 6-5 the R and p values for evaluating correlations of IOP values with age for preoperative and 1,3 and 6 months postoperative in PRK data

| | Pre | | 1M Post | | 3M Post | | 6MPost | |
|---------------|---------|---------|---------|---------|---------|---------|---------|---------|
| | R Value | p Value | R Value | p Value | R Value | p Value | R Value | p Value |
| CVSIOP (mmHg) | -0.043 | 0.738 | -0.129 | 0.318 | -0.148 | 0.252 | -0.013 | 0.922 |
| bIOP (mmHg) | -0.106 | 0.411 | -0.174 | 0.177 | -0.199 | 0.121 | -0.051 | 0.695 |
| bIOP2 (mmHg) | -0.154 | 0.232 | -0.133 | 0.301 | -0.168 | 0.191 | -0.048 | 0.712 |

In LASIK data, CVSIOP was correlated with CCT in all groups. bIOP was not correlated with CCT and bIOP2 was not correlated with CCT only in preoperative data. The postoperative CCT was negatively correlated with bIOP2, Figure 6-19. Detailed analysis provided in Table 6-6.

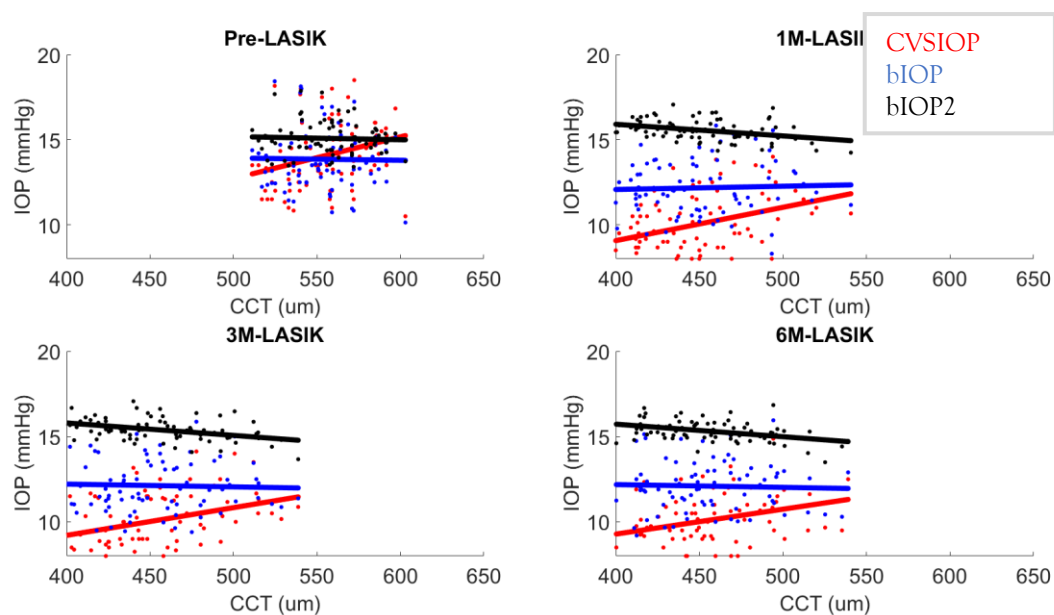


Figure 6-19 The correlation of IOP values with CCT in LASIK data for preoperative and 1,3 and 6 months postoperative

Table 6-6 the R and p values for evaluating correlations of IOP values with CCT for preoperative and 1,3 and 6 months postoperative in LASIK data

| | Pre | | 1M Post | | 3M Post | | 6M Post | |
|---------------|---------|---------|---------|---------|---------|---------|---------|---------|
| | R Value | p Value | R Value | p Value | R Value | p Value | R Value | p Value |
| CVSIOP (mmHg) | 0.277 | 0.013 | 0.364 | 0.001 | 0.325 | 0.003 | 0.305 | 0.006 |
| bIOP (mmHg) | -0.017 | 0.880 | 0.039 | 0.732 | -0.036 | 0.754 | -0.036 | 0.748 |
| bIOP2 (mmHg) | -0.043 | 0.703 | -0.370 | 0.001 | -0.384 | 0.000 | -0.412 | 0.000 |

In LASIK data, there was no correlation with age in all groups and all measurements, Figure 6-20. The detailed analysis is provided in Table 6-7. Correlations remained weak in all and especially with bIOP and bIOP2.

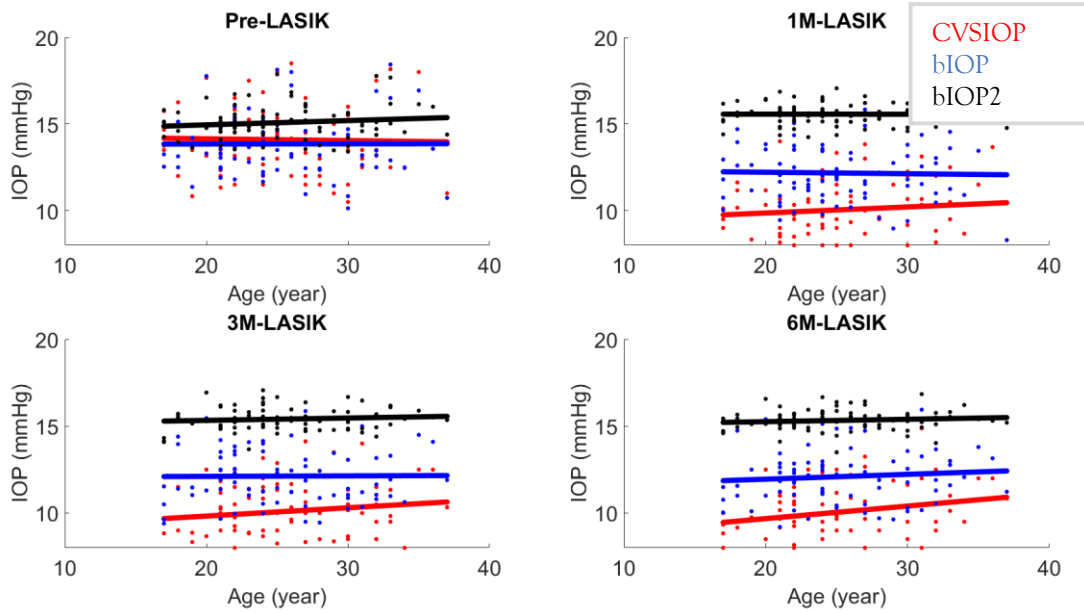


Figure 6-20 The correlation of IOP values with age in LASIK data for preoperative and 1,3 and 6 months postoperative

Table 6-7 the R and p values for evaluating correlations of IOP values with age for preoperative and 1,3 and 6 months postoperative in LASIK data

| Age/ LASIK | Pre | | 1M Post | | 3M Post | | 6MPost | |
|---------------|---------|---------|---------|---------|---------|---------|---------|---------|
| | R Value | p Value | R Value | p Value | R Value | p Value | R Value | p Value |
| CVSIOP (mmHg) | -0.025 | 0.826 | 0.094 | 0.407 | 0.135 | 0.231 | 0.218 | 0.052 |
| bIOP (mmHg) | 0.003 | 0.981 | -0.025 | 0.824 | 0.009 | 0.937 | 0.090 | 0.427 |
| bIOP2 (mmHg) | 0.125 | 0.270 | -0.002 | 0.983 | 0.102 | 0.369 | 0.112 | 0.323 |

In SMILE data, correlation with CCT was weak with bIOP in all cases. The bIOP correlation was not significant in pre-op and six months post-op, but it was significant in other groups. CVSIOP was also not significantly correlated with CCT in this case, Figure 6-21. Detailed analysis provided in Table 6-8

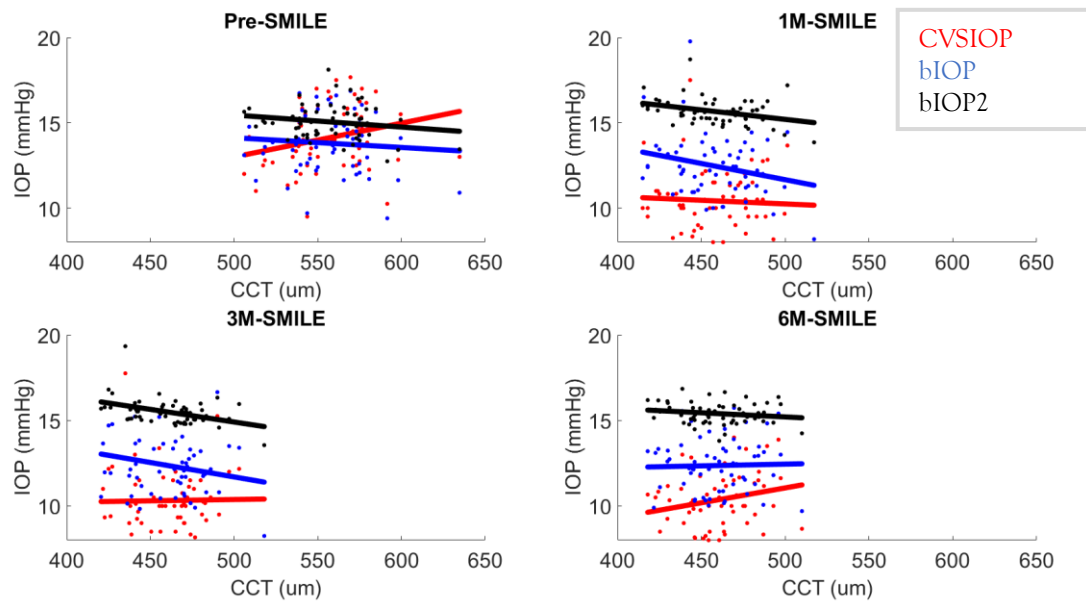


Figure 6-21 The correlation of IOP values with CCT in SMILE data for preoperative and 1,3 and 6 months postoperative

Table 6-8 the R and p values for evaluating correlations of IOP values with CCT for preoperative and 1,3 and 6 months postoperative in SMILE data

| CCT/ SMILE | Pre | | 1M Post | | 3M Post | | 6MPost | |
|------------------|------------|------------|------------|------------|------------|------------|------------|------------|
| | R Value | p Value | R Value | p Value | R Value | p Value | R Value | p Value |
| CVSIOP (mmHg) | 0.251 | 0.053 | -0.055 | 0.674 | 0.018 | 0.892 | 0.229 | 0.079 |
| bIOP (mmHg) | -0.079 | 0.548 | -0.243 | 0.061 | -0.197 | 0.131 | 0.027 | 0.835 |
| bIOP2 (mmHg) | -0.169 | 0.196 | -0.348 | 0.006 | -0.426 | 0.001 | -0.167 | 0.202 |

The correlation with age in SMILE group, similar to others, remained not significant with all measurements and all groups, Figure 6-22. Detailed analysis is provided in Table 6-9.

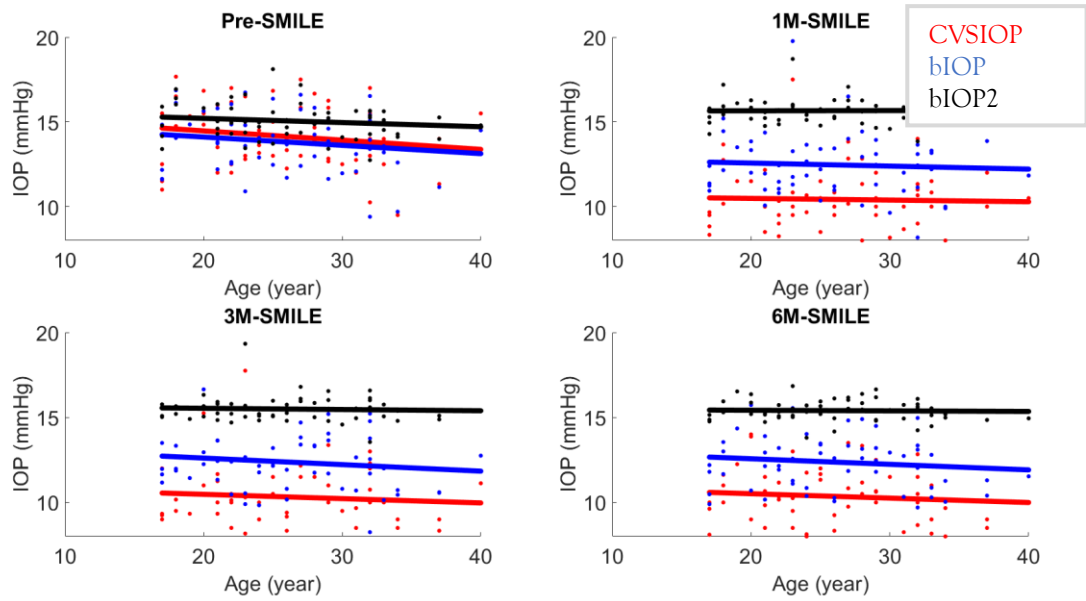


Figure 6-22 The correlation of IOP values with age in SMILE data for preoperative and 1,3 and 6 months postoperative

Table 6-9 the R and p values for evaluating correlations of IOP values with age for preoperative and 1,3 and 6 months postoperative in SMILE data

| Age/ SMILE | Pre | | 1M Post | | 3M Post | | 6MPost | |
|---------------|---------|---------|---------|---------|---------|---------|---------|---------|
| | R Value | p Value | R Value | p Value | R Value | p Value | R Value | p Value |
| CVSIOP (mmHg) | -0.176 | 0.179 | -0.032 | 0.806 | -0.083 | 0.527 | -0.098 | 0.456 |
| bIOP (mmHg) | -0.173 | 0.187 | -0.058 | 0.658 | -0.126 | 0.337 | -0.127 | 0.332 |
| bIOP2 (mmHg) | -0.151 | 0.249 | 0.011 | 0.936 | -0.059 | 0.657 | -0.035 | 0.791 |

CXL Data

Dataset 2

Dataset 2 includes 37 KC patients who undergo CXL with mean age of 22.0 ± 5.0 (14 - 31) and CCT of 482.5 ± 30.5 (447 - 567) microns. The three mean IOP values for CVSIOP was 13.6 ± 2.2 (10.5 - 20.0) mmHg, with bIOP of 15.1 ± 2.0 (12.5 - 21.1) mmHg and bIOP2 of 16.1 ± 1.0 (14.5 - 18.8) mmHg. Correlation with age was not significant for CVSIOP (R: -0.1834, p: 0.2773), bIOP (R: -0.2587, p: 0.1221) and bIOP2 (R: -0.1011, p: 0.5514). Correlation with CCT was significant for CVSIOP (R: 0.3938, p: 0.0159) and insignificant for bIOP (R: 0.0609, p: 0.7205) and bIOP2 (R: 0.0525, p: 0.7578), Figure 6-23.

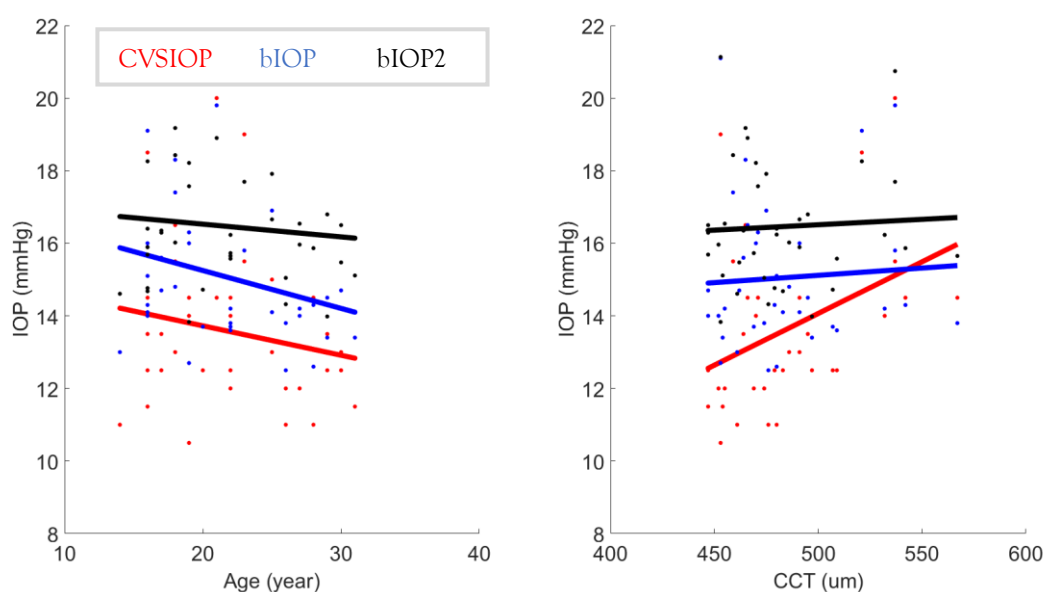


Figure 6-23 Correlation of IOP values from CVSIOP, bIOP and bIOP2 with CCT (left) and age (right) in Pre CXL Dataset 2

In dataset 2 post CXL, mean CCT was 487 ± 29 (444 - 569) microns with CVSIOP of 14.0 ± 2.4 (9.5 - 21.5) mmHg, bIOP of 15.5 ± 2.1 (11.9 - 21.5) mmHg and bIOP2 of 16.1 ± 1 (14.4 - 19.0) mmHg. The correlation with age was not significant for CVSIOP (R: -0.1952, p: 0.2469), bIOP (R: -0.2511, p: 0.1338) and bIOP2 (R: -0.0396, p: 0.8162). CCT was significantly correlated with CVSIOP (R: 0.3955, p: 0.0154) but not significant with bIOP (R: 0.1107, p: 0.5144) and bIOP2 (R: 0.1177, p: 0.4877), Figure 6-24.

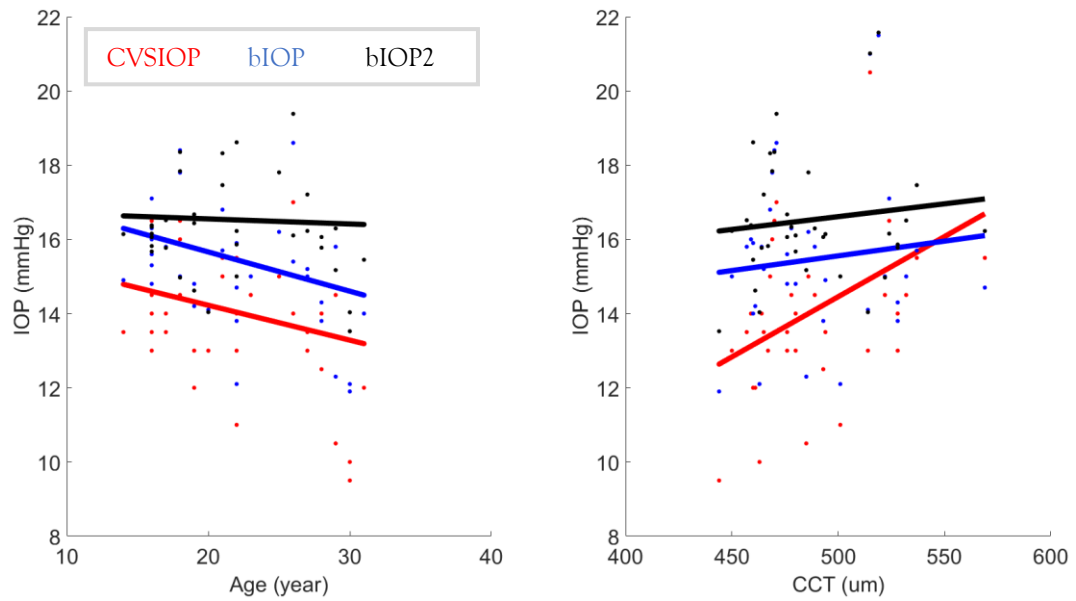


Figure 6-24 Correlation of IOP values from CVSIOP, bIOP and bIOP2 with CCT (left) and age (right) in Post CXL Dataset 2

The mean differences of CVSIOP was -0.47 ± 2.32 (-8.5 - 4.5) mmHg (p: 0.230), bIOP was -0.41 ± 2.09 (-7.4 - 4.1) mmHg (p:0.245), and bIOP2 -0.04 ± 0.99 (-2.86 -1.91) mmHg (p: 0.815). It clearly shows that bIOP2 improved on both standard deviations and mean differences in comparison to bIOP when pre and post-CXL data were compared.

Dataset 3

Dataset 3 includes 21 KC patients who undergo CXL with mean age of 29.2 ± 7.2 (18 - 41) years and CCT of 484 ± 31 (421 - 544) microns. The mean measurements of CVSIOP was 13.1 ± 2.9 (7.5 -18.5) mmHg, with bIOP of 14.4 ± 2.6 (9.8 -19.9) mmHg and bIOP2 of 15.9 ± 1.0 (14.4 -18.0) mmHg. The correlation with age was not significant for CVSIOP (R: -0.0704, p: 0.7616), bIOP (R: -0.1823, p: 0.4291) and bIOP2 (R: -0.0915, p: 0.6934). Correlations with CCT was significant for CVSIOP (R: 0.4417, p: 0.0450) but not significant for bIOP (R: 0.2212, p: 0.3353) and bIOP2 (R: 0.0639, p: 0.7830), Figure 6-25.

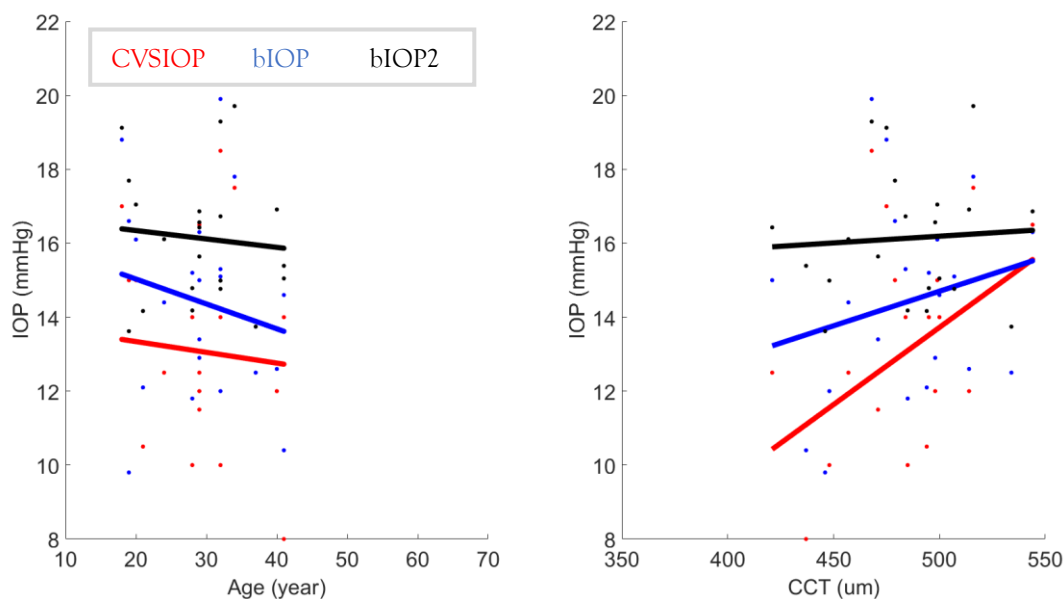


Figure 6-25 Correlation of IOP values from CVSIOP, bIOP and bIOP2 with CCT (left) and age (right) in Pre CXL Dataset 3

In post CXL data, mean CCT was 455 ± 43 (332 -523) microns, with CVSIOP of 14.1 ± 2.4 (9.5 -19) mmHg, bIOP of 16.0 ± 2.1 (11.2 -19.5) mmHg and bIOP2 of 16.5 ± 1.2 (13.8 -18.6) mmHg. The correlation with age was not significant for CVSIOP (R: 0.1793, p: 0.4368), bIOP (R: 0.0436, p: 0.8513) and bIOP2 (R: 0.3455, p: 0.1251). Correlation with CCT was significant with CVSIOP (R: 0.4760, p: 0.0292) but not significant for bIOP (R: 0.1988, p: 0.3875) and bIOP2 (R: -0.1962, p: 0.3941), Figure 6-26.

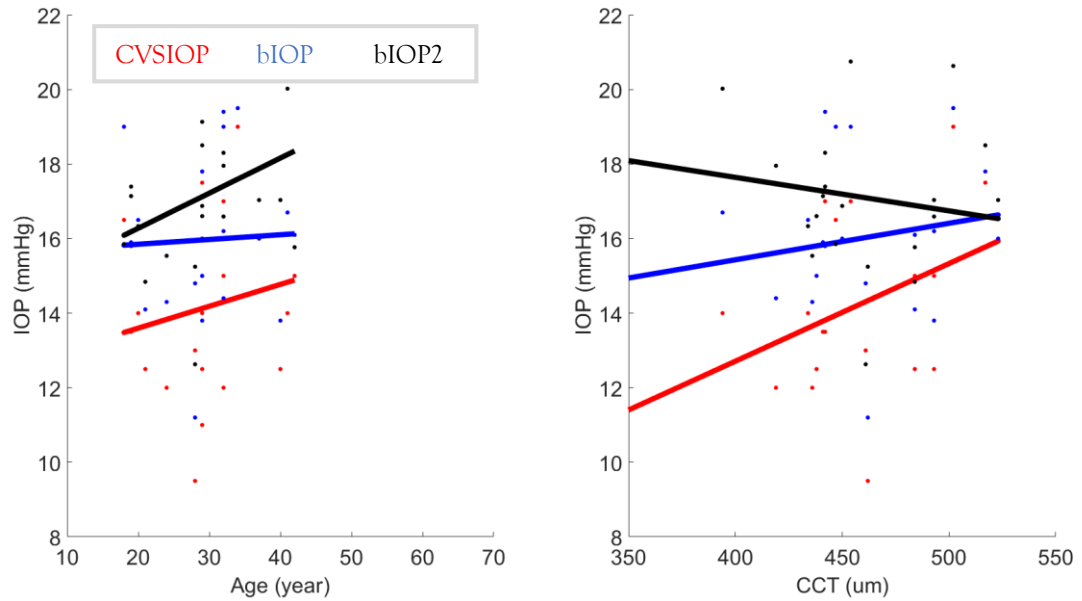


Figure 6-26 Correlation of IOP values from CVSIOP, bIOP and bIOP2 with CCT (left) and age (right) in Post CXL Dataset 2

The differences between pre and post for CVSIOP were $-1.07 \pm 2.22 (-6 -1.5)$ mmHg (p:0.64), with bIOP of $-1.56 \pm 2.07 (-6.3 -1.2)$ mmHg (p:0.004), and bIOP2 of $-0.59 \pm 1.18 (-2.69 -1.9)$ mmHg (p:0.053). This clearly shows that EIOP improved on standard deviation and the mean differences in comparison to bIOP.

Dataset 4

This dataset includes 69 KC eyes undergo CXL with mean age of 26.1 ± 8.8 (13 -56) years, CCT of 481.5 ± 37.8 (404 -565) microns, CVSIOP of 11.8 ± 2.5 (6 -19) mmHg, bIOP was 13.3 ± 2.4 (7.8 -21.1) mmHg and bIOP2 of 15 ± 1.2 (11.8 -18.5) mmHg. The correlation with CCT for Corvis ST IOP was significant (R:0.318, p:0.0077) while both bIOP2 (R:0.0393, p:0.7486) and bIOP (R:0.0133, p:0.9138) remained insignificant. The correlation with age for Corvis ST IOP (R:-0.0193, p:0.8752), bIOP2 (R:0.0064, p:0.9585) and bIOP (R:-0.0508, p:0.6782) was not significant, Figure 6-27.

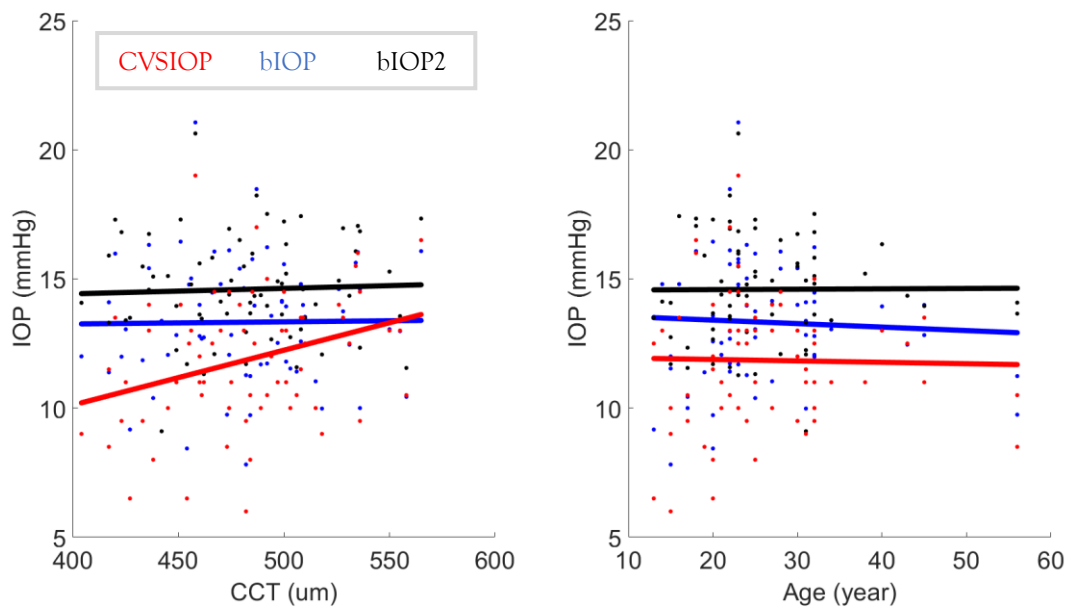


Figure 6-27 Correlation of IOP values from CVSIOP, bIOP and bIOP2 with CCT (left) and age (right) in Pre CXL Dataset 4

One month post operative data demographics showed mean age of 26.3 ± 8.8 (13 -56) years, CCT of 466.8 ± 42.3 (358 -572) microns, CVSIOP of 14.1 ± 2.8 (5.5 -22) mmHg, bIOP of 15.8 ± 2.9 (8.4 -24.2) mmHg and bIOP2 of 16.1 ± 1.6 (13.5-21.3) mmHg. The correlation with CCT was not significant for CVSIOP (R:0.1001, p:0.413), bIOP2 (R: -0.15, p:0.2187) and bIOP (R:-0.1984, p:0.1022). The correlation with age for CVSIOP (R:0.122, p:0.318), bIOP2 (R:0.1393, p:0.2537) and bIOP (R:0.0424, p:0.7296) remained insignificant, Figure 6-28.

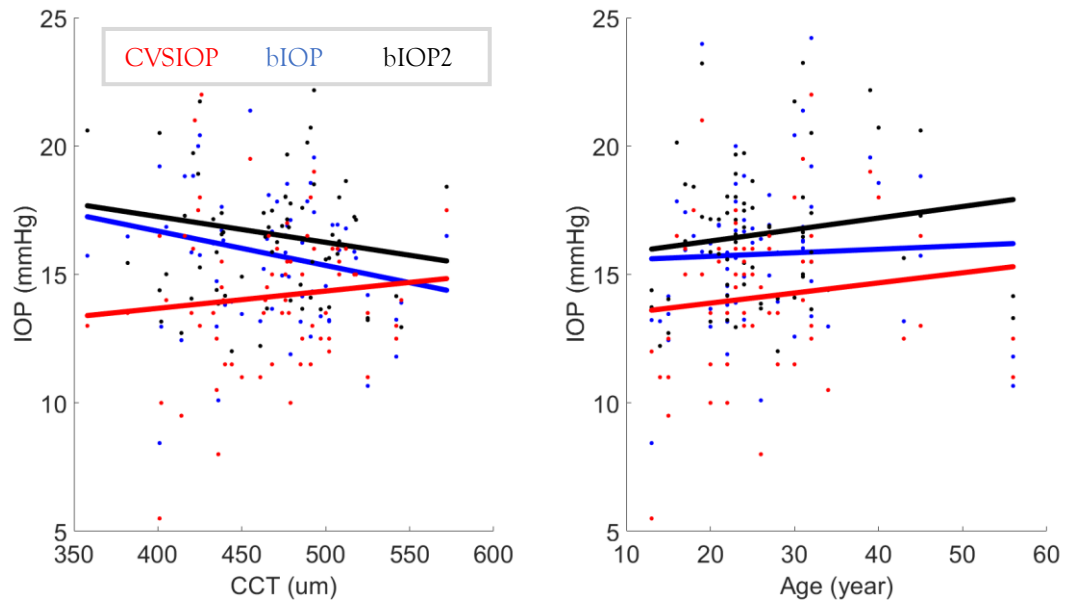


Figure 6-28 Correlation of IOP values from CVSIOP, bIOP and bIOP2 with CCT (left) and age (right) in Post CXL Dataset 4

The differences between pre and post for CVSIOP were -2.3 ± 3.1 (-12.5 -2.5) mmHg ($p < 0.001$), with bIOP of -2.5 ± 3 (-12.6 -2.9) mmHg ($p < 0.001$), and bIOP2 of -1.2 ± 1.6 (-5 -2.6) mmHg ($p < 0.001$). This clearly shows that EIOP improved on standard deviation and the mean differences in comparison to bIOP.

Glaucoma Patients

Dataset 2

Dataset 2 includes healthy, Normal Tension Glaucoma (NTG), HTG and OHT. Healthy group with 37 patients had mean age of 72.2 ± 10.4 (51.0 -87.0) years, CCT of 554 ± 33 (487 -626) microns and IOP was measured using GAT and Corvis ST. The CVSIOP was 15.4 ± 2.9 (10.5 -26.5) mmHg with bIOP of 13.4 ± 2.8 (7.7 -23.6) mmHg, bIOP2 of 15.0 ± 1.7 (12.3 -21.7) mmHg, GAT of 16.4 ± 1.7 (12.3 -21.7) mmHg and adjusted GAT (AdjGAT) of 15.4 ± 1.7 (12.3 -21.7) mmHg. CVSIOP ($p:0.830$, $R:-0.036$), GAT ($p:0.350$, $R:0.165$) and bIOP2 ($p:0.116$, $R:-0.263$) showed no significant correlations with CCT, whereas bIOP ($p:0.035$, $R:-0.347$) and AdjGAT ($p:0.000$, $R:-0.685$) values were correlated. Correlation with age was not significant in CVSIOP ($p:0.724$, $R:0.060$), bIOP ($p:0.981$, $R:0.004$), bIOP2 ($p:0.860$, $R:-0.030$), GAT ($p:0.109$, $R:-0.280$) and AdjGAT ($p:0.903$, $R:0.022$), Figure 6-29.

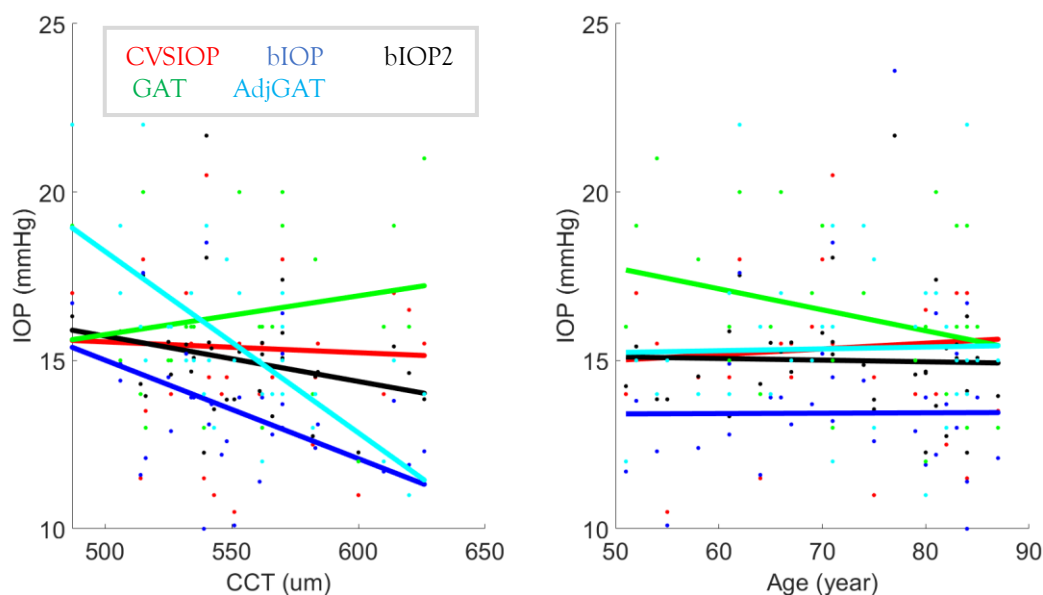


Figure 6-29 Correlation of IOP values from CVSIOP, bIOP and bIOP2 with CCT (left) and age (right) in healthy group of Dataset 2

In NTG group with 33 patients had mean age of 75.7 ± 9.7 (47.0 -87.0) years and CCT of 504 ± 34 (430 -573) microns. Mean IOP measurements for CVSIOP was 13.4 ± 2.4 (8.5 - 17.5) mmHg, with bIOP of 12.9 ± 2.3 (8.9 -18.3) mmHg, bIOP2 of 14.4 ± 1.0 (12.3 - 16.6) mmHg, GAT of 13.7 ± 1.0 (12.3 -16.6) mmHg and AdjGAT of 16.3 ± 1.0 (12.3 - 16.6) mmHg. Correlation with CCT was significant for AdjGAT ($p:0.000$, $R:-0.650$) and not significant in GAT ($p:0.621$, $R:0.100$), bIOP ($p:0.172$, $R:-0.243$), CVSIOP ($p:0.319$, $R:0.179$) and bIOP2 ($p:0.230$, $R:-0.215$). Age was not correlated significantly with bIOP ($p:0.608$, $R:-0.093$), CVSIOP ($p:0.790$, $R:0.048$), bIOP2 ($p:0.082$, $R:-0.308$), GAT ($p:0.187$, $R:-0.262$) and AdjGAT ($p:0.823$, $R:-0.045$), Figure 6-30.

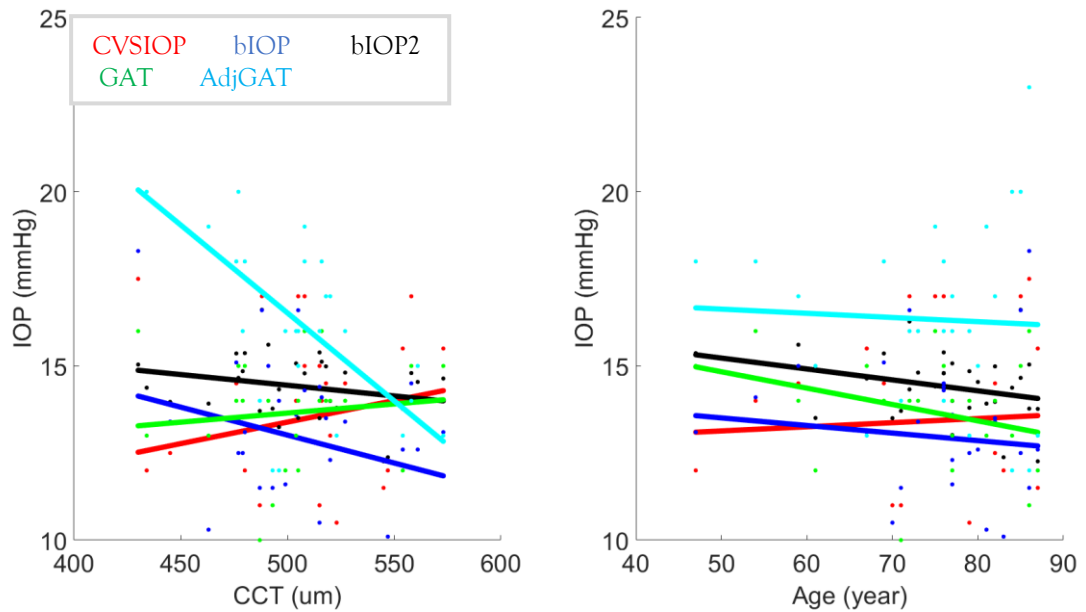


Figure 6-30 Correlation of IOP values from CVSIOP, bIOP and bIOP2 with CCT (left) and age (right) in NTG group of Dataset 2

In HTG group with 41 cases, patients had mean age of 71.4 ± 10.3 (38.0 -91.0) years and CCT of 523 ± 31 (451 -597) microns. Mean IOP measurements showed bIOP of 14.8 ± 3.1 (10.8 -25.8) mmHg, CVSIOP of 15.8 ± 3.6 (11.0 -27.5) mmHg, bIOP2 of 15.8 ± 1.9 (13.0 -22.6) mmHg, GAT of 17.2 ± 1.9 (13.0 -22.6) mmHg and AdjGAT of 18.6 ± 1.9 (13.0 -22.6) mmHg. Correlation with CCT was significant with GAT ($p:0.011$, $R: 0.437$) and insignificant with bIOP ($p:0.648$, $R:0.073$), CVSIOP ($p:0.052$, $R:0.306$), bIOP2 ($p:0.516$, $R:0.104$) and AdjGAT ($p:0.568$, $R:0.105$). Age had no correlation with bIOP ($p:0.835$, $R:-0.034$), CVSIOP ($p:0.949$, $R:0.010$), bIOP2 ($p:0.588$, $R:-0.087$), GAT ($p:0.780$, $R:-0.051$) and AdjGAT ($p:0.831$, $R:0.039$), Figure 6-31.

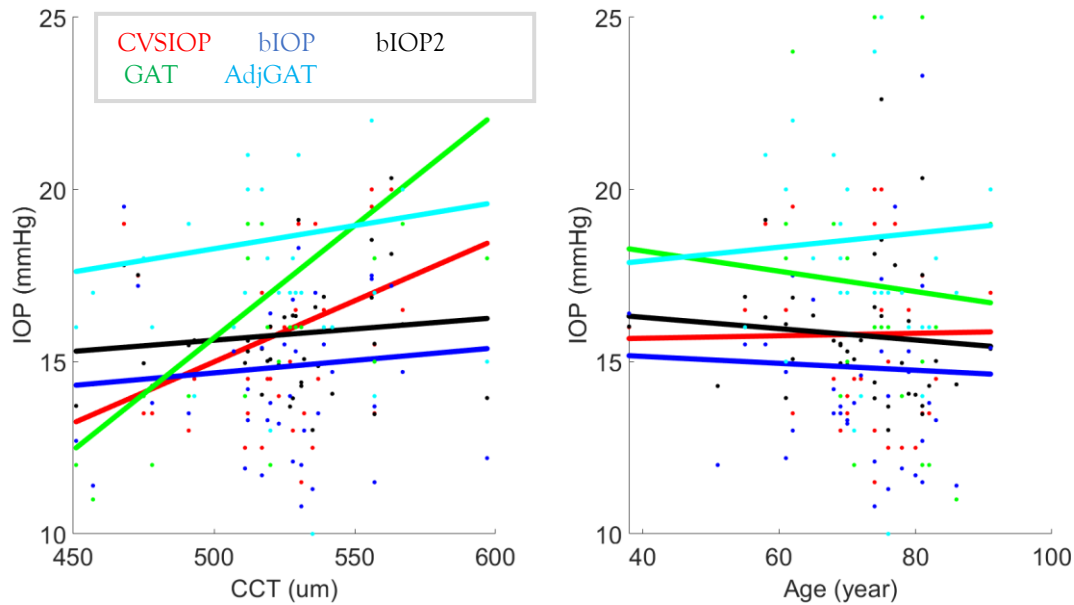


Figure 6-31 Correlation of IOP values from CVSIOP, bIOP and bIOP2 with CCT (left) and age (right) in HTG group of Dataset 2

Patients with OHT were 45 cases with mean age of 60.3 ± 12.1 (20.0 -85.0) years and CCT of 547 ± 53 (352 -640) microns. IOP measurements showed mean bIOP of 17.0 ± 4.1 (10.4 -29.1) mmHg, CVSIOP of 18.8 ± 4.8 (8.5 -30.5) mmHg, bIOP2 of 17.6 ± 2.4 (13.6 -23.8) mmHg, GAT of 22.0 ± 2.4 (13.6 -23.8) mmHg and AdjGAT of 20.7 ± 2.4 (13.6 -23.8) mmHg. There was significant correlations with CCT for CVSIOP ($p:0.026$, $R:0.332$) and AdjGAT ($p:0.001$, $R:-0.521$) and no correlation with bIOP ($p:0.940$, $R:0.012$), bIOP2 ($p:0.811$, $R:-0.037$) and GAT ($p:0.809$, $R:-0.041$). Age had significant correlation with CVSIOP ($p:0.042$, $R:0.304$) and no significant correlation with bIOP ($p:0.249$, $R:0.176$), bIOP2 ($p:0.411$, $R:0.125$), GAT ($p:0.974$, $R:-0.005$) and AdjGAT ($p:0.404$, $R:0.141$), Figure 6-32.

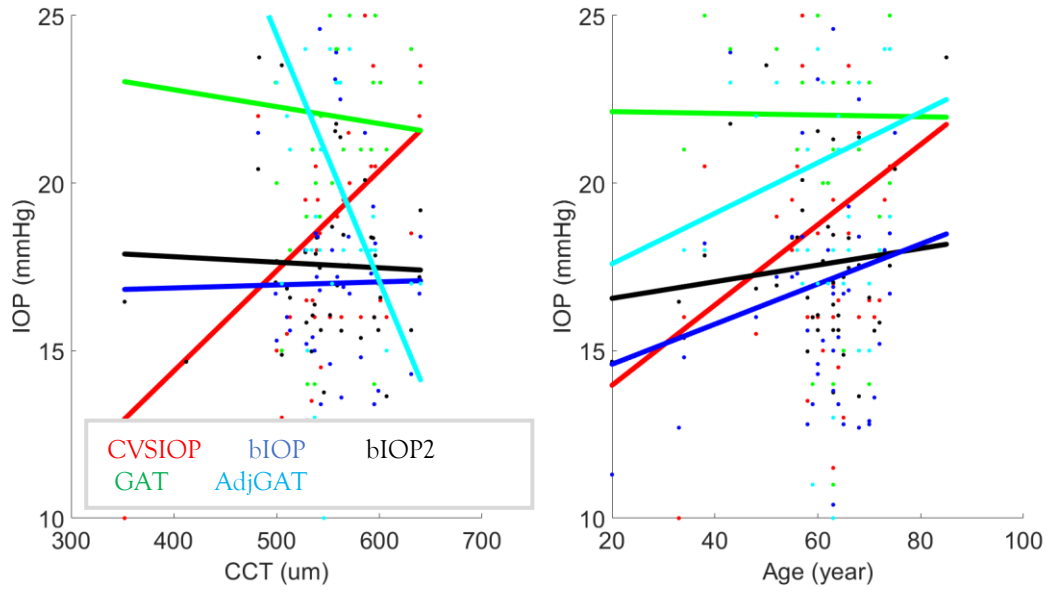


Figure 6-32 Correlation of IOP values from CVSIOP, bIOP and bIOP2 with CCT (left) and age (right) in OHT group of Dataset 2

Keratoconus Patients

Dataset2

This data includes 143 KC eyes with mean age of 33.9 ± 14.9 (14.0 -80.0) years, CCT of 495 ± 40 (315 -597) microns, bIOP of 14.1 ± 2.0 (9.6 -20.0) mmHg, CVSIOP of 13.1 ± 2.3 (7.0 -20.5) mmHg, bIOP2 of 15.5 ± 1.1 (12.5 -19.0) mmHg. Both bIOP ($p:0.771$, $R:0.025$) and bIOP2 ($p:0.123$, $R:-0.130$) were not correlated with CCT while CVSIOP ($p:0.000$, $R:0.385$) correlation was significant. Correlartin with age followed similar pattern were bIOP ($p:0.317$, $R:0.084$) and bIOP2 ($p:0.309$, $R:0.086$) were not correlated and CVSIOP ($p:0.011$, $R:0.213$) was significantly correlated, Figure 6-33.

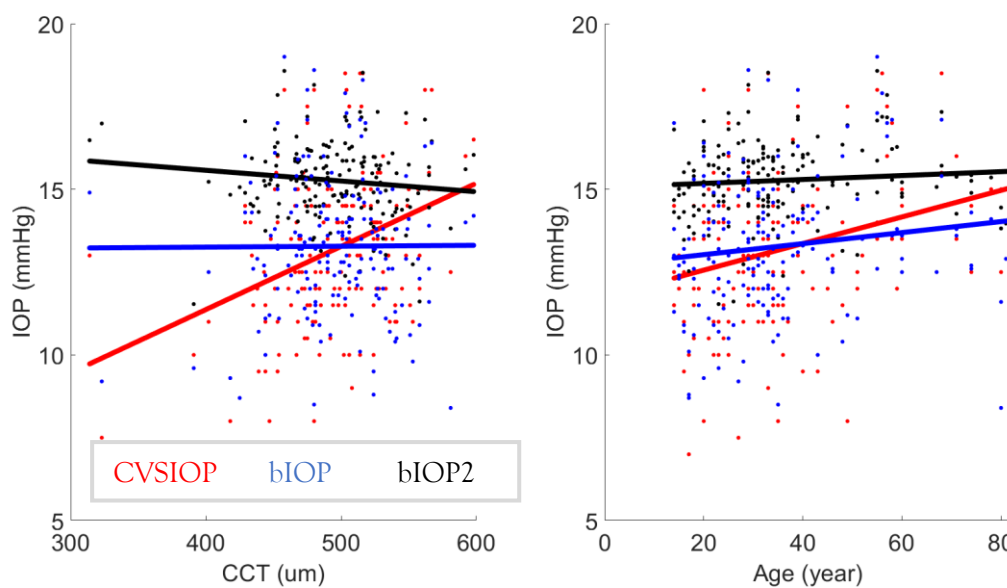


Figure 6-33 Correlation of IOP values from CVSIOP, bIOP and bIOP2 with CCT (left) and age (right) in KC Dataset 2

Comparison of IOP values with the healthy group (based on disease severity) showed no significant differences with FFKC ($p: 0.1100$), Mild ($p: 0.3252$), Moderate ($p: 0.2390$) and Severe ($p: 0.7709$) groups for bIOP2. However, bIOP was significantly different in all cases ($p<0.001$), Figure 6-34.

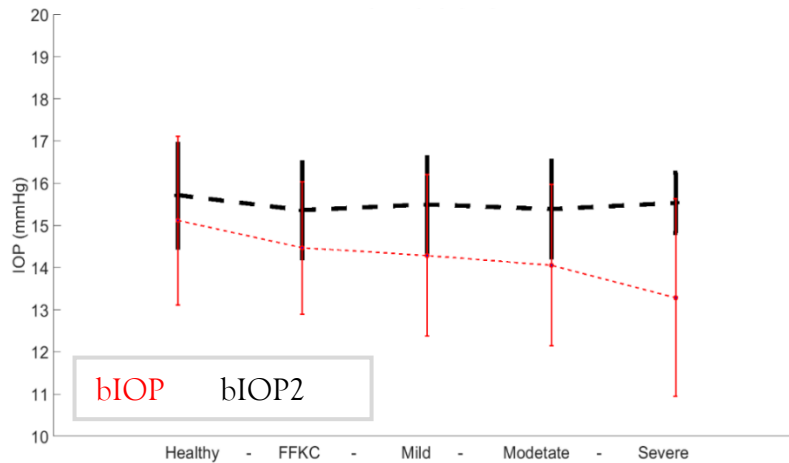


Figure 6-34 The changes in bIOP2 and bIOP in healthy, FFKC, Mild, Moderate and Severe keratoconic cases in Dataset 2

Dataset 3

This dataset consist of 363 KC eyes with mean age of 33.2 ± 10.8 (13.0 -72.0) years, CCT of 492 ± 40 (345 -590) microns, bIOP of 13.5 ± 2.3 (7.4 -23.4) mmHg, CVSIOP of 12.3 ± 2.5 (6.0 -23.5) mmHg, bIOP2 of 15.5 ± 1.1 (11.5 -20.2) mmHg. The correlation with CCT was not significant in bIOP ($p:0.549$, $R:-0.032$) and it was significant with both bIOP2 ($p:0.009$, $R:-0.137$) and CVSIOP ($p:0.000$, $R:0.311$). Correlation with age was not significant with bIOP ($p:0.111$, $R:-0.084$), CVSIOP ($p:0.874$, $R:0.008$) and bIOP2 ($p:0.891$, $R:-0.007$), Figure 6-35.

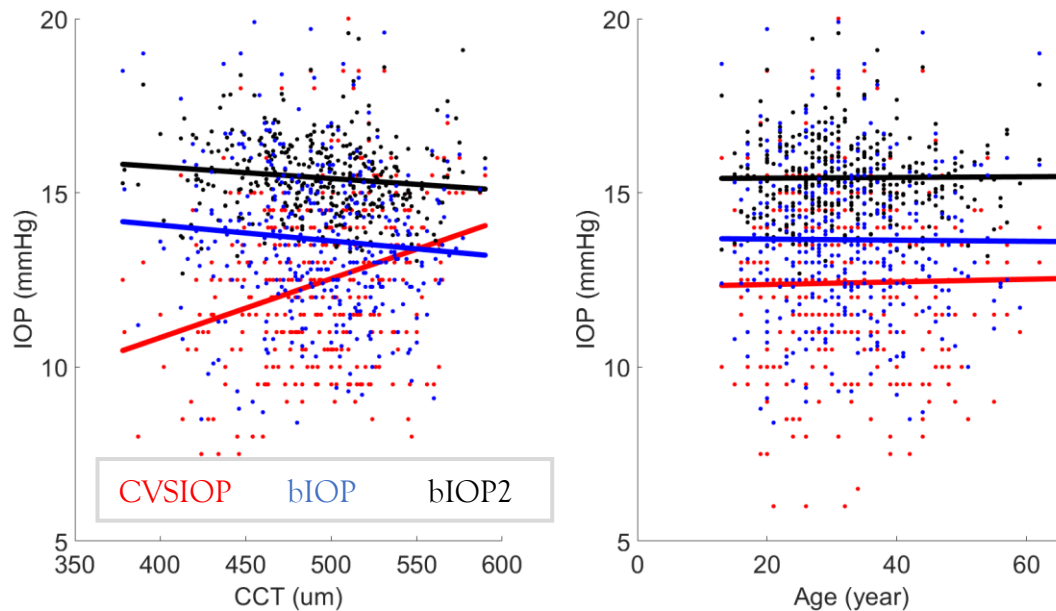


Figure 6-35 Correlation of IOP values from CVSIOP, bIOP and bIOP2 with CCT (left) and age (right) in KC Dataset 3

The comparison of IOP values with the healthy group (based on disease severity) showed significant differences with FFKC ($p: 0.0083$) group, and no significant differences with

Mild ($p: 0.1553$), Moderate ($p: 0.7524$) and Severe ($P: 0.7698$) KC cases for bIOP2. IOP was significantly different ($p < 0.001$) in all cases with bIOP values, Figure 6-36.

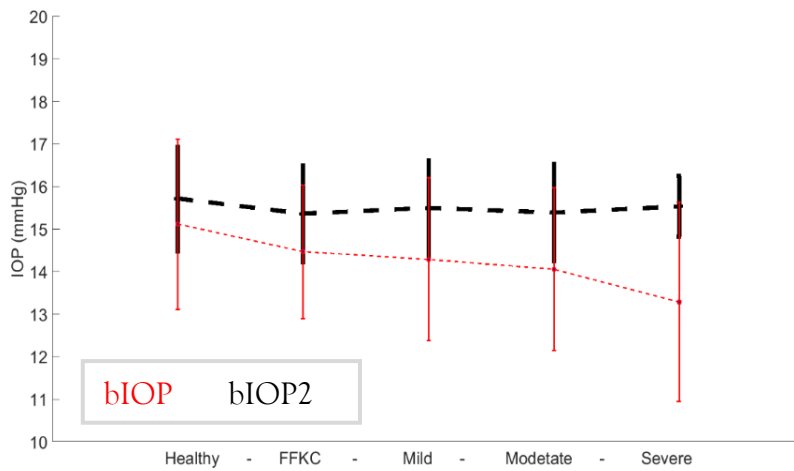
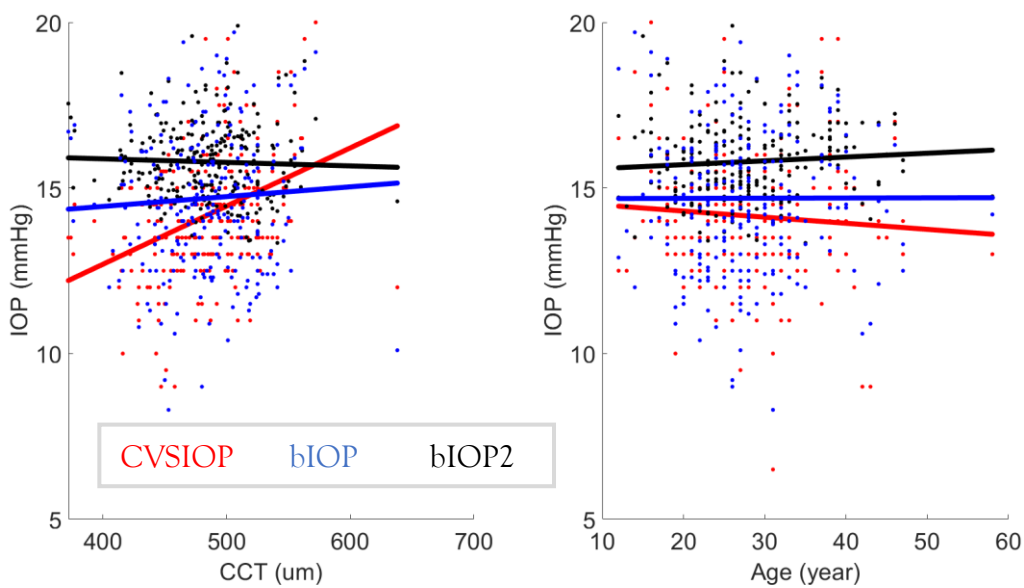


Figure 6-36 The changes in bIOP2 and bIOP in healthy, FFKC, Mild, Moderate and Severe keratoconic cases in Dataset 3

Dataset 4

This dataset consist of 227 KC eyes with mean age of 27.6 ± 7.5 (12.0 -58.0) years, CCT of 482 ± 40 (374 -636) microns, bIOP of 15.6 ± 1.9 (8.5 -23.3) mmHg, CVSIOP of 14.2 ± 2.1 (6.5 -21.5) mmHg and bIOP2 of 15.9 ± 1.1 (13.3 -19.9) mmHg. Correlation with CCT was not significant for bIOP ($p:0.204$, $R:-0.085$) and bIOP2 ($p:0.533$, $R: -0.042$) but sificant with CVSIOP ($p:0.000$, $R:0.339$). Correlation with age was signfiicnat for bIOP ($p:0.033$, $R:-0.142$) and insignificant for CVSIOP ($p:0.540$, $R: -0.041$) and bIOP2 ($p:0.529$, $R:0.042$), Figure 6-37.



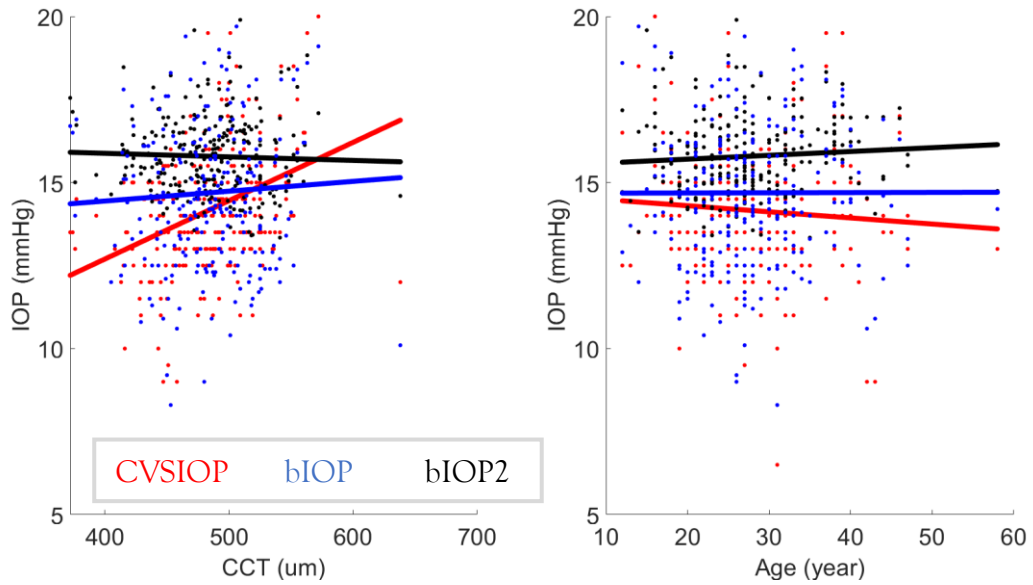


Figure 6-37 Correlation of IOP values from CVSIOP, bIOP and bIOP2 with CCT (left) and age (right) in KC Dataset 4

The comparison of IOP values with the healthy group (based on disease severity) showed bIOP was not significantly different in FFKC (p: 0.9856), Mild (p: 0.3665), Moderate (p: 0.1882) and Severe (p: 0.0893) groups. Similarly bIOP2 showed no significant differences with FFKC (p: 0.0829), Mild (p: 0.3673), Moderate (p: 0.4374) and Severe (p: 0.1849) cases, Figure 6-38.

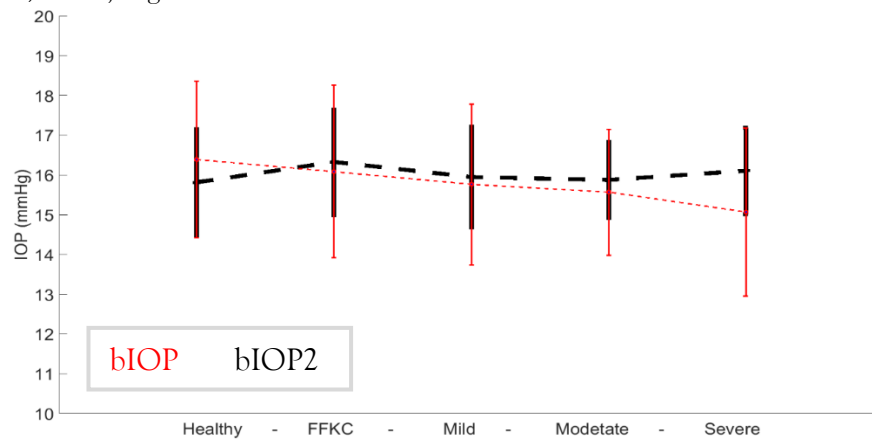


Figure 6-38 The changes in bIOP2 and bIOP in healthy, FFKC, Mild, Moderate and Severe keratoconic cases in Dataset 4

Dataset 5

Consist of 14 KC eyes with mean age of 33.6 ± 12.2 (20.0 -66.0) years, CCT of 484 ± 22 (451 - 529) microns, bIOP of 13.9 ± 1.8 (11.8 -16.7) mmHg, CVSIOP of 12.6 ± 2.0 (10.0 - 15.5) mmHg and bIOP2 of 15.3 ± 1.1 (13.4 -17.1) mmHg. Correlation with CCT was significant with CVSIOP (p:0.021, R:0.608) but not significant with bIOP2 (p:0.145, R:0.410) and bIOP (p:0.148, R:0.407). There was no correlation with age in bIOP (p:0.233, R:-0.341), CVSIOP (p:0.618, R:-0.146) and bIOP2 (p:0.699, R:-0.114), Figure 6-39.

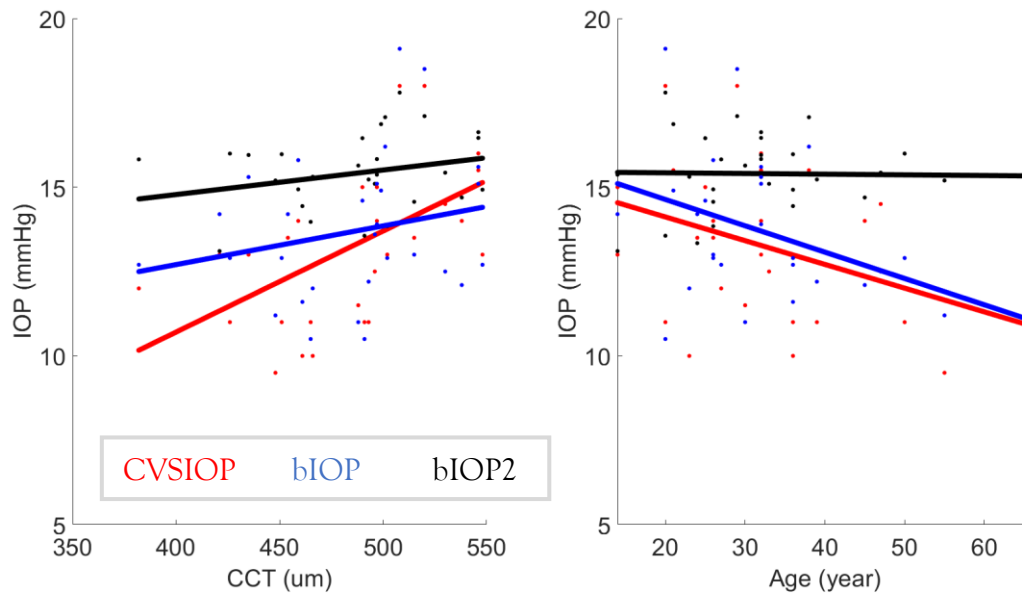


Figure 6-39 Correlation of IOP values from CVSIOP, bIOP and bIOP2 with CCT (left) and age (right) in KC Dataset 5

The comparison of IOP values with the healthy group (based on disease severity) showed no significant differences with bIOP2 in FFKC ($p: 0.4398$), Mild ($p: 0.1625$), Moderate ($p: 0.6866$) and Severe ($p: 0.5159$) groups. Whereas the bIOP was significant in Mild ($p: 0.0050$) group and not significant in FFKC ($p: 0.1723$), Moderate ($p: 0.0878$) and Severe ($p: 0.0969$), Figure 6-40.

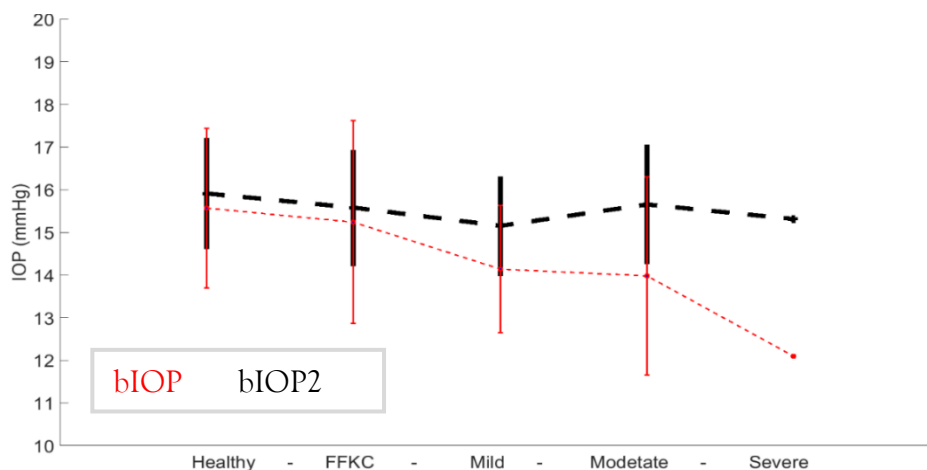


Figure 6-40 The changes in bIOP2 and bIOP in healthy, FFKC, Mild, Moderate and Severe keratoconic cases in Dataset 5

Dataset 6

Dataset 6 consist of 143 KC eyes with mean age of 34.1 ± 12.1 (12.0 -66.0) years, CCT of 490 ± 38 (396 -602) microns, bIOP of 13.7 ± 2.4 (7.1 -21.1) mmHg, CVSIOP of 12.5 ± 2.3 (6.0 -19.0) mmHg and bIOP2 of 15.1 ± 1.3 (12.0 -19.1) mmHg. Correlation with CCT was not significant with CVSIOP ($p:0.971$, $R:-0.003$) and significant with bIOP ($p:0.000$, $R:-0.369$) and bIOP2 ($p:0.001$, $R:-0.278$). There was no significant

correlation with age and bIOP ($p:0.052$, $R:-0.163$), CVSIOP ($p:0.492$, $R:-0.058$) or bIOP2 ($p:0.821$, $R:-0.019$), Figure 6-41.

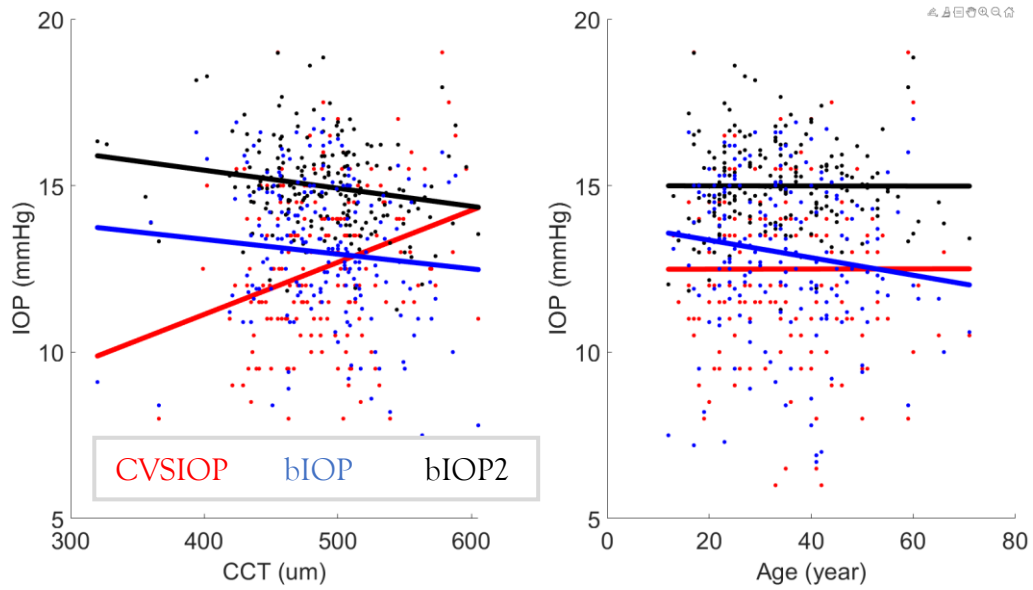


Figure 6-41 Correlation of IOP values from CVSIOP, bIOP and bIOP2 with CCT (left) and age (right) in KC Dataset 6

The comparison with mean values between different groups (based on disease severity) showed bIOP was significantly different ($p<0.001$) in all cases. bIOP2 was not significant in FFKC ($p: 0.0505$) and significant in Mild ($p: 0.0179$), Moderate ($p<0.01$) and Severe ($p: 0.0386$), Figure 6-42.

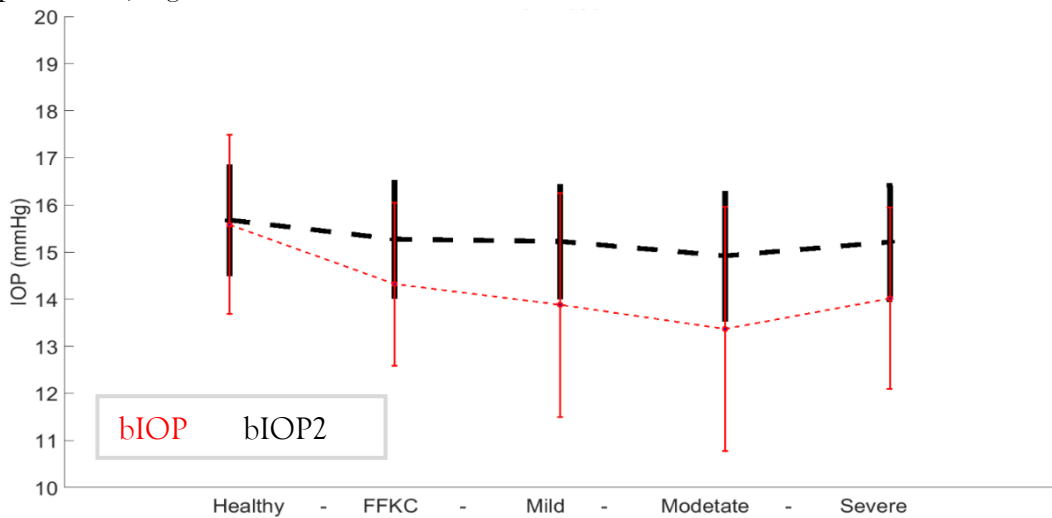


Figure 6-42 The changes in bIOP2 and bIOP in healthy, FFKC, Mild, Moderate and Severe keratoconic cases in Dataset 6

Dataset 7

Dataset 7 consist of 405 KC eyes with mean age of 27.1 ± 10.5 (10.0 -81.0) years, CCT of 484 ± 43 (297 -636) microns, bIOP of 15.0 ± 2.1 (8.6 -22.0) mmHg, CVSIOP of 13.6 ± 2.3 (6.0 -23.5) mmHg and bIOP2 of 15.5 ± 1.1 (12.6 -20.1) mmHg. CCT was

significantly correlated with CVSIOP ($p:0.000$, $R:0.323$) and not significant with both bIOP ($p:0.155$, $R:-0.07$) and bIOP2 ($p:0.774$, $R:-0.014$). Age was significantly correlated with bIOP ($p:0.000$, $R:-0.186$) and not significant with CVSIOP ($p:0.403$, $R:-0.042$) and bIOP2 ($p:0.082$, $R:-0.086$), Figure 6-43.

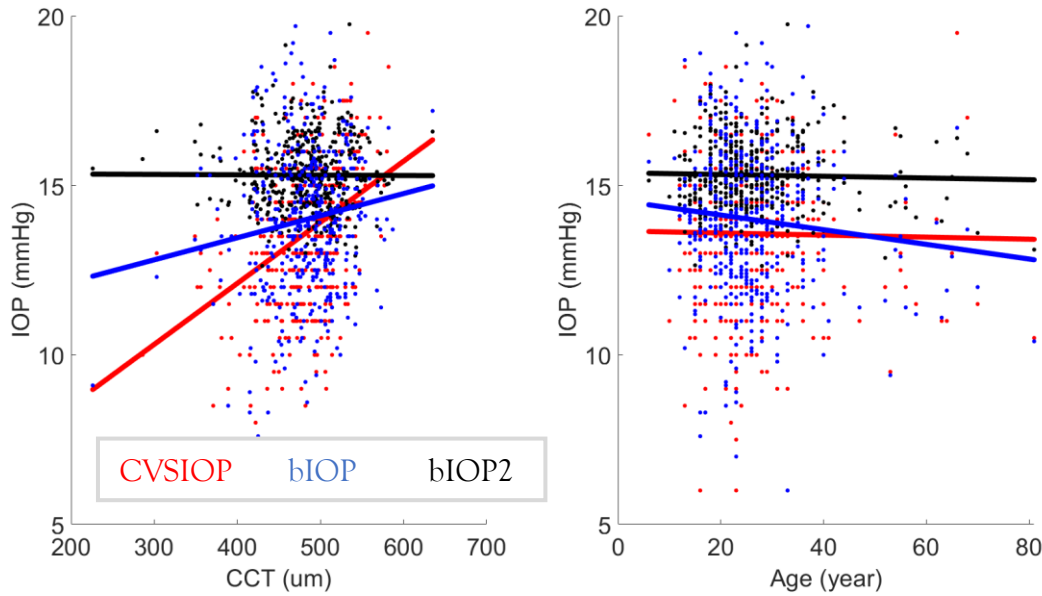


Figure 6-43 Correlation of IOP values from CVSIOP, bIOP and bIOP2 with CCT (left) and age (right) in KC Dataset 7

The comparison of patients at different stages of the disease with the healthy group showed no significant difference in bIOP2 with FFKC ($p: 0.3692$), Mild ($p: 0.5531$), Moderate ($p: 0.8557$) and Severe ($p: 0.0903$). On the other hand, bIOP was not significantly different in FFKC ($p: 0.9718$) and Mild ($p: 0.1322$) group, but the moderate ($p: 0.0209$) and severe ($p: 0.0004$) groups were significant, Figure 6-44.

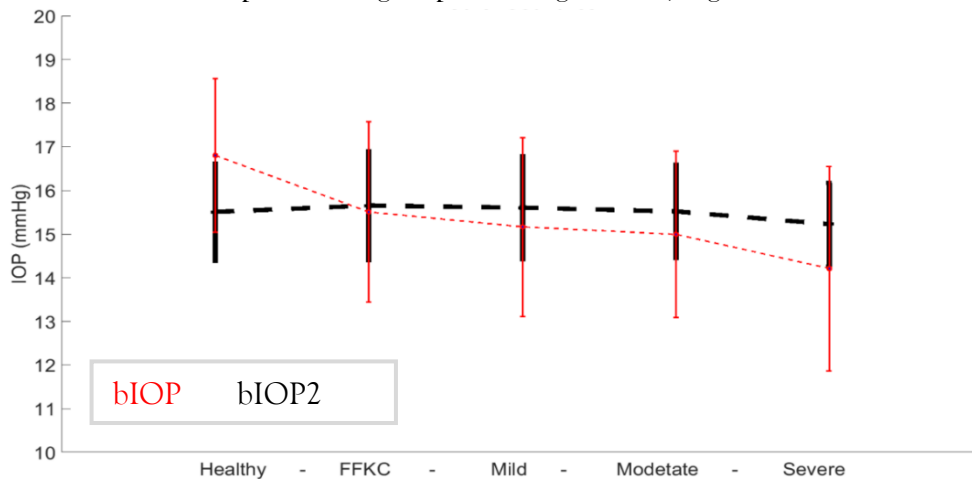


Figure 6-44 The changes in bIOP2 and bIOP in healthy, FFKC, Mild, Moderate and Severe keratoconic cases in Dataset 7

Dataset 8

Combining all cases, 1522 KC eyes of patients with mean age of 31.1 ± 11.7 (10.0 -83.0) years, CCT of 487 ± 40 (297 -636) microns, bIOP of 14.3 ± 2.3 (6.1 -23.4) mmHg, CVSIOP of 13.1 ± 2.4 (4.5 -23.5) mmHg, bIOP2 of 15.5 ± 1.1 (11.5 -20.2) mmHg. The correlation were significant with CCT for bIOP ($p:0.000$, $R:-0.113$), CVSIOP ($p:0.000$, $R:0.246$) and bIOP2 ($p:0.000$, $R:-0.120$). Age was not significantly correlated with bIOP2 ($p:0.343$, $R:-0.024$) and CVSIOP ($p:0.075$, $R:-0.046$) and it was significant in bIOP ($p:0.000$, $R:-0.171$), Figure 6-45.

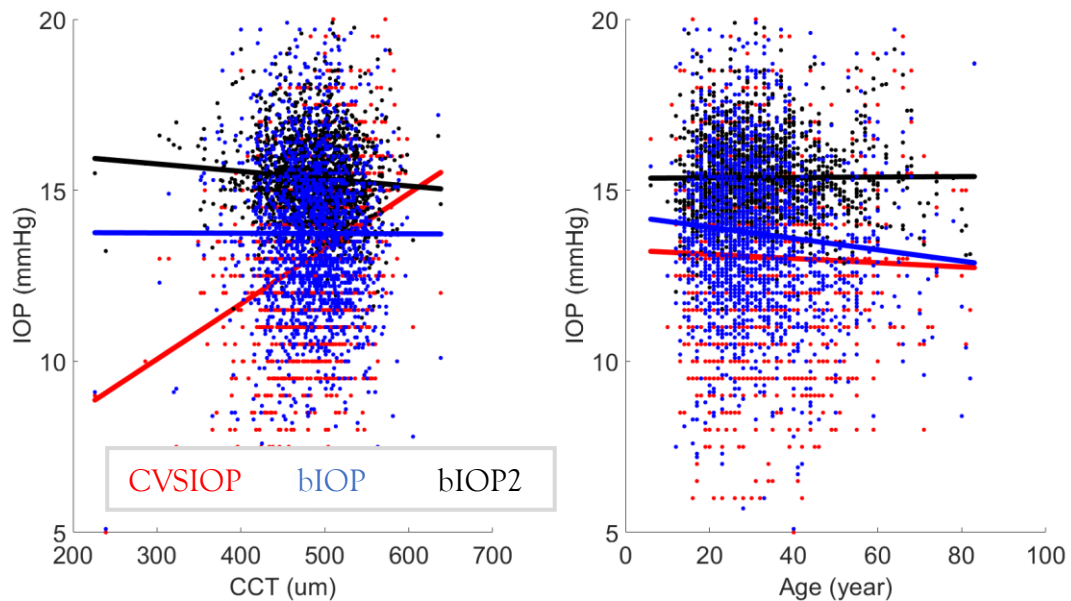


Figure 6-45 Correlation of IOP values from CVSIOP, bIOP and bIOP2 with CCT (left) and age (right) in KC Dataset 8

The comparison between the healthy IOP values with disease stages showed no significant difference in bIOP2 with FFKC ($p: 0.1052$), Mild ($p: 0.3909$), Moderate ($p: 0.1051$) and Severe ($p: 0.0676$) groups. This comparison was found significant ($p < 0.01$) between bIOP values in all groups, Figure 6-46.

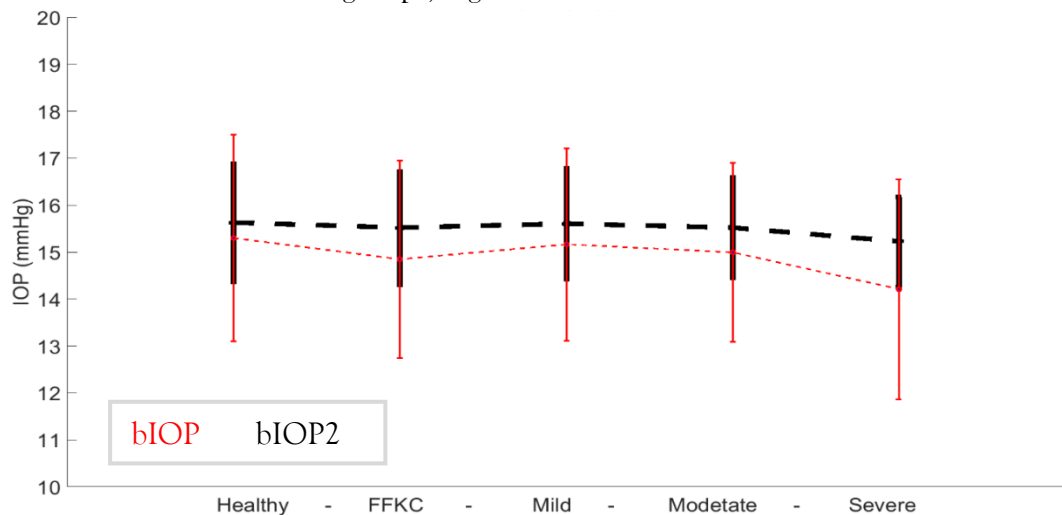


Figure 6-46 The changes in bIOP2 and bIOP in healthy, FFKC, Mild, Moderate and Severe keratoconic cases in Dataset 8

bIOP2-KC Equation

Dataset 2

This dataset includes 143 KC eyes with a mean age of 33.9 ± 14.9 (14 -80) years, CCT of 495.3 ± 40.1 (315 -597) microns, bIOP2 of 15.5 ± 1.1 (12.5 -19) mmHg and bIOP2KC of 15.4 ± 1.1 (12.3 -19.4) mmHg. bIOP2-kc (p:0.8716, R:0.0137) correlation with CCT was weaker than bIOP2 (p:0.1229, R:-0.1296). The correlation with age slightly improved in bIOP2-kc (p:0.3768, R:0.0747). compared to bIOP2 (p:0.3088, R:0.0857). The differences between the IOP values of the two equations were not significant (p:0.5043), Figure 6-47.

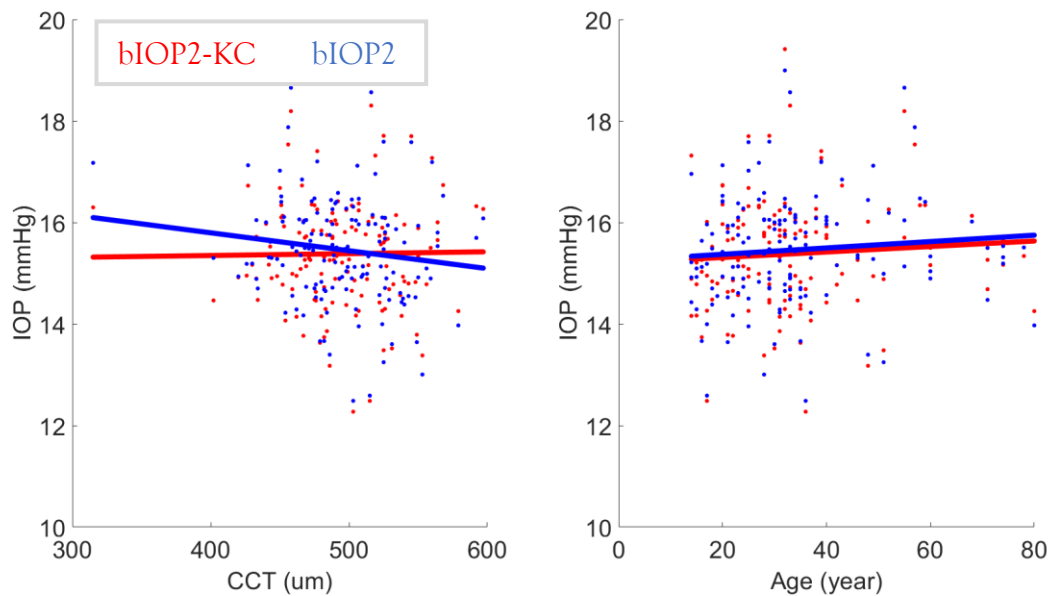


Figure 6-47 Correlation of IOP values from bIOP2 and bIOP2-KC with CCT (left) and age (right) in KC Dataset 2

The differences between IOP values in each group separated based on disease severity were compared to healthy and remained close to the previously calculated values in section 4.5.1.1.7. Hence the numbers are not presented again for this section as the conclusion remained the same, Figure 6-48.

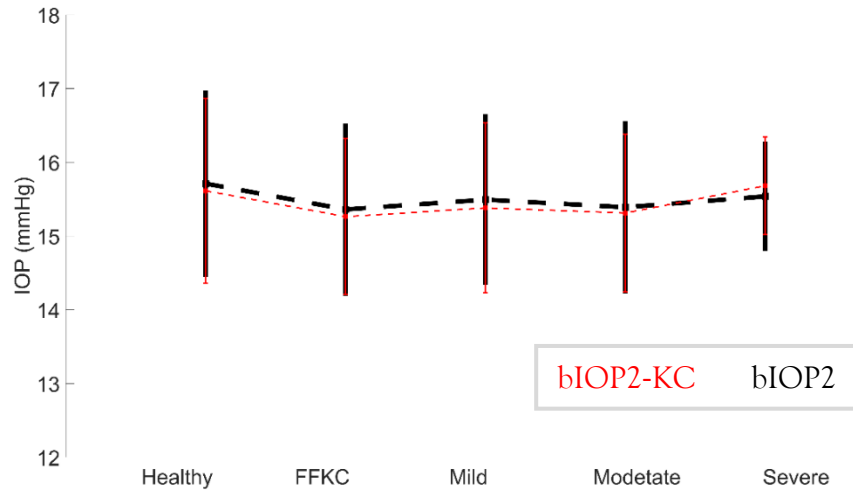


Figure 6-48 The changes in bIOP2 and bIOP2-KC in healthy, FFKC, Mild, Moderate and Severe keratoconic cases in Dataset 2

Dataset 3

This dataset includes 363 KC eyes with a mean age of 33.2 ± 10.8 (13 -72) years, CCT of 492.2 ± 40.5 (345 -590) microns, bIOP2 of 15.5 ± 1.1 (11.5 -20.2) mmHg and bIOP2KC of 15.5 ± 1.1 (11.4 -19.9) mmHg. The correlation with CCT improved in bIOP2kc ($p:0.1116$, $R:-0.0842$) compared to bIOP2 ($p:0.009$, $R:-0.1369$). Correlation with age remained the same for both bIOP2kc ($p:0.745$, $R:-0.0172$) and bIOP2 ($p:0.8913$, $R:-0.0072$). The differences between the IOP values of the two equations were not significant ($p:0.3333$), Figure 6-49.

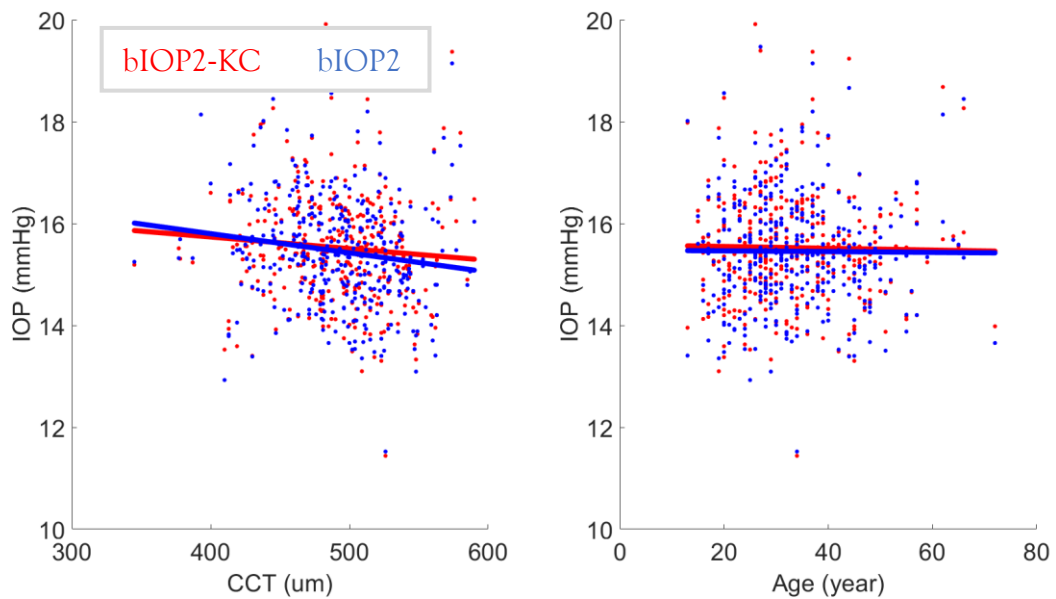


Figure 6-49 Correlation of IOP values from bIOP2 and bIOP2-KC with CCT (left) and age (right) in KC Dataset 3

The differences between IOP values in each group separated based on disease severity were compared to healthy and remained close to the previously calculated values in section 4.5.1.1.7. Hence the numbers are not presented again for this section as the conclusion remained the same, Figure 6-50.

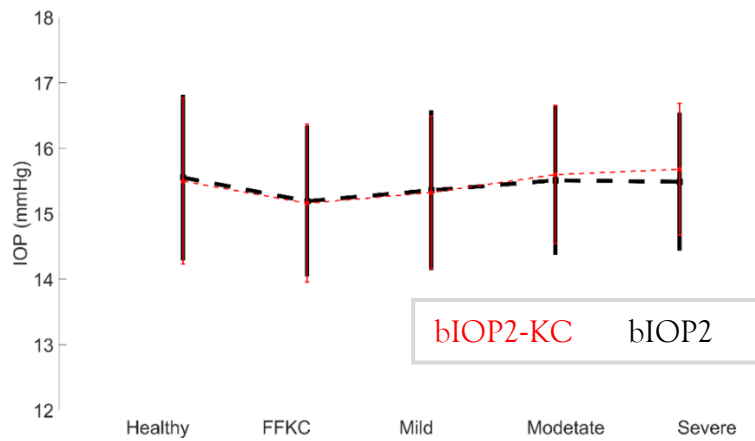


Figure 6-50 The changes in bIOP2 and bIOP2-KC in healthy, FFKC, Mild, Moderate and Severe keratoconic cases in Dataset 3

Dataset 4

This dataset includes 227 KC eyes with a mean age of 27.6 ± 7.5 (12 -58) years, CCT of 482.1 ± 39.7 (374 -636) microns, bIOP2 of 15.9 ± 1.1 (13.3 -19.9) mmHg and bIOP2KC of 15.9 ± 1.1 (13.3 -20.2) mmHg. The correlation with CCT remained insignificant while bIOP2 ($p:0.5335$, $R:-0.0415$) showed negative correlations and bIOP2KC ($p:0.3577$, $R:0.0616$) showed positive correlations. Correlations with age remained the same for both bIOP2 ($p:0.5294$, $R:0.042$) and bIOP2KC ($p:0.5078$, $R:0.0444$). The differences between the IOP values of the two equations were not significant ($p:0.5689$), Figure 6-51.

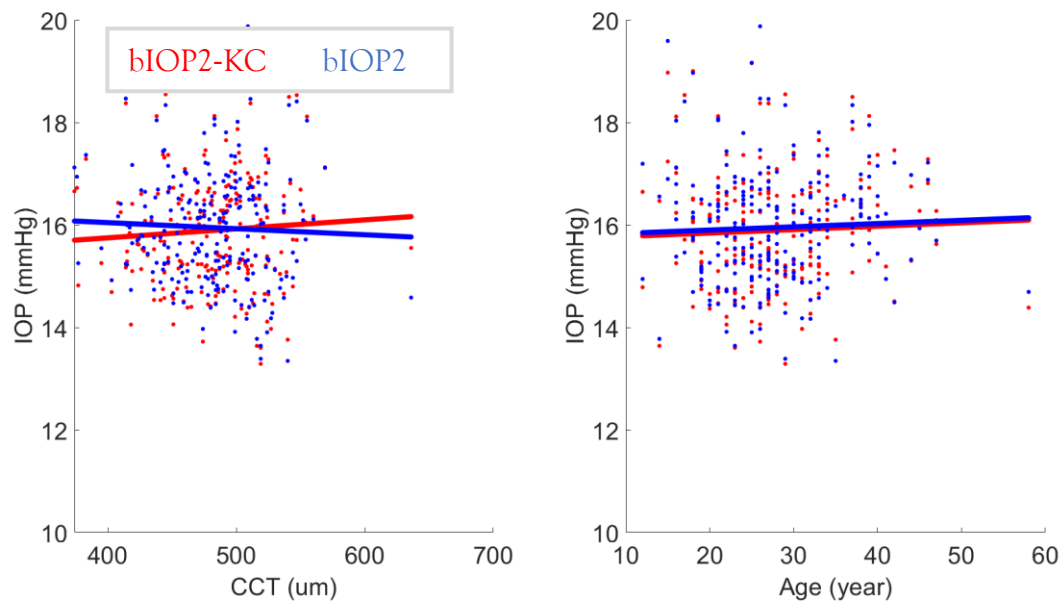


Figure 6-51 Correlation of IOP values from bIOP2 and bIOP2-KC with CCT (left) and age (right) in KC Dataset 4

The differences between IOP values in each group separated based on disease severity were compared to healthy and remained close to the previously calculated values in section 4.5.1.1.7. Hence the numbers are not presented again for this section as the conclusion remained the same, Figure 6-52.

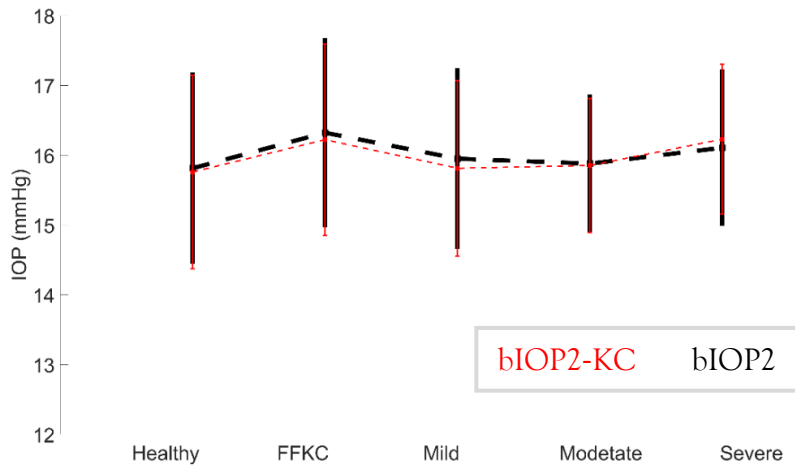


Figure 6-52 The changes in bIOP2 and bIOP2-KC in healthy, FFKC, Mild, Moderate and Severe keratoconic cases in Dataset 4

Dataset 5

This dataset includes 14 KC eyes with a mean age of 33.6 ± 12.2 (20 -66) years, CCT of 483.9 ± 21.9 (451 -529) microns, bIOP2 of 15.3 ± 1.1 (13.4 -17.1) mmHg and bIOP2KC of 15.2 ± 1.2 (13 -17.2) mmHg. The correlation with CCT for bIOP2 ($p:0.1449$, $R:0.4104$) and for bIOP2KC ($p:0.1159$, $R:0.4394$) remained the same. Similarly, the correlations with age for bIOP2 ($p:0.6986$, $R:-0.1138$) and bIOP2KC ($p:0.6415$, $R:-0.1366$) did not change. The differences between the IOP values of the two equations were not significant ($p:0.8362$), Figure 6-53.

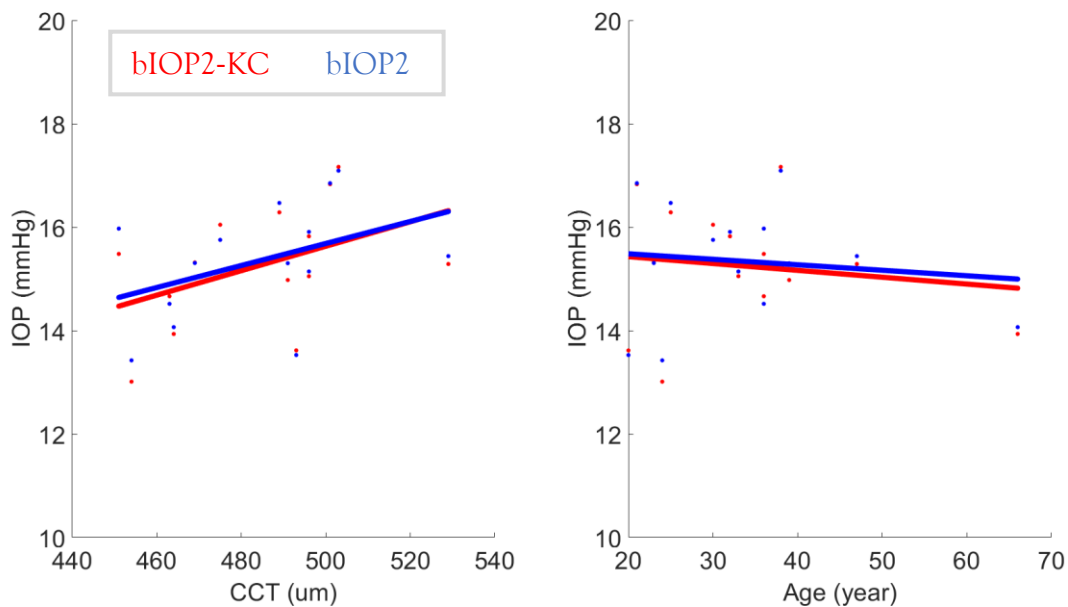


Figure 6-53 Correlation of IOP values from bIOP2 and bIOP2-KC with CCT (left) and age (right) in KC Dataset 5

The differences between IOP values in each group separated based on disease severity were compared to healthy and remained close to the previously calculated values in

section 4.5.1.1.7. Hence the numbers are not presented again for this section as the conclusion remained the same, Figure 6-54.

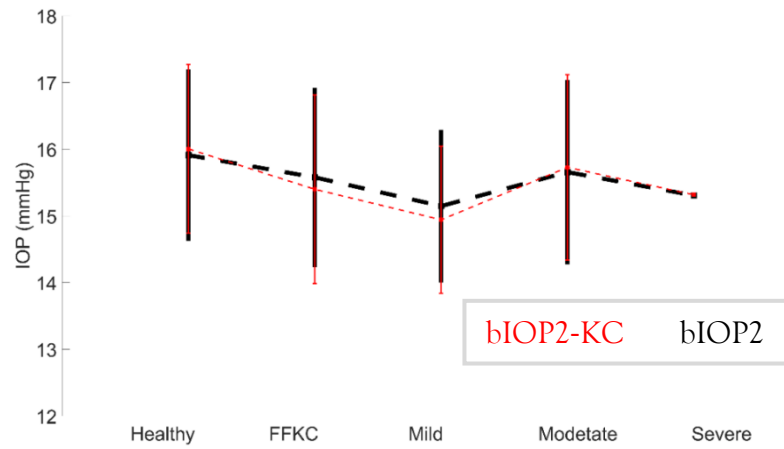


Figure 6-54 The changes in bIOP2 and bIOP2-KC in healthy, FFKC, Mild, Moderate and Severe keratoconic cases in Dataset 5

Dataset6

This dataset includes 143 KC eyes with a mean age of 34.1 ± 12.1 (12 -66) years, CCT of 490 ± 38.5 (396 -602) microns, bIOP2 of 15.1 ± 1.3 (12 -19.1) mmHg and bIOP2KC of 15.2 ± 1.2 (12.6 -19.2) mmHg. The correlation with CCT improved in bIOP2KC (p:0.042, R:-0.1715) compared to bIOP2 (p:0.0008, R:-0.2775). The correlations with age remained the same for both bIOP2 (p:0.8205, R:-0.0191) and bIOP2KC (p:0.7416, R:-0.028). The differences between the IOP values of the two equations were not significant (p:0.2901), Figure 6-55.

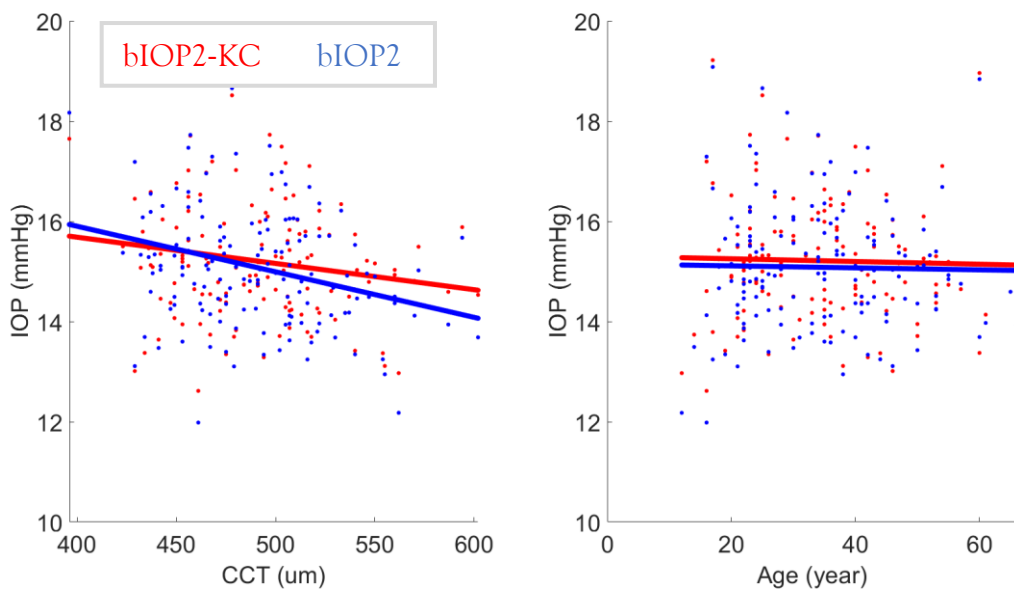


Figure 6-55 Correlation of IOP values from bIOP2 and bIOP2-KC with CCT (left) and age (right) in KC Dataset 6

The differences between IOP values in each group separated based on disease severity were compared to healthy and remained close to the previously calculated values in section 4.5.1.1.7. Hence the numbers are not presented again for this section as the conclusion remained the same, Figure 6-56.

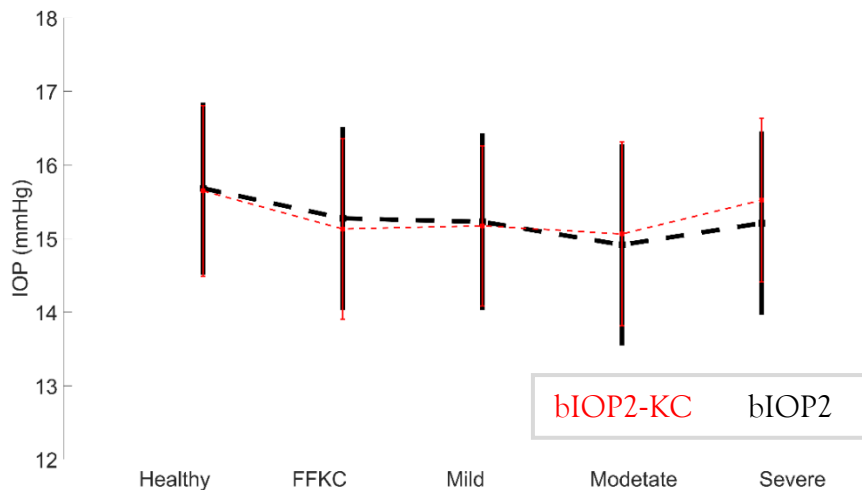


Figure 6-56 The changes in bIOP2 and bIOP2-KC in healthy, FFKC, Mild, Moderate and Severe keratoconic cases in Dataset 6

Dataset 7

This dataset includes 402 KC eyes with a mean age of 27.2 ± 10.5 (10 -81) years, CCT of 484 ± 42.6 (297 -636) microns, bIOP2 of 15.5 ± 1.1 (12.6 -20.1) mmHg and bIOP2KC of 15.5 ± 1.1 (12.8 -20.2) mmHg. The correlations remain insignificant while bIOP2 ($p:0.7629$, $R:-0.0151$) showed negative correlation and bIOP2KC ($p:0.071$, $R:0.0904$) had a positive correlation with CCT. Correlations with age remained insignificant for bIOP2 ($p:0.0818$, $R:-0.0869$) and significant for bIOP2KC ($p:0.0313$, $R:-0.1077$) while they both have a similar correlation with age. The differences between the IOP values of the two equations were not significant ($p:0.4406$), Figure 6-57.

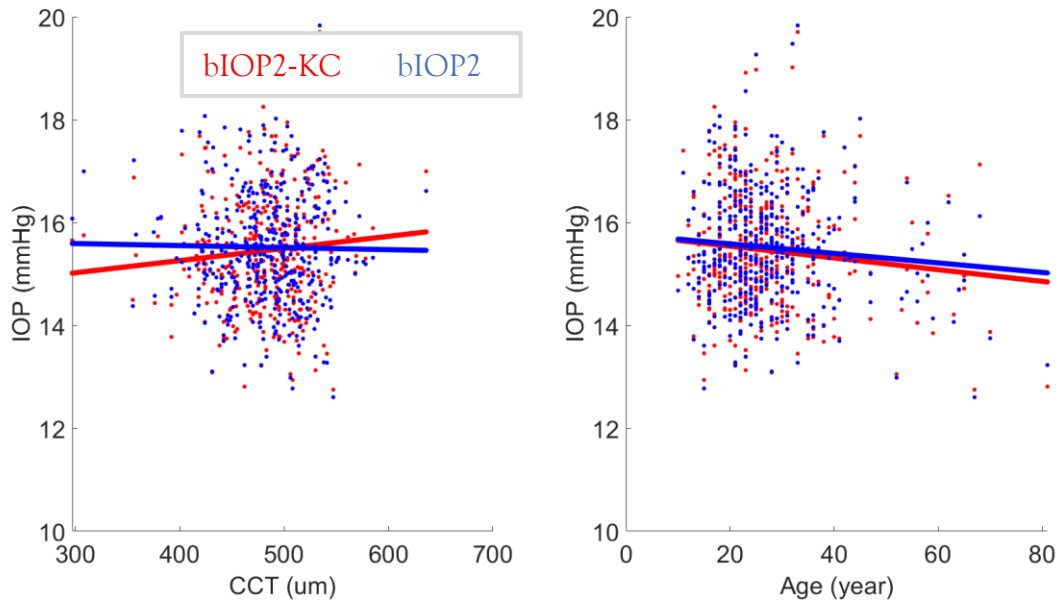


Figure 6-57 Correlation of IOP values from bIOP2 and bIOP2-KC with CCT (left) and age (right) in KC Dataset 7

The differences between IOP values in each group separated based on disease severity were compared to healthy and remained close to the previously calculated values in section 4.5.1.1.7. Hence the numbers are not presented again for this section as the conclusion remained the same, Figure 6-58.

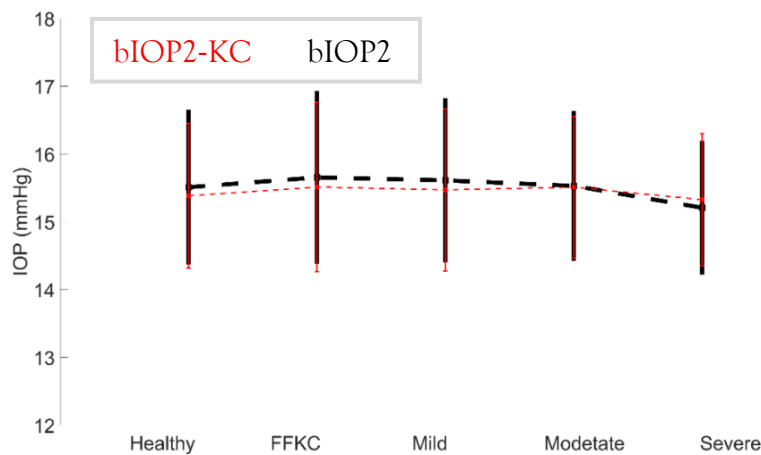


Figure 6-58 The changes in bIOP2 and bIOP2-KC in healthy, FFKC, Mild, Moderate and Severe keratoconic cases in Dataset 7

Dataset 8

Combining of KC datasets resulted in 1522 KC eyes with a mean age of 31.1 ± 11.7 (10 - 83) years, CCT of 486.9 ± 40.4 (297 - 636) microns, bIOP2 of 15.5 ± 1.1 (11.5 - 20.2) mmHg and bIOP2KC of 15.5 ± 1.1 (11.4 - 20.2) mmHg. There was no correlation with CCT for bIOP2KC ($p:0.4228$, $R:-0.0207$) while bIOP2 ($p:0.000$, $R:-0.1204$) showed weak significant negative correlations. The correlation with age remained the same for

both bIOP2KC ($p:0.4248$, $R:-0.0206$) and bIOP2 ($p:0.3432$, $R:-0.0243$). The differences between the IOP values of the two equations were not significant ($p:0.9375$), Figure 6-59.

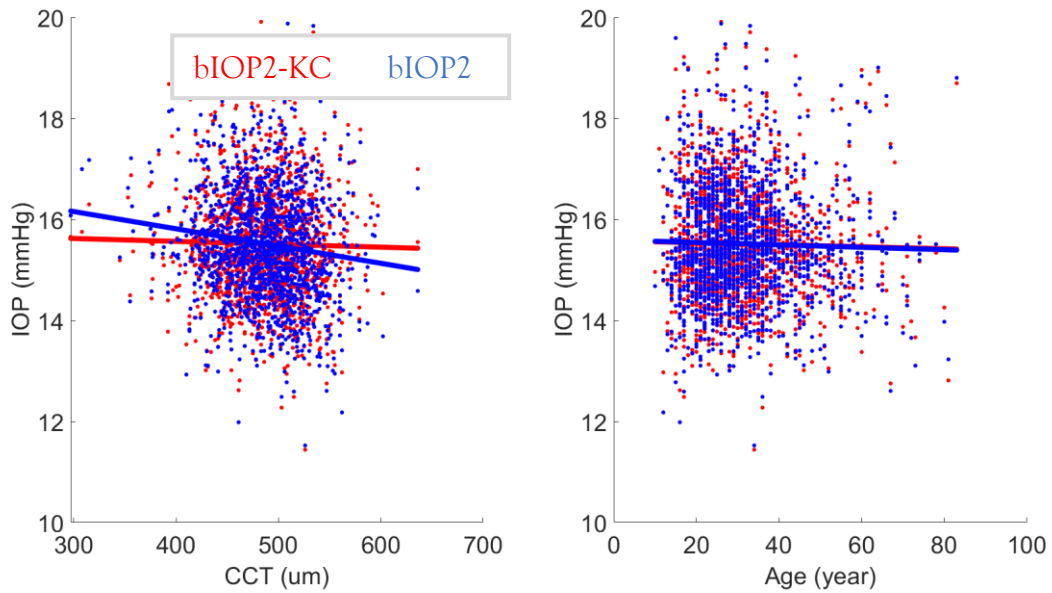


Figure 6-59 Correlation of IOP values from bIOP2 and bIOP2-KC with CCT (left) and age (right) in KC Dataset 8

The differences between IOP values in each group separated based on disease severity were compared to healthy and remained close to the previously calculated values in section 4.5.1.1.7. Hence the numbers are not presented again for this section as the conclusion remained the same, Figure 6-60.

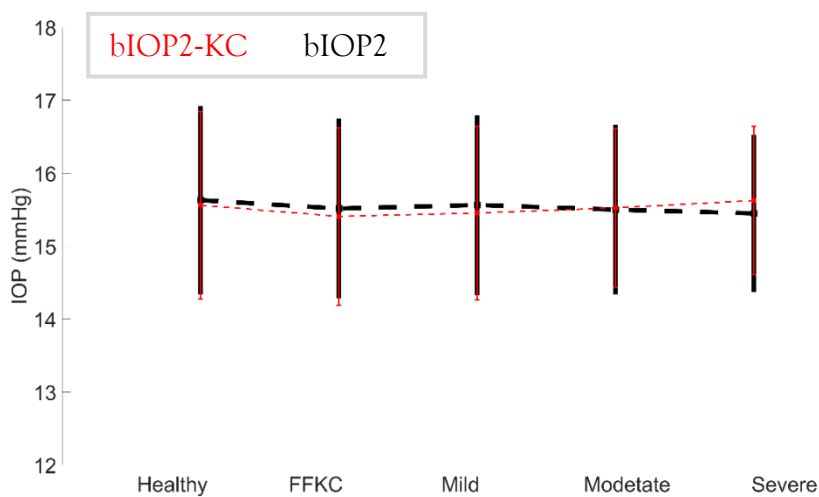


Figure 6-60 The changes in bIOP2 and bIOP2-KC in healthy, FFKC, Mild, Moderate and Severe keratoconic cases in Dataset 8

Section B - Stress-Strain Index (SSI2)

SSI Healthy Equation

Healthy Patients

Dataset 2

It included 239 patients with a mean age of 37.5 ± 16.3 (7-85) years, CCT of 547 ± 32 (464 - 644) microns, bIOP of 15.7 ± 1.2 (13.0-21.1) mmHg, bIOP2 of 15.1 ± 2.0 (8.7-21.9) mmHg, SSI of 0.96 ± 0.19 (0.58-1.64) and SSI2-H of 1.00 ± 0.20 (0.45-1.72). Correlation with CCT for SSI was $R:0.171$ ($p:0.008$), and became weaker for SSI2-H, which was $R:0.004$ ($p:0.955$). Correlation with age for SSI was $R:0.549$ ($p:0.000$) and for SSI2-H was $R:0.931$ ($p:0.000$). Correlation with bIOP2 for SSI and SSI2-H was $R:0.445$ ($p:0.000$) and $R:-0.163$ ($p:0.012$). The SSI2-H had a weaker negative correlation and SSI2-H stronger positive correlation, Figure 6-61.

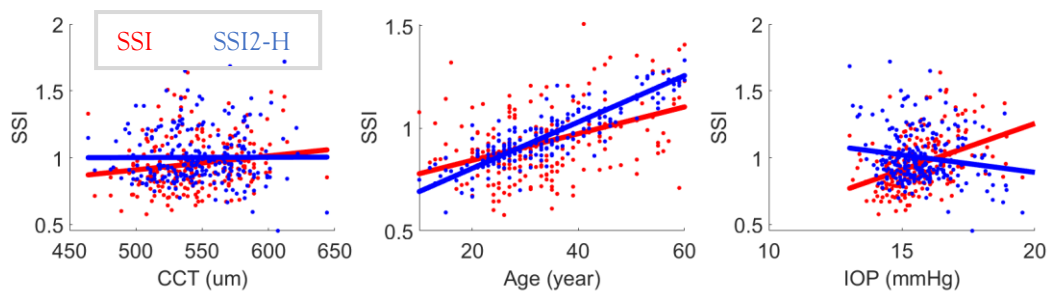


Figure 6-61 The correlation of SSI and SSI2-H with CCT (left), age (middle) and IOP (right) in Dataset 2

Dataset 3

It included 326 patients with a mean age of 34.5 ± 9.8 (7-62) years, CCT of 548 ± 33 (447 - 661) microns, bIOP of 15.6 ± 1.2 (12.6-21.8) mmHg, bIOP2 of 14.9 ± 2.2 (10.1 - 27.1) mmHg, SSI of 1.01 ± 0.20 (0.52-1.71) and SSI2-H of 1.02 ± 0.14 (0.59-1.48). The correlation with CCT for SSI was significant with $R:0.145$ ($p:0.009$), and for SSI2-H was insignificant with $R:-0.007$ ($p:0.899$). Correlation with age for SSI was $R:0.174$ ($p:0.002$) and for SSI2-H was $R:0.710$ ($p:0.000$). Correlation with bIOP2 for SSI and SSI2-H was $R:0.387$ ($p:0.000$) and $R:-0.048$ ($p:0.391$). SSI showed significant correlations with IOP while SSI2-H remained insignificant and weaker, Figure 6-62.

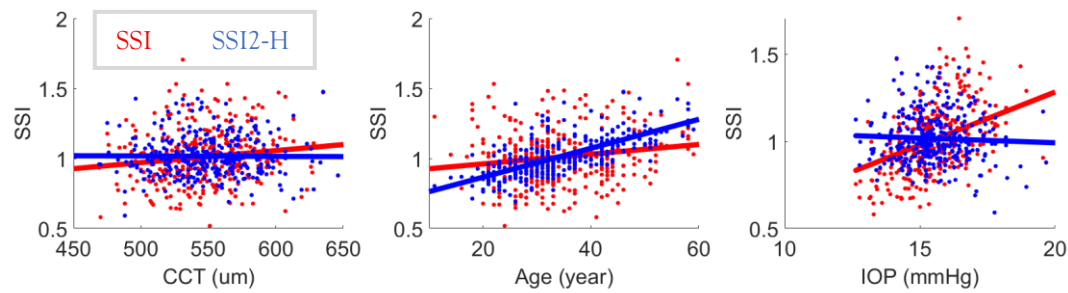


Figure 6-62 The correlation of SSI and SSI2-H with CCT (left), age (middle) and IOP (right) in Dataset 3

Dataset 4

It included 182 patients with a mean age of 27.1 ± 5.3 (19-47) years, CCT of 553 ± 27 (470 - 633) microns, bIOP of 15.8 ± 1.3 (12.2-19.4) mmHg, bIOP2 of 16.4 ± 2 (12.3-22.2) mmHg, SSI of 1.02 ± 0.20 (0.52-1.73) and SSI2-H of 1.00 ± 0.11 (0.79-1.31). Correlation with CCT for SSI was $R: -0.013$ ($p: 0.864$), and for SSI2-H was $R: 0.018$ ($p: 0.812$) and both remained weak. Correlation with age for SSI was $R: 0.266$ ($p: 0.000$) and for SSI2-H was $R: 0.730$ ($p: 0.000$). Correlation with bIOP2 for SSI and SSI2-H was $R: 0.617$ ($p: 0.000$) and $R: 0.026$ ($p: 0.730$). SSI showed a large positive correlation with IOP while there was no correlation with SSI2-H, Figure 6-63.

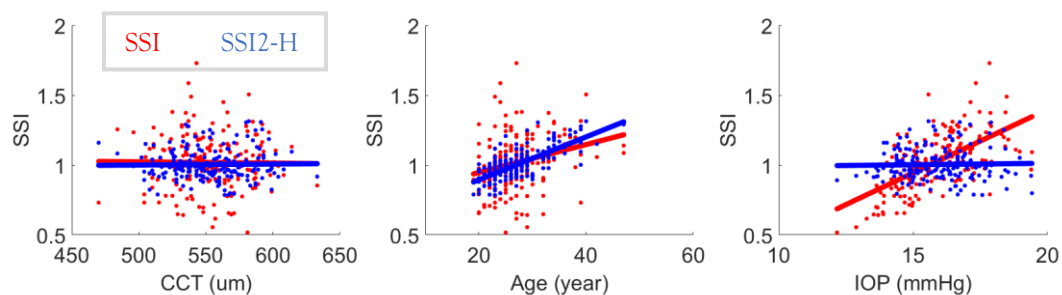


Figure 6-63 The correlation of SSI and SSI2-H with CCT (left), age (middle) and IOP (right) in Dataset 4

Dataset 5

It included 47 patients with a mean age of 33.6 ± 8.6 (12-54) years, CCT of 554 ± 33 (459 - 615) microns, bIOP of 15.9 ± 1.3 (12.9-18.6) mmHg, bIOP2 of 15.6 ± 1.9 (11.5 - 19.1) mmHg, SSI of 0.90 ± 0.13 (0.56-1.15) and SSI2-H of 0.96 ± 0.09 (0.68-1.17). Correlation with CCT for SSI was $R: 0.008$ ($p: 0.958$), and for SSI2-H was $R: -0.231$ ($p: 0.118$) and both remained insignificant. Correlation with age for SSI was $R: 0.209$ ($p: 0.158$) and for SSI2-H was $R: 0.749$ ($p: 0.000$). Correlation with bIOP2 for SSI and SSI2-H was $R: 0.745$ ($p: 0.000$) and $R: 0.008$ ($p: 0.958$). SSI showed significant positive correlations with IOP while there was no correlation with SSI2-H, Figure 6-64.

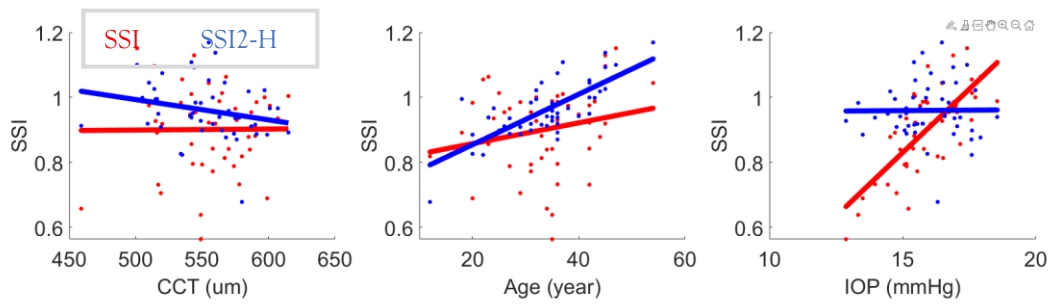


Figure 6-64 The correlation of SSI and SSI2-H with CCT (left), age (middle) and IOP (right) in Dataset 5

Dataset 6

It included 122 patients with a mean age of 34.5 ± 14.1 (0-80) years, CCT of 552 ± 32 (473 - 645) microns, bIOP of 15.7 ± 1.1 (13.4-19.6) mmHg, bIOP2 of 15.6 ± 1.9 (10.1 - 22.8) mmHg, SSI of 0.93 ± 0.19 (0.53-1.79) and SSI2-H of 1.00 ± 0.16 (0.65-1.62). Correlation with CCT for SSI was $R:0.125$ ($p:0.169$), and for SSI2-H was $R:-0.056$ ($p:0.529$) and remained insignificant for both. Correlation with age for SSI was $R:0.466$ ($p:0.000$) and for SSI2-H was $R:0.911$ ($p:0.000$). Correlation with bIOP2 for SSI and SSI2-H was $R:0.506$ ($p:0.000$) and $R:0.097$ ($p:0.286$). Significant positive correlations were observed in SSI while SSI2-H was not correlated, Figure 6-65.

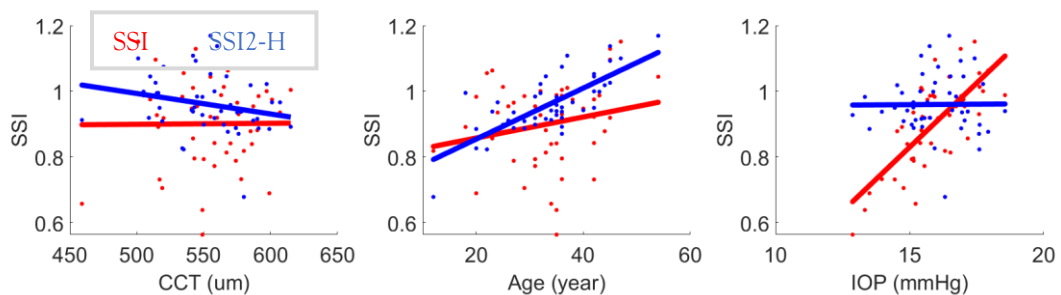


Figure 6-65 The correlation of SSI and SSI2-H with CCT (left), age (middle) and IOP (right) in Dataset 6

Dataset 7

It included 78 patients with a mean age of 26.2 ± 5.6 (11-44) years, CCT of 523 ± 28 (456 - 617) microns, bIOP of 15.5 ± 1.1 (13.1-18.7) mmHg, bIOP2 of 16.8 ± 1.8 (12.1 - 22.5) mmHg, SSI of 0.9 ± 0.25 (0.52-1.66) and SSI2-H of 1.0 ± 0.13 (0.81-1.55). Correlation with CCT was significant for both where for SSI was $R:0.258$ ($p:0.023$), and for SSI2-H was $R:0.402$ ($p:0.000$). Correlation with age for SSI was $R:0.035$ ($p:0.763$) and for SSI2-H was $R:0.463$ ($p:0.000$). Correlation with bIOP2 for SSI and SSI2-H was $R:0.429$ ($p:0.000$) and $R:-0.062$ ($p:0.590$). SSI2-H was not correlated with IOP while SSI had significant positive correlations, Figure 6-66.

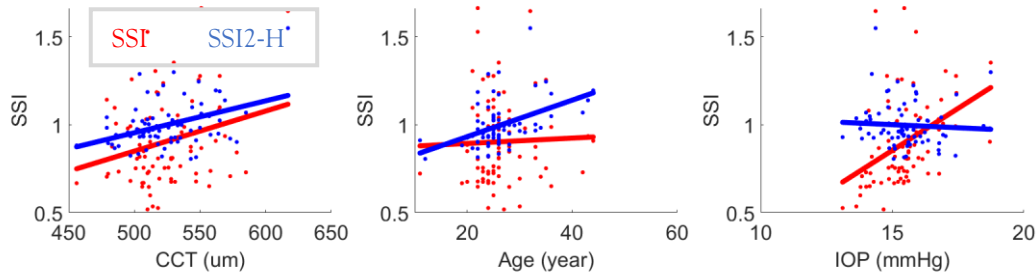


Figure 6-66 The correlation of SSI and SSI2-H with CCT (left), age (middle) and IOP (right) in Dataset 7

Dataset 8

Combining all datasets resulted in 1410 patients with a mean age of $35.2 \pm 14(0-91)$ years, CCT of $545 \pm 32(447-661)$ microns, bIOP of $15.6 \pm 1.3(12.2-22.8)$ mmHg, bIOP2 of $15.3 \pm 2.2(7.7-27.1)$ mmHg, SSI of $1 \pm 0.22(0.52-1.87)$ and SSI2-H of $1.03 \pm 0.17(0.45 - 1.74)$. Correlation with CCT for SSI was significant with $R:0.111$ ($p:0.000$), while SSI2-H was not correlated with $R:-0.003$ ($p:0.899$). Correlation with age for SSI was $R:0.419$ ($p:0.000$) and for SSI2-H was $R:0.841$ ($p:0.000$). Correlation with bIOP2 for SSI and SSI2-H was $R:0.471$ ($p:0.000$) and $R:0.000$ ($p:0.999$). This shows that SSI is highly correlated with IOP, while SSI2-H has no correlation at all and is more representative of tissue's material behaviour, Figure 6-67.

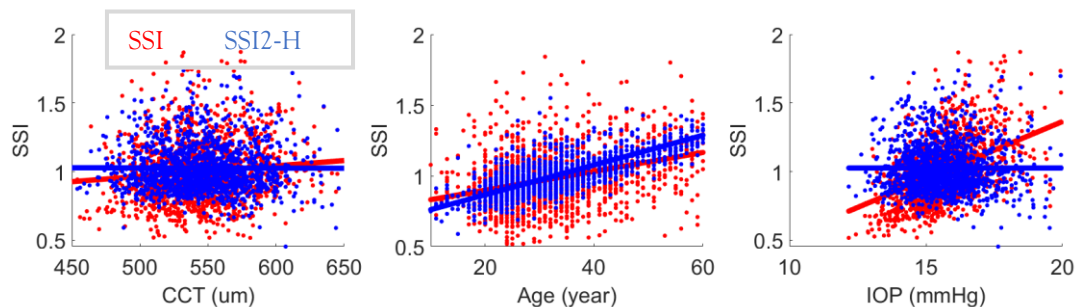


Figure 6-67 The correlation of SSI and SSI2-H with CCT (left), age (middle) and IOP (right) in Dataset 8

PRK Surgery

Dataset 2

It includes 53 patients who undergo SMILE surgery with a mean CCT of 558 ± 30 (496 - 636) microns, age of 26.8 ± 5.1 (17-39) years, bIOP of 14.4 ± 2.1 (10.1-19.2) mmHg, bIOP2 of 15.4 ± 1.2 (12.7-18.5) mmHg, SSI of 0.98 ± 0.14 (0.75-1.46) and SSI2-H of 0.86 ± 0.12 (0.54-1.16). After SMILE these values changed to a mean CCT of 451 ± 39 (371-543) microns, age of 27.4 ± 5.2 (17-40) years, bIOP of 13.8 ± 2 (9.4 - 17.7) mmHg, bIOP2 of 16 ± 0.9 (14.1-17.9) mmHg, SSI of 0.97 ± 0.18 (0.73-1.52) and SSI2-H of 0.84 ± 0.08 (0.66-1.03). To evaluate the performance of SSI values, $(\text{Pre SSI} - \text{Post SSI}) / \text{Pre SSI}$ was calculated. This value for SSI was 0.126 ± 0.102 and for SSI2-H was 0.010 ± 0.111 . Bland Altman plots are provided to visualise these changes, Figure 6-68.

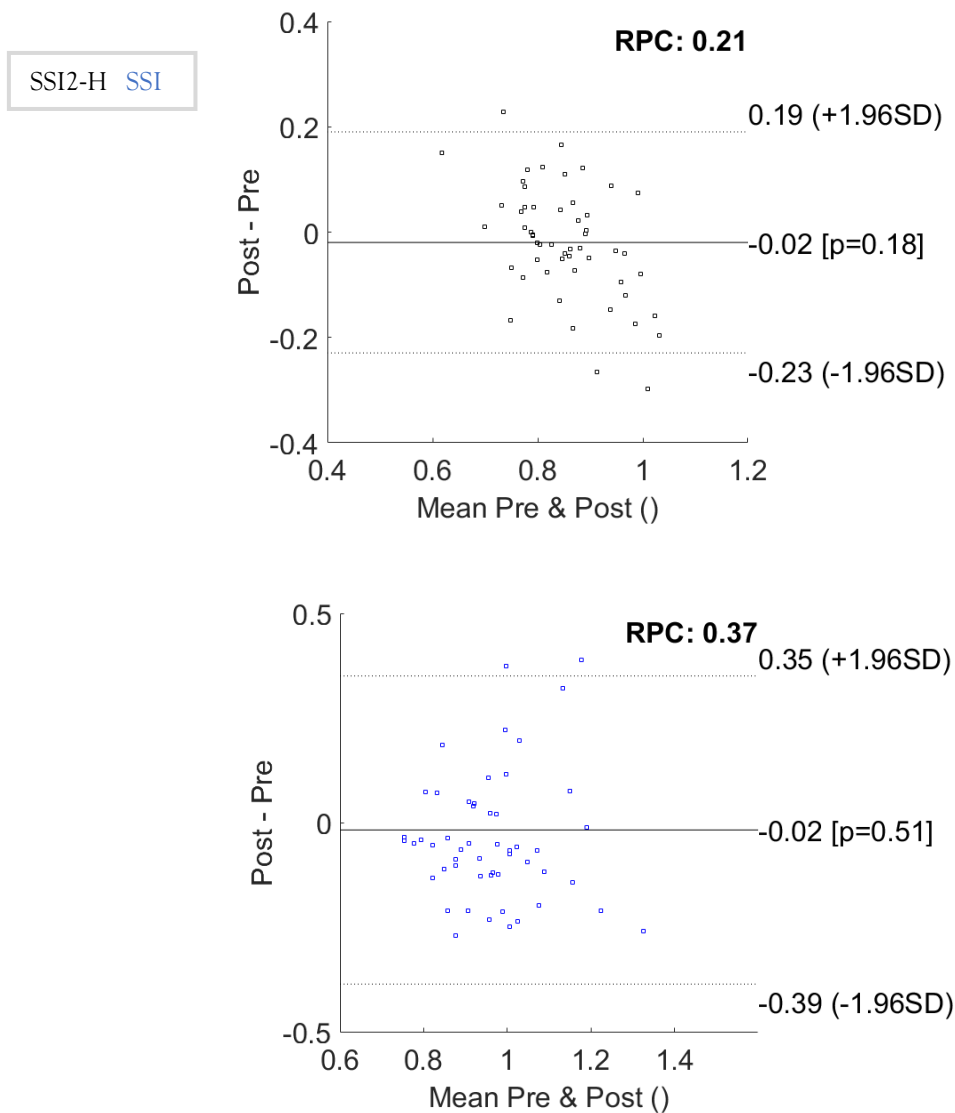


Figure 6-68 Bland Altman plot for SSI2-H (top) and SSI (bottom) comparing the pre and post PRK surgery results in Dataset 2

Further, the correlations between changes in CCT and SSI/SSI2-H were evaluated. The correlation for SSI was $R:-0.342$ ($p:0.011$) and for SSI2-H was $R:-0.007$ ($p:0.961$). SSI, in this case, was significantly correlated with changes in CCT while SSI2-H did not correlate, Figure 6-69.

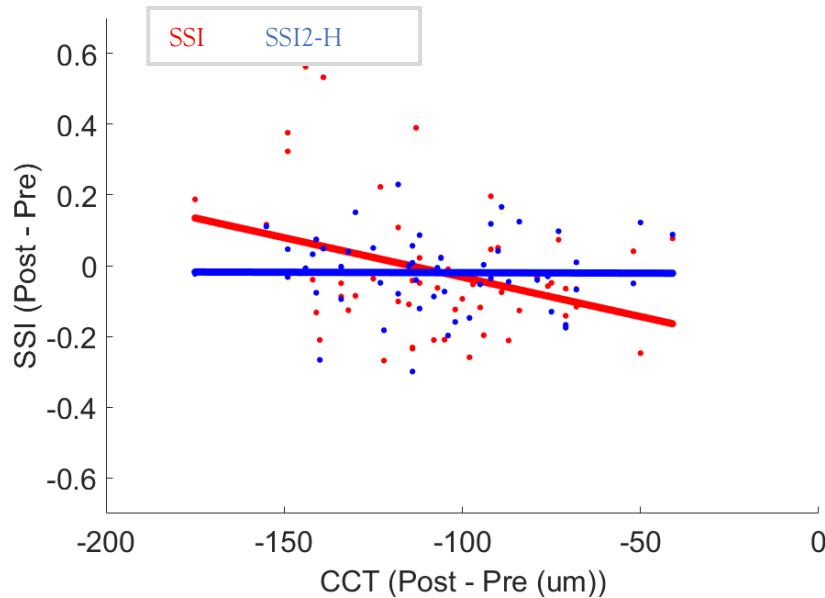


Figure 6-69 The evaluation of correlation in changes in CCT with changes in SSI and SSI2-H in PRK group of Dataset 2

Correlations with CCT before surgery for SSI was $R:-0.042$ ($p:0.765$) and for SSI2-H was $R:-0.116$ ($p:0.404$) and insignificant in both cases. Age correlation with SSI was $R:0.096$ ($p:0.490$) and with SSI2-H was $R:0.577$ ($p:0.000$). Correlation of bIOP2 with SSI was strong and significant with $R:0.345$ ($p:0.011$) while SSI2-H had a similar correlation in the negative direction with $R:-0.341$ ($p:0.012$), Figure 6-70.

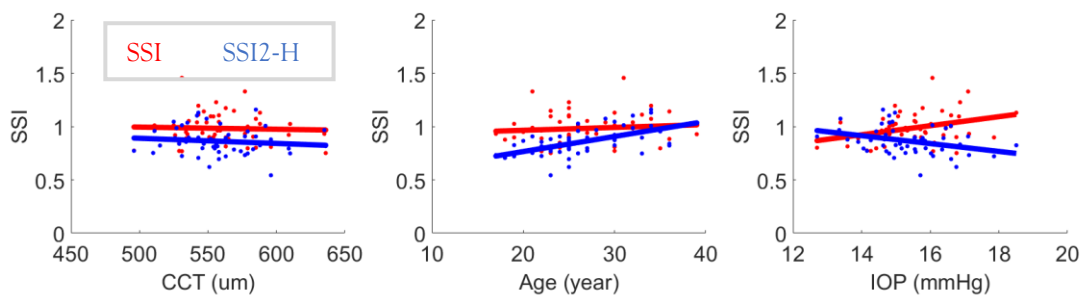


Figure 6-70 The correlation of SSI and SSI2-H with CCT (left), age (middle) and IOP (right) in pre-surgery PRK group of Dataset 2

Correlations with CCT before surgery for SSI was $R:-0.070$ ($p:0.617$) and for SSI2-H was $R:-0.014$ ($p:0.920$) and both remained insignificant. Age correlation with SSI was negative with $R:-0.05$ ($p:0.972$) and with SSI2-H was positive with $R:0.633$ ($p:0.000$). Correlation of bIOP2 with SSI was substantial and significant with $R:0.590$ ($p:0.000$)

while SSI2-H had weak and insignificant correlations with $R:-0.115$ ($p:0.408$), Figure 6-71.

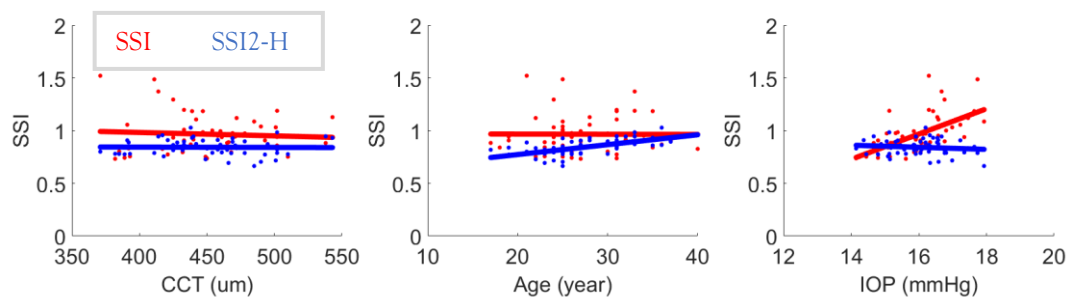


Figure 6-71 The correlation of SSI and SSI2-H with CCT (left), age (middle) and IOP (right) in post-surgery PRK group of Dataset 2

SSI2-KC Equation

Keratoconus Patients

Dataset 2

It included 143 patients with a mean age of 33.9 ± 14.9 (14-80) years, CCT of 495 ± 40 (315-597) microns, bIOP of 14.1 ± 2 (9.6-20) mmHg, bIOP2 of 15.5 ± 1.1 (12.5-19) mmHg, SSI of 0.89 ± 0.37 (0.47-4.5) and SSI2-KC of 0.76 ± 0.22 (0.38-2). Correlation with CCT for SSI was high and significant with $R:0.222$ ($p:0.008$), while for SSI2-KC it remained insignificant and weak with $R:0.027$ ($p:0.750$). Correlation with age for SSI was $R:0.132$ ($p:0.117$) and for SSI2-KC was $R:0.747$ ($p:0.000$). Correlation with bIOP2 for SSI was large and significant with $R:0.199$ ($p:0.017$) while SSI2-KC was not correlated and insignificant with $R:0.008$ ($p:0.921$), Figure 6-72.

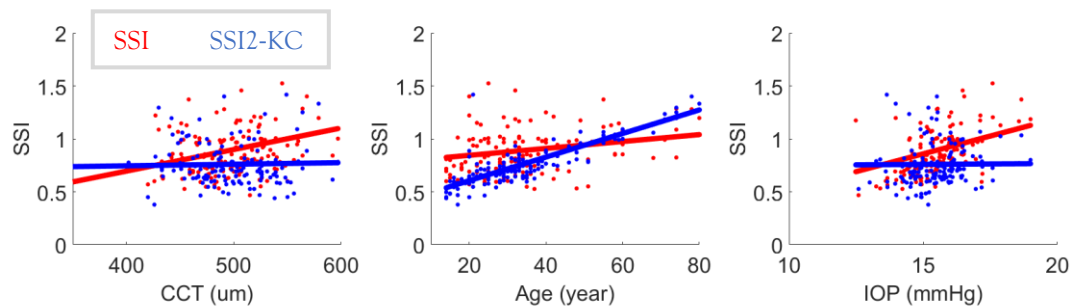


Figure 6-72 The correlation of SSI and SSI2-KC with CCT (left), age (middle) and IOP (right) in Dataset 2

When comparing the changes in SSI and SSI2-KC with disease progression, it is clear that SSI2-KC followed a clear trend. In severe cases, corneal biomechanics changed and became softer than less severe or healthy patients. However, SSI changes were inconsistent and particularly in the Moderate group had a large standard deviation. SSI2-KC showed a more significant softening in Mild, Moderate and Severe cases, Figure 6-73. The detailed analysis for means, standard deviations and statistical comparison of SSI/ SSI2-KC values to the healthy group is provided in Table 6-10.

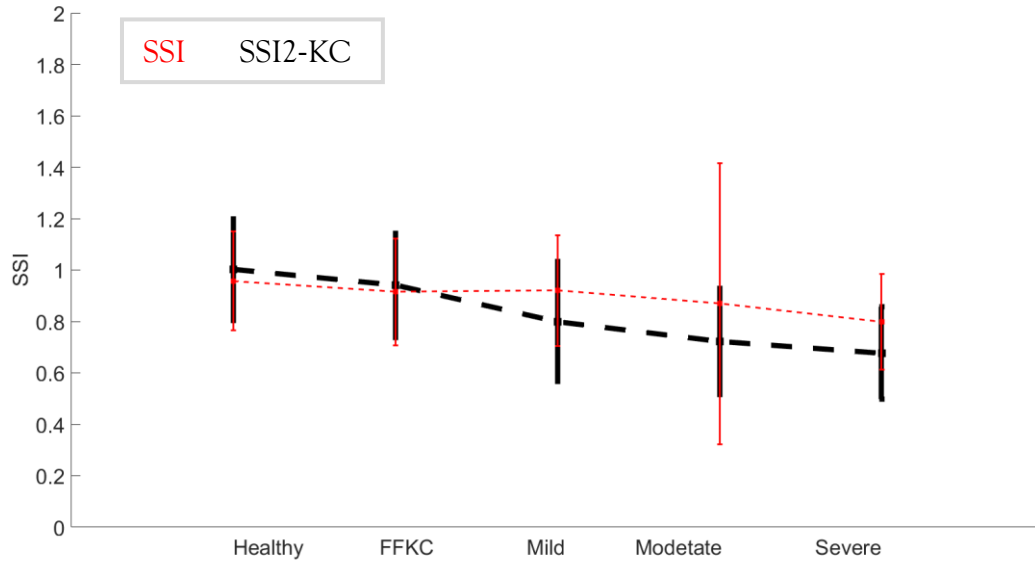


Figure 6-73 The changes in SSI2-KC and SSI in healthy, FFKC, Mild, Moderate and Severe keratoconic cases in Dataset 2

Table 6-10 Showing the mean, standard deviation (SD) and statistical comparison with the healthy group for SSI / SSI2-KC in the same format as shown here in Dataset 2

| | | | | | |
|----------------|----------|-------------|-------------|-------------|-------------|
| Mean | 0.96/1 | 0.92/0.94 | 0.92/0.8 | 0.87/0.72 | 0.8/0.68 |
| SD | 0.19/0.2 | 0.21/0.2 | 0.21/0.23 | 0.55/0.21 | 0.19/0.18 |
| p value | 1/1 | 0.217/0.019 | 0.136/0.001 | 0.000/0.000 | 0.007/0.001 |

Dataset 3

It included 363 patients with a mean age of 33.2 ± 10.8 (13-72) years, CCT of 492 ± 40 (345-590) microns, , bIOP of 13.5 ± 2.3 (7.4-23.4) mmHg, bIOP2 of 15.5 ± 1.1 (11.5-20.2) mmHg, SSI of 0.9 ± 0.24 (0.43-2.19) and SSI2-KC of 0.73 ± 0.16 (0.29-1.31). Correlation with CCT for SSI was $R:0.328$ ($p:0.000$), and for SSI2-KC was $R:0.203$ ($p:0.000$) where both are significant. Correlation with age for SSI was $R:0.144$ ($p:0.006$) and for SSI2-KC was $R:0.699$ ($p:0.000$). Correlation with bIOP2 for SSI was large and significant with $R:0.526$ ($p:0.000$) while SSI2-KC remained insignificant and not correlated with $R:0.043$ ($p:0.418$), Figure 6-74.

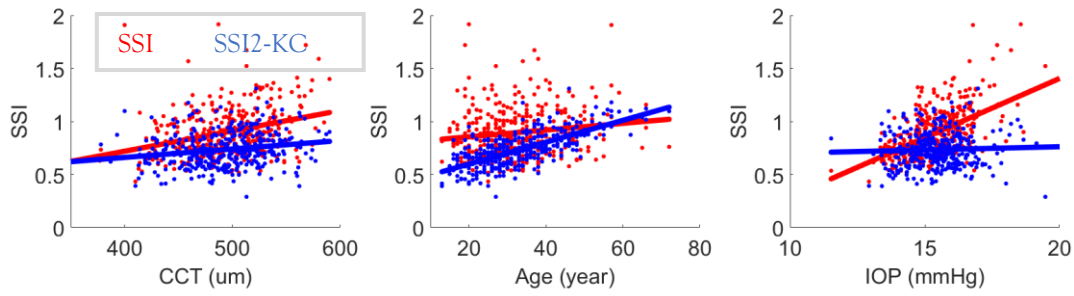


Figure 6-74 The correlation of SSI and SSI2-KC with CCT (left), age (middle) and IOP (right) in Dataset 3

When comparing the changes in SSI and SSI2-KC with disease progression, it is clear that both equations followed a clear trend. In severe cases, corneal biomechanics changed and became softer than less severe or healthy patients. SSI2-KC showed a more significant softening in Mild, Moderate and Severe cases, Figure 6-75. The detailed analysis for means, standard deviations and statistical comparison of SSI values to the healthy group is provided in Table 6-11.

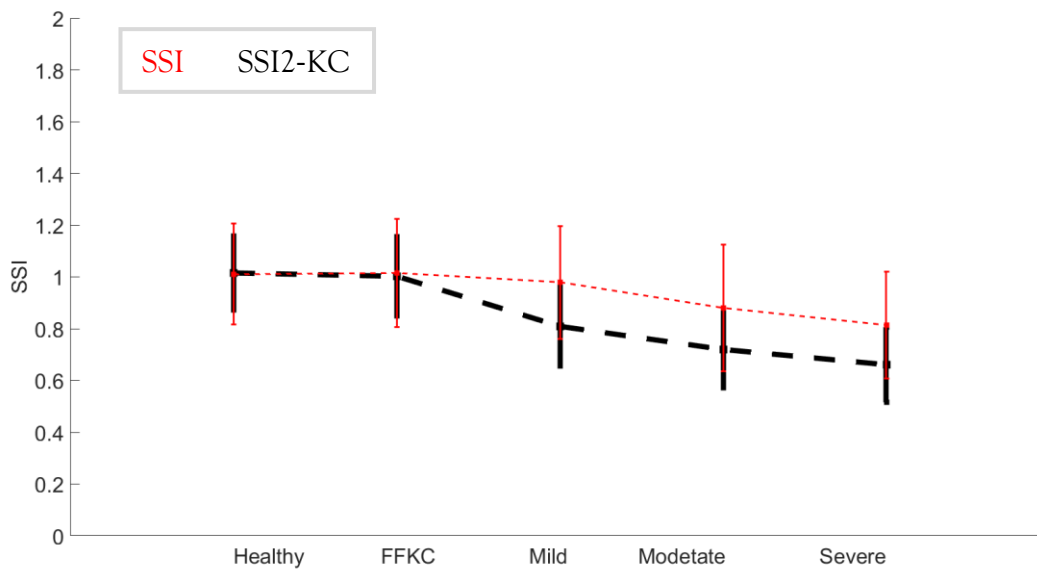


Figure 6-75 The changes in SSI2-KC and SSI in healthy, FFKC, Mild, Moderate and Severe keratoconic cases in Dataset 3

Table 6-11 Showing the mean, standard deviation (SD) and statistical comparison with the healthy group for SSI / SSI2-KC in the same format as shown here in Dataset 3

| | | | | | |
|-------------|-----------|-----------|-----------|-----------|-----------|
| Mean | 1.01/1.02 | 1.02/1 | 0.98/0.81 | 0.88/0.72 | 0.81/0.66 |
| SD | 0.2/0.14 | 0.21/0.15 | 0.22/0.15 | 0.24/0.15 | 0.21/0.15 |

| | | | | | |
|---------|-----|-------------|-------------|-------------|-------------|
| p value | 1/1 | 0.815/0.237 | 0.053/0.000 | 0.000/0.000 | 0.000/0.000 |
|---------|-----|-------------|-------------|-------------|-------------|

Dataset 4

It included 227 patients with a mean age of 27.6 ± 7.5 (12-58) years, CCT of 482 ± 40 (374 -636) microns, bIOP of 15.6 ± 1.9 (8.5-23.3) mmHg, bIOP2 of 15.9 ± 1.1 (13.3-19.9) mmHg, SSI of 0.91 ± 0.24 (0.51-1.77) and SSI2-KC of 0.74 ± 0.14 (0.34-1.14). Correlation with CCT for SSI was large and significant with $R:0.291$ ($p:0.000$), while for SSI2, it remained weak and insignificant with $R:0.054$ ($p:0.417$). Correlation with age for SSI was $R:0.238$ ($p:0.000$) and for SSI2-KC was $R:0.603$ ($p:0.000$). Correlation with bIOP2 for SSI was large and significant with $R:0.637$ ($p:0.000$) and for SSI2-KC it became weak and insignificant $R:0.098$ ($p:0.141$), Figure 6-76.

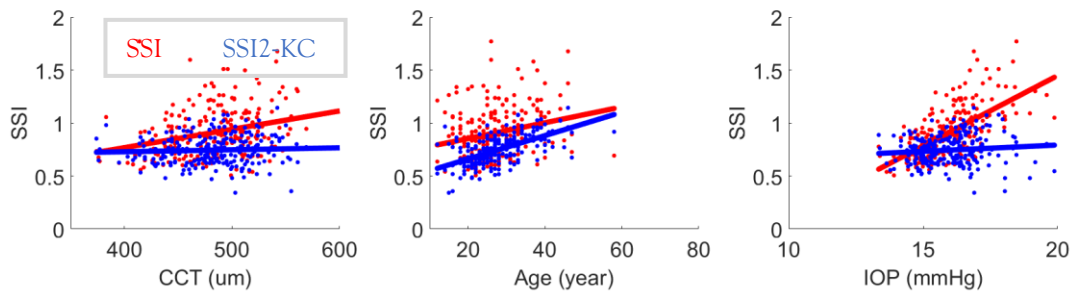


Figure 6-76 The correlation of SSI and SSI2-KC with CCT (left), age (middle) and IOP (right) in Dataset 4

When comparing the changes in SSI and SSI2-KC with disease progression, it is clear that SSI2-KC equation followed a clear trend. In severe cases, corneal biomechanics changed and became softer than less severe or healthy patients. SSI did not follow any trend, and it increased and decreased in various group. SSI2-KC showed a more significant softening in Mild, Moderate and Severe cases, Figure 6-77. The detailed analysis for means, standard deviations and statistical comparison of SSI values to the healthy group is provided in Table 6-12.

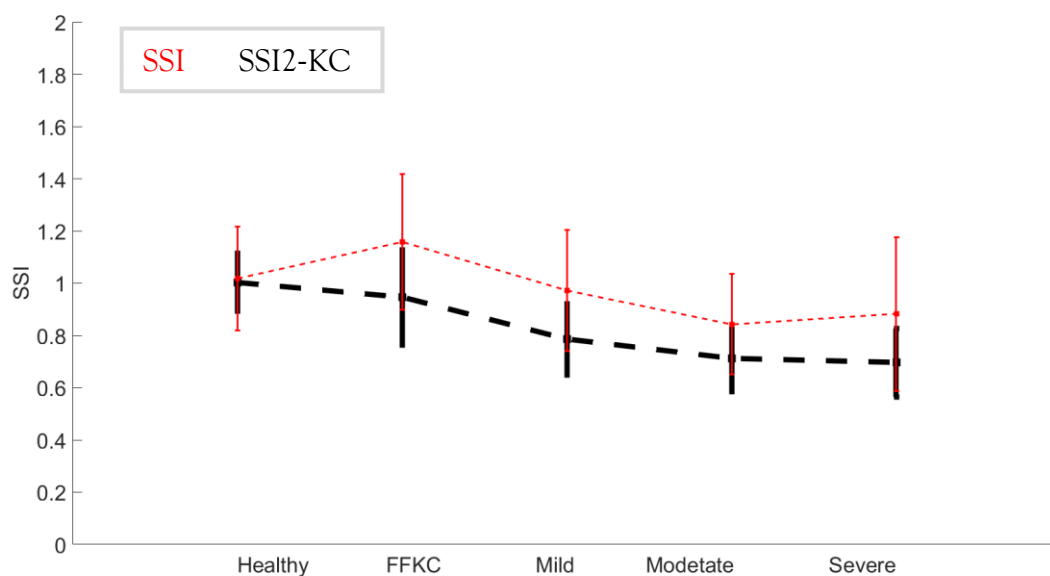


Figure 6-77 The changes in SSI2-KC and SSI in healthy, FFKC, Mild, Moderate and Severe keratoconic cases in Dataset 4

Table 6-12 Showing the mean, standard deviation (SD) and statistical comparison with the healthy group for SSI / SSI2-KC in the same format as shown here in Dataset 4

| | | | | | |
|----------------|----------|-------------|-------------|-------------|-------------|
| Mean | 1.02/1 | 1.16/0.95 | 0.97/0.79 | 0.84/0.71 | 0.88/0.7 |
| SD | 0.2/0.11 | 0.26/0.18 | 0.23/0.14 | 0.19/0.13 | 0.29/0.13 |
| p value | 1/1 | 0.001/0.022 | 0.037/0.000 | 0.000/0.000 | 0.000/0.000 |

Dataset 5

It included 14 patients with a mean age of 33.6 ± 12.2 (20-66) years, CCT of 484 ± 22 (451 - 529) microns, bIOP of 13.9 ± 1.8 (11.8-16.7) mmHg, bIOP2 of 15.3 ± 1.1 (13.4 - 17.1) mmHg, SSI of 0.82 ± 0.19 (0.46-1.12) and SSI2-KC of 0.73 ± 0.14 (0.52-1.09). Correlation with CCT for SSI was strong with $R:0.546$ ($p:0.044$), and for SSI2-KC weak and insignificant with $R:0.239$ ($p:0.410$). Correlation with age for SSI was $R:0.108$ ($p:0.714$) and for SSI2-KC was $R:0.821$ ($p:0.000$). Correlation with bIOP2 for SSI was large and significant with $R:0.821$ ($p:0.000$) while SSI2-KC remained not correlated with $R:0.012$ ($p:0.968$), Figure 6-78.

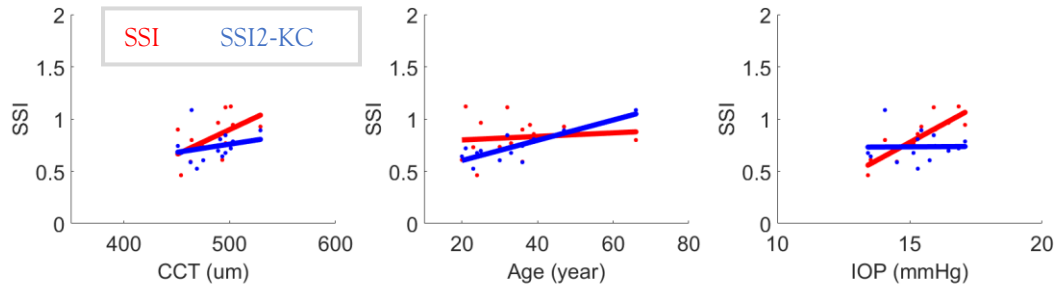


Figure 6-78 The correlation of SSI and SSI2-KC with CCT (left), age (middle) and IOP (right) in Dataset 5

When comparing the changes in SSI and SSI2-KC with disease progression, it is clear that both equations followed a trend. They both reduced with disease severity; however, SSI changes are small. SSI2-KC showed a more significant softening in Mild, Moderate and Severe cases, Figure 6-79. The detailed analysis for means, standard deviations and statistical comparison of SSI values to the healthy group is provided in Table 6-13.

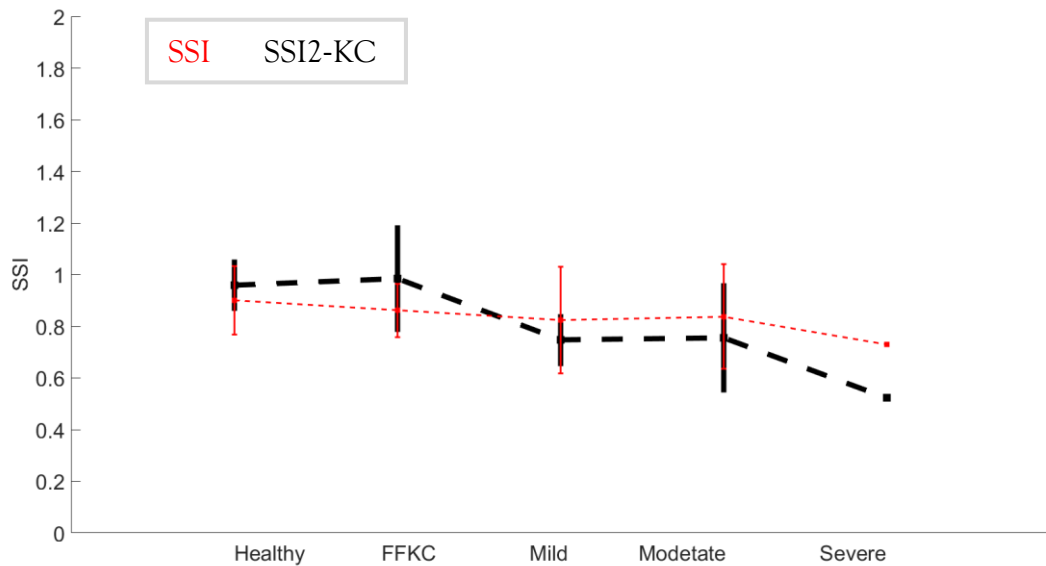


Figure 6-79 The changes in SSI2-KC and SSI in healthy, FFKC, Mild, Moderate and Severe keratoconic cases in Dataset 5

Table 6-13 Showing the mean, standard deviation (SD) and statistical comparison with the healthy group for SSI / SSI2-KC in the same format as shown here in Dataset 5

| | | | | | |
|---------|-----------|-------------|-------------|-------------|-------------|
| Mean | 0.9/0.96 | 0.86/0.98 | 0.82/0.75 | 0.84/0.76 | 0.73/0.52 |
| SD | 0.13/0.09 | 0.1/0.2 | 0.21/0.09 | 0.2/0.2 | 0/0 |
| p value | 1/1 | 0.354/0.959 | 0.277/0.075 | 0.402/0.145 | 0.194/0.097 |

Dataset 6

It included 143 patients with a mean age of 34.1 ± 12.1 (12-66) years, CCT of 490 ± 38 (396-602) microns, bIOP of 13.7 ± 2.4 (7.1-21.1), bIOP2 of 15.1 ± 1.3 (12-19.1), SSI of 0.73 ± 0.18 (0.42-1.36) and SSI2-KC of 0.68 ± 0.15 (0.33-1.15). Correlation with CCT for SSI was $R:0.082$ ($p:0.330$), and for SSI2-KC was $R:0.049$ ($p:0.560$) where both are small and insignificant. Correlation with age for SSI was $R:0.116$ ($p:0.166$) and for SSI2-KC was $R:0.785$ ($p:0.000$). Correlation with bIOP2 for SSI was strong and significant with $R:0.667$ ($p:0.000$) while SSI2-KC remained insignificant with $R:0.125$ ($p:0.125$), Figure 6-80.

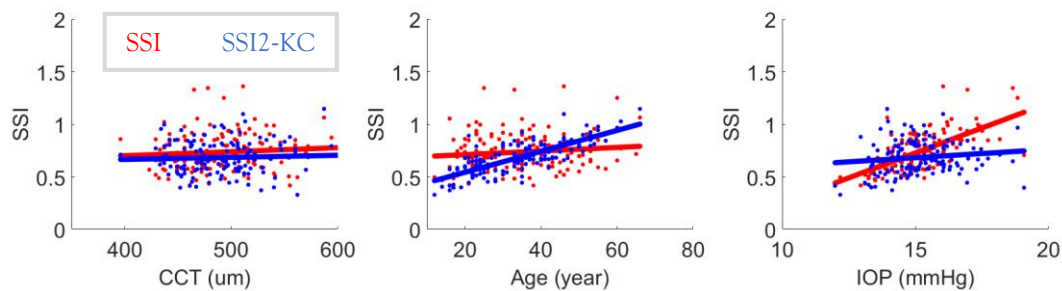


Figure 6-80 The correlation of SSI and SSI2-KC with CCT (left), age (middle) and IOP (right) in Dataset 6

When comparing the changes in SSI and SSI2-KC with disease progression, it is clear that both equations followed a clear trend. In severe cases, corneal biomechanics changed and became softer than less severe or healthy patients. SSI2-KC showed a more significant softening in Mild, Moderate and Severe cases, Figure 6-81. The detailed analysis for means, standard deviations and statistical comparison of SSI values to the healthy group is provided in Table 6-14.

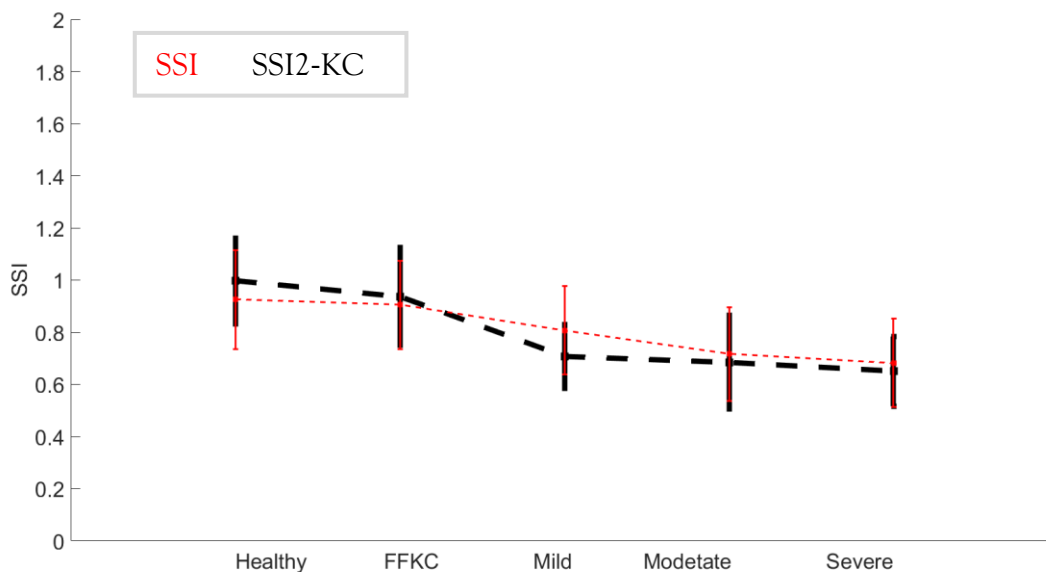


Figure 6-81 The changes in SSI2-KC and SSI in healthy, FFKC, Mild, Moderate and Severe keratoconic cases in Dataset 6

Table 6-14 Showing the mean, standard deviation (SD) and statistical comparison with the healthy group for SSI / SSI2-KC in the same format as shown here in Dataset 6

| | | | | | |
|---------|-----------|-------------|-------------|-------------|-------------|
| Mean | 0.93/1 | 0.90/0.94 | 0.81/0.71 | 0.72/0.69 | 0.68/0.65 |
| SD | 0.19/0.16 | 0.17/0.19 | 0.17/0.12 | 0.18/0.18 | 0.17/0.13 |
| p value | 1/1 | 0.647/0.039 | 0.000/0.000 | 0.000/0.000 | 0.000/0.000 |

Dataset 7

It included 402 patients with a mean age of 27.2±10.5(10-81) years, CCT of 484±43(297-636) microns, bIOP of 15±2.1(8.6-22) mmHg, bIOP2 of 15.5±1.1 (12.6 - 20.1) mmHg, SSI 0.82±0.19(0.39-1.66) and SSI2-KC of 0.7±0.14 (0.34 - 1.35). Correlation with CCT for SSI was large and significant with R:0.321 (p:0.000), and for SSI2-KC was weaker but still significant with R:0.176 (p:0.000). Correlation with age for SSI was R:0.134 (p:0.007) and for SSI2-KC was R:0.775 (p:0.000). Correlation with bIOP2 for SSI was large and significant with R:0.580 (p:0.000) while SSI2-KC remained not correlated with R:-0.042 (p:0.405), Figure 6-82.

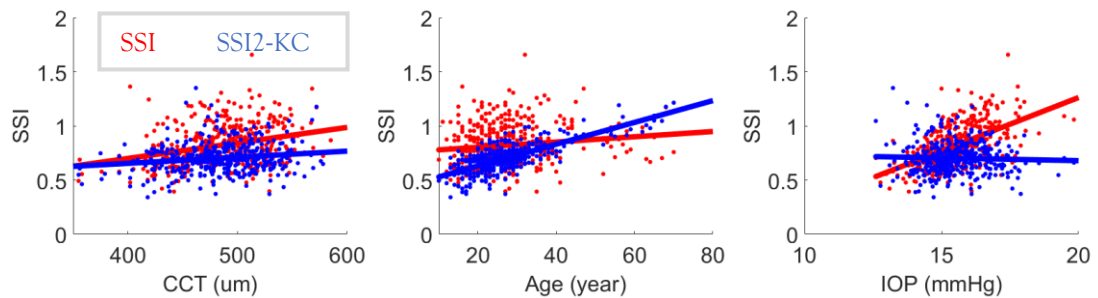


Figure 6-82 The correlation of SSI and SSI2-KC with CCT (left), age (middle) and IOP (right) in Dataset 7

When comparing the changes in SSI and SSI2-KC with disease progression, it is clear that both equations followed a clear trend. In severe cases, corneal biomechanics changed and became softer than less severe or healthy patients. SSI2-KC showed a more significant softening in Mild, Moderate and Severe cases, Figure 6-83. The detailed analysis for means, standard deviations and statistical comparison of SSI values to the healthy group is provided in Table 6-15.

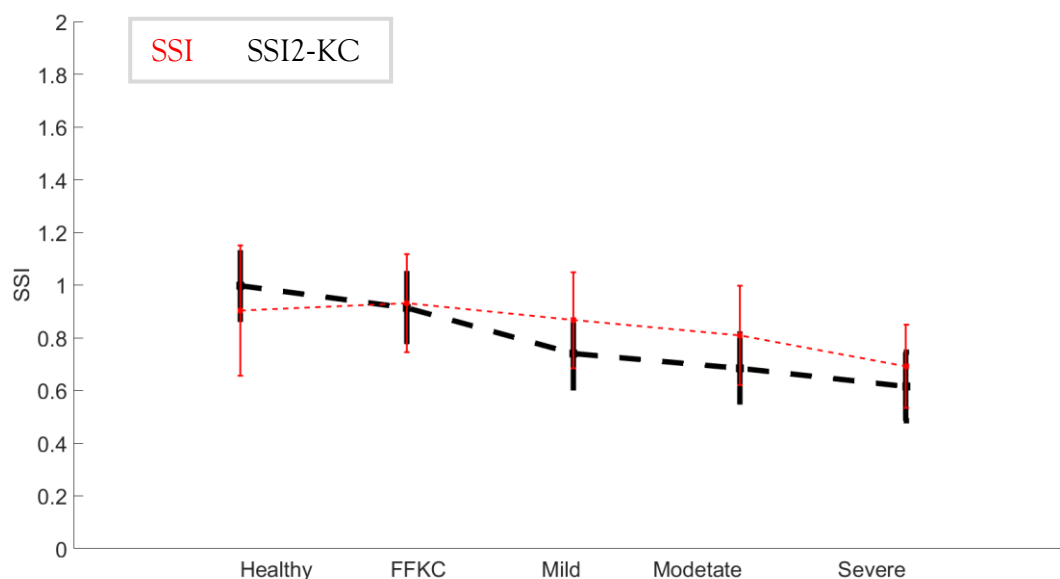


Figure 6-83 The changes in SSI2-KC and SSI in healthy, FFKC, Mild, Moderate and Severe keratoconic cases in Dataset 7

Table 6-15 Showing the mean, standard deviation (SD) and statistical comparison with the healthy group for SSI / SSI2-KC in the same format as shown here in Dataset 7

| | | | | | |
|----------------|-----------|-------------|-------------|-------------|-------------|
| Mean | 0.9/1 | 0.93/0.91 | 0.87/0.74 | 0.81/0.69 | 0.69/0.62 |
| SD | 0.25/0.13 | 0.19/0.13 | 0.18/0.13 | 0.19/0.13 | 0.16/0.13 |
| p value | 1/1 | 0.059/0.000 | 0.671/0.000 | 0.012/0.000 | 0.000/0.000 |

Dataset 8

Combining all datasets resulted in 1522 patients with a mean age of 31.1 ± 11.7 (10-83) years, CCT of 487 ± 40 (297-636) microns, bIOP of 14.3 ± 2.3 (6.1-23.4) mmHg, bIOP2 of 15.5 ± 1.1 (11.5-20.2) mmHg, SSI of 0.86 ± 0.25 (0.1-4.5) and SSI2-KC of 0.73 ± 0.16 (0.29 - 2). Correlation with CCT for SSI was strong with $R:0.257$ ($p:0.000$), and for SSI2-KC weaker with $R:0.131$ ($p:0.000$). Correlation with age for SSI was $R:0.164$ ($p:0.000$) and for SSI2-KC was $R:0.716$ ($p:0.000$). Correlation with bIOP2 for SSI was strong with $R:0.516$ ($p:0.000$) while SSI2-KC was weaker with $R:0.068$ ($p:0.008$) but still significant, Figure 6-84.

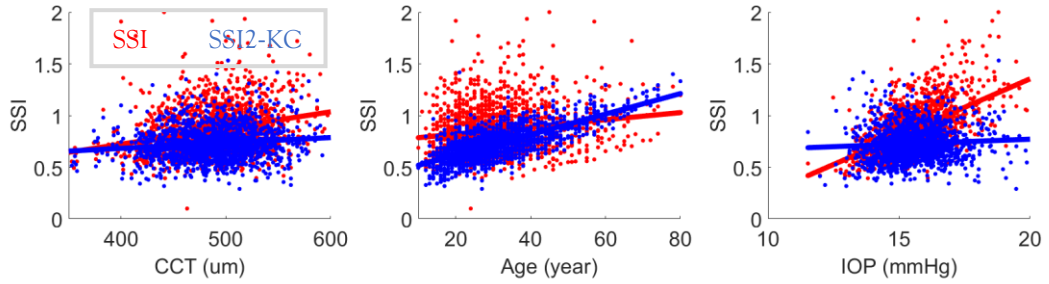


Figure 6-84 The correlation of SSI and SSI2-KC with CCT (left), age (middle) and IOP (right) in Dataset 8

When comparing the changes in SSI and SSI2-KC with disease progression, it is clear that both equations followed a clear trend. In severe cases, corneal biomechanics changed and became softer than less severe or healthy patients. SSI2-KC showed a more significant softening in Mild, Moderate and Severe cases, Figure 6-85. The detailed analysis for means, standard deviations and statistical comparison of SSI values to the healthy group is provided in Table 6-16.

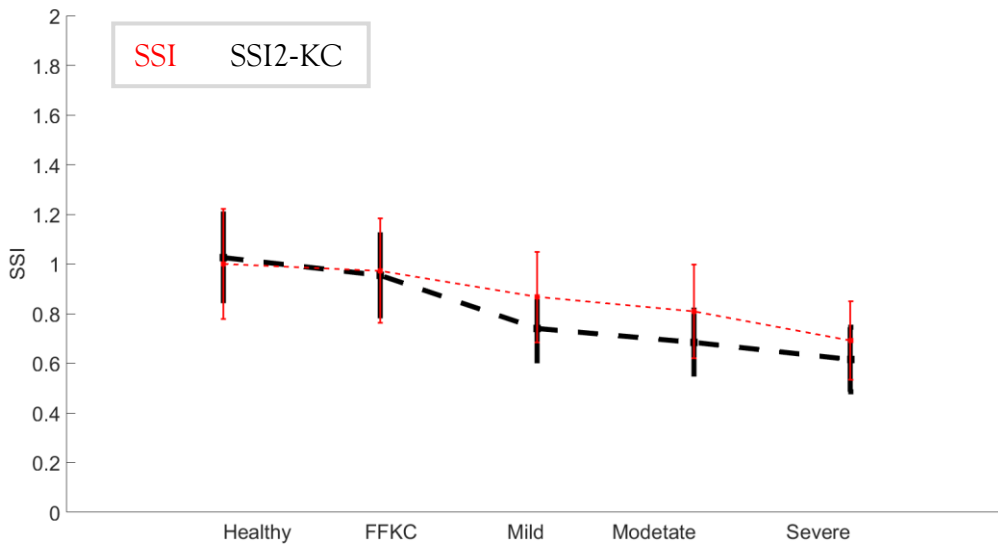


Figure 6-85 The changes in SSI2-KC and SSI in healthy, FFKC, Mild, Moderate and Severe keratoconic cases in Dataset 8

Table 6-16 Showing the mean, standard deviation (SD) and statistical comparison with the healthy group for SSI / SSI2-KC in the same format as shown here in Dataset 8

| | | | | | |
|------|-----------|-----------|-----------|-----------|-----------|
| Mean | 1/1.03 | 0.97/0.95 | 0.87/0.74 | 0.81/0.69 | 0.69/0.62 |
| SD | 0.22/0.17 | 0.21/0.16 | 0.18/0.13 | 0.19/0.13 | 0.16/0.13 |

| | | | | | |
|---------|-----|-------------|-------------|-------------|-------------|
| p value | 1/1 | 0.023/0.000 | 0.000/0.000 | 0.000/0.000 | 0.000/0.000 |
|---------|-----|-------------|-------------|-------------|-------------|

Crosslinked Corneas

Dataset 2

Dataset 2 consists of 37 patients who undergo CXL with a mean CCT of 483 ± 30 (447 - 567) microns, age of 21.9 ± 5 (14-31) years, bIOP of 15 ± 2 (12.5-21.1) mmHg, bIOP2 of 16.1 ± 1 (14.5-18.8) mmHg, SSI of 0.87 ± 0.14 (0.61-1.22) and SSI2-KC of 0.62 ± 0.09 (0.41-0.87). After crosslinking these values changed to a mean CCT of 487 ± 29 (444-569) microns, bIOP of 15.5 ± 2.1 (11.9-21.5) mmHg, bIOP2 of 16.1 ± 1 (14.4-19) mmHg, SSI of 0.97 ± 0.14 (0.7-1.26) and SSI2-KC 0.7 ± 0.08 (0.55-0.88). In SSI, 24.3% of patients showed softening after crosslinking, whereas with SSI2-KC 8.1% showed softening, Figure 6-86.

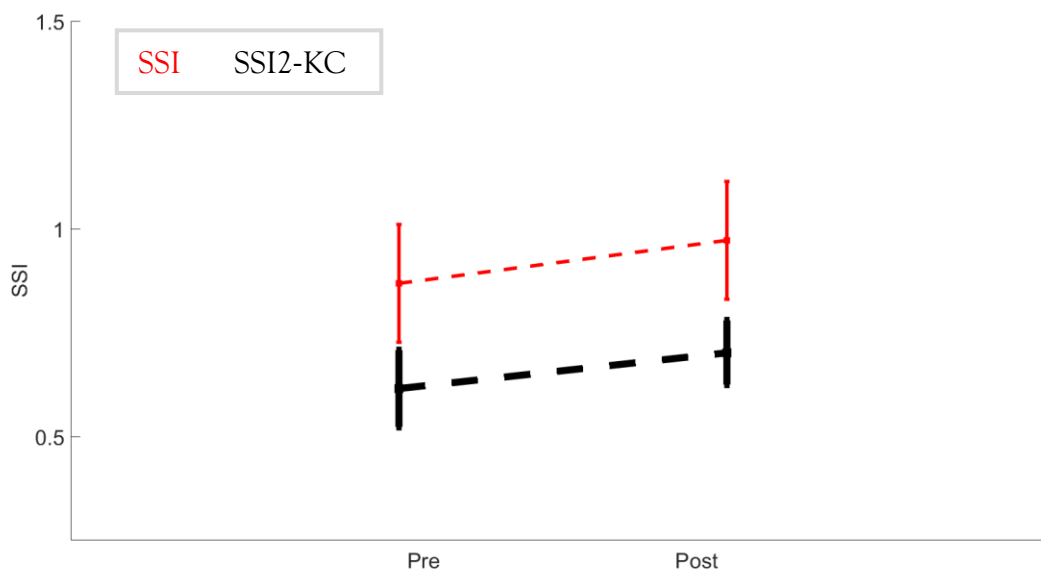


Figure 6-86 The mean and standard deviation of pre-CXL and post-CXL data for SSI and SSI2-KC in the CXL Dataset 2

Correlations with CCT before crosslinking for SSI was strong with $R:0.415$ ($p:0.011$) while SSI2-KC remained insignificant with $R:0.269$ ($p:0.107$). Age correlation with SSI was $R:-0.070$ ($p:0.679$) and with SSI2-KC was $R:0.283$ ($p:0.090$). The correlation of bIOP2 with SSI was strong with $R:0.313$ ($p:0.059$) while SSI2-KC remained uncorrelated with $R:-0.037$ ($p:0.828$), Figure 6-87.

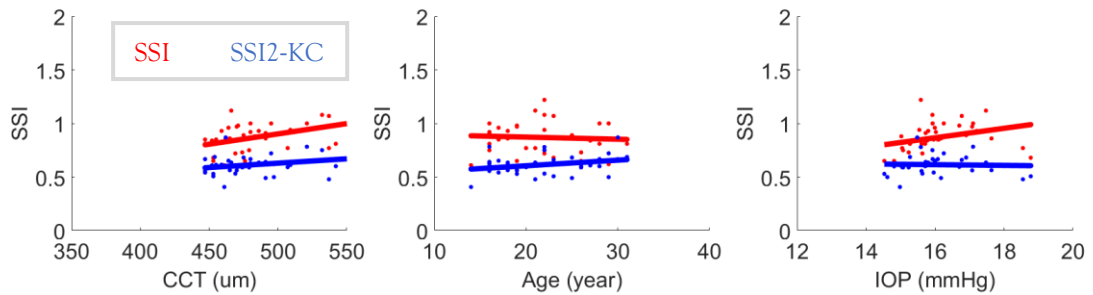


Figure 6-87 The correlation of SSI and SSI2-KC with CCT (left), age (middle) and IOP (right) in the pre-surgery group of CXL Dataset 2

Correlations with CCT after crosslinking for SSI was $R:0.150$ ($p:0.377$) and for SSI2-KC was $R:0.047$ ($p:0.782$) where both remained insignificant. Age correlation with SSI was $R:-0.242$ ($p:0.149$) and with SSI2-KC was $R:0.203$ ($p:0.228$). Correlation of bIOP2 with SSI and SSI2-KC were $R:0.206$ ($p:0.222$) and $R:-0.263$ ($p:0.116$). While both remained insignificant, SSI2-KC had a negative and SSI had a positive correlation, Figure 6-88.

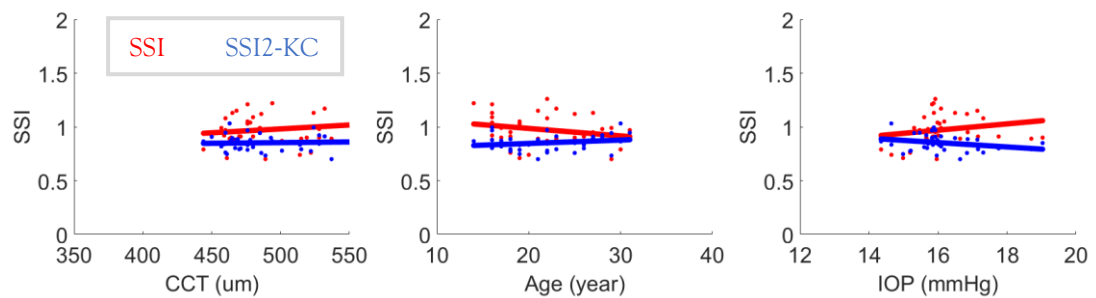


Figure 6-88 The correlation of SSI and SSI2-KC with CCT (left), age (middle) and IOP (right) in the post-surgery group of CXL Dataset 2

Dataset 3

Dataset 3 consist of 21 patients who undergo CXL with a mean CCT of 484 ± 31 (421 - 544) microns, age of 29.2 ± 7.2 (18-41) years, bIOP of 14.4 ± 2.6 (9.8-19.9) mmHg, bIOP2 of 15.9 ± 1 (14.4-17.9) mmHg, SSI of 0.77 ± 0.11 (0.6-1.09) and SSI2-KC of 0.62 ± 0.11 (0.42-0.83). After crosslinking these values changed to a mean CCT of 455 ± 43 (332-523) microns, bIOP of 16 ± 2.1 (11.2-19.5) mmHg, bIOP2 of 16.5 ± 1.1 (13.8-18.6) mmHg, SSI of 0.83 ± 0.22 (0.57-1.43), SSI2-KC of 0.65 ± 0.13 (0.44-0.98). In SSI, 33.3% of patients showed softening after crosslinking, whereas with SSI2-KC 19% showed softening, Figure 6-89.

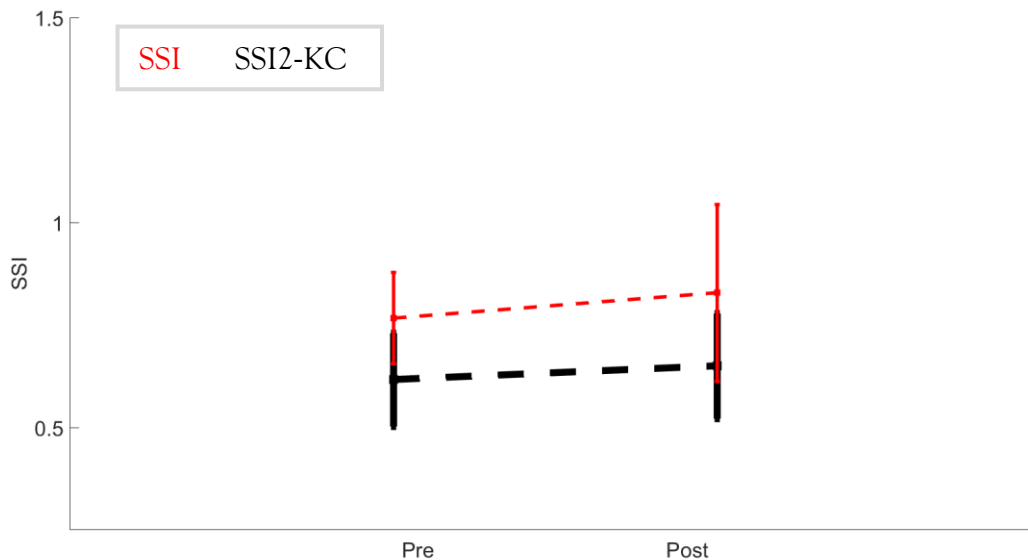


Figure 6-89 The mean and standard deviation of pre-CXL and post-CXL data for SSI and SSI2-KC in the CXL Dataset 3

Correlations with CCT before crosslinking for SSI was $R:0.196$ ($p:0.396$) and for SSI2-KC was $R:0.158$ ($p:0.494$) where both remained insignificant. Age correlation with SSI was $R:0.305$ ($p:0.180$) and with SSI2-KC was $R:0.784$ ($p:0.000$). Correlation of bIOP2 with SSI was strong but insignificant with $R:0.328$ ($p:0.146$) while SSI2-KC was weaker and also insignificant with $R:-0.124$ ($p:0.593$), Figure 6-90.

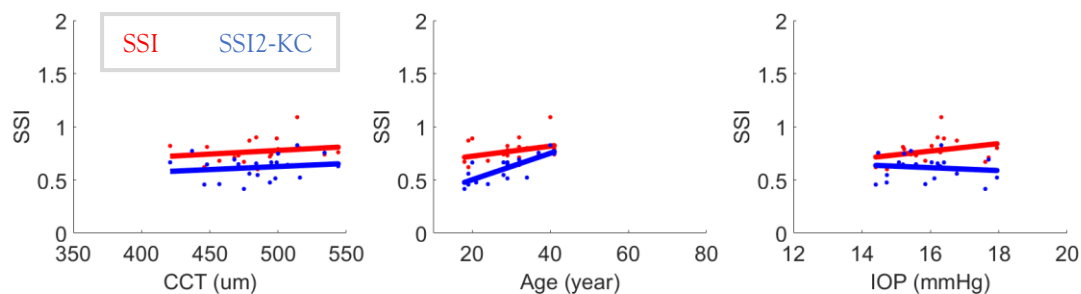


Figure 6-90 The correlation of SSI and SSI2-KC with CCT (left), age (middle) and IOP (right) in the pre-surgery group of CXL Dataset 3

Correlations with CCT after crosslinking for SSI was $R:0.265$ ($p:0.258$) and for SSI2-KC was $R:0.044$ ($p:0.851$) where both are insignificant. Age correlation with SSI was $R:0.530$ ($p:0.016$) and with SSI2-KC was $R:0.737$ ($p:0.000$). Correlation of bIOP2 with SSI and SSI2-KC were $R:0.330$ ($p:0.156$) and $R:0.169$ ($p:0.464$). SSI2-KC showed a weaker correlation with IOP, Figure 6-91.

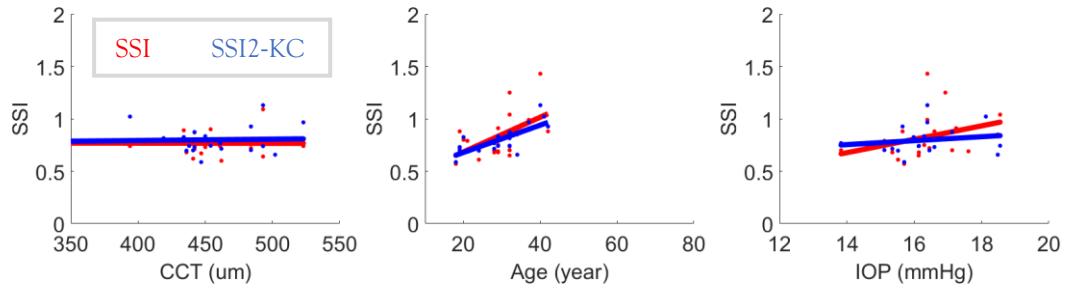


Figure 6-91 The correlation of SSI and SSI2-KC with CCT (left), age (middle) and IOP (right) in post-surgery group of CXL Dataset 3

Dataset 4

This dataset includes 69 CXL eyes with a mean age of 26.1 ± 8.8 (13 -56) years, CCT of 481 ± 38 (404 - 565) microns, bIOP of 13.3 ± 2.4 (7.8 -21.1) mmHg, bIOP2 of 14.9 ± 1.2 (11.7 -18.5) mmHg, SSI2-KC of 0.578 ± 0.142 (0.276 -0.97) and SSI of 0.739 ± 0.192 (0.461 -1.296). After surgery these values changed to a mean age of 26.3 ± 8.8 (13 -56) years, CCT of 467 ± 42 (358 - 572) microns, bIOP of 15.8 ± 2.9 (8.4 - 24.2) mmHg, bIOP2 of 16.1 ± 1.6 (13.5 -21.3) mmHg, SSI2-KC of 0.612 ± 0.137 (0.307 -0.993) and SSI of 0.855 ± 0.278 (0.508 -1.618). In SSI, 18.8% of patients showed softening after crosslinking, whereas with SSI2-KC 26.1% showed softening, Figure 6-92.

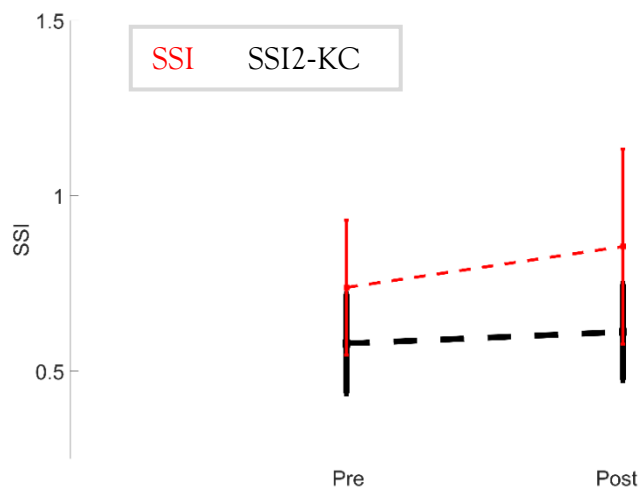


Figure 6-92 The mean and standard deviation of pre-CXL and post-CXL data for SSI and SSI2-KC in the CXL Dataset 4

In pre-surgery data, the correlation with CCT for SSI2-KC was $R:0.204$ ($p:0.093$), which is weaker than SSI with $R:0.348$ ($p:0.003$). Correlation with IOP for SSI2-KC was weak with $R:0.150$ ($p:0.218$) while SSI had strong correlations with $R:0.652$ ($p:0.000$).

Correlation with age for SSI2-KC was $R:0.706$ ($p:0.000$), and for SSI it was insignificant with $R:0.070$ ($p:0.567$), Figure 6-93.

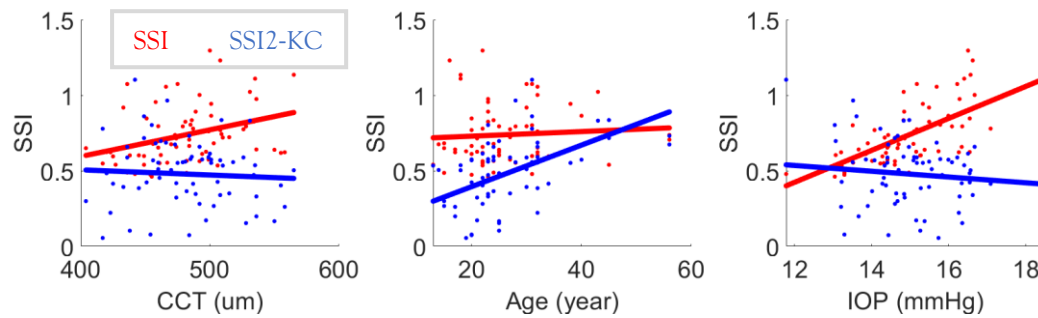


Figure 6-93 The correlation of SSI and SSI2-KC with CCT (left), age (middle) and IOP (right) in the pre-surgery group of CXL Dataset 4

Correlation with CCT remained weaker after the surgery for SSI2-KC with $R:0.216$ ($p:0.075$) than SSI with $R:0.227$ ($p:0.061$). Age correlation was stronger in SSI2-KC with $R:0.720$ ($p:0.000$) than SSI with $R:0.138$ ($p:0.257$). SSI2-KC was not significantly correlated with IOP with $R:0.123$ ($p:0.312$) while SSI had strong correlations with $R:0.515$ ($p:0.000$), Figure 6-94.

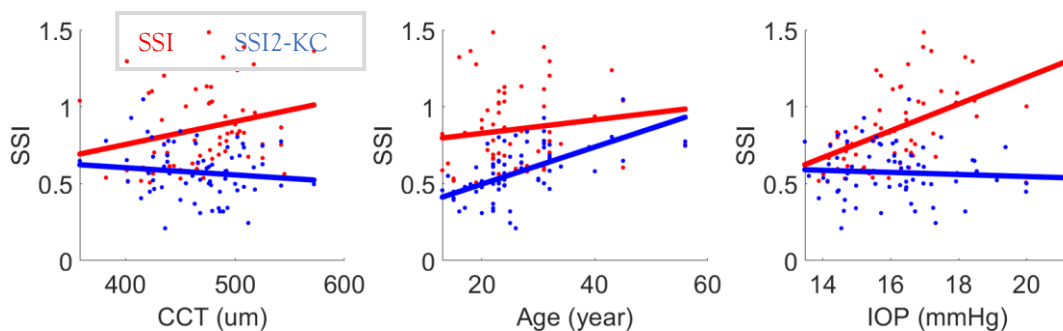


Figure 6-94 The correlation of SSI and SSI2-KC with CCT (left), age (middle) and IOP (right) in the post-surgery group of CXL Dataset 4

SSI-PLS for post LASIK and SMILE

Dataset 2

Dataset 2 consists of 47 patients who undergo LASIK with a mean CCT of 549 ± 34 (476 - 632) microns, age of 35.6 ± 7.4 (21-47) years, bIOP of 14.9 ± 2.2 (11.2-22.5) mmHg, bIOP2 of 15.7 ± 1.4 (13.8-18.8) mmHg, SSI of 1.04 ± 0.25 (0.56-1.67) and SSI2-H of 1.01 ± 0.13 (0.7-1.36). After LASIK these values changed to a mean CCT of 475 ± 51 (348 -583) microns, bIOP of 13.4 ± 1.8 (8.8-17.3) mmHg, bIOP2 of 15.4 ± 0.9 (13.8-17.2) mmHg, SSI of 0.95 ± 0.21 (0.64-1.44) and SSI2-PLS of 0.98 ± 0.1 (0.77-1.17). To evaluate the performance of SSI values, (Pre SSI - Post SSI)/ Pre SSI was calculated. This value for SSI was 0.066 ± 0.161 and for SSI2 was 0.028 ± 0.074 . Bland Altman plots are provided to visualise these changes, Figure 6-95.

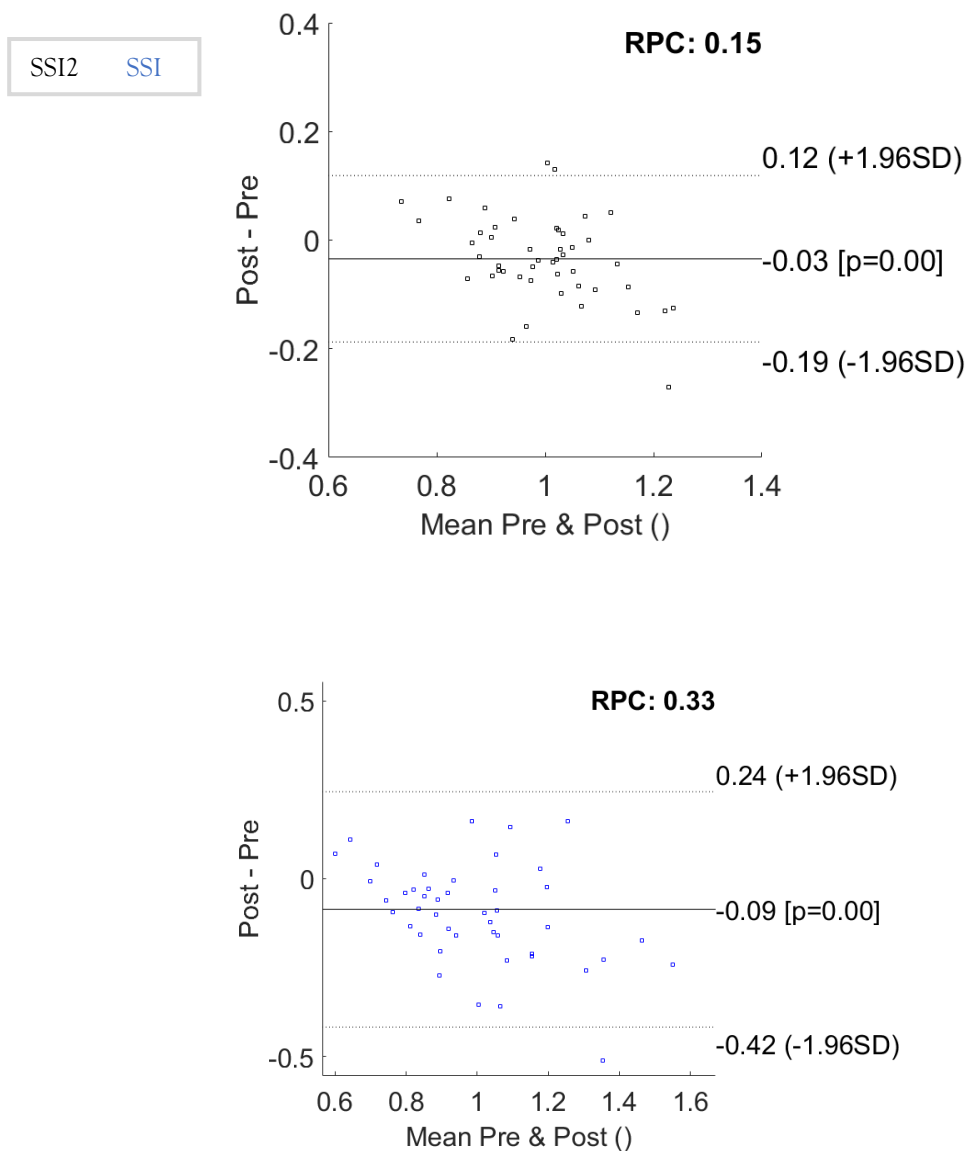


Figure 6-95 Bland Altman plot for (top) SSI2 and (bottom) SSI comparing the pre and post LASIK surgery results in Dataset 2

Further, the correlations between changes in CCT and SSI/SSI2 were evaluated. The correlation for SSI was $R:-0.349$ ($p:0.170$) and for SSI2 was $R:0.069$ ($p:0.792$). This showed SSI2 changes were not significantly influenced by changes in CCT and this value was weaker than SSI, Figure 6-96.

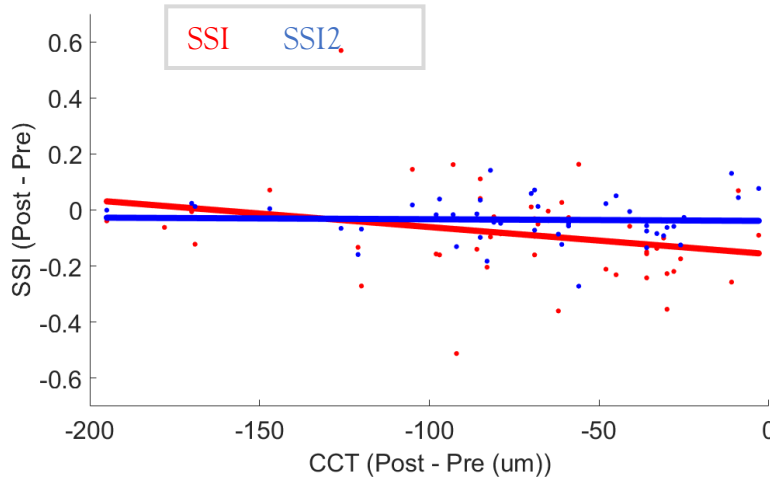


Figure 6-96 The evaluation of correlation in changes in CCT with changes in SSI and SSI2 in the LASIK group of Dataset 2

Correlation with CCT before surgery for SSI was $R:0.083$ ($p:0.579$) and for SSI2-H was $R:0.054$ ($p:0.719$) where both were insignificant. Age correlation with SSI was $R:0.298$ ($p:0.422$) and with SSI2-H was $R:0.572$ ($p:0.000$). The correlation of bIOP2 with SSI was significant and strong with $R:0.504$ ($p:0.000$) and SSI2-H was not correlated with $R:0.029$ ($p:0.847$), Figure 6-97.

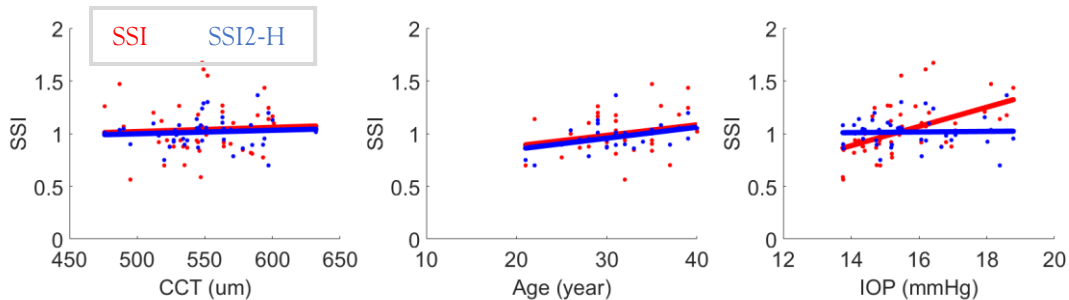


Figure 6-97 The correlation of SSI and SSI2-H with CCT (left), age (middle) and IOP (right) in the pre-surgery LASIK group of Dataset 2

Correlations with CCT after surgery for SSI became strong and significant with $R:0.442$ ($p:0.002$) while SSI2-PLS remained insignificant with $R:0.229$ ($p:0.121$). Age correlation with SSI was $R:0.222$ ($p:0.135$) and with SSI2-PLS was $R:0.704$ ($p:0.000$). Correlation of bIOP2 with SSI remained strong and significant with $R:0.351$ ($p:0.016$) while SSI2-PLS remained weak and insignificant with $R:-0.097$ ($p:0.516$), Figure 6-98.

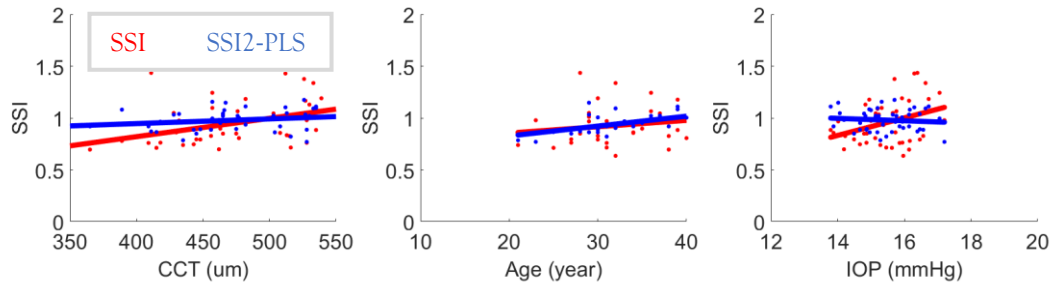
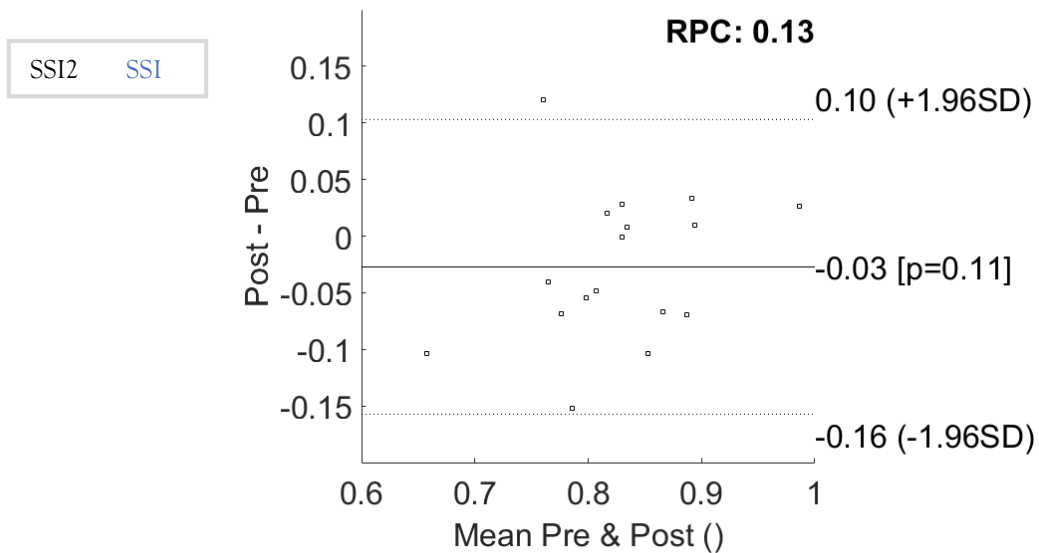


Figure 6-98 The correlation of SSI and SSI2-PLS with CCT (left), age (middle) and IOP (right) in the post-surgery LASIK group of Dataset 2

Dataset 2 further includes 17 patients who undergo SMILE surgery with a mean CCT of 548 ± 22 (515-595) microns, age of 24.1 ± 4.5 (18-31) years, bIOP of 16.8 ± 1.3 (14.5 - 19) mmHg, bIOP2 of 16.6 ± 0.8 (15.2-18.1) mmHg, SSI of 1.01 ± 0.13 (0.84-1.3) and SSI2-H of 0.84 ± 0.07 (0.7-0.97). After SMILE these values changed to a mean CCT of 450 ± 26 (409-499) microns, age of 24.8 ± 4.3 (19-32) years, bIOP of 16.2 ± 1.5 (14.3-19.1) mmHg, bIOP2 of 16.6 ± 1 (15.1-19.3) mmHg, SSI of 0.86 ± 0.11 (0.68-1.07) and SSI2-PLS of 0.81 ± 0.09 (0.61-1). To evaluate the performance of SSI values, $(\text{Pre SSI} - \text{Post SSI}) / \text{Pre SSI}$ was calculated. This value for SSI was 0.137 ± 0.136 and for SSI2 was 0.031 ± 0.083 . Bland Altman plots are provided to visualise these changes, Figure 6-99.



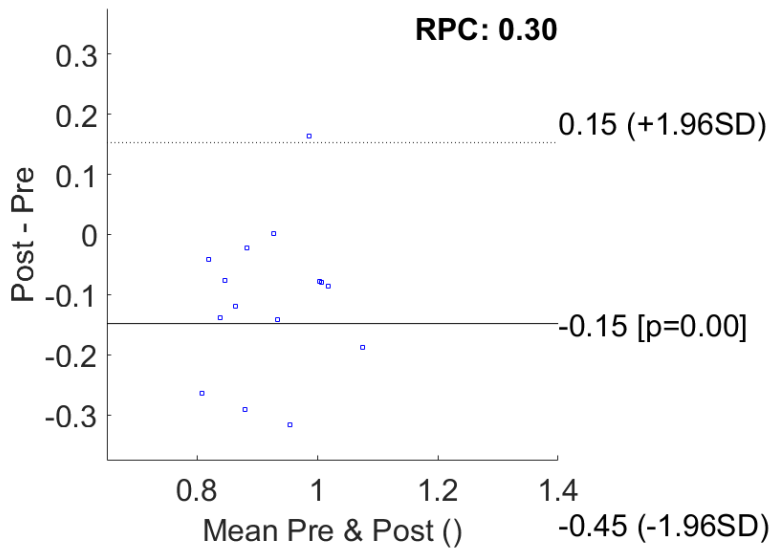


Figure 6-99 Bland Altman plot for SSI2 (top) and SSI (bottom) comparing the pre and post SMILE surgery results in Dataset 2

Further, the correlations between changes in CCT and SSI/SSI2 were evaluated. The correlation for SSI was $R:0.069$ ($p:0.792$) and for SSI2 was $R:-0.349$ ($p:0.170$). Both remained insignificant while SSI showed a weaker positive correlation and SSI2 showed a stronger negative correlation, Figure 6-100.

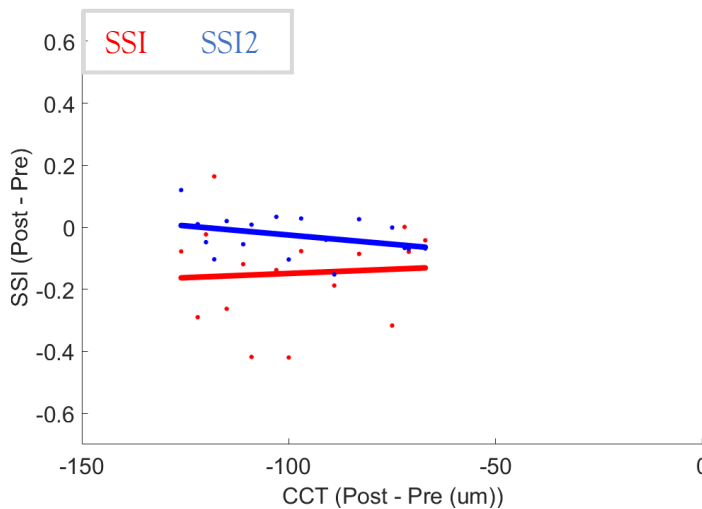


Figure 6-100 The evaluation of correlation in changes in CCT with changes in SSI and SSI2 in SMILE group of Dataset 2

Correlations with CCT before surgery for SSI was $R:0.187$ ($p:0.472$) and for SSI2-H was weaker with $R:0.024$ ($p:0.927$) where both remained insignificant. Age correlation with SSI was negative with $R:-0.059$ ($p:0.822$) and with SSI2-H was $R:0.583$ ($p:0.014$). Correlation of bIOP2 with SSI was weak and positive with $R:0.138$ ($p:0.598$) and SSI2-H showed a stronger negative correlation with $R:-0.415$ ($p:0.098$) but insignificant, Figure 6-101.

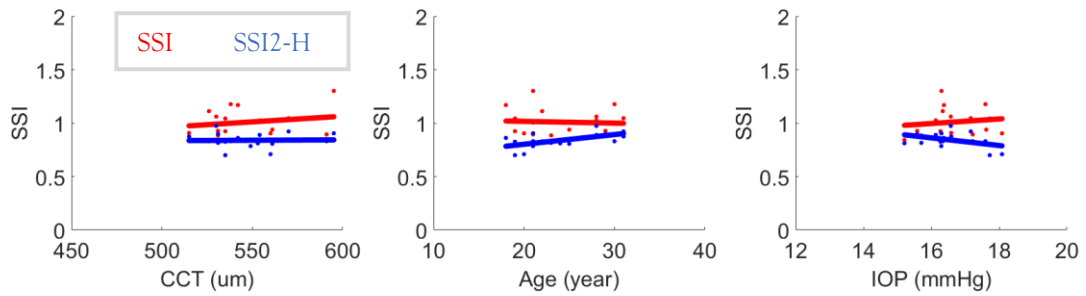


Figure 6-101 The correlation of SSI and SSI2-H with CCT (left), age (middle) and IOP (right) in the pre-surgery SMILE group of Dataset 2

Correlations with CCT after surgery for SSI was $R:0.214$ ($p:0.409$) and for SSI2-PLS was weaker and negative with $R:-0.184$ ($p:0.480$). Age correlation with SSI was negative with $R:-0.239$ ($p:0.356$) and SSI2-PLS remained positive with $R:0.644$ ($p:0.005$). Correlation of bIOP2 with SSI and SSI2-PLS were $R:0.816$ ($p:0.000$) and $R:-0.534$ ($p:0.027$). Both were significant where SSI was positively correlated and SSI2-PLS negatively, Figure 6-102.

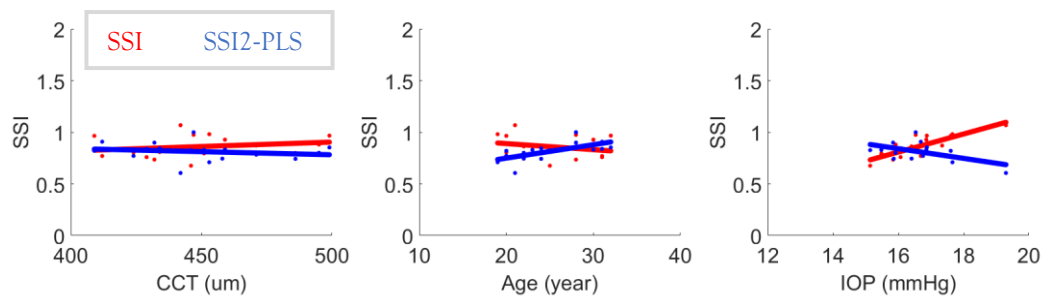


Figure 6-102 The correlation of SSI and SSI2-PLS with CCT (left), age (middle) and IOP (right) in the post-surgery SMILE group of Dataset 2

Dataset 3

Dataset 3 consists of 43 patients who undergo LASIK with a mean CCT of 560 ± 27 (510- 605) microns, age of 25 ± 5.2 (17-36) years, bIOP of 13.8 ± 1.6 (11.2-18.8) mmHg, bIOP2 of 15.2 ± 1 (13.7-17.9) mmHg, SSI of 0.98 ± 0.13 (0.66-1.33) and SSI2-H of 0.83 ± 0.09 (0.54-1.03). After LASIK these values changed to a mean CCT of 451 ± 31 (400-530) microns, age of 25.4 ± 5.4 (17-37) years, bIOP of 12.1 ± 1.5 (8.7-16.2) mmHg, bIOP2 of 15.3 ± 0.6 (14-17.2) mmHg, SSI of 0.85 ± 0.08 (0.72-1.11) and SSI2-PLS of 0.82 ± 0.08 (0.68-1.01). To evaluate the performance of SSI values, (Pre SSI - Post SSI)/ Pre SSI was calculated. This value for SSI was 0.126 ± 0.102 and for SSI2 was 0.010 ± 0.111 . Bland Altman plots are provided to visualise these changes, Figure 6-103.

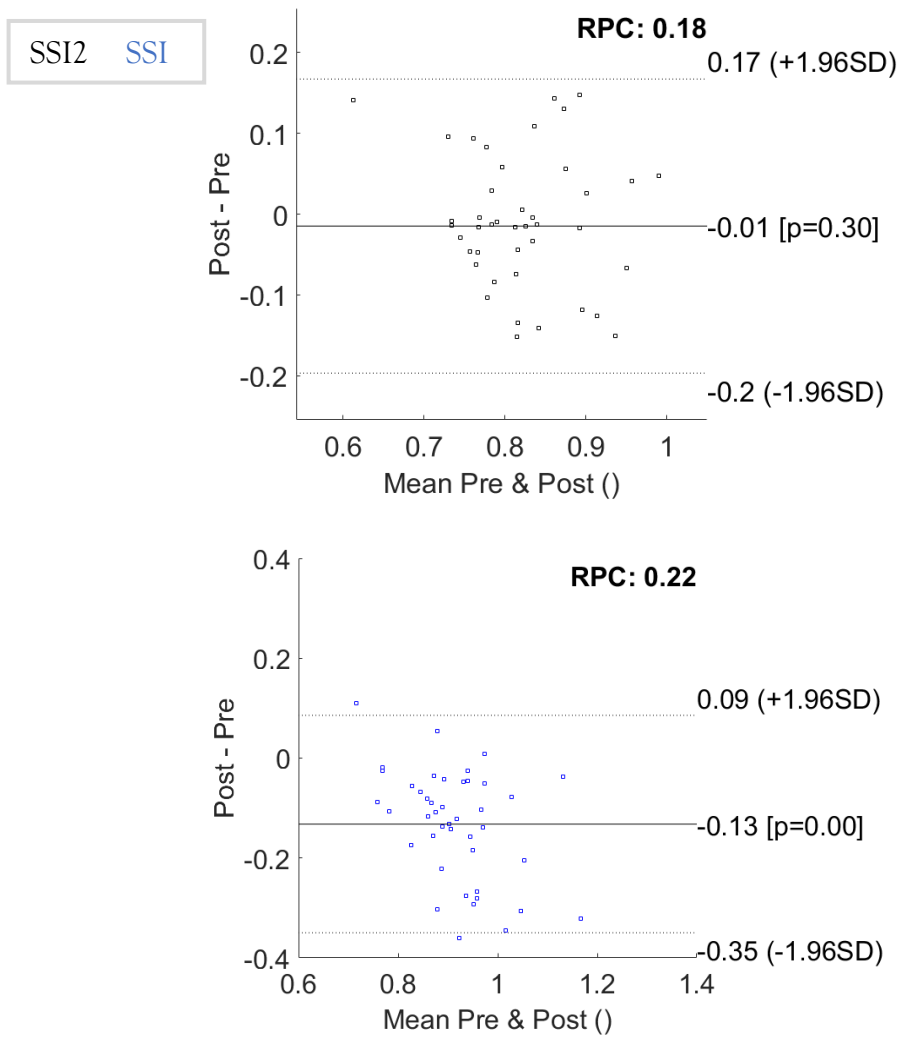


Figure 6-103 Bland Altman plot for SSI2 (top) and SSI (bottom) comparing the pre and post LASIK surgery results in Dataset 3

Further, the correlation between changes in CCT and SSI were evaluated. The correlation for SSI was R:0.245 (p:0.114) and for SSI2 R:0.222 (p:0.152). Both were insignificant and positively correlated with the reduction of CCT, Figure 6-104.

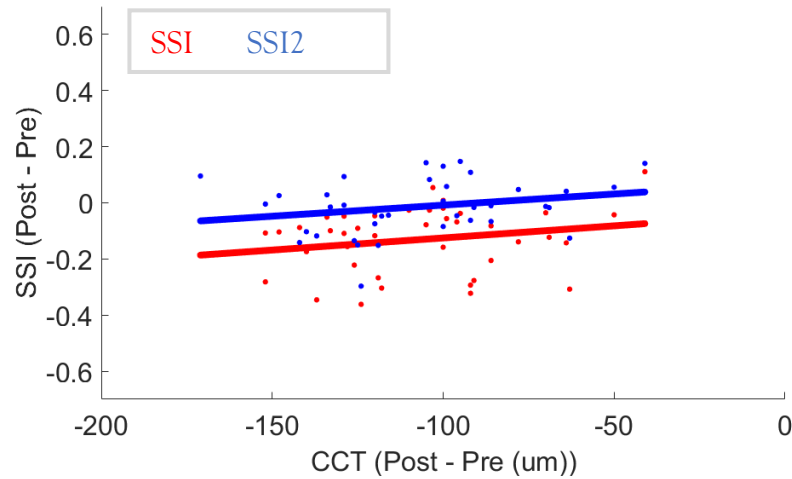


Figure 6-104 The evaluation of correlation in changes in CCT with changes in SSI and SSI2 in the LASIK group of Dataset 3

Correlations with CCT before surgery for SSI was $R:0.096$ ($p:0.541$) and for SSI2-H was $R:-0.131$ ($p:0.403$) where both were insignificant. Age correlation with SSI was $R:0.183$ ($p:0.240$) and with SSI2-H was $R:0.659$ ($p:0.000$). Correlation of bIOP2 with SSI was strong and significant with $R:0.784$ ($p:0.000$) and for SSI2-H it remained insignificant and weakly correlated with $R:0.070$ ($p:0.656$), Figure 6-105.

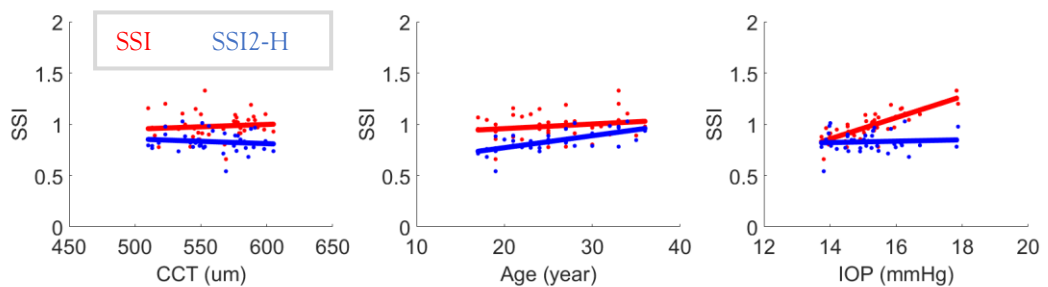


Figure 6-105 The correlation of SSI and SSI2-H with CCT (left), age (middle) and IOP (right) in the pre-surgery LASIK group of Dataset 3

Correlations with CCT after surgery for SSI was $R:0.218$ ($p:0.160$) and for SSI2-PLS was $R:0.1795$ ($p:0.250$) where both remained insignificant. Age correlation with SSI was $R:-0.028$ ($p:0.859$) and with SSI2-PLS was $R:0.558$ ($p:0.000$). Correlation of bIOP2 with SSI remained significant with $R:0.316$ ($p:0.039$) and for SSI2-PLS remained insignificant with $R:-0.057$ ($p:0.718$), Figure 6-106.

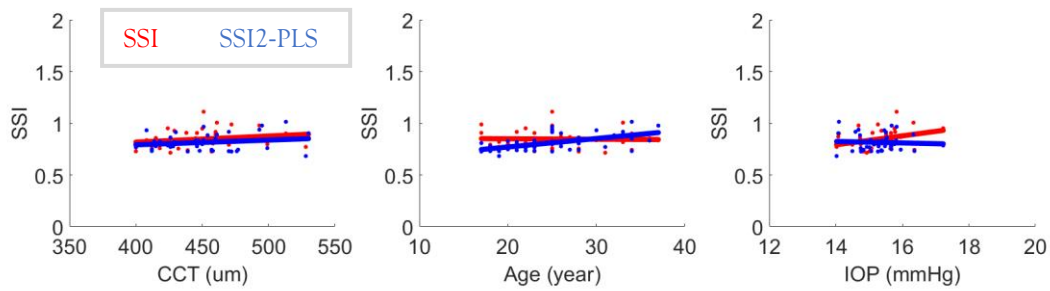
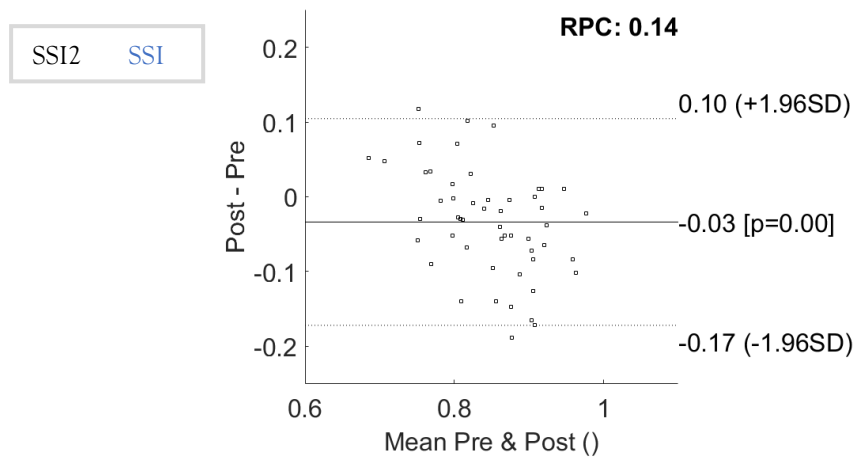


Figure 6-106 The correlation of SSI and SSI2-PLS with CCT (left), age (middle) and IOP (right) in the post-surgery LASIK group of Dataset 3

Dataset 3 includes 52 patients who undergo SMILE surgery with a mean CCT of 556 ± 24 (506-611) microns, age of 26.5 ± 5.4 (17-40) years, bIOP of 14.3 ± 1.9 (10.3 - 18.4) mmHg, bIOP2 of 15.5 ± 1.1 (13.6-18) mmHg, SSI of 1.03 ± 0.14 (0.79-1.37) and SSI2-H of 0.86 ± 0.09 (0.66-1.01). After SMILE these values changed to a mean CCT of 461 ± 23 (416-508) microns, bIOP of 13 ± 1.7 (9.2-17.4) mmHg, bIOP2 of 15.7 ± 0.7 (14.6 - 17.4) mmHg, SSI of 0.89 ± 0.1 (0.7-1.21) and SSI2-PLS of 0.83 ± 0.06 (0.71-0.97). To evaluate the performance of SSI values, $(\text{Pre SSI} - \text{Post SSI}) / \text{Pre SSI}$ was calculated. This value for SSI was 0.127 ± 0.111 and for SSI2 was 0.033 ± 0.081 . Bland Altman plots are provided to visualise these changes, Figure 6-107.



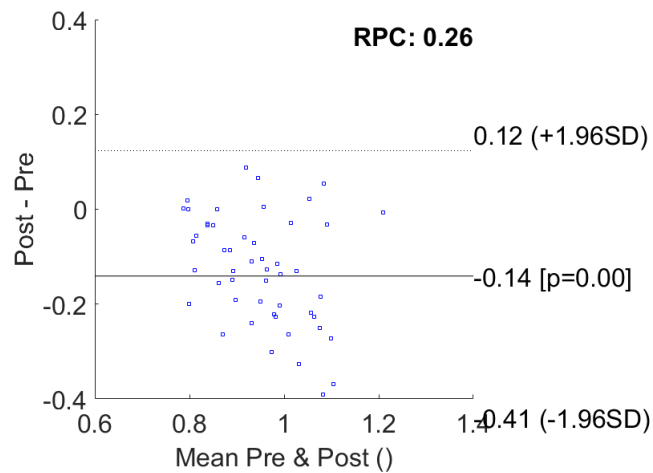


Figure 6-107 Bland Altman plot for SSI2 (top) and SSI (bottom) comparing the pre and post SMILE surgery results in Dataset 3

Further, the correlation between changes in CCT and SSI were evaluated. The correlation for SSI was $R:-0.055$ ($p:0.696$) and for SSI2 $R:0.191$ ($p:0.175$). Both changes in SSI and SSI2 were insignificant and weakly correlated with changes in CCT, Figure 6-108.

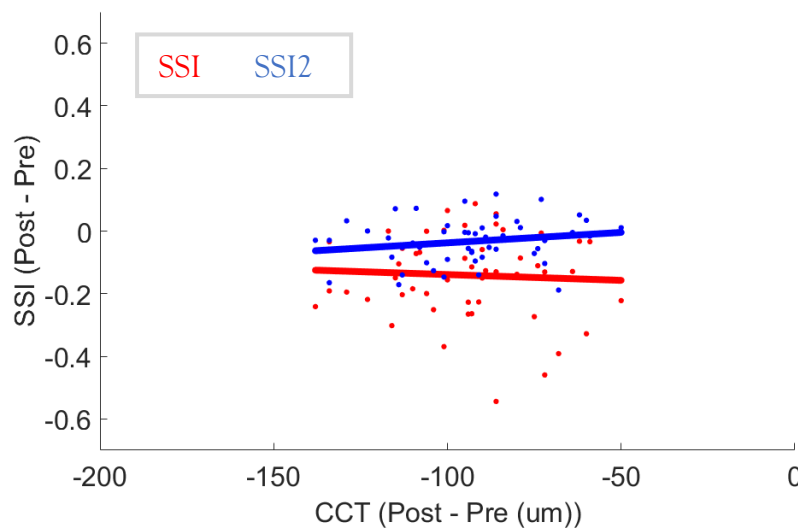


Figure 6-108 The evaluation of correlation in changes in CCT with changes in SSI and SSI2 in SMILE group of Dataset 3

Correlation with CCT before surgery for SSI was $R:0.061$ ($p:0.667$) and for SSI2-H was $R:-0.085$ ($p:0.547$) and both showed insignificant correlations. Age correlation with SSI was negative with $R:-0.239$ ($p:0.087$) and with SSI2-H was $R:0.594$ ($p:0.000$). Correlation of bIOP2 with SSI was strong and significant with $R:0.651$ ($p:0.000$) and for SSI2-H it was weaker but still significant with $R:-0.362$ ($p:0.008$), Figure 6-109.

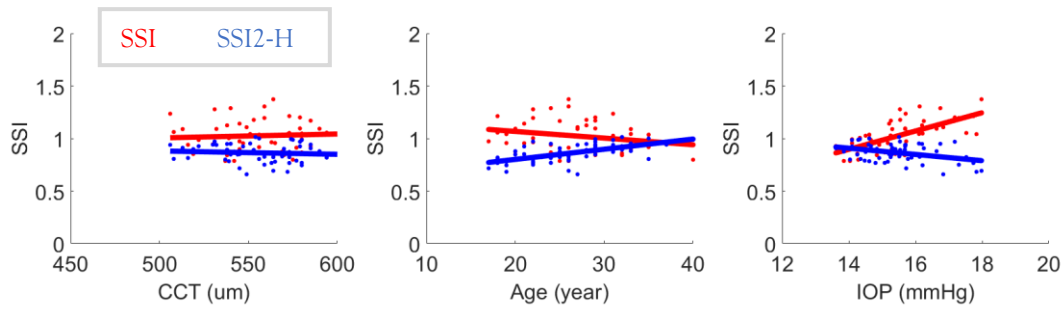


Figure 6-109 The correlation of SSI and SSI2-H with CCT (left), age (middle) and IOP (right) in the pre-surgery SMILE group of Dataset 3

Correlation with CCT before surgery for SSI was strong and significant with $R:0.489$ ($p:0.000$) and for SSI2-PLS it was weak and insignificant with $R:-0.036$ ($p:0.799$). Age correlation with SSI remained negative with $R:-0.286$ ($p:0.040$) and with SSI2-PLS was strong with $R:0.628$ ($p:0.000$). Correlation of bIOP2 with SSI remained strong and significant with $R:0.453$ ($p:0.000$) while SSI2-PLS became weakly correlated and insignificant with $R:-0.148$ ($p:0.295$), Figure 6-110.

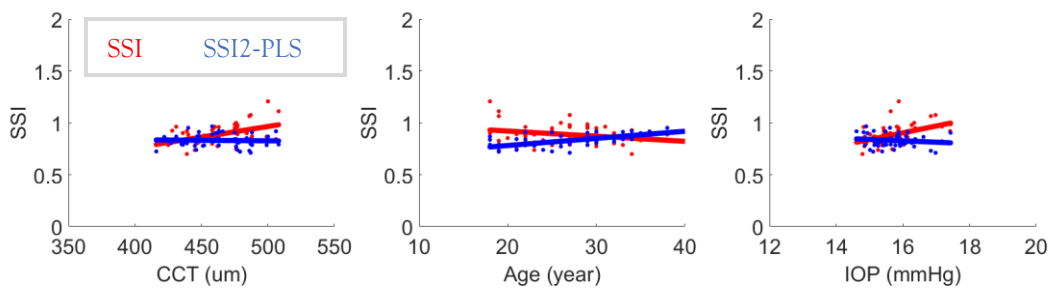


Figure 6-110 The correlation of SSI and SSI2-PLS with CCT (left), age (middle) and IOP (right) in the post-surgery SMILE group of Dataset 3